

DISS. ETH NO. 30149

- I. **Synthesis and Biological Assessment of Analogs of the Marine Macrolide (–)-Zampanolide.**
- II. **Studies Towards the Synthesis of Core-Modified Analogs of β -Lactam Antibiotics: Exploring Reactions of Isocyanates with Aliphatic Imines and Synthesis of New β -Sultam Derivatives.**

A thesis submitted to attain the degree of
DOCTOR OF SCIENCES
(Dr. sc. ETH Zurich)

Presented by

Etienne Victor Cotter

MSc in Interdisciplinary Sciences, ETH Zurich

Born on September 28th, 1994

Accepted on the recommendation of

Prof. Dr. Jonathan Hall, examiner

Prof. Dr. Karl-Heinz Altmann, co-examiner

2024

„Da steh' ich nun, ich armer Tor,
Und bin so klug als wie zuvor!
Heiße Magister, heiße Doktor gar,
Und ziehe schon an die zehen Jahr'
Herauf, herab und quer und krumm
Meine Schüler an der Nase herum –
Und sehe, daß wir nichts wissen können!“

– Johann Wolfgang von Goethe, Faust (1808)

Acknowledgements

Als Erstes möchte ich mich bei Prof. Dr. *Karl-Heinz Altmann* bedanken, der mir grosse wissenschaftliche Freiheiten gab und gleichzeitig sehr viel Zeit und Energie investierte, mich bei jeglichen Fragen zu unterstützen. Danke für deine Geduld in den vielen lehrreichen Gesprächen und für deine hilfreichen Korrekturen, dadurch habe ich mich stets weiterentwickeln können.

I would like to thank Prof. Dr. *Jonathan Hall* for not only taking the co-examination of my thesis, but for accepting to do it for the last four PhDs from our lab, within a month!

Ein grosses Dankeschön geht auch an meinen externen Koexaminator Prof. Dr. *Karl Gademann*.

Special thanks goes to my H494 lab mates, *Carolina Caso*, *Simone Berardozzi*, *Melanie Zechner* and *Simon Glauser*, who created a great scientific environment, but at the same time made me feeling like home. I am very grateful for Simone's supervision during my Master Thesis and throughout my PhD. Carolina went through the good and bad times from start to finish, I was very fortunate having you on my side for this journey.

Dank gilt ebenfalls der Töggeli- und der Tenniscrew für die willkommene Abwechslung: Töggele; *Simone Berardozzi*, *Philipp Waser*, *Christian Bold*, *Simon Glauser*, *Bernhard Pfeiffer*, *Etienne Bonvin*, *Carolina Caso* and *Jennifer Müller*. Tennis; *Simone Berardozzi*, *Philipp Waser*, *Bernhard Pfeiffer*, *Etienne Bonvin* and *Thomas Frossard*. Dä hole mer no!!

Gleiches gilt für die regelmässigen Teilnehmer des wöchentlichen LOC Fussballs, welches ich mit Freuden die letzten Jahre organisieren durfte und mir oft geholfen hat den Kopf frei zu kriegen.

Merci auch den regelmässigen Happy Hour Teilnehmern die für unzählige, lustige Mittwochabende gesorgt haben, sei es in der Alumni Lounge, im Loch Ness, beim frischen Max, im Café Porta d'Oro oder *via Zoom*: *Philipp Waser*, *Carolina Caso*, *Christian Bold*, *Anna Parera Sadurni*, *Jennifer Müller*, *Melanie Zechner*, *Simone Berardozzi*, *Etienne Bonvin*, *Sara Guidicelli*, *Ines Canivete Cuissa*, *Juliane Habiger*, *Thomas Frossard* and *Barbara Stoessel*.

Ein besonderes Dankeschön geht an *Kurt Hauenstein*, die gute Seele der Gruppe. Du hast nie einen Gefallen ausgeschlagen, warst immer sofort bereit zu helfen und dank dir lief das ganze Labor einwandfrei. Ich habe die Zeit und die Gespräche mit dir sehr genossen.

Zusätzlich möchte ich *Philipp* für all seine Hilfe bei jeglichen theoretischen und praktischen Fragen danken, dein fotografisches Gedächtnis hat mich oft weiter gebracht!

Many thanks also to our collaborators Prof. Dr. *Sereina Riniker* and Dr. *Felix Pultar* (ETH, IMPS) and to Dr. *José Fernando Díaz* and his group (CIB, Madrid). I had a great time in and outside the

lab during my research stay in Madrid. Special thanks goes to *Rebeca Paris*, Dr. *Daniel Lucena-Agell*, *Rafael Hortigüela*, *Oscar F. Blanco* and Dr. *Marian A. Oliva* for teaching me the biochemical assays and showing me around in Madrid.

Meinem NMR-Service Team Chef Dr. *Bernhard Pfeiffer* möchte ich für die vielen Tipps und Tricks danken, wie auch für die *in silico* Analysen, die er für uns durchgeführt hat.

I would like to thank my Master and PhD students, who also contributed to this thesis with their dedication and hard work: *Plinio Scapozza*, *Alina Lelke* and *Rebeca Paris*.

Für das ausgezeichnete Gruppenklima möchte ich mich bei den aktuellen und ehemaligen Gruppenmitgliedern bedanken: *Saiyyna Stepanova*, *Alexandre Perera*, *Jasmine Schürmann*, *Yurii Lipisa*, *Lukas Leu*, *Patrick Eisenring* und *Alexandre Bory*.

Danke auch all denen die im Hintergrund agieren und mir die Arbeit an der ETH erleichtert haben: *Sylvia Peleg* (Administration), dem gesamten MoBiAS-Team, dem SMOCC Team, dem LOC NMR Service und allen Mitarbeiter/innen des HCI-Shops.

Die Wichtigsten zum Schluss; meine Familie und Freunde. Ich danke euch von ganzem Herzen für eure Unterstützung und euer Verständnis während meiner fast 10 Jahren an der ETH. Ihr wart der Grund, warum ich dies alles gut überstanden habe! Besonderer Dank geht an meine langjährigen Freunde *David* und *Endrit*, die mich schon seit meiner Kindheit begleiten.

Im Speziellen meinen Eltern *Peter* und *Heidi*, die mich immer und mit allem, was nötig war unterstützt haben, ohne je selbst etwas zu verlangen, möchte ich danken. Gleiches gilt auch für meine Geschwister *Calvin* und *Danielle*, ich bin sehr froh euch zu haben. Zusätzlich bedanke ich mich bei *Peter* und *Miquel* für ihre Hilfe bei den Deckblättern für die Publikationen.

Zu guter Letzt bedanke ich mich von Herzen bei meiner Freundin *Sabrina*, mit der ich unzählige schöne Momente erleben durfte und mir so immer wieder neue Kraft gegeben hat. Danke auch für dein Verständnis, wenn ich den Kopf wieder einmal mit Arbeit voll hatte und du mich auf andere Gedanken gebracht hast.

Table of Contents

| | |
|---|-----------|
| Abstract | i |
| Zusammenfassung | vi |
| Abbreviations and Dimension Units | xi |
| 1 Natural Products in Drug Discovery | 1 |
| 2 Synthesis and SAR Studies of (-)-Zampanolide Analogs | 3 |
| 2.1 Introduction | 3 |
| 2.1.1 Isolations and Structures of Zampanolides..... | 3 |
| 2.1.2 Microtubule Structure and Function..... | 5 |
| 2.1.3 Microtubule Modulators..... | 6 |
| 2.1.4 Biological Activity and Mode of Action | 10 |
| 2.1.5 Total Syntheses of Zampanolide | 13 |
| 2.1.6 Stereoselective Aza-Aldol Reaction for the Construction of Zampanolides | 20 |
| 2.1.7 Structure-Activity Relationship (SAR) Studies | 21 |
| 2.2 Results and Discussion | 27 |
| 2.2.1 Synthesis and Structure-Activity Relationship Studies of C(13)- Desmethylene-(-)-Zampanolide Analogs (Publication 1) | 27 |
| 2.2.2 Synthesis and Structure-Activity Relationship Studies of Dioxane- and Oxathiane-Based Analogs of (-)-Zampanolide (Publication 2) | 50 |
| 2.2.3 Additional Information on Publication 2..... | 65 |
| 2.2.4 Side Chain-Modified Analogs | 72 |
| 2.3 Conclusion and Outlook | 80 |
| 3 Studies Towards the Synthesis of Core-Modified Analogs of β-Lactam Antibiotics ... | 84 |
| 3.1 Introduction | 84 |
| 3.1.1 β -Lactam Antibiotics..... | 85 |
| 3.1.2 Antibacterial Resistance..... | 88 |
| 3.2 1,3-Diazetidione- and β -Sultam-Based Analogs of β -Lactam Antibiotics | 90 |
| 3.2.1 Studies Towards the Synthesis of 1,3-Diazetidione-based Analogs of β - Lactam Antibiotics | 91 |

Table of Contents

| | | |
|----------|--|------------|
| 3.2.2 | Studies Towards the Synthesis of β -Sultam-Based Analogs of β -Lactam Antibiotics..... | 116 |
| 3.3 | Conclusion and Outlook | 132 |
| 4 | Experimental Part..... | 136 |
| 4.1 | General..... | 136 |
| 4.2 | Synthesis and SAR Studies of (-)-Zampanolide Analogs..... | 138 |
| 4.2.1 | Synthesis and Structure-Activity Relationship Studies of C(13)-Desmethylene-(-)-Zampanolide Analogs (Publication 1) | 138 |
| 4.2.2 | Synthesis and Structure-Activity Relationship Studies of Dioxane- and Oxathiane-Based Analogs of (-)-Zampanolide (Publication 2) | 199 |
| 4.2.3 | Side chain-modified analogs | 280 |
| 4.3 | Studies Towards the Synthesis of Core-Modified Analogs of β -lactam Antibiotics .. | 301 |
| 4.3.1 | Studies Towards the Synthesis of 1,3-Diazetidione-Based Analogs of β -Lactam Antibiotics | 301 |
| 4.3.2 | Studies Towards the Synthesis of β -Sultam-Based Analogs of β -Lactam Antibiotics..... | 377 |
| 5 | Bibliography | 405 |
| | Curriculum Vitae..... | 416 |

Abstract

The marine natural product (-)-zampanolide (**A1**) inhibits the growth of human cancer cells by microtubule stabilization with IC_{50} values in the single digit nanomolar range. A number of total syntheses of **A1** have been reported, but the SAR around this compound has remained underexplored.

The first part of this PhD thesis describes the synthesis and biological evaluation of core- and side chain-modified zampanolide analogs **A2-A12** (Figure 1).

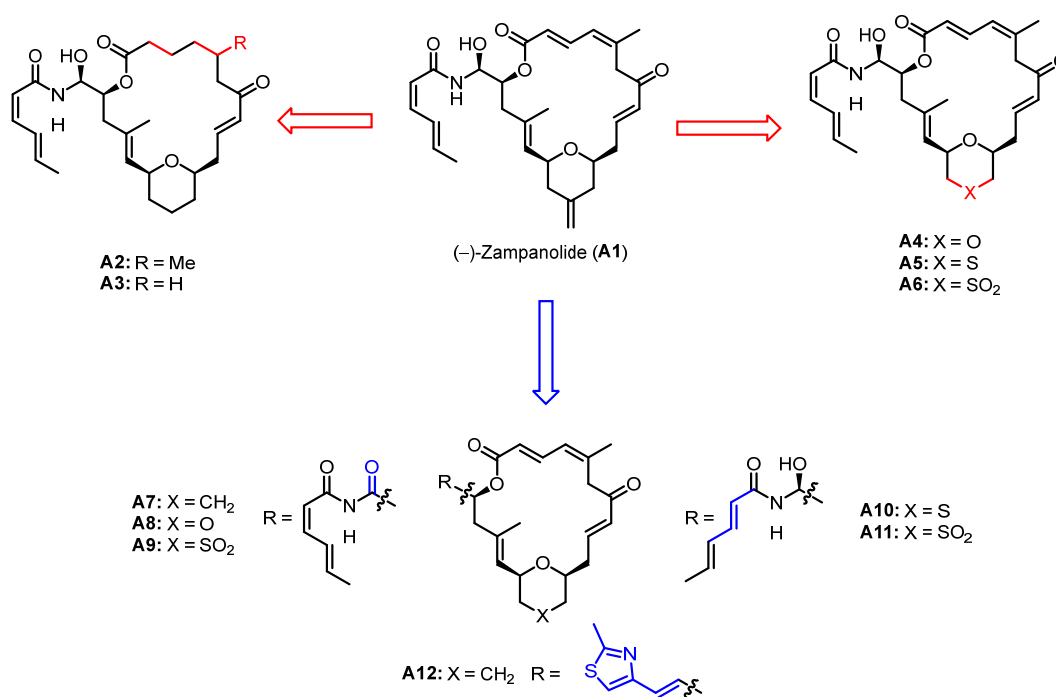
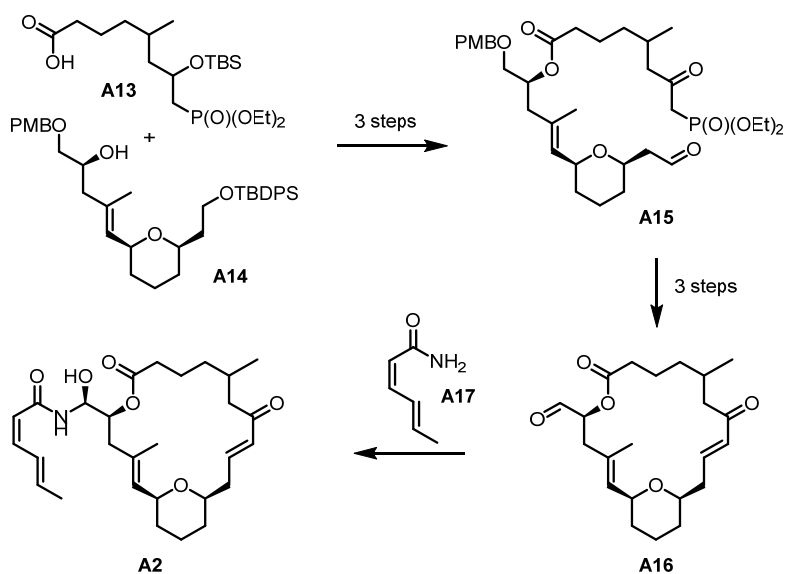


Figure 1: Structure of (-)-zampanolide (**A1**), core-modified (**A2-A6**) and side chain-modified (**A7-A12**) analogs.

The global synthetic strategy followed for all zampanolide analogs prepared is exemplified in **Scheme 1** for the synthesis of **A2**. Acid **A13** was esterified with alcohol **A14**, followed by global desilylation and oxidation to give **A15**. Macrocyclization of the latter by an *E*-selective *HWE* reaction, followed by PMB-cleavage and oxidation delivered **A16**, which was then submitted to a stereoselective aza-aldol reaction with *Z,E*-sorbamide (**A17**) to furnish **A2**.



Scheme 1: Global synthetic strategy for the synthesis of zampanolide analogs **A2-A12** (exemplified for the synthesis of **A2**).

Applying the general strategy exemplified in **Scheme 1** to the synthesis of dioxane- and oxathiane/oxathiane-dioxide-based analogs required access to alcohols **A18** and **A19** (**Figure 2**)

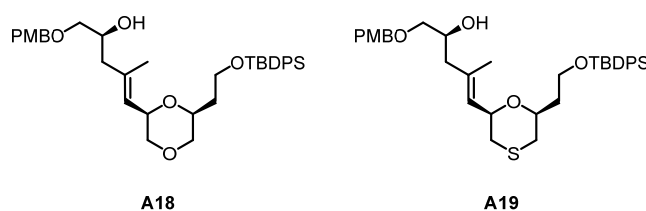
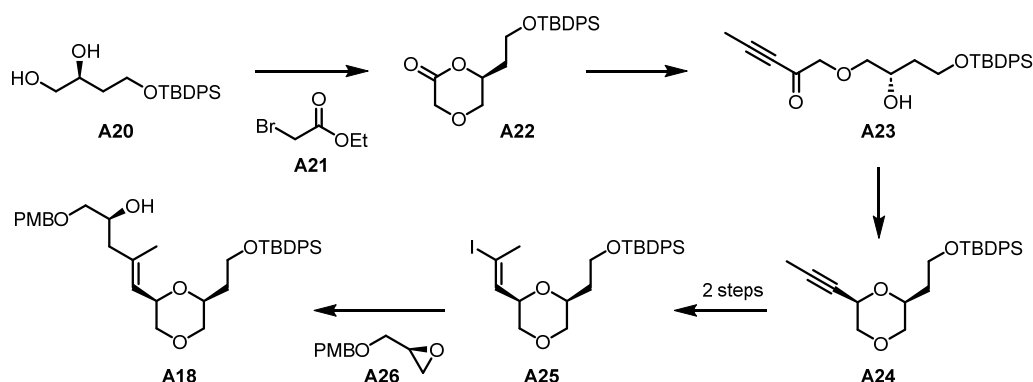


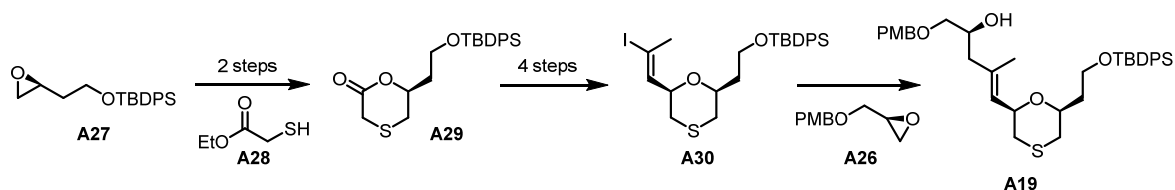
Figure 2: Structures of alcohols **A18** and **A19**.

Dioxane **A18** could be accessed from (*S*)-malic acid in 16% yield over 10 steps *via* known diol **A20** (**Scheme 2**). While the elaboration of **A22** into 2,6-*syn*-disubstituted dioxane **A24** had been previously described in the group in very low yield, a significantly improved route could be established.



Scheme 2: Synthesis of dioxane alcohol **A18**.

Oxathiane **A19** was synthesized from D-aspartic acid *via* known epoxide **A27** in 18% yield over 10 steps (**Scheme 3**). A major challenge posed the epoxide-opening of **A26** with vinyl iodide **A30**, which could be overcome by the use of a combination of lithium- and copper-based reagents.



Scheme 3: Synthesis of oxathiane alcohol **A19**.

Side chain-modified analogs **A7-A9** were obtained by DMP oxidation of hemiaminals **A2**, **A4** and **A6**, respectively. Analogs **A10** and **A11** were prepared *via* stereoselective aldol reaction between the required precursor aldehyde and *E,E*-sorbamide. The zampanolide-epothilone hybrid **A12** was obtained *via* Wittig reaction with aldehyde **A16**.

The antiproliferative potencies of partially saturated analogs **A2** and **A3** were roughly 30-40-fold lower than for **A1**. Dioxane- and oxathiane-based analogs **A4** and **A5** were equipotent with **A1**, while oxathiane-dioxide **A6** was 50-100-fold less active; **A10** and **A11** were 3-12-fold less potent than **A5** and **A6**. Side chain-imide analogs **A7-A9** were 1-2 orders of magnitude less active than **A1**. Surprisingly, **A12** has IC_{50} values only in the low micromolar range.

The second part of this PhD thesis discusses the attempted synthesis of new analogs of β -lactam antibiotics, where the β -lactam ring was to be replaced either by an *N*-acyl-1,3-diazetidione or a β -sultam moiety (**Figure 3**). Conceptually, such compounds were assumed to be sufficiently reactive to undergo opening of the 4-membered ring by penicillin binding proteins. At the same time, it was hypothesized that **A31** and **A32** could be slowly reversible inhibitors of Ser- β -

lactamases, as their reaction with the catalytic Ser residue would result in the formation of a protein-bound carbamate or sulfonic ester, respectively. The latter would be expected to be hydrolyzed much more slowly than the usual ester intermediate formed upon reaction with conventional β -lactam antibiotics.

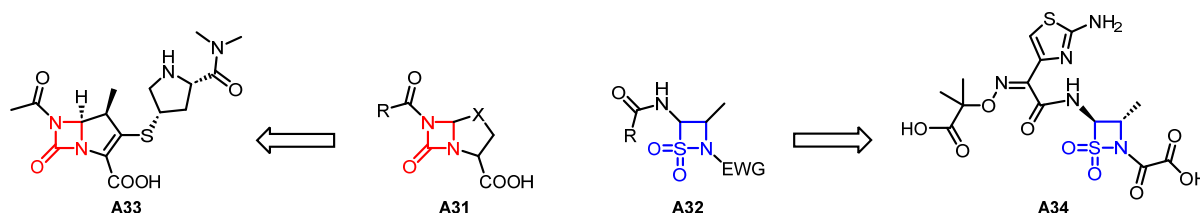
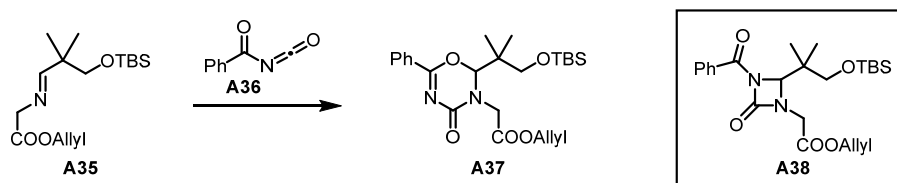


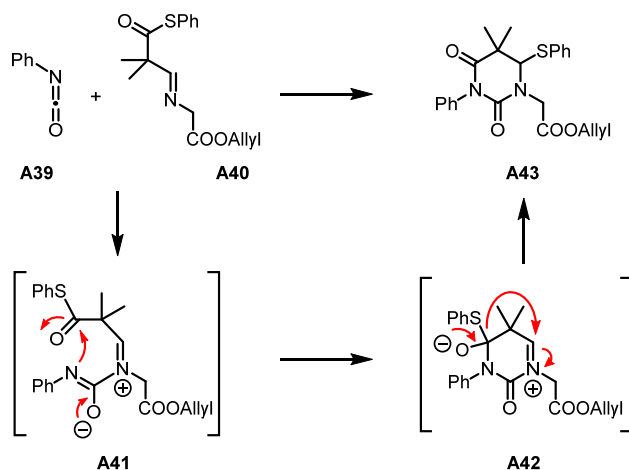
Figure 3: General structures of targeted dual penicillin binding protein/ β -lactamase inhibitors **A31/A32** and specific target structures **A33/A34**.

For analogs of type **A31**, the specific target structure to be pursued was meropenem analog **A33** (**Figure 3**), which was planned to be accessed *via* [2+2]-cycloaddition of acetyl isocyanate and an appropriate imine as enabling key step. However, this strategy could not be implemented. As shown in subsequent model studies, the reaction of imine **A35** with benzoyl isocyanate (**A36**) only produced the [4+2]-cycloaddition product **A37**, while the alternative [2+2]-cycloaddition product **A38** was not observed (**Scheme 4**).



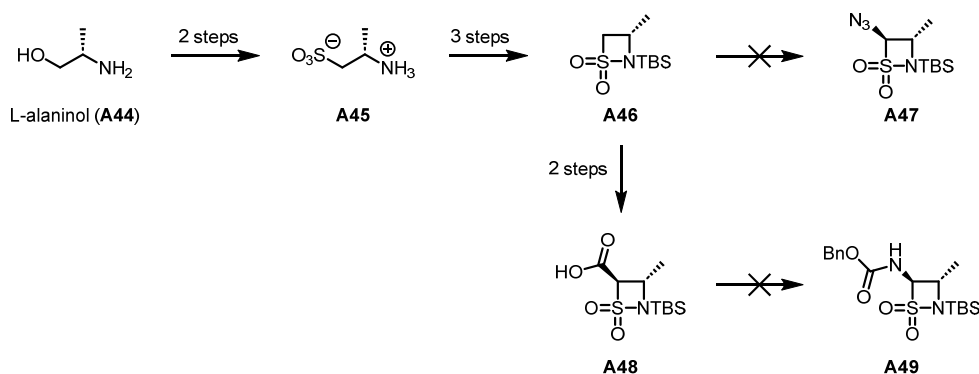
Scheme 4: Reaction of benzoyl isocyanate (**A36**) with imine **A35**.

The reaction of phenyl isocyanate (**A39**) with imine **A40** led to formation of 5,5-dimethyl dihydropyrimidine-2,4-dione **A43**, presumably *via* a (4+2)-cycloaddition/rearrangement pathway (**Scheme 5**). Phenyl-substituted derivatives of **A43** were obtained in reactions with *p*-substituted phenyl isocyanates in similar yields, independent of the nature of the *para*-substituent.



Scheme 5: Synthesis of 5,5-dimethyldihydropyrimidine-2,4-dione-**A43**.

For time reasons, efforts towards the synthesis of β -sultam **A34** had to be paused at the stage of acid **A48** (**Scheme 6**). The latter was obtained from L-alaninol (**A44**) *via* sulfonic acid **A45**; **A45** was sequentially chlorinated, cyclized and silylated to give β -sultam **A46**. Attempted α -azidation of **A46** with TsN_3 or trisylN_3 did not deliver the desired azide **A47**. In contrast, **A46** could be converted into acid **A48** *via* acylation with methyl chloroformate and subsequent ester hydrolysis. At this point, the transformation of carboxylic acid **A48** into Cbz-protected amine **A49** *via* a one-pot acyl azide formation/*Curtius* rearrangement sequence has still been unsuccessful.



Scheme 6: Synthesis of β -sultams **A46** and **A48**.

Zusammenfassung

Der marine Naturstoff (-)-Zampanolid (**A1**) inhibiert das Wachstum von menschlichen Krebszellen durch Mikrotubulistabilisierung mit IC_{50} -Werten im einstelligen nanomolaren Bereich. Während eine Reihe von Totalsynthesen des (-)-Zampanolid (**A1**) beschrieben sind, existieren vergleichsweise wenige Studien zur Untersuchung von Struktur-Aktivitäts-Beziehungen für diesem Naturstoff.

Der erste Teil dieser Dissertation beschäftigt sich mit der Synthese und der biologischen Evaluierung der Zampanolid-Analoga **A2-A12** (**Abbildung 1**), die durch strukturelle Modifikationen sowohl am Makrolacton-Grundkörper wie auch in der Seitenkette charakterisiert sind.

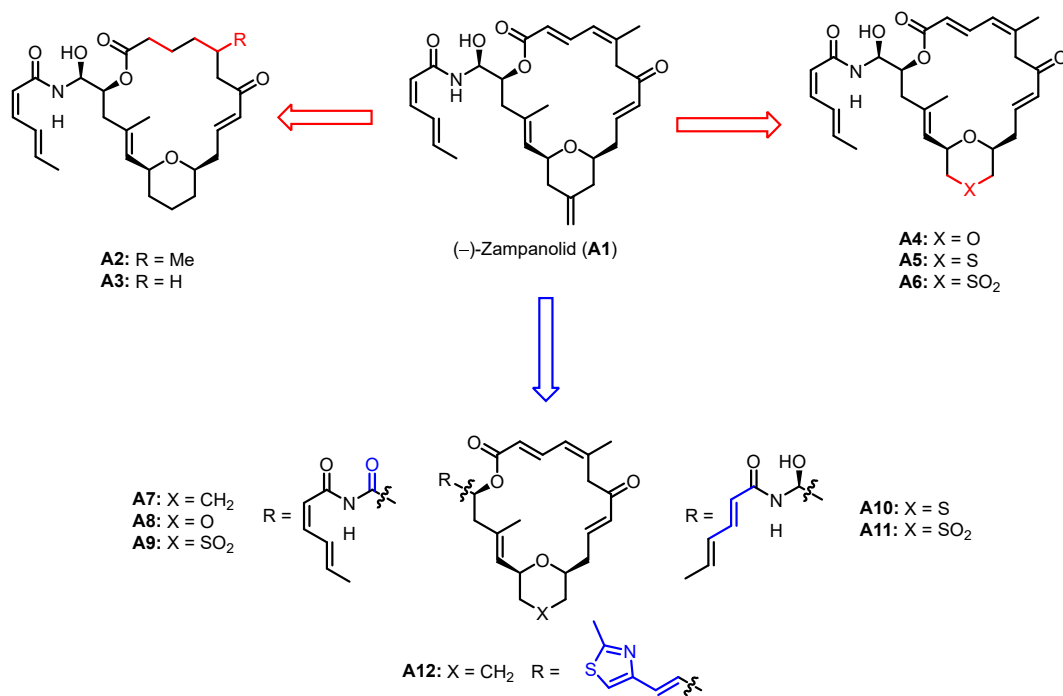
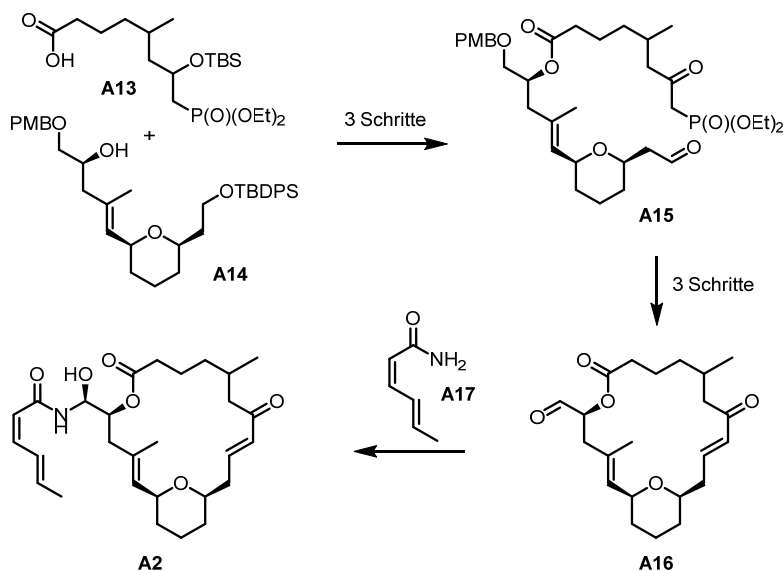


Abbildung 1: Struktur von (-)-Zampanolid (**A1**), Grundkörper-modifizierten (**A2-A6**) und Seitenkette-modifizierten Analoga (**A7-A12**).

Die grundlegende Synthesestrategie, welche für die Synthese aller hier beschriebenen Zampanolid-Analoga verfolgt wurde, ist in **Schema 1** am Beispiel der Verbindung **A2** dargelegt. Die Veresterung der Carbonsäure **A13** mit dem Alkohol **A14** und anschließende Desilylierung und Oxidation führten zum Aldehyd **A15**. Dieser wurde mittels *E*-selektiver *HWE* Reaktion, PMB-Entschützung und Oxidation in den makrozyklischen Aldehyd **A16** überführt. Eine stereoselektive

Aza-Aldol Reaktion zwischen **A16** und *Z,E*-Sorbamid (**A17**), zum Aufbau der Hemiaminal-Gruppierung, lieferte schliesslich das gewünschte Analogon **A2**.



Schema 1: Globale Synthesestrategie für die Synthese der Zampanolid-Analoga **A2-A12** am Beispiel der Synthese von **A2**.

Die Synthese der Dioxan- und Oxathian/Oxathiadioxid-basierten Analoga **A4-A6** erforderte die Herstellung der Alkohole **A18** und **A19** (**Abbildung 2**).

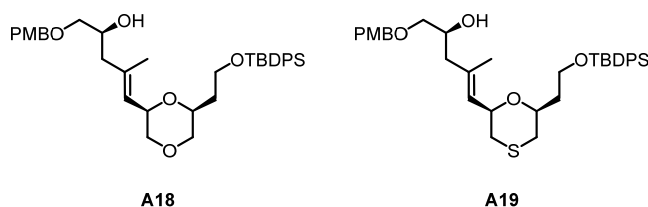
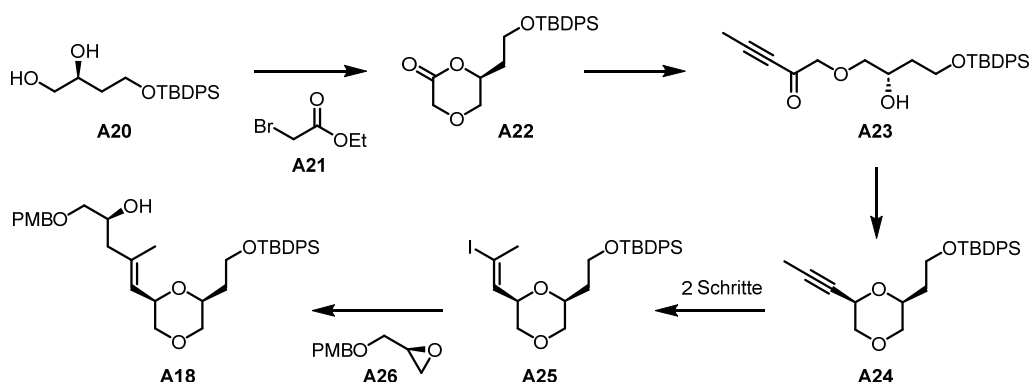


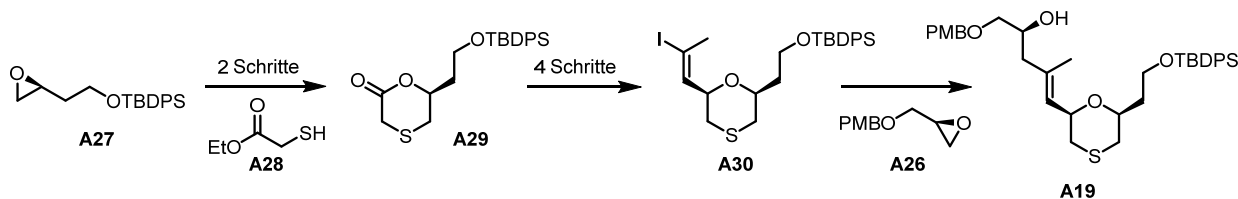
Abbildung 2: Strukturen der Alkohole **A18** und **A19**.

Dioxan **A18** konnte ausgehend von L-Äpfelsäure *via* Diol **A20** in zehn Schritten und einer Gesamtausbeute von 16% hergestellt werden (**Schema 2**). Die Überführung des Dioxanons **A22** in das 2,6-*syn*-disubstituierte Dioxan **A24** war bereits früher in der Forschungsgruppe untersucht worden, konnte allerdings nur in sehr geringer Ausbeute realisiert werden. Im Rahmen dieser Dissertation konnte nun ein deutlich verbesserter Ansatz für die Überführung von **A22** in **A24** etabliert werden.



Schema 2: Synthese von Dioxan **A18**.

Oxathian **A19** wurde ausgehend von D-Asparaginsäure *via* Epoxid **A27** in zehn Schritten und einer Gesamtausbeute von 18% hergestellt (**Schema 3**). Dabei stellte die Öffnung von Epoxid **A26** durch das Vinyljodid **A30** eine grosse Herausforderung dar, welche durch die Verwendung einer Kombination von Lithium- und Kupferreagenzien überwunden werden konnte.



Schema 3: Synthese von Oxathian Alkohol **A19**.

Die Imid-Analoga **A7-A9** wurden durch DMP-Oxidation der Hemiaminale **A2**, **A4** bzw. **A6** erhalten. Die Analoga **A10** und **A11** waren aus den dafür erforderlichen makrozyklischen Aldehydvorläufern über eine stereoselektive Aza-Aldol-Reaktion mit *E,E*-Sorbamid zugänglich. Das Zampanolid-Epothilon-Hybrid **A12** wurde durch eine *Wittig*-Reaktion mit Aldehyd **A16** hergestellt.

Die antiproliferative Aktivität der teilgesättigten Analoga **A2** und **A3** war etwa 30-40-mal geringer als diejenige von **A1**. Die Dioxan- und Oxathian-basierten Analoga **A4** und **A5** waren äquipotent mit **A1**, während das Oxathiandioxid **A6** 50-100-mal weniger aktiv war; **A10** und **A11** waren 3-12-mal weniger wirksam als **A5** und **A6**. Imid-Analoga **A7-A9** waren 1-2 Grössenordnungen weniger aktiv als **A1**. Überraschenderweise wies **A12** IC_{50} -Werte im niedrigen mikromolaren Bereich auf.

Der zweite Teil dieser Dissertation befasst sich mit dem Versuch, neue Analoga von β -Lactam-Antibiotika zu synthetisieren, bei denen der β -Lactam-Ring entweder durch einen *N*-Acyl-1,3-diazetidion oder durch einen β -Sultam-Ring ersetzt werden sollte (**Abbildung 3**).

Es wurde angenommen, dass solche Verbindungen ausreichend reaktiv wären, um eine Öffnung des 4-gliedrigen Rings durch Penicillin-bindende Proteine zu ermöglichen. Gleichzeitig wurde erwartet, dass **A31** und **A32** langsam-reversible Inhibitoren von Ser- β -Lactamasen sein könnten, da ihre Reaktion mit dem katalytischen Ser-Rest zur Bildung eines proteingebundenen Carbamats bzw. eines Sulfonsäureesters führen würde. Letztere dürften sehr viel langsamer hydrolysiert werden als das übliche Ester-Zwischenprodukt, das bei der Reaktion mit herkömmlichen β -Lactam-Antibiotika entsteht.

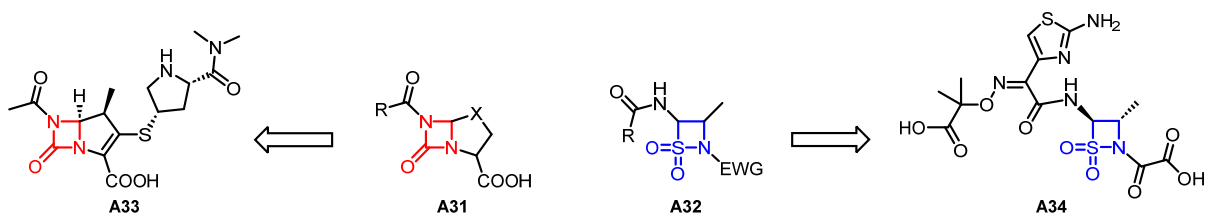
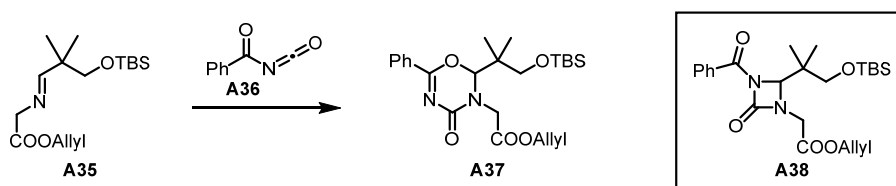


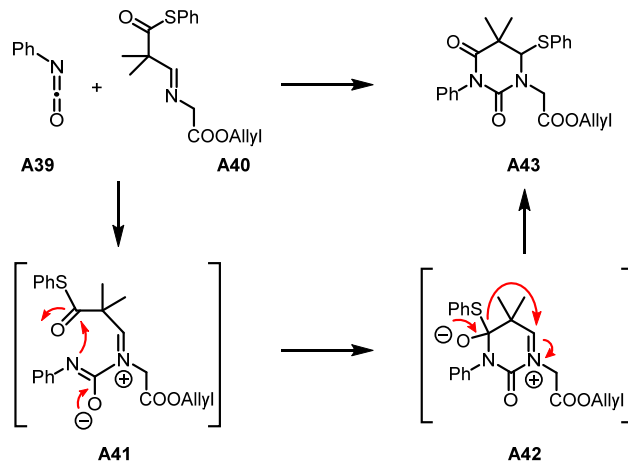
Abbildung 3: Generelle Strukturen der geplanten dualen Penicillin-bindenden Protein/ β -Lactamase Inhibitoren **A31/A32** und Strukturen der spezifischen Zielmoleküle **A33/A34**.

Bei den Analoga des Typs **A31** wurde als spezifische Zielstruktur die Synthese des Meropenem-Analogons **A33** angestrebt, das über eine [2+2]-Cycloaddition von Acetylisocyanat und einem geeigneten Imin als Schlüsselschritt zugänglich gemacht werden sollte. Diese Strategie konnte jedoch nicht umgesetzt werden. Wie in anschließenden Modellstudien gezeigt wurde, führte die Reaktion zwischen Imin **A35** und Benzoylisocyanat (**A36**) nur zum [4+2]-Cycloadditionsprodukt **A37**, während das alternative [2+2]-Cycloadditionsprodukt **A38** nicht erhalten wurde (**Schema 4**).



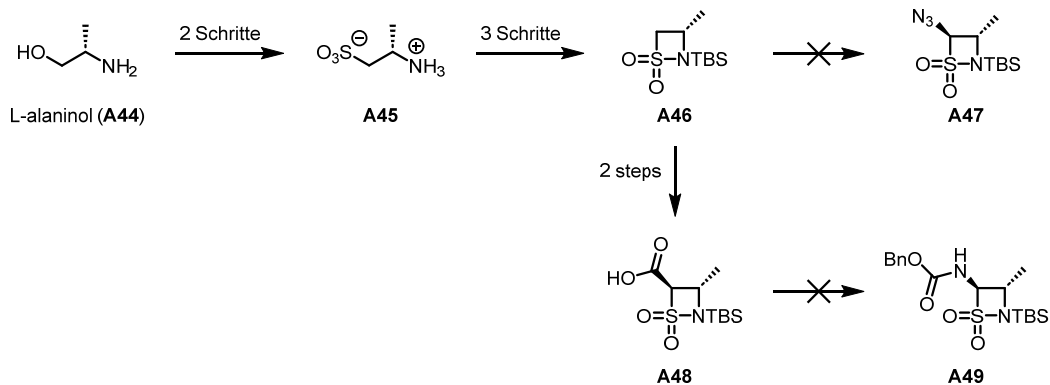
Schema 4: Reaktion zwischen Benzoylisocyanat (**A36**) und Imin **A35**.

Die Reaktion zwischen Phenylisocyanat (**A39**) und Imin **A40** ergab 5,5-Dimethyldihydropyrimidin-2,4-dion **A43**, vermutlich über eine (4+2)-Cycloadditions-/Umlagerungssequenz (**Schema 5**). Phenylsubstituierte Derivate von **A49** wurden in Reaktionen mit *p*-substituierten Phenylisocyanaten in ähnlichen Ausbeuten erhalten, unabhängig von der Art des *para*-Substituenten.



Schema 5: Synthese von 5,5-Dimethyldihydropyrimidin-2,4-dion **A43**.

Aus Zeitgründen mussten die Bemühungen zur Synthese von β -Sultam **A34** auf der Stufe der Carbonsäure **A48** unterbrochen werden (**Schema 6**). Letztere wurde aus L-Alaninol (**A44**) *via* Sulfonsäure **A45** hergestellt; **A45** wurde dann durch Chlorierung, Zyklisierung und Silylierung in das β -Sultam **A46** übergeführt. Die versuchte α -Azidierung von **A46** mit TsN_3 oder TrisylN_3 führte nicht zum gewünschten Azid **A47**. Hingegen konnte **A46** durch Acylierung mit Chlorameisensäuremethylester und anschließender Esterhydrolyse in die Carbonsäure **A48** überführt werden. Die Umwandlung der Carbonsäure **A48** in das Cbz-geschützte Amin **A49**, über eine Acyl-Azidbildung/*Curtius*-Umlagerungssequenz, war bisher noch nicht erfolgreich.



Schema 6: Synthese der β -Sultame **A46** und **A48**.

Abbreviations and Dimension Units

A

| | |
|-----------|---|
| $[a]_D^T$ | specific rotation at temperature T at the sodium D line |
| Å | Ångström |
| Ac | acetyl |
| ADC | antibody drug conjugate |
| AML | acute myeloid leukemia |
| AMR | antimicrobial resistance |
| ALL | acute lymphoblastic leukemia |
| app. | apparent |
| atm | atmosphere |
| aqu. | aqueous |

B

| | |
|-------|-------------------------------|
| BINOL | 1,1'-bi-2-naphthol |
| Bn | benzyl |
| Boc | <i>tert</i> -butyloxycarbonyl |
| br | broad |
| Bu | butyl |

C

| | |
|------|-------------------------|
| °C | degree Celsius |
| ca. | about, approximately |
| cat. | catalytic |
| COSY | correlated spectroscopy |
| CSA | camphorsulfonic acid |

D

| | |
|----------|---|
| δ | NMR chemical shift in ppm |
| d | doublet |
| DAZ | 1,3-diazetidione |
| DBU | 1,8-diazabicyclo[5.4.0]undec-7-ene |
| DCC | <i>N,N'</i> -dicyclohexylcarbodiimide |
| DDQ | 2,3-dichloro-5,6-dicyano-1,4-benzoquinone |
| DEAD | diethyl azodicarboxylate |
| DFT | density functional theory |
| DIBAL-H | diisobutylaluminum hydride |
| DIPEA | <i>N,N</i> -diisopropylethylamine |
| DIPA | diisopropylamine |
| DMAP | 4-dimethylamino pyridine |
| DMF | <i>N,N</i> -dimethylformamide |
| DMP | Dess-Martin periodinane |

| | |
|------------------|---|
| DMSO | dimethyl sulfoxide |
| DOX | 2,3-dihydro-1,3,5-oxadiazin-4-one |
| DPPA | diphenylphosphoryl azide |
| dr | diastereomeric ratio |
| DTT | dithiothreitol |
| E | |
| EDCI | 1-ethyl-3-(3-dimethylaminopropyl)carbodiimide |
| <i>ee</i> | enantiomeric excess |
| EI | electron ionization |
| EGTA | 3,12-bis(carboxymethyl)-6,9-dioxa-3,12-diazatetradecane-1,14-dioic acid |
| <i>ent</i> | enantiomeric |
| ESI | electrospray ionization |
| eq. | equivalent |
| equiv. | equivalent |
| <i>epi</i> | epimeric |
| Et | ethyl |
| EtOAc | ethyl acetate |
| F | |
| FC | flash chromatography |
| FDA | U. S. Food and Drug Administration |
| G | |
| g | gram |
| G1/G2 | gap 1/gap 2 |
| GDP | guanosine diphosphate |
| GI ₅₀ | half maximal growth inhibition concentration |
| GTP | guanosine triphosphate |
| H | |
| h | hour |
| HATU | hexafluorophosphate azabenzotriazole tetramethyl uranium |
| HBTU | hexafluorophosphate benzotriazole tetramethyl uranium |
| HCTU | hexafluorophosphate chlorobenzotriazole tetramethyl uranium |
| HMBC | heteronuclear multiple bond correlation |
| HPLC | high-performance liquid chromatography |
| HR-FABMS | high resolution fast-atom bombardment mass spectrometry |
| HRMS | high resolution mass spectrometry |

| | |
|-------------------|--|
| HSQC | heteronuclear single quantum coherence |
| HWE | Horner-Wadsworth-Emmons |
| Hz | Hertz (s^{-1}) |
| I | |
| <i>i</i> | <i>iso</i> |
| IC ₅₀ | half maximal inhibitory concentration |
| IR | infrared |
| J | |
| <i>J</i> | coupling constant |
| K | |
| K _b | binding constant |
| K _{bapp} | apparent binding constant |
| KHMDS | potassium bis(trimethylsilyl)amide |
| L | |
| LA | Lewis acid |
| LAH | lithium aluminum hydride |
| LDA | lithium diisopropylamide |
| LiHMDS | lithium bis(trimethylsilyl)amide |
| LLS | longest linear sequence |
| M | |
| m | multiplet |
| M | molar |
| MAP | microtubule-associated protein |
| MDA | microtubule-destabilizing agent |
| MDR | multidrug-resistant |
| Me | methyl |
| Mes | mesityl |
| mg | milligram |
| MHz | megahertz |
| MIC | minimum inhibitory concentration |
| min | minute |
| mL | milliliter |
| mM | millimole per liter |
| mmol | millimole |
| μL | microliter |
| μM | micromole per liter |
| mol% | mole percent |
| MRSA | methicillin-resistant <i>Staphylococcus aureus</i> |
| MS | molecular sieves or mass spectrometry |
| Ms | methanesulfonyl |

| | |
|---------------------|--|
| MSA | microtubule-stabilizing agent |
| MT | microtubules |
| MTA | microtubule-targeting agents |
| MTT | 3-(4,5-dimethylthiazol-2-yl)-2,5-diphenyltetrazolium bromide |
| N | |
| NAG | <i>N</i> -acetylglucosamine |
| NaHMDS | sodium bis(trimethylsilyl)amide |
| NAM | <i>N</i> -acetylmuramic acid |
| NaPi | monosodium phosphate |
| n.d. | not determined |
| ng | nanogram |
| NIS | <i>N</i> -iodosuccinimide |
| nM | nanomol per liter |
| NOESY | nuclear Overhauser effect spectroscopy |
| NMR | nuclear magnetic resonance |
| NP | natural product |
| P | |
| <i>p</i> | <i>para</i> |
| PCC | pyridinium chlorochromate |
| PDC | pyridinium dichromate |
| Pg | protecting group |
| Pgp | P-glycoprotein |
| Ph | phenyl |
| Piv | pivaloyl |
| PMB | <i>para</i> -methoxybenzyl |
| ppm | parts per million |
| PPTS | pyridinium <i>para</i> -toluenesulfonate |
| Pr | propyl |
| PTSA | <i>para</i> -toluenesulfonic acid |
| py | pyridine |
| Q | |
| q | quartet |
| quint. | quintet |
| R | |
| RAR | rearrangement |
| RCM | ring-closing metathesis |
| Red-Al [®] | sodium bis(2-methoxyethoxy)aluminumhydride |
| R _f | retention factor |
| RP | reversed-phase |

| | |
|----------------|---|
| rr | regioisomeric ratio |
| R _t | retention time |
| rt | room temperature |
| S | |
| s | second or singlet |
| SAR | structure-activity relationship |
| Ser | serine |
| sol. | solution |
| sat. | saturated |
| T | |
| t | triplet |
| <i>t</i> | <i>tert</i> |
| TBAF | tetra- <i>n</i> -butylammonium fluoride |
| TBAI | tetra- <i>n</i> -butylammonium iodide |
| TCBC | 2,4,6-trichlorobenzoyl chloride |
| TBDPS | <i>tert</i> -butyldiphenylsilyl |
| TBS | <i>tert</i> -butyldimethylsilyl |
| TEMPO | 2,2,6,6-tetramethylpiperidin-1-yloxy |
| TES | triethylsilyl |
| TfO | trifluoromethanesulfonate |
| TFA | trifluoroacetic acid |
| THF | tetrahydrofuran |
| THP | tetrahydropyran |
| TIPS | triisopropylsilyl |
| TLC | thin layer chromatography |
| TMS | trimethylsilyl |
| trisyl | 2,4,6-triisopropylbenzenesulfonyl |
| Triton B | benzyltrimethylammonium hydroxide |
| tRNA | transfer RNA |
| Ts (tosyl) | <i>para</i> -toluenesulfonyl |
| TsOH | <i>para</i> -toluene sulfonic acid |
| TTL | tubulin tyrosine ligase |
| U | |
| UV | ultraviolet |
| Z | |
| ZI | zwitterionic iminium intermediate |

1 Natural Products in Drug Discovery

Organisms lacking any physical means of protection are forced to find other ways to protect themselves. They do so by producing bioactive natural products (NPs)¹, serendipitously creating a highly prolific source of lead structures for drug discovery and development.^[1,2] NPs have been used to treat disease for centuries, e.g. the extracts of the roots of the May apple, *Podophyllum peltatum*,^[3,4] were used to treat skin cancers and venereal warts by the American Indians and in traditional Asian medicine.^[5] The main bioactive component podophyllotoxin was first isolated in 1881 by *Podwyssotzki*^[3]. The chemical formula of podophyllotoxin was not determined until 1930, and its chemical structure, configuration (1973),^[6] and mode of action (1977)^[7] were established later.^[5] Even though podophyllotoxin was not approved as anticancer agent, two derived compounds, etoposide, and teniposide, are in clinical use today.^[8–10]

The importance of NPs in drug discovery is reflected by the fact that more than one third (38%) of the approved drugs between 1981 and 2019 (including biopharmaceuticals and vaccines) are NPs or are derived from them (**Figure 4**).^[11]

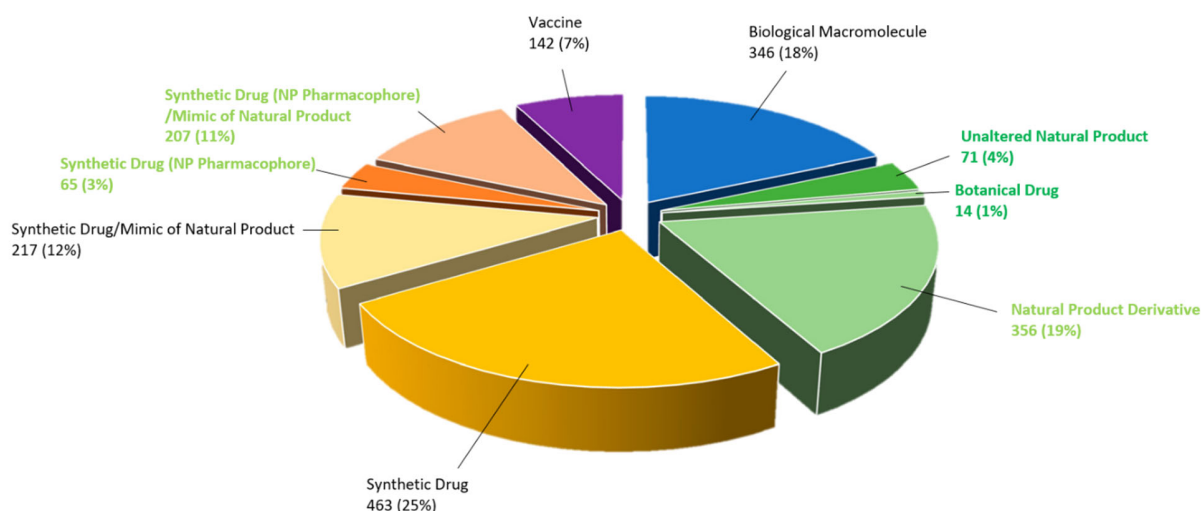


Figure 4: All new FDA approved drugs from January 1981 to September 2019. Natural product categories are shown in dark green and natural product derived categories are shown in light green. (Adapted with permission from ref. [11])

In relation to this thesis, it is particularly notable that nearly half of the oncology drugs that entered the market during this period were either unaltered NPs (7%) or natural product derived (41%). Likewise, NPs/NP derivatives are highly represented in the category of antibacterials, with

¹ In this thesis, the term natural product refers to secondary metabolites.

more than half of the antibiotics that entered the market between 1981 and 2019 being either natural products (7%) or compounds derived from NPs (49%).^[11]

The pronounced ability of NPs to act as protein ligands has been hypothesized to originate from their natural involvement in a great number of NP-protein interactions during their own biosynthesis and in the NP-dependent modulation of biological processes. This inherent protein-binding ability makes NPs pre-validated lead structures for chemical biology and medicinal chemistry research.^[12] NPs tend to have more complex molecular structures compared to artificial small molecules and therefore occupy more chemical space, so they will remain a key player in drug discovery.^[13]

2 Synthesis and SAR Studies of (-)-Zampanolide Analogs

2.1 Introduction

2.1.1 Isolations and Structures of Zampanolides

The marine natural product (-)-zampanolide (**E1**) (**Figure 5**) was first isolated in 1996 by *Tanaka* and *Higa* from the sponge *Fasciospongia rimosa* near Cape Zampa off the coast of Okinawa, Japan (**Figure 6**).^[14] The compound was found to exhibit cell toxicity against various human cancer cell lines with IC₅₀ values in the range of 2-10 nM. The molecular structure of **E1**, including the relative stereochemistry of the macrocyclic core, was determined by HR-FABMS and extensive NMR spectroscopy; the configuration at C(20) was not assigned by *Tanaka & Higa*. The absolute and full relative configuration of **E1** was established subsequently through total synthesis of the corresponding (+)-enantiomer by *Smith* and co-workers in 2001.

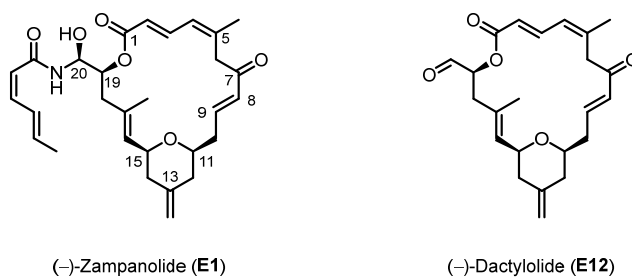


Figure 5: Structure of (-)-zampanolide (**E1**) and (-)-dactylolide (**E2**).^[14,15]

Key features of the structure of **E1** are (1) a highly unsaturated 20-membered macrolactone core with an embedded *syn*-2,6-disubstituted tetrahydropyran ring bearing an exocyclic methylene group and (2) an unusual linear hemiaminal group connecting the macrolide core with a (*Z,E*)-sorbamide side chain. Such a linear hemiaminal motif is rare in natural products and only a handful of other examples are known in the literature, including pederin^[16,17], mycalamides^[17,18], spergualin^[19], and echinocadin B^[20]. In 2009, (-)-zampanolide (**E1**) was reisolated from the Togan sponge *Cacospongia mycofijiensis* (**Figure 6**) by *Northcote* and co-workers.^[21] They confirmed the previously reported antiproliferative properties of the compound against various cancer cell lines and, more importantly, they showed that **E1** acts as a microtubule-stabilizing agent (MSA) arresting cells in the G2/M phase of the cell cycle. The biological activity of **E1** will be discussed in more detail in chapter 2.1.4.



Figure 6: Location (left, cape Zampa, Japan) and sources of isolation (right, top: sponge *Fasciospongia Rimosa*, bottom: sponge *Cacospongia mycofijiensis*) of the marine natural product (–)-zampanolide (**E1**).^[14,21]

More recently, the same group isolated four new natural congeners of **E1**, which they now call zampanolide A (**E1** is referred as (–)-zampanolide in this thesis), from *Cacospongia mycofijiensis*, i.e. zampanolides B (**E3**), C (**E4**), D (**E5**), and E (**E6**) (**Figure 7**).^[15]

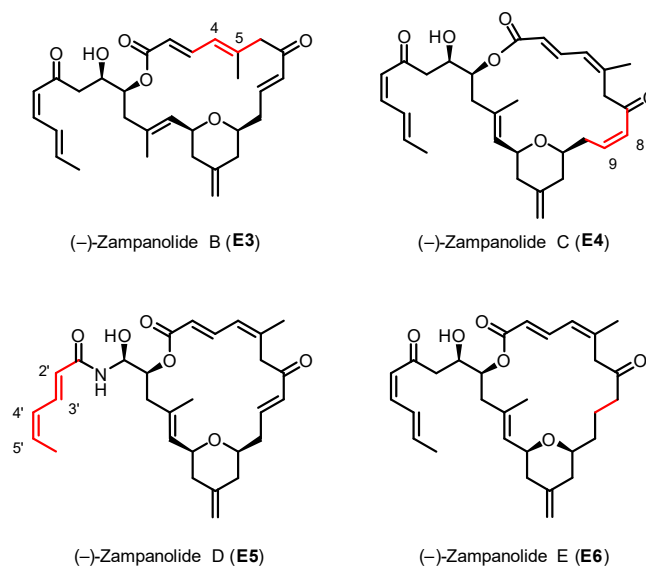


Figure 7: Structures of zampanolides B-E (**E3-E6**).^[15]

In addition to zampanolides B-E, *Northcote* and co-workers also reported the first isolation of (-)-dactylolide (**E2**), which only comprises the macrolide core of **E1**, from the same extract. While no studies have been published on the biosynthesis of **E1**, the isolation of **E2** lends support to a prior hypothesis that this compound could be a biogenetic precursor of **E1**,^[22,23] although it had never been reported in the literature. Conversely, *Riccio* and co-workers in 2001 had described the isolation of (+)-dactylolide (*ent*-**E2**) from the Vanuatan sponge *Dactylospongia sp.*^[24] It should be noted, though, that doubts have been raised about the sign of the specific rotation reported by *Riccio* for the compound isolated, which in fact might have been (-)-dactylolide (**E2**).

To put the discussion of the cellular effects of **E1** in a broader context, the next sections will review the basic features of the microtubule system in cells and the effects resulting from disturbing this system by small molecules.

2.1.2 Microtubule Structure and Function

Three different types of filaments are essential for the spatial organization of the cytoskeleton of eukaryotic cells: *intermediate filaments*, providing mechanical strength and resistance to shear stress, *actin filaments*, defining the shape of the cell and being responsible for its rapid remodeling ability, and *microtubules*, which are involved in many cellular processes, such as positioning of organelles, maintenance of the cellular shape, intracellular transport, cell division and mitosis.^[25,26]

Microtubules (MTs) are hollow, tube-shaped protein assemblies composed of α - and β -tubulin heterodimers. They typically consist of 13 protofilaments with an outer diameter of 24 nm (**Figure 8**). Within the protofilaments the heterodimers are arranged in a head-to-tail fashion, thus creating an intrinsic polarity within the MT; the plus and the minus end.^[27,28]

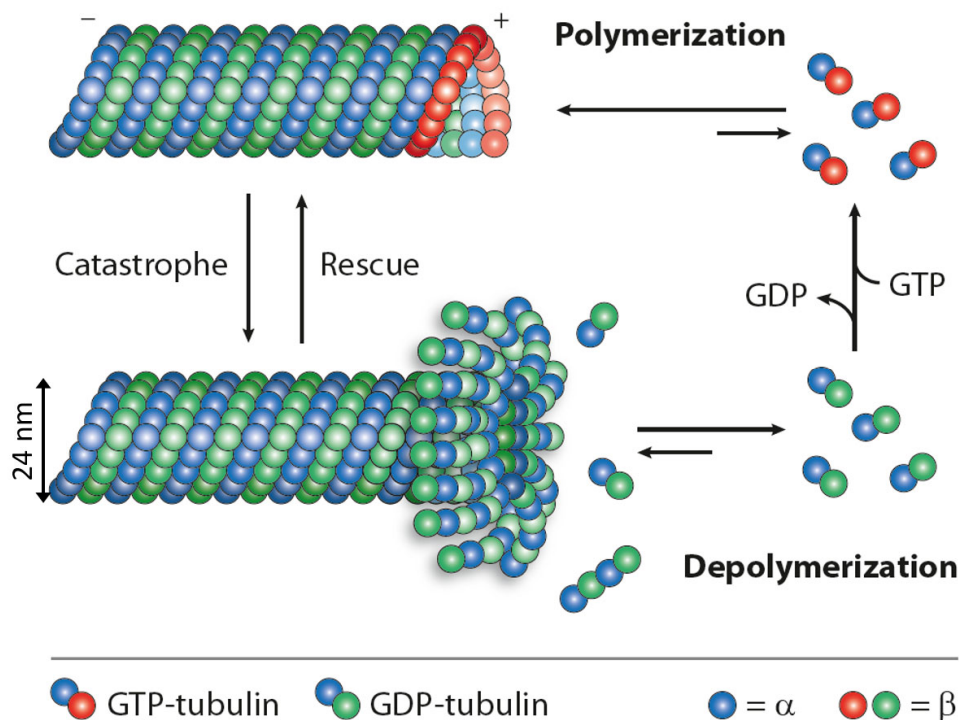


Figure 8: Structure and dynamic properties of microtubules. α/β -Tubulin heterodimers are added (polymerization) or released (depolymerization) at the plus-end. Polymerization makes use of GTP-tubulin (blue/red spheres), whereas GDP-tubulin is released upon depolymerization (blue/green spheres), which can be activated again for polymerization with reaction with GTP. Changing from the polymerization to the depolymerization state is called *catastrophe* and the reverse event is called *rescue*. (Figure reprinted with permission from ref. [29])

Proper functioning of MTs is closely related to two dynamic processes called *dynamic instability* and *treadmilling*.^[30–32] The former refers to the interchange of slow growing and fast shrinkage cycles. This process predominantly takes place at the exposed β -tubulin at the plus end. Changing from the growing to the shrinking phase is called *catastrophe*, whereas the opposite event is called *rescue*.^[30,33–35] On the other hand, *treadmilling* does not lead to a net change in microtubule mass, but rather consists of a simultaneous loss of tubulin subunits at the minus end and an addition of tubulin subunits at the plus end.^[32] In cells, these essential dynamic processes are regulated by microtubule-associated proteins (MAPs).^[27,28,36]

2.1.3 Microtubule Modulators

The dynamic features of the MT system can be disrupted by small molecules that are referred to as microtubule-targeting agents (MTAs) or microtubule modulators. The compounds can be classified into two categories: microtubule-stabilizing agents (MSAs) and microtubule-destabilizing agents (MDAs). MSAs favor the polymerization of tubulin heterodimers into

microtubules or prevent already assembled microtubules from depolymerization, whereas MDAs behave as antagonist. In cells, both classes of compounds can block mitosis by preventing proper formation of the mitotic spindle, which depends on intact MT dynamics.^[37–39] Mitotic arrest eventually leads to uncontrolled cell division and finally to apoptosis (**Figure 9**).^[37,38] Their ability to inhibit cell growth with high potency makes microtubule modulators an important class of anticancer agents.^[38]

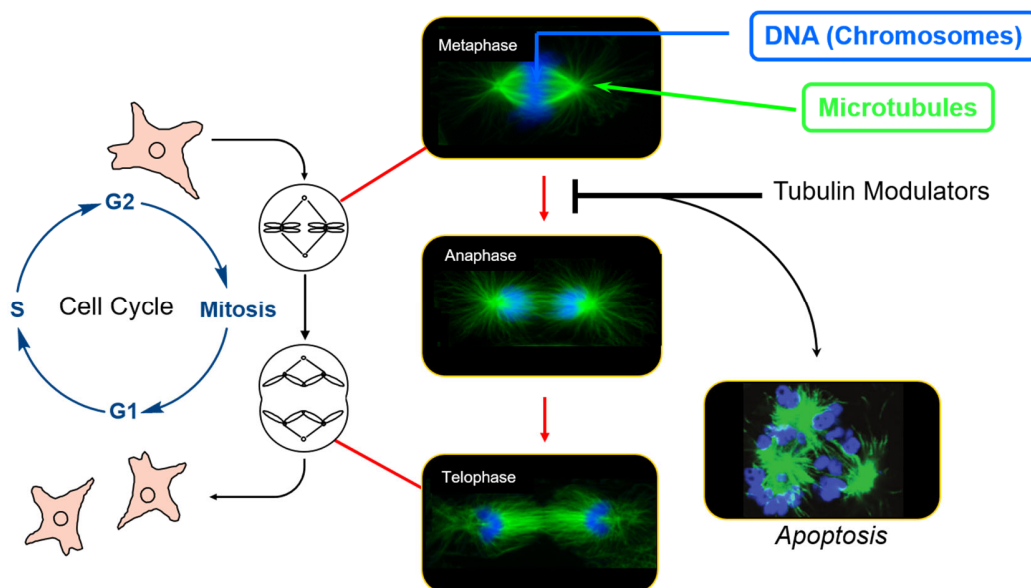


Figure 9: Cell division with focus on normal and tubulin modulator disrupted mitosis.

Currently, six binding sites for MTAs on tubulin are known: the vinca, maytansine, taxane, laulimalide/peloruside (all located on the β -tubulin subunit), colchicine (located at the interface of the α -tubulin and β -tubulin subunits) and the pironetin site (located on the α -tubulin subunit), which are named after the compound(s) first discovered to bind to the respective site (**Figure 10**).^[40]

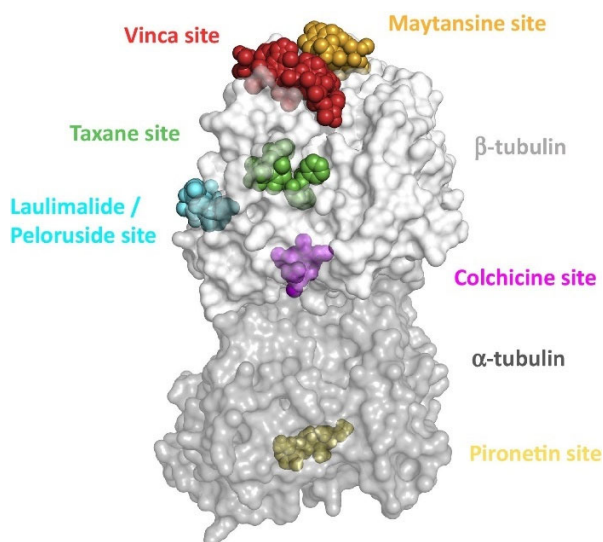


Figure 10: The six known binding sites for MTAs on $\alpha\beta$ -tubulin. The binding sites are named after the first compounds identified binding to the respective site. Four out of six sites are located on the β -tubulin subunit, one is located on the α -tubulin subunit and one is located at the interface of them. (Figure reprinted with permission from ref.[40])

MSAs bind either to the taxane or to the laulimalide/peloruside site, whereas MDAs bind to one of the other four binding sites. There are seven MDAs that are FDA-approved chemotherapeutics; in addition, eight compounds are approved as part of an antibody drug conjugate (ADC) (as of April 2023).^[41]As (-)-zampanolide (**E1**) belongs to the class of MSAs, they are discussed in more detail in section 2.1.3.1.

2.1.3.1 Microtubule-Stabilizing Agents

As the name implies, microtubule-stabilizing agents stabilize microtubules, i.e. they can prevent their disassembly under normally destabilizing conditions; at the same time, they can also promote their formation under conditions where assembly would not usually take place.^[42] Interestingly, natural products and their derivatives are the only source of all potent MSAs known to date (**Figure 11**). The most prominent MSA is the diterpenoid alkaloid taxol (**E7**), which was also the first compound to be recognized as an MSA in 1979,^[43] 8 years after its first isolation from the stem bark of the western yew tree (*Taxus brevifolia*).^[44] It took another 13 years until taxol was approved by the FDA (as Taxol[®]) as drug for the treatment of ovarian cancer.^[45] This also marks the introduction of MSAs into clinical cancer therapy. The drug was later approved for the treatment of breast (1994) and non-small cell lung cancer (1999). Today, the bulk material for clinical use is produced by semi-synthetic means, due to its low abundance in nature and complex total synthesis.^[46] There are only five FDA-approved MSA chemotherapeutics on the market and no ADC (as of April 2023).^[41] All of them bind to the taxane-binding site.

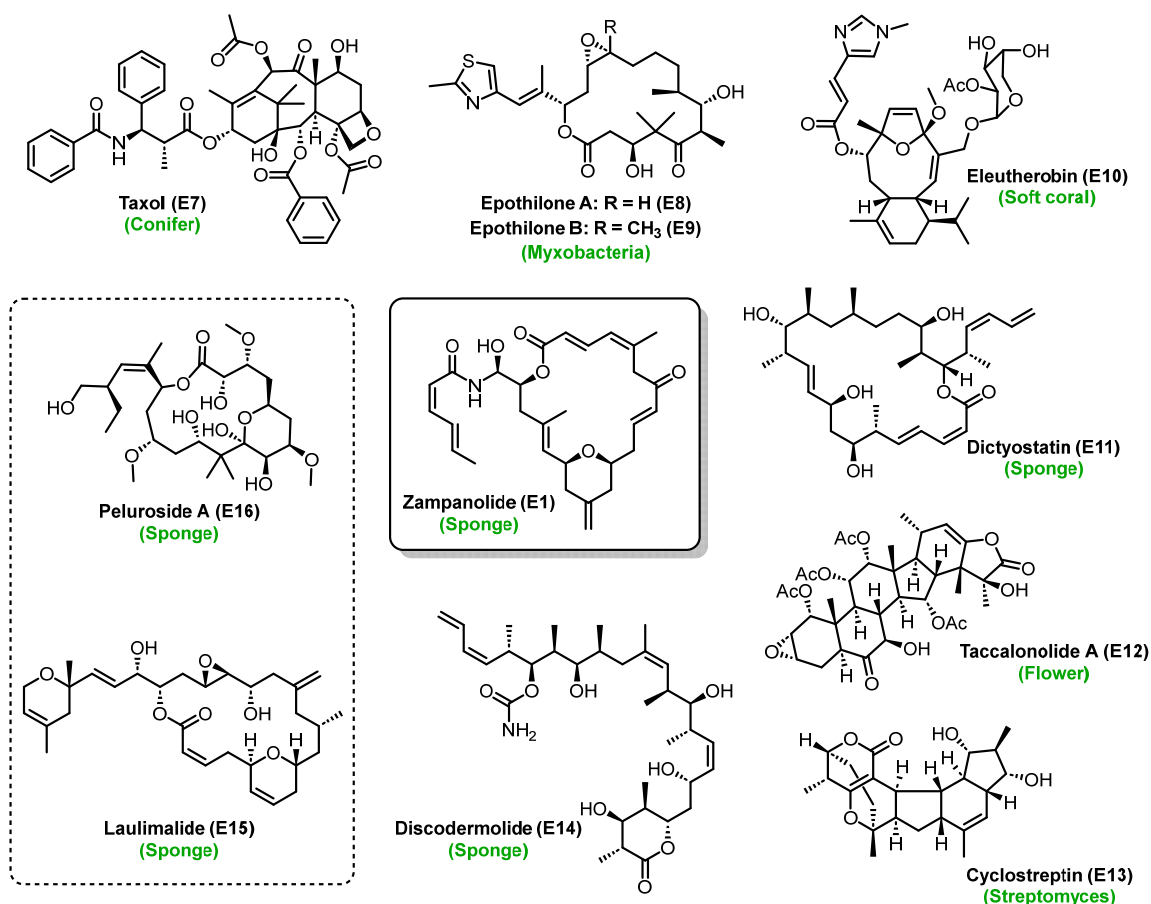


Figure 11: The currently known MSAs, all being natural products (source of isolation in green). All apart from peloruside and laulimalide (in dashed bracket on the bottom left) bind to the taxane binding site on tubulin.

Taxol is a very potent MSA and as such suffers from peripheral neurotoxicity and myelosuppression as mechanism-related side effects.^[36,47] In addition, it is characterized by poor water solubility and it shows high affinity for the P-glycoprotein (P-gp) efflux pump, leading to a lack of oral bioavailability and more importantly, to the development of resistance.^[36,46,48] After a drought of 16 years after the elucidation of taxol's mechanism of action, a series of other natural products were recognized to be potent MSAs after 1995 (ordered according to their year of identification as MSA): epothilones A (**E8**) and B (**E9**),^[49] discodermolide (**E14**),^[50] eleutherobin (**E10**) and its structural relatives sarcodictyins A and B,^[51,52] laulimalide (**E15**),^[53] cyclostreptin (formerly known as FR182877 or WS9885B) (**E13**),^[54] peloruside A (**E16**),^[55] dictyostatin (**E11**),^[56] taccalonolides (e.g. **E12**)^[57] and (-)-zampanolide (**E1**)^[21]. With the exception of laulimalide and peloruside A, all of these compounds bind to the taxol-binding site on β -tubulin; the former also bind to β -tubulin but to another, distinct site. These compounds share the same molecular mechanism of microtubule stabilization *via* helix induction of the otherwise disordered M-loop.

This mode of action is explained in more detail on the example of (–)-zampanolide (**E1**) in section 2.1.4.2.

2.1.4 Biological Activity and Mode of Action

2.1.4.1 Inhibition of Cancer Cell Growth

As already alluded to in section 2.1.1, (–)-zampanolide (**E1**) was shown, in the context of the isolation work, to exhibit high antiproliferative activity against four human cancer cell lines (P388, A549, HT29, and MEL28),^[14] with IC₅₀ values ranging from 2 to 10 nM. *Northcote* and co-workers later confirmed these results and reported IC₅₀ values against four additional human cancer cell lines: 4.3 nM against HL-60 (leukemia), 14.3 nM against 1A9 (ovarian), 7.1 nM against A2780 (ovarian), and 7.5 nM against A2780 AD, which is a multidrug-resistant variant of the A2780 cell line that overexpresses the P-gp efflux pump.^[21] The latter finding is of particular interest, as it suggests that, in contrast to taxol (**E7**), (–)-zampanolide (**E1**) is not a substrate for the P-gp efflux pump. Therefore, (–)-zampanolide (**E1**) represents an interesting lead structure for drug discovery targeting the inhibition of the growth of multidrug-resistant tumors.

Northcote and co-workers also showed that treatment of 1A9 cells with **E1** led to arrest of the cell cycle in the G2/M phase and to apoptosis. In addition, the formation of microtubule bundles was observed in interphase cells and multiple asters were detected in dividing cells. Finally, the compound led to a dose-dependent shift of the soluble tubulin/polymerized tubulin ratio in cells towards the polymerized state. This effect was also confirmed biochemically using purified tubulin preparations in an extracellular context. These findings led to the conclusion that **E1** belongs to the group of MSAs.^[21]

The ability of **E1** to overcome P-gp-mediated multidrug-resistance, was further confirmed by *Cerchiatti* and co-workers in 2015,^[58] who showed that **E1** inhibited several AML (acute myeloid leukemia) and ALL (acute lymphoblastic leukemia) cell lines with high potency (GI₅₀ values < 1 nM). This included the P-gp-overexpressing KG-1a (AML) and CCRF-CEM/VBL (ALL) cell lines. Of the four recently isolated natural congeners of **E1** (i.e. **E3-E6**, **Figure 7**), three showed virtually identical potency as **E1** against HL60 human leukemia cells (3-5 nM vs. 3 nM).^[15]

Recently, the first *in vivo* study with (–)-zampanolide (**E1**) in tumor-bearing mice was reported by *Risinger* and coworkers.^[59] While intratumoral injection of **E1** led to a substantial decrease in tumor volume, systemic administration showed no such effect and even a single i.p. dose of 1 mg/kg was found to be highly toxic. Thus, no therapeutic window could be established in these

experiments for the treatment of mice bearing tumors with (–)-zampanolide (**E1**). It is unclear, however, if these findings can be extrapolated to other tumor types, especially to liquid tumors, for which the corresponding cell lines are highly sensitive to **E1** *in vitro*. Likewise, a more favorable profile may be achievable for specific analogs of **E1**.

2.1.4.2 Binding to Microtubules

While *Northcote* and co-workers established the tubulin/microtubule system as the molecular target of **E1**,^[21] they did not investigate the molecular interactions of the compound with tubulin. This was only done in subsequent collaborative work between the groups of *Diaz*, *Northcote*, and *Altmann*.^[60] Employing displacement experiments with the fluorescent taxol derivative Flutax-2, it was shown that **E1** binds covalently to the taxane-binding site. Specifically, while **E1** was readily able to displace Flutax-2 from weakly cross-linked microtubules, preincubation of microtubules with **E1** (for as short a time period as 30 min) and subsequent treatment with Flutax-2 did not lead to any displacement of **E1**. On the other hand, no competition for tubulin-binding was observed between **E1** and the non-taxol site binder peloruside A (**E16**, **Figure 11**). Further experiments (mass spectrometric analysis of tryptic digests of zampanolide-modified β -tubulin derived from cross-linked microtubules) suggested that the covalent attachment of **E1** may involve reaction of the side chains of β Asn228 or β His229 with C(3) of the enoate moiety of **E1**. This assumption was proven incorrect later, however (*vide infra*). Independent of this, similar results were obtained with soluble tubulin heterodimers, thus suggesting that the binding mode of **E1** is similar for soluble tubulin and tubulin in its microtubule-assembled state.

The exact binding mode of **E1** to β -tubulin was firmly established in 2013 by *Steinmetz* and co-workers, who obtained a high resolution (1.8 Å) X-ray crystal structure of a tubulin-zampanolide complex. This structure represented the first molecular picture ever of an MSA in complex with tubulin that was derived from experimental data.^[61] The β -tubulin-**E1** complex in the crystals is part of a larger protein assembly that comprises two $\alpha\beta$ -tubulin heterodimers (T), the stathmin-like protein RB₃ (R), and tubulin tyrosine ligase (TTL) (T₂R-TTL). The structure confirmed the covalent binding of **E1** to the His229 side chain in the taxane binding site (**Figure 12**). However, in contrast to the previous computational predictions, C(9) of the enone moiety in the macrolactone ring was identified as the Michael acceptor, rather than C(3). The structure of the protein in its **E1**-bound state is essentially identical to the free, non-ligated state. As the sole and marked exception, the M-loop, which includes amino acids 272-287 is largely disordered in the non-ligated state, whereas binding of **E1** induces the formation of a short α -helix involving residues Arg278 to Tyr283 (**Figure 12B**). Helix induction is mediated by several hydrophobic and

hydrophilic interactions between the hemiaminal-tethered side chain of **E1** and residues in the M-loop; hydrogen bonding occurs between OH20 and O1' of (-)-zampanolide (**E1**) and the carbonyl oxygen and the amino group of β Thr276, respectively. A structured M-loop is also observed in microtubules and it is the source of favorable lateral tubulin interactions between protofilaments, which are essential for microtubule stability.^[62,63] The M-loop is unstructured in non-ligated tubulin heterodimers (and also in the non-ligated T2R-TTL complex; *vide supra*).

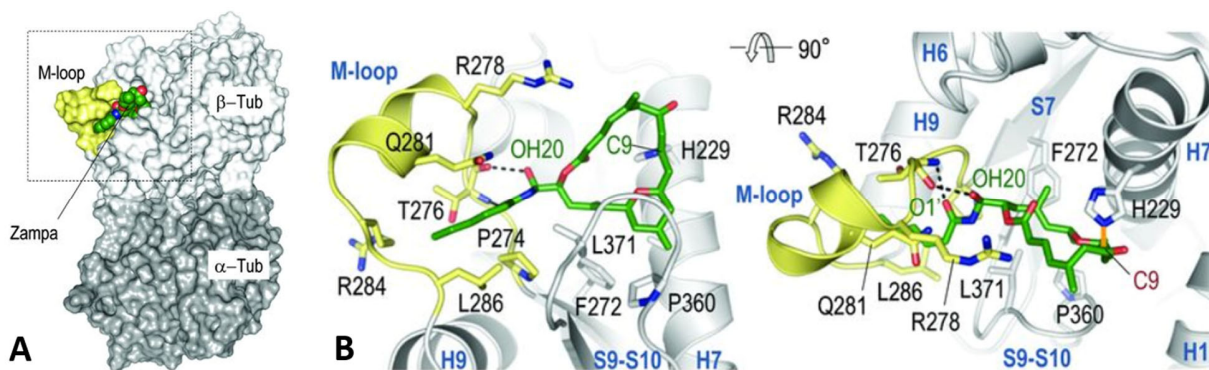


Figure 12: Crystal structure of (-)-zampanolide (**E1**) bound to the taxane site of $\alpha\beta$ -tubulin. **A:** Overview of the $\alpha\beta$ -tubulin-zampanolide complex with $\alpha\beta$ -tubulin in gray (M-loop in yellow) and (-)-zampanolide (**E1**) as green spheres. **B:** Close-up views of **E1** (green sticks) in the taxane binding site (grey cartoon, interacting residues are shown as sticks). Oxygen and nitrogen atoms are shown in red and blue, carbon atoms are either green (for **E1**) or gray/yellow for β -tubulin. Dashed lines represent hydrogen bonds and the covalent bond between C(9) of **E1** and Ne^2 of His229 of β -tubulin is depicted as orange line. (A = Ala, C = Cys, D = Asp, E = Glu, F = Phe, G = Gly, H = His, I = Ile, K = Lys, L = Leu, M = Met, N = Asn, P = Pro, Q = Gln, R = Arg, S = Ser, T = Thr, V = Val, W = Trp, Y = Tyr.) (Reprinted with permission from Ref ^[61])

Soluble tubulin heterodimers, with the M-loop in an unordered state, are characterized by a curved or kinked arrangement of α - and β -tubulin monomers. In contrast, these monomeric subunits are aligned straight in the microtubule-assembled state, with the M-loop in a partially helical conformation. Based on the structural data discussed above, (-)-zampanolide (**E1**) has been suggested to promote tubulin assembly by facilitating the curved-to-straight transition in unassembled tubulin *via* M-loop organization, thereby reducing the entropic cost associated with the assembly process. At the same time, complex formation between **E1** and existing microtubules raises the energetic cost for the straight-to-curved transition, thus resulting in a higher barrier for disassembly.^[61] Diaz and co-workers have published a study on zampanolide-ligated, soluble $\alpha\beta$ -tubulin, which supports this model.^[64]

In the same work of Steinmetz and co-workers, a tubulin-epothilone A complex was resolved as well, showing a similar M-loop organization effect.^[61] In 2016, Yang and co-workers reported a crystal structure of taccalonolide AJ bound to the taxane site of tubulin, which also induced a

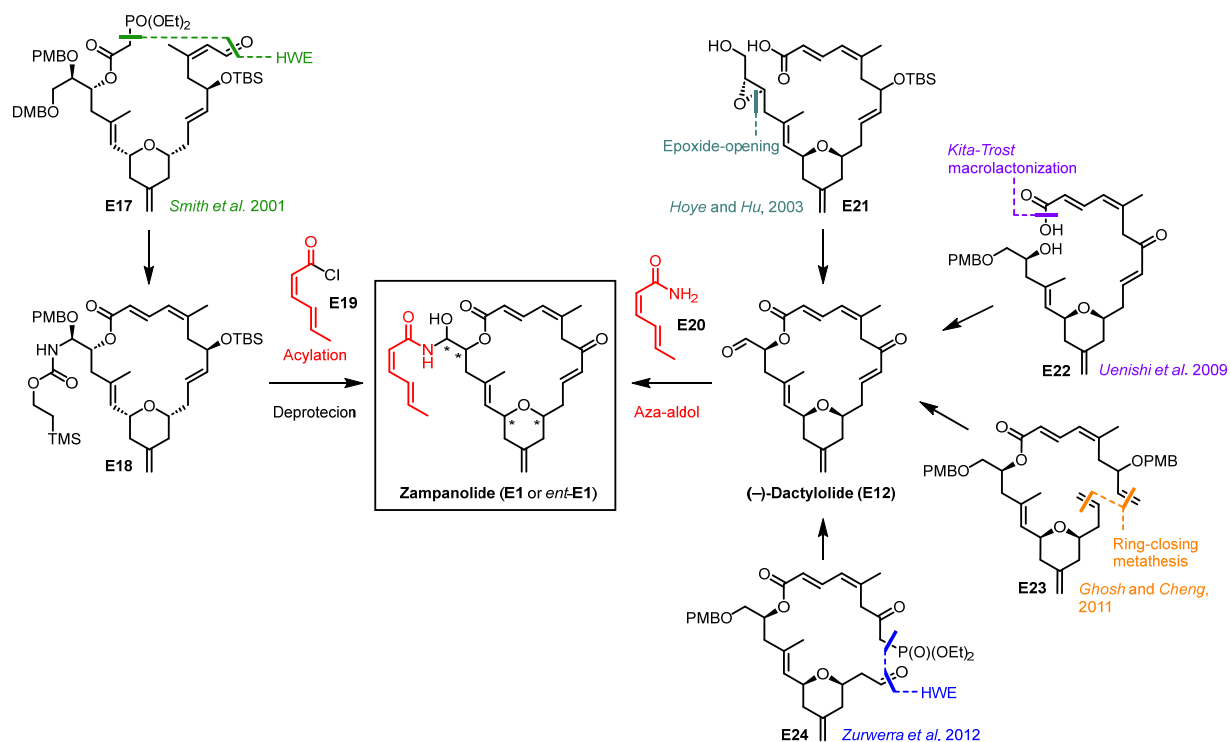
short α -helix in the M-loop.^[65] More recently, Wang and co-workers published x-ray crystallographic investigations on ixabepilone, epothilone B, and epothilone D and confirmed the previous findings of Steinmetz *et al.*^[66] They also summarized the binding modes for most of the taxane-site binders.

In summary, (–)-zampanolide (**E1**) is a covalent MSA and potent inhibitor of cancer cell growth *in vitro*. Of note, it is able to overcome multidrug-resistance mediated by the P-gp efflux pump. As such, **E1** could be a promising lead for anticancer drug discovery. While a preliminary *in vivo* study with **E1** in a single tumor model in mice could not establish a therapeutic window upon systemic administration, antitumor activity was observed upon intratumoral injection. Given its mode of action, the toxicity of **E1** is not too surprising; even clinically employed tubulin modulators are characterized by relatively narrow therapeutic windows. Additional experiments will be required to gain a more general understanding of the *in vivo* pharmacology of **E1**. At the same time, deficiencies in its profile might be mitigated by structural modifications.

2.1.5 Total Syntheses of Zampanolide

Given the distinct biological activity of **E1** in combination with its challenging molecular structure, it is not surprising that **E1** has been the target of several total synthesis campaigns. The first successful total synthesis of (+)-zampanolide (*ent*-**E1**) was reported by Smith and co-workers in 2001.^[67] This was followed by several reports on syntheses of (–)-zampanolide (**E1**).^{[22,68–71][68]} A global summary of the macrocyclization methods employed in these syntheses and their final steps are depicted in **Scheme 7**.

Smith and co-workers relied on an intramolecular *HWE* reaction with **E17** to close the macrocycle and the *HWE* product was further elaborated into carbamate **E18**.^[67] The latter was acylated with (2*Z*,4*E*)-sorblyl chloride (**E19**) and deprotected to give (+)-zampanolide (*ent*-**E1**). All reported syntheses of (–)-zampanolide (**E1**) made use of (–)-dactylolide (**E2**) as an advanced intermediate, to which the sorbamide part of the side chain was attached by an aza-aldol reaction. The macrocycle was closed in four different ways: (1) by epoxide-opening from **E21** (Hoye and Hu);^[70] (2) by *Kita-Trost* macrolactonization of **E22** (Uenishi *et al.*);^[22] by ring-closing olefin metathesis with **E23** (Ghosh and Cheng,^[71] see also Hoye and Hu^[70]); or by an intramolecular *HWE* reaction of **E24** (Zurwerra *et al.*).^[68]



Scheme 7: Macrocyclization methods and last steps in the successful total syntheses of zampanolide. [22,67–71]

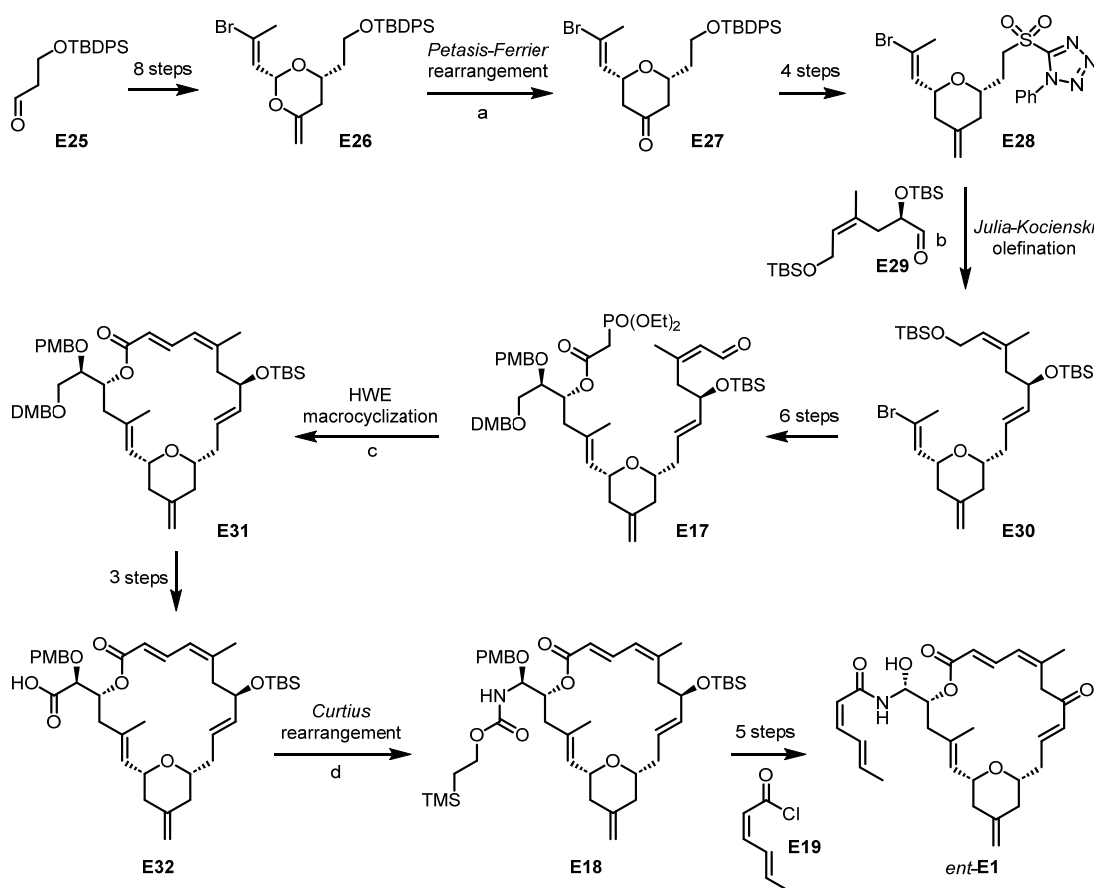
Additionally, several successful total syntheses of (-)-dactylolide (**E2**)^[72–76] and (+)-dactylolide (*ent*-**E2**)^[77–80] have been reported without their conversion into the corresponding zampanolide. Only successful syntheses of zampanolide will be discussed in this section.

2.1.5.1 Synthesis of (+)-Zampanolide by Smith

As discussed in section 2.1.1, the absolute configuration of **E1** was not determined upon first isolation of the compound by *Tanaka* and *Higa*.^[14] In the absence of this information, the first total synthesis of zampanolide by *Smith* and co-workers arbitrarily targeted what turned out to be non-natural (+)-zampanolide (*ent*-**E1**). This became obvious only after the successful synthesis by comparing the specific rotations of synthetic and natural material.^[14,67,81]

A summary of *Smith's* synthesis is outlined in **Scheme 8**. Aldehyde **E25** was elaborated into enol acetal **E26** in 8 steps. Treatment of **E26** with Me_2AlCl triggered a *Petasis-Ferrier* rearrangement to yield the desired pyranone **E27**. The ketone moiety in **E27** was then transformed into an *exo*-methylene group under standard *Wittig* conditions, followed by deprotection of the TBDPS-protected alcohol, addition of the thiotetrazole moiety under *Mitsunobu* conditions, and oxidation of the resulting sulfide to give sulfone **E28**. A *Julia-Kocienski* olefination connected **E28**

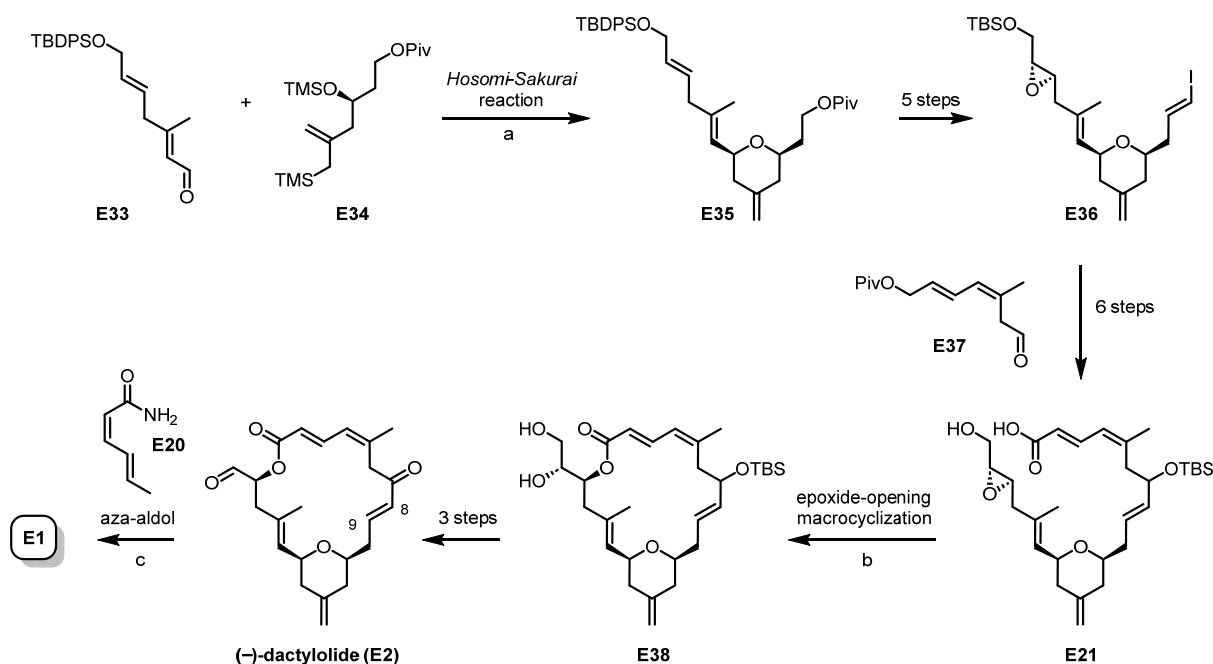
with olefin **E29** to give vinyl bromide **E30**, which was converted into aldehyde **E17** in 6 steps. Macrocyclization *via* an *HWE* reaction mediated by NaHMDS furnished macrolactone **E31** in good yield (72%). Liberation of the primary hydroxy group followed by its oxidation gave carboxylic acid **E32**. Carbamate **E18** was obtained from carboxylic acid **E32** *via in situ* acyl azide formation and subsequent *Curtius* rearrangement with retention of configuration. The carbamate nitrogen was acylated with (2*Z*,4*E*)-sorbyl chloride (**I19**), followed by sequential carbamate- and TBS-cleavage, oxidation of the ensuing alcohol and finally DDQ-mediated cleavage of the PMB group revealed *ent*-**E1**. Epimerization at C(20) was observed (dr: 1.3:1) in this last step (PMB-cleavage). The NMR data of the major isomer was identical to the NMR data reported for natural (–)-zampanolide (**E1**)^[14], but the sign for the specific rotation was inverted (+102 ° vs. –101 °), which proving that the synthesis of the wrong enantiomer was accomplished.



Scheme 8: Summarized synthesis of (+)-zampanolide (*ent*-**E1**) by Smith.^[67,81] *Petasis-Ferrier* RAR: a) (i) Me₂AlCl, CH₂Cl₂, –78 to 0 °C; (ii) NaHCO₃, NEt₃, 0 °C to rt, 59%; *Julia-Kocienski* olefination: b) (i) KHMDS, THF, –78 °C; (ii) **E29**, –78 °C to rt, 88%; *HWE* macrocyclization: c) NaHMDS, THF, –78 to 0 °C, 72%; *Curtius* RAR: d) (i) DIPEA, *i*-BuOCOCl, rt; (ii) NaN₃, H₂O, 0 °C; (iii) toluene, Δ; (iv) TMSCH₂CH₂OH, Δ, 75%.

2.1.5.2 Synthesis of (-)-Zampanolide by Hoyo and Hu

The first total synthesis of (-)-zampanolide (**E1**) was reported by Hoyo and Hu in 2003 (Scheme 9).^[70] CSA-catalyzed *Hosomi-Sakurai* cyclization of advanced building blocks **E33** and **E34** furnished the 2,6-*syn*-disubstituted tetrahydropyran ring in **E35** with excellent diastereoselectivity. Then, **E35** was elaborated into vinyl iodide **E36** in 6 steps. Lithiated **E36** was then reacted with aldehyde **E37** and the ensuing free hydroxy group was TBS protected. Afterwards, a sequence of pivalate removal, oxidation of the liberated hydroxy group and cleavage of the primary TBS-ether gave carboxylic acid **E21**. The macrocycle was closed *via* Ti(O*i*Pr)₄-catalyzed intramolecular epoxide opening by the carboxylate group to deliver lactone diol **E38** in moderate yield (40%). Desilylation and chemoselective oxidation of the allylic alcohol, using *Bobbitt's* salt, furnished the corresponding enone. Oxidative diol cleavage of this enone gave (-)-dactylolide (**E2**). Finally, the aza-aldol reaction of **E2** with (2*Z*,4*E*)-sorbamide served to complete the side chain at C(19). To this end, (2*Z*,4*E*)-sorbamide (**E20**) was treated with DIBAL-H and the mixture was reacted with (-)-dactylolide (**E2**) to yield (-)-zampanolide (**E1**) and its C(20)-epimer as a 1:1 mixture (no yield reported in ref. [70]).

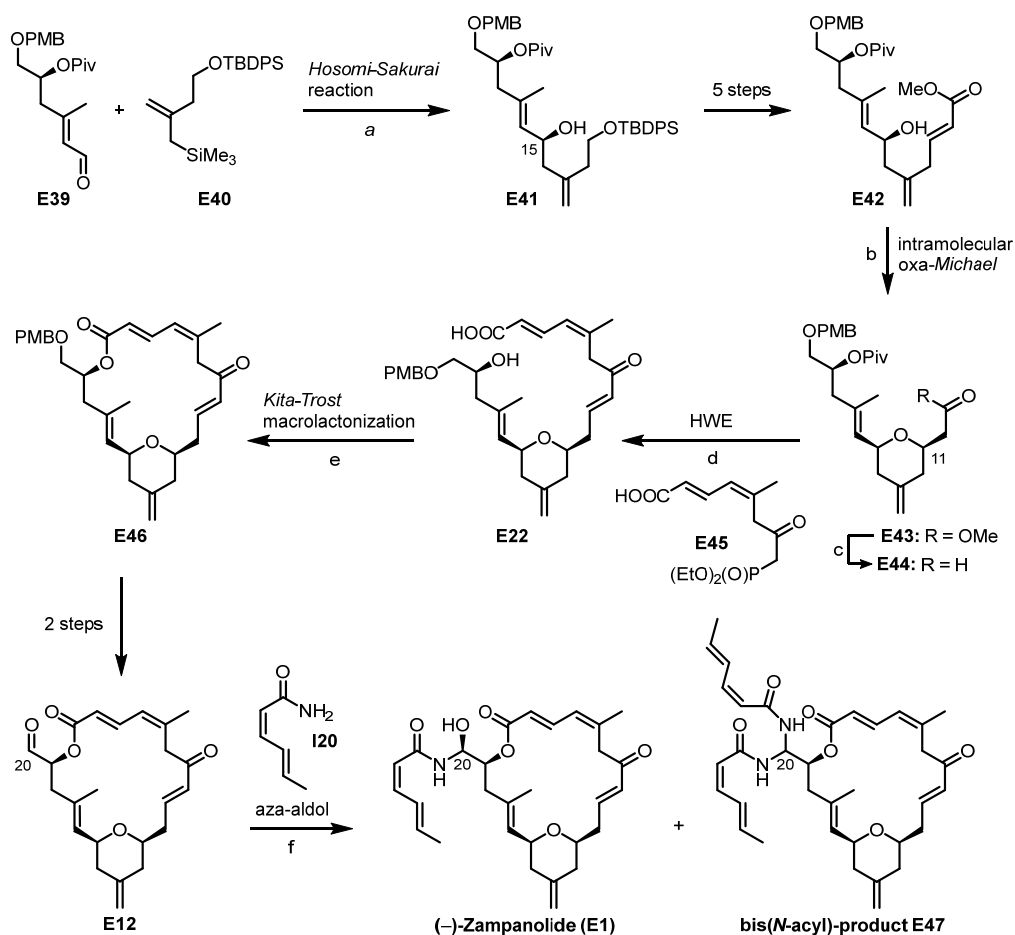


Scheme 9: Summarized synthesis of (-)-zampanolide (**E1**) by Hoyo and Hu.^[70] *Hosomi-Sakurai* reaction: a) CSA (5 mol%), Et₂O, rt, 78%; epoxide-opening macrocyclization: b) Ti(O*i*Pr)₄, CH₂Cl₂, 75 °C, 40% (30% recovered starting material); aza-aldol reaction: c) (2*Z*,4*E*)-sorbamide (**E20**), DIBAL-H, THF, rt, no yield reported.

Hoye and Hu also reported an alternative synthesis of (–)-dactylolide (**E2**), which featured an intermolecular $\text{Ti}(\text{O}i\text{Pr})_4$ -catalyzed epoxide opening reaction to establish the ester bond and macrocyclization *via* RCM at C(8)-C(9) (not shown here).^[70]

2.1.5.3 Synthesis of (–)-Zampanolide by Uenishi

Uenishi and co-workers reported the second total synthesis of **E1** in 2009 (**Scheme 10**).^[22] Alcohol **E41** was obtained from aldehyde **E39** and terminal olefin **E40** *via* Hosomi-Sakurai reaction. This transformation furnished the desired allylic alcohol **E41** in 47% yield together with 42% of its C(15) epimer (*epi*-**E41**); the latter could be converted into **E41** by Mitsunobu inversion. This material was then transformed into enoate **E42** in 5 steps, before the THP ring was closed *via* LiHMDS-mediated intramolecular *oxa-Michael* reaction to furnish **E43**. Noteworthy, low stereoselectivity was observed for this latter transformation, which gave the desired **E43** in 60% yield along with 34% of its C(11) epimer (*epi*-**E43**). After DIBAL-H-mediated reduction of **E43**, the corresponding aldehyde **E44** was coupled with β -ketophosphonate **E45** in an *HWE* reaction to give **E22**. Then, the macrocycle was closed under *Kita-Trost* esterification conditions to yield **E46** in 48% yield. Sequential PMB-ether cleavage and oxidation gave (–)-dactylolide (**E2**). The *aza*-aldol reaction of **E2** with (2*Z*,4*E*)-sorbamide was carried out with CSA as a catalyst, to give (–)-zampanolide (**E1**) in low yield (12%) with no intrinsic stereoselectivity (12% of *epi*-**E1**). The main product of the reaction was the bis(*N*-acyl)-product **E47** (16% yield). Furthermore, 35% of the unreacted (–)-dactylolide (**E2**) was reisolated.

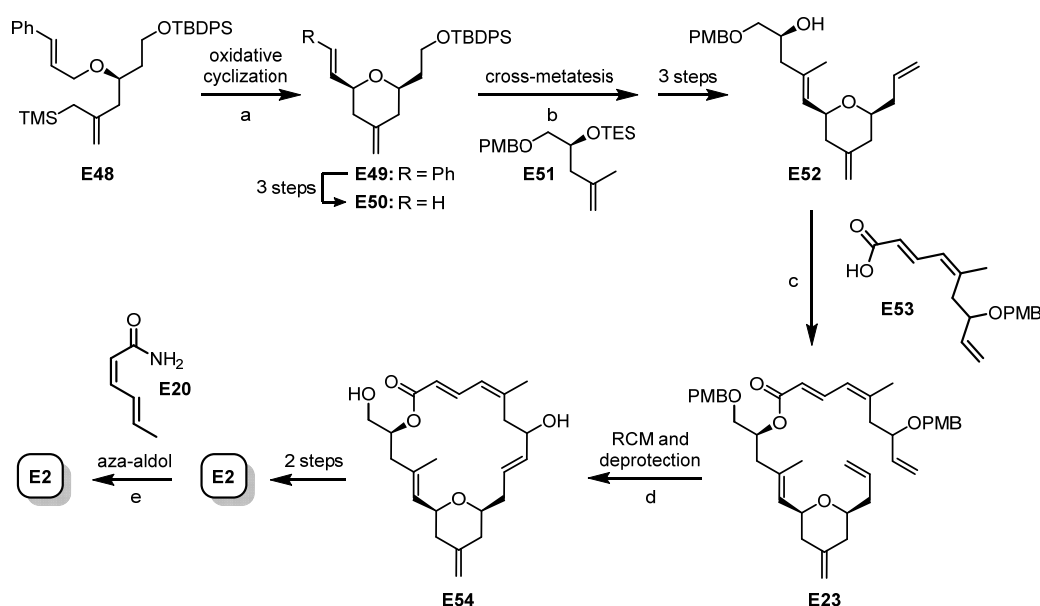


Scheme 10: Summarized synthesis of (-)-zampanolide (**E1**) by Uenishi.^[22] Hosomi-Sakurai reaction: a) SnCl_4 , CH_2Cl_2 , -78°C , 47% (+ 42% C(15) *epi*-**E41**); intramolecular oxa-Michael reaction: b) LiHMDS, TMEDA, toluene, rt, 60%, (additional 34% *epi*-**E43**); reduction: c) DIBAL-H, CH_2Cl_2 , -78°C , 92%; HWE reaction: d) Cs_2CO_3 , *i*-PrOH, rt, 89%; Trost-Kita macrolactonization: e) ethoxyacetylene, $[\text{RuCl}_2(p\text{-cymene})]_2$, acetone, then CSA, toluene, 48%; aza-aldol reaction: f) (2*Z*,4*E*)-sorbamide (**E20**), CSA, CH_2Cl_2 , rt 12%, (additional 12% *epi*-**E1**, 35% recovered **E2** and 16% bis(*N*-acyl)-product **E47** (16%).

2.1.5.4 Synthesis of (-)-Zampanolide by Ghosh

In 2011 Ghosh and co-workers reported a total synthesis of **E1** that featured a novel DDQ/PPTS-mediated intramolecular oxidative cyclization approach for the transformation of **E48** into THP-derivative **E49** (Scheme 11).^[69,71] **E49** was subsequently elaborated in 3 steps into terminal alkyne **E50**, which was submitted to cross-metathesis with **I51** in the presence of Grubbs II catalyst to give a mixture of *E/Z* olefins (1.7:1). The isomers were separable after desilylation and the *Z*-olefin was photochemically isomerized into the desired *E*-olefin. Sequential chemoselective oxidation of the primary hydroxy group with TEMPO and PIDA, followed by Wittig olefination delivered **I52**. Carboxylic acid **I53** was esterified with alcohol **I52** under Yamaguchi conditions to furnish **E23**. Macrocyclization *via* RCM using Grubbs II catalyst followed by PMB-ether cleavage

with DDQ gave diol **E54** in 65% yield over 2 steps. Oxidation of the latter with DMP furnished (–)-dactylolide (**E2**), which was submitted to a (*S*)-TRIP-catalyzed aza-aldol reaction to deliver (–)-zampanolide (**E1**) in 51% yield. Noteworthy, only 18% of the C(20) epimer was isolated, thus revealing a moderate stereoselectivity (2.8:1) of the (*S*)-TRIP-catalyzed aza-aldol reaction in favor of **E1**. This contrasts with the outcome of the DIBAL-H-mediated and CSA-catalyzed variants that had been reported by *Hoye and Hu* and by *Uenishi* and co-workers, respectively, which had been non-selective.

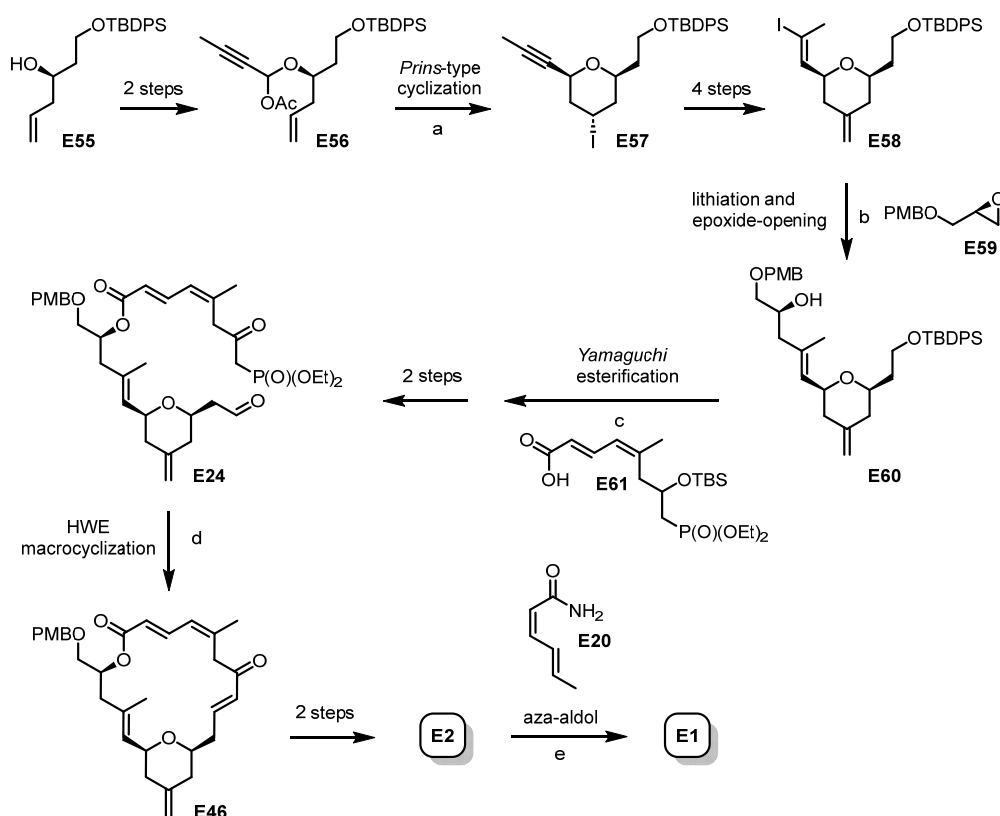


Scheme 11: Summarized synthesis of (–)-zampanolide (**E1**) by *Ghosh*.^[69,71] Oxidative cyclization: a) DDQ, PPTS, MeCN, –38 °C, 81%, cross-metathesis: b) Grubbs II catalyst, CH₂Cl₂, reflux, *E/Z* = 1.7:1, 57%; *Yamaguchi* esterification: c) TCBC, NEt₃, DMAP, toluene, rt, 91%; RCM and deprotection: d) (i) Grubbs II catalyst, benzene, 60 °C; (ii) DDQ, CH₂Cl₂, H₂O, rt, 65% over two steps; aza-aldol reaction: e) (2*Z*,4*E*)-sorbamide (**E20**), (*S*)-TRIP, CH₂Cl₂, rt, 51% (additional 18% of C(20) epimer *epi*-**E1**).

2.1.5.5 Synthesis of (–)-Zampanolide by *Altmann*

The total synthesis of **E1** reported by *Altmann* and co-workers in 2011 was based on macrocycle formation by an intramolecular *HWE* reaction with an α -phosphono ketone (as opposed to the cyclization with an α -phosphono ester as in *Smith's* approach) (**Scheme 12**).^[68,72] Esterification of **E55** with 2-butynoic acid followed by partial ester reduction and acylation gave acetal **E56**. The THP ring was then furnished *via* TMSI-mediated *Prins*-type cyclization, to yield the desired 2,6-*syn*-disubstituted product **E57** in 85% yield as a single diastereoisomer. This intermediate was further elaborated into vinyl iodide **E58** in 4 steps. Lithium-halogen exchange with *t*-BuLi, followed by BF₃·OEt₂-promoted epoxide opening of **E59** gave rise to alcohol **E60**. The latter was coupled with carboxylic acid **E61** (synthesized in 10 steps from 2-butynol) under *Yamaguchi*

conditions. After global desilylation, the ensuing diol was oxidized to β -ketophosphonate **E24**, which, in the presence of $\text{Ba}(\text{OH})_2$, underwent *E*-selective intramolecular *HWE* reaction to produce macrolactone **E46** in high yield (85%). PMB-ether cleavage gave (–)-dactylolide (**E2**), which was submitted to DIBAL-H-mediated aza-aldol reaction as reported by *Hoye and Hu* [70] to give (–)-zampanolide (**E1**) in 18% yield and its C(20) epimer *epi*-**E1** in 12% yield.



Scheme 12: Summarized synthesis of (–)-zampanolide (**E1**) by *Altmann*.^[68,72] *Prins*-type cyclization: a) TMSI, 2,6-dimethylpyridine, CH_2Cl_2 , -19°C , 85%; lithiation and epoxide-opening: b) *t*-BuLi, **E59**, $\text{BF}_3\cdot\text{OEt}_2$, toluene, -85 to -78°C , 61%; *Yamaguchi* esterification: c) **E61**, TCBC, Et_3N , DMAP, toluene, rt, 85%; *HWE* reaction: d) $\text{Ba}(\text{OH})_2$, THF/ H_2O 40:1, 0°C to rt, 85%; aza-aldol reaction: e) **E20**, DIBAL-H, THF, rt, 18%, (additional 12% C(20) epimer *epi*-**E1**).

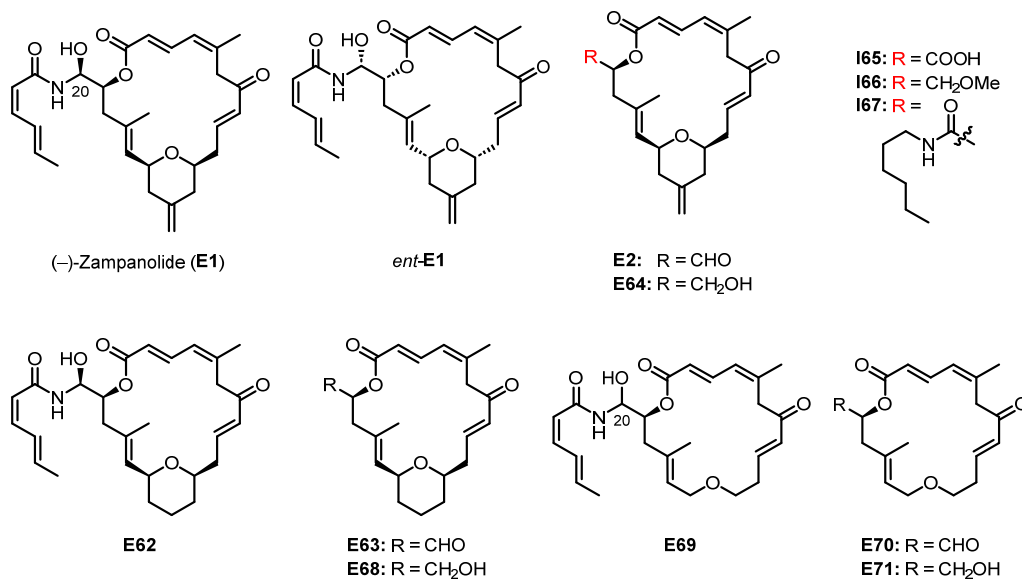
2.1.6 Stereoselective Aza-Aldol Reaction for the Construction of Zampanolides

The non-selective aza-aldol reaction was the major bottleneck in the syntheses of (–)-zampanolide (**E1**), which was very unsatisfactory, as it was the last step of a long synthesis and the requisite precursor thus very precious. The *Altmann* group reported a stereoselective method for the desired construction of the *N*-acyl hemiaminal moiety in zampanolides in 2020 (**Scheme 13**).^[82] In this procedure, **E2** was reacted with an *in situ* formed (*S*)-BINAL-(2*Z*,4*E*)-sorbamide complex to deliver **E1** in 81% yield as a single diastereoisomer. This was a significant improvement compared to the non-selective version using DIBAL-H, which gave **E1** in 18%.^[68,72] This method

to its carboxylic acid (**E65**), methyl ether (**E66**) or amide (**E67**) analogs led to a big drop in activity, which was reported in the same study by *Altmann* and co-workers.

The findings by Uenishi *et al.* on the C(20)-*R* epimer of **E1** and of *Ding* and *Jennings* on **E2** were subsequently confirmed by the *Altmann* group in their early SAR work, which is summarized in **Table 1** together with data for **E62** and **E63**, which were investigated only more recently. One of the most pertinent findings in the early stages of this work was the recognition that the removal of C(13) methylene group from (-)-dactylolide (**E63**) (or the corresponding alcohol **E68**) had no impact on antiproliferative activity. This finding was later extended to the corresponding zampanolide analog **E62**; as shown by the data in **Table 1**, this compound is at least equipotent with **E1** across all cell lines investigated. In contrast, (+)-zampanolide (*ent*-**E1**) is four orders of magnitude less active than **E1** at least against the ovarian cancer cell lines A2780 or its multidrug-resistant variant A2780 AD (the only cell lines investigated).^[82]

Rather intriguingly, *Altmann* and co-workers also found that monocyclic analogs **E69-E71** (which were epimeric mixtures at C(20)) were no more than ca. 25-80-fold less potent than the corresponding parent compounds **E1**, **E2**, and **E64**, respectively. This was surprising, given that the removal of the THP moiety would be expected to cause a significant decrease in structural rigidity.

Table 1: Antiproliferative activity of (-)-zampanolide (**E1**), (-)-dactylolide (**E2**) and selected analogs against human cancer cell lines (IC₅₀ [nM]).^[68,82]

| Compound | A549 (lung) | MCF-7 (breast) | PC-3 (prostate) | A2780 (ovarian) | A2780 AD (MDR ovarian) ^[a] |
|---------------------------|----------------|-------------------|--------------------|-----------------------------|--|
| E1 | 3.2 ± 0.4 | 6.5 ± 0.7 | 2.9 ± 0.4 | 1.9 ± 0.01 ^[b] | 2.2 ± 0.2 ^[b] |
| C(20)-epi-E1 | 53 ± 5.9 | 42 ± 9.3 | 50 ± 12 | | |
| <i>ent</i> - E1 | | | | 10500 ± 1138 ^[c] | 11445 ± 70 ^[c] |
| E2 | 301 ± 4.3 | 247 ± 2.6 | 751 ± 69 | 602 ± 100 ^[b] | 1236 ± 180 ^[b] |
| E64 | 127 ± 2.9 | 106 ± 3.6 | 320 ± 26 | | |
| E65 | 9732 ± 260 | 7624 ± 303 | 9338 ± 242 | | |
| E66 | 1072 ± 103 | 1489 ± 83 | 1274 ± 117 | | |
| E67 | 973 ± 90 | 1138 ± 72 | 829 ± 27 | | |
| E62 | 1.0 ± 0.2 | | | 1.7 ± 0.4 ^[c] | 3.53 ^[c] |
| E63 | 149 ± 12.8 | 68 ± 5.6 | | | |
| E68 | 189 ± 19.3 | 114 ± 10.2 | 104 ± 4.1 | | |
| E69 ^[d] | | 165 ± 13 | 218 ± 7 | | |
| E70 | 3921 ± 216 | 2894 ± 144 | 4021 ± 102 | | |
| E71 | 2378 ± 70 | 3891 ± 102 | 3051 ± 178 | | |

^[a]Multidrug-resistant cell line overexpressing the Pgp efflux pump.^[83,84] ^[b]Data from ref. [60]. ^[c]Data from ref. [82]. ^[d]**E69** was obtained as a 1.6:1 epimeric mixture at C(20).

Building on *Altmann's* findings, *Chen* and co-workers subsequently investigated a whole series of monocyclic desTHP analogs of zampanolide (**E72-E77**) with simplified (i.e. achiral) side chains (**Figure 13**).^[85-88] Three of these analogs (**E72-S**, **E73-R**, and **E74-R**) showed submicromolar antiproliferative activity against docetaxel-sensitive and resistant cancer cell lines. The activity of all other compounds was in the low single digit micromolar range.^[85,86]

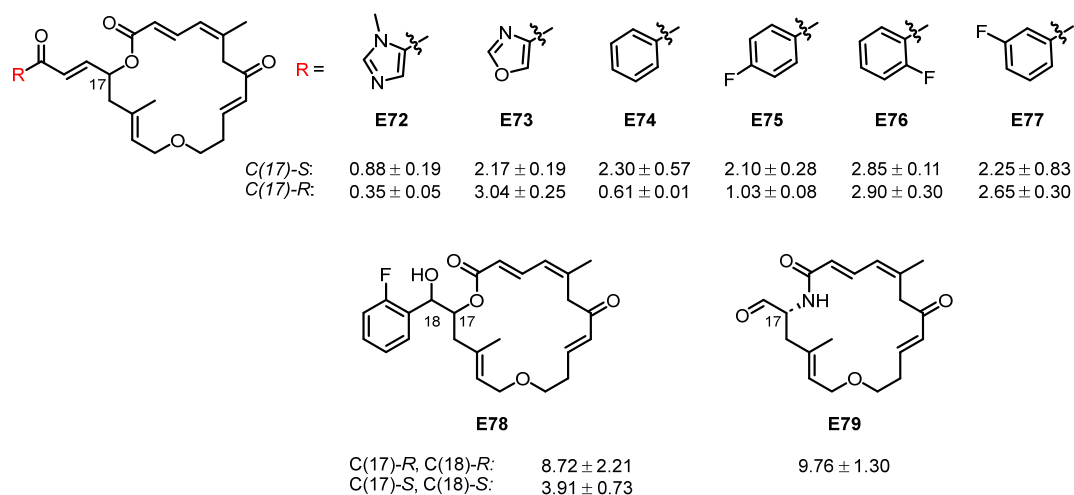


Figure 13: Structures of monocyclic desTHP zampanolide/dactyloolide analogs **E72-E79** and antiproliferative activity against the prostate cancer cell line PC-3 (IC_{50} [nM]).^[85-88]

In follow up studies, *Chen* and co-workers reported data for 2-fluorobenzyl alcohol **E78**^[87] and macrolactam **E79**^[88]; these compounds showed slightly decreased potencies compared to the aryl enoates (**Figure 13**).

The discovery of the potent antiproliferative activity of 13-desmethylene zampanolide (**E62**) led the *Altmann* group to investigate the effects of the replacement of the THP moiety by other heterocycles. So far, this has included the incorporation of *N*-substituted morpholine moieties (analog **E80-E83**)^[89] or of an oxazole ring (analog **E84**)^[90] (**Figure 14**). Three main reasons made such compounds desirable targets: (1) the additional heteroatoms were believed to increase the solubility of the compounds; (2) the same heteroatoms would also offer the potential for additional hydrogen bonding interactions with the protein; and (3) the secondary amino group of the morpholine ring would offer a handle for the attachment of conjugate groups, such as e.g. tumor-targeted antibodies, fluorophores etc. While *N*-substituted morpholine-zampanolides **E80** (*N*-acetylated), **E81** (*N*-benzoylated) and **E82** (*N*-mesylated) showed similar antiproliferative activity as **E1** across all four tested cell lines (A549, PC-3, MCF-7, HeLa), *N*-tosylated morpholine analog **E83** was significantly less active.^[89] Unfortunately, all efforts towards the corresponding unsubstituted parent compound were futile. Dactyloolide analog **E84** was ca. two orders of

magnitude less potent than the corresponding THP-based dactylolide alcohol **E64**.^[90] Unfortunately, **E84** could not be elaborated into the corresponding oxazole-zampanolide analog.

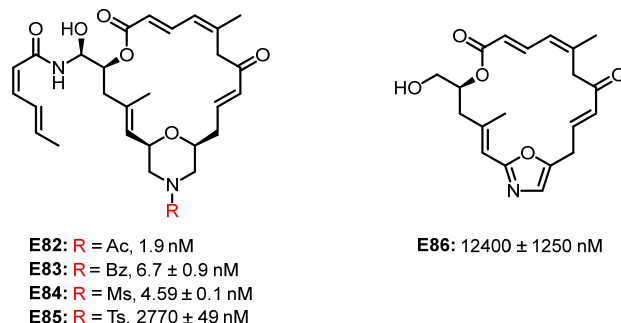


Figure 14: Structures and IC₅₀ values of morpholine based zampanolide/dactylolide alcohol analogs **E80-E83/E84** against lung cancer cell line A549.^[89,90]

Taylor and co-workers reported that C(17)-desmethyl-13-desmethylene zampanolide **E87** is 17-57-fold less active against PC3, A549 and 1A9 cell lines compared to **E1** (Figure 15).^[91] Noteworthy, **E87** was tested as a 1.5:1 diastereomeric mixture at C(20). The global synthetic strategy was based on the reported total synthesis of **E1** by Altmann and co-workers (cf. Scheme 12): acid **E61** was coupled with a C(17)-desmethyl-C(13)-methylene alcohol analog of **E60** (cf. Scheme 12). The latter was obtained from (*R*)-aspartic acid in 6 steps. More recently the same group reported the activity of the non-macrocyclic zampanolide analog **E88** (Figure 15).^[92] This analog was drastically less potent against the same three cell lines mentioned above.

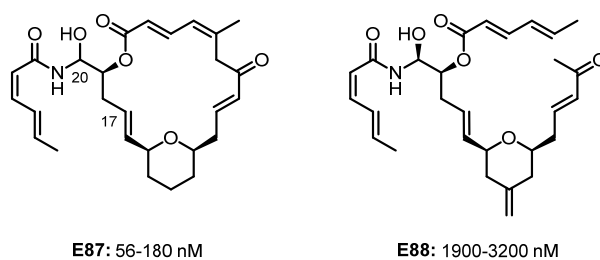


Figure 15: Structures and range of GI₅₀ values (against PC3, A549 and 1A9 cells) of C(17)-desmethyl-13-desmethylene zampanolide **E87** (1.5:1 diastereomeric mixture at C(20)) and non-macrocyclic zampanolide analog **E88**. **E88** was not active against A549 cells in the tested concentration range (>6000 nM).^[92]

As alluded to earlier, Northcote and co-workers have recently reported the isolation of a new set of natural congeners of **E1** (i.e. zampanolides B-E, **E3-E6**) and they have tested the activity of these compounds against HL60 human leukemia cells.^[15] Inversion of the configuration of either the C(4)-C(5) (analog **E3**) or the C(8)-C(9) (analog **E4**) double bond does not lead to a change in potency compared to **E1**; only a marginally lowered IC₅₀ value was found for zampanolide D (**E5**),

which features an *EZ* diene configuration in the sorbamide part of the side chain (vs. the *ZE* arrangement in **E1**).

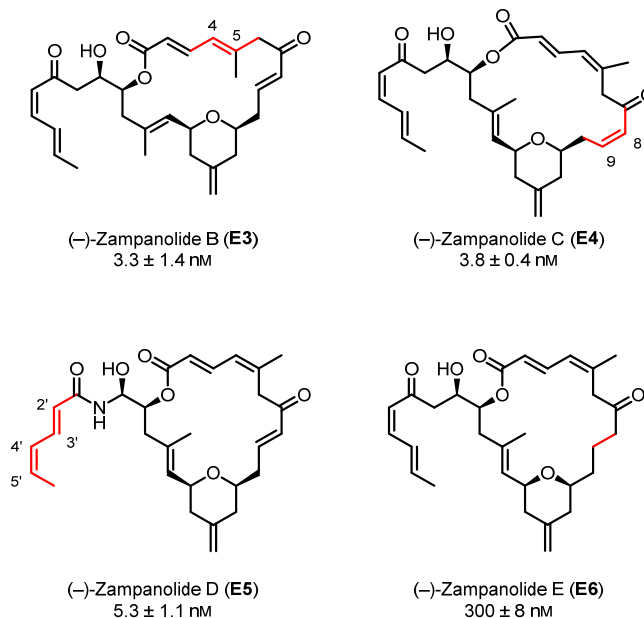


Figure 16: Structures of zampanolides B-E (**E3-E6**) and antiproliferative activity against the human leukemia cell line HL-60 (IC_{50} [nM]).^[15]

Somewhat surprisingly, even zampanolide E (**E6**), which lacks the C(8)-C(9) double bond responsible for covalent binding to tubulin, still exhibits profound inhibition of cancer cell growth (ca. 91-fold lower than **E1**). Thus, zampanolide E is still a potent substrate for microtubule stabilization even if in a non-covalent manner “only” and despite its decrease in structural rigidity compared to **E1**.

To date, there is still no report about an analog with superior potency over the parental compound (-)-zampanolide (**E1**). While limited SAR studies have been reported, there are still a lot of open questions about the biological importance of certain moieties of **E1**.

2.2 Results and Discussion

2.2.1 Synthesis and Structure-Activity Relationship Studies of C(13)-Desmethylene-(–)-Zampanolide Analogs (Publication 1)

Based on:

T. M. Brütsch,* E. Cotter,* D. Lucena-Agell, M. Redondo-Horcajo, C. Davies, B. Pfeiffer, S. Pagani, S. Berardozi, J. F. Díaz, J. H. Miller, K. H. Altmann, *Chem. Eur. J.* **2023**, *29*, e202300703. (*co-first authors)^[93]

E. Cotter's contributions: conceptualization with T. M. Brütsch, S. Berardozi and K.-H. Altmann; synthetic investigations (analogs **R7** and **R8**) with T. M. Brütsch (analogs **R6**, **R9** and compound **R47**) and S. Pagani (compound **R47**); Brütsch; publication writing with K.-H. Altmann and J. F. Díaz; cover page.

Introduction

Natural products represent a critical source of lead structures for drug discovery and development and a substantial fraction of drugs approved for the treatment of human diseases are either unmodified natural products or derived from a natural product lead.^[11,94–96] The overwhelming majority of these compounds originate from terrestrial plants, fungi or bacteria; in comparison, the impact of natural products obtained from marine organisms so far has been much less pronounced, at least partly due to their more limited availability from the natural sources.^[97,98] At the same time, many marine natural products display unique structures and bioactivities,^[99–101] which makes them highly attractive starting points for drug discovery^[102–106] and/or valuable tools for chemical biology.^[107,108] In this context, the total chemical synthesis of marine natural products and, in particular, the chemical synthesis of analog structures is of central importance,^[109–112] as it allows to mitigate the problem of limited material supply from the producing organisms.

As a case in point, (–)-zampanolide (**R1**) (**Figure 17**) is a marine macrolide that was first isolated in 1996 by *Tanaka* and *Higa* from the marine sponge *Fasciospongia rimosa* and shown to be a potent inhibitor of cancer cell growth *in vitro* with IC₅₀ values in the low nanomolar range (2–10 nM).^[14]

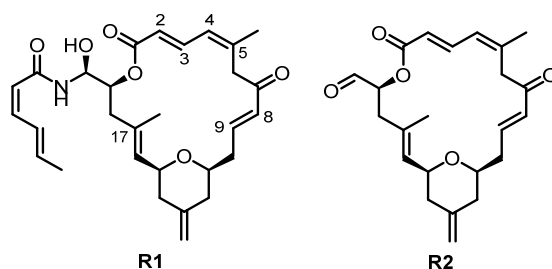


Figure 17: Structures of (-)-zampanolide (**R1**) and of (-)-dactylolide (**R2**).

Structurally, (-)-zampanolide (**R1**) features a dioxabicyclo[15.3.1]heneicosane core, including a polyunsaturated macrolactone ring and a *syn*-2,6-disubstituted tetrahydropyran unit bearing an exocyclic methylene group. The core is linked to a (*Z,E*)-sorbamide-derived side chain by way of a (linear) hemiaminal moiety; only few other natural products are known to incorporate this intriguing structural motif.^[15–20]

After the biology of (-)-zampanolide (**R1**) had not been further investigated for several years after its discovery, it was re-isolated from a different sponge, *Cacospongia mycofijiensis* by Northcote and co-workers in 2009.^[21] Mode-of-action studies with the compound then revealed that **R1** was a potent microtubule-stabilizing agent (MSA), thus exerting its antiproliferative effects through the same mechanism as the established anticancer drugs paclitaxel, taxotere, cabacitaxel, or ixabepilone.^[46] In contrast to the latter, however, (-)-zampanolide (**R1**) binds to β -tubulin in a covalent fashion, as has been demonstrated by biochemical^[60] as well as structural studies.^[61] Covalent bond formation involves 1,4-addition of β -His229 to C(9) of the enone moiety in the macrocycle.^[61]

(-)-Zampanolide (**R1**) has been the target of multiple successful total synthesis campaigns,^[22,68,113,114] including the synthesis of (+)-zampanolide (*ent*- **R1**) by *Smith* and co-workers,^[81] which established the complete relative and absolute configuration of the natural product (which had not been fully elucidated by *Tanaka* and *Higa*).^[14] In addition to the total synthesis of **R1**, numerous synthetic studies have targeted (-)-dactylolide (**R2**) (**Figure 17**),^[22,68,73,113,114] which has served as an advanced intermediate in all^[22,68,113,114] but one total synthesis of **R1**.^[81] This compound is significantly less potent than **R1**,^[68,73,81] thus highlighting the importance of the C(19) side chain for microtubule-stabilization and antiproliferative activity. Other aspects of the zampanolide SAR that have been investigated by means of synthetic analogs are the importance of the tetrahydropyran ring,^[68,85–90] of the C(13) methylene group^[68] and of the methyl group at C(17).^[91] Of particular importance in the context of the current study is *Taylor's* work on 13-desmethylene-17-desmethyl(-)-zampanolide (**R5**),^[91] which was found to be a 17- to 57-fold less potent cell growth inhibitor than **R1** (for a 1.5:1 diastereomeric mixture

at C(20); tested against 3 cancer cell lines). Unfortunately, none of the singly modified congeners (either 13-desmethylene(-)-zampanolide (**R3**) or 17-desmethyl(-)-zampanolide) was reported in that study, which made it difficult to discern the effect of each of the individual modifications. We have recently shown that the removal of the C(13) methylene group in (-)-zampanolide (**R1**) has no discernible impact on antiproliferative activity.^[82] As the synthesis of 13-desmethylene zampanolide (**R3**, **Figure 18**) includes 3 fewer steps than the synthesis of the parent natural product **R1** (at least when employing the strategy that we have developed for the total synthesis of **R1**),^[68] we have based our subsequent SAR work on the 13-desmethylene macrocycle and we have used 13-desmethylene (-)-zampanolide (**R3**) as a reference comparator to assess the effect of other modifications.

Following this approach, we have investigated the importance of the methyl groups at C(5) and C(17), of the C(2)-C(3) and C(4)-C(5) double bonds, individually and in combination, and of the enone double bond between C(8) and C(9) for microtubule-binding and antiproliferative activity.

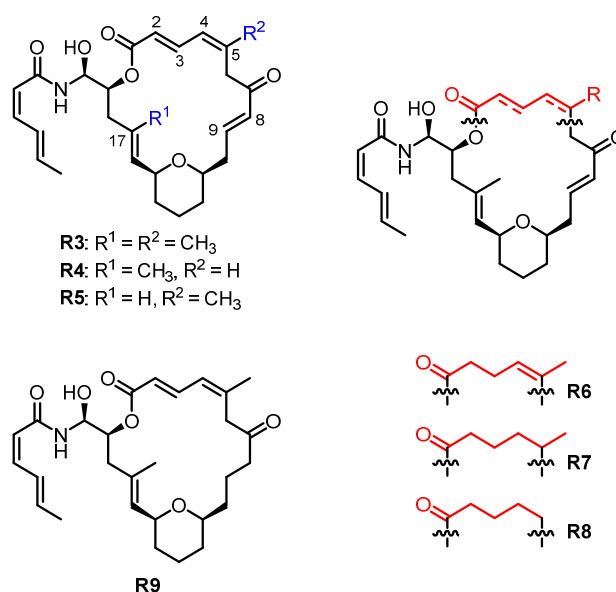


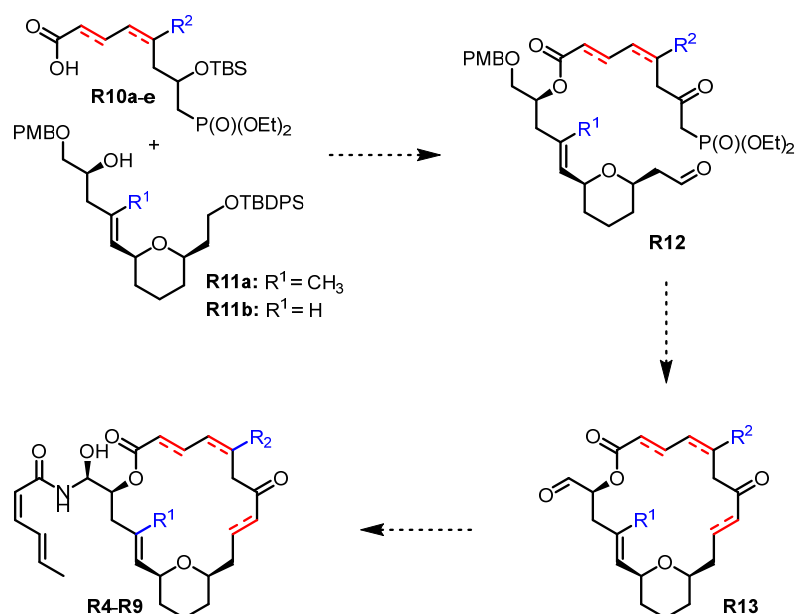
Figure 18: Structure of 13-desmethylene (-)-zampanolide (**R3**) and of targeted analogs (**R4-R8**) for SAR studies.

Inspection of the structure of the complex between **R1** and β -tubulin shows the C(17) methyl group to be located in a hydrophobic environment, although it is unclear to what extent it actually contributes to the binding affinity of **R1**; in contrast, the C(5) methyl group appears not to be important for tubulin binding, but these questions needed to be addressed experimentally.^[61] Partial or complete removal of the double bonds from the conjugated system between C(1) and C(5) should provide information on the importance of conformational rigidity in this part of the structure for microtubule-binding affinity and antiproliferative activity. Finally, the removal of

the C(8)-C(9) double bond in analog **R9** at first glance may appear as counterintuitive, as it is required for covalent binding to β -tubulin.^[61] However, the investigation of **R9** was meant to assess the inherent binding affinity of **R1** for microtubules in the absence of covalent attachment. The corresponding analogs **R5-R9** (**Figure 18**) were all prepared *via* a unified global strategy. Analog **R4** could not be prepared for reasons that will be discussed in detail below.

Results and Discussion

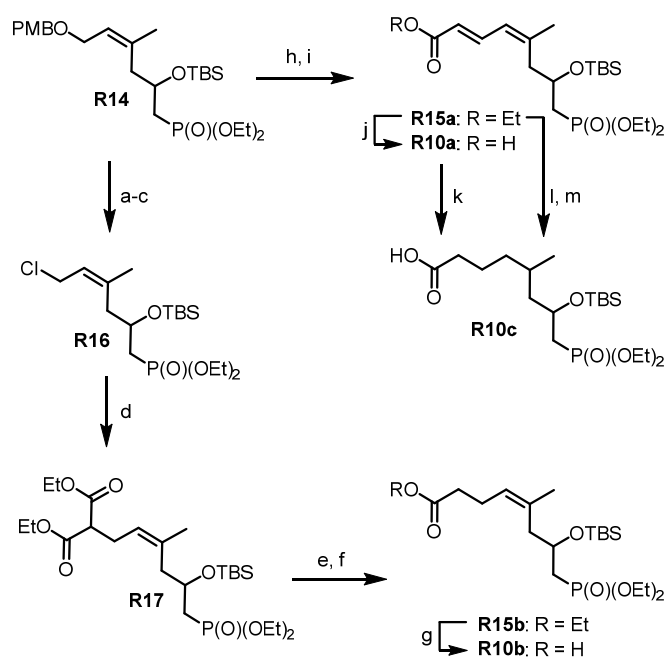
Synthetic planning. The synthesis of all analogs was to be based on our previously developed approach towards the total synthesis of (-)-zampanolide (**R1**),^[68] which we had also followed for the synthesis of **R3** and a series of morpholino-zampanolides.^[89] According to this overall strategy, the ester products resulting from acylation of alcohols **R11** with acids **R10** would be elaborated into keto-aldehydes **R12** (**Scheme 14**); the latter were expected to undergo *E*-selective intramolecular *HWE* reaction to form the corresponding macrolactones. PMB-removal and oxidation would then furnish aldehydes **R13**, which would be reacted with (*Z,E*)-sorbamide in a stereoselective aza-aldol reaction recently developed in our laboratory,^[82] to provide analogs **R4-R8**. Analog **R9** was envisioned to be accessible from the macrocyclization product *en route* to **R3**^[68,82] by selective reduction of the enone double bond, for example by means of the Stryker reagent.



Scheme 14: Global strategy for the synthesis of zampanolide analogs **R4-R9**. **R10a** is the precursor acid for analogs **R5** and **R9**, **R10b-d** are the precursor acids for analogs **R6-R8**, respectively, and **R10e** is the precursor acid for analog **R4** (*cf.* **Figure 18**).

Synthesis of acids R10. The synthesis of acid **R10a** via phosphonate **R14** and ester **R15a** (Scheme 15) has been reported previously.^[68] **R10a** was required as a precursor for the synthesis of analogs **R5** and **R9**.

Partially saturated acid **R10b** was obtained from phosphonate **R14**,^[68] which was submitted to oxidative PMB-removal with DDQ (Scheme 15). The reaction gave a mixture of the expected allylic alcohol and the corresponding aldehyde; treatment of this mixture with DIBAL-H in CH₂Cl₂ at -78 °C yielded the desired alcohol in 56% yield over 2 steps. Mesylation of the primary hydroxy group followed by *in situ* reaction of the ensuing mesylate with LiCl then furnished allylic chloride **R16** in close to quantitative yield.



Scheme 15: Synthesis of acids **R10a-c**: a) a) DDQ, CH₂Cl₂/H₂O (20:1), rt; b) DIBAL-H, CH₂Cl₂, -78 °C, 56% over two steps; c) MsCl, LiCl, 2,6-lutidine, 0 °C, 98%; d) Na, diethyl malonate, EtOH, reflux, 86%; e) KOH, EtOH, rt, 98%, f) Et₃N, toluene, reflux, 85%; g) 2M NaOH, EtOH, rt, 97%; h) i. DDQ, CH₂Cl₂/H₂O (20:1), 0 °C; ii. (COCl)₂, DMSO, Et₃N, CH₂Cl₂, -78 °C to rt, 88% over two steps; i) (EtO)₂P(O)CH₂COOEt, *n*-BuLi, THF, 0 °C; j) 1M NaOH, EtOH, 0 °C, 94% over two steps; k) H₂, 10% Pd/C, EtOH, rt, 78%; l) H₂, 10% Pd/C, EtOH, rt, 95%; m) 1M NaOH, EtOH, 0 °C to rt, 95%.

While attempts at the direct formation of ethyl ester **R15b** by alkylation of the Li-enolate of ethyl acetate (formed with LiHMDS) with **R16** were unsuccessful, reaction of **R16** with the Na-enolate of diethyl malonate (formed with sodium in ethanol) gave substituted malonate **R17** in 86% yield after 5 min at reflux.

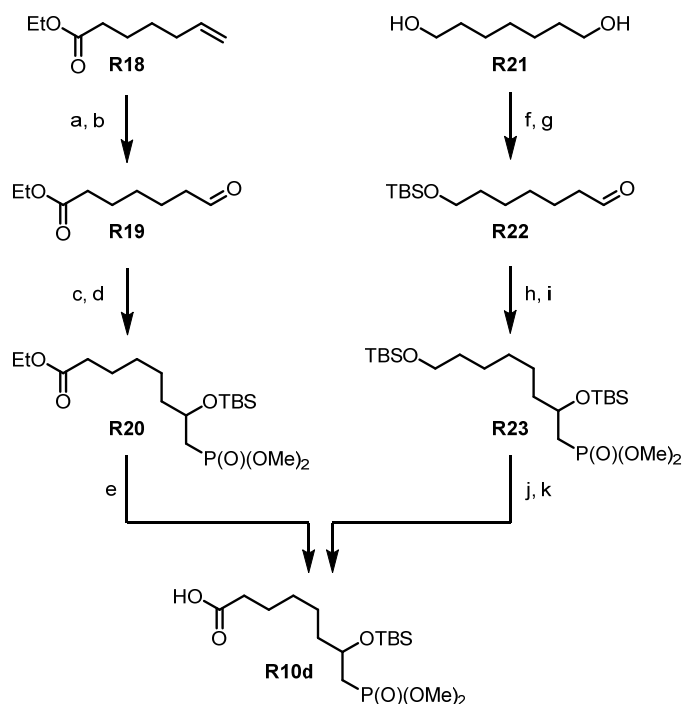
As *Krapcho* decarboxylative conditions (NaCl, DMSO/H₂O, 120-170 °C)^[115] only led to decomposition, **R17** was hydrolyzed to the corresponding mono acid, which was then treated with Et₃N in toluene to induce decarboxylation. This two-step process gave ethyl ester **R15b** in

83% yield (from **R17**). Finally, saponification of **R15b** with NaOH/EtOH provided acid **R10b** in excellent yield (97%).

Fully saturated acid **R10c** was obtained from **R10a** by hydrogenation under standard conditions (H₂, 10% Pd/C, EtOH) in 78% yield as an inseparable mixture of diastereoisomers (**Scheme 15**). Alternatively, hydrogenation of ester **R15a** followed by saponification of the fully saturated product with aqueous NaOH gave **R10c** in 90% overall yield.

Two different approaches were elaborated towards fully saturated acid **R10d** (**Scheme 16**), which would serve as a building block for the most extensively modified zampanolide analog investigated in this study, i.e. **R8**. Our first generation approach towards **R10d** started from commercially available ethyl hept-6-enoate (**R18**), which was converted into aldehyde **R19** in 24% overall yield by hydroboration/oxidation and further oxidation of the resulting primary alcohol with pyridinium chlorochromate (PCC). Addition of lithiated dimethyl methylphosphonate to **R19** at -100 °C in THF followed by TBS-protection (TBSCl, DMAP) then gave the fully protected β-hydroxy phosphonate **R20** in moderate overall yield (10%). Ester hydrolysis with aqueous NaOH finally furnished the desired acid **R10d** in 72% yield. While this route would have provided sufficient amounts of analog **R8** for biological testing, the poor yield for the transformation of **R19** into **R20** led us to seek an alternative, more efficient route towards acid **R10d**.

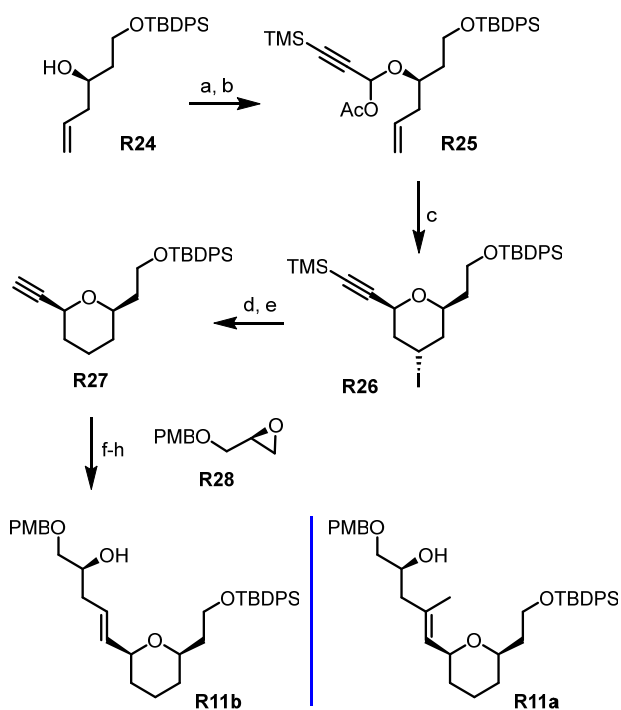
As depicted in **Scheme 16**, the alternative route started with the conversion of heptane-1,7-diol (**R21**) into aldehyde **R22** by mono-TBS protection followed by Swern oxidation of the mono-TBS ether. While the overall yield for this transformation (35% for two steps) still leaves room for improvement, aldehyde **R22** could be transformed into phosphonate **R23** in 85% yield by reaction with LiCH₂P(O)(OCH₃)₂ followed by DMAP-catalyzed silylation of the newly formed hydroxy group (vs. 10% for the conversion of **R19** into **R20** under the same conditions).



Scheme 16: Synthesis of acid **R10d**: a) i. BH_3 , THF, 0°C to rt; ii. H_2O_2 , 1M NaOH, 76% over two steps; b) PCC, CH_2Cl_2 , 0°C to rt, 32%; c) dimethyl methylphosphonate, *n*-BuLi, THF, -100°C , 35%; d) TBSCl, imidazole, DMAP, DMF, 29%; e) 1M NaOH, EtOH, 0°C to rt 72%; f) TBSCl, Et_3N , CH_2Cl_2 , 0°C to rt, 54%; g) $(\text{COCl})_2$, DMSO, Et_3N , CH_2Cl_2 , -78 to 0°C , 65%; h) dimethyl methylphosphonate, *n*-BuLi, THF, -100°C ; i) TBSCl, imidazole, DMAP, DMF, 85% (two steps); j) CSA (20 mol%), $\text{CH}_2\text{Cl}_2/\text{MeOH}$ (1:1), 0°C to rt, quant.; k) i. DMP, NaHCO_3 , CH_2Cl_2 , rt; ii. NaClO_2 , NaH_2PO_4 , 2-methyl-2-butene, *t*-BuOH/ H_2O , 0°C to rt, 93% (two steps).

Selective liberation of the primary hydroxy group with catalytic amounts (20 mol%) of camphorsulfonic acid in $\text{CH}_2\text{Cl}_2/\text{MeOH}$ (1:1) followed by Dess-Martin oxidation^[116] of the resulting free alcohol and subsequent Pinnick oxidation^[117] of the ensuing aldehyde provided acid **R10d** in excellent yield (93% over 3 steps). Acid **R10d** could thus be obtained from heptane-1,7-diol (**R21**) in 6 steps with an overall yield of 23%, compared to 2% for the 5-step sequence from ethyl hept-7-enoate (**R18**).

Synthesis of alcohol R11b. The synthesis of alcohol **R11b** was devised around THP-ring formation by a Prins-type cyclization as the central step (**Scheme 17**). The requisite cyclization precursor **R25** could be obtained from homoallylic alcohol **R24** by Steglich esterification with 3-TMS-propionic acid followed by DIBAL-H reduction at -78°C and *in situ* acetylation of the ensuing hemiacetal with acetic anhydride/DMAP; **R24** had also been an intermediate in the preparation of alcohol **R11a**, in the context of our work on (–)-zampanolide (**R1**)^[68] and 13-desmethylene(–)-zampanolide (**R3**).^[82]



Scheme 17: Synthesis of alcohol **R11b**: a) 3-TMS-propionic acid, DCC, DMAP, CH_2Cl_2 , $-20\text{ }^\circ\text{C}$, 38%; b) DIBAL-H, then Ac_2O , pyridine, DMAP, CH_2Cl_2 , $-78\text{ }^\circ\text{C}$, 89%; c) TMSI, 2,6-dimethylpyridine (20 mol%), CH_2Cl_2 , $-20\text{ }^\circ\text{C}$ to rt, 88%; d) Bu_3SnH , AIBN (10 mol%), toluene, reflux, 87%; e) K_2CO_3 , MeOH, rt, 98%; f) **R28**, *n*-BuLi, $\text{BF}_3\cdot\text{Et}_2\text{O}$, THF, $-78\text{ }^\circ\text{C}$, 83%; g) LiAlH_4 , THF, $50\text{ }^\circ\text{C}$, 56%; h) TBDPSCl, imidazole, DMF, rt, 92%.

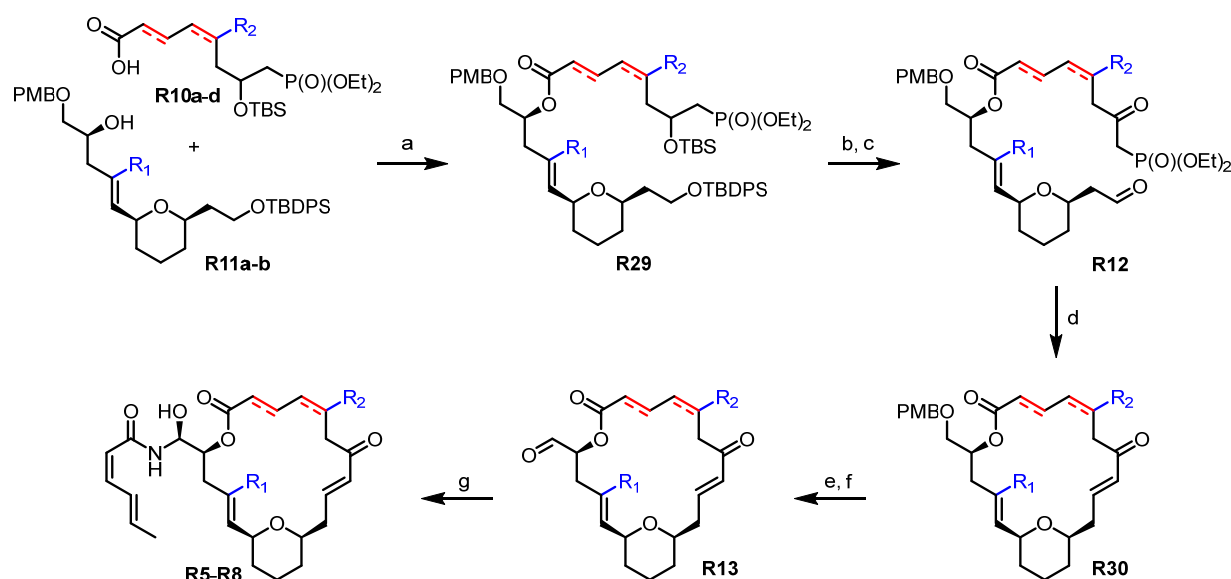
Somewhat surprisingly, and in contrast to our experience with the coupling of **R24** and 3-butynoic acid,^[68] the esterification step proved not to be straightforward and even under optimized conditions (dropwise addition of a solution of DCC/DMAP in CH_2Cl_2 to a solution of **R24** and 3-TMS-propionic acid in CH_2Cl_2 at $-20\text{ }^\circ\text{C}$) provided the desired ester **R25** only in 38% yield (on multigram-scale). As a major side product, the TMS-ether of **R24** was isolated in 29% yield, from which **R24** could be readily recovered by treatment with aqueous HCl. While the esterification of **R24** with propionic acid was slightly more efficient (44% yield), subsequent attempts at Prins cyclization with the terminal alkyne unprotected were unsuccessful. In contrast, treatment of **R25** with TMSI gave the 4-iodo tetrahydropyran **R26** in 88% yield as a single stereoisomer. Radical deiodination of **R26** with Bu_3SnH /AIBN followed by TMS-cleavage with K_2CO_3 /MeOH then provided alkyne **R27** in high overall yield (85% from **R26**).

In analogy to our previous synthesis of alcohol **R11a**,^[68] the projected elaboration of alkyne **R27** into **R11b** was to involve its conversion into a terminal vinyl iodide followed by iodine-lithium exchange and reaction of the ensuing vinyl lithium species with epoxide **R28**^[118] (**Scheme 17**). Unfortunately, hydrozirconation/iodination of **R27** gave the desired vinyl iodide only in poor yield and with low selectivity. Moreover, treatment of the mixture of vinyl iodides in toluene with

n-BuLi followed by addition of epoxide **R28** in the presence of $\text{BF}_3 \cdot \text{Et}_2\text{O}$ led to a complex mixture of products.

As an alternative to the use of a vinylmetal in the epoxide opening reaction, we then investigated the reaction of lithiated alkyne **R27** and epoxide **R28** in the presence of $\text{BF}_3 \cdot \text{Et}_2\text{O}$ in THF.^[119] In the event, the corresponding homopropargylic alcohol was obtained in excellent yield (83%). Hydroalumination of the latter with LAH after aqueous work-up delivered the desired *E* olefin as a single stereoisomer, albeit with concomitant loss of the TBDPS protecting group. However, the resulting diol could be selectively mono TBDPS-protected by reaction with TBDPSCl to give alcohol **R11b** in 50% overall yield from alkyne **R27**.

Elaboration of analogs R5-R8. As depicted in **Scheme 18**, the elaboration of acids **R10a-d** and alcohols **R11a-b** into analogs **R5-R8** followed the overall strategy outlined in **Scheme 14**. Thus, esterification of an acid **R10** with an alcohol **R11** under Yamaguchi conditions^[120] delivered an ester **R29** in yields between 74% and 88%. Global desilylation of **R29** with $\text{HF} \cdot \text{pyridine}$ (73% to 90%) followed by DMP oxidation^[116] of the resulting diols gave crude phosphono-aldehydes **R13** in excellent overall yields (86% to 98%).



Scheme 18: Final steps of the synthesis of (-)-zampanolide analogs **R5-R8**: a) 2,4,6-Trichlorobenzoyl chloride, NEt_3 , DMAP, toluene, rt, 74-88%; b) $\text{HF} \cdot \text{py}$, THF, 0 °C to rt, 73-90%; c) DMP, CH_2Cl_2 , rt, 86-98%; d) $\text{Ba}(\text{OH})_2$ THF/ H_2O (40:1), rt, 64-76%; e) DDQ, $\text{CH}_2\text{Cl}_2/\text{H}_2\text{O}$ (5:1), rt, 62-97%; f) DMP, CH_2Cl_2 , 67-95%; g) (*S*)-BINOL, LiAlH_4 , EtOH (*Z,E*)-sorbamide, THF, rt, 15-75 min, 24-71%. For the structures of analogs **R5-R8**, cf. **Figure 18**. For the structures of alcohols **R11a/b**, of acids **R10a-c**, and of acid **R10d**, cf. **Scheme 14**, **Scheme 15** and **Scheme 16**, respectively. Analog **R5** is derived from acid **R10a** and alcohol **R11b**, analogs **R6-R8** are all derived from alcohol **R11a** and acids **R10b**, **R10c** and **R10d**, respectively.

Gratifyingly, when treated with $\text{Ba}(\text{OH})_2 \cdot \text{H}_2\text{O}$ in wet THF^[35] all phosphono-aldehydes **R12** underwent efficient intramolecular *HWE* reaction, to form macrolactones **R30** in yields between 64% and 76%. PMB-cleavage with DDQ and subsequent DMP oxidation of the resulting free alcohols furnished (–)-dactylolide analogs **R13**.

With (–)-dactylolide analogs **R13** in hand, the stage was set for the diastereoselective aza-aldol reaction that would complete the hemiaminal linked side chain at C(19). Following a protocol that we have recently reported for the stereoselective addition of (*Z,E*)-sorbamide to dactylolide analogs,^[82] aldehydes **R13** were reacted with an *in situ* formed (*S*)-BINAL-sorbamide complex to deliver zampanolide analogs **R5-R8** in yields between 24% (**R8**) and 71% (**R6**) and dr's of >93:7 (at C(20)) after flash column chromatography and subsequent NP-HPLC purification. As an exception, analog **R8** was only purified by flash column chromatography, as decomposition was observed during attempted NP- or RP-HPLC purification; likewise, slow retro aza-*ene* reaction was detectable for **R8** in CDCl_3 solution. Analog **R7** was obtained as an inseparable 1.4:1 mixture of diastereoisomers at C(5).

For analog **R5**, the relative and absolute configuration of all stereocenters could be confirmed by X-ray crystallography (**Figure 19**);² notably, no other crystal structure of a zampanolide-type molecule has been reported in the literature so far. Most importantly, the structural data firmly establish that the asymmetric aza-aldol reaction between aldehydes **R13** and the amide transfer reagent derived from sorbamide and (*S*)-BINOL produces an (*S*)-configured C(20) stereocenter. It is also worth noting that the crystal structure of **R5** shows an *s-trans* conformation of the enone moiety, which is in line with previous findings by Taylor and co-workers on the conformational preferences of (–)-dactylolide (**R2**) in DMSO solution (with a *ca.* 70% fraction of *s-trans* conformers present in the conformational equilibrium).^[91,121] Interestingly, however, the reaction of zampanolide with His229 of β -tubulin must occur from an *s-cis* conformation, based on the configuration of the newly formed stereocenter in the adduct.^[61]

² Deposition Number 1499285 contains the supplementary crystallographic data for this paper (for **R5**). These data are provided free of charge by the joint Cambridge Crystallographic Data Centre and Fachinformationszentrum Karlsruhe [Access Structures](#) service.

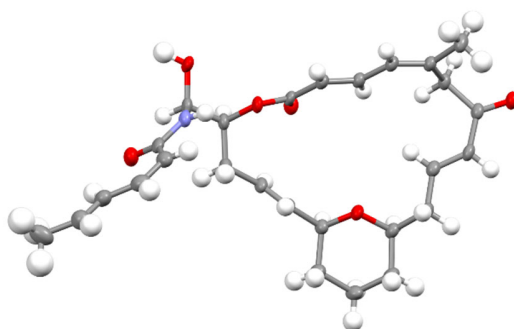
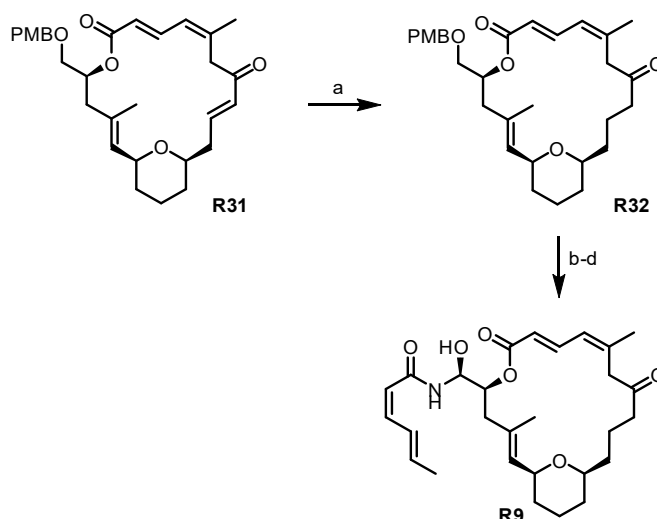


Figure 19: X-Ray crystal structure of 13-desmethylene-17-desmethyl-(-)-zampanolide (**R5**).

Analog **R9** was obtained from macrolactone **R31**, which we had previously prepared as part of our synthesis of 13-desmethylene-(-)-zampanolide (**R3**) (**Scheme 19**).^[82] Selective reduction of the enone double bond in **R31** with Stryker's reagent^[122] furnished macrocyclic ketone **R32** in 65% yield. The latter was then elaborated into analog **R9** by PMB-cleavage, DMP oxidation and aza-aldol reaction in 32% overall yield. Analog **R9** was obtained with a dr of 88:12.



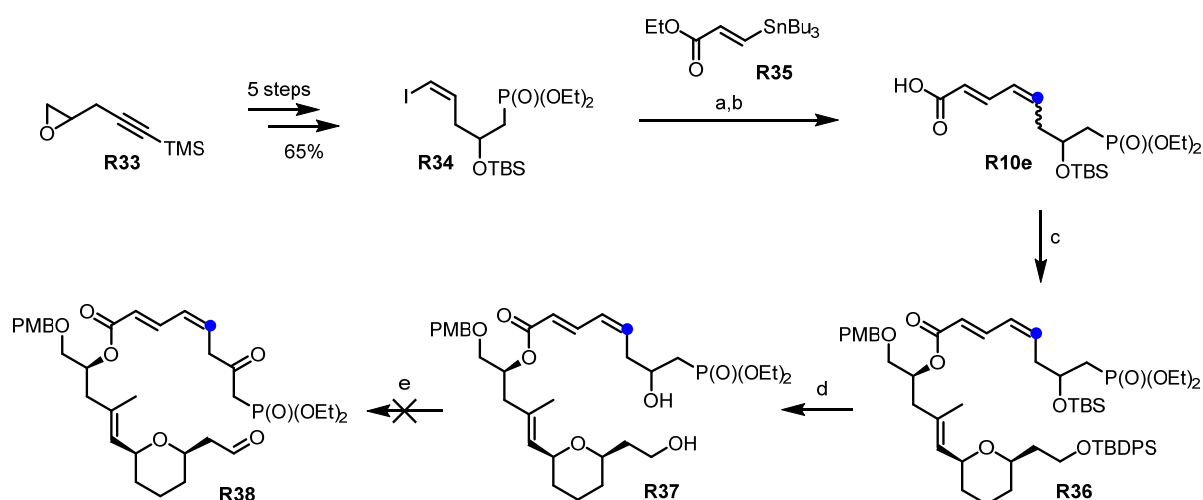
Scheme 19: Synthesis of analog **R9**: a) $(\text{PPh}_3\text{CuH})_6$, toluene, -40°C , 65%; b) DDQ, $\text{CH}_2\text{Cl}_2/\text{H}_2\text{O}$ (5:1), rt, 79%; c) DMP, CH_2Cl_2 , 74%; d) (*S*)-BINOL, LiAlH_4 , EtOH, (*Z,E*)-sorbamide, THF, rt, 15-75 min, 54%.

Studies towards the synthesis of analog **R4**: Synthesis of 5-desmethyl-13-desmethylene-(-)-dactylolide

Attempted macrocyclization by intramolecular HWE olefination. As for the synthesis of analogs **R5-R9**, our initial plan for the synthesis of analog **R4** was based on the general strategy outlined in **Scheme 14** and thus envisaged the assembly of the heavy atom framework of the macrocycle by the esterification of alcohol **R11a** with acid **R10e**. As depicted in **Scheme 20**, acid **R10e** was assembled by Stille coupling of ester **R35**^[123] and vinyl iodide **R34** as the key step. The latter could

be accessed from (racemic) epoxide **R33**^[124] in 5 steps, including $\text{BF}_3 \cdot \text{Et}_2\text{O}$ -mediated epoxide opening with lithium diethylphosphite in THF at -78°C , TBS-protection of the ensuing free hydroxy group, TMS-removal with K_2CO_3 in methanol, reaction of the terminal triple bond with NIS in the presence of catalytic AgNO_3 in acetone, to produce an iodoalkyne, and, finally, treatment of the latter with 2-nitrobenzenesulfonylhydrazide and Et_3N (as an *in situ* source of diimide^[125]); **R34** was obtained in excellent overall yield (65%), although it was contaminated with *ca.* 20% of the corresponding alkyl iodide, resulting from over-reduction of the precursor iodoalkyne. Stille coupling of this material with **R35** produced the corresponding *E/Z*-enoate in 70% yield, with the alkyl iodide contaminant being readily separable at this stage by flash chromatography. Saponification of the coupling product with aqueous sodium hydroxide in ethanol then gave the desired carboxylic acid **R10e** in 68% yield, on a 300 mg scale. Surprisingly, when the reaction was repeated on a 1 g scale under ostensibly identical conditions, extensive isomerization of the C(4)-C(5) double bond was observed, leading to a *ca.* 1:1 mixture of **R10e** and its *E/E* isomer. The reasons for this discrepancy are unclear and no efforts were made to finetune the reaction conditions such as to prevent isomerization also on a larger scale.

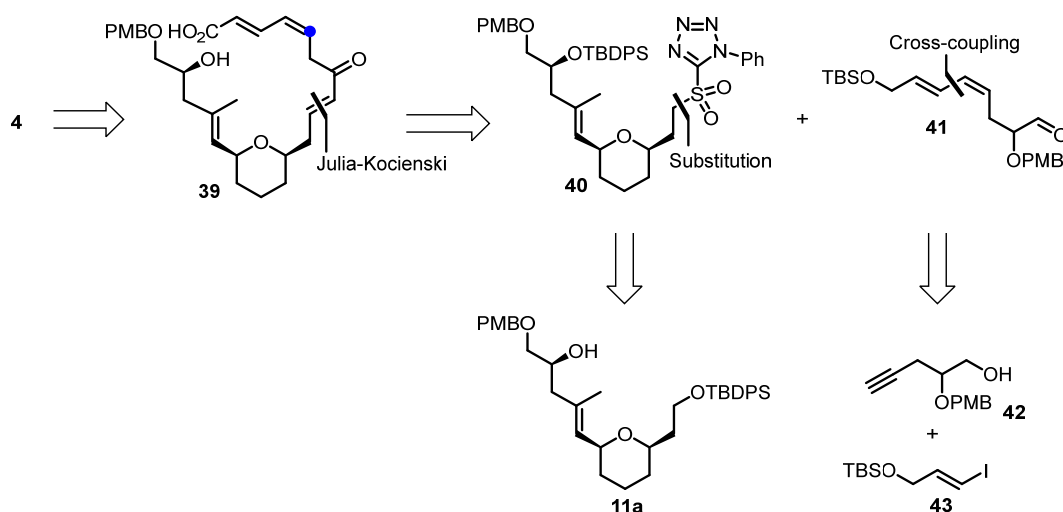
As for the previous analogs described, the esterification of **R10e** with alcohol **R11a** was performed under Yamaguchi conditions,^[120] which furnished ester **R36** in 69% yield. When the esterification was performed with a mixture of **R10e** and its *E/E*-isomer a mixture of the corresponding esters was obtained in 68% total yield without noticeable change in isomer ratio. Gratifyingly, the desired ester **R36** was separable from its *E/E* isomer at this stage by column chromatography.



Scheme 20: a) **R35**, Pd_2dba_3 , DIPEA, NMP, rt, dark, 70%; b) NaOH, EtOH, rt, 76% (up to 50% isomerization of the *Z*-double bond); c) 2,4,6-Trichlorobenzoyl chloride, Et_3N , toluene, DMAP, rt, 68%; d) $\text{HF} \cdot \text{py}$, py, THF, rt, 98%; e) DMP, CH_2Cl_2 , rt, decomposition.

Ester **R36** was then submitted to global desilylation with pyridine-buffered HF•pyridine in THF to yield diol **R37** in 98% yield. However, while oxidation of this diol with DMP did occur (as indicated by in-process reaction monitoring with TLC-MS and NMR), the desired keto aldehyde could not be isolated after work-up. More specifically, the organic layer turned dark red during work-up and no product-related signals could be detected in the ¹H-NMR spectrum of the crude material recovered from the organic phase. In order to avoid problems that might be related to aqueous work-up conditions, activated Ba(OH)₂ in wet THF was added directly to the reaction mixture after completion of the DMP oxidation. Unfortunately, immediate decomposition was observed and none of the desired macrocycle could be isolated.

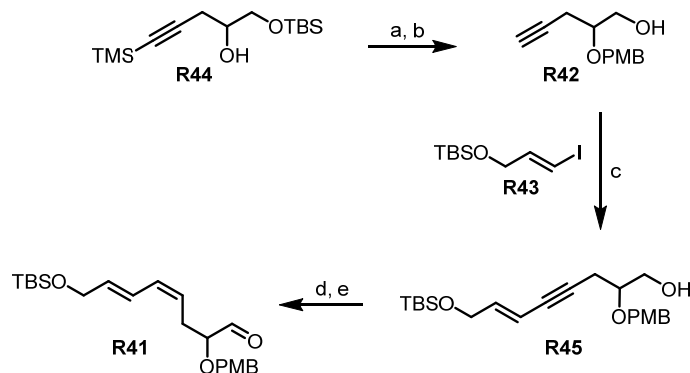
Macrolactonization approach. In light of the difficulties encountered with the *HWE*-based macrocyclization approach towards 13-desmethylene-5-desmethyl(-)-zampanolide (**R4**), we started to explore an alternative overall strategy that would involve macrocyclic ring-closure by macrolactonization rather than double bond formation between C(8) and C(9) (**Scheme 21**). The requisite *seco* acid **R39** was envisioned to be prepared by means of *Julia-Kocienski* olefination^[126] from aldehyde **R41** and sulfone **R40**.



Scheme 21: Macrolactonization-based retrosynthesis of zampanolide analog **R4**.

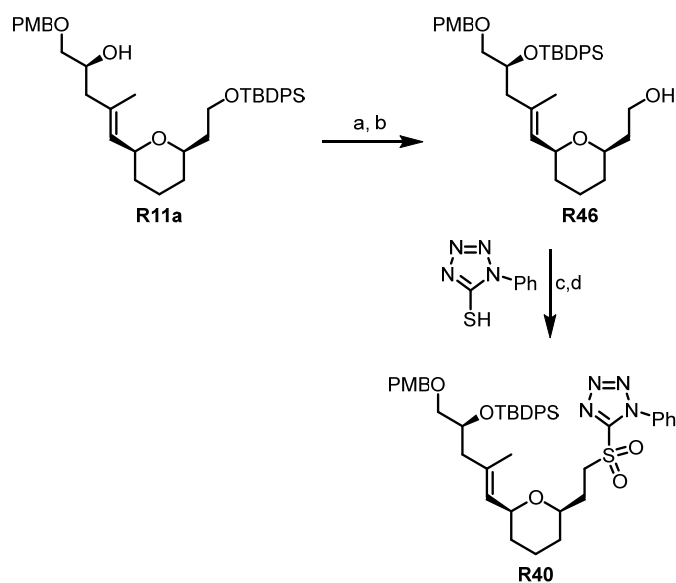
Aldehyde **R41** was projected to be obtained by Sonogashira cross-coupling^[127] of **R42** and **R43** followed by semireduction of the triple bond. Sulfone **R40** would be obtained from alcohol **R11a** following previous work by Smith and co-workers.^[81] In the forward direction, the elaboration of aldehyde **R41** made use of homopropargylic alcohol **R44**,^[128] which was transformed into **R42** by PMB-protection and subsequent desilylation with TBAF•3H₂O in THF in 74% overall yield (**Scheme 22**).

Sonogashira coupling^[127] of **R42** with vinyl iodide **R43**^[129] efficiently delivered enyne **R45** (98% yield). The alkyne moiety was then selectively reduced to the *Z* double bond with freshly prepared Zn/Cu/Ag composite that was activated with TMSCl.^[130] To obtain full conversion, the reaction had to be heated to 55 °C for three days, thus furnishing the corresponding diene in 84% yield.



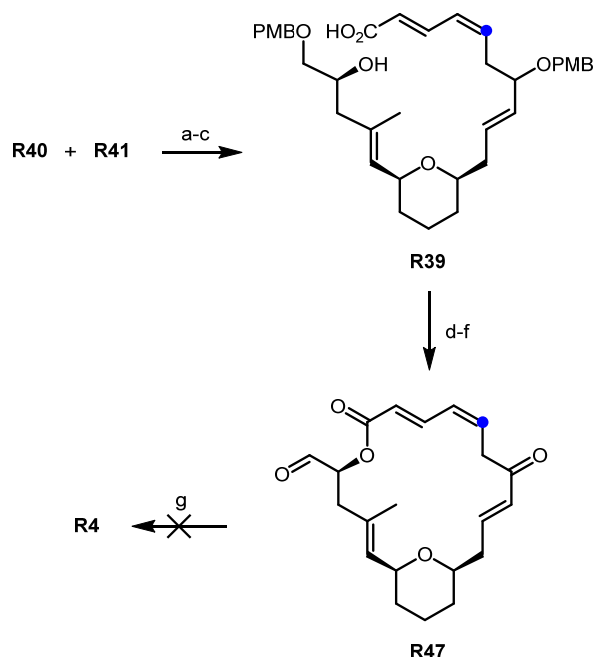
Scheme 22: Synthesis of aldehyde **R41**: a) PMB-trichloroacetimidate, TfOH (2.0 mol%), Et₂O, rt, 93%; b) TBAF•3H₂O, THF, rt, 80%; c) **R43**, Pd(PPh₃)₄, CuI, Et₃N, MeCN, 45 °C, 98%; d) Zn/Cu/Ag, TMSCl, MeOH, THF, H₂O, 55 °C, 3 d, 84%; e) DMP, NaHCO₃, CH₂Cl₂, rt 69%.

Finally, the ensuing diene was oxidized under buffered Dess-Martin conditions to give aldehyde **R41**, which proved to be rather unstable. The conversion of alcohol **R11a** into sulfone **R40** in a first step involved TBDPS-protection of the free secondary hydroxy group, followed by selective cleavage of the primary TBDPS-ether with TBAF/AcOH, to furnish **R46** in 52% overall yield (**Scheme 23**). Treatment of **R46** with 1-phenyl-1*H*-tetrazol-5-thiol under Mitsunobu conditions^[131] then furnished a thioether that was oxidized to the corresponding sulfone **R40** with hydrogen peroxide in the presence of catalytic amounts of (NH₄)₆Mo₇O₂₄•4H₂O in ethanol.^[81] Sulfone **R40** was obtained in 80% overall yield from alcohol **R46**.



Scheme 23: a) Synthesis of sulfone **R40**: TBDPSCl, imidazole, CH_2Cl_2 , rt, 91%; b) TBAF/AcOH, THF, 57%; c) 1-Phenyl-1H-tetrazol-5-thiol, PPh_3 , DEAD, THF, 0 °C, 92%; d) H_2O_2 (aq.), $(\text{NH}_4)_6\text{Mo}_7\text{O}_{24} \cdot 4 \text{H}_2\text{O}$ (10 mol%), EtOH, rt, 88%.

The *Julia-Kocienski* olefination of **R40** and aldehyde **R41** proceeded smoothly and delivered the desired olefin in 82% yield as a single isomer (**Scheme 24**). Double desilylation with $\text{HF} \cdot \text{pyridine}$ then gave the corresponding free diol in 64% yield; selective oxidation of the allylic hydroxy group with MnO_2 followed by immediate Pinnick oxidation of the ensuing aldehyde subsequently furnished acid **R39**. To avoid isomerization of the *E,Z*-dienal, a Pinnick-Lindgren oxidation was employed that used resorcinol as a scavenger.^[132] While the reaction was slow and took up to five days to reach >90% conversion, no isomerization of the *Z*-double bond occurred under the modified Pinnick conditions and *seco* acid **R39** was isolated in 74% overall yield (based on the preceding diol). Gratifyingly, treatment of *seco* acid **R39** with 2,4,6-trichlorobenzoic acid, Et_3N and DMAP^[120] led to smooth macrolactonization (69% yield); simultaneous cleavage of the two PMB-ether groups with DDQ followed by DMP oxidation of the resulting diol then furnished 5-desmethyl-13-desmethylene-(–)-dactylolide (**R47**) in 39% overall yield from **R39**. Unfortunately, all attempts to convert **R47** into 13-desmethylene-5-desmethyl-(–)-zampanolide (**R4**) by applying our stereoselective aza-aldol reaction protocol^[82] proved to be futile. Only decomposition of the starting material **R47** was observed.



Scheme 24: Final steps in the synthesis of 13-desmethylene-5-desmethyl(-)-dactylolide (**R47**): a) **R40**, KHMDS; THF, $-78\text{ }^{\circ}\text{C}$, then aldehyde **R41**, 82%; b) $\text{HF}\cdot\text{py}$, THF, rt, 64%; c) MnO_2 , CH_2Cl_2 , rt, then NaClO_2 , resorcinol, *t*-BuOH, acetate buffer pH 4.0, 5 d, 74%; d) 2,4,6-Trichlorobenzoyl chloride, Et_3N , THF, rt, DMAP, Et_3N , toluene, 69%; e) DDQ, CH_2Cl_2 /buffer (5:1), pH 7.2, rt, 65%; f) DMP, NaHCO_3 , CH_2Cl_2 , rt, 87%; g) (*S*)-BINOL, LiAlH_4 , EtOH, (*Z,E*)-sorbamide, THF, rt, decomposition.

Cellular effects of zampanolide analogs R5-R9. As touched upon in the introduction, we have shown previously that 13-desmethylene(-)-zampanolide (**R3**) was an equally potent growth inhibitor of A549, A2780 and A2780 AD cells as natural (-)-zampanolide (**1**).^[82] In this study we have now extended the profiling of **R3** to five additional cancer cell lines (HL-60, 1A9, MCF-7, PC-3, and HT29; **Table 2**) and the data obtained have re-confirmed that **R3** is a highly potent inhibitor of cancer cell proliferation *in vitro*; in all cases investigated so far, the activity of **R3** was at least comparable with that of natural (-)-zampanolide (**R1**). These results are in agreement with and extend previous findings on 13-desmethylene(-)-dactylolide (**R3**)^[68] and they clearly indicate that the C(13)-exomethylene group is not essential for the biological activity of zampanolide-type structures.

Of the different analogs of **R3**, the two dihydro derivatives **R6** and **R9** showed dramatically different activities (**Table 2**). While 8,9-dihydro analog **R9** was consistently several hundred-fold less potent than **R3**, the 2,3-dihydro derivative **R6** retained at least double-digit nanomolar potency against all 6 cell lines investigated here. For 4 of these cell lines (A2780, A2780 AD, HL-60, 1A9), the IC_{50} 's for analog **R6** were no more than 3-fold higher than for the parent compound **R3**; a slightly more pronounced decrease in potency (6-fold) was observed against HT29 cells, while A549 cells were 44-fold less sensitive to **R6** than **R3**.

The potency loss incurred by **R9** is not too surprising, as the compound lacks the reactive enone system that is responsible for the covalent interaction of (–)-zampanolide (**R1**) with tubulin; but the data provide additional experimental confirmation that the covalent nature of the interaction of **R1** (and **R3**, for that matter) with the protein is truly essential for high cellular potency. This conclusion has also been reached independently by *Taufa et al.* based on the activity of the recently isolated zampanolide E (8,9-dihydro-(–)-zampanolide) against HL-60 cells.^[15] Based on the cell cycle and microtubule bundling data discussed below, the residual activity of **R9** and zampanolide E is most likely due to non-covalent binding to tubulin; but we cannot completely exclude the involvement of other cellular targets.

The high potency of **R6** is intriguing, as the formal reduction of the double bond would be expected to increase the flexibility of the structure and, thus, enhance the entropic cost of target binding. However, we have previously found for other bioactive macrocycles (3-deoxy-2,3-didehydro-epothilone A,^[133] rhizoxin F (M. Liniger, C. Neuhaus, K.-H. Altmann, unpublished data) that the formal reduction of *E* double bonds was associated only with a moderate loss in cellular potency.

Removing both the C(2)-C(3) and the C(4)-C(5) double bond simultaneously, led to a further 3-12-fold decrease in potency for analog **R7** (compared to **R6**); interestingly, no further drop in activity was observed upon removal of the C(5) methyl group from **R7** (i. e. for analog **R8**). While analogs **R7** and **R8** thus appear to be one to two orders of magnitude less potent than **R3**, both compounds still exhibit profound antiproliferative activity. Given the removal of the two C-C double bonds from the dienoate system in the northern part of the structure of **R3**, this finding is quite remarkable. It should also be noted that analog **R7** represents a 1.4:1 mixture of diastereoisomers at C(5); if one of these isomers were substantially more potent than the other, the IC₅₀ values of the former could be up to 2.4-fold lower than those for the mixture.

The removal of the C(17) methyl group (analog **R5**) was associated with a 6-26-fold potency loss vs. **R3** (**Table 2**). The compound, thus, is somewhat less potent than **R6**, but it still exhibits high antiproliferative activity. For reasons that cannot be discerned, the IC₅₀ values obtained here for **R5** against A549 and 1A9 cells are lower than those reported by Taylor and co-workers, even if one takes into account that Taylor's study was performed with a 1.5:1 epimeric mixture at C(20). Finally, for all analogs, similar activity was observed against the ovarian cancer cell line A2780 and its Pgp-overexpressing, multidrug-resistant A2780 AD variant.^[83,84] Similar findings have been made previously for natural (–)-zampanolide (**R1**)^[60] and for **R3**.^[82] The ability of zampanolide-type structures to overcome Pgp-mediated multidrug-resistance may be a direct consequence of their covalent mode of action, which leads to irreversible intracellular retention.

If, in addition, they may also be intrinsically poor substrates for the Pgp-efflux pump has not been determined.

As discussed above, C(5)-desmethyl-C(13)-desmethylene(-)-zampanolide (**R4**) was not accessible through either of the two strategies investigated. However, experiments with C(5)-desmethyl-C(13)-desmethylene(-)-dactylolide (**R47**) on 1A9 and HT29 cells revealed a *ca.* 10-fold and 30-fold loss in potency, respectively, relative to (-)-dactylolide (**R2**) (IC₅₀'s 1A9 cells: **R47**, 8.34 ± 0.95 βM; **R2**, 0.82 ± 0.14 βM. IC₅₀s HT29 cells: **R47**, 10.56 ± 0.28 βM; **R2**, 0.359 βM ± 0.083 βM). These potency differences are comparable with those observed between **R5** and **R3**, which may suggest that the activities of **R5** and the elusive **R4** may be similar. However, this conclusion has to be considered tentative, as it is not clear if the same macrocycle modification in (-)-dactylolide (**R2**) and (-)-zampanolide (**1**) leads to the same relative change in potency.

Table 2. Antiproliferative activity of (-)-zampanolide (**R1**) and zampanolide analogs **R3**, and **R5-R9** against human cancer cell lines (IC₅₀ [nM]).^[a]

| Cpd | A549 (lung) | A2780 (ovarian) | A2780 AD ^[b] (ovarian) | HL-60 (leukemia) | 1A9 (ovarian) | HT29 (colon) | MCF-7 ^[c] (breast) | PC3 ^[c] (prostate) |
|-----------|-------------------------|-------------------------|--------------------------------------|---------------------|------------------|-----------------|----------------------------------|----------------------------------|
| R1 | 3.2 ± 0.4 ³⁵ | 1.9 ± 0.2 ³⁰ | 2.2 ± 0.3 ³⁰ | 4.1 ± 0.5 | 15 ± 8 | 1.87 ± 0.38 | n.d. | n.d. |
| R3 | 1.0 ± 0.2 | 1.7 ± 0.4 | 3.53 ± 1.97 | 2.5 ± 0.6 | 12 ± 5 | 1.24 ± 0.20 | < 1.5 | < 1.5 |
| R5 | 15 ± 5 | 13 ± 1 | 20 ± 4 | 26 ± 6 | 90 ± 23 | 32.9 ± 2.56 | n.d. | n.d. |
| R6 | 44 ± 10 | 5.2 ± 0.6 | 12 ± 3 | 5.9 ± 1 | 16 ± 5 | 10.85 ± 0.49 | n.d. | n.d. |
| R7 | 133 ± 6 | 65 ± 21 | 72 ± 28 | n.d. | n.d. | n.d. | n.d. | n.d. |
| R8 | 120 ± 8 | 110 ± 21 | 94 ± 4 | n.d. | n.d. | n.d. | n.d. | n.d. |
| R9 | 1056 ± 50 | 820 ± 20 | 1860 ± 890 | 2910 ± 34 | 9386 ± 2435 | 684 ± 77 | n.d. | n.d. |

^[a]Cells were exposed to compounds for 48 h (A549, A2780, A2780AD, HL60) or 72 h (1A9, HT29, MCF-7, PC3); n.d. = not determined. ^[b]Multidrug-resistant cell line overexpressing the Pgp efflux pump.^[83,84] ^[c]These experiments were conducted at ProQuinase GmbH, Freiburg, Germany.

The antiproliferative activity of zampanolide analogs is reflective of their effects on the cellular microtubule network and on cell cycle progression. As shown in **Figure 20**, 13-desmethylene(-)-zampanolide (**R3**) at a concentration of 25 nM induced microtubule bundling in interphase cells similar to what was observed with 200 nM taxol and what had been reported for (-)-zampanolide (**R1**). Likewise, microtubule bundling was also observed with analogs **R5** and **R6** at similar concentrations (see experimental section 4.2.1.4.2 **Figure 49**).

In comparison, and as expected from its significantly lower growth inhibitory activity, 13-desmethylene-8,9-dihydro(-)-zampanolide (**R9**) led to microtubule bundling only at substantially higher concentrations (5 μM) (**Figure 20**). Nevertheless, this finding indicates that

the antiproliferative effects of **R9** are still mediated through interaction with the tubulin/microtubule system (at least partly). Notably, the effects of short term exposure (6 h) of A549 cells to 5 μM of **R9** were fully reversible, as was also the case for taxol; in contrast, no reversibility was observed with **R3**, **R5**, or **R6**, all of which incorporate the reactive enone system that enables covalent attachment to β -tubulin.

In line with their effects on the microtubule cytoskeleton, the treatment of A549 cells with analogs **R3**, **R5**, or **R6** led to cell cycle arrest in the G2/M phase at low nanomolar concentrations (**Figure 21**), as has also been demonstrated for (-)-zampanolide (**R1**).^[21] Mitotic arrest was also observed with analog **R9**, but only at much higher compound concentrations (25 μM) (**Figure 21**).

Binding to microtubules and promotion of tubulin polymerization. In order to gain some basic understanding of the effects of the various modifications of **R3** on the interaction of the corresponding zampanolide analogs with tubulin, we have investigated their ability to displace the fluorescent taxol analog Flutax-2 from preformed cross-linked microtubules.^[134]

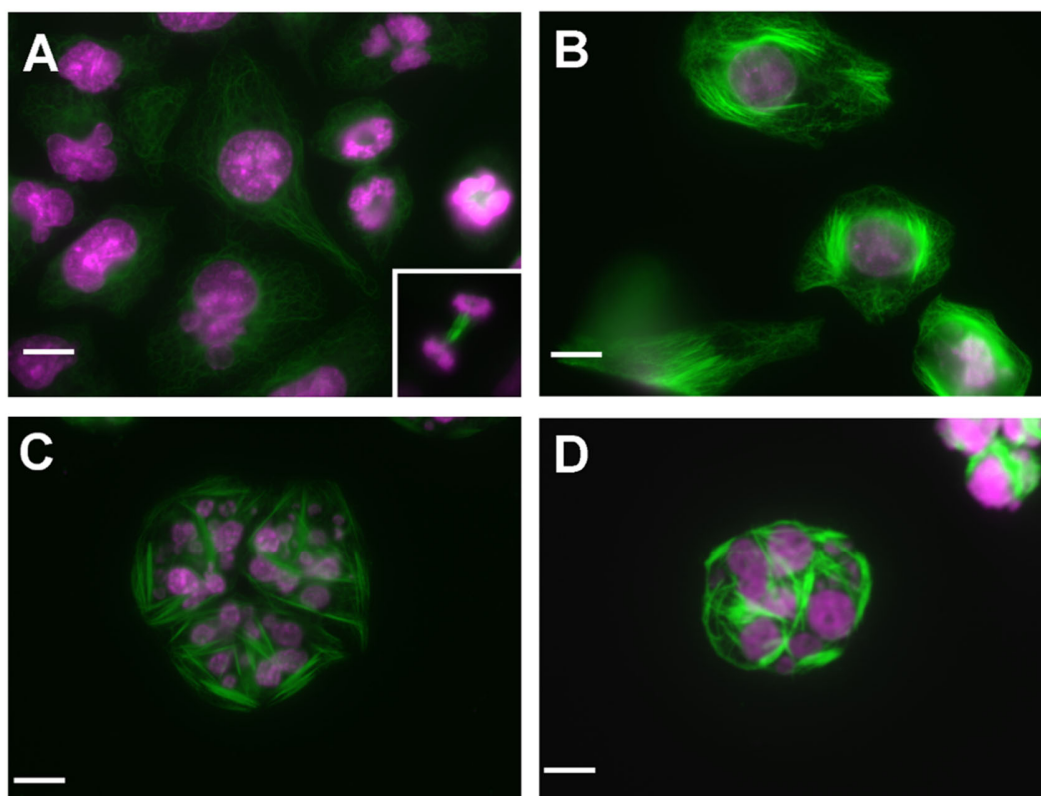


Figure 20: Microtubule bundling in A549 cells induced by 13-desmethylene-(-)-zampanolide (**R3**) and its 8,9-dihydro derivative (**R9**). Microtubule (green) and DNA (pink) staining of A549 lung carcinoma cells. Cells were treated with DMSO (negative control) (A); taxol (200 nM, positive control) (B); **R3** (25 nM) (C); or 5 μM of **R9** (D). Microtubules

were immunostained with an α -tubulin monoclonal antibody; DNA was stained with Hoechst 33342. Scale bar = 10 μm .

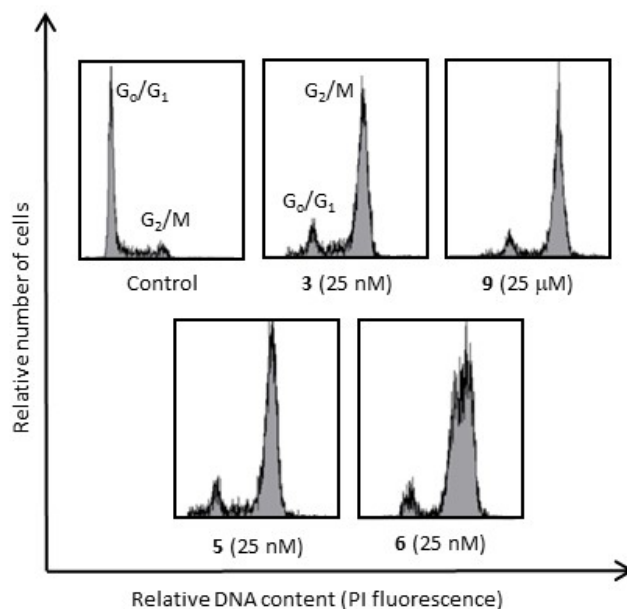


Figure 21: Cell cycle histograms of A549 lung carcinoma cells treated with compounds **R3**, **R5**, **R6**, or **R9**. Shown are the lowest ligand concentrations that induce maximal arrest in the G2/M phase.

For non-covalent microtubule binders, the concentration-dependent displacement of Flutax-2 (at a fixed concentration) allows to determine thermodynamic binding constants (K_b); conducting these experiments with a covalent microtubule ligand (which is formally treated like a reversible ligand) only gives what we refer to as apparent binding constants (K_{bapp}). These apparent binding constants do not reflect an equilibrium binding situation, as they depend on both the intrinsic binding affinity of the ligand for tubulin *and* the rate of the subsequent reaction of the ligand with the protein. Thus, K_{bapp} values are less informative than true binding constants K_b and they cannot be directly compared to each other or to true K_b values. However, if one assumes that the tubulin-bound conformation of all zampanolide analogs investigated here is similar and that this leads to a similar rate constant for the conversion of the initial non-covalent complex into the covalent adduct, then the differences in K_{bapp} between different zampanolide analogs provide at least an approximate measure for the differences in intrinsic binding affinity. Independent of these assumptions, K_{bapp} values provide a measure for the efficiency of the overall reaction of zampanolide analogs with polymerized tubulin.

The K_{bapp} values for zampanolide analogs **R3**, **R5**, **R6**, **R7**, and **R8** are summarized in **Table 3**; for analog **R9** the value is a true thermodynamic binding constant. It is immediately obvious that

analogs **R5-R8** are all less efficient than 13-desmethylene-(–)-zampanolide (**R3**) in displacing Flutax-2 from stabilized microtubules. In comparison to **R3**, the smallest difference in K_{bapp} values (ca. 3.6-fold) was observed for 13-desmethylene-2,3-dihydro-(–)-zampanolide (**R6**), for all other analogs K_{bapp} was more than 10-fold reduced. The data indicate that all modifications to **R3** compromise the microtubule-binding affinity of the corresponding analogs to some extent.

Table 3: Apparent microtubule binding constants K_{bapp} of (–)-zampanolide (**R1**) and analogs **R3** and **R5-R9** for microtubules at 35 °C.

| Cpd | K_{bapp} [$10^6 M^{-1}$] ^[a] |
|-------------------------|---|
| 1 ^[b] | 214 ± 9.3 |
| 3 | 24 ± 2 |
| 5 | 1.9 ± 0.4 |
| 6 | 7 ± 2 |
| 7 | 0.47 ± 0.07 |
| 8 | 2.29 ± 0.2 |
| 9 | 0.061 ± 0.001 |

^[a]Determined by the displacement of the fluorescent taxoid Flutax-2 from stabilized microtubules.^[134] ^[b]Data are from ref.[60].

Conclusions

C(13)-Desmethylene-(–)-zampanolide (**R3**) is an equipotent, synthetic congener of the marine microtubule stabilizer (–)-zampanolide (**R1**). In this study, we have investigated the importance of individual double bonds and of the C(17) methyl group in **R3** (and, by inference, in **R1**) for its antiproliferative activity and interactions with microtubules. To this end, we have prepared five analogs of **R3/R1**, including the known C(13)-desmethylene-C(17)-desmethyl-(–)-zampanolide (**R5**),^[91] based on a global strategy that we had previously elaborated for the total synthesis of **R1** and **R3**. The successful and efficient preparation of these analogs attests to the robustness of our synthetic approach; in particular, the intramolecular *HWE* reaction of phosphono aldehydes **R12**, which has also been adopted by others,^[85–88,91] in all cases provided the desired macrocycles in good yields. In addition, the C(20) stereocenter could be established with high selectivity, employing a putative (*S*)-BINOL-based amide transfer reagent that we have recently developed. As the only exception, 5-desmethyl-(–)-dactyloolide (**R47**) could not be converted into the corresponding zampanolide analog **R4**, which has remained elusive in this study. Likewise, a macrolactonization-based approach had to be developed to access **R47**, as the ω -oxo β -keto

phosphonate **R 38** as the requisite precursor for an *HWE*-based macrocyclization could not be obtained in this case by oxidation of the corresponding diol **R37**.

C(13)-Desmethylene-(–)-zampanolide (**R3**) proved to be an equally potent inhibitor of cancer cell growth as (–)-zampanolide (**R1**) across a panel of 6 tumor cell lines. All structural modifications of **R3** investigated here led to a decrease in cellular potency, albeit to a different extent. Overall, the best tolerated modification was the formal reduction of the C(2)-C(3) double bond; with the exception of one cell line, the corresponding analog **R6** was no more than 6-fold less active than **R3**. A more pronounced, but still moderate loss in potency was caused by the removal of the C(17)-methyl group.

All synthetic zampanolides, including 13-desmethylene-(–)-zampanolide (**R3**) were less efficient in displacing the fluorescent taxoid Flutax-2 from the taxol binding site on stabilized microtubules, as judged by their apparent binding constants K_{bapp} . The interpretation of the displacement data is not straightforward, as the derived K_{bapp} values are not equilibrium binding constants. However, they seem to suggest that all modifications, including the removal of the C(13) methylene group, reduce the stability of the initial, non-covalent ligand-tubulin complex relative to natural (–)-zampanolide (**R1**). This conclusion is in line with the fact that both the C(13)-methylene or the C(17)-methyl group are located in hydrophobic pockets in the protein.^{3[61]} In addition, as has been elegantly demonstrated by Taylor and co-workers by means of computational and solution NMR studies on C(17)-desmethyl-(–)-dactyloolide, the removal of the C(17)-methyl group leads to greater conformational flexibility in the C(14)-C(19) segment of the macrocycle,^[91] which may additionally compromise microtubule-binding affinity. Enhanced conformational flexibility may also explain the reduced binding affinity of analogs **R6- R8**, although for **R6** the decrease in K_{bapp} vs. **R3** is rather moderate. This assumption is supported by the results of macrocycle conformational sampling using the Schrödinger OPLS4 force field and subsequent clustering of 3000 to 5000 conformations for each analog based on macrocycle atoms.⁴ According to these computations, all analogs of **R3** generally exhibit greater conformational flexibility than **R1** in the regions surrounding the modifications, but not in other parts of the structure. For analog **R5**, these observations are nicely aligned with the results of Taylor's work.^[91] Conformational flexibility was found to be most pronounced for analog **R9**, while the sampled conformational space is virtually identical for **R1** and **R3**.

³ In spite of its location in a hydrophobic pocket, we had previously assumed that the C(13) methylene group of **R1** was not involved in major interactions with the protein.^[90] In light of the binding data for **R3** this view may need to be revised.

⁴ The computational work was carried out by Dr. Bernhard Pfeiffer and is described in the Supporting Information of ref. [93].

In spite of its 10-fold lower K_{bapp} , compared to **R1**, C(13)-desmethylene-(–)-zampanolide (**R3**) is equipotent with **R1** on cells; likewise, analogs **R5** and **R6** exhibit high cellular potency. We believe that the correlation between apparent binding constants and cellular activity is blurred by the irreversible binding of analogs **R5- R8** to microtubules, as compounds with only moderately reduced K_{bapp} may achieve levels of tubulin labelling approaching those of **R1** within the timeframe of the cellular experiments. More detailed studies will be necessary to consolidate (or refute) this hypothesis (see, however, ref. [59]).

Finally, it needs to be noted that *Johnson, Risinger* and co-workers have recently reported the first *in vivo* data with (–)-zampanolide (**R1**) in tumor-bearing mice.^[59] In this study, **R1** was found to exhibit profound antitumor activity when administered intratumorally; however, even a single i.p. dose of 1 mg/kg proved to be highly toxic without showing any antitumor activity. The absence of a systemic therapeutic window for **R1** is disappointing. However, given the unique mechanism of action of zampanolide-type structures and their activity against MDR tumor cells still makes the continued evaluation of analogs of **R1** a worthwhile undertaking. In this context, the *in vivo* evaluation of some of the analogs described in this study would help to understand if structurally modified and somewhat less potent analogs of **R1** could offer an acceptable therapeutic window.

2.2.2 Synthesis and Structure-Activity Relationship Studies of Dioxane- and Oxathiane-Based Analogs of (–)-Zampanolide (Publication 2)

Based on:

E. Cotter, S. Glauser, A. Lelke, P. Scapozza, S. Berardozi, D. Lucena-Agell, R. Hortigüela, M. A. Oliva, J. Fernando Díaz, K.-H. Altmann, *ChemRxiv*, **2024**, DOI 10.26434/CHEMRXIV-2024-NWB48.^[135]

E. Cotter's contributions: conceptualization with S. Glauser, S. Berardozi and K.-H. Altmann, synthetic investigations (analogs **O5-8**) with S. Glauser (analog **O4**), A. Lelke (analogs **O4, O5** and **O6**) and P. Scapozza (analog **O4**); supervision of A. Lelke and P. Scapozza (analogs **O4-O6**) with S. Berardozi; biochemical investigations (analogs **O5-O8**) with D. Lucena-Agell and R. Hortigüela; publication writing with K.-H. Altmann and M. A. Oliva.

Introduction

(–)-Zampanolide (**O1**) (**Figure 22**) is a marine macrolide that was first isolated in 1996 by *Tanaka* and *Higa* from the marine sponge *Fasciospongia rimosa* collected at cape Zampa off the coast of Okinawa, Japan.^[14] It features a bicyclic core structure including a 20-membered macrolactone ring, which carries an unusually stable linear *N*-acyl hemiaminal-containing side chain.^[14] (–)-Zampanolide (**O1**) is a potent microtubule-stabilizing agent (MSA) and it inhibits the growth of human cancer cells with IC₅₀ values in the low nanomolar range (2-10 nM).^[21] The antiproliferative effect of **O1** is thus based on the same mechanism of action that characterizes the clinical cancer drugs taxol, docetaxel, cabazitaxel, or ixabepilone.^[46] However, in contrast to the latter, **O1** binds to β -tubulin covalently; attachment to the protein involves 1,4-addition of the β -His229 side chain to C(9) of the enone moiety in the macrocycle.^[60,61] The relative and absolute configuration of **O1** was established in early synthetic work by *Smith* and co-workers on (+)-zampanolide (*ent*-**O1**) in 2001,^[81] which over the years was followed by several total syntheses of the natural product **O1**.^[22,113,114] Synthetic work has also been expended on a variety of analogs of **O1** in the context of structure-activity relationship (SAR) studies. This has included investigations of modifications of the C(19)-side chain,^[68,74,81] the tetrahydropyran ring,^[68,82,85,87,89,90,136] and, most recently, the macrolide backbone.^[93,137]

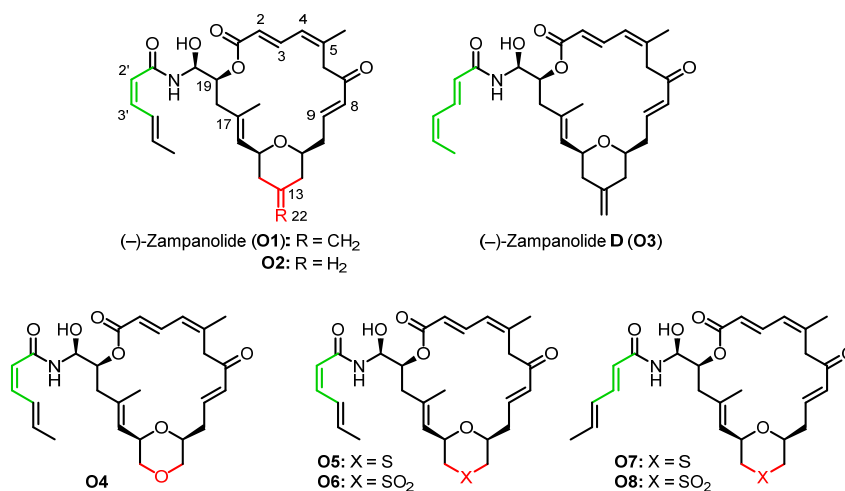


Figure 22: Structures of (-)-zampanolide (**O1**) and of (-)-zampanolide analogs **O4-O8**.

As part of these studies, work in our own laboratory has revealed that 13-desmethylene(-)-zampanolide (**O2**) (**Figure 22**) inhibits human cancer cell growth with the same potency as **O1**. Based on this finding, we embarked on a program directed at the replacement of the tetrahydropyran (THP) ring by alternative heterocycles containing additional heteroatoms, which we hoped would lead to improved solubility. At the same time, such additional heteroatoms offer the potential for new hydrogen bonding with the protein. In an initial step, the implementation of this program involved the synthesis of morpholine-based analogs of **O1/O2**; unfortunately, while we were able to prepare a number of *N*-substituted morpholino-zampanolides, all efforts towards the corresponding unsubstituted parent compound proved futile. In this work, we have expanded our SAR investigations to substitution of the C(13) in **O2** with oxygen or sulfur, either at the sulfide or the sulfone oxidations state (**Figure 22**). In this context, it is interesting to note that only few natural products are known that incorporate an oxathiane moiety,^[138–140] thus making the corresponding zampanolide analogs **O4-O8** rather unique structurally.

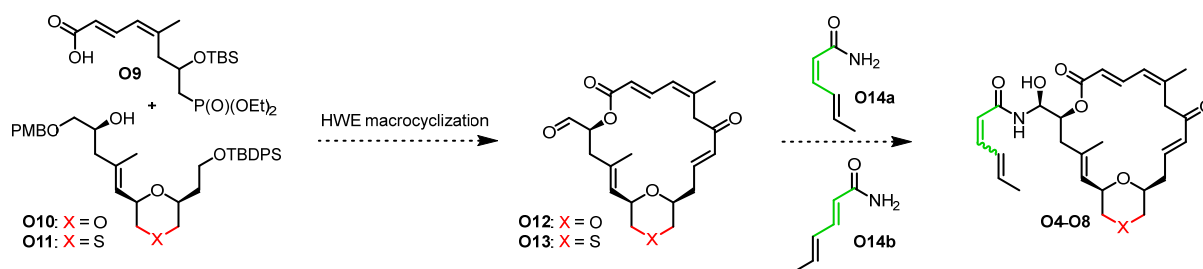
As will be shown below, the replacement of C(13) in **2** by O or S is very well tolerated. Building on these findings and with sufficient amounts of the requisite precursor aldehyde in hand, we have used the oxathiane-based scaffold to prepare analogs **O6** and **O7**, whose side chains incorporate an *E,E*-configured sorbamide moiety. This line of investigation was triggered by the recent discovery of zampanolide D (**O3**); in contrast to all other natural zampanolides, **O3** features an *E,E*-configured side chain (as opposed to the usual *Z,E* configuration). Notwithstanding this unusual side chain configuration, **O3** essentially retains the antiproliferative activity of **O1** against HL-60 cells (5.3 nM vs. 3.2 nM of **O1**).^[15] However, the effect of the change in side chain configuration on microtubule binding and the antiproliferative activity against cell

lines derived from solid tumors have not been reported. These questions were to be addressed through zampanolide D analogs **O7** and **O8**.

Results and Discussion

Global Synthetic Strategy

Zampanolide analogs **O4–O8** were all to be prepared according to the same convergent approach that we had successfully followed in our total synthesis of **O1** and of different types of previous analogs (**Scheme 25**).^[68,89,93] Thus dioxane- and oxathiane-based alcohols **O10** and **O11**, respectively, would be esterified with acid **O9** and the esters would then be elaborated into aldehydes **O12** and **O13** *via* an intramolecular *HWE* reaction as the macrocyclization step.

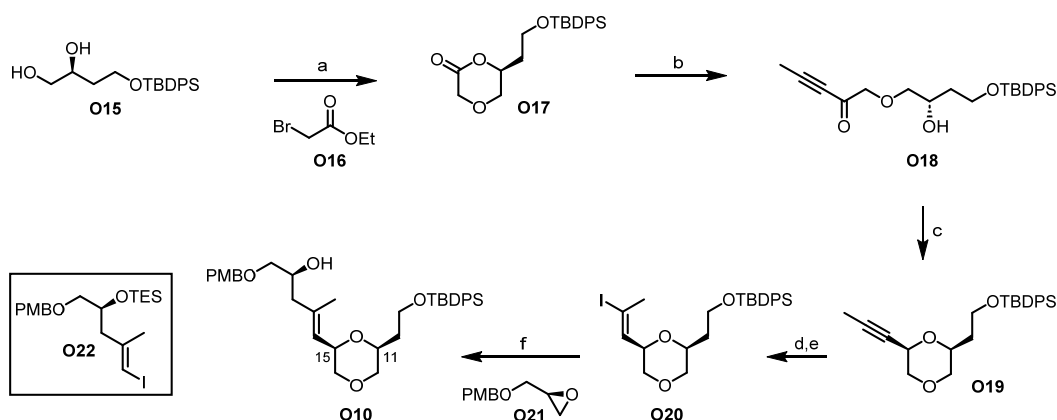


Scheme 25: Global strategy for the synthesis of zampanolide analogs **O4–O8**.

Aldehydes **O12** and **O13** would then undergo a stereoselective aza-aldol reaction with sorbamides **O14a** and **O14b**, respectively.^[82] While acid **O9** was known, alcohols **O10** and **O11** were not and synthetic routes needed to be developed to access these key intermediates. These syntheses will be discussed in the next section.

Synthesis of alcohols **O10** and **O11**

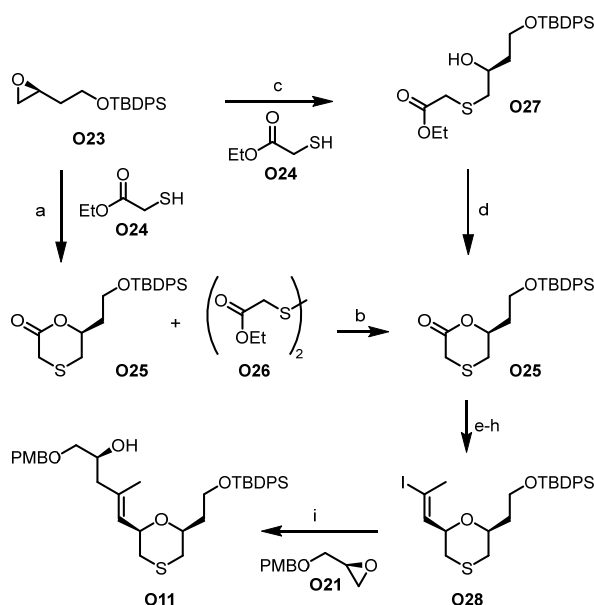
The synthesis of alcohol **O10** proceeded through diol **O15**, which was prepared in 4 steps and 63% overall yield from (*S*)-malic acid. Diol **O15** was elaborated into dioxanone **O17** by first forming a di-*n*-butyl stannylene acetal (through reaction with dibutyltin oxide in MeOH), which then underwent *in situ* regioselective alkylation with ethyl bromoacetate/TBAI followed by lactonization to furnish dioxanone **O17** in 67% overall yield (**Scheme 26**).^[141,142]



Scheme 26: a) i. Bu_2SnO , MeOH, 70 °C, 18 h; ii. TBAI, ethyl bromoacetate (**O16**), toluene, reflux, 3 h, 67%; b) *Z/E*-bromopropene, *n*-BuLi, THF, -78 °C, 2 h, then **O17**, -78 °C, 1 h; c) triethylsilane, TFA, CH_2Cl_2 , -78 to -40 °C, 2.5 h, 76% over two steps; d) CuCN, *n*-BuLi, Bu_3SnH , MeOH, THF, -78 to -15 °C, 16 h; e) NIS, THF, -17 °C, 20 min, 73% over two steps; f) *n*-BuLi, toluene, -78 °C, 1 h, then **O21**, $\text{BF}_3 \cdot \text{OEt}_2$, -100 to -78 °C, 3 h, 69%.

Lactone **O17** was then transformed into hydroxy ketone **O18** by 1,2-addition of *in situ* formed propynyllithium^[143] followed by *cis*-selective reductive cyclization with triethylsilane and TFA^[144] to give dioxane **O19** in 76% over two steps. Stannylcupration/iodination of alkyne **O19** furnished the corresponding *E* vinyl iodide^[68] **O20** in good yield (73%). Lithiation of **O20** with *n*-BuLi and subsequent reaction of the ensuing vinyl lithium species with PMB-protected (*R*)-glycidol (**O21**)^[118] in the presence of $\text{BF}_3 \cdot \text{OEt}_2$ at -100 °C delivered alcohol **O10** in 66% yield. The desired *cis*-configuration of the C(11)- and C(15)- substituents in **O10** was confirmed by NOE-experiments. It should be noted here that early attempts at the synthesis of **O10** had involved the addition of the vinyl lithium derived from vinyl iodide **O22** to lactone **O17**, followed by reduction of the addition product with triethylsilane and TFA. As the product formed in the addition step was found to be very labile, it was immediately submitted to the reduction step. Using this approach, however, alcohol **O10** was obtained in only in 5% yield from **O22**.

The synthesis of alcohol **O11** made use of epoxide **O23** as an early intermediate, which was accessible in 3 steps and 71% overall yield from D-aspartic acid.^[145] Epoxide **O23** was then elaborated into oxathianone **O25** by reaction with ethyl thioglycolate (**O24**) in an epoxide opening/lactonization sequence (**Scheme 27**). Initial experiments focused on a one-pot process for this transformation, employing conditions that have been reported by Romdhani-Younes and co-workers for the one-pot synthesis of 1,4-oxathian-2-ones from ethyl thioglycolate and various epoxides with benzyltrimethylammonium hydroxide (Triton B) as catalyst.^[146]



Scheme 27: a) Triton B, ethyl thioglycolate (**O24**), 4Å MS, toluene, reflux, 40 h; b) DTT, Et₃N, CH₂Cl₂, rt, 3 h, 56% of **O25** and 21% of **O27** over two steps; c) DBU, ethyl thioglycolate (**O24**), THF, -65 °C, 10 min, then **O23**, BF₃•OEt₂, THF, -65 °C, 30 min, 84%; d) *p*-TsOH•H₂O, 4Å MS, toluene, reflux, 40 h, 91%; e) *Z/E*-bromopropene, *n*-BuLi, THF, -78 °C, 2 h, then **O25**, -78 °C, 2 h; f) triethylsilane, TFA, CH₂Cl₂, -78 to -40 °C, 2.5 h, 56% over two steps; g) CuCN, *n*-BuLi, Bu₃SnH, MeOH, THF, -78 to -15 °C, 2 h; h) NIS, THF, -17 °C, 20 min, 92% over two steps; i) *t*-BuLi, toluene, -78 to -45 °C, 20 min, then Li(2-th)CuCN, -78 to -45 °C, 30 min, then **O21**, BF₃•OEt₂, -45 °C to rt, 2 h, 63%.

Best results were obtained when using 1 equiv. of Triton B and 5 equiv. of ethyl thioglycolate (**O24**) in the presence of 4Å MS in toluene (see **Table 6** in section 2.2.3 for details). However, even under these conditions, the reaction was slow (no full conversion after 40 h) and the product could not be separated from inadvertently formed disulfide **O26**. Disulfide formation could not be fully suppressed even when the solvent was thoroughly degassed and the reaction performed under argon. Treatment of the reaction mixture with DTT followed by basic aqueous workup to remove **O24** finally gave oxathianone **O25** in 56% yield after flash chromatography. In addition, 21% of non-cyclized thioether **O27** was isolated.

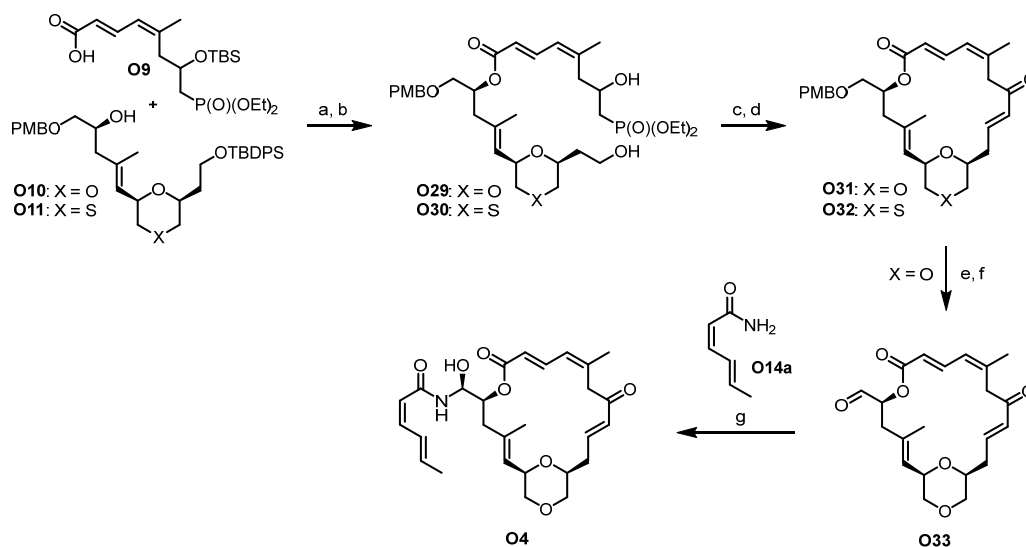
In light of the incomplete conversion of **O27** into **O25**, we explored whether a stepwise approach, with isolation of the intermediate thioether **O27**, would deliver **O25** in higher yields. Thus, ethyl thioglycolate (**O24**) was pre-treated with base before the addition of epoxide **O23** and BF₃•OEt₂. Among the various bases investigated (Et₃N, NaH, NaOEt, *t*-BuLi, DBU) *t*-BuLi in combination with BF₃•OEt₂ at -78 °C in THF proved to be optimal and delivered thioether **O27** in 84% yield after 45 min of total reaction time (see **Table 7** in section 2.2.3 for condition screening). While yields declined somewhat under these conditions for larger scales (0.7 g; 71%), using DBU and BF₃•OEt₂ at -65 °C in THF gave **O27** in 80% yield on a 13 g scale. Ester **O27** could be cyclized smoothly with TsOH•H₂O and 4Å MS in refluxing toluene to furnish oxathianone **O25** in 91% yield.

Oxathianone **O25** was then transformed into vinyl iodide **O28** in 4 steps and 52% overall yield in analogy to the synthesis of **O17** from **O20** (see experimental section 4.2.2.2.3 for details). Unfortunately, attempts to elaborate **O28** into **O11** under the conditions that had allowed the formation of alcohol **O10** from vinyl iodide **O20** were unsuccessful. Changing the alkyllithium reagent from *n*-BuLi to *t*-BuLi and using 1.6 equiv. of *t*-BuLi, epoxide **O23**, and BF₃•OEt₂ each, the desired alcohol **O11** was obtained in 28-30% yield (see **Table 8** in section 2.2.3 for condition screening). Gratifyingly, when catalytic amounts of Li(2-th)CuCN instead of stoichiometric amounts of BF₃•OEt₂ were added to the reaction mixture, the yield increased to 47% (**Scheme 27**). Even better yields (59-63%) were observed when 1.5 equiv. of Li(2-th)CuCN were used in gram scale reactions. The desired *cis*-configuration of the C(11)- and C(15)-substituents in **O11** was confirmed by NOE-experiments. In summary, alcohol **O10** could be accessed from (*S*)-malic acid in 16% yield over 10 steps and oxathiane alcohol **O11** was synthesized from D-aspartic acid in 18% yield over 10 steps.

Synthesis of zampanolide analogs **O4-O8**

As depicted in **Scheme 28**, esterification of acid **O9** with alcohols **O10** or **O11** under Yamaguchi conditions^[120] and subsequent silyl-ether cleavage with HF•py gave diols **O29** and **O30**, respectively, in 68% and 93% overall yield. Oxidation of **O29** and **O30** with DMP gave the corresponding keto aldehydes, which were immediately submitted to Ba(OH)₂ in THF to induce macrocyclization by intramolecular *HWE* reaction, thus delivering macrolactones **O31** and **O32**, respectively, in 68% and 63% yield.

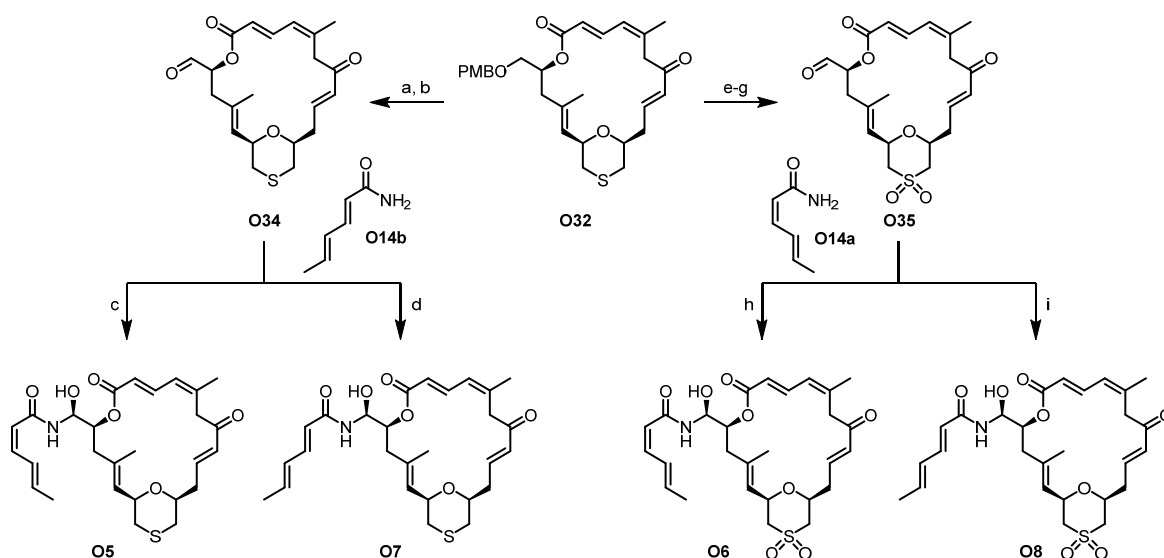
DDQ-mediated PMB-cleavage from dioxane-containing macrolactone **O31** followed by DMP oxidation of the ensuing alcohol then furnished aldehyde **O33** (**Scheme 28**), which was converted into zampanolide analog **O4** in a diastereoselective aza-aldol reaction with an *in situ* formed (*S*)-BINAL-(*2Z,4E*)-sorbamide complex under conditions that we have previously elaborated.^[82] After purification by flash column chromatography and subsequent NP-HPLC, dioxane-based zampanolide analog **O4** was obtained as a single diastereoisomer (at C(20)) in 46% yield.



Scheme 28: a) 2,4,6-Trichlorobenzoyl chloride, Et₃N, DMAP, toluene, rt to 60 °C, 4-16 h; b) HF•py, THF, 0 °C to rt, 16 h, 68% (for **O29**), 93% (for **O30**) over two steps; c) DMP, CH₂Cl₂, rt, 1-2 h; d) Ba(OH)₂, THF/H₂O (40:1), rt, 20 min, 68% (for **O31**), 63% (for **O32**) over two steps; e) DDQ, CH₂Cl₂/H₂O (5:1), rt, 1 h, 84%; f) DMP, CH₂Cl₂, 2.5 h, 85%; g) (*S*)-BINOL, LiAlH₄, EtOH, (*Z,Z*,*4E*)-sorbamide (**O14a**), THF, rt, 40 min, 46%.

Following the same sequence of steps as described above for the elaboration of dioxane **O31** into **O4**, oxathiane-based zampanolide analog **O5** was obtained from **O32** in 26% overall yield (**Scheme 29**). When aldehyde **O34** was reacted with (*2E,4E*)-sorbamide (**O14b**) in the aza-aldol step (*2'-E,4'-E*)-zampanolide analog **O7** was obtained in 38% yield.⁵

⁵ 38% is the chemical yield of the reaction. This material contained 13 mol-% of **O5** and 22 mol-% of (*2E,4E*)-sorbamide. The presence of **O5** was due to contamination of **O14b** with **O14a**. After extensive purification, **O7** was isolated without detectable impurities in 5% yield (1.2 mg) (see experimental section 4.2.2.4 for details).



Scheme 29: a) DDQ, CH₂Cl₂/H₂O (5:1), rt, 5 h, 72%; b) DMP, CH₂Cl₂, 2 h, 91%; c) (*S*)-BINOL, LiAlH₄, EtOH, (*2Z,4E*)-sorbamide (**O14a**), THF, rt, 75 min, 40%; d) (*S*)-BINOL, LiAlH₄, EtOH, (*2E,4E*)-sorbamide (**O14b**), THF, rt, 75 min, 38%⁵; e) mCPBA, CH₂Cl₂, -35 °C, 2 h, 78%; f) DDQ, CH₂Cl₂/H₂O (5:1), rt, 3 h, 87%; g) DMP, CH₂Cl₂, 2 h, 77%; h) (*S*)-BINOL, LiAlH₄, EtOH, (*2Z,4E*)-sorbamide (**O14a**), THF, rt, 45 min, 58%; i) (*S*)-BINOL, LiAlH₄, EtOH, (*2E,4E*)-sorbamide (**O14b**), THF, rt, 45 min, 34%.

To access oxathiane-dioxide-based zampanolide analogs **O6** and **O8**, **O32** was first oxidized with mCPBA to the corresponding sulfone, which was then elaborated into aldehyde **O35** (52% overall yield from **O32**). Stereoselective aza-aldol reaction with either **O14a** or **O14b** finally furnished **O6** and **O8** in 58% and 34% yield, respectively.

Interestingly, when diol **O30** was reacted with 3.3 equiv. of DMP (rather than the standard 2.2 equiv.), treatment of the crude reaction mixture with Ba(OH)₂ gave the expected macrocycle **O32** in only 20% yield (vs. 63% when 2.2 equiv. of DMP were used). In addition, the reaction produced thioacetals **O37a** and **O37b** as an inseparable 1.8:1 mixture in 27% yield (**Figure 23**).

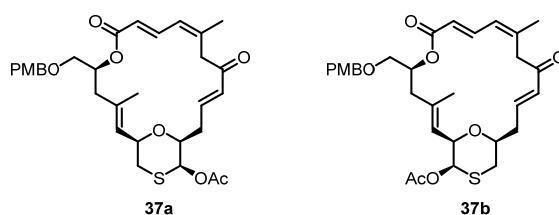
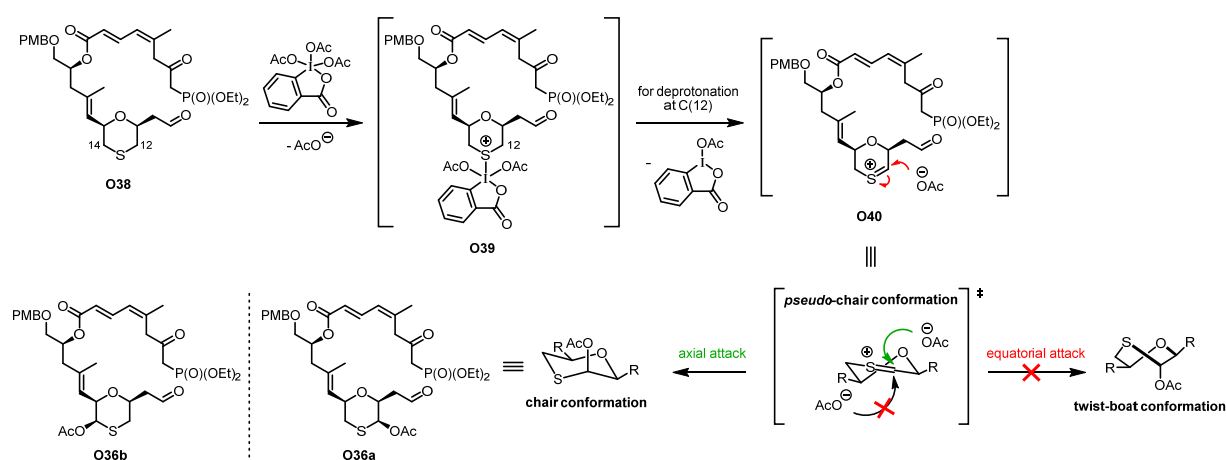


Figure 23: Structures of monothioacetals **O37a** and **O37b**.

The all-*cis* configuration in **O37a** and **O37b** was proven by NOESY-spectroscopy. Similar α -oxidations of sulfides by hypervalent iodine species have been reported previously,^[147–151] but only in the presence of a metal catalyst. Attempts to reduce the thioacetal groups with Et₃SiH/TFA

at low temperature gave **O32** in very low yields only (9-11%) (see **Table 9** in section 2.2.3 for condition screening).

A possible mechanism for the oxidation of the oxathiane ring α to the sulfur atom is shown in **Scheme 30** at the stage of keto aldehyde **O38**. The fact that oxidation of **O30** with only 2.2 equiv. of DMP in the subsequent step delivered macrocycle **O32** in 68% yield clearly suggests that oxidation to the keto aldehyde occurs before oxidation of the oxathiane ring. According to this mechanism, which is related to the mechanism of alcohol oxidation by DMP, nucleophilic displacement of one of the acetate units in DMP by the thioether group leads to sulfonium intermediate **O39**.



Scheme 30: Proposed mechanism for the formation of **O37a** and **O37b**.

Subsequent deprotonation at C(12) or C(14) by displaced acetate anion followed by (or concomitant with) cleavage of the sulfur-iodine bond results in the formation of sulfenium intermediate **O40**, which is then attacked by a second acetate anion originating from DMP to give monothioacetals **O36a** or **O36b**. In accordance with the Fürst-Plattner rule,^[152] only products arising from axial attack on sulfenium intermediate **O40** are observed.

Cellular effects of zampanolide analogs

As shown by the data summarized in **Table 4**, dioxane- and oxathiane-based zampanolide analogs **O4** and **O5**, respectively, are essentially equipotent inhibitors of cancer cell proliferation as **O1** across all 5 cell lines investigated. In contrast, the replacement of the sulfide moiety in analog **O5** by a sulfone group results in a significant decrease in activity of between 50- and 100-fold for analog **O6**.

Changing the configuration of the C(2′)-C(3′) double bond in the C(19) side chain in **O5** or **O6** from *Z* to *E* leads to moderately reduced potencies; thus, (*E,E*)-zampanolide **7** is 4-12-fold less potent than **O5**, while **O8** is 3-6-fold less potent than **O6**. These findings are in line with the reported (small) differences in growth inhibitory activity between (–)-zampanolide (**O1**) and zampanolide D (**O3**) against HL-60 cells.^[15]

Table 4. Antiproliferative activity of (–)-zampanolide (**O1**) and zampanolide analogs **O4–O8** against human cancer cell lines (IC₅₀ [nM]).^[a]

| Cpd | A549 (lung) | A2780 (ovarian) | A2780 AD ^[b] (ovarian) | HeLa (cervical) | HeLa β-III ^[c] (cervical) |
|-----------|----------------|--------------------|--------------------------------------|--------------------|---|
| O1 | 1.8 ± 0.7 | 0.7 ± 0.1 | 0.5 ± 0.1 | 0.8 ± 0.1 | 3.6 ± 0.4 |
| O4 | 1.6 ± 0.2 | 1.7 ± 0.1 | 1.9 ± 0.1 | 0.6 ± 0.0 | 0.9 ± 0.0 |
| O5 | 1.8 ± 0.9 | 0.5 ± 0.1 | 0.6 ± 0.0 | 0.7 ± 0.1 | 3.0 ± 0.2 |
| O6 | 214.4 ± 25.1 | 50.4 ± 5.1 | 1479.7 ± 77.7 | 34.4 ± 2.2 | 80.6 ± 1.3 |
| O7 | 10.7 ± 0.7 | 5.2 ± 0.7 | 7.5 ± 0.4 | 5.7 ± 0.6 | 13.0 ± 1.1 |
| O8 | 656.8 ± 138.7 | 264.5 ± 15.5 | 13117.1 ± 558.8 | 204.0 ± 11.6 | 351.0 ± 47.4 |

^[a]Cells were exposed to compounds for 48 h (A549, A2780, A2780AD, HeLa and HeLa β-III); ^[b]Multidrug-resistant cell line overexpressing the Pgp efflux pump;^[83,84] ^[c]Taxol-resistant cell line overexpressing the βIII tubulin isotype.^[153,154]

Intriguingly, a significant loss in activity was observed for oxathiane-dioxide-based analogs **O6** (29-fold) and **O8** (50-fold) against the Pgp-overexpressing, multidrug-resistant ovarian cancer cell line A2780AD^[83,84] relative to the drug-sensitive parental A2780 line. No difference in activity against A2780 and A2780AD cells was observed for **O4**, **O5**, or **O7**; the same is true for natural (–)-zampanolide (**O1**)^[68] and almost all of our previously reported analogs,^[68,87,89,93] whose cellular potency is not affected by Pgp-overexpression. It has been suggested that the cellular potency of covalent microtubule inhibitors is inherently insensitive to overexpression of the Pgp efflux pump.^[60] Finally, for βIII-tubulin-overexpressing HeLa β-III cells^[153,154] all compounds show a slight trend towards lower activity compared to HeLa cells with normal expression levels of βIII-tubulin. Whether this trend is truly significant is unclear at this point.

Binding of zampanolide analogs to microtubules

In order to assess the microtubule-binding affinity of analogs **O4–O8** and establish a possible relationship with their cellular activity, we have investigated their ability to displace the

fluorescent taxol analog Flutax-2 from cross-linked microtubules.^[134] As discussed previously,^[93] the binding data obtained for covalent binders in a displacement assay do not represent *bona fide* thermodynamic binding constants. Rather, this assay produces what we call apparent binding constants (K_{bapp}).^[93] While K_{bapp} values cannot be reliably compared to each other or to true K_b 's, they are indicative of the efficiency of the overall reaction of a covalent ligand with polymerized tubulin.

Table 5 summarizes the K_{bapp} values for (-)-zampanolide (**O1**) and zampanolide analogs **O4-O8**. For dioxane-based zampanolide analog **O4**, its K_{bapp} is virtually identical with that of natural **O1**; thus, the substitution of the C(13)-C(22) ethylene unit in the natural product by oxygen has no obvious impact on binding efficiency.

Table 5. Apparent microtubule binding constants K_{bapp} of (-)-zampanolide (**O1**) and analogs **O4-O8** at 26 °C.

| Cpd | K_{bapp} [10^6 M ⁻¹] ^[a] |
|-----------|--|
| O1 | 15.9 ± 0.6 ^[b] |
| O4 | 21.3 ± 1.9 |
| O5 | 7.4 ± 0.2 |
| O6 | 0.3 ± 0.0 |
| O7 | 1.9 ± 0.1 |
| O8 | 0.09 ± 0.00 |

^[a]Determined by the displacement of the fluorescent taxoid Flutax-2 from stabilized microtubules.^[134] ^[b]For reasons that are not entirely clear this value is *ca.* 14-fold lower than reported in ref. [60].

Likewise, the binding efficiency of oxathiane-based analog **5** is largely uncompromised relative to **O1**. The K_{bapp} 's of **O4** and **O5** are in range with the one reported for C(13)-desmethylene-zampanolide (**2**) (24×10^6 M⁻¹).^[93] While this may appear unsurprising, it should be remembered that the incorporation of sulfur in a cyclohexane ring (or a THP ring for that matter) leads to distinct geometric changes (reduced C-S-C bond angle vs. C-C-C or C-O-C, which is associated with enhanced puckering; increased distance between the two carbons at the sulfur atom). The K_{bapp} for (*E,E*)-zampanolide analog **O7** is somewhat lower than for **O5**, which parallels the difference in antiproliferative activity between the compounds (**Table 4**). It should be kept in mind, however, that the relationship between microtubule-binding affinity and cellular potency is not straightforward and it is unclear if the reduced cellular potency of **O7** is a direct consequence of its lower K_{bapp} . What is clear, however, is that sulfones **O6** and **O8** not only exhibit significantly reduced growth inhibitory activity compared to their parent sulfides but also bind to

microtubules with strongly reduced efficiency. In fact, the K_{bapp} 's for **O6** and **O8** are similar to the K_b for 13-desmethylene-8,9-dihydro-zampanolide, which cannot bind to microtubules covalently. Based on this observation, it may be speculated that **O6** and **O8** no longer bind to tubulin in a covalent fashion, possibly due to an unfavorable non-covalent binding mode that would impair nucleophilic attack by the β His229 side chain and that could be induced by the sulfone moiety. However, this speculation needs to be investigated experimentally.

Structure of the complex of **O4** with β -tubulin

We performed soaking experiments with **O4** on crystals of the macromolecular complex T₂R-TTL, which is composed of two α,β -tubulin heterodimers (T₂), the stathmin-like protein RB3 (R) and the tubulin tyrosine ligase (TTL).^[61] Unequivocal difference electron densities were observed at the taxane site of both β -tubulin units in the complex (chains B and D, **Figure 24A-B**) and the corresponding structure could be refined to 2.20 Å resolution.

The structures of the tubulin/(-)-zampanolide (**O1**) and the tubulin/**O4** complex superimposed very well with a rmsd of the intermediate domain of 0.091 over 40 C α . Similar to natural zampanolide (**O1**), **O4** is covalently linked to His229 (through C(8) (labelled as C18 in **Figure 24C**) and the NE2 atom of the histidine side chain. As for the tubulin/(-)-zampanolide (**O1**) complex, hydrogen bonds are formed between the carbonyl oxygen of the sorbamide unit (labelled as O1 in **Figure 24C**) and the NH group of T276 as well as the C(20)-OH group (labelled as OH2 in **Figure 24C**) and the main chain carbonyl oxygens of T276 and Q281, respectively (**Figure 24C**). Both complexes feature the rearrangement of part of the M-loop (R278-Y283) into a short helix, which is a hallmark of tubulin stabilization by (-)-zampanolide (**O1**) or epothilones.^[61] However, as a notable unique feature, **O4** is involved in a water-mediated interaction with A233 through the dioxane oxygen that replaces the C(13)-C(22) ethylene unit in (-)-zampanolide (**O1**) (**Figure 24C**).

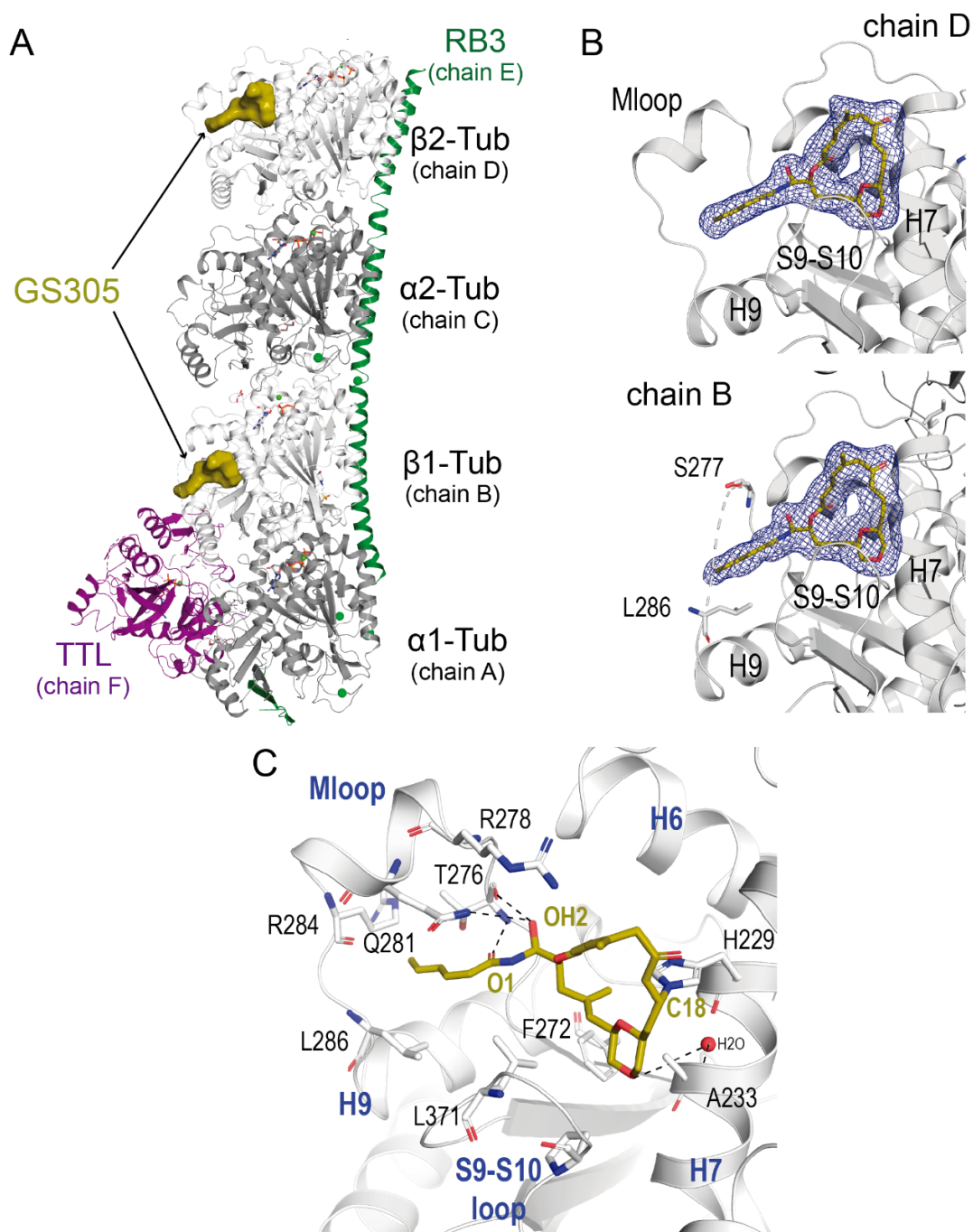


Figure 24: **A.** Global view of the T_2R -TTL-**O4** complex structure. Proteins are in ribbon representation (α -tubulin in grey, β -tubulin in white, RB3 in green and TTL in purple). The compound is in surface representation bound at the taxane site of both β -tubulin chains within the complex. **B.** The sigma A weighted 2mFo-DFc (dark blue) electron density map counteracted at 3.0 sigma of **O4** (stick representation in yellow) at each of the taxane sites within the complex. In chain D the M loop is folded into an α -helix, whereas in chain B it is disordered from S277 to L286. **C.** Close view of the interactions of **O4** with tubulin in chain D. The β -tubulin subunit is in white cartoon representation, with residues involved in hydrogen bonding or hydrophobic interactions shown in sticks. Oxygen and nitrogen atoms are colored in red and blue, respectively. Water molecule is represented as red sphere. Hydrogen bonds are represented by black broken lines and tubulin secondary structure elements are labelled in blue.

Remarkably, while the tubulin/(-)-zampanolide (**O1**) structure was obtained by preparing the tubulin/**O1** adduct prior to crystallization, in the case of **O4**, folding of the M loop was induced within the crystal during soaking of the compound (incubation time of about 20 min). Finally, it should also be noted that in contrast to **O1**, which is only found in the D-chain of its complex with T₂R-TTL, clear densities were observed for **O4** at both β -tubulin chains in the macromolecular complex. Whereas the M-loop is fully ordered in chain D, it is less well defined in chain B (**Figure 24B**).

Conclusions

In this work we have prepared a group of new analogs of the antimitotic marine natural product (-)-zampanolide (**O1**) where the natural 2,6-disubstituted 4-methylenetetrahydropyran unit has been replaced by a corresponding dioxane, oxathiane, or oxathiane-dioxide ring. While the synthesis of these analogs followed the same overall strategy that we had established for the total synthesis of the natural product, specific routes had to be developed towards the requisite heterocycle-containing alcohol building blocks **O10** and **O11**. Dioxane-containing building block **O10** was prepared in 10 steps and 16% overall yield from (*S*)-malic acid; the formation of the dioxane ring involved the regioselective alkylation of a 1,2-stannylene acetal with ethyl bromoacetate followed by lactonization. Oxathiane-containing alcohol **O11** was accessed from D-aspartic acid in 10 steps and 18% overall yield. Here, the construction of the oxathiane ring was achieved most efficiently through a stepwise epoxide opening/lactonization sequence. No major difficulties were encountered in the *HWE*-based macrocyclization step or for the final stereoselective aza-aldol reaction, thus attesting to the robustness of our overall approach. Of note, however, oxidation of the oxathiane ring α to the sulfur atom occurred when excess DMP was used to establish the keto aldehyde motif in the macrocyclization precursor.

The dioxane- and oxathiane-based zampanolide analogs **O4** and **O5**, respectively, both bind to microtubules with similar efficiency as natural (-)-zampanolide (**O1**) or 13-desmethylene-zampanolide (**O2**) and they are equipotent cell growth inhibitors. Thus, the replacement of the C(13)-C(22)-ethylene unit in **O1** by oxygen or sulfur is well tolerated. While this may be considered unsurprising in light of the previously reported potent activity of 13-desmethylene-zampanolide (**O2**) (where the C(13)-C(22)-ethylene unit is replaced by a CH₂-group, **Figure 22**), we are not aware of any previous studies on the effects of a tetrahydropyran to dioxane or oxathiane exchange in bioactive natural products. Interestingly, the second oxygen atom in dioxane-based analog **O4** engages in a new water-mediated hydrogen bond that might compensate for the loss of hydrophobic interactions due to the presence of a polar moiety. Intriguingly, in contrast to the replacement of the C(13)=CH₂ group in **O1** by oxygen or sulfur, a

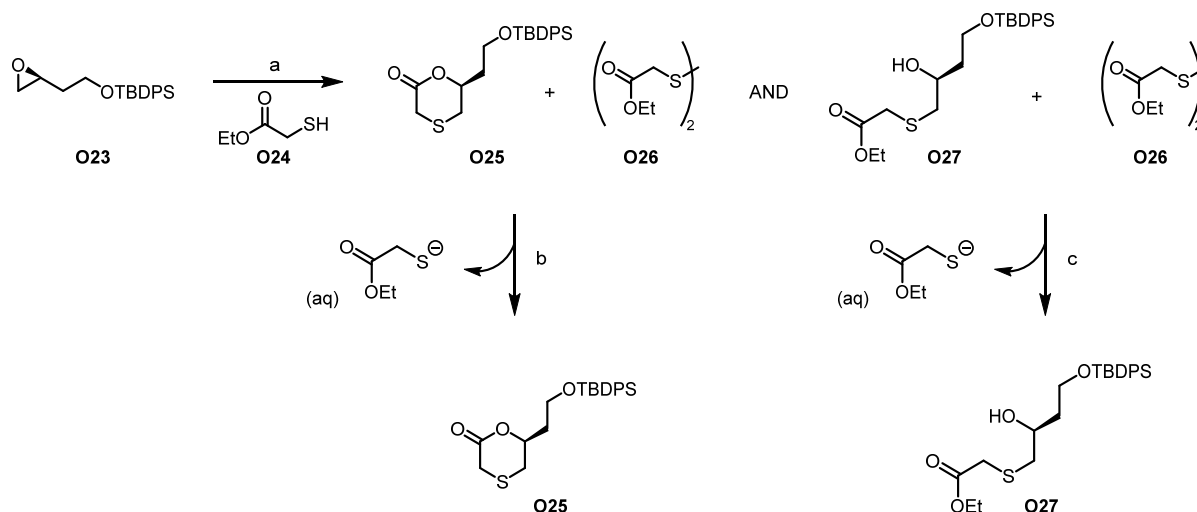
sulfonyl group is not well tolerated; it leads to a substantial loss in antiproliferative activity and strongly interferes with microtubule-binding. In addition, the corresponding analogs **O6** and **O8** are highly susceptible to Pgp-mediated efflux, which has not been observed for other zampanolide-type structures. The molecular underpinnings of this disparate behavior will need to be elucidated.

In summary, we have expanded the synthetic chemistry and SAR knowledge base on the marine natural product zampanolide to dioxane-, oxathiane-, and oxathiane-dioxide-based congeners. Through this work, we have also broadened the diversity of potent zampanolide-derived structures that could be of interest for *in vivo* pharmacological profiling.⁶

⁶ First *in vivo* experiments with **O1** have recently been reported by Johnson, Risinger and co-workers: L. Takahashi-Ruiz, J. D. Morris, P. Crews, T. A. Johnson, A. L. Risinger, *Molecules* **2022**, *27*, 4244. While the compound showed antitumor activity when administered intratumorally, even a single i.p. dose of 1 mg/kg was highly toxic. The *in vivo* evaluation of some of the analogs described in this study would help to understand if these observations are due to a class effect or if structurally modified analogs of **O1** could offer an acceptable therapeutic window.

2.2.3 Additional Information on Publication 2

In this chapter, additional experimental information is provided on the work described in the previous chapter, such as cross-referenced schemes, table, figures etc.



Scheme 31: One-pot procedure for the formation of **O25** from **O23** and **O24**. a) Triton B, **O24**, 4Å MS, toluene, reflux, 40 h; b) DTT, Et₃N, DCM, rt, 3 h, 56% over two steps. c) DTT, Et₃N, DCM, rt, 3.5 h, 21% over two steps.

The first attempt to convert epoxide **O23** into oxathianone **O25** (**Scheme 31**) proceeded in low yield (14%) with concomitant thioether intermediate **O27** isolation (18%) (**Table 6**, entry 1). Beside the unsatisfactory yield, oxathianone **O25** was obtained as a mixture with disulfide **O26** (**Scheme 31**), which is formed through oxidative dimerization of ethyl thioglycolate (**O24**). To eliminate residual oxygen, the solvent was degassed for the next reaction attempt (**Table 6**, entry 2). However, this proved ineffective in preventing disulfide formation, as indicated by reaction monitoring *via* ¹H-NMR spectroscopy. Gratifyingly, **O26** was sequestered effectively to **O24** by DTT-mediated reduction and consecutive basic workup with a 2M aqueous NaOH solution, delivering clean **O25** and **O27** (**Scheme 31**). Attempts to enforce full consumption of epoxide **O23**, by increasing the equivalents of Triton B and thiol **O24**, as well as prolonged reaction times (**Table 6**, entries 2 and 3) failed. By trapping ethanol, that is released upon lactonization of **O27**, the yield of cyclic **15** was sought to increase. Thus, 4Å molecular sieves (MS) were employed (**Table 6**, entry 3), which led to an improved yield of **O25** (55% instead of 32%, **Table 6**, entries 2 and 3, respectively). However, it must be noted that more than one reaction parameter was changed (also load of Triton B and thiol **O24** increased), which is why the increase in yield may not be solely a result of the added MS. For all reactions presented in **Table 6**, unreacted epoxide **O23** was present in the reaction mixture and in the crude mixture after aqueous workup

(according to $^1\text{H-NMR}$ spectroscopic analysis). Thus, the unsatisfactory yield obtained for **O25** and **O27** was concluded to originate from incomplete starting material consumption.

Table 6: Conditions investigated for the Triton B-catalyzed opening of epoxide **O23** with ethyl thioglycolate (**O24**).^[a]

| Entry | Scale | Triton B ^[b] | Thiol O24 | Time | Yields ^[c] of O27/O25 | Remarks |
|-------|--------|-------------------------|------------------|------|---|----------------------------------|
| 1 | 100 mg | 0.15 eq. | 3.0 eq. | 24 h | 18% / 14% ^[d] | - |
| 2 | 500 mg | 0.35 eq. | 3.5 eq. | 68 h | 45% ^[d] and 32% ^[d] | solvent degassed |
| 3 | 150 mg | 1.0 eq. | 5.0 eq. | 40 h | 21% and 55% | solvent degassed, 4Å MS added |

^[a]For all reactions, a mixture of epoxide **O23**, thiol **O24** and Triton B in toluene was heated under reflux for the specified time period. ^[b]The amount of Triton B present was continuously increased during the reaction by portionwise addition. Indicated is the number of equiv. reached after complete addition. ^[c]Isolated yields after flash column chromatography. ^[d]Compound isolated as a mixture with disulfide **O26**. The yield is based on $^1\text{H-NMR}$ spectroscopic analysis of the mixture.

It was explored whether lactone **O25** could be obtained in higher yields, if epoxide opening and lactonization were performed in two separate steps. Heating a mixture of **O23**, **O24** and Et_3N in toluene under reflux for 18 h gave clean **O27**, yet in low yield (15%). Furthermore, low conversion (70% of **O23** reisolated) was observed (**Table 7**, entry 1). A prolonged reaction time (60 h vs. 24 h) led to a significant improvement of the yield (33% vs. 15%) (**Table 7**, entry 2). Attempts with NaH failed to deliver thioether **O27**; analysis of the crude material by $^1\text{H-NMR}$ spectroscopy revealed no significant consumption of **O23** (**Table 7**, entry 3). Given that a significantly reduced reaction time for deprotonation (5 min instead of 1 h) and heating of the mixture under reflux did not lead to opening of **O23** (**Table 7**, entry 4), the use of NaH was not further pursued. Likewise, NaOEt did not give access to **O27** (**Table 7**, entry 5).

Table 7: Conditions investigated for the opening of epoxide **O23** with ethyl thioglycolate (**O24**).

| Entry | Scale | Conditions ^[a] | Yield of O27 ^[b] | Remarks |
|-------|--------|---|------------------------------------|--|
| 1 | 120 mg | Et_3N (2.5 eq.), O24 (2.0 eq.), toluene, 18 h, reflux | 15% | 70% of O23 reisolated ^[c] |
| 2 | 250 mg | Et_3N (2.5 eq.), O24 (2.0 eq.), toluene, 60 h, reflux | 33% | 53% of O23 reisolated ^[c] |
| 3 | 120 mg | i.) NaH (1.2 eq.), O24 (1.0 eq.), THF, 1 h, 0 °C to rt | n.d. ^[d] | No conversion of O23 ^[e] |

| ii.) O23 , THF, 24 h, rt | | | | |
|---------------------------------|-----------|--|---------------------|---|
| 4 | 120 mg | i.) NaH (1.2 eq.), O24 (1.0 eq.), THF, 5 min, 0 °C to rt ii.) O23 , THF, 24 h, rt to reflux | n.d. ^[d] | No conversion of O23 ^[e] |
| 5 | 150 mg | i.) NaOEt (1.1 eq.), O24 (1.0 eq.), EtOH, 5 min, rt ii.) O23 , EtOH, 16 h, rt | 0% | Decomposition ^[f] |
| 6 | 100 mg | BF₃•OEt₂ (0.4 eq.), O24 (4.0 eq.), CH ₂ Cl ₂ , 18 h, rt | 0% | 91% TBDPS-OH isolated |
| 7 | 100 mg | i.) <i>t</i> -BuLi (1.1 eq.), BF₃•OEt₂ (1.0 eq.), O24 (1.1 eq.), THF, 10 min, –78 °C ii.) O23 , THF, 35 min, –78 °C | 85% | |
| 8 | 720 mg | i.) <i>t</i> -BuLi (1.1 eq.), BF₃•OEt₂ (1.0 eq.), O24 (1.1 eq.), THF, 10 min, –78 °C ii.) O23 , THF, 6 h, –78 to –10 °C | 71% | |
| 9 | 100 mg | i.) DBU (1.5 eq.), BF₃•OEt₂ (1.5 eq.), O24 (1.2 eq.), THF, 10 min, –65 °C ii.) O23 , THF, 30 min, –65 °C | 84% | |
| 10 | 12'000 mg | i.) DBU (1.5 eq.), BF₃•OEt₂ (1.5 eq.), O24 (1.2 eq.), THF, 10 min, –65 °C ii.) O23 , THF, 30 min, –65 °C | 80% | |

^[a]For all reactions (except for entries 1, 2 and 6) **O24** was pretreated with base under the conditions given in “i.”, before **O23** (1.0 eq.) was added under the conditions given in “ii.” ^[b]Isolated yield after flash column chromatography. ^[c]Material isolated as a mixture with **O24** and **O26**. ^[d]n.d. = not determined, no purification was conducted, no yield was calculated. ^[e]¹H-NMR spectroscopic analysis of the crude mixture after aqu. workup indicated no conversion of **O23**. ^[f]Reaction monitoring by TLC indicated formation of **O27** and decomposition may have occurred upon aqu. workup.

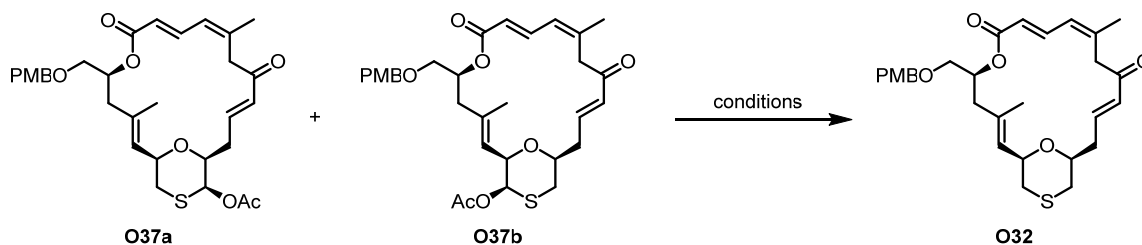
Attempts with **BF₃•OEt₂** in CH₂Cl₂ did not furnish **O27**, but loss of the protecting group was observed (91% according to isolated TBDPS-OH) (**Table 7**, entry 6). Gratifyingly, deprotonation of thiol **O24** with *t*-BuLi, followed by addition of epoxide **O26** together with **BF₃•OEt₂** gave rise to thioether **O27** in high yield (85%) (**Table 7**, entry 7) and no desilylation was observed under these conditions (significantly lower temperature compared to entry 6). Markedly, the yield was found to slightly drop (71% vs. 85%) when the reaction was conducted on a bigger scale (720 mg vs. 100 mg, **Table 7**). Replacing the highly reactive *t*-BuLi with DBU was considered favorable especially in light of reactions on larger scales (>10 g). Thus, DBU was used under similar conditions as established for the *t*-BuLi-mediated reaction (**Table 7**, entry 9). Gratifyingly, virtually the same

| | | | |
|----|---------|---|-----|
| 7 | 50 mg | i.) <i>t</i> -BuLi (2.0 eq.), BF ₃ •OEt ₂ (2.5 eq.), THF, -78 °C, 30 min ii.) O21 (2.5 eq.), -90 to -78 °C, 4 h | - |
| 8 | 50 mg | i.) <i>t</i> -BuLi (2.0 eq.), BF ₃ •OEt ₂ (2.5 eq.), Et ₂ O, -78 °C, 30 min ii.) O21 (2.5 eq.), -90 to -78 °C, 4 h | - |
| 9 | 50 mg | i.) <i>t</i> -BuLi (1.6 eq.), BF ₃ •OEt ₂ (1.6 eq.), toluene, -78 °C, 30 min ii.) O21 (1.6 eq.), -90 to -78 °C, 8 h | 12% |
| 10 | 50 mg | i.) <i>t</i> -BuLi (1.6 eq.), BF ₃ •OEt ₂ (1.6 eq.), toluene, -78 °C, 30 min ii.) O21 (1.6 eq.), -90 to -40 °C, 5 h | 30% |
| 11 | 50 mg | i.) <i>t</i> -BuLi (1.6 eq.), BF ₃ •OEt ₂ (1.6 eq.), toluene, -78 °C, 30 min ii.) O21 (1.6 eq.), -90 to -10 °C, 4 h | 7% |
| 12 | 500 mg | i.) <i>t</i> -BuLi (1.6 eq.), BF ₃ •OEt ₂ (1.6 eq.), toluene, -78 °C, 30 min ii.) O21 (1.6 eq.), -40 °C, 2 h | 28% |
| 13 | 50 mg | i.) <i>t</i> -BuLi (1.7 eq.), toluene, -78 to -45 °C, 20 min ii.) Li(2-th)CuCN (0.07 eq.), -78 to -45 °C, 30 min iii.) O21 (1.5 eq.), -78 to 0 °C, 3 h | 47% |
| 14 | 1000 mg | i.) <i>t</i> -BuLi (1.7 eq.), -78 to -45 °C, 20 min ii.) Li(2-th)CuCN (1.1 eq.), -78 to -45 °C, 30 min iii.) O21 (1.5 eq.), -78 to 0 °C, 3 h | 59% |
| 15 | 3250 mg | i.) <i>t</i> -BuLi (1.7 eq.), -78 to -45 °C, 20 min ii.) Li(2-th)CuCN (1.1 eq.), -78 to -45 °C, 30 min iii.) O21 (1.5 eq.), -78 to 0 °C, 3 h | 63% |

^[a]For all reactions **O28** was pretreated with base under the conditions given in "i.", before **O21** was added under the conditions given in "ii.". For entries 3 and 13-15, additional treatment with conditions given in "ii" preceded addition of **O21** under conditions given in "iii."; ^[b]Isolated yield after flash column chromatography. "-" refers to unidentifiable product(s).

The attempts to reduce thioacetals **O37a/O37b** to thioether **O32** are summarized in **Table 9**. Of the tested conditions, only the combination of TFA and Et₃SiH in CH₂Cl₂ at low temperature gave desired **O32**, but still in low yields (9-11%) (**Table 9**, entries 5 and 6).

Table 9: Conditions investigated for the reduction of **O37a/O37b** to **O32**.



| Entry | Scale | Reagents | Conditions | Yield of O32 ^[a] |
|-------|-------|--|--|-----------------------------|
| 1 | 30 mg | TMSOTf, Et ₃ SiH | MeCN, rt, 24 h | - |
| 2 | 20 mg | AcOH, Et ₃ SiH | CH ₂ Cl ₂ , rt, 24 h | - |
| 3 | 20 mg | H ₂ N-NH ₂ ·AcOH | DMF, rt, 3h | - |
| 4 | 15 mg | TFA, Et ₃ SiH | CH ₂ Cl ₂ , rt, 1 h | - |
| 5 | 20 mg | TFA (15 eq.), Et ₃ SiH (10 eq.) | CH ₂ Cl ₂ , -78 to -40 °C, 6 h | 11% |
| 6 | 15 mg | TFA (15 eq.), Et ₃ SiH (30 eq.) | CH ₂ Cl ₂ , -40 °C, 3 h | 9% |

^[a] “-” refers to unidentifiable product(s).

Cell Growth Inhibition (MTT assay) and Binding to Microtubules

The cell growth inhibition (MTT assay) and binding to microtubules were conducted as described in experimental section 4.2.1.4. An illustration of cell growth inhibition of A549 cells by oxathiane zampanolide analog **O5** is shown in **Figure 25**.

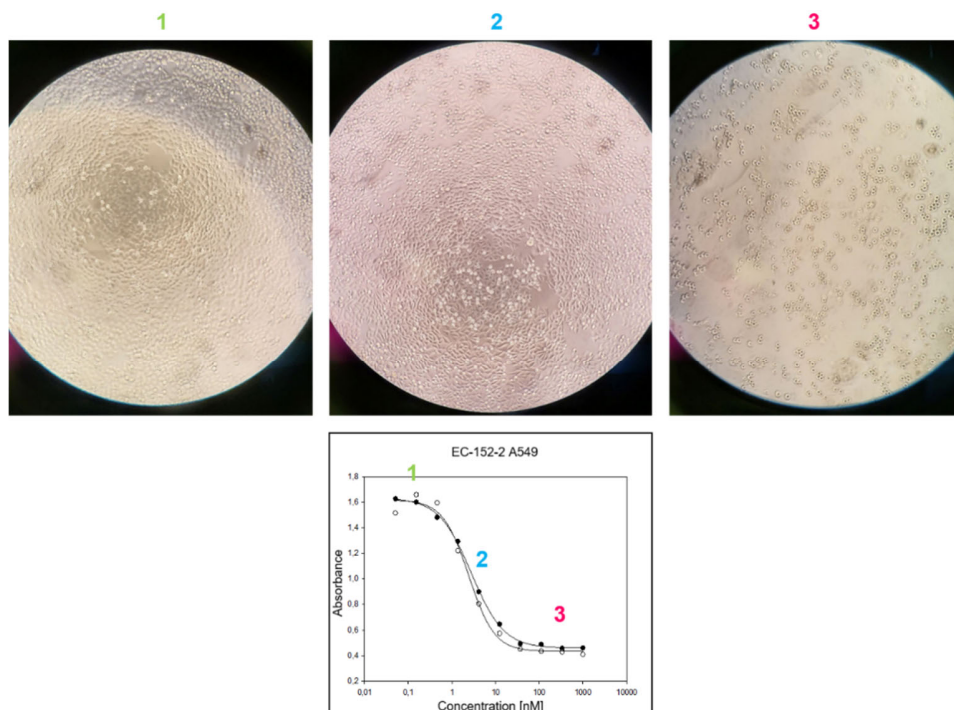


Figure 25: Illustration of cell growth inhibition of A549 cells by oxathiane zampanolide analog **O5** (named EC-152-2 in the figure). Pictures of cell plates obtained through a microscope lens with a 20X zoom, representing the three different sections (1-3) of the inhibition curve shown (top). Section **1**, (low concentration of reagent) shows mostly

resting cells (monolayer of elongated cells) with only few cells in mitosis (spherical cells detached from the surface); section 2 (half maximum inhibitory concentration range for **O5**) shows dividing and non-dividing cells in a *ca.* 1:1 ratio; section 3 (high concentration of reagent) shows mostly cells trapped in mitosis.

Induction of Tubulin Polymerization

As alluded to in section 2.1.3.1, microtubule-stabilizing agents can promote the assembly of soluble tubulin heterodimers into (MSA-bound) microtubule polymers under conditions that do not otherwise support microtubule formation. A compound's ability to induce tubulin polymerization, thus, represents a functional measure for the strength of its interactions with microtubules. DMSO was used as blank and (–)-zampanolide (**O1**) was used as reference compound. The used GAB buffer induces polymerization of tubulin even in the absence of a MSA (glycerol mediated), so that even the blank (no compound but DMSO added) shows some degree of polymerization over time (black line in **Figure 26**). The induction of tubulin polymerization by **O1** and zampanolide analogs **O5-O8** is depicted in **Figure 26**. Noteworthy, analog **O5** (red line) performed better than parental **O1** (orange line), whereas all other compounds triggered less polymerization than **O1**.

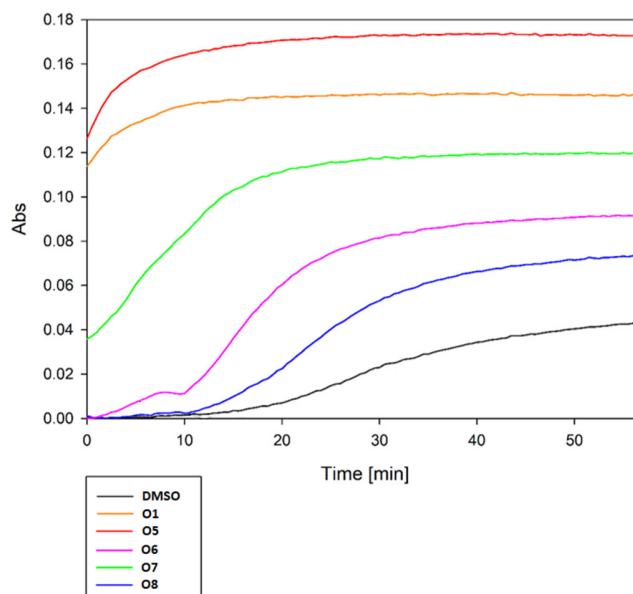


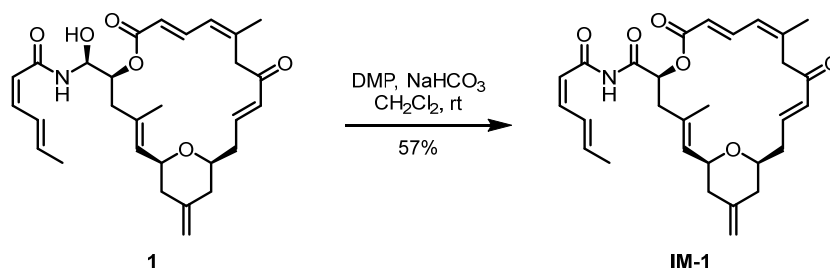
Figure 26: Induction of tubulin polymerization by (–)-zampanolide (**O1**) and by oxathiane- and oxathiane-dioxide-based zampanolide analogs **O5-O8**. Tubulin (25 μM) was polymerized in GAB buffer in the presence of 27.5 μM of test compound at 37°C for *ca.* 60 min. The absorbance at 350 nm was measured on a Multiskan plate reader in a 30-second interval. All measurements were carried out in technical duplicate and the average of the two is shown here.

2.2.4 Side Chain-Modified Analogs

2.2.4.1 Imide-Based Analogs of R7, O4 and O6

As highlighted earlier, a unique structural feature of (-)-zampanolide (**1**) is the C(20) hemiaminal unit that links the macrocyclic core to the nitrogen of *Z,E*-sorbamide. At the same time, this entity is a potential source of chemical and perhaps metabolic instability. Thus, *Smith* and co-workers showed early on that (+)-zampanolide (*ent*-**1**) in benzene at 85 °C quantitatively afforded dactylolide and sorbamide *via* retro *aza-ene* reaction after 105 min.^[81] Similar observations were also reported by *Altmann* and co-workers for certain morpholino-zampanolides;^[155] likewise, for some of the zampanolide analogs described in this thesis (**R7** and **R8**), the formation of the corresponding dactylolide variant was observed upon prolonged NMR data acquisition in CDCl₃ solution. The significance of these findings for the stability of the hemiaminal moiety in biological systems (cell culture, *in vivo*) is unclear at this point, as no data on this question are available. It should be noted, however, that **1** and C(20)-*epi*-**1** show significantly different cellular activity, which strongly suggests that only limited cleavage of the hemiaminal moiety can occur in cell proliferation experiments.

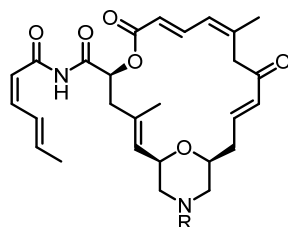
Independent of its importance as a putative chemical/metabolic weak-spot, *Altmann* and co-workers became interested in the investigation of imide-based analogs of **1**, with **IM-1** as the prototypical example, where the hemiaminal hydroxy group is oxidized to a carbonyl group. At the very least, this modification would improve synthetic accessibility relative to the corresponding hemiaminal-based congeners. Thus, *Berardozzi* and *Altmann* prepared imide **IM-1** by oxidation of **1** with DMP in 57% yield (**Scheme 32**, unpublished work).



Scheme 32: Preparation of imide **IM-1** by oxidation of (-)-zampanolide (**1**) (*Berardozzi* and *Altmann*, unpublished work).

Intriguingly, **IM-1** was found to be a slightly less potent inhibitor of cancer cell growth *in vitro* than **1**, although only one cell line was investigated (A2780; IC₅₀ 12 nM for **IM-1** vs. 4 nM for **1**). Similarly, *Bold et al.* found that imide-containing *N*-acetyl-morpholino-zampanolide **IM-2** was an

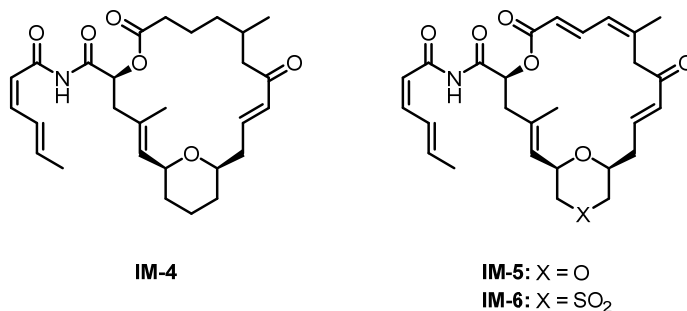
equipotent cell growth inhibitor as the parent hemiaminal **E80** across three different cancer cell lines (**Table 10**). In intriguing contrast, however, *N*-tosyl derivative **IM-3** was significantly less potent than hemiaminal **E83** (**Table 10**).^[155]



IM-2: R = Ac
IM-3: R = Ts

Figure 27: Morpholine-zampanolides investigated by *Bold et al.*^[155]

In light of the relative paucity of data on zampanolide analogs with imide-based side chains in general and the opposite cellular effects observed for this modification in combination with different core macrocycles, it was of interest to study the microtubule-binding affinity and antiproliferative activity of imide-based analogs of **R7**, **O4** and **O6** as **IM-4**, **IM-5** and **IM-6** (**Figure 28**). These compounds were prepared by DMP oxidation of the corresponding hemiaminals **R7**, **O4** and **O6** in 17-55% yield (see experimental section 4.2.3.1 for details) (**Figure 27**). No efforts were made on trying to oxidize oxathiane-based analogs, due to potential problems with oxidation of the oxathiane ring.



IM-4

IM-5: X = O
IM-6: X = SO₂

Figure 28: Imide-based zampanolide analogs **IM-4-5**.

The data for inhibition of cancer cell growth by imide-based zampanolide analogs **IM-1-6** together with those of parent hemiaminals are summarized in **Table 10**. Imides **IM-4** and **IM-5** were roughly one order of magnitude less potent compared to **R7** and **O4**, respectively, which was also observed for **IM-1** vs. **1**. For the oxathiane-dioxide based compound **IM-6** the drop in activity compared to **O6** was strongly dependent on the tested cell line (up to 8-101-fold).

Table 10. Antiproliferative activity of (-)-zampanolide (**1**), zampanolide analogs **E80**, **E83**, **R7**, **O4**, **O6**, and zampanolide imide analogs **IM-1-6** against human cancer cell lines (IC₅₀ [nM]).^[a]

| Cpd | A549 (lung) | A2780 (ovarian) | A2780 AD ^[b] (ovarian) | HeLa (cervical) |
|-------------|--------------------------|----------------------------|--------------------------------------|---------------------------|
| 1 | n.d. | 0.81 ± 0.01 ^[c] | 2.68 ± 0.21 ^[c] | n.d. |
| IM-1 | n.d. | 12 ± 1 ^[c] | 19 ± 11 ^[c] | n.d. |
| E80 | 1.9 ^[d] | n.d. | n.d. | 1.3 ± 0.1 ^[d] |
| IM-2 | 4.2 ^[d] | n.d. | n.d. | 1.0 ^[d] |
| E83 | 2770 ± 49 ^[d] | n.d. | n.d. | 1673 ± 155 ^[d] |
| IM-3 | n.d. | n.d. | n.d. | 186 ^[d] |
| R7 | 133 ± 6 ^[e] | 65 ± 21 ^[e] | 72 ± 28 ^[e] | n.d. |
| IM-4 | 1262 ± 51 | 794 ± 78 | 1098 ± 5 | n.d. |
| O4 | 1.6 ± 0.2 | 1.7 ± 0.1 | 1.9 ± 0.1 | 0.6 ± 0.0 |
| IM-5 | 26 ± 7 | 31 ± 3 | 23 ± 0 | n.d. |
| O6 | 214 ± 25 | 50 ± 5 | 1480 ± 78 | 34 ± 2 |
| IM-6 | 7434 ± 974 | 2385 ± 56 | 12056 ± 860 | 3446 ± 237 |

^[a]Cells were exposed to compounds for 48 h; n.d. = not determined; ^[b]Multidrug-resistant cell line overexpressing the Pgp efflux pump;^[83,84] ^[c]Data from *Berardozzi and Altmann*, unpublished work; ^[d]Data from ref. [155]; ^[e]Data from ref. [93];

Table 11 shows the apparent binding affinity (K_{bapp}) of imide-based zampanolide analogs **IM-1-6** together with those of parent hemiaminals. The same trends as in the cytotoxicity data were obtained; K_{app} for **IM-4** is one order of magnitude lower compared to **R7**, values for **IM-5** and **O4** are similar and comparable to **1**, affinity of **O6** was two orders of magnitude lower than **1** and **IM-6** was not able to fully displace Flutax-2 even at a concentration of 25 μ M.

Table 11: Apparent microtubule binding constants K_{bapp} of (-)-zampanolide (**1**), zampanolide analogs **E80**, **E83**, **R7**, **O4**, **O6**, and zampanolide imide analogs **IM-1-6** at 35 °C.

| Cpd | K_{bapp} [10^6 M ⁻¹] ^[a] |
|--------------------------|---|
| 1 / IM-1 | 93.4 ± 0.37 ^[b,c] / 109.0 ± 0.85 ^[c] |
| E80 / IM-2 | 61.6 ^[d] / 15.8 ^[d] |
| E83 / IM-3 | no displacement ^[e] / no displacement ^[e] |

| | |
|------------------|--|
| R7 / IM-4 | $0.47 \pm 0.07^{[f]} / 0.054 \pm 0.006$ |
| O4 / IM-5 | $30.4 \pm 3.4 / 2.03 \pm 0.2$ |
| O6 / IM-6 | $0.52 \pm 0.03 / \text{no displacement}^{[e]}$ |

^[a]Determined by the displacement of the fluorescent taxoid Flutax-2 from stabilized microtubules;^[134] ^[b]For reasons that are not entirely clear this value is *ca.* 6-fold higher than the one reported in ref. [135]; ^[c]Data from *Berardozzi* and *Altmann*, unpublished work; ^[d]Data from ref. [155]; ^[e]not sufficient displacement in the tested concentration range (0 – 25 μM) was observed; ^[f]Data from ref. [93].

2.2.4.2 Zampanolide-Epothilone Hybrids⁷

An alternative approach to zampanolide analogs lacking the potentially problematic hemiaminal moiety was suggested by closer inspection of the crystal structures of tubulin-bound **1** and epothilone A (**2**), respectively. A comparison of these structure reveals that the C(19) side chain of **1** and the C(15) side chain of epothilone A (**2**) occupy the same space and can be readily overlaid. For both MSAs, the interaction with the respective side chains leads to partial helical structuring of the M-loop (see section 2.1.4.2) (**Figure 29**).

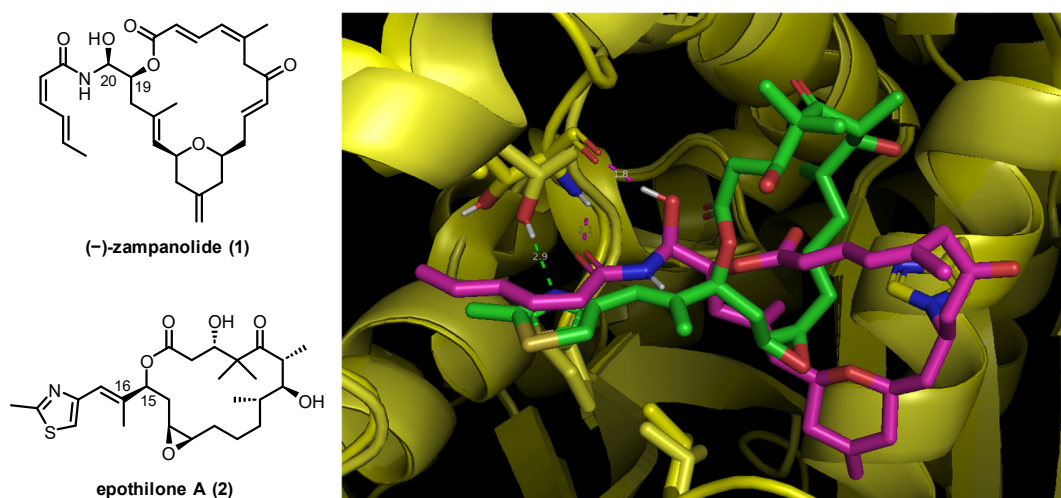


Figure 29: Overlay of (-)-zampanolide (**1**, pink) and epothilone A (**2**, green) in the taxane binding pocket (yellow). Nitrogen atoms are shown in blue, oxygen atoms in red and sulfur atoms in yellow. Supramolecular interactions between the side chains and the M-loop of the tubulin are shown in pink/green dashed lines and the corresponding distances are given in Å.

Based on these observations, the replacement of the C(20) side chain in zampanolide by the C(15) side chain in epothilones thus emerged as a plausible approach towards potent zampanolide analogs with potentially increased chemical/metabolic stability. This led to the design of zampanolide-epothilone hybrid structures **H1** and **H3**, which combine the 13-desmethylene zampanolide core with modified versions of the epothilone side chain (**Figure 30**). Hybrid **H1** was shown to be able to dock into the taxane-binding using Glide from the Schrödinger Software package.⁸

⁷ The experiments described in this section were performed by Rebeca Paris under my supervision.

⁸ Dockings studies were performed by Dr. Bernhard Pfeiffer.

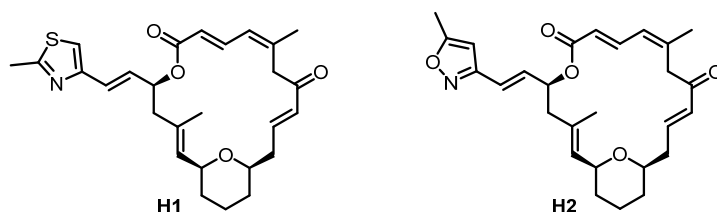
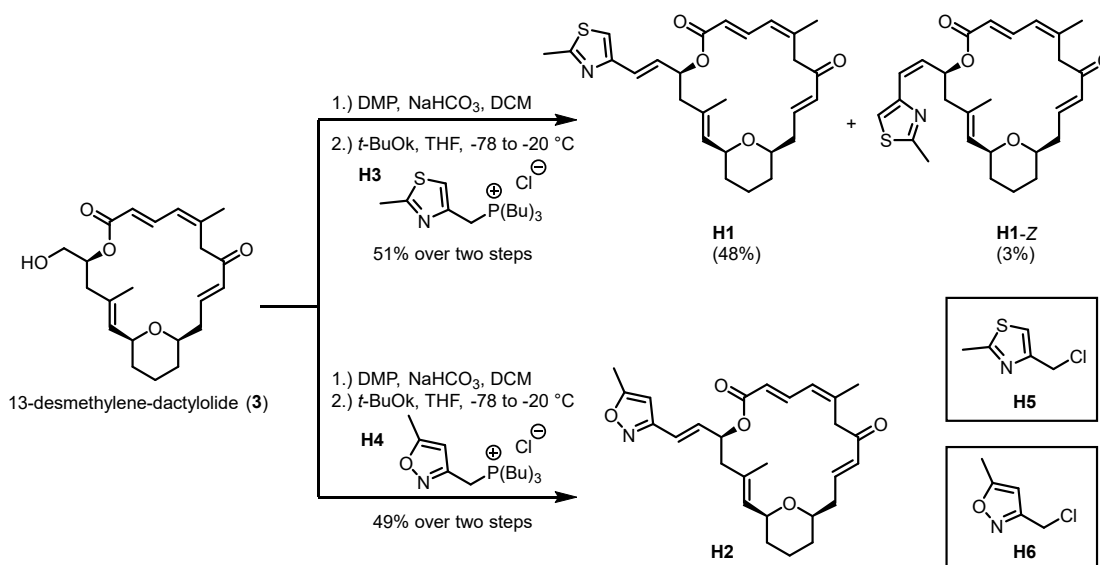


Figure 30: Structures of zampanolide-epothilone hybrids **H1** and **H2**.

The C(16)-methyl group in epothilones has been previously shown to be non-essential for potent antiproliferative activity.^[156,157] The absence of this group in **H1** and **H2**, thus, was not expected to negatively affect their antiproliferative activity; at the same time, the stereoselective construction of the disubstituted *E* double bond in **H1** and **H2** was deemed to be somewhat more straightforward than for a methylated variant. More importantly, the absence of the methyl group also avoids any unfavourable interactions with the protein relative to the zampanolide side chain. Conceptually, analogs **H1** and **H2** are related to the monocyclic zampanolide analogs reported by Chen (**E72-E77**, section 2.1.7, **Figure 13**).^[85,86] These analogs had different aryl enoate side chains installed and showed single digit micromolar to submicromolar antiproliferative activity, which is still decent given the fact that their core was monocyclic (desTHP).

The design of hybrid structures **H2** was additionally driven by previous observations on isoxazole-containing epothilone analogs, which in several cases had been shown to be more potent cell growth inhibitors than the corresponding thiazole-based congeners.^[157–159] For a later phase of the project it was also planned to construct tool compounds for biochemical studies by replacing the methyl group attached to the heterocycle in either **H1** or **H2** by a bulky fluorophore-containing chain (should hybrids **H1** or **H2** (or both) retain sufficient potency). It was thus of interest to determine if and how the position of a methyl group on the heterocycle in zampanolide-epothilone hybrids would affect their cellular activity; this would then guide the design of the fluorophore containing probes. In this context, it should be noted that for thiazole-based epothilone analogs larger substituents at position C(2) of the thiazole ring lead to significantly reduced cellular potency,^[160] while the size tolerance is substantially higher for the C(5) position of the isoxazole ring (K.-H. Altmann, personal communication).

Both **H1** and **H2** were synthesized from 13-desmethylene dactyloide alcohol (**3**) *via* oxidation with DMP and subsequent Wittig reaction of the crude aldehyde with phosphonium salts **H3**^[161] and **H4**^[162] (**Scheme 33**); the latter were obtained from chlorides **H5** and **H6** by reaction with P(Bu)₃ in DMF in 89% and 85% yield, respectively.



Scheme 33: Synthesis of **H1**, and **H2**.

Thiazole analog **H1** and isoxazole analog **H2** were obtained in 49-51% yield over two steps from 13-desmethylene dactylolide alcohol (**3**) (**Scheme 33**). Excellent stereoselectivity for the desired *E* isomer was observed in both cases. For **H1**, a separable 18:1 *E/Z* mixture was obtained in the Wittig reaction, from which **H1-E** could be isolated in 48% yield; the corresponding *Z* isomer **H1-Z** could also be isolated in 3% yield. For **H2**, only the desired *E* isomer was obtained.

The data for antiproliferative activity and the affinity for microtubule binding of zampanolide-epothilone hybrids **H1** and **H2** together with their parent compounds (–)-zampanolide (**1**) and epothilone A (**2**) are shown in **Table 12**. Compounds **H1-E**, **H1-Z** and **H2** exhibited very similar antiproliferative activity against A549 cells with IC₅₀ around 4 μM compared, which is significantly reduced compared to the *ca.* 2 nM IC₅₀ of their parental compounds **1** and **2**. The same trend was also observed for the microtubule binding affinity (K_{app}); which were in the range of 10⁴ (**H1-E**, **H1-Z** and **H2**) compared to 10⁷ for **1** and **2**. It should be noted that the binding constant for epothilone A (shown in **Table 12**) is a real binding constant (K_b instead of K_{app}), as this compound binds non-covalently to the taxane-binding site of tubulin.^[163]

Table 12. Antiproliferative activity (IC_{50})^a and apparent microtubule binding constants (K_{bapp})^b of (-)-zampanolide (**1**), epothilone A (**2**) and zampanolide-epothilone hybrids **H1-E**, **H1-Z** and **H2**.

| Cpd | IC_{50} [nM] | K_{bapp} [$10^6 M^{-1}$] |
|-------------|---------------------|------------------------------|
| 1 | 1.8 ± 0.7^c | 15.9 ± 0.6^c |
| 2 | 2.0 ± 0.38^d | 31.7 ± 3.1^e |
| H1-E | 4136.61 ± 22.36 | 0.057 ± 0.003 |
| H1-Z | 4190.72 ± 34.43 | 0.082 ± 0.014 |
| H2 | 4138.73 ± 18.24 | 0.053 ± 0.003 |

^aA549 cells were exposed to compounds for 48 h; ^bDetermined by the displacement of the fluorescent taxoid Flutax-2 from stabilized microtubules;^[134] ^cData from ref. [135]; ^dData from ref. [157]; ^eValue from ref. [163] represents a real binding constant K_b (**2** is a non-covalent binder of the taxane-binding site); ^fnot sufficient displacement in the tested concentration range (0 – 150 μM) was obtained.

2.3 Conclusion and Outlook

The first part of this PhD thesis describes the synthesis and biological evaluation of new analogs of the antimitotic marine natural product (–)-zampanolide (**1**). This work has addressed the effects of (1) backbone reduction/demethylation (analogs **R7** and **R8**); (2) the replacement of the THP moiety in **1** by other heterocycles (analogs **O4**, **O5** and **O6**); and (3) modifications of the C(19)-side chain (analogs **O7/O8**, **IM-4/IM-5/IM-6** and **H1/H2**) on microtubule-binding affinity and antiproliferative activity (**Scheme 31**).

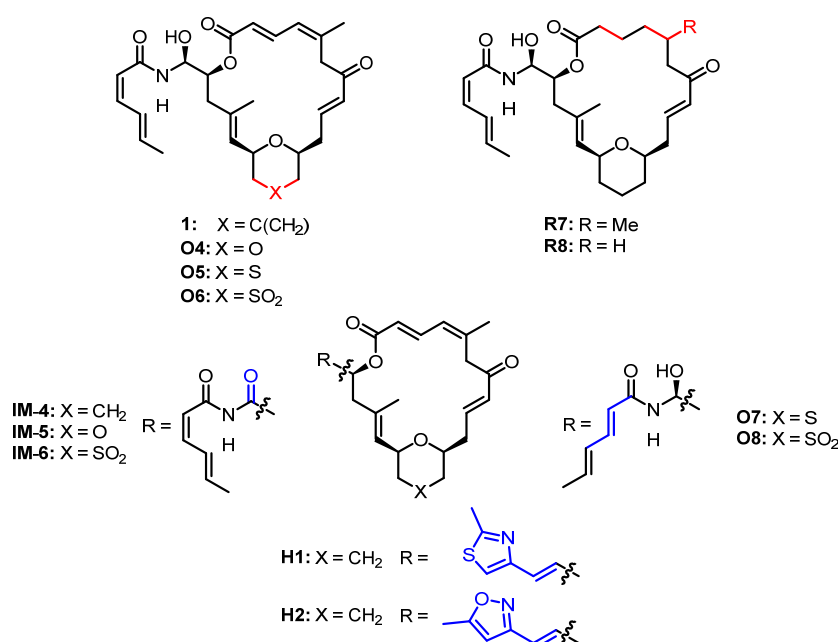
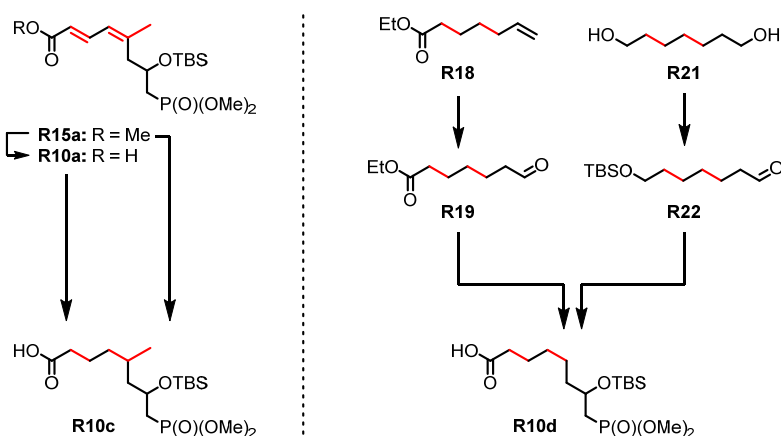


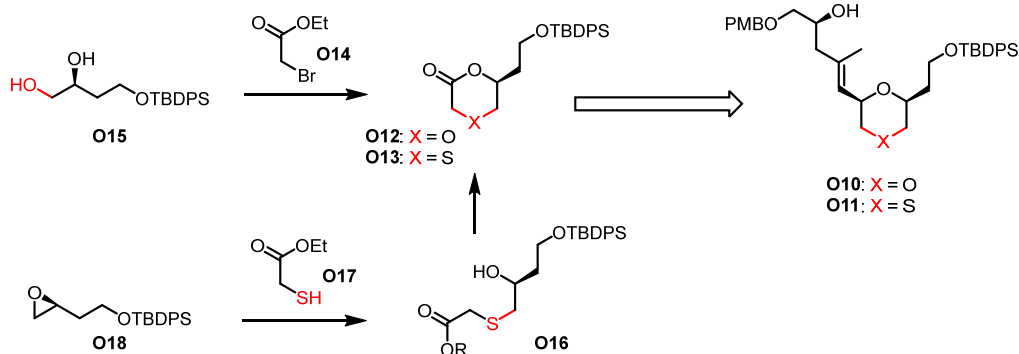
Figure 31: Structure of (–)-zampanolide (**1**), core-modified (**O4/O5/O6** and **R7/R8**) and side chain-modified (**IM-4/IM-5/IM-6**, **O6/O7** and **H1/H2**) analogs.

While the synthesis of these analogs followed the same global approach that had been established in the group for the total synthesis of the natural product, specific routes had to be developed towards the synthesis of the requisite carboxylic acid building blocks **R10c/R10d** and alcohol building blocks **O10/O11**. Fully saturated carboxylic acid **R10c** was accessed *via* reduction of known carboxylic acid **R10a** or by a reduction/hydrolysis sequence from known ester **R-15a**, in high yields in both cases. Two different approaches were elaborated towards saturated C(5)-desmethyl acid **R10d**; (1) from ethyl hept-6-enoate (**R18**) in five steps with an overall yield of 2% and (2) from heptane-1,7-diol (**R21**) in six steps with an overall yield of 23% (**Scheme 34**).



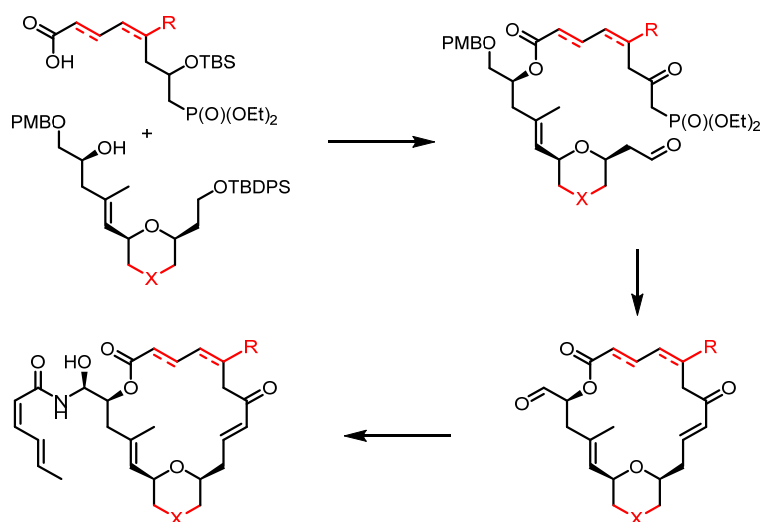
Scheme 34: Carboxylic acids **R10c/R10d** and their starting materials **R15a/R15b** and **R18/R21**.

Dioxane-containing building block **O10** was prepared in 10 steps and 16% overall yield from (*S*)-malic acid; the formation of the dioxane ring involved the regioselective alkylation of a 1,2-stannylene acetal with ethyl bromoacetate (**O14**) followed by lactonization (**Scheme 35**). Oxathiane-containing alcohol **O11** was accessed from *D*-aspartic acid in 10 steps and 18% overall yield. Here, the construction of the oxathiane ring was achieved most efficiently through a stepwise epoxide opening/lactonization sequence (**Scheme 35**).



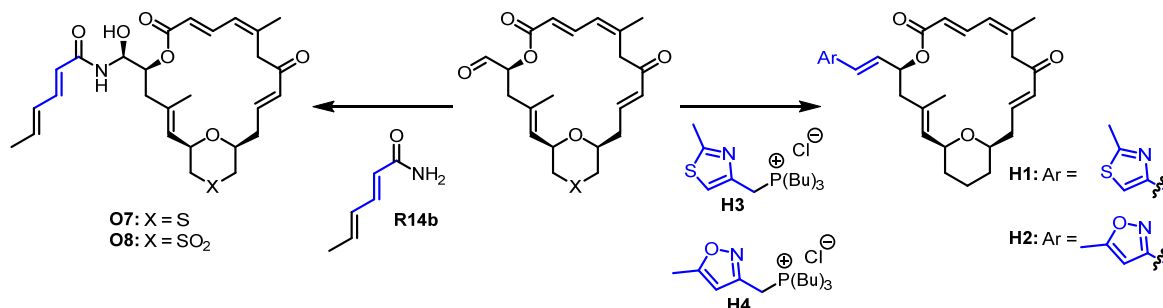
Scheme 35: Alcohols **O10/O11** and their starting materials **O15/O18**.

No major difficulties were encountered in the process of building block assembly. This attests to the robustness of the overall synthetic approach, including macrocyclization by intramolecular *HWE* reaction and side chain elaboration by stereoselective aza-aldol reaction (**Scheme 36**).



Scheme 36: Global synthetic strategy for the synthesis of all reported zampanolide analogs.

Analogs **IM-4**, **IM-5** and **IM-6** with imide-based side chains were obtained by DMP oxidation of hemiaminals **R7**, **O4** and **O6**, respectively. *E,E*-sorbamide side chain-analogs **O7** and **O8** were prepared *via* stereoselective aldol reaction between the required precursor aldehyde and *E,E*-sorbamide (**R14b**) (**Scheme 37**). Zampanolide-epothilone hybrids **H1** and **H2** were obtained *via* Wittig reaction of aldehyde **A16** and Wittig salts **H3** or **H4** (**Scheme 37**).



Scheme 37: Last step in the synthesis of analogs **O7/O8** and **H1/H2**.

The antiproliferative potencies of partially saturated analogs **R7** and **R8** were roughly 30-40-fold lower than for **1**. The reduced antiproliferative activity of these analogs correlates with their reduced (apparent) microtubule-binding affinity, which is likely caused by enhanced conformational flexibility.

In contrast, dioxane- and oxathiane-based analogs **O4** and **O5** were equipotent with **1**, while oxathiane-dioxide **O6** was 50-100-fold less active; **O7** and **O8** were 3-12-fold less potent than **O5** and **O6**. In line with their effects on cell proliferation, **O4** and **O5** both bind to microtubules with similar strength as natural (–)-zampanolide (**1**), while the sulfonyl moiety in **O6** and **O8** strongly

interferes with microtubule-binding. The molecular underpinnings of this disparate behavior will need to be elucidated; I note, however, that preliminary data by our collaborators seem to suggest that **O6** and **O8** are no longer covalent binders to tubulin or that at least their reaction with the protein is much slower than for **1**. These data need to be confirmed.

Imide-based analogs **A7-A9** were 1-2 orders of magnitude less active than **A1**. For this modification, it has yet to be determined whether the replacement of the *N*-acyl hemiaminal moiety by an imide group offers any metabolic stability advantage that might outweigh their reduced potency *in vivo*.

Surprisingly, **H1** and **H2** were found to be much less potent cell growth inhibitors than **1** and they are significantly worse binders of microtubules. This is in spite of the fact that the zampanolide and epothilone A side chains occupy highly similar positions in the structures of the corresponding tubulin complexes. The poor activity of **H1** and **H2** is difficult to rationalize at this point. An interesting question to address here, as for sulfones **O6**, **O8**, would be if **H1** and **H2** still covalently interact with tubulin. It is at least conceivable that the structural changes in **O6**, **O8**, **H1**, and **H2** could lead to changes (if ever so subtle) in the positioning of these analogs in the initial non-covalent tubulin complexes that would prevent efficient attack of the His229 side chain on the enone moiety.

In summary, the work conducted in this PhD thesis has significantly expanded the synthetic chemistry and SAR knowledge base on the marine natural product zampanolide. It needs to be seen if this natural product could indeed serve as a viable lead for drug discovery. In this context, I note that **1**, in the first *vivo* study ever published on the compound, was recently found to exhibit profound antitumor activity in tumor-bearing mice upon intratumoral administration. However, even low level *i.p.* dosing proved to be toxic and no antitumor activity was observed, but only a single tumor model was evaluated. Further studies with **1** and modified analogs would be required to determine the true potential of these compounds as antitumor agents. The work described in this PhD thesis contributes to the diversity of potent zampanolide-derived structures that could be of interest for such *in vivo* studies

3 Studies Towards the Synthesis of Core-Modified Analogs of β -Lactam Antibiotics

3.1 Introduction

The inhibition of bacterial growth and survival by clinically employed antibiotics is based on four major modes of action: Inhibition of protein synthesis, inhibition of DNA/RNA synthesis, inhibition of folate biosynthesis and inhibition of cell wall synthesis (**Figure 32**).

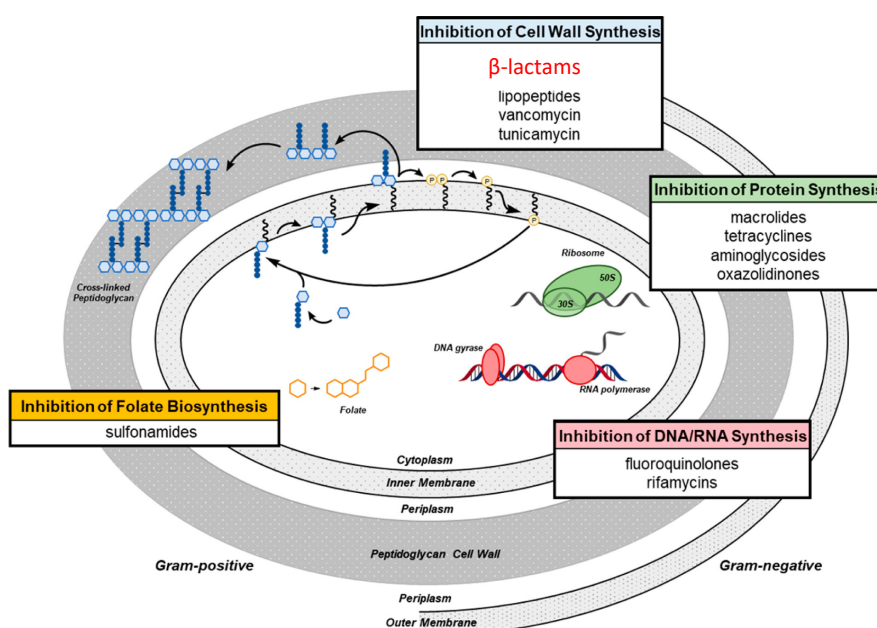


Figure 32: The four main modes of action of widely used antibiotics (adapted with permission from ref. [164]).

Inhibition of protein synthesis: Ribosomes are macromolecular machines, which are essential for protein synthesis *via* mRNA translation. The difference in the structure of the ribosomal small (30S vs. 50S) and big (40S vs. 60S) subunit between prokaryotes and eukaryotes set the basis for targeting protein synthesis by antibacterials.^[164–166] Aminoglycoside and tetracycline antibiotics bind to the small subunit,^[164,165] the former change the conformation of this subunit leading to mistranslation,^[167] the latter prevent binding of aminoacyl-tRNA and therefore inhibit mRNA translation.^[168,169] Macrolide and oxazolidinones antibiotics bind to the big subunit;^[164,165] the former primarily block the exit tunnel of the growing peptide,^[170,171] the latter bind to the A-site pocket at the peptidyl transferase center and thereby prevent the peptidyl-tRNA to be translocated from the A- to the P-site.^[172–174]

Inhibition of DNA/RNA synthesis: Quinolone antibiotics target bacterial gyrase enzymes.^[164,165] These enzymes are involved in unwinding DNA, which is essential to prevent excessive supercoiling during replication and transcription.^[175] On the other hand, differences between bacterial and eukaryotic RNA polymerases are exploited to selectively inhibit the bacterial variant by rifamycins.^[176–178]

Inhibition of folate biosynthesis: *p*-Amino benzoic acid is a precursor in the biosynthesis of folate, an essential nutrient for bacteria. Sulfonamides are structure mimics of the former, which competitively bind to dihydropteroate synthase and thus inhibit the biosynthesis of folate.^[164,165]

Inhibition of cell wall synthesis: Cross linking of the bacterial cell wall is vital, this process is inhibited by β -lactams (discussed in more detail in the next section)^[179] and vancomycin^[180] antibiotics. On the other hand, tunicamycin blocks *N*-glycosylation in the lipid carrier cycle^[181] and lipopeptides e.g. daptomycin is inserted into the cell membrane of gram-positive bacteria leading to holes in the membrane.^[182]

3.1.1 β -Lactam Antibiotics

Among the wide range of antibiotics employed for the treatment of bacterial infections, the β -lactam family is the most prominent (**Figure 33A**).^[183] As the name indicates the characteristic structural feature of β -lactam antibiotics is a four-membered ring containing a nitrogen atom and an adjacent carbonyl group (colored red in **Figure 33**). All subclasses of β -lactam antibiotics bear a second 5- or 6-membered ring fused to the β -lactam moiety, except for the monobactams. In 1928 Sir *Alexander Fleming*, in St. Mary's Hospital in London, observed that forgotten Petri dishes of a culture of *Staphylococcus* were infected by a fungus.^[184] Its morphology suggested that it was a penicillium and its characteristics resembled closely to *Penicillium rubrumm* (later corrected to *Penicillium rubens*)^[185]; intriguingly, the fungal colonies were surrounded by a transparent halo.^[184] The lysis and reduced growth of the bacterial colony in proximity of the fungus suggested an ability to produce some sort of antibacterial substance. Four years later (1932) Fleming published his findings on the antibacterial activity of a "Mould broth filtrate" from a penicillium, which he named "penicillin".^[184] In 1939 *Florey*, *Chain* and *Heatly* isolated penicillin and tested it first in mice and in 1941 treated an Oxford policeman with a severe infection, the first human to receive penicillin treatment.^[186] Even though the administration resulted in a big improvement, unfortunately, they ran out of supply and the policeman died a few weeks later. After that, other patients were treated with great success, but pharmaceutical companies in the UK were unable to produce big quantities of penicillin because of World War II commitments.^[186]

Thus, *Florey* and *Heatley* traveled to the US with their mold samples, where finally large quantities of penicillin could be produced to treat the Allied Armed Forces in 1943.^[186] Only later it became clear that "penicillin" isolated from *Penicillium* molds was a mixture of four active compounds (penicillin I-IV, **Figure 33B**).^[187,188] *Fleming*, *Chain* and *Florey* were awarded with the Nobel Prize in Physiology or Medicine in 1945 for the discovery and research on penicillin. After the discovery of penicillins, other natural β -lactam antibiotics were discovered, including the cephalosporins (cephem), clavams (oxapenam), carbapenems and monobactams (**Figure 33A**) as earlier classes.^[189]

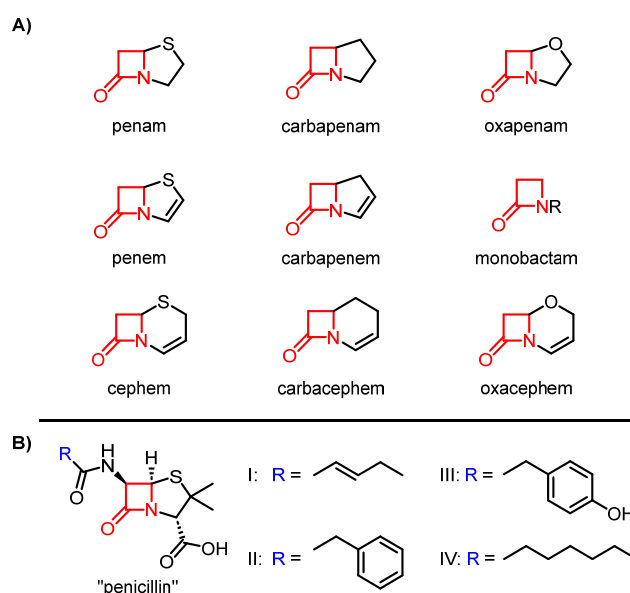


Figure 33: **A)** Core structures of β -lactam antibiotics; **B)** Structures of penicillins I-IV, active compounds in the "Mould broth filtrate" referred as "penicillin" by *Fleming*.^[184]

β -Lactams continue to be the most widely used class of antibacterials, with annual global sales of 15 billion USD in 2013, corresponding to a 65% share of the total antibiotics market.^[190,191] In particular, carbapenems possess broad-spectrum activity and high potency against Gram-positive and Gram-negative bacteria, which often make them "antibiotics of last resort".^[190,192] The global threat of antimicrobial resistance (AMR) will be discussed in more detail in section 3.1.2.

As mentioned in the previous section, β -lactam antibiotics interfere with cell wall synthesis. The bacterial cell wall is a mesh-like layer of peptidoglycan polymers. Peptidoglycan polymers are composed of disaccharide units NAG and NAM, which carry a pentapeptide side chain attached to the NAM sugar (**Figure 34**). The latter mediates essential cross-linking between peptidoglycan strands, which is critical for cell wall stability.^[193]

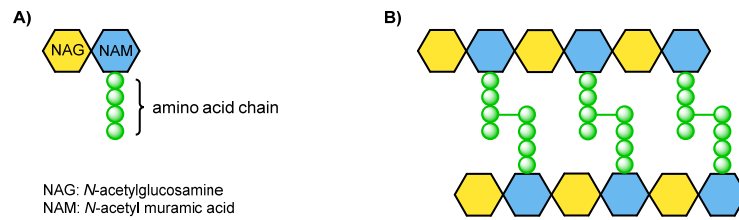


Figure 34: Schematic representation of a bacterial cell wall, NAG (*N*-acetylglucosamine) shown in yellow, NAM (*N*-acetylmuramic acid) in blue and amino acids as green spheres. **A)** Peptidoglycan monomer; **B)** Peptidoglycan bilayer with cross-linked peptide side chains. (Adapted from ref ^[193])

During cross-linking, a D-alanine residue of the donor strand is attacked by a serine residue in the transpeptidase domain of a penicillin binding protein (PBP, also called DD-peptidase) (acylation), followed by attack of the ϵ -amino group of a lysine (can differ depending on bacterial strain) residue in the acceptor strand to establish the peptide cross-link (amide bond formation) and reconstitution of the free PBP (**Figure 35A**).^[179] In the presence of compounds that are able to bind to the active site of the transpeptidase domain of a PBP crosslinking is inhibited, which ultimately leads to bacterial cell death. In the case of β -lactam antibiotics, the serine residue in the active site of the PBP attacks carbonyl carbon of the β -lactam ring, leading to ring opening and formation of a highly stable PBP ester. Therefore, the transpeptidase activity of the bound PBP is essentially eliminated (**Figure 35B**).^[179]

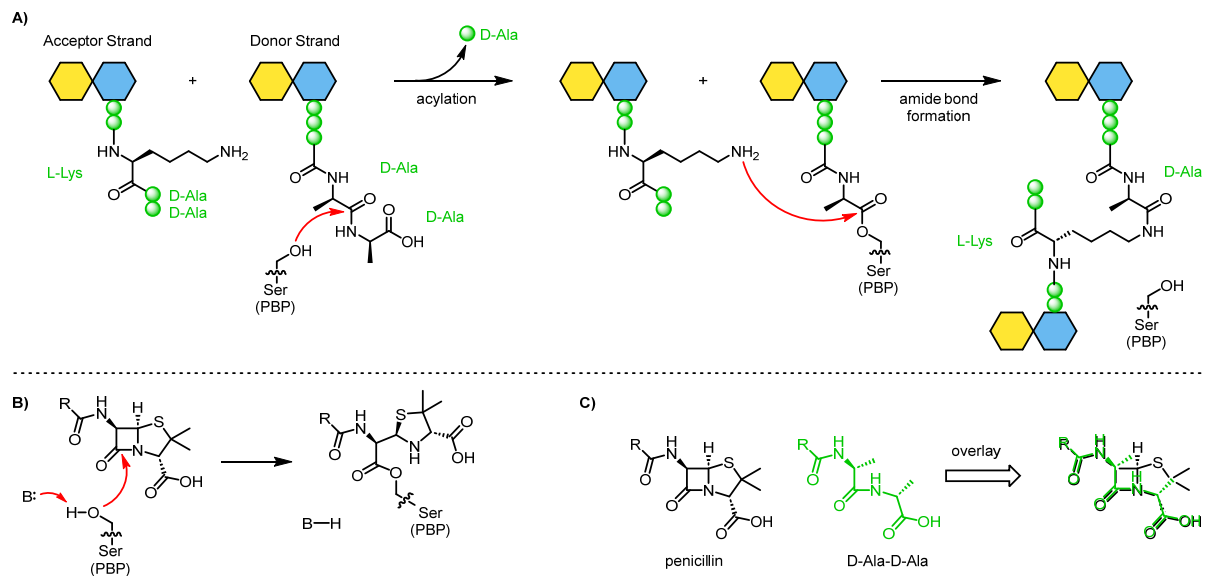


Figure 35: NAG (*N*-acetylglucosamine) shown in yellow, NAM (*N*-acetylmuramic acid) in blue and amino acids as green spheres. **A)** Exemplified mechanism of penicillin binding protein (PBP) mediated cross-linking of peptidoglycan layers. **B)** Acylation of PBP with by a β -lactam antibiotic. **C)** Structural similarity of penicillins and D-Ala-D-Ala dimer. Adapted with permission from refs. ^[179,190]

The structural similarity of penicillins and the enzyme substrate D-Ala-D-Ala unit in the enzyme substrate is the basis for the inhibition of cross-linking of PBPs by penicillins and related compounds (**Figure 35C**).^[190] On top of these structural similarities, the high electrophilicity of the carbonyl group of the β -lactam moiety is essential for potent PBP inhibition. The release of ring strain upon nucleophilic ring opening greatly contributes to the enhanced reactivity of β -lactams compared to linear amides (or amides groups in larger rings).^[190]

3.1.2 Antibacterial Resistance

Pathogens can be intrinsically resistant to antibiotics or they can become resistant by either gene mutations or plasmid mediated horizontal gene transfer.^[194] Multidrug-resistant pathogens are undermining the successful treatment of patients with bacterial infections^[195] and antimicrobial resistance (AMR) poses a major threat to human health around the globe.^[196] In 2019 an estimated 13.7 million people died because of a bacterial infection worldwide.^[197] 4.95 million of these infection-related deaths were associated with AMR.^[198] There are several mechanisms of bacterial resistance to antibiotics, which are summarized in **Figure 36**. Of these, only the inactivation of antibiotics by chemical modification is discussed, as it is the major cause of resistance against β -lactam antibiotics.

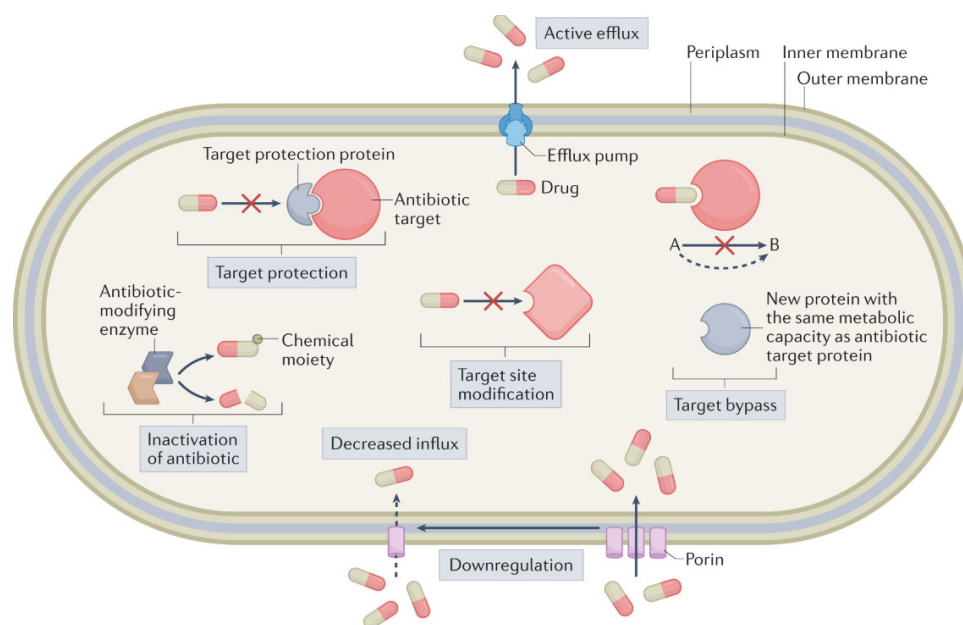


Figure 36: Overview of different mechanisms of antimicrobial resistance (reprinted with permission from ref. [194])

The inactivation of β -lactam antibiotics is mediated by different classes of β -lactamase enzymes, which open the β -lactam ring (**Figure 37**). As the hydrolysis product is unable to bind to penicillin binding proteins, the antibiotic is thus rendered ineffective.

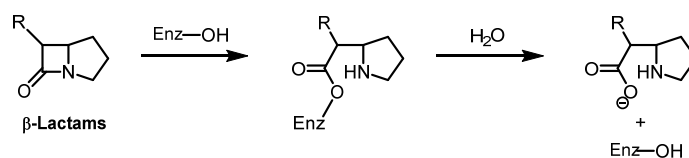


Figure 37: Mechanism of β -lactam inactivation by β -lactamases.

While this problem can often be overcome by combined treatment with a β -lactam antibiotic and a β -lactamase inhibitor, effective inhibitors are not available for all types of β -lactamases. There are four classes of β -lactamases (A-D): classes A, C and D are serine hydrolases, whereas class B members are zinc-dependent metalloenzymes.^[194] New variants of β -lactamases are discovered continuously, which increases the demand for new treatments even more. Hospitals are predestined hotspots for spreading resistant pathogens. It has been shown that longer hospital stays lead to an infection with resistant pathogens more often than short stays.^[199] Furthermore, different bacterial species within the same intensive care unit often share the same antibiotic resistance gene, in most cases a β -lactamase gene.^[200] Another cause of the resistance crisis is inappropriate prescribing; treatment indication, choice of agent or duration of antibiotic therapy incorrect resulting in an incomplete antibacterial treatment. This can lead to increased virulence and can contribute to strain diversification.^[201,202] A major driver of antimicrobial resistance is the overuse of antibiotics in animal farming, where they are used to accelerate animal growth and suppress infections/diseases within crowded herds.^[203] Despite difficulties in gathering data for the estimation of veterinary antibiotics use per country (see ref. [203] for more details), *Van Boeckel* (ETH) and co-workers were able to give an estimate of the numbers for 2020 and a prediction for 2030.^[203] In 2020 an estimated 99'502 tons of antibiotics (active ingredient) were administered globally, with China (33%), Brazil (11%; largest meat exporter in the world), USA (6%), India (5%) and Australia (4%) being on top of the list. Despite efforts of the World Organization for Animal Health (WOAH) to curtail the use of antibiotics in this sector, the predicted usage growth by 2030 is 8%.

The combination of a huge administration volume of antibiotics and the absence of promising new compounds in the pipeline,^[204] creates an urgent global public health threat and research in this field is therefore highly desirable.^[205]

3.2 1,3-Diazetidione- and β -Sultam-Based Analogs of β -Lactam Antibiotics

As highlighted above, there exists a distinct need for the discovery of new structural types of antibiotics, in order to address the global AMR threat. Within this context, it had been one of the objectives of this PhD thesis to investigate the synthesis (and eventual biological assessment) of new analogs of β -lactam antibiotics, where the β -lactam ring was replaced either by an *N*-acyl-1,3-diazetidione or a β -sultam moiety, respectively (**Figure 38**).

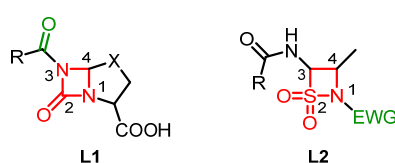


Figure 38: General structures of targeted dual penicillin binding protein/ β -lactamase inhibitors **L1** and **L2**. R = alkyl, aryl, benzyl; X = C, O or S; EWG = C(O)C(O)OH or SO₃H

Conceptually, such compounds were assumed to be sufficiently reactive to undergo β -lactam-opening and inhibit of PBPs, due to the presence of an acyl group on N(3) in **L1** and of an electron-withdrawing group on the sultam nitrogen in **L2**. At the same time, **L1** or **L2** were considered potential slowly reversible inhibitors of Ser- β -lactamases, as their reaction with the catalytic Ser residue would result in the formation of a protein-bound carbamate or sulfonic ester intermediate, respectively. The latter would be expected to be hydrolyzed much more slowly than the usual ester intermediate formed upon reaction with conventional β -lactam antibiotics (**Figure 39**; cf. also **Figure 37**).^[206]

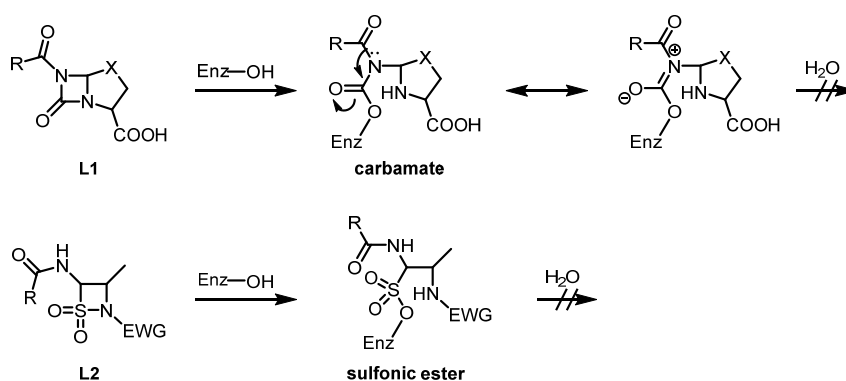


Figure 39: Proposed mechanism of inactivation of β -lactamases by generalized target structures **L1** (1,3-diazetidione, top) and **L2** (β -sultam, bottom).

Work carried out towards structures of type **L1** and **L2** will be discussed in chapters 3.2.1 and 3.2.2, respectively. However, to put this work in context, prior work on such structures will be briefly reviewed in the early sections of those chapters.

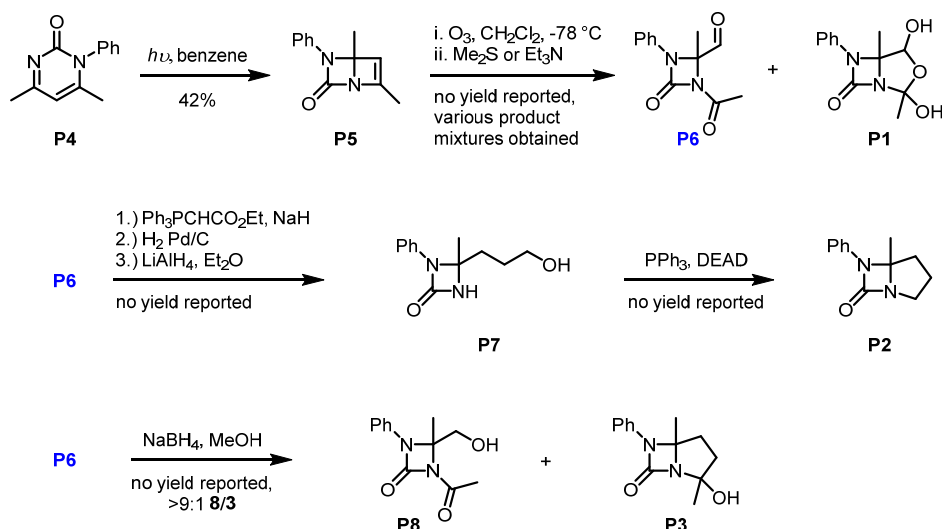
3.2.1 Studies Towards the Synthesis of 1,3-Diazetidione-based Analogs of β -Lactam Antibiotics

3.2.1.1 1,3-Diazetidiones as Potential Antibiotics: Prior work

The use of a 1,3-diazetidione moiety as a pharmacophore in new antibiotics/ β -lactamase inhibitors has been proposed previously.^[206–213] However, work in this area has mostly included computational studies;^[206–209,212,213] only very limited synthetic efforts have been reported.^[210,211] Importantly, none of these previous studies has included structures of type **L1**, bearing an acyl group on N(3) of the diazetidinone ring, which I hypothesized would impart the necessary reactivity on the internal carbonyl group.

In summary, computational studies conducted by *Nangia* and co-workers and *Muñoz* and co-workers suggested that the 1,3-diazetidione moiety based on electrostatic and structural arguments should be able to react with PBPs and Ser- β -lactamases,^[207,212] and that for the reaction with Ser- β -lactamases the resulting enzyme-bound carbamate would hydrolyze more slowly than the enzyme-bound ester resulting from β -lactam^[206,208,209,213].

Nangia and co-workers also reported the synthesis of bicyclic 1,3-diazetidiones **P1**, **P2** and **P3** (**Scheme 38**).^[210] The 1,3-diazetidione moiety in these analogs was established by a light induced electrocyclic reaction with **P4**, which provided **5** in 42% yield. Ozonolysis of **P6** followed by reductive workup gave **P6** and **P1**. The former was then elaborated into analogs **P2** in four steps and into **P3** in one step, respectively (**Scheme 38**). Noteworthy, no experimental protocols, yields or spectroscopic data were provided for most of these transformations. No biological assessment of these compounds has been reported.



Scheme 38: 1st generation of bicyclic 1,3-diazetidone compounds (**P1-P3**) by Nangia and co-workers.^[210]

In subsequent work, Nangia and co-workers also reported the synthesis of analogs **P9-P17** (Figure 40), which were again synthesized *via* intermediate **P6**.^[211] Importantly, the structures of **P10** and **P16** could be confirmed by X-ray crystallography.

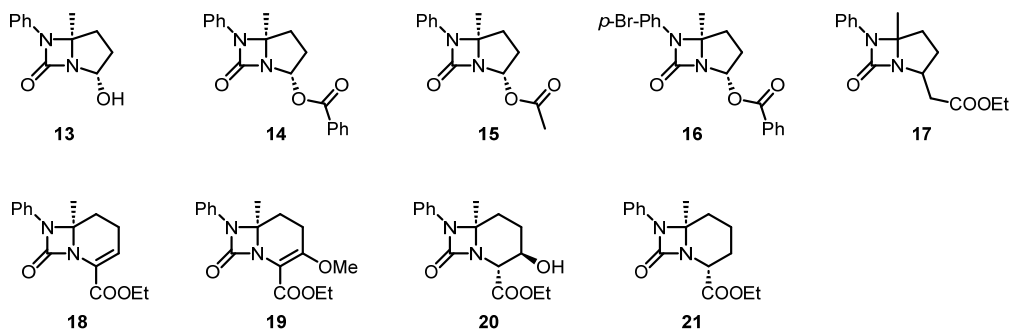


Figure 40: 2nd generation of bicyclic 1,3-diazetidone compounds (**P9-P17**) by Nangia and co-workers.^[211]

Limited data on bacterial growth inhibition by **P9-P17** are provided in ref [211]. No MICs are provided, instead, growth inhibition percentages against *Bacillus subtilis* at different concentrations (150-330 $\mu\text{g}/\text{ML}$) are compared to ampicillin and benzylpenicillin. Compounds **P10**, **P16** and **P21** showed higher inhibition percentages than ampicillin and benzylpenicillin at the same concentration. No other bacterial strains were investigated. As alluded to in ref. [211], further investigations would need to be conducted to consolidate and expand on these data.

3.2.1.2 Experimental and Theoretical Studies on the Reactions of Aliphatic Imines with Isocyanates (Publication 3)

Based on:

E. Cotter, F. Pultar, S. Riniker, K.-H. Altmann, *Chem. Eur. J.* **2024**, e202304272.^[214]

E. Cotter's contributions: conceptualization with K.-H. Altmann; synthetic investigations; publication writing with K.-H. Altmann and F. Pultar; cover page.

Introduction

The emergence of antimicrobial resistance (AMR) poses one of the major global health problems for the coming decades.^[196,215,216] To meet this threat, the development of new antibiotics is urgently required; ideally, these drugs should be based on new structural scaffolds and/or should act on new antibacterial targets in order at least to retard the emergence of resistance.^[205,217] Before this background, we have been interested in the synthesis and eventual biological investigation of core-modified analogs **D2** of natural-derived β -lactam antibiotics of types **D1a** and **D1b**, where the 3-(acylamino)- β -lactam ring is replaced by an N(3)-acylated 1,3-diazetidione moiety (**Figure 41**).

Compounds **D2** were conceived based on the hypothesis that they could still react with and inactivate penicillin-binding proteins (PBPs)^[218] but would also act as covalent reversible inhibitors of β -lactam-inactivating serine β -lactamases (classes A, C and D).^[219] Inactivation would be due to the formation of a less hydrolytically susceptible carbamate upon reaction with the active site serine.^[220,221] These general concepts have been previously advocated by others^[206–213] and their possible viability is supported by some computational^[206–209,212,213] as well as a limited set of experimental data.^[210,211] However, none of these previous studies has included analogs bearing acyl substituents on N(3) of the 1,3-diazetidione ring, which we considered important in order to enhance the reactivity of the urea type endocyclic carbonyl group in 1,3-diazetidiones. The specific target structure chosen to assess the concept outlined above, based on a combination of synthetic and bioactivity considerations, was 1,6-diazabicyclo[3.2.0]hept-2-en-7-one derivative **D3**, which is related to meropenem (**Figure 41**).

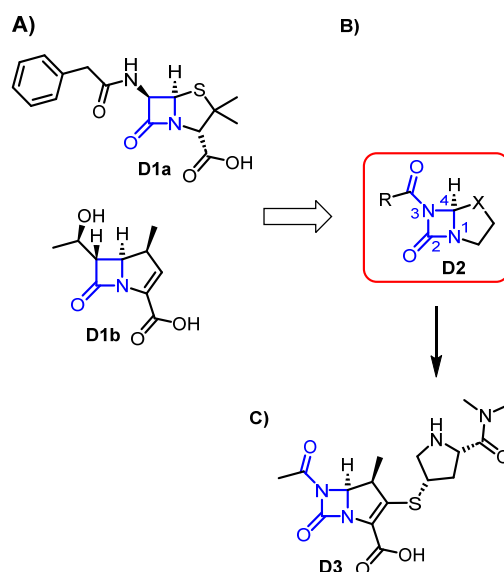
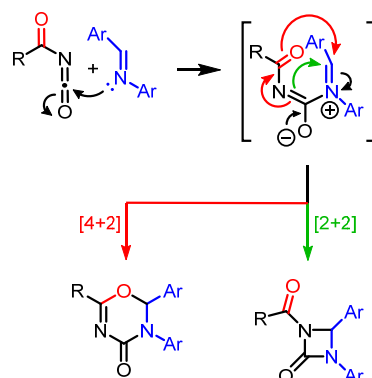


Figure 41: A) Structures of penicillin G (**D1a**) and meropenem (**D1b**) as examples of prototypical β -lactam antibiotics. B) General structure of diazetidinone-based β -lactam analogs. C) Structure of meropenem analog **D3**.

Synthetically, the *N*-acyl 1,3-diazetidione system in meropenem analog **D3** was thought to be accessible *via* [2+2]-cycloaddition of an acyl isocyanate with an appropriate imine, based on earlier studies by *Arbuzov* and co-workers in the 1960's.^[222–224] According to *Arbuzov's* findings, the reaction of acyl isocyanates with imines can either lead to 1,3-diazetidiones *via* [2+2] cycloaddition or to 2,3-dihydro-4*H*-1,3,5-oxadiazin-4-ones *via* [4+2]-cycloaddition, depending on the exact reaction conditions (**Scheme 39**). Both reactions are believed to proceed *via* a zwitterionic iminium intermediate, which is formed upon attack of the imine nitrogen on the isocyanate carbonyl. This intermediate can then progress either to a four-membered 1,3-diazetidione or a six-membered dihydro-oxadiazinone depending on the attacking nucleophile (green arrows or red arrows in **Scheme 39**, respectively). However, no dedicated mechanistic studies, either experimental or computational, have been reported for reactions between acyl isocyanates and imines. The formation of 2,3-dihydro-4*H*-1,3,5-oxadiazin-4-ones has also been observed by *Tsuge* and co-workers^[225,226] and by *Neidlein* and *Bottler*,^[227] while neither of these groups reported the formation of 1,3-diazetidiones. Although we felt encouraged by *Arbuzov's* results, we were also cognizant of the fact that all imines investigated in his studies and also those investigated by *Tsuge* or *Neidlein* were derived from substituted benzaldehydes (or once from pyridine-2-carboxaldehyde and once from pyridine-4-carboxaldehyde)^[225] and anilines.



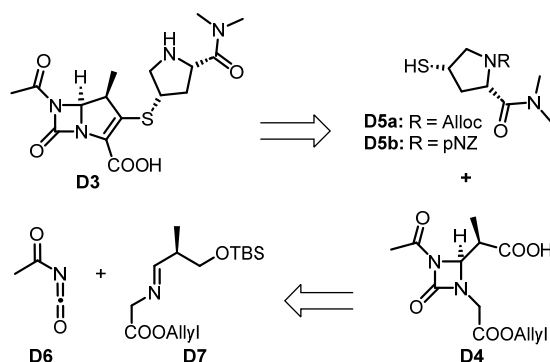
Scheme 39: Possible pathways for the reaction of acyl isocyanates with imines according to *Arbuzov* and co-workers.^[222,223]

In this paper, we now report on the reactions of acyl isocyanates with a series of imines derived from aliphatic aldehydes and allyl glycinate, which were meant to produce 1,3-diazetidiones that could be further elaborated into **D3** or related carbapenem analogs. In addition, we have also studied the reaction of these imines with differently substituted phenyl isocyanates. However, the desired 1,3-diazetidiones were never obtained; instead, the only cycloaddition products observed were those formed *via* a [4+2] reaction pathway. These experimental findings could be rationalized by DFT calculations.

Results and Discussion

Experimental work

As depicted in **Scheme 40**, meropenem analog **D3** was to be obtained from carboxylic acid **D4** and thiols **D5a** or **D5b** according to methodology that has been developed by *Kondo* and co-workers for the synthesis of 1- β -methylcarbapenems (and that will be discussed in more detail below).^[228]



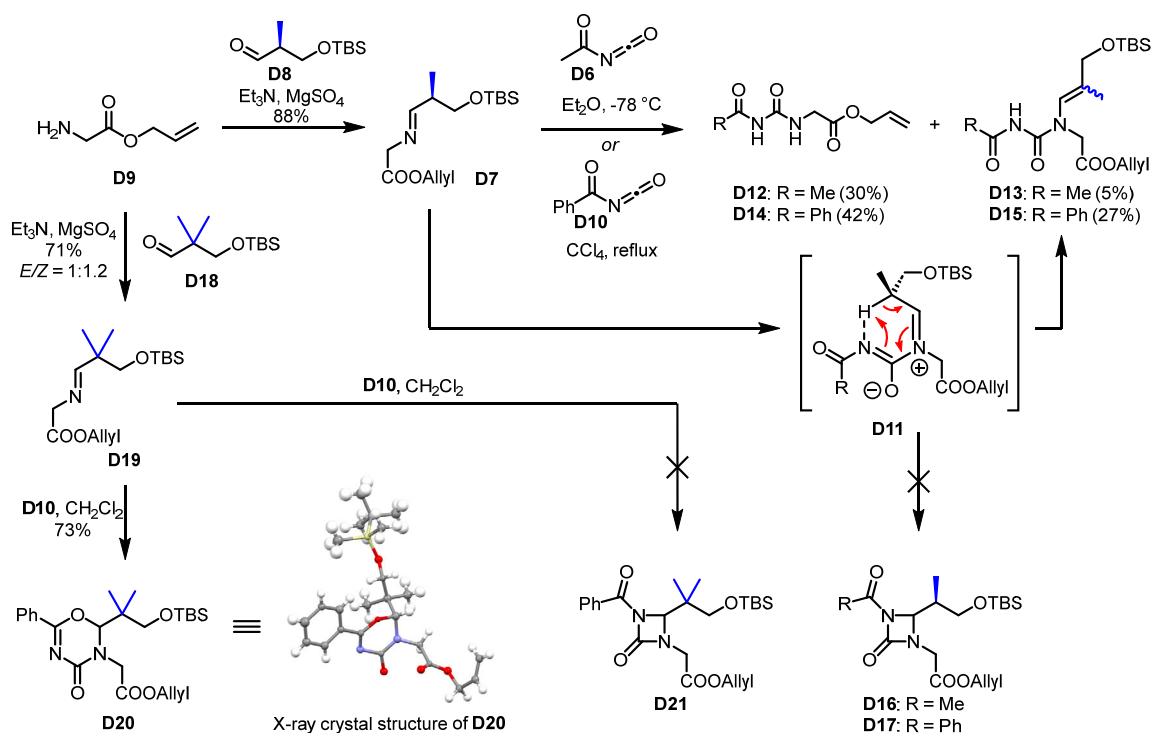
Scheme 40: Global retrosynthesis of meropenem analog **D3**. pNZ = *para*-nitrobenzyloxycarbonyl.

Following the general approach discussed above for the construction of the N(3)-acyl 1,3-diazetidione moiety, carboxylic acid **D4** was envisioned to be accessed from *in situ* generated acetyl isocyanate (**D6**) and imine **D7** *via* thermal [2+2]-cycloaddition followed by TBS-removal and oxidation.

Our synthetic work commenced with the preparation of imine **D7** from aldehyde **D8**^[229] and allyl glycinate (**D9**)^[230,231] (**Scheme 41**). Condensation of **D8** and **D9** in the presence of Et₃N and MgSO₄ gave crude **D7** in 88% yield (as a 8.3:1 mixture with **D8** (11%));⁹ while unreacted amine **D9** was removed in the aqueous work-up, attempts to remove **D8** by silica gel chromatography led to hydrolysis of **D7**.

In initial experiments, attempts to react the mixture of **D7** and **D8** with acetyl isocyanate (**D6**) (formed *in situ* from acetamide and (COCl)₂)^[232] only gave acetyl urea **D12** in 20-40% yield together with small amounts of enamide **D13** (2-5%) (after aqueous work-up). When commercial benzoyl isocyanate (**D10**) was reacted with imine **D7**, approximately equal amounts of benzoyl urea **D14** and enamide **D15** were isolated as an inseparable mixture (42% and 27% chemical yield, respectively; *E/Z* = 4:1 for **D15**) (**Scheme 41**); the structures of **D12** and **D14** were confirmed by X-ray crystallography. Importantly, the reaction of **D7** neither with **D6** nor with **D10** produced any detectable amounts of the desired diazetidinones **D16** or **D17**, respectively.

⁹ The yields reported for products that could only be obtained as mixtures with another component are true chemical yields. They were calculated based on the molar fraction of the product in the mixture as determined by NMR spectroscopy.



Scheme 41: Reactions of acyl isocyanates with imine **D7** and **D19**.^{10,11]}

Several explanations are possible for the formation of ureas **D12** and **D14**: (1) The presence of residual amine **D9** in the imine material (*vide supra*) would directly lead to urea formation by reaction with the isocyanates. (2) Alternatively, amine **D9** could be released either from imine **D7** or from putative intermediates **D11** by reaction with either residual acetamide from the *in situ* preparation of **D6** or with benzamide, which is contained in commercial preparations of **D10** (up to 20%). It should be noted, however, that commercial trichloroacetyl isocyanate, which is >95% pure, also gave the corresponding urea product. (3) Finally, ureas **D12** and **D14** may only be formed upon aqueous work-up through hydrolysis of intermediates **D11**.¹² As for the formation of enamides **D13** and **D15**, we assume that these products arise from proton loss from the initial

¹⁰ Imines **D7**, **D19**, **D30**, **D32** and **D48** are shown as *E* isomers based on literature precedent for related structures: a) W. Van Brabandt, G. Verniest, D. De Smaele, G. Duvey, N. De Kimpe, *J. Org. Chem.* **2006**, *71*, 7100–7102.; b) N. Piens, H. Goossens, D. Hertsen, S. Deketelaere, L. Crul, L. Demeurisse, J. De Moor, E. Van den Broeck, K. Mollet, K. Van Hecke, V. Van Speybroeck, M. D’hooghe, *Chem. Eur. J.* **2017**, *23*, 18002–18009; c) S. A. Shehzadi, A. Saeed, F. Lemièrre, B. U. W. Maes, K. Abbaspour Tehrani, *Eur. J. Org. Chem.* **2018**, *2018*, 78–88; and based on Nuclear Overhauser Enhancement Spectroscopy (NOESY) for compounds **D30**, **D32** and **D48**.

¹¹ Due to these limitations, no coordinates for this structure (**D20**) have been deposited in the Cambridge Crystallographic Data Centre (CCDC).

¹² Based on reaction monitoring by ¹H NMR, the ureas were already formed during the reaction. However, we cannot strictly exclude that hydrolysis of **D11** occurred in the process of taking samples and/or during NMR acquisition.

addition product **D11**, possibly through an intramolecular 1,5-proton shift to the original isocyanate nitrogen (**Scheme 41**).

It is also conceivable, however, that imine isomerization to the enamine precedes nucleophilic attack on the isocyanate or that both mechanisms are operative in parallel. Independent of the operating mechanism, the results of these orientating experiments led us to conclude that imine **7** was not a suitable precursor for the preparation of the desired diazetidinones.

Therefore, we considered it important to investigate the reaction of acyl isocyanates with imines such as **D19** (**Scheme 41**). The latter contains a *gem*-dimethyl group at the imine α -carbon,¹³ which excludes isomerization to an enamine and also prevents enamide formation from the initial putative iminium intermediate. With this alternative pathway blocked, we envisioned that diazetidinone formation would become a more favorable reaction pathway. Reaction of aldehyde **D18**^[233] with amine **D9** gave imine **D19** in 63% yield as an inseparable 5:1 mixture with **D18** (13%) (**Scheme 41**).

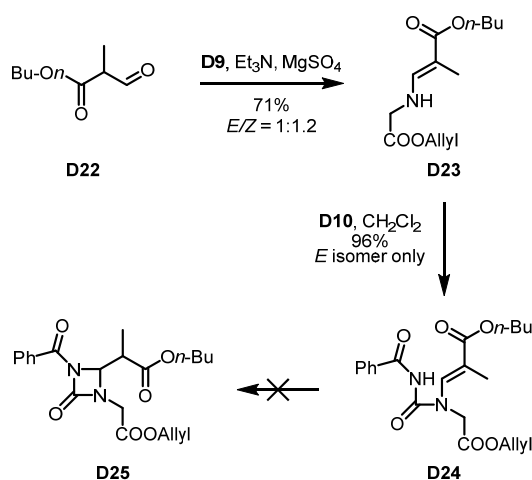
Treatment of this material with trichloroacetyl isocyanate led to a complex mixture of products, including allyl ((2,2,2-trichloroacetyl)carbamoyl)glycinate and aldehyde **D18**, along with other unidentified structures. In contrast, when imine **D19** was treated with benzoyl isocyanate (**D10**), the [4+2]-cycloaddition product **D20** was obtained in 73% yield; the corresponding [2+2]-cycloaddition product **D21** was not observed.

As discussed in the Introduction, *Arbuzov* and co-workers have reported competition between [4+2] and [2+2]-cycloaddition in the reaction of acyl isocyanates and imines^[222,223] with the preferred pathway being dependent on different reaction parameters such as temperature and solvent but also the nature of the imine and the acyl isocyanate. Unfortunately, in our case, changing solvents or temperature never led to formation of the desired 1,3-diazetidione. Although disappointing, our observations are in line with the fact that four-membered ring formation has only been reported for reactions of acyl isocyanates with imines derived from (substituted) benzaldehydes.^[222,223] It should also be noted that the spectroscopic discrimination between potential four- and six-membered ring products was challenging. For a given reaction, both types of products exhibit the same molecular mass and contain only few hydrogen atoms in the heterocyclic core, thus making analysis by ¹H or standard 2D NMR spectroscopy difficult; furthermore, no reference values for ¹³C NMR shifts are available in the literature for either type of structure. ¹⁵N NMR spectroscopy was inconclusive and, likewise, manual assignment of IR

¹³ Carbapenems with *gem*-dimethyl substitution have been reported to exhibit antibiotic activity, although actual data are not included in the corresponding publication. The compounds were simply noted "...[to exhibit] considerable activities against a number of Gram positive and Gram negative organisms": Shibuya, M.; Kubota, S. *Tetrahedron Lett.* **1981**, *22*, 3611–3614.

vibration frequencies to either an imine or a ketone moiety was ambiguous (in contrast to computational assignment, *vide infra*). Finally, although hampered by the tendency of the compound to decompose, X-ray crystallography unequivocally confirmed the six-membered ring structure of **D20**. While the quality of the crystals and their size did not allow the unambiguous assignment of atom types, the presence of a six-membered rather than a four-membered ring could be established.¹¹

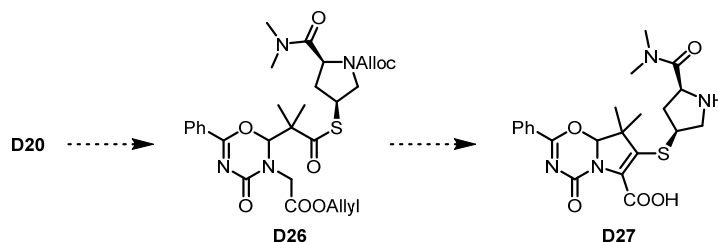
Trying to build on the insights gained from the experiments of imine **D7** with isocyanates, we also investigated the reaction of α,β -unsaturated ester enamine **D23** with benzoyl isocyanate (**D10**) (**Scheme 42**). We hypothesized that enamide **D24** that would be formed in this reaction could be induced to undergo intramolecular 1,4-addition to form a diazetidinone ring. (The use of racemic *n*-butyl ester aldehyde **D22** rather than a shorter chain alkyl ester was solely based on its more straightforward synthesis).^[234] Enamine **D23** was obtained from ester aldehyde **D22** by reaction with amine **D9** under the same conditions as those employed for the formation of **D7**; enamine **D23** was obtained as a 1:1.2 mixture of *E/Z* isomers in 71% yield (**Scheme 42**). Simple stirring of **D23** with 5 equiv. of benzoyl isocyanate (**D10**) in CH_2Cl_2 at room temperature gave enamide **D24** in excellent yield (96%) as the *E* isomer exclusively. Unfortunately, however, the compound did not undergo 4-*exo-trig* ring closure to the desired diazetidinone **D25** under any of the conditions investigated, including the addition of $\text{BF}_3\cdot\text{OEt}_2$ or various *Brønsted* bases as well as variations in solvent and temperature (see section 3.2.1.3 for details).



Scheme 42: Attempted synthesis of **D25** via intramolecular 1,4-addition.

Given the difficulties encountered while targeting the desired 1,3-diazetidiones, we turned our attention to the further elaboration of the obtained 2,3-dihydro-4*H*-1,3,5-oxadiazin-4-ones. Although not within our original target scope, we hypothesized that compounds derived from **D20** with its unusual 2,3-dihydro-4*H*-1,3,5-oxadiazin-4-one core might still be reactive with

protein nucleophiles and when embedded into the proper structural context might exhibit some β -lactamase inhibitory potential. We thus decided to pursue elaboration of **D20** into the meropenem-type dihydro-oxadiazinone **D27** (**Scheme 43**) as an alternative target structure. The synthesis of **D27** was to proceed through thioester **D26**, which would be elaborated into **D27** based on formation of the pyrroline ring *via* Dieckmann-type cyclization according to Kondo and co-workers (in analogy what had been foreseen for the synthesis of **D3**).^[228]



Scheme 43: Structure of meropenem-type dihydro-oxadiazinone **D27** envisioned to be accessible from **D20** *via* thioester **D26**.

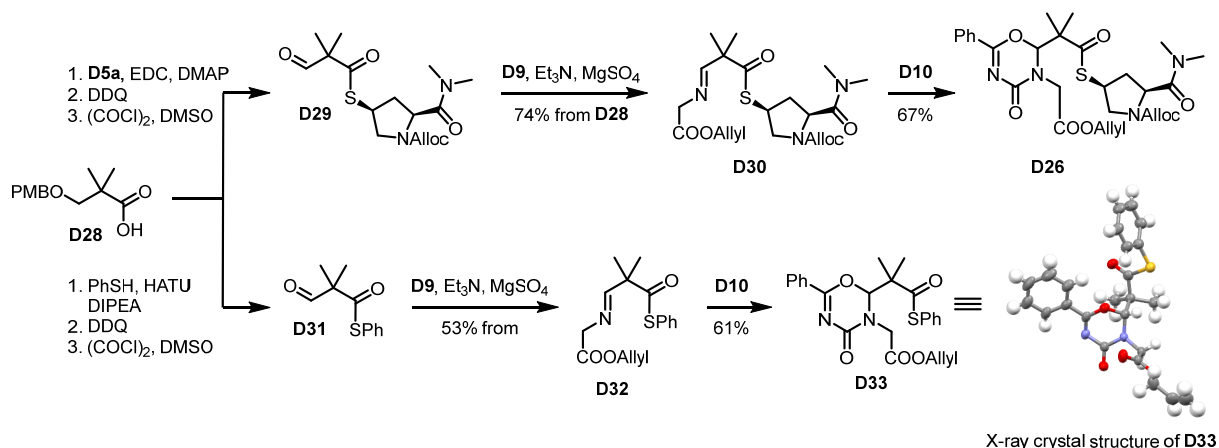
Thioester **D26** was planned to be obtained from **D20** by desilylation, oxidation of the resulting primary alcohol to a carboxylic acid, and subsequent thioesterification with **D5a** or **D5b**. However, while desilylation of **D20** with TBAF was straightforward and gave the corresponding free alcohol in 72% yield (**D55**; see experimental section 4.3.1.3), the attempted oxidation of the latter to the corresponding aldehyde with DMP or under Swern conditions only led to decomposition (not shown here).

These findings are in line with the observed instability of **D20**, which rapidly decomposed even upon storage in the freezer. In light of these observations, no further attempts were made at the conversion of **D20** into acid **D26**. Rather, an alternative strategy for the synthesis of **D27** was devised, where thioester formation was to precede the cycloaddition reaction (**Scheme 44**).

Thus, acid **D28** was obtained from the corresponding aldehyde^[235] by Pinnick oxidation followed by thioesterification with thiol **D5a** to furnish the corresponding thioester (**D58**; see experimental section 4.3.1.5) in excellent overall yield (95%). Thiol **D5a** was prepared from *trans*-4-hydroxy-L-proline in 4 steps and 40% overall yield (see experimental section 4.3.1.1).¹⁴ Oxidative cleavage of the PMB-ether with DDQ followed by Swern oxidation of the ensuing primary alcohol (**D59**; see experimental section 4.3.1.5) and condensation of the resulting aldehyde **D29** with amine **D9**

¹⁴ Thiol **D5a** has been reported in the literature multiple times, but no experimental protocols for the preparation of the compound have been published: a) Ref. [228] b) O. Sakurai, T. Ogiku, M. Takahashi, M. Hayashi, T. Yamanaka, H. Horikawa, T. Iwasaki, *J. Org. Chem.* **1996**, *61*, 7889–7894. c) M. Seki, K. Kondo, T. Iwasaki, *Synlett*, 1995, 1995, 315–316. d) K. T. M. Sungawa, A. Sasaki, H. Matsumura, K. Goda, *Chem. Pharm. Bull.* **1994**, *42*, 1381–1387. e) M. Sunagawa, H. Matsumura, A. Sasaki, H. Yamaga, Y. Kitamura, Y. Sumita, H. Nouda, *J. Antibiot.* **1997**, *50*, 621–627.

furnished imine **D30** in 74% overall yield from **D28**. Upon treatment of **D30** with 3 equiv. of benzoyl isocyanate (**D10**) in CH₂Cl₂, only the [4+2]-cycloaddition product **D26** was isolated in 67% yield (as a 7:1 mixture with benzamide); none of the [2+2]-cycloaddition product was observed.



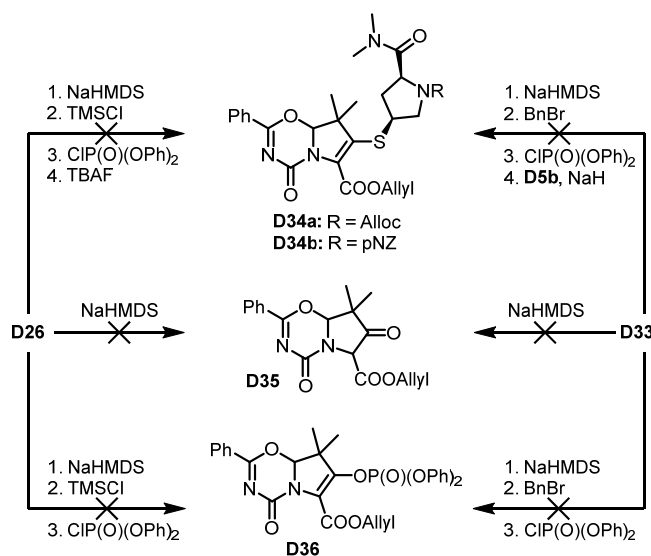
Scheme 44: Synthesis of 2,3-dihydro-4*H*-1,3,5-oxadiazin-4-ones **D26** and **D33**.^{10,15}

In analogy to Kondo's work on the synthesis of 1- β -methylcarbapenems,^[228] sequential treatment of thioester **D26** with NaHMDS, TMSCl, CIP(O)(OPh)₂ and TBAF was expected to result in 5-membered ring formation *via* Dieckmann-type cyclization followed by enol phosphate formation and re-addition of thiol **D5a** to produce **D34a** (**Scheme 45** and **Scheme 49**).

Unfortunately, none of the desired cyclization/re-addition product **D34a** was observed under these conditions. Likewise, attempts to isolate the five-membered ring either as keto ester (**D35**) or as enol phosphate (**D36**), which could have been further processed into thioenol ether **D34**, were unsuccessful (**Scheme 45**). No Dieckmann cyclization product was observed under any of the conditions investigated (see **Table 14** in section 3.2.1.3). The only identifiable products isolated from these reactions were thiol **5a** and the corresponding thiophosphate (**DS10**; see experimental section 4.3.1.5) both in ca. 15-35% yield.

To investigate if a better thiol leaving group would enable Dieckmann cyclization, phenyl thioester-containing imine **D32** was prepared from acid **D28** in analogy to the synthesis of **D26**. Reaction of **D32** with benzoyl isocyanate (**D10**) gave 2,3-dihydro-4*H*-1,3,5-oxadiazin-4-one **D33** in 31% overall yield from **D28** (**Scheme 44**). Gratifyingly, in contrast to **D20**, X-ray crystallography unequivocally confirmed the molecular structure of **D33**, including the assignment of all atom types.¹⁵

¹⁵ Crystals of **D33** contained two *N*-Alloc conformers in a 9:1 ratio. Only the major conformer is shown in **Scheme 44**, but an overlay of both conformers is shown in **Figure 56** in the experimental section 4.3.1.8.



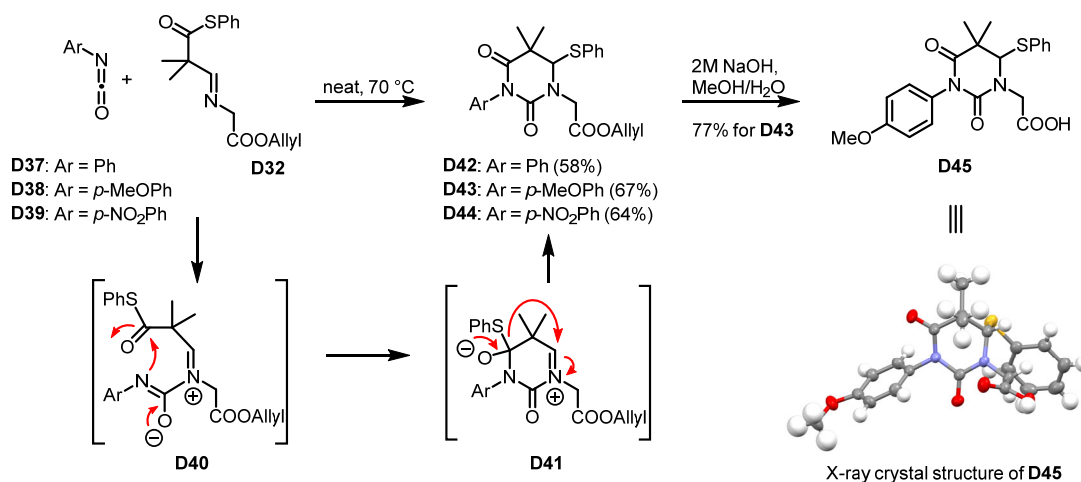
Scheme 45: Dieckmann-type cyclization attempts. pNZ = para-nitrobenzyloxycarbonyl.

Interestingly, in contrast to **D10**, trichloroacetyl or (mono)chloroacetyl isocyanate did not undergo cycloaddition under identical conditions. Unfortunately, like **D26**, thioester **D33** could not be converted into **D34b**, **D35** or **D36** (Scheme 45). The corresponding reactions only returned starting material **D33** either alone (27%) or as mixture with imine **D32**, the corresponding aldehyde and benzyl phenyl sulfide (see Table 15 in section 3.2.1.3).

In light of the complete absence of [2+2]-cycloaddition products from the reactions of imines **D19**, **D30** and **D32** with acyl isocyanates, we turned towards the evaluation of the reaction of imine **D32** with simple aryl isocyanates that lack the carbonyl group between the aryl and the isocyanate moieties, thereby rendering the undesired [4+2]-cycloaddition pathway impossible (Scheme 46). The preparation of 1,3-diazetidinsones from phenyl isocyanate and 1,2-bis-(benzylidene-amino)ethane^[236] or heterocyclic formamidines,^[237] respectively, has been reported previously. However, as for the reactions of acyl isocyanates with imines, we are not aware of any reports on the reactions of phenyl isocyanate with imines derived from aliphatic aldehydes.

In initial experiments, no reaction was observed upon treatment of imine **D32** with 5 equiv. of phenyl isocyanate at -78 °C to rt in CH₂Cl₂, Et₂O or MeCN. However, when using 5 equiv. of phenyl isocyanate (**D36**) neat, traces of a new product with the desired mass appeared and the same observation was made at 70 °C in CCl₄. Upon further variation of reaction conditions, it was found that the reaction of **D37** with 5 equiv. of neat **D41** at 70-80 °C yielded 5,5-dimethyl dihydropyrimidine-2,4-dione **D42** in 58% yield, rather than the desired diazetidinone (Scheme 46). The outcome of the cycloaddition reaction was independent of the electron-donating/-withdrawing properties of a *para* substituent on the aryl group. Similar yields of **D42**, **D43** and

D44 were obtained for the reaction of **D32** with phenyl isocyanate (**D37**), *p*-methoxyphenyl isocyanate (**D38**), or *p*-nitrophenyl isocyanate (**D39**), respectively, under identical conditions (58-64%) (**Scheme 46**).



Scheme 46: Synthesis of 5,5-dimethyldihydropyrimidine-2,4-diones **42-45**.

The structure of **D43** was unequivocally established by X-ray crystallography of the derived acid **D45**, which was obtained from **D43** by treatment with NaOH/MeOH. In accordance with the formation of **D43** from **D32** and *p*-methoxyphenyl isocyanate (**D38**), reaction of the latter with imine **D30** (neat at 70 °C) gave 5,5-dimethyldihydropyrimidine-2,4-dione **D46** in 67% yield (**Figure 42**). Importantly, the reaction of imine **D32** and benzyl isocyanate (**D47**) furnished **D48** in 59% yield (**Figure 42**), thus indicating that the formation of 5,5-dimethyldihydropyrimidine-2,4-diones from imines and isocyanates is not limited to aryl isocyanates.

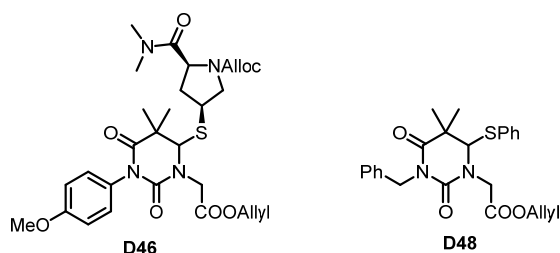


Figure 42: Products obtained from reactions of imine **D30** with *p*-methoxyphenyl isocyanate (**D38**) (**D46**) and of imine **D32** with benzyl isocyanate (**D47**) (**D48**).

A possible mechanism for the formation of 5,5-dimethyldihydropyrimidine-2,4-diones from imines **D30/D32** and aryl isocyanates **D37-D39** or benzyl isocyanate (**D47**) is depicted in **Scheme 46**. After formation of zwitterionic intermediate **D40**, the former isocyanate nitrogen attacks the thioester group to form six-membered *S,O*-hemiacetal **D41**. The latter collapses with re-

formation of the carbonyl group and ejection of a thiolate anion, which adds to the iminium moiety to give the final 5,5-dimethyldihydropyrimidine-2,4-dione. Whether the reaction takes place concerted or in a stepwise fashion would need to be determined.

The final conditions elaborated for the reactions of imines **D30** and **D32** with aryl isocyanates (neat at 70 °C, **Scheme 46**) were subsequently also applied to the reaction of **D32** with benzoyl isocyanate (**D10**), which had previously been conducted at 0 °C in CH₂Cl₂ and produced **D33** in 61% yield (**Scheme 44**). No significant change in reaction outcome was observed if **D32** was reacted neat with **D10** either at room temperature or at 70 °C; **D33** was obtained as the major product in both cases (41% yield and 54% yield, respectively). Again, no formation of the four-membered ring product was observed.

Finally, in order to determine if [2+2]-cycloaddition may occur between aryl isocyanates and imines that do not incorporate a thioester group, we investigated the reaction of isocyanates **D37-D39** with imine **D49** (**Figure 43**).

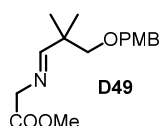


Figure 43: Structure of imine **D49**.¹⁰

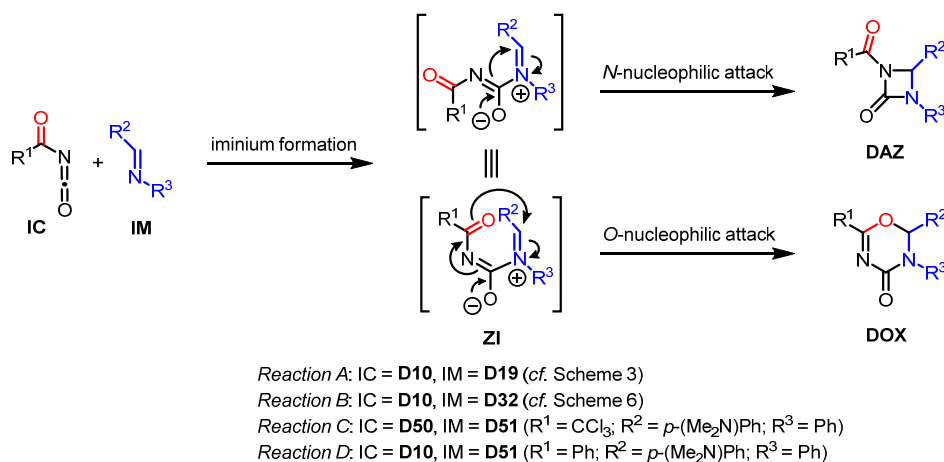
However, in no case did heating of imine **D49** with isocyanates to 80 °C either neat or in CCl₄ or ClC₂H₄Cl as solvents result in any conversion (based on reaction monitoring by ¹H NMR spectroscopy). When the temperature was raised to 200 °C, decomposition was predominant and up to 21% of the aldehyde component of the imine could be isolated next to unidentified side products.

DFT Calculations

To rationalize our experimental findings and support proposed mechanisms, we studied the reactions between benzoyl isocyanate (**D10**) and imines **D19** or **D32**, respectively (**Scheme 47**, reactions A and B), using DFT calculations. By locating all stationary points of the proposed mechanism, we can compare the barrier heights and relative product stabilities.¹⁶ For comparison, we also included the reactions of N-[4-(dimethylamino)benzylidene]aniline (**D51**) with trichloroacetyl isocyanate (**D50**) and with benzoyl isocyanate (**D10**) (**Scheme 47**, reactions C

¹⁶ We also investigated concerted mechanisms that would directly transform starting isocyanates (IC) and imines (IM) into 1,3-diazetidiones (DAZ) or dihydro-oxadiazinones (DOX). However, for all reactions investigated, we were unable to locate a corresponding transition state (results not shown). This finding, in conjunction with other products of related reactions that can be explained *via* a common zwitterionic iminium intermediate (ZI) (for example those shown in **Scheme 46**) led us to focus on a stepwise reaction mechanism.

and D), which have been reported previously by *Arbuzov* and co-workers.^[222,223] Reactions A and B were selected because they had both furnished the respective dihydro-oxadiazinones **D20** and **D33** as the major products (73% and 61% yield, respectively), which greatly simplified the computational setup.



Scheme 47: Mechanistic hypotheses considered for reactions A–D. Reactions A and B produced dihydro-oxadiazinones DOX and no 1,3-diazetidiones DAZ, while reactions C and D were reported by *Arbuzov*^[222,223] to give mixtures of DAZ and DOX.

Reactions C and D were chosen because among all examples reported by *Arbuzov*, they provided the highest levels of four-membered ring formation. It is noteworthy, however, that even for the reactions of imine **D51** with either **D10** or **D50**, formation of the six-membered ring product was competitive and could be the chief reaction pathway, depending on reaction conditions.

In the proposed mechanism, isocyanates (IC) and imines (IM) react to form an intermediate zwitterionic iminium species (ZI). *N*-Centered or *O*-centered nucleophilic attack then yields *N*(3)-acyl-1,3-diazetidiones (DAZ) or 2,3-dihydro-4*H*-1,3,5-oxadiazin-4-ones (DOX), respectively (**Scheme 47**).

Given the relative size, number of rotatable bonds, and possibly shallow potential energy surface of the reactions investigated, we anticipated the importance of rigorous conformational sampling of all species, including transition state structures. Accordingly, we set up a computational pipeline using autodE v.1.3.2^[238] with xtb/6.5.1^[239] as *lmethod* and ORCA/5.0.3^[240,241] as *hmethod*. This workflow was recently reported to perform well on a large array of organic and inorganic reaction classes,^[238] including examples with multiple low-energy conformers. Default values were used for DFT-related parameters defined by autodE except for the optimization convergence criterion, which was set to TightOpt. Furthermore, pruning of small-ring transition states was deactivated. An example Python script is provided in the SI. In brief, low energy conformers of reactants were generated with the ETKDG algorithm^[242] implemented in RDKit

v.2022.09.1.^[243] Resulting conformers were optimized using xtb v.6.5.1 (GFN2-xTB Hamiltonian)^[244] followed by ORCA v.5.0.3^[240] on the PBE0/def2-SVP^[245–247] level of theory with the RIJCOSX^[248] approximation. Dispersion interactions were included using the D3 correction^[249] with Becke-Johnson damping.^[250] Solvation effects were included using CPCM^[251] (ORCA) and the GBSA model^[252] (xtb) with parameters appropriate for dichloromethane. Transition state candidates were located *via* a constrained optimization of initial guesses generated by an adaptive path search algorithm at the same level of theory.¹⁷ Transition state conformers were generated using a randomize and relax algorithm^[238] and optimized at the same level of theory. We subsequently performed frequency calculations on the converged structures of all stationary points to confirm true minima (no imaginary frequencies). True transition states were confirmed through the presence of one strong imaginary mode connecting product and starting material.¹⁸ For final single point calculations on all stationary points, the basis set was expanded to def2-TZVP.^[253] Gibbs free energies were estimated using scaled frequencies^[254] ($\lambda_{harm} = 0.96$) and the quasi-RRHO approach.^[255] We simulated multiple replicates of each run to account for stochastic processes in the pipeline (e.g. conformer generation) and report average results. Using this approach, we successfully localized the relevant stationary points for all four reactions. **Figure 44** shows the resulting energy profiles for reactions A and C (for the energy profiles of reactions B and D and transition state structures for all four reactions and coordinate files of all stationary points consult the supporting information of the publication ref. [256] or experimental section 4.3.1.9).

Relative product stability of four-membered **DAZ-A** (i.e. **D21**, **Scheme 41**) versus six-membered **DOX-A** (i.e. **D20**, **Scheme 41**) was found to differ by around 1.1 kcal/mol. However, the barrier heights for transition state **TS-II-A** leading to **DAZ-A** was found to be 13.4 kcal/mol higher than the corresponding barrier of **TS-III-A** leading to **DOX-A**. This finding is consistent with our observation that reaction A exclusively yielded **DOX-A**, but no diazetidinone. In contrast, the corresponding barrier heights for reaction C differ by only 1.5 kcal/mol (13.1 vs. 11.6 kcal/mol), slightly favoring formation of **DOX-C**. Relative product stability, on the other hand, favors the formation of **DAZ-C** by 7.3 kcal/mol. These results are consistent with reports by *Arbuzov*^[18,19] who observed product mixtures for reaction C, with product ratios DAZ/DOX depending on solvent and temperature. Such changes in reaction parameters are expected to shift the free potential energy surface, with certain conditions favoring the formation of **DAZ-C** over **DOX-C** and *vice versa*. It is also conceivable that higher temperature might lead to thermodynamic

¹⁷ Consult the autodE v.1.0.0b3 changelog online for more information.

¹⁸ autodE uses a threshold of 40 cm⁻¹ to consider a mode significant.

product control over kinetic product control that we hypothesize is dominant at lower temperatures. Similar conclusions were derived for reactions B and D (consult the supporting information of the publication ref. [256]).

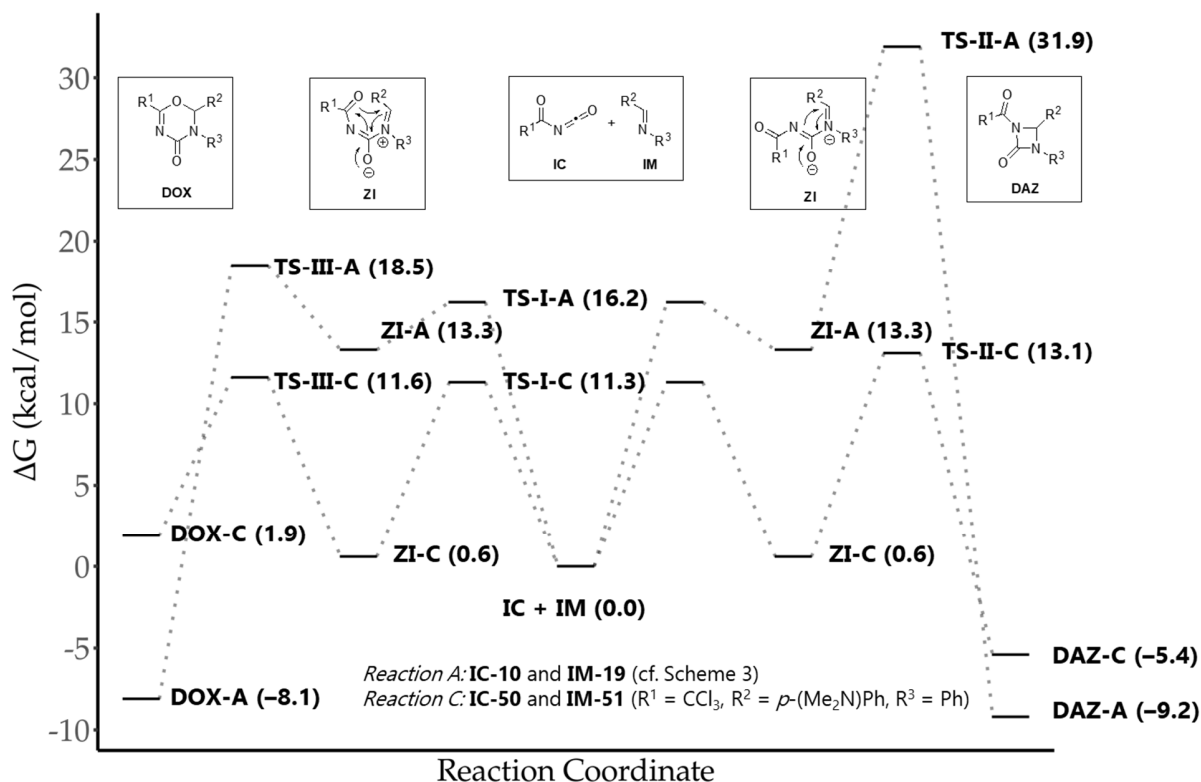


Figure 44: Reaction energy profiles for reactions A and C on the PBE0/def2-TZVP(D3BJ)-CPCM(dichloromethane) level of theory. The educt state isocyanate (IC) (IC-10 = D10 and IC-50 = D50) and imine (IM) (IM-19 = D19 and IM-51 = D51) is shown in the middle. The first step of the reaction (iminium formation, ZI) is the same for both directions. Subsequent *N*-centered nucleophilic attack to yield 4-membered ring DAZ is shown on the right, whereas *O*-centered nucleophilic attack to yield six-membered ring DOX is shown on the left. Gibbs free energies are provided in parentheses and are average values over four independent runs and reported relative to the respective starting materials IC and IM. The plot was visualized using EverPlot v.1.3.^[257] DAZ-A (D21)/DAZ-C and DOX-A (D20)/DOX-C refer to the 1,3-diazetidiones and dihydro-oxadiazinones, respectively, from reactions A and C. For transition state structures see supporting information of ref. [256] or experimental section 4.3.1.9.

While the barrier height for TS-II-B is 14.9 kcal/mol higher than for TS-III-B, the corresponding difference for reaction D is only 7.2 kcal/mol, suggesting that competitive reaction pathways could be operative for different reaction conditions. These computational results help rationalize why our attempts to access *N*(3)-acyl 1,3-diazetidiones *via* the reaction of acyl isocyanates with imines D19, D30, or D32 have remained unsuccessful. At the same time, they support the proposed mechanism outlined in Scheme 47, which might enable future improvements in this class of reactions.

Automatic IR Alignments

As alluded to earlier, it was not possible to unequivocally differentiate between DAZ and DOX products by means of ^1H and ^{13}C NMR spectroscopy due to the small number of NMR active atoms in the relevant regions of the molecules. Furthermore, the use of X-ray diffraction was limited by the availability of suitable crystals, which prevented routine assignment of reaction products. In light of these difficulties, we were interested whether a distinction between DAZ and DOX products was possible with our recently published computational workflow that relies on alignment of experimentally recorded IR spectra with theoretically predicted reference spectra of candidate structures.^[258–260] The IRSA algorithm takes the random error of theory into account alongside the experimental peak pattern. The workflow results in unbiased alignment scores that correlate with the probability of a correct match. This protocol has been successfully applied to differentiate configurational as well as constitutional isomers of a broad variety of molecules.^[258–260]

Theoretical reference spectra of structures **DAZ-A** (i.e. **D21**) and **DOX-A** (i.e. **D20**) (**Figure 45**) were obtained using a modified version of the procedure described in ref (64). In brief, conformers were generated using the ETKDG algorithm,^[261] optimized with MMFF94s,^[262,263] and clustered using the Butina algorithm^[264] as implemented in RDKit v.2022.09.1.^[243] Resulting cluster centroids were geometry pre-optimized at the RI-BP86/def2-SVP(D3BJ)^[249,250,265–267] level of theory using ORCA/5.0.3.^[240,241] Geometry pre-optimized conformers were clustered again, and remaining centroids optimized with the def2-TZVP basis set followed by frequency calculation at the same level of theory. Theoretical spectra of remaining cluster centroids were Boltzmann-weighted based on their estimated Gibbs free energy (*vide supra*) and broadened assuming a Lorenz shape and a bandwidth of 12 cm^{-1} to give theoretical references. The theoretical spectra were aligned using the published IRSA package (<https://github.com/rinikerlab/irsa>) in the range $1900\text{--}500\text{ cm}^{-1}$. **Figure 45A** and **B** show aligned reference spectra of **DAZ-A** and **DOX-A** next to the experimental spectrum of **D20**.¹⁹

The theoretical reference spectrum of dihydro-oxadiazinone **DOX-A** matches the overall peak shape of the experimental spectrum of the product obtained from the reaction of benzoyl isocyanate (**D10**) and imine **D19** (**Figure 45B**).

¹⁹ Consult the supporting information of the publication^[214] or section 4.3.1.10 for the comparison of experimental data with unaligned theoretical reference spectra. Theoretical reference spectra as well as coordinate files of geometry-optimized structures are also provided there.

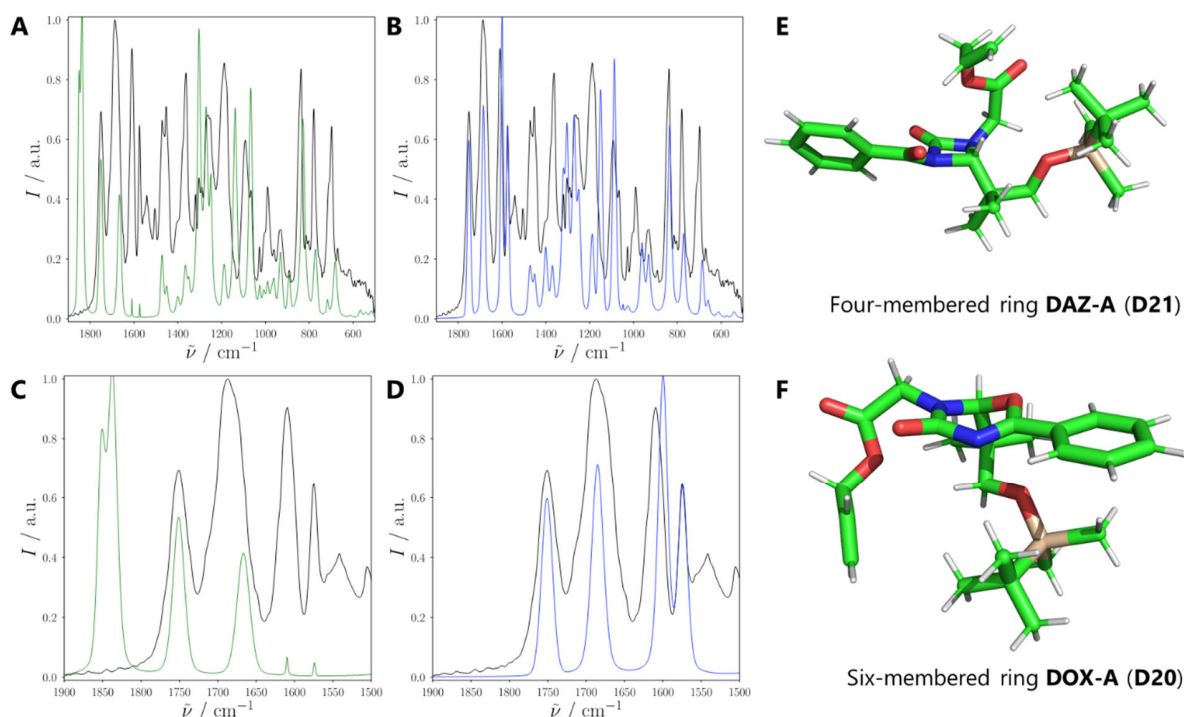


Figure 45: (A,B) IRSA-aligned theoretical spectra for four-membered **DAZ-A (D21)** (green) and six-membered **DOX-A (D20)** (blue) together with the experimentally recorded IR spectrum of **D20** (black). Alignment of the experimental spectrum with the theoretical spectrum of structure **DAZ-A** yields a Pearson coefficient $r_p = 0.01$ and Spearman coefficient $r_s = 0.13$. Corresponding values for alignment with the theoretical spectrum of **DOX-A** are $r_p = 0.19$ and $r_s = 0.38$. Inlets (C,D) of the range 1900–1500 cm^{-1} region. Further shown are low-energy conformers for **DAZ-A** (E) and **DOX-A** (F)

Especially the vibrational modes between 1900–1500 cm^{-1} (**Figure 45D**) are explained very well by the theoretical spectrum. In contrast, the theoretical reference spectrum calculated for diazetidinone **DAZ-A** matches the experimental spectrum poorly (**Figure 45A** and **C**). These ostensible differences are captured quantitatively in the Pearson and Spearman correlation coefficients r_p and r_s . While the spectrum calculated for **DOX-A** has relatively high correlation scores of 0.19 and 0.38, the corresponding coefficients are 0.01 and 0.13 for the spectrum calculated for **DAZ-A**. These findings clearly illustrate that our workflow allows the reliable distinction between DAZ and DOX products on the basis of IR spectroscopy in conjunction with computational chemistry methods.

Next, we set out to rationalize the major differences in the spectra calculated for possible structural candidates. We visualized the major modes calculated for six-membered candidate **DOX-A** in the 1900–1500 cm^{-1} part of the IR spectrum and found that they correspond to stretching vibrations of the allylic carbonyl group (1740 cm^{-1}) and the carbonyl group of the six-membered ring (DOX) (1670 cm^{-1}), as well as rocking vibrations of the subunit comprised of the heterocyclic core and phenyl side chain (1590 cm^{-1} and 1570 cm^{-1}) (**Figure 45D**). In contrast,

major bands for four-membered **DAZ-A** in the same spectral region correspond to stretching vibrations of the carbonyl group located within the four-membered ring (DAZ) (1830 cm^{-1}) as well as in the exocyclic allyloxycarbonyl (1750 cm^{-1}) and benzoyl groups (1660 cm^{-1}) (**Figure 45C**). Inspection of the geometries of low-energy conformers for **DAZ-A** and **DOX-A** (**Figure 45E** and **F**) revealed that while the exocyclic phenyl group of **DOX-A** is in the same plane as the six-membered ring (**Figure 45F**), the exocyclic benzoyl group in **DAZ-A** is out of the plane defined by the four-membered ring (**Figure 45E**). These differences in geometry suggest the presence of an extended π -system in **DOX-A** that has no correspondence in **DAZ-A**, thus offering an explanation for the presence of the two strong bands around 1600 cm^{-1} , which are absent in the theoretical spectrum of **DAZ-A**. Carbonyl groups incorporated in small rings typically show vibration frequencies at higher wave numbers than those embedded in acyclic chains or medium-sized rings. For example, *Arbuzov* reported that it was possible to distinguish the formal [2+2] adduct from the formal [4+2] adduct *via* IR band assignment of involved carbonyl groups (1780 cm^{-1} and 1690 cm^{-1} for DAZ vs. 1670 cm^{-1} for DOX).^[222,223] However, for compounds of increased structural complexity that feature additional carbonyl groups, as in the cases investigated here, and due to the scarcity of literature data for the heterocyclic cores, the magnitude of the shift was difficult to predict *a priori* without a theoretical reference. In contrast, the presented IRSA method provides a simple way to gauge experimental data against theoretical references in an unbiased way, thus aiding the structural elucidation of complex substrates.

Conclusions

This work was originally motivated by the question whether the [2+2]-cycloaddition of acyl isocyanates with functionalized imines would constitute a suitable path towards the synthesis of N(3)-acyl-1,3-azetidione-based analogs **D2** of classical β -lactam antibiotics. While the reaction of acyl isocyanates with imines derived from aromatic aldehydes and anilines has been studied in the past, their reaction with functionalized, non-aromatic imines, to the best of our knowledge, has not been investigated. Unfortunately, the projected [2+2]-cycloadditions *en route* to **D2** were not observed, at least for those pairs of isocyanates and functionalized imines that we have investigated here. While α -monosubstituted imines underwent neither [2+2] nor [4+2]-cycloaddition, [4+2]-cycloaddition did occur with α,α -disubstituted imines. These findings are in agreement with results of DFT calculations, which showed a large difference between the activation barriers for the formation of a 1,3-diazetidione (DAZ) and a 2,3-dihydro-1,3,5-oxadiazin-4-one (DOX) ring from a common zwitterionic iminium intermediate (ZI). In contrast, this difference in energy barriers was found to be significantly smaller for an acyl

isocyanate/imine pair that had been reported previously to undergo [2+2]-cycloaddition under appropriate experimental conditions.

While the six-membered ring structure of the cycloaddition products **D20** and **D33** could ultimately be assigned on the basis of X-ray crystallography, we could also show that the automated alignment of theoretical and experimental IR spectra by means of the recently developed IRSA algorithm provides an efficient approach to distinguish between 1,3-diazetidione- and 2,3-dihydro-4*H*-1,3,5-oxadiazin-4-one-derived structures.

Intriguingly, the reactions of imines bearing a thioester moiety in the 2-position with aryl isocyanates or benzyl isocyanate gave neither 1,3-diazetidiones nor dihydro-oxadiazinones; rather, these reactions produced 5,5-dimethyl-6-(aryl-/alkylthio)-dihydropyrimidine-2,4-diones in good yields. The reaction most likely follows an alternative [4+2]-cycloaddition pathway, with displacement of the thiol component of the ester in the ring-closing step followed by addition of the thiol to the iminium moiety.

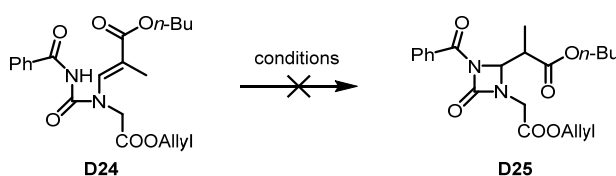
In summary, the work described here provides new insights into the reaction of isocyanates with imines, even though the envisaged 1,3-diazetidiones were not observed. Of particular note, 6-(aryl-/alkylthio)-dihydropyrimidine-2,4-diones, such as **D42-D44**, **D46** and **D48**, to the best of our knowledge, have not been reported in the literature but may be of interest as intermediates in the synthesis of new bioactive heterocycles.

3.2.1.3 Additional Information on Publication 3

In this chapter, additional experimental information is provided on the work described in the previous chapter, such as cross-referenced schemes, table, figures etc. that appear in the Supporting Information of the publication (paper 3).^[214]

Table 13 summarizes the conditions that were investigated for the attempted transformation of **D24** into **D25**.

Table 13: Screening of conditions for the projected intramolecular aza Michael addition to form diazetidinone **D25** from enamide **D24**.

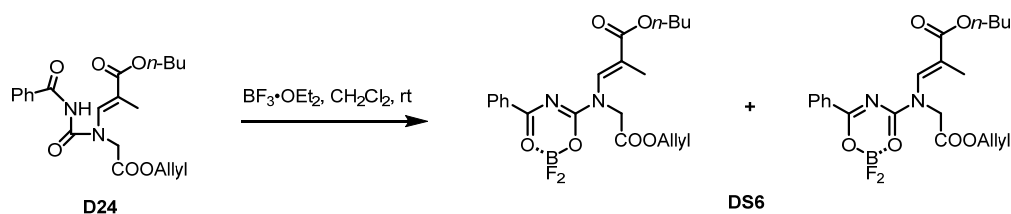


| Entry | Conditions | Time [h] | Outcome ^a |
|-------|---|----------------------------|-------------------------------------|
| 1 | DBU, CH ₂ Cl ₂ | 18 h at rt | - |
| 2 | NaOEt, EtOAc | 16 h at reflux | Hydrolyzed to D23 (76%) |
| 3 | DBU, CH ₂ Cl ₂ | 18 at reflux | - |
| 4 | DABCO, CH ₂ Cl ₂ | 3 h at rt + 16 h at reflux | Traces of D23 |
| 5 | Et ₃ N, CH ₂ Cl ₂ | 3 h at rt + 18 h at reflux | Traces of D23 |
| 6 | LiHMDS, THF | 18 h at rt + 4 h at reflux | - |
| 7 | DBU, THF | 5 h at reflux | - |
| 8 | DIPEA, CH ₂ Cl ₂ | 18 h at rt | D23 (42%) + D24 (22%) |
| 9 | BF ₃ •OEt ₂ , CH ₂ Cl ₂ | 18 h at rt | DS6 (66%) |

^a "-" refers to unidentifiable product(s).

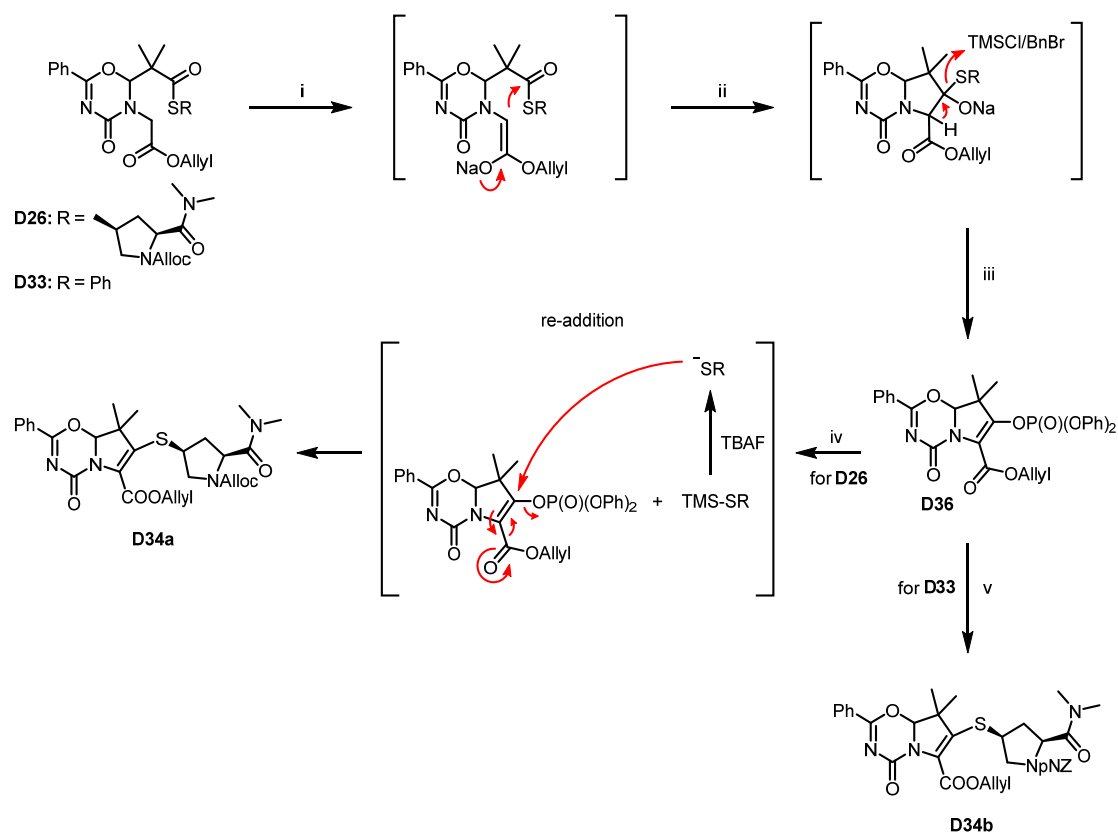
The product obtained upon treatment of **D24** with BF₃•OEt₂ in CH₂Cl₂ at rt (**Table 13**, Entry 9) was tentatively assigned structure **DS6** (2.3:1 mixture of isomers, **Scheme 48**) based on 1D-NMR

spectroscopy (^1H , ^{13}C , ^{19}F , ^{11}B), 2D-NMR spectroscopy (COSY, HSQC and HMBC), HRMS and IR-spectroscopy.



Scheme 48: Tentative structure **DS6**.

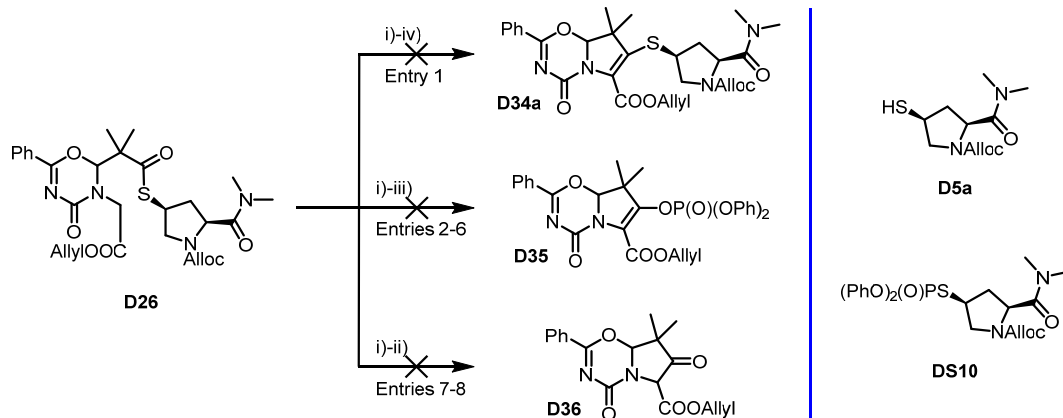
The proposed mechanism for the attempted one-pot^[24] or stepwise^[37c] Dieckmann-type cyclization of **D26** or **D33** into **D34** is depicted in **Scheme 49**.



Scheme 49: Envisioned one-pot^[24] or stepwise^[37c] Dieckmann-type cyclization, enol phosphorylation, and re-addition approach to transform **D26** or **D33** into **D34**. i) NaHMDS, THF, -30°C , 5 min; ii) TMSCl (for **D26**) or BnBr (for **D33**), -30°C , 5 min; iii) CIP(O)(OPh)_2 , 0°C , 2.5 h; iv) TBAF, DMF, 5°C , 72 h; v) **D5b**, NaH, -20°C , 2 h. (See **Table 14** and **Table 15** for screening of conditions)

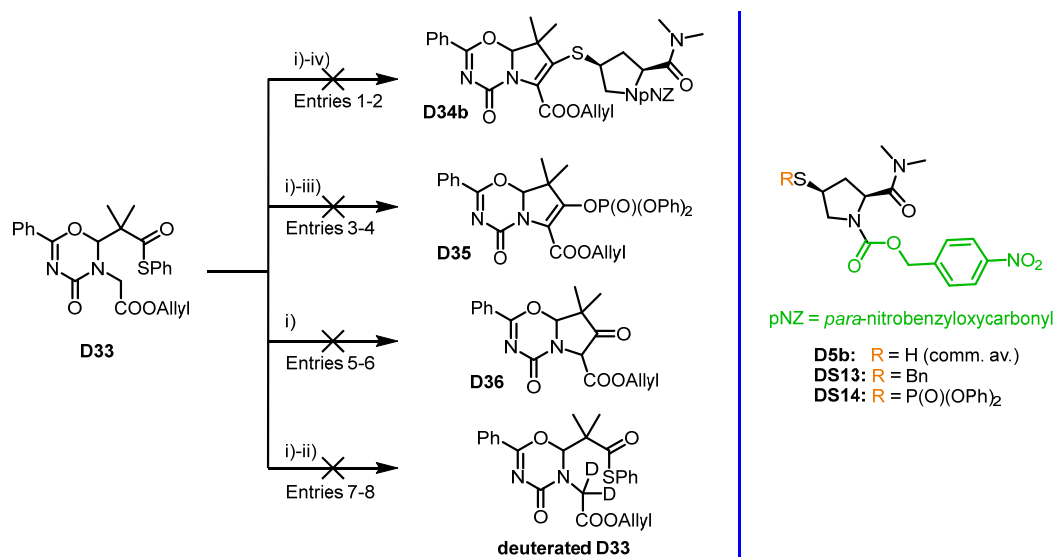
Table 14 and **Table 15** show the conditions investigated for the attempted transformation of **D26** into **D34a**, **D35** or **D36** and of **D33** into **D34b**, **D35**, **D36** and deuterated **D33**.

Table 14: Conditions for the intended Dieckmann-type cyclization of thioester **D26** towards **D34**, **D35** and **D36**



| Entry | Scale [mg] | i) | ii) | iii) | iv) | Outcome ^a |
|-------|------------|---------------------------------------|--|---|-----------------------|--|
| 1 | 170 | NaHMDS (2.2 eq.), THF, -30 °C, 5 min | TMSCl (1.1 eq.), -30 °C, 5 min | CIP(O)(OPh) ₂ (1.1 eq.), 0 °C, 2.5 h | TBAF, DMF, 5 °C, 72 h | Thiophosphate DS10 (15%) & thiol D5a (31%) |
| 2 | 40 | " | " | " | Nothing added | - |
| 3 | 80 | " | " | " | " | Thiophosphate DS10 (15%) |
| 4 | 75 | " | " | " 16 h instead of 2.5 h | " | Thiophosphate DS10 (35%) |
| 5 | 35 | NaHMDS (3.0 eq.), THF, -30 °C, 15 min | TMSCl (1.5 eq.), -30 °C, 15 min | CIP(O)(OPh) ₂ (3.0 eq.), 0 °C, 3 h | " | Traces of thiophosphate DS10 |
| 6 | 35 | " | ZnI ₂ (1.1 eq.), -30 °C, 15 min | " | " | - |
| 7 | 20 | NaHMDS (2.2 eq.), THF, -30 °C, 45 min | TMSCl (1.1 eq.), 2 h + TMSCl (1.1 eq.), 3 h -30 °C | - | " | Thiol D5a (16%) |
| 8 | 20 | NaHMDS (2.2 eq.), THF, -30 °C, 45 min | ZnI ₂ (0.6 eq.), 2 h + ZnI ₂ (0.6 eq.), 3 h -30 °C | - | " | Thiol D5a (90%, containing unknown aromatic impurities) |

^a "-" refers to unidentifiable product(s).

Table 15: Conditions for the intended Dieckmann-type cyclization of thioester **D33** for forming **D34b**, **D35**, **D36** or deuterated **D33**.

| Entry | Scale [mg] | i) | ii) | iii) | iv) | Outcome ^a |
|-------|------------|--|---|---|--|--|
| 1 | 125 | NaHMDS (2.2 eq.), THF/toluene (1:4), -20 °C, 1 h | BnBr (1.1 eq.), 0.5 h, -20 °C | CIP(O)(OPh) ₂ (1.1 eq.), -20 °C, 1.5 h | D5b (1.0 eq.), NaH (1.0 eq.), -20 °C, 2 h | Mix of D33 , Bn-S-Ph, D32 , D29 & mix of D5b , DS13 and DS14 |
| 2 | 125 | NaH (2.3 eq.), THF/toluene (1:4), -20 °C, 1 h | " | " | " | " |
| 3 | 150 | NaHMDS (2.2 eq.), THF/toluene (1:1), -20 °C, 1 h | BnBr (1.1 eq.), 0.5 h, -20 °C | CIP(O)(OPh) ₂ (1.1 eq.), -20 °C, 1.5 h | Nothing added | Mix of Bn-S-Ph & BnBr & unknown species |
| 4 | 150 | NaH (2.3 eq.), THF/toluene (1:1), -20 °C, 1 h | " | " | " | D33 (27%), D14 (11%) |
| 5 | 40 | NaHMDS (2.2 eq.), THF/toluene (1:4), -20 °C, 2 h | Nothing added | Nothing added | Nothing added | - |
| 6 | 40 | NaH (2.3 eq.), THF/toluene (1:4), -20 °C, 2 h | " | " | " | D14 (10%) |
| 7 | 70 | NaHMDS (2.2 eq.), THF/toluene (1:1), -20 °C, 3 h | Quenched with MeOD or D₂O | " | " | - |
| 8 | 70 | NaH (2.3 eq.), THF/toluene (1:1), -20 °C, 3 h | " | " | " | - |

^a "-" refers to unidentifiable product(s).

3.2.2 Studies Towards the Synthesis of β -Sultam-Based Analogs of β -Lactam Antibiotics

β -Sultams are derivatives of 1,2-thiazetidine 1,1-dioxide (**S1**, **Figure 46**) (also referred to as ethansultame), a compound that was described by *Kohler* as early as 1897, but the analytical data was limited to a melting point and elemental analysis.^[268] It was then synthesized and characterized by NMR and IR spectroscopy for the first time only in 1972 by *Berre* and *Petit* (see chapter 3.2.2.3).^[269]

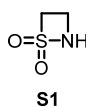
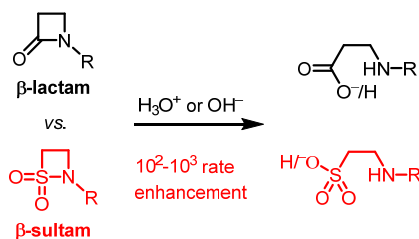


Figure 46: Structure of 1,2-thiazetidine 1,1-dioxide (**S1**).

Based on their structural similarity with β -lactams, β -sultams have been proposed in the literature as potential new antibiotics more than once.^[270–273] Quite surprisingly, however, no targeted efforts have been described towards the synthesis of β -sultam-based analogs of clinically relevant β -lactam antibiotics. In order to provide the basic background for the work performed in this PhD thesis, the reactivities of β -sultams, their relevant biological activities, and approaches towards their synthesis shall be briefly summarized in the following chapters.

3.2.2.1 β -Sultams: Structural Properties and Reactivity

Page and co-workers, in the context of extensive studies on the reactivity of monocyclic β -sultams,^[274–276] have shown that they have the capacity to inhibit Ser- β -lactamases.^[272,273,277,278] As part of this work, *Page* and co-workers found that *N*-alkyl- or *N*-aryl-substituted monocyclic β -sultams are 10^2 - 10^3 -fold more susceptible to acid- or base-catalyzed hydrolysis than their β -lactam counterparts.^[275] These experimental findings are in line with subsequent computational studies by *Novak* and co-workers,^[279] which suggest that the enhanced reactivity of *N*-substituted β -sultams compared to the corresponding β -lactams is due to a combination of less efficient resonance stabilization of the S-N bond and increased ring strain in the case of β -sultams. Interestingly, the reactivity order observed between *N*-substituted β -sultams and β -lactams is reversed for acyclic sulfonamides and the corresponding carboxamides, with the former being much less reactive than the latter; overall, *N*-alkyl/aryl substituted β -sultams are hydrolyzed 10^7 - 10^9 times faster than linear sulfonamides (**Scheme 50**).^[275]

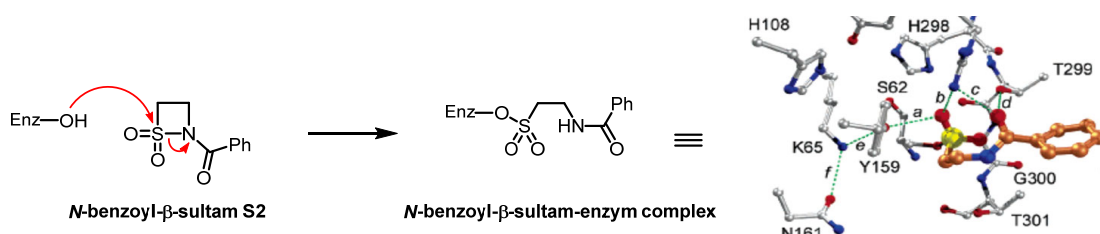


Scheme 50: Acid/base catalyzed hydrolytic ring-opening of β -lactams vs. β -sultams.^[275]

In spite of their reactivity towards $\text{H}_3\text{O}^+/\text{OH}^-$, however, *N*-aryl β -sultams do not efficiently react with other O, N, or S nucleophiles in aqueous solution, i. e. no competing alcoholysis, aminolysis or thiolysis is observed. In contrast, the more reactive *N*-benzoyl- β -sultam **S2** (Scheme 51) does undergo alcoholysis in aqueous solution, but not aminolysis or thiolysis.^[276]

3.2.2.2 Inhibition of Penicillin Binding Proteins and β -Lactamases by β -Sultams

Most importantly in the context of this PhD thesis, *N*-benzoyl- β -sultam **S2** and also *para*-substituted derivatives thereof have been shown to be active site-directed irreversible inhibitors of the penicillin binding protein DD-peptidase R61 of *Streptomyces*.^[277] The mechanism of inhibition involves nucleophilic ring opening of the β -sultam by the side chain of the active site serine of the peptidase, resulting in the formation of a stable sulfonate adduct (Scheme 51). The rate of inactivation was increased or decreased, compared to *N*-benzoyl- β -sultam **S2**, depending on the properties of the *p*-substituent of the benzoyl group; electron withdrawing groups (Cl, NO_2), respectively decreased vs. electron donating group (OMe) increased. In contrast to linear *N*-acyl sulfonamide inhibitors of Ser hydrolases, which acylate the active site serine, only S-N bond cleavage occurs in the reaction of R61 DD-peptidase with *N*-aroyl β -sultams. The formation of the serine-derived sulfonate was ultimately established by X-ray crystallography (Scheme 51). No data on the antibacterial activity of *N*-aroyl β -sultams have been reported but they have been pointed out to be "relatively hydrolytically labile", which probably impairs their activity in biological systems.^[277]



Scheme 51: Sulfonation of β -lactamases with *N*-benzoyl- β -sultam **S2** and crystal structure of the ensuing complex. (Adapted with permission from ref. [277])

N-Aroyl β -sultams **S2** and related structures have also been demonstrated to irreversibly inhibit the class C P99 β -lactamase from *Enterobacter cloacae*, while no inhibition was observed for the metallo-enzyme class B β -lactamase Bacillus cereus 569/H (BCII).^[278] As for the DD peptidase, the inhibition of the P99 lactamase involves the initial formation of a sulfonate derivative of the active site serine; however, in this case this adduct is not stable and over time undergoes β -elimination to form dehydroalanine. Again, no data are available on the performance of these compounds on bacteria.

In 2013 *Sieber* and co-workers assessed a collection of (monocyclic) β -sultam probes (**S3/S4**, **S5-S10** and **11/12**) (see section 3.2.2.3, **Scheme 53**) by activity-based protein profiling (ABBP) in *Burkholderia cenocepacia*, *B. thailandensis*, *Listeria welshimeri* and *L. monocytogenes* bacteria. Target engagement was analyzed *via* gel-based and gel-free mass spectrometry (MS); neither β -lactamases nor PBPs were found to engage in a covalent interaction with any of the tested β -sultams.^[280] Furthermore, none of the probes showed any antibacterial activity.

Apart from the probes investigated in *Sieber's* study, the only β -sultams for which testing against bacteria has been reported are **S13** and **S14** (**Figure 47**), which were found to be inactive.^[270,281] It should be noted, however, that the β -lactam analog of **S13**, i. e. penicillanic acid, is also devoid of antibacterial activity.

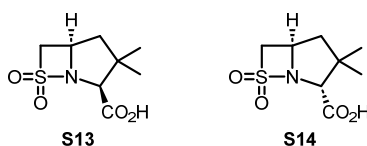


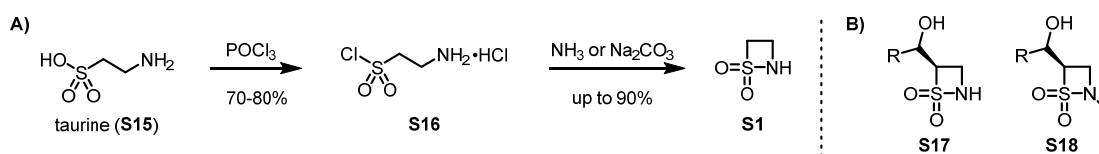
Figure 47: Structures of **S13** and **S14**.

Notwithstanding the latter finding, the data summarized in this section clearly indicate that appropriately designed β -sultams could hold the potential to be dual PBP/ β -lactamase inhibitors. All studies so far were conducted with simple β -sultams, which do not resemble a β -lactam antibiotic in its substitution pattern and its whole structural complexity. In fact, no targeted efforts toward the synthesis of β -sultam-based analogs of clinically used β -lactam antibiotics have been reported. As has also been pointed out by *Page* and co-workers the rates of either PBP or β -lactamase inactivation by β -sultams could be improved by incorporating appropriate protein recognition elements into their structures.^[277] At the same time, such modifications could also reduce the susceptibility of such compounds towards hydrolysis, thus enhancing their stability in biological systems.

3.2.2.3 Literature Precedents of Synthesis of β -sultams

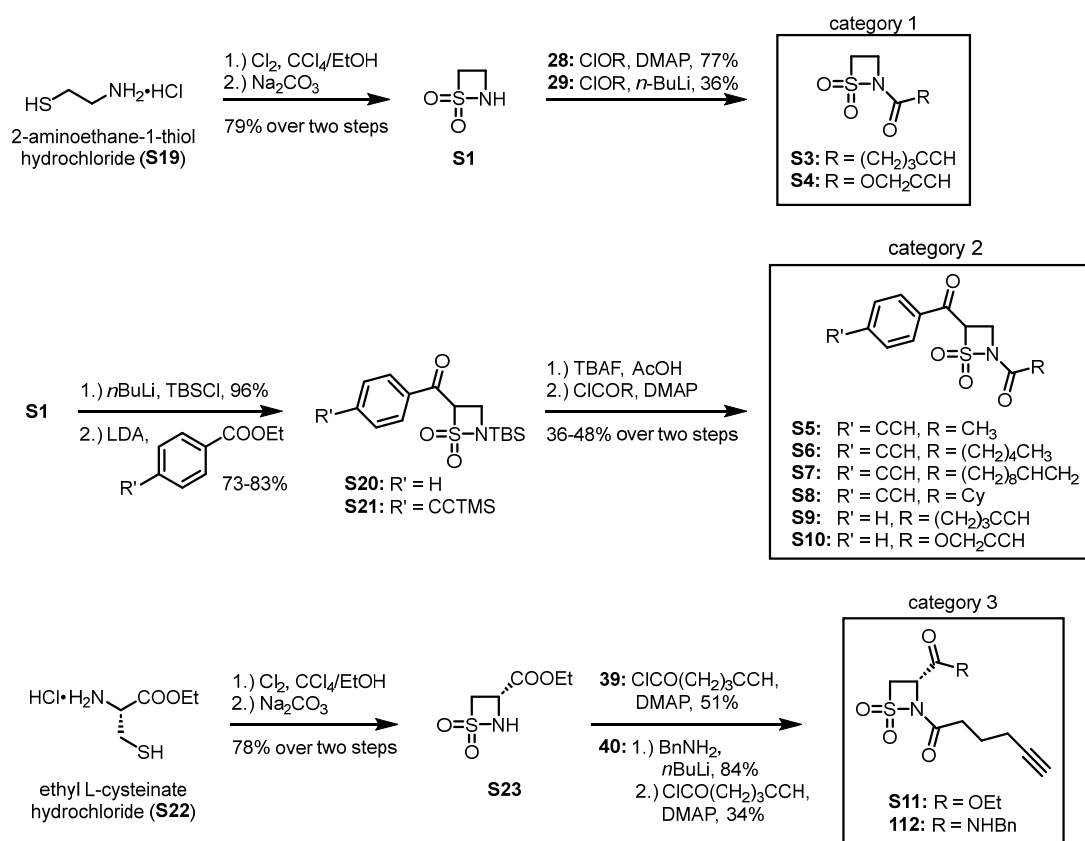
This section focuses on synthetic approaches, which were relevant for this thesis, rather than covering all synthetic efforts reported towards β -sultams. For a more general summary on (β -)sultam chemistry consult reviews in refs [271,282,283].

As previously mentioned, *Berre* and *Petit* reported the synthesis and characterization by NMR and IR spectroscopy of 1,2-thiazetidine 1,1-dioxide (**S1**, **Scheme 52A**) in 1972.^[269] Chlorination of taurine (**S15**) gave **S16**, which was submitted to base-catalyzed cyclization to afford **S1** in up to 72% yield. Following the same lines, *Otto* and co-workers synthesized mono and bicyclic β -sultams. They also made major contributions in exploring chemistry around this structural moiety.^[49,284–294] Apart from preliminary investigations on the antibacterial potency of 4-(α -hydroxyalkyl)- β -sultams (in the type of **S17** and **S18**, **Scheme 52B**), which showed no activity, no other biological assays were reported.^[292]



Scheme 52: A) First synthesis of 1,2-thiazetidine 1,1-dioxide **S1**;^[269] **B)** 4-(α -hydroxyalkyl)- β -sultams **S17** and **S18**.^[292]

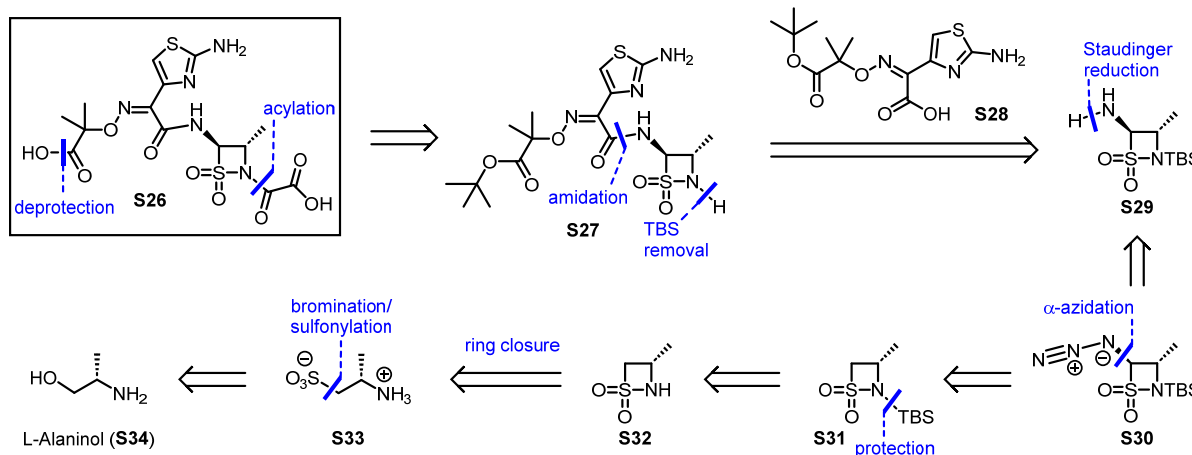
In 2013 *Sieber* and co-workers synthesized a collection of β -sultams (**Scheme 53**). 2-Aminoethane-1-thiol hydrochloride was sequentially chlorinated and cyclized to give β -sultam **S1** in 79% yield over two steps. The secondary amine of the β -sultam moiety of **S1** was acylated either with hex-5-ynoyl chloride or with ethynyl carbonochloridate to give **S3** (77%) and **S4** (36%) respectively. These two compounds built category 1. Key intermediate **S1** was also used for the synthesis of the compounds belonging to category 2 (**S5-S10**). Thus, **S1** was *N*-TBS-protected followed by α -acylation with ethyl benzoate or ethyl 4-((trimethylsilyl)ethynyl)benzoate to give **S21** and **S22** in 73-83% yield. These intermediates were desilylated and acylated with various acyl chlorides to deliver compounds **S5-S10** in 36-48% yield over two steps. Category 3 compounds were obtained following the same overall synthetic strategy as for compounds of category 1, but the synthesis commenced from ethyl L-cysteine and analog **S24** required an additional amidation step with benzylamine.



Scheme 53: Synthesis and structures of β-sultams **S3/S4**, **S5-S10** and **S11/S12** by Sieber and co-workers.^[280]

3.2.2.4 Objective

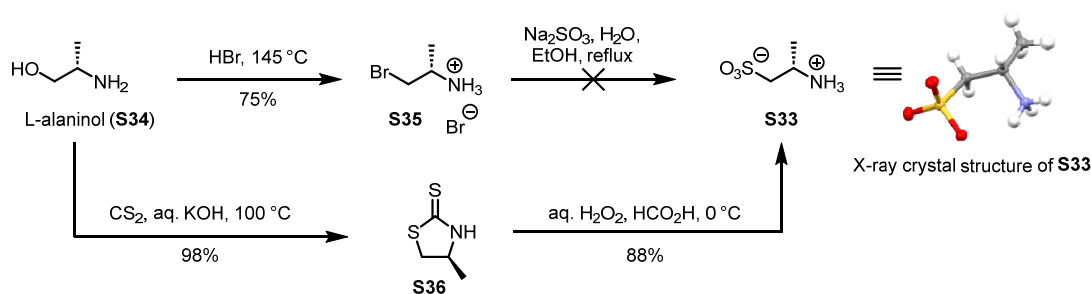
The synthetic strategy of β-sultam **S26** was to be based on its previously reported synthesis by Otto and co-workers.^[286] Commercially available L-alaninol (**S34**) would be sequentially brominated and sulfonated to give sulfonic acid **S33**, which would be cyclized to give **S32** in a next step (**Scheme 54**). The nitrogen of the β-sultam would be TBS-protected leading to **S31**. A first key step would be the α-azidation to give azide **S30**. Primary amine **S29** would be obtained *via* a Staudinger reduction. Amidation of commercially available acid **S28** and amine **S29** followed by TBS-removal would deliver **S27**. The latter would be acylated at N(1) followed by hydrolysis of the *tert*-butyl ester to furnish β-sultam **S26**.



Scheme 54: Retrosynthesis of monocyclic β -sultam analog **S26**.

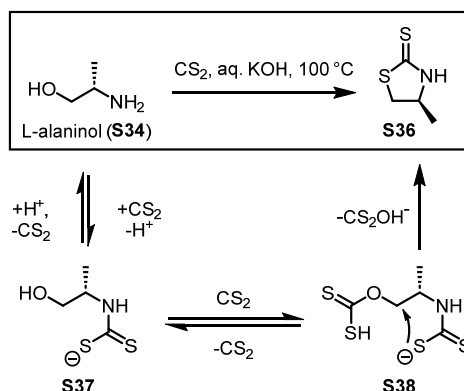
3.2.2.5 Synthesis of (*S*)-3-Methyl Ethylsultam (**S32**)

The synthesis of **S32** commenced with the bromination of L-alaninol (**S34**) with aqu. HBr (48%) at 145 °C,^[295] which furnished alkyl bromide **S35** in 75% chemical yield as an inseparable mixture with unreacted L-alaninol (**S34**) (3:1) (**Scheme 55**). Attempted sulfonation of **S35** by treatment with 0.6 equivalents of sodium sulfite in H₂O/EtOH under reflux, as reported by *Prager* and co-workers,^[296] did not afford sulfonic acid **S33**. Employing an excess of sodium sulfite (3.0 eq.) under otherwise similar conditions, as reported by *Otto* and co-workers,^[286] was likewise unsuccessful. A two-step approach towards **S33** from L-alaninol, *via* thiazolidine-2-thione **S36**, has been reported by *Xu* and co-workers (**Scheme 55**).^[297] Following *Xu*'s approach, reaction of L-alaninol with carbon disulfide in aqu. KOH at reflux delivered **S36** in 98% yield. Oxidation and hydrolysis of the latter with *in situ* formed performic acid in water then afforded **S33** in excellent yield (88%).



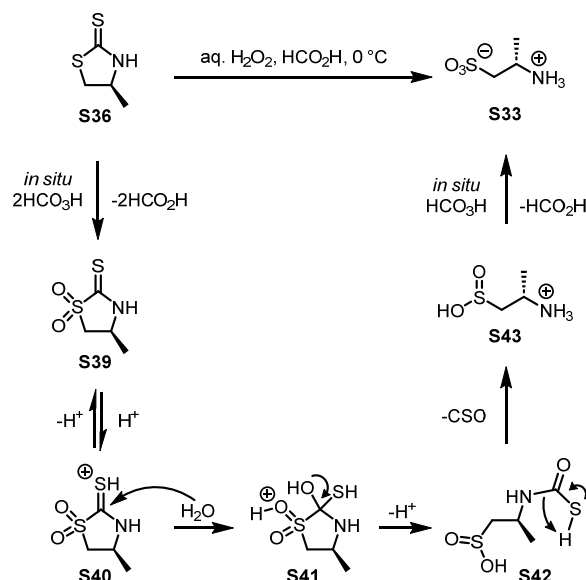
Scheme 55: Synthesis of sulfonic acid **S33** starting from L-alaninol (**S34**).

A proposed mechanism for the transformation of L-alaninol (**S34**) into thiazolidine-2-thione **S36** is shown in **Scheme 56**.^[298] Dithiocarbamic acid **S37** can react with a second molecule of carbon disulfide to give **S38**, which undergoes intramolecular nucleophilic substitution to deliver the desired **S36** and loss of hydrogen dithiocarbonate.



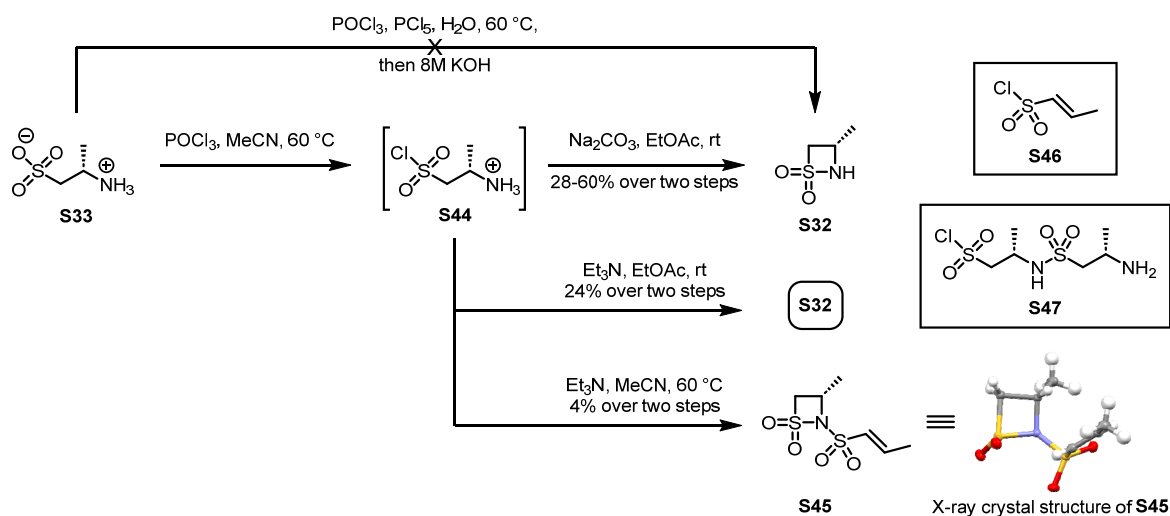
Scheme 56: Proposed mechanism for the transformation of L-alaninol (**S34**) into thiazolidine-2-thione **S36**.^[298]

Xu and coworkers have proposed a mechanism for the oxidation of **S36** to sulfonic acid **S33** (**Scheme 57**).^[297] According to this proposal, performic acid oxidizes **S36** to thiazolidine-2-thione 1,1-dioxide **S39**, which undergoes acid-catalyzed addition of water to form tetrahedral intermediate **S41**. The latter undergoes ring-opening to yield **S42**, which forms sulfinic acid **S43** by loss of carbonyl sulfide. Finally, the latter is oxidized to sulfonic acid **S33**.



Scheme 57: Proposed mechanism for the transformation of thiazolidine-2-thione **S36** into sulfonic acid **S33**.^[297]

Submitting **S33** to a one-pot chlorination-cyclization sequence with POCl₃, PCl₅ and aqu. KOH, as reported by *Otto* and coworkers for the synthesis of **S32**, gave only traces of the desired *β*-sultam **S32** (**Scheme 58**).^[286] It was also attempted to isolate **S44**, but it was not clear if the chlorination was successful, as analysis by ¹H-NMR spectroscopy and TLC was not conclusive. At this point, it was not clear, if **S32** had not been formed or if the workup conditions might have led to hydrolysis or loss of product in the aqueous phase. Thus, a slightly different approach was pursued^[299] that involved reaction of **S33** with POCl₃ in acetonitrile at 60 °C, isolation of **S44** by trituration with Et₂O after solvent removal and cyclization of the latter with either Na₂CO₃ or Et₃N in ethyl acetate (**Scheme 58**). Both bases performed comparably on a 0.3 g scale and delivered **S32** in yields of 28% and 24%, respectively. Only Na₂CO₃ was used for scale-up and the yield of **S32** increased with increasing scale: 28% (0.15 g), 44% (1.0 g), and 60% (4.0 g) over two steps from **S33**. Interestingly, when Et₃N was directly added to the reaction mixture obtained from **S33** and POCl₃ after 10 hours, no **S32** could be isolated. The only product obtained after FC, albeit in very low yield (4%), was **S45** (**Scheme 58**). The latter was believed to be formed upon sulfonylation of **S32** with *in situ* formed vinyl sulfonyl chloride **S46**. The latter could originate from an Et₃N-catalyzed elimination of the sulfonamide moiety in **S47** (dimerization product of **S44**). The structure of **S45** was confirmed by means of X-ray crystallography (**Scheme 58**).

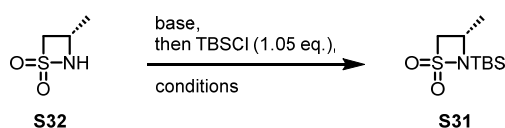


Scheme 58: Synthesis of *β*-sultam **S32** from **S33**.

3.2.2.6 Studies Towards the Synthesis of Amine **S29**

In preparation of the functionalization of the C(4) position in **S32**, the protection of the sulfonamide nitrogen in **S32** was investigated. *Otto* and co-workers reported the *N*-TBS-

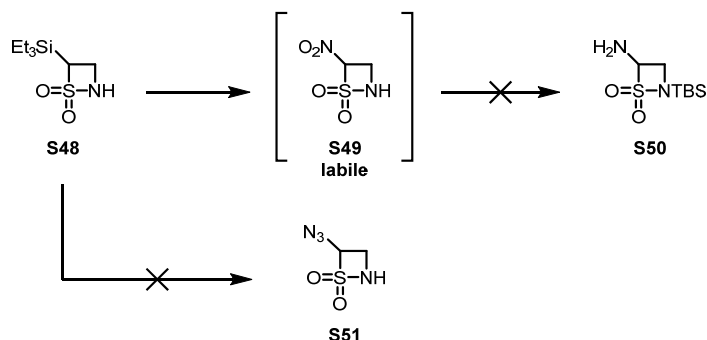
protection of similar β -sultams *via* deprotonation with *n*-BuLi in THF at -78 °C and subsequent reaction of the resulting anions with TBSCl to afford the respective *N*-TBS derivatives in 49-71% yield.^[286] The same conditions were also used by *Sieber* and co-workers for the *N*-silylation of 1,2-thiazetidine 1,1-dioxide (**S1**) in 96% yield (*cf.* **Scheme 53** in section 3.2.2.3). However, when **S32** was sequentially treated with *n*-BuLi and TBSCl, **S31** was only obtained in 33% and 11% of **S32** was reisolated (**Table 16**, Entry 1). Performing the deprotonation with *t*-BuLi or LDA instead of *n*-BuLi, gave **S31** in 50% and 60% yield, respectively, and virtually no **S32** was re-isolated (**Table 16**, Entries 2 and 3). When **S32** was pre-treated with Et₃N in CH₂Cl₂ for 10 min and then reacted with TBSCl at rt for 48 h; **S31** was obtained in 52% yield and 11% of **S32** could be re-isolated (**Table 16**, Entry 4). Increasing the scale of the reaction with LDA as base led to increased yields of **S31** of 86-98% under otherwise identical reaction conditions (**Table 16**, Entries 3 and 5-7).

Table 16: Conditions investigated for the TBS-protection of **S32**.

| Entry | Scale | Base | Conditions | Yields of S31 and S32 |
|-------|--------|--------------------------------------|--|-----------------------|
| 1 | 25 mg | <i>n</i> -BuLi (1.05 eq.), 10 min | THF, -78 °C, 4 h | 33%, 11% |
| 2 | 21 mg | <i>t</i> -BuLi (0.60 eq.), 10 min | THF, -78 °C, 1 h | 50%, <1% |
| 3 | 24 mg | LDA (0.60 eq.), 10 min | THF, -78 °C, 1 h | 60%, 0% |
| 4 | 50 mg | Et ₃ N (1.20 eq.), 10 min | CH ₂ Cl ₂ , rt, 48 h | 52%, 11% |
| 5 | 300 mg | LDA (1.05 eq.), 10 min | THF, -78 °C, 4 h | 86%, 5% |
| 6 | 500 mg | LDA (1.05 eq.), 10 min | THF, -78 °C, 3 h | 95%, 0% |
| 7 | 500 mg | LDA (1.05 eq.), 10 min | THF, -78 °C, 2 h | 98%, 0% |

With sufficient material of **S31** in hand, its projected α -azidation was investigated next. Unsuccessful attempts at α -azidation or α -amination of β -sultam **S48** have been previously reported by *Szymonifka* and *Heck* (**Scheme 59**).^[300] On the other hand, α -silylation and α -methylation of ethylsultam (**S1**) proved to be possible. Furthermore, *Otto* and co-workers, *Page*

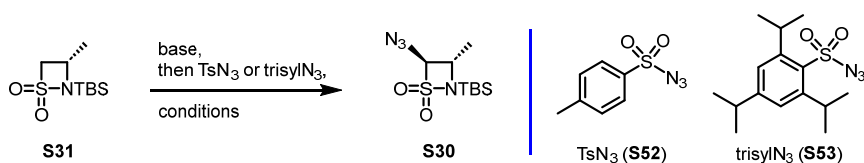
and co-workers and *Sieber* and co-workers all have reported the successful α -acylation, α -silylation and α -methylation of *N*-protected ethylsultam analogs.^[280,285,286]



Scheme 59: Attempted α -azidation or α -amination of β -sultam **S48** by *Szymonifka* and *Heck*.^[300]

When **S31** was treated with LDA in THF at $-78\text{ }^{\circ}\text{C}$ for 2-30 min followed by addition of TsN_3 (**S52**) (11 wt% commercial solution in toluene), no **S30** was observed and part of the starting material was re-isolated (**Table 17**, Entries 1-3). In addition, partial desilylation of **S31** to **S32** occurred. Similar results were obtained with *t*-BuLi or NaH as bases and when applying higher temperatures (**Table 17**, Entries 3-6). In order to exclude potential problems with the quality of the commercial TsN_3 (**S52**) solution, experiments were also carried out with trisyl N_3 (2,4,6-triisopropylbenzenesulfonyl azide) (**S53**).^[301,302] The latter was synthesized from 2,4,6-triisopropylbenzenesulfonyl chloride and NaN_3 in one step.^[302] However, as with **S52**, the formation of **S30** was not observed with **S53**.

Table 17: Conditions investigated for the attempted α -azidation of **S31**.

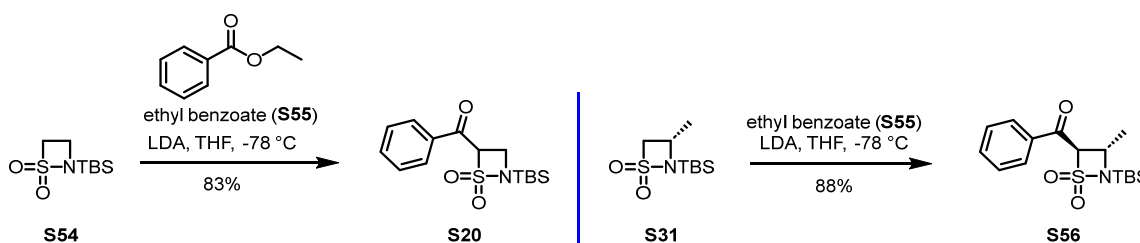


| Entry | Scale | Base | Conditions | Yields of S30 , S31 and S32 |
|-------|-------|--|---|--|
| 1 | 50 mg | LDA (1.1 eq.), 2 min | TsN_3 (1.1 eq.) THF, $-78\text{ }^{\circ}\text{C}$ to rt, 18 h | 0%, 20%, 27% |
| 2 | 30 mg | LDA (<i>in situ</i>) (2.0 eq.), 30 min | TsN_3 (2.5 eq.) THF, $-78\text{ }^{\circ}\text{C}$ to rt, 18 h | 0%, n.d. ^a |

| | | | | |
|----|-------|-------------------------------------|--|-----------------------|
| 3 | 30 mg | <i>n</i> -BuLi (1.3 eq.), 15 min | TsN ₃ (2.0 eq.) THF, -78 °C to rt, 18 h | 0%, 22%, 0% |
| 4 | 30 mg | <i>t</i> -BuLi (1.3 eq.), 15 min | TsN ₃ (2.0 eq.) THF, -78 °C to 50 °C, 18 h | 0%, 10%, 36% |
| 5 | 30 mg | NaH (1.3 eq.), 15 min | TsN ₃ (2.0 eq.) THF, -78 °C to 50 °C, 18 h | 0%, n.d. ^a |
| 6 | 30 mg | NaH (0.9 eq.), 15 min | TsN ₃ (2.0 eq.) THF, -78 °C to 50 °C, 18 h | 0%, n.d. ^a |
| 7 | 20 mg | NaH (1.1 eq.), 15 min | trisylN ₃ (1.3 eq. as solution) THF, -78 °C to 50 °C, 18 h | 0%, n.d. ^a |
| 8 | 20 mg | KHMDS (1.1 eq.), 15 min | trisylN ₃ (2.0 eq. as sol.) THF, -78 °C to 50 °C, 18 h | 0%, n.d. ^a |
| 9 | 20 mg | NaH (1.1 eq.), 15 min | trisylN ₃ (1.5 eq. as solid) THF, -78 °C to 50 °C, 18 h | 0%, n.d. ^a |
| 10 | 20 mg | KHMDS (1.1 eq.), 15 min | trisylN ₃ (1.5 eq. as solid) THF, -78 °C to 50 °C, 18 h | 0%, n.d. ^a |

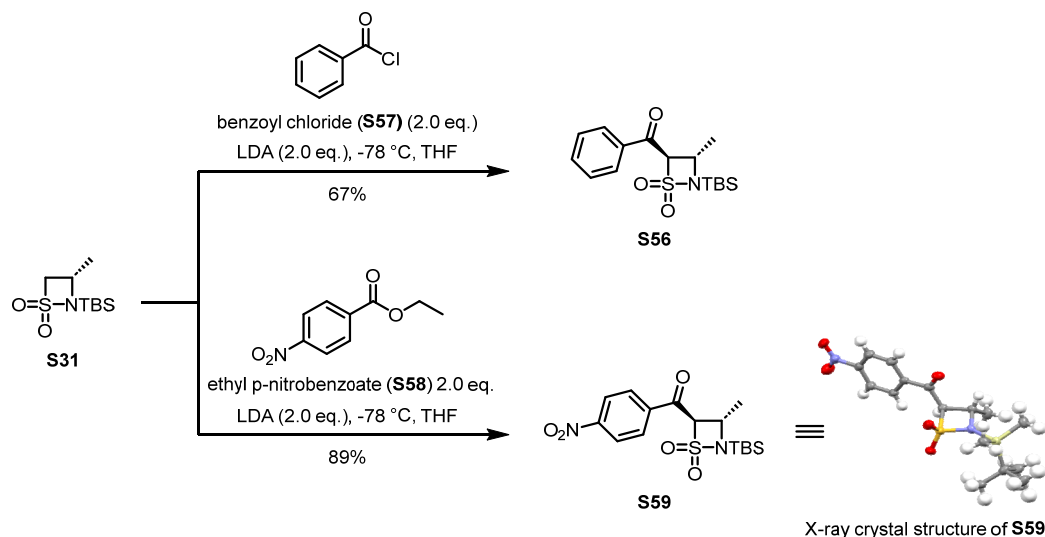
^a n.d. = not determined, ¹H-NMR spectrum of crude product after aqu. workup showed no hint for product formation, thus no isolation efforts were conducted.

In order to determine, if the intended α -deprotonation of **S31** did indeed occur, experiments were performed where **S31** was reacted with base and the reaction was quenched with deuterated solvents. Unfortunately, these experiments remained inconclusive. However, as shown in **Scheme 60**, α -benzylation of **S31** under the conditions reported by *Sieber* and co-workers for the benzylation of *N*-TBS ethanesultam (**S54**) with ethyl benzoate (**S55**) (LDA, ethyl benzoate (**S55**), THF, -78 °C; cf. **Scheme 53** in section 3.2.2.3) proceeded smoothly and yielded **S56** in 88% yield as a single diastereoisomer. This finding indicates that lack of deprotonation could not have been the cause of the failed azidation attempts with **S31**.

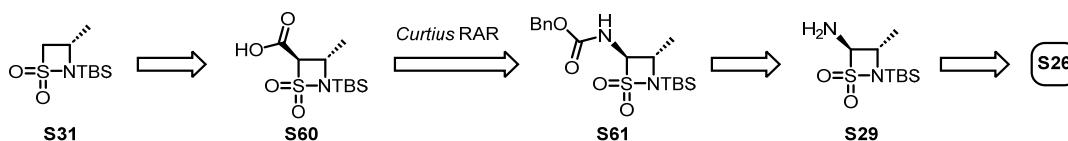


Scheme 60: Reported benzylation of **S54** to give **S20**^[280] and benzylation of **S31** to give **S56**.

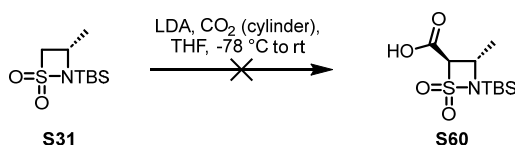
Aroylation of **S31** was also possible with benzoyl chloride (**S57**), to give **S56** in 67% yield, and with ethyl *p*-nitrobenzoate (**S58**), to furnish **S59** in 89% yield (**Scheme 61**). The structure of **S59** was confirmed by X-ray crystallography. Thus, as expected, acylation occurred *trans* to the methyl group.



As α -azidation of **S31** had been unsuccessful, but α -acylation was readily possible, a revised strategy towards **S29** was devised. According to this modified approach, **S31** would be converted into carboxylic acid **S60**, either directly or *via* an ester intermediate, which would be transformed into carbamate **S61** by means of a *Curtius* rearrangement (**Scheme 62**). The latter, would be converted into primary amine **S29** and elaborated into **S26** as outlined in **Scheme 54** in section 3.2.2.4.



As *Otto* and co-workers had described the successful carboxylation of **S54** with LDA/CO₂,^[285] these conditions were also explored for the synthesis of **S60** from **S31**. However, the attempted carboxylation of **S31** with LDA and CO₂ remained unsuccessful (**Scheme 63**).

**Scheme 63:** Attempted carboxylation of **S31** to give **S60**.

As an alternative to the direct carboxylation of **S31**, **S60** was then considered to be accessed *via* methyl ester **S62** (**Scheme 64**). To this end, **S31** was treated with *in situ* formed LDA for 2-30 min and either dimethyl dicarbonate, methyl cyanofomate or methyl chloroformate were added to the reaction mixture at $-78\text{ }^{\circ}\text{C}$ in THF (**Table 18**). Using dimethyl dicarbonate as the electrophile did not yield **S62** (**Table 18**, Entry 1); similar observations were made when methyl cyanofomate (Mander's reagent, used for selective C-acylations)^[303] was used (**Table 18**, Entry 2). Gratifyingly, the use of methyl chloroformate (2 eq.) and LDA (2 eq.) did result in the formation of **S62**. However, the compound was obtained as an inseparable mixture with the doubly acylated product **S63** in 40% and 22% yield, respectively (**Table 18**, Entry 3). This mixture was submitted to LiOH-mediated hydrolysis to deliver carboxylic acid **S60** in 25% yield over two steps (**Scheme 64**). The structure of **S63** was confirmed by X-ray crystallography (**Scheme 64**); likewise, the four-membered ring structure of **S60** was confirmed by X-ray crystallography, but the quality of the crystals and their size did not allow the unambiguous assignment of atom types. Lowering the amount of LDA (1.1 eq. vs. 2.0 eq.) and methyl chloroformate (1.3 eq. vs. 2 eq.) led to lower yields of **S62** and **S63** (**Table 18**, Entry 4 vs. Entry 3). The conditions from **Table 18**, entry 3 gave the best result and were therefore were used for the reaction on a 300 mg scale (vs. 20 mg in **Table 18**, entry 3). Disappointingly, the reaction gave **S62** in 12% and **S63** in 56% chemical yield as an inseparable mixture. Thus, the reaction could not be scaled up efficiently for these particular reaction conditions.

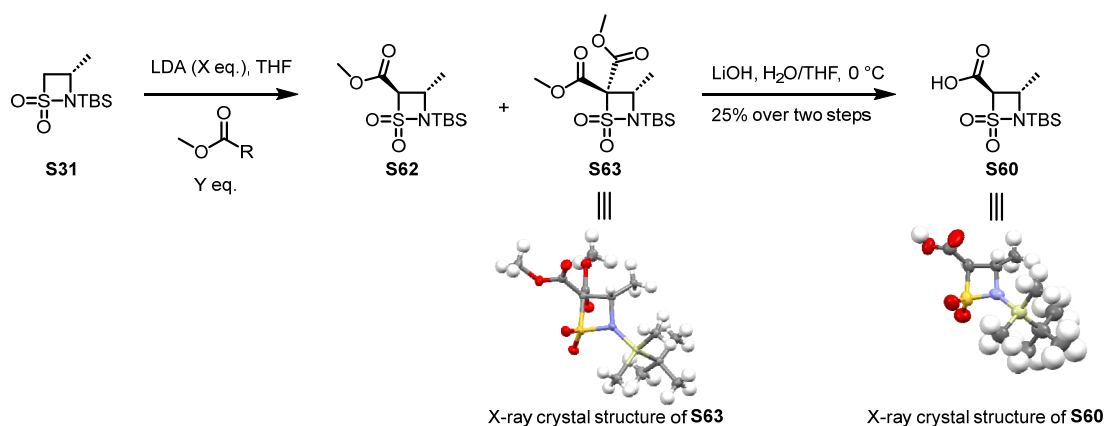
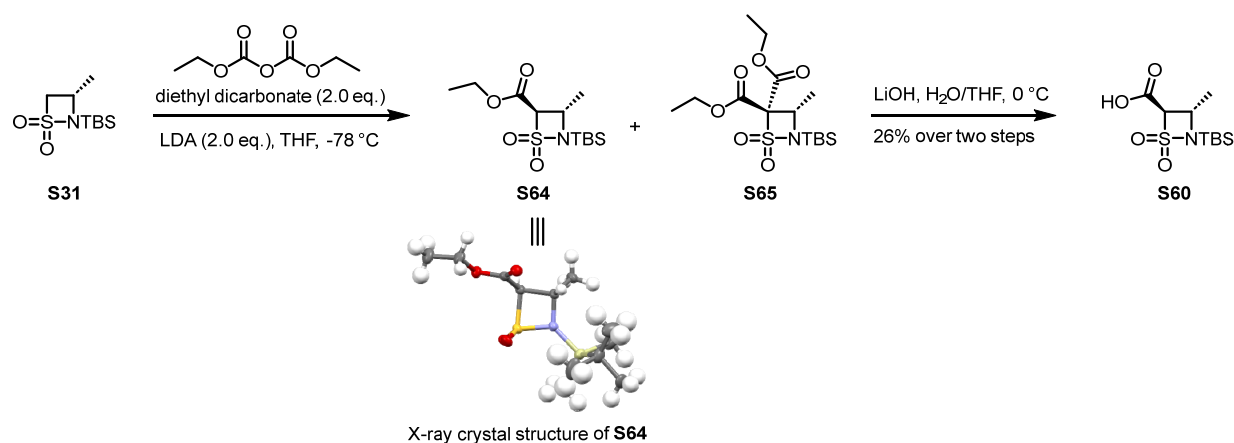
**Scheme 64:** Two step synthesis of acid **S60** from **S31** *via* methyl ester **S62**.

Table 18: Conditions investigated for the formation of **S62** from **S31**.

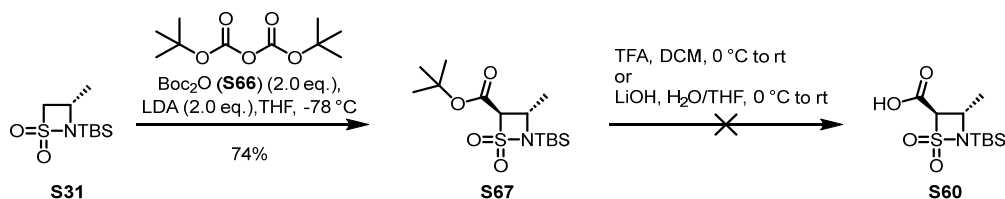
| Entry | Scale | R | X | Y | Time and temperature | Yields of S62 , S63 and S31 |
|-------|--------|-----|-----|-----|----------------------------|--|
| 1 | 50 mg | OMe | 2.0 | 2.0 | 1 h at -78 °C + 16 h at rt | 0% and 0%, n.d. |
| 2 | 20 mg | CN | 2.0 | 2.0 | 2 h at -78 °C | Traces of 28/29 , 0% |
| 3 | 20 mg | Cl | 2.0 | 2.0 | 2 h at -78 °C | 40%, 22%, 0% |
| 4 | 30 mg | Cl | 1.1 | 1.3 | 2 h at -78 °C + 1 h at rt | 5% ^[a] , 2% ^[a] , 37% |
| 5 | 300 mg | Cl | 2.0 | 2.0 | 2 h at -78 °C | 12%, 56%, 23% |

n.d. = ¹H-NMR spectrum of crude mixture after aq. workup showed no hint of product formation, thus no purification was performed. ^[a] estimated yield, unknown impurities not subtracted.

S31 could also be converted into **S60** *via* ethyl ester **S64** (**Scheme 65**). The LDA-mediated acylation of **S31** (50 mg/100 mg scale) with diethyl dicarbonate gave a mixture of **S64** (<46%/<57% yield) and **S65** (<13%/<37%yield) together with unknown impurities that could not be removed. Treatment of this mixture with LiOH in H₂O/THF gave **S60** in 26% yield over two steps (for both scales). The structure of **S64** was confirmed by X-ray crystallography. Larger quantities of **S60** were produced *via* the mixture of **S64/S65** by several parallel reactions (100 mg of **S31** each) in order to prevent potential scalability issues.

**Scheme 65:** Two step synthesis of acid **S60** from **S31** *via* ethyl ester **S64**.

LDA-mediated acylation of **S31** with Boc₂O gave (**S66**) *t*-butyl ester **S67** in 74% and no double-acylation was observed (**Scheme 66**). Unfortunately, **S67** could not be converted into **S60** under acidic or basic conditions.



Scheme 66: Attempted two step synthesis of acid **S31** from **S31** via *t*-butyl ester **S67**.

Interestingly, the comparison of the X-ray crystal structures of mono-acylated β -sultams **S59**, **S60** and **S64** with that of doubly acylated **S63** revealed distinctly different conformations of the 4-membered ring. For the mono-acylated structures, the four-membered ring is almost planar in all three cases, with the ester/acid group and the methyl group in an eclipsed conformation. For doubly acylated **S63**, the ring adopts an envelope conformation, which puts the substituents in positions 3 and 4 slightly staggered conformation (**Figure 48**).

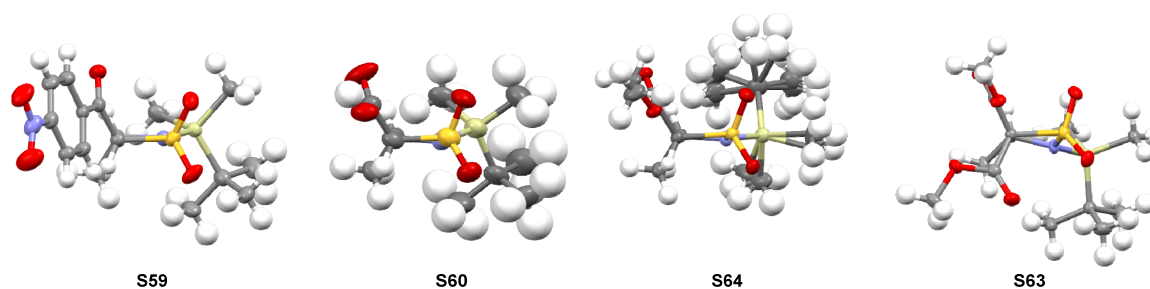
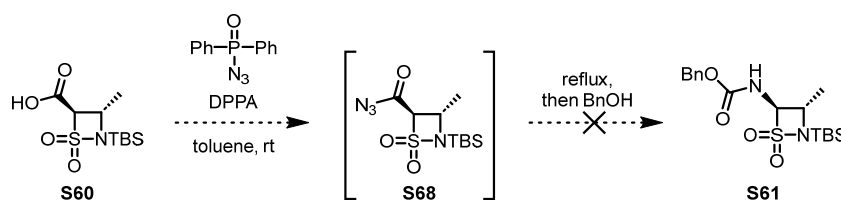


Figure 48: Comparison of the X-ray crystal structures of mono-acylated β -sultam **S59**, **S60** and **S64** with that of doubly acylated **S63**.

With acid **S60** available in sufficient quantities, its conversion into Cbz-protected amine **S61** via a one-pot azidation/*Curtius* rearrangement sequence was then investigated. Thus, **S60** was (1) stirred with diphenylphosphoryl azide (DPPA) in toluene at rt for 4 h to form azide **S68**; (2) the reaction mixture was heated to reflux for 30 min, to induce *Curtius* rearrangement; and (3) benzyl alcohol was added at rt and stirring was continued for 1 h, to form carbamate **S61** from the isocyanate product of the rearrangement (**Scheme 67**). Unfortunately, no carbamate **S61** was obtained. The reaction was monitored by TLC and $^1\text{H-NMR}$ spectroscopy; no formation of **S68** or **S61** was observed and no starting material could be reisolated.



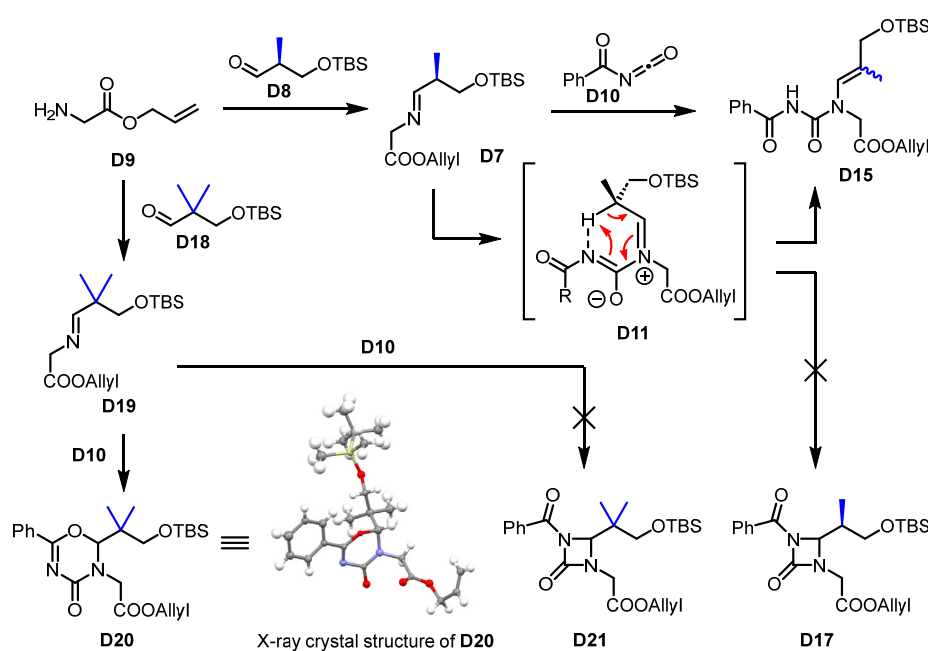
Scheme 67: Attempted *Curtius* rearrangement to transform **S60** into **S61**.

It is unclear at this point, what caused the reaction to fail and additional experiments would have to be conducted in order to determine if the *Curtius* approach is not viable indeed. However, no such further experiments were possible within the time frame of this PhD thesis.

3.3 Conclusion and Outlook

The original goal of the work described in this chapter of the dissertation was the synthesis (and eventual biological assessment) of new analogs of β -lactam antibiotics, where the β -lactam ring would be replaced either by an *N*-acyl-1,3-diazetidione or a β -sultam moiety.

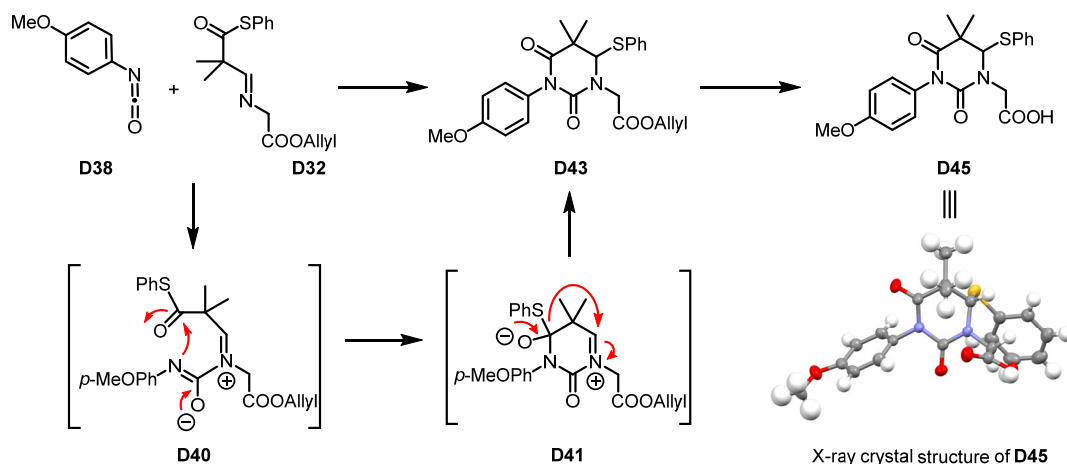
Unfortunately, the projected [2+2]-cycloadditions *en route* to *N*-acyl-1,3-diazetidione (e.g. **D17** or **D21**) were not observed, at least for those pairs of isocyanates and functionalized imines that I investigated. α -Monosubstituted imine **D7** underwent neither [2+2] nor [4+2]-cycloaddition, but instead gave enamides (e.g. **D15**). Only [4+2]-cycloaddition occurred with α,α -disubstituted imines (e.g. **D19**), to give 2,3-dihydro-1,3,5-oxadiazin-4-ones (e.g. **D20**) (**Scheme 68**). These experimental observations could subsequently be rationalized by DFT calculations conducted in the group of Prof. *Sereina Riniker* at ETH Zurich; the calculations showed a large difference between the activation barriers for the formation of a 1,3-diazetidione and a 2,3-dihydro-1,3,5-oxadiazin-4-one ring from a common zwitterionic iminium intermediate.



Scheme 68: Reactions of benzoyl isocyanate (**D10**) with imines **D7** and **D19**.

Intriguingly, the reactions of imines bearing a thioester moiety in the 2-position (e.g. **D32**) with aryl isocyanates (e.g. **D38**) or benzyl isocyanate gave neither 1,3-diazetidiones nor dihydro-oxadiazinones; rather, these reactions produced 5,5-dimethyl-6-(aryl-/alkylthio)-dihydropyrimidine-2,4-diones (e.g. **A48**) in good yields. The reaction most likely follows an alternative (4+2)-cycloaddition pathway, with displacement of the thiol component of the ester

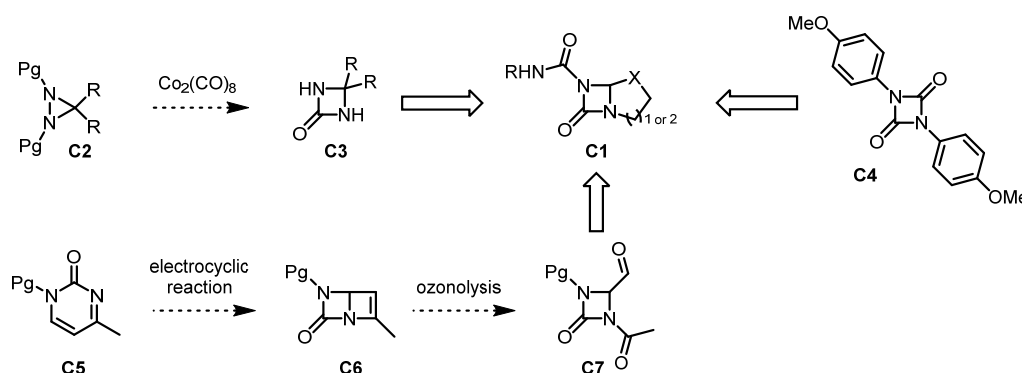
in the ring-closing step followed by addition of the thiol to the iminium moiety (**Scheme 69**). Differently phenyl-substituted derivatives of **D43** were obtained in reactions with other *p*-substituted phenyl isocyanates in similar yields, independent of the nature of the *para*-substituent.



Scheme 69: Synthesis of 5,5-dimethyldihydropyrimidine-2,4-dione **D45**.

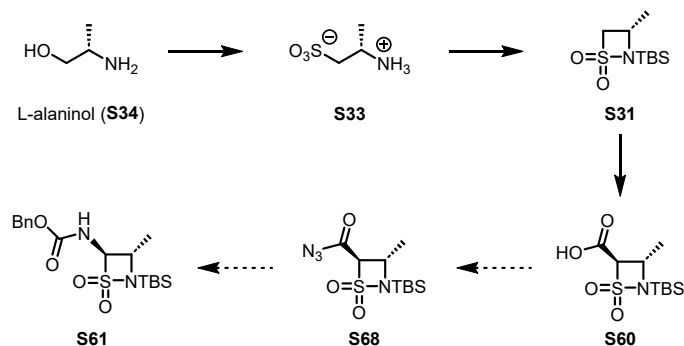
Even though the envisaged 1,3-diazetidiones were not observed, new insights into the reaction of isocyanates with imines were gained. Of particular note, 6-(aryl-/alkylthio)-dihydropyrimidine-2,4-diones, such as **D42-D45**, **D46** and **D48**, to the best of my knowledge, have not been reported in the literature but may be of interest as intermediates in the synthesis of new bioactive heterocycles.

Alternative synthetic strategies towards bicyclic 1,3-diazetidiones (**C1**) could make use of (1) diaziridines with a general structure **C2**, which would be transformed into 1,3-diazetidiones **C3** (based on ref. [304]); (2) reported double PMB-protected 1,3-diazetidione **C4**, by partial deprotection, reduction, alkylation (order of steps could also be altered) and cyclization; (3) an electrocyclic reaction with **C5** to give **C6**, which would be transformed into **C7** by means of ozonolysis (based on ref. [305]) (**Scheme 70**).



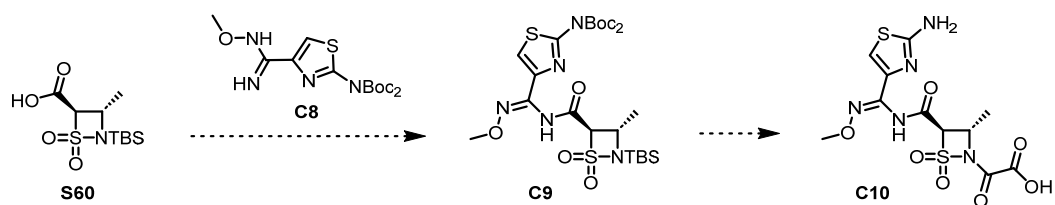
Scheme 70: Ideas towards bicyclic 1,3-diazetidiones **C1**.

β -Sultam **S31** could be accessed from sulfonic acid **S33** by sequential chlorination and base-catalyzed cyclization in good yields (**Scheme 71**). While α -azidation of **S31** was not successful, α -acylation with various acyl electrophiles was achieved e.g. an acylation-hydrolysis sequence furnished carboxylic acid **S60**. The latter could not yet be elaborated into amide **S61** *via* one-pot azidation/*Curtius* rearrangement sequence. At this point it is not clear, which step of this sequence is in fact problematic, thus a stepwise approach with isolation of the intermediate acyl-azide **S68** might be informative. Alternatively, a light-induced *Curtius* rearrangement protocol could be attempted.



Scheme 71: Synthetic strategy towards **S61**.

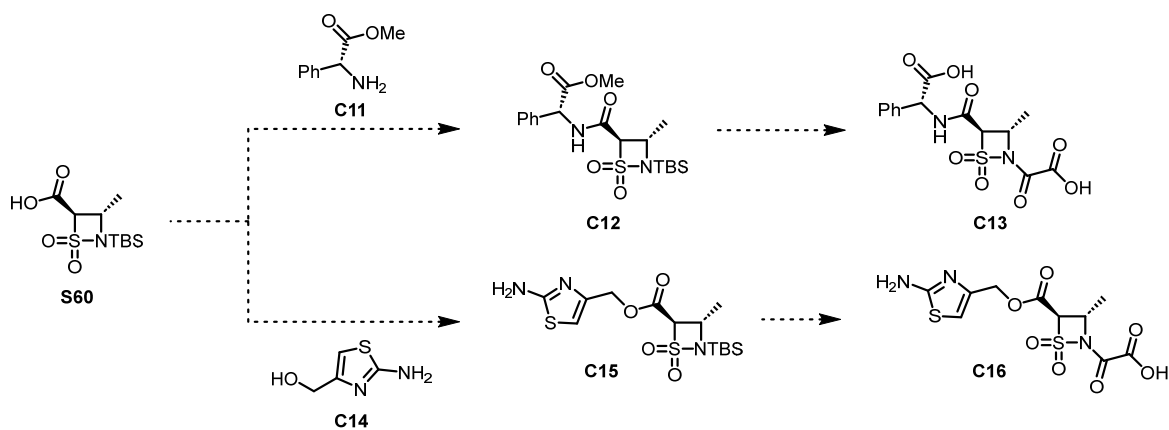
Should **S61** not be accessible or should the free α -amino sultam turn out to be unstable, the chemistry established up to this point could potentially be exploited for the synthesis of **C10** as an alternative target structure mimicking the globular structure of the original target compound **A34** (see **Figure 3** in Abstract), but incorporating an inverted amide bond and a simpler oxime moiety (**Scheme 72**).



Scheme 72: Synthetic strategy towards alternative target structures **C10**.

It has been shown by *Treuner* and coworkers that the corresponding simplification of the oxime moiety (compared to **A34**) did not lead to a significant drop in antibacterial activity in other β -lactam antibiotics.^[306]

More simplified versions of **C10** would be **C13** or **C16** (**Scheme 73**).



Scheme 73: Synthetic strategies towards alternative target structures **C13** and **C16**.

Indeed, carboxylic acid **S60** has been successfully transformed into amide **C12** with methyl (*R*)-2-amino-2-phenylacetate (**C11**) (**Scheme 73**). Efforts towards the synthesis of **C13** are currently ongoing.

4 Experimental Part

4.1 General

All reactions were performed under an argon atmosphere using flame-dried glassware and standard syringe/septa techniques. CH₂Cl₂, THF and Et₂O used for reactions were distilled under argon prior to use (CH₂Cl₂ from CaH₂, THF and Et₂O from Na/benzophenone). All other absolute solvents were purchased as anhydrous grade from Acros (puriss.; dried over molecular sieves; H₂O <0.005%) and used without further purification. Solvents for extractions, flash column chromatography (FC) and thin layer chromatography (TLC) were either purchased as commercial grade and distilled prior to use or purchased as HPLC grade. All other commercially available reagents were used without further purification. Reaction mixtures were magnetically stirred and monitored by TLC performed on Merck TLC aluminum sheets (silica gel 60 F254). Spots were visualized with UV light ($\lambda = 254$ nm) or through staining with KMnO₄/K₂CO₃. DMP workup solution refers to a 0.1M sodium thiosulfate and 1M sodium bicarbonate aq. solution.

Purification of products by **FC** was performed using either Sigma-Aldrich or SiliCycle silica gel 60 for preparative column chromatography (particle size 40-63 μm).

¹H- and ¹³C-NMR spectra were recorded on a Bruker AV-400 400 MHz or on a Bruker AV-500 500 MHz spectrometer at rt. Chemical shifts (δ) are reported in ppm and are referenced to CHCl₃ (δ 7.26 ppm for ¹H, δ 77.23 ppm for ¹³C), to DMSO (δ 2.50 ppm for ¹H, δ 39.52 ppm for ¹³C) or to MeOH (δ 3.31 ppm for ¹H, δ 49.00 ppm for ¹³C). All ¹³C-NMR spectra were measured with complete proton decoupling. Data for NMR spectra are reported as follows: s = singlet, d = doublet, t = triplet, q = quartet, quint = quintet, sept = septet, m = multiplet, br = broad signal, app. = apparent.

Infrared (IR) spectra were recorded on a Jasco FT/IR-6200 instrument. Absorption bands are given in wavenumbers in cm⁻¹.

Optical rotations were measured on a Jasco P-1020 polarimeter at the sodium D line with a 10 or 100 mm path length cell and are reported as follows: $[\alpha]_D^{20}$: (concentration (g/100 ml), and solvent).

High resolution mass spectra (HRMS) were recorded on a Bruker maXis (ESI) or on a Micromass (Waters) AutoSpec Ultima spectrometer (EI), respectively, by the ETH Zürich MS service.

Normal phase HPLC analysis were performed using the following combinations of devices: Analytical HPLC, Elite LaChrom equipped with column oven L-2350, PDA detector L-2455, autosampler L-2200, pump L-2130 and Luna® 3 μm NH₂, 100 Å, 150 x 4.6 mm; Preparative HPLC,

Gilson equipped with fraction collector FC-204, UV-Vis detector UV-Vis-156, pumps 331 and 332 and Luna[®] 5 μm NH₂, 100 Å, 150 x 21.2 mm.

Reversed phase HPLC analysis were performed using the following combinations of devices: Analytical HPLC, Elite LaChrom equipped with column oven L-2350, PDA detector L-2455, autosampler L-2200, pump L-2130 and Symmetry[®] C18 column, 3.5 μm , 100 x 4.6 mm or Agilent 1100 Series equipped with G13779A degasser, G1311A QuatPump, G1315B DAD-detector, G1313A Auto injector and ZORBAX SB-18 RRHT column, 1.8 μm 4.6 mm ID X 50 mm; Preparative HPLC, Gilson equipped with PLC 2050, Liquid Handler GX-241, verity 4020 and Symmetry[®] C18 column, 5 μm , 100 x 19 mm.

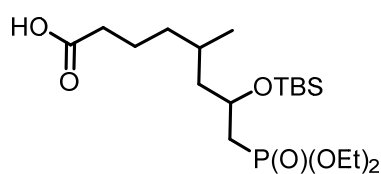
Quantum mechanical computations were performed on the Euler cluster of ETH Zurich.

4.2 Synthesis and SAR Studies of (-)-Zampanolide Analogs

4.2.1 Synthesis and Structure-Activity Relationship Studies of C(13)-Desmethylene-(-)-Zampanolide Analogs (Publication 1)

Literature known compounds **R10a**,^[72] **R11a**,^[60] **R14**,^[72] **R24**,^[72] **R28**,^[60] **R31**,^[60] **R44**^[128] and (*Z,E*)-sorbamide^[60] were prepared according to literature procedures.

4.2.1.1 Synthesis of acid **R10c**



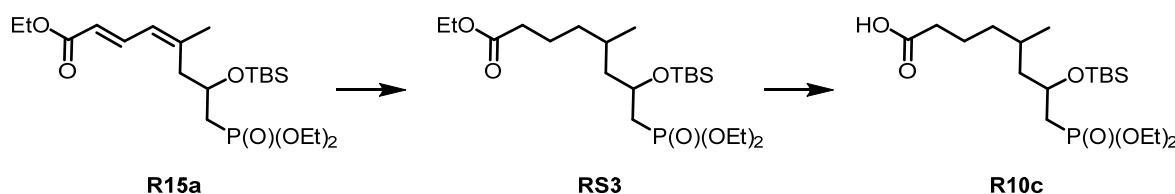
R10c

7-((*tert*-Butyldimethylsilyl)oxy)-8-(diethoxyphosphoryl)-5-methyloctanoic acid (**R10c**).

From acid **R10a**

To a solution of **R10a** (1.00 g, 2.38 mmol, 1.0 equiv.) in EtOH (22 mL), Pd/C 10% (0.51 g, 0.48 mmol, 0.20 equiv.) was added under argon. The flask was flushed with hydrogen (3 vacuum-hydrogen cycles) and the mixture was stirred at rt for 4 h. After complete conversion of the starting material the hydrogen was replaced by argon (5 vacuum-argon cycles) and the mixture was filtered over celite. The solvent was removed under reduced pressure. The residue was purified by column chromatography (1:1 EtOAc/hexane) to give **R10c** (0.79 g, 1.86 mmol, 78 %) as a colorless oil.

From ester **R15a**

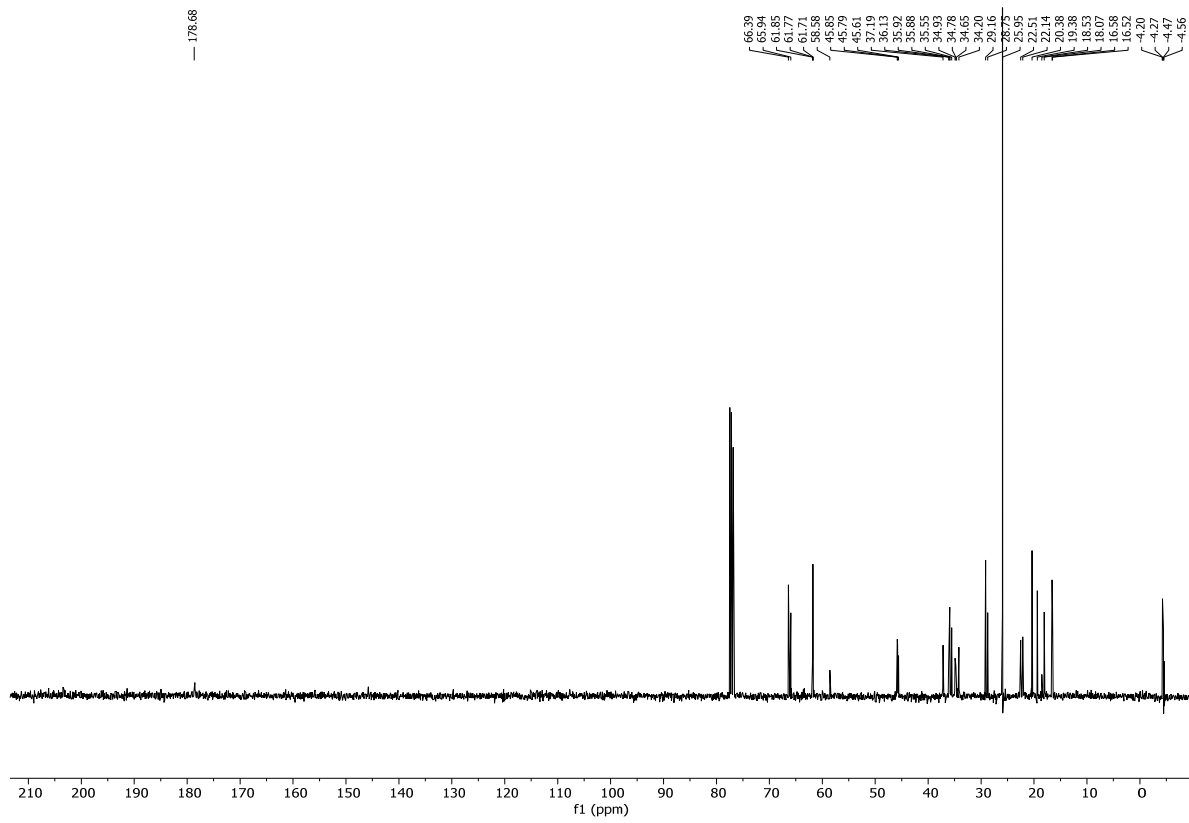
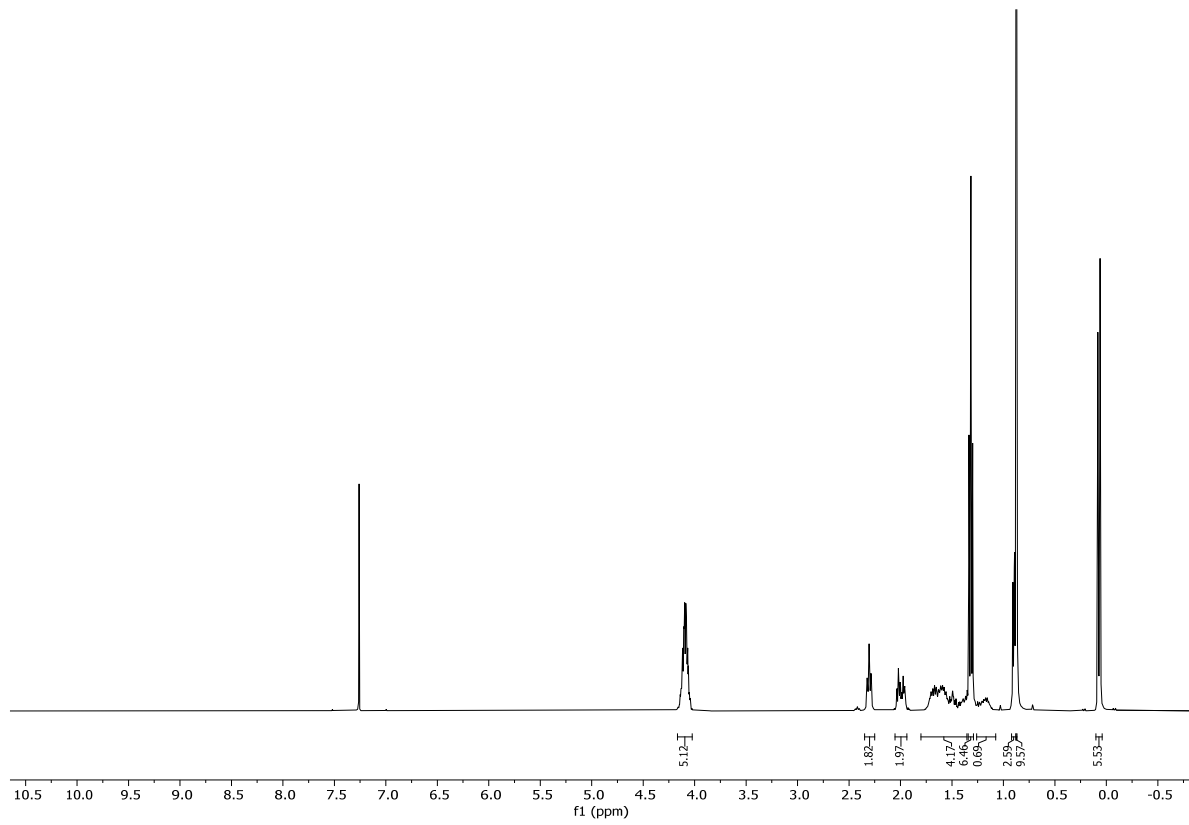


To a solution of **R15a** (0.30 g, 0.67 mmol, 1.0 equiv.) in EtOH (6 mL), Pd/C 10% (0.14 mg, 0.13 mmol, 0.20 equiv.) was added under argon. The flask was flushed with hydrogen (3 vacuum-hydrogen cycles) and the mixture was stirred at rt for 4 h. After complete conversion of the

starting material the hydrogen was replaced by argon (5 vacuum-argon cycles) and the mixture was filtered over celite. The solvent was removed under reduced pressure to give fully sat. aqu. ester **RS3** (0.29 g, 0.63 mmol, 95%).

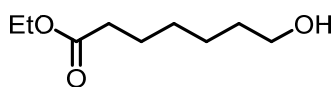
To a solution of crude ester **RS3** (0.29 g, 0.63 mmol, 1.00 equiv.) in EtOH (5 mL) was added 1M NaOH (1.90 mL, 1.90 mmol, 3.00 equiv.) at 0 °C. The cooling bath was removed after 5 min and the yellow solution at was stirred at rt for 24 h. The reaction was then quenched by the addition of 2M HCl (1 mL, 1.90 mmol, 3.00 equiv.). Subsequently, EtOAc (25 mL) and brine (25 mL) were added, the phases were separated, and the aqueous phase was extracted with EtOAc (4 x 25 mL). The combined organic extracts were dried over MgSO₄ and evaporated under reduced pressure. The residue was dried in high vacuum to give crude **R10c** (0.25 g, 0.60 mmol, 95% hydrolyzes only or 90% over two steps) which was used in the next step without further purification.

TLC: R_f = 0.55 (EtOAc/hexane 1:5 + 1% acetic acid). **¹H-NMR** (400 MHz, CDCl₃): δ = 4.09 (d, *J* = 10.0, 7.1, 3.4 Hz, 5H), 2.35 – 2.25 (m, 2H), 2.05 – 1.94 (m, 2H), 1.80 – 1.36 (m, 4H), 1.32 (t, *J* = 7.0 Hz, 6H), 1.26 – 1.08 (m, 1H), 0.92 – 0.88 (m, 3H), 0.87 (d, *J* = 1.9 Hz, 10H), 0.10 – 0.04 (m, 6H). **¹³C-NMR** (101 Hz, CDCl₃): δ = 178.7, 66.4, 65.9, 61.9, 61.8, 61.7, 58.6, 45.9, 45.8, 45.6, 37.2, 36.1, 35.9, 35.9, 35.6, 34.9, 34.8, 34.7, 34.2, 29.2, 28.8, 26.0, 22.5, 22.1, 20.4, 19.4, 18.5, 18.1, 16.6, 16.5, -4.2, -4.3, -4.5, -4.6. **IR** (neat): $\tilde{\nu}$ = 2954, 2930, 2857, 1726, 1472, 1463, 1391, 1370, 1251, 1204, 1178, 1097, 1024, 962, 921, 835, 807, 774, 661, 549 cm⁻¹. **HRMS** (ESI): calcd for C₁₉H₄₁NaO₆PSi [(M+Na)⁺]: 447.2302; found: 447.2298.



4.2.1.2 Synthesis of acid R10d

4.2.1.2.1 From ethyl 6-heptenoate

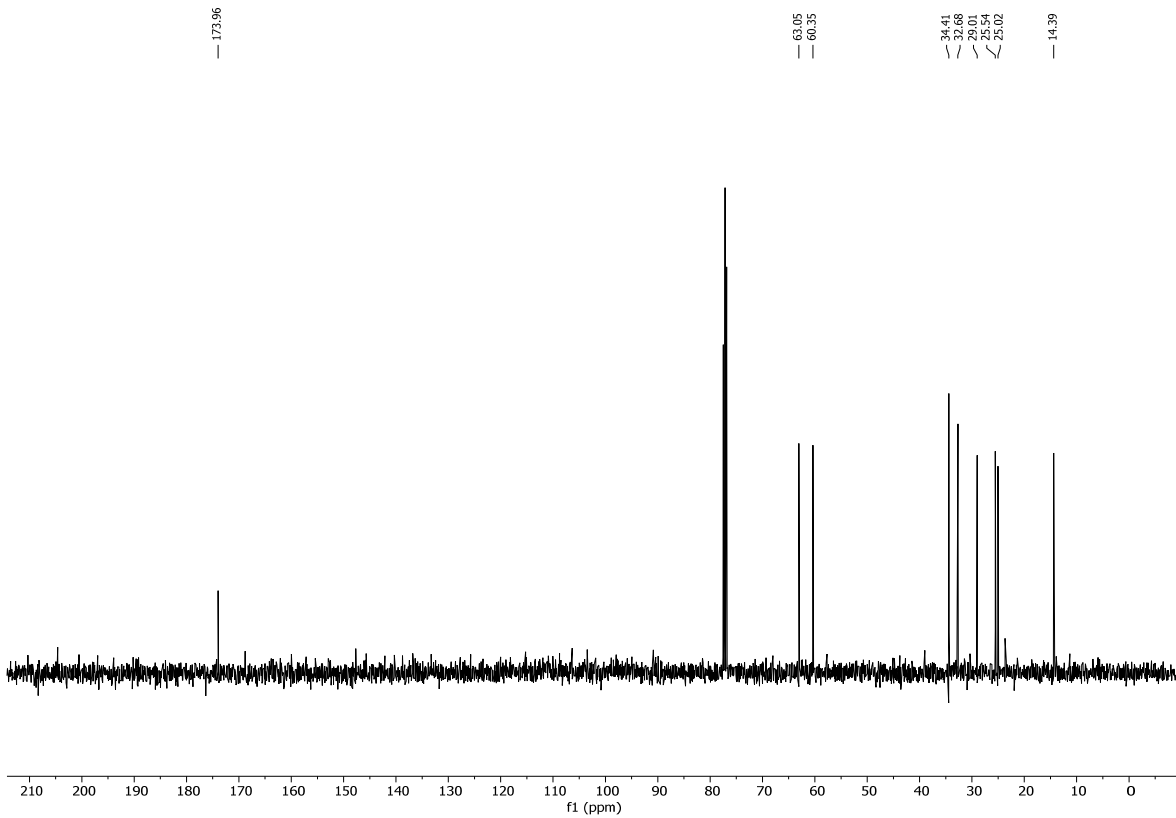
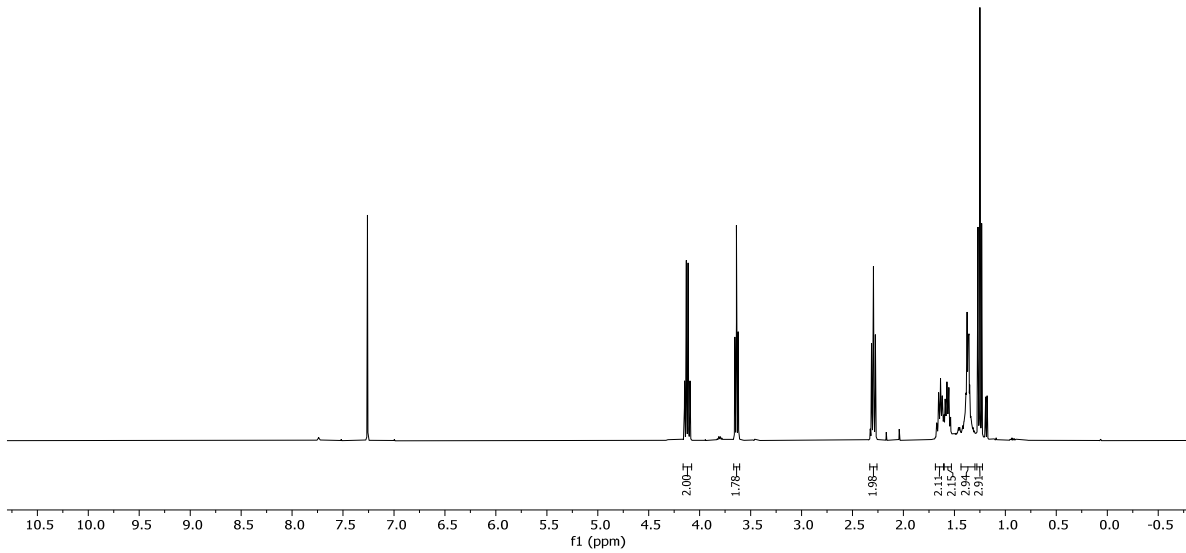


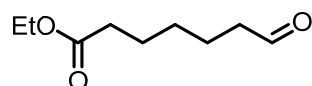
RS4

Ethyl 7-hydroxyheptanoate (RS4).²⁰ BH₃ (1M in THF, 3.96 mL, 3.96 mmol, 0.33 equiv.) was added to a solution of ethyl 6-heptenoate (1.30 mL, 11.89 mmol, 1.00 equiv.) in THF (2 mL) in 60 min at 0 °C. After stirring for 2 h at 0 °C and 2 h at 25 °C, hydrogen peroxide (30 %, 4.58 mL, 12.26 mmol, 1.03 equiv.) and sodium hydroxide (1M, 4.89 mL, 4.89 mmol, 0.41 equiv.) were added simultaneously at 10-22 °C and the mixture was stirred for 2 h. The solution was then diluted with Et₂O (30 mL) and the layers were separated. The aqueous layer was extracted with Et₂O (3 x 15 mL), then sat. aqu. with potassium carbonate and extracted with 150 mL THF. The combined organic extracts were dried over MgSO₄ and concentrated under reduced pressure. The residue was purified by FC (EtOAc/hexane 1:2) to give hydroxy ester **RS4** (1.57 g, 9.01 mol, 76%) as a colorless oil.

TLC (EtOAc/hexane 1:2): R_f = 0.25. **¹H-NMR** (400 MHz, CDCl₃): δ = 4.12 (q, *J* = 7.2 Hz, 2H), 3.64 (t, *J* = 6.6 Hz, 2H), 2.30 (t, *J* = 7.6 Hz, 2H), 1.69 – 1.61 (m, 2H), 1.60 – 1.53 (m, 2H), 1.37 (qt, *J* = 4.2, 2.0 Hz, 3H), 1.25 (t, *J* = 7.2 Hz, 3H). **¹³C-NMR** (101 MHz, CDCl₃): δ = 174.0, 63.1, 60.4, 34.4, 32.7, 29.0, 25.5, 25.0, 14.4. **HRMS** (ESI): calcd for C₉H₁₈NaO₃ [(M+Na)⁺]: 197.1148; found: 197.1148.

²⁰ Compound **RS4** was first reported by Mori *et al.*^[72] ¹H-NMR-spectroscopic data have been reported by Ballini *et al.*^[73] ¹³C data have not been reported (based on the information available in SciFinder). The procedure used here has not been described previously.

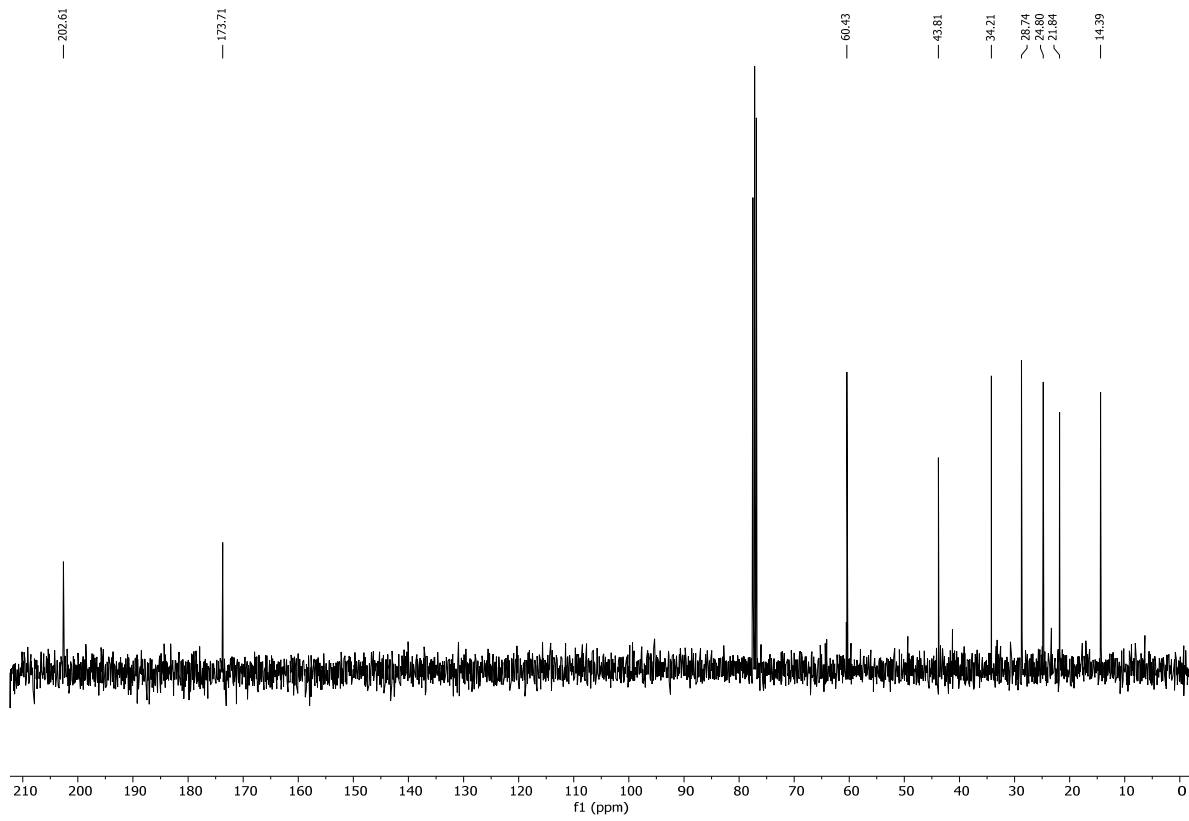
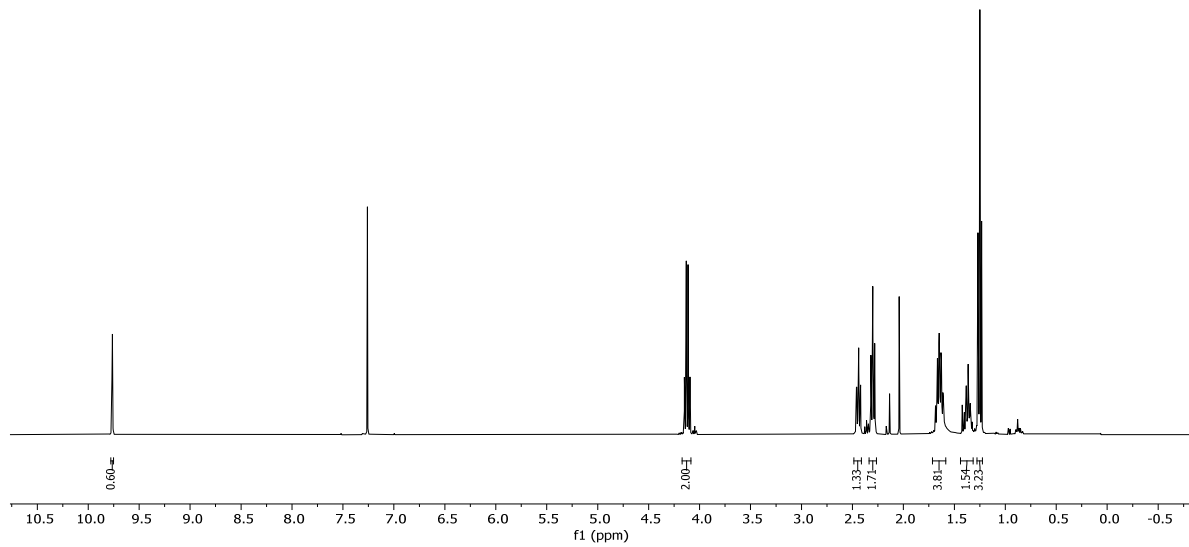


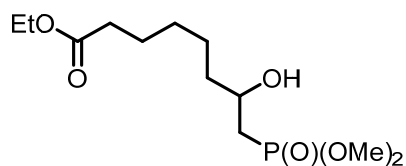
**R19**

Ethyl 7-oxoheptanoate (R19).²¹ To a mixture PCC (3.88 g, 18.02 mmol, 2.00 equiv.) and molecular sieves (3Å, 1.5 g) in CH₂Cl₂ (57 mL), **RS4** (1.57 g, 9.01 mmol, 1.00 equiv.) was added at 0 °C. The mixture was stirred at rt until the reaction was complete (2 h, TLC). The solvent was evaporated and the residue was filtered through a small pad of silica gel with EtOAc/hexane 1:5 as eluent. The filtrate was concentrated to give the virtually pure aldehyde **R19** (0.50 g, 2.90 mmol, 32%) as a colorless oil.

TLC (EtOAc/hexane 1:2): R_f = 0.50. **¹H-NMR** (400 MHz, CDCl₃): δ = 9.76 (t, J = 1.7 Hz, 1H), 4.12 (qd, J = 7.2, 1.7 Hz, 2H), 2.44 (td, J = 7.3, 1.8 Hz, 1H), 2.30 (t, J = 7.5 Hz, 2H), 1.64 (tddd, J = 10.1, 7.2, 5.0, 2.1 Hz, 4H), 1.44 – 1.32 (m, 2H), 1.25 (td, J = 7.1, 2.0 Hz, 3H). **¹³C-NMR** (101 MHz, CDCl₃): δ = 202.6, 173.7, 60.4, 43.8, 34.2, 28.7, 24.8, 21.8, 14.4.

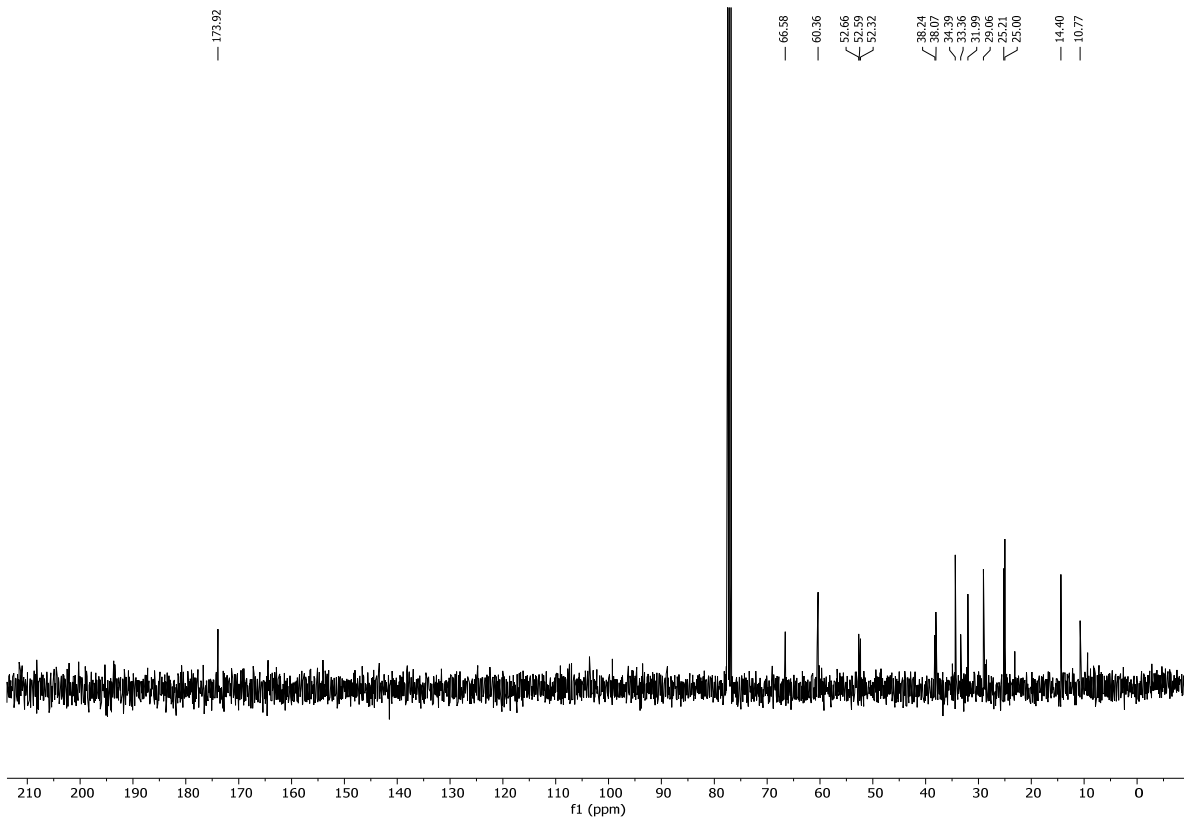
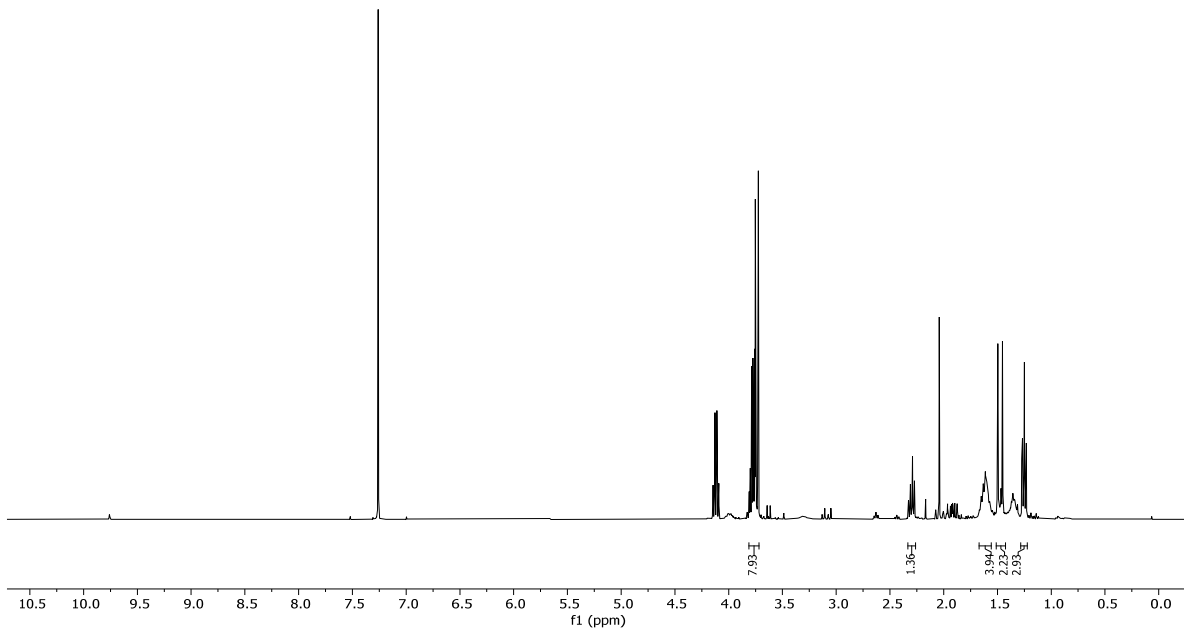
²¹ Compound **R19** was prepared according to Ballini *et al.*^[73] Ref.[73] includes ¹H-NMR data, ¹³C data have been reported by Mostyn *et al.*^[74]

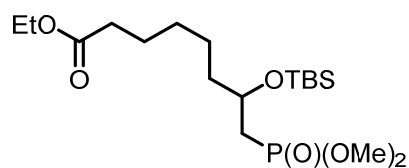


**RS5**

Ethyl 8-(dimethoxyphosphoryl)-7-hydroxyoctanoate (RS5). To a solution of dimethyl phosphonate (0.42 mL, 3.91 mmol, 1.34 equiv.) in THF (9 mL) was added *n*-BuLi (1.96 mL, 3.16 mmol, 1.08) at $-80\text{ }^{\circ}\text{C}$. The resulting yellow solution was stirred for 1 h at $-80\text{ }^{\circ}\text{C}$ and then cooled to $-100\text{ }^{\circ}\text{C}$ (N_2/EtOH). Then, a solution of **R19** (0.50 g, 2.90 mmol, 1 equiv.) in THF (17 mL), was added dropwise and the resulting solution was stirred for 1 h at $-100\text{ }^{\circ}\text{C}$ before sat. aq. NaHCO_3 (20 mL) was added. The mixture was allowed to warm to rt and after addition of EtOAc (15 mL) and H_2O (15 mL), the layers were separated. The aqueous layer was extracted with EtOAc (3×25 mL). The combined organic layers were dried over MgSO_4 , filtered, and concentrated under reduced pressure. Purification of the residue by FC (EtOAc) afforded alcohol **RS5** (0.30 g, 1.01, 35%) as a colorless liquid. The $^1\text{H-NMR}$ spectrum shows traces of EtOAc.

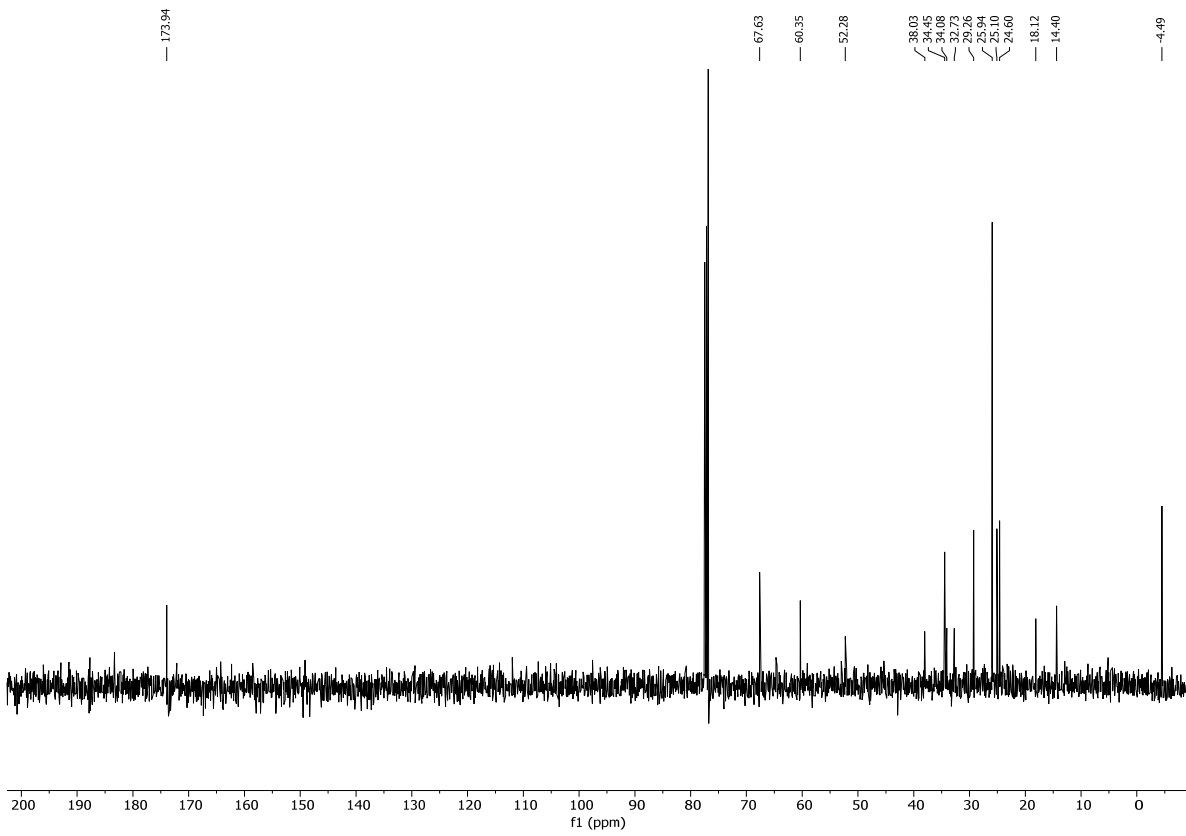
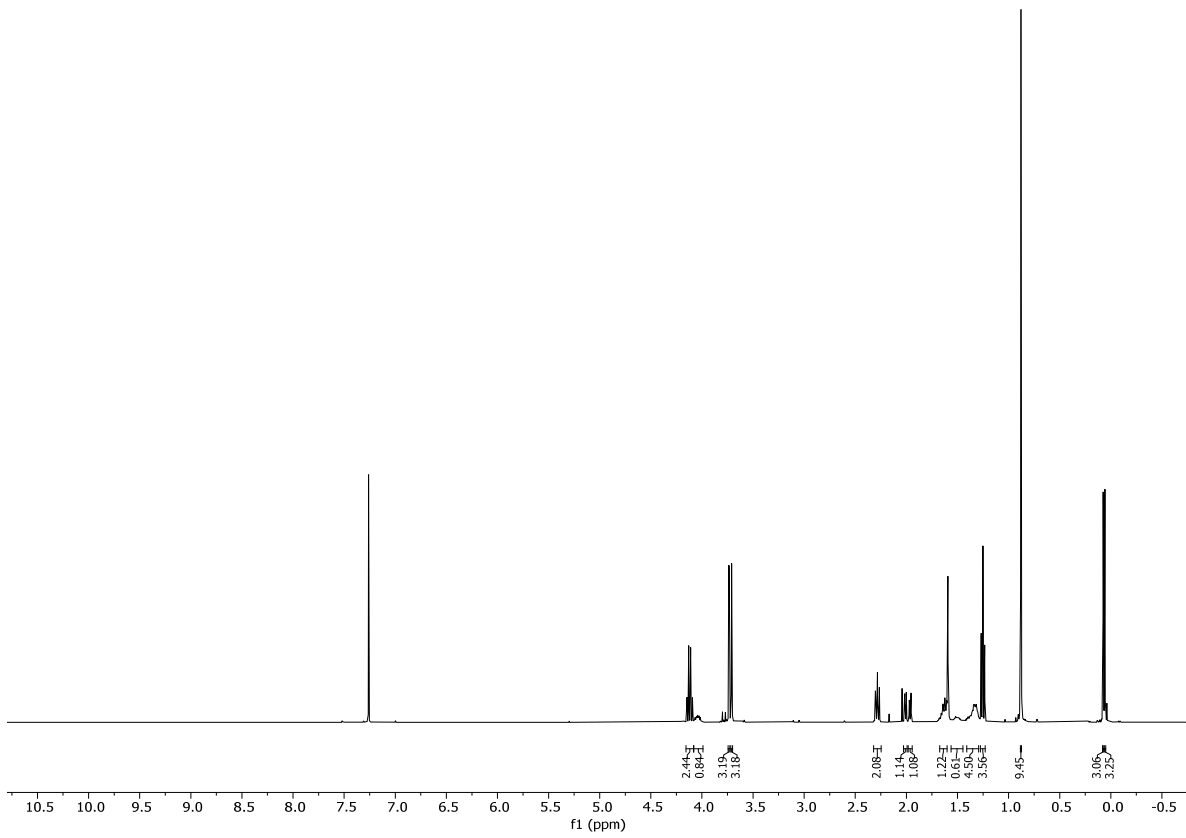
TLC (EtOAc): $R_f = 0.15$. **$^1\text{H-NMR}$** (400 MHz, CDCl_3): $\delta = 3.81 - 3.72$ (m, 8H), 2.33 – 2.26 (m, 1H), 1.61 (ddd, $J = 17.0, 12.1, 8.1$ Hz, 4H), 1.51 – 1.42 (m, 2H), 1.25 (td, $J = 7.1, 2.6$ Hz, 3H). **$^{13}\text{C-NMR}$** (101 MHz, CDCl_3): $\delta = 173.9, 66.6, 60.4, 52.7, 52.6, 52.3, 38.2, 38.1, 34.39, 33.4, 32.0, 29.1, 25.2, 25.0, 14.4, 10.8$. **IR** (neat): $\tilde{\nu} = 2934, 1732, 1634, 1463, 1246, 1183, 1095, 1055, 1028, 828\text{ cm}^{-1}$.

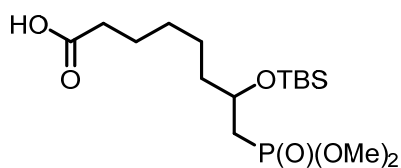


**R20**

Ethyl 7-((*tert*-butyldimethylsilyl)oxy)-8-(dimethoxyphosphoryl)octanoate (R20). To a solution of **RS5** (0.30 g, 1.01 mmol, 1.00 equiv.) in DMF (3 mL) were added sequentially imidazole (0.38 g, 5.55 mmol, 5.50 equiv.), DMAP (0.11 g, 0.93 mmol, 0.92 equiv.) and TBSCl (0.42 g, 2.77 mmol, 2.74 equiv.) at rt. The mixture was stirred for 1.5 d; H₂O (10 mL) and Et₂O (10 mL) were then added, the phases were separated and the aqueous phase was extracted with Et₂O (3 x 10 mL). The combined organic extracts were then washed with H₂O (2 x 10 mL), dried over MgSO₄ and concentrated under reduced pressure. Purification of the residue by FC (EtOAc/hexane 1:1) afforded TBS-ether **R20** (0.12 g, 0.29 mmol, 29%) as a colorless oil.

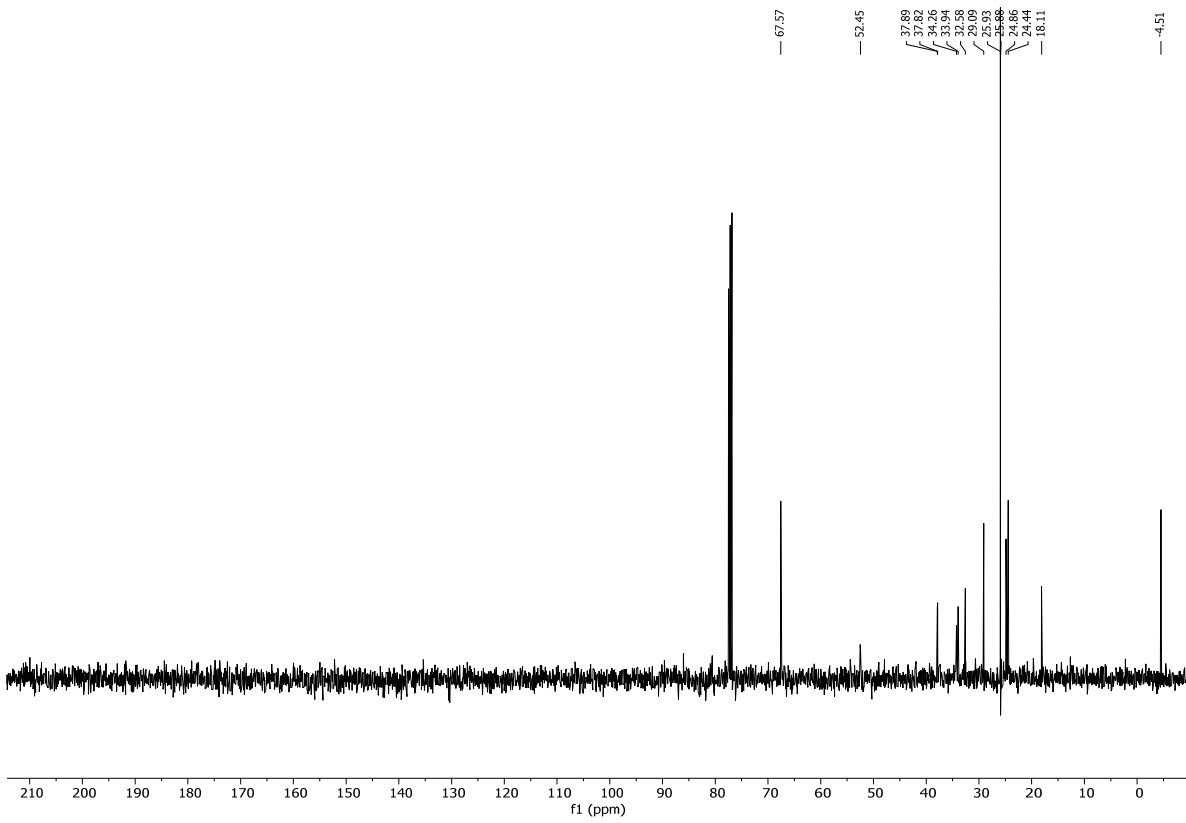
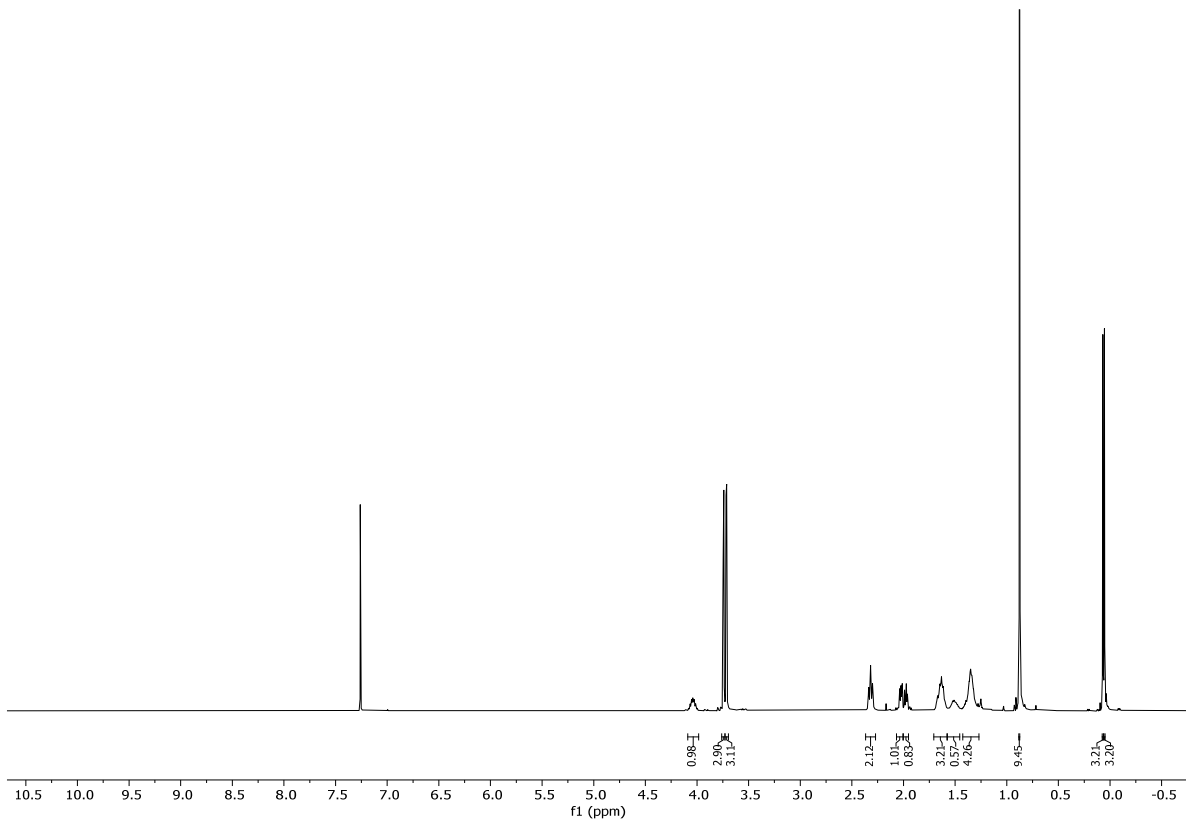
TLC (EtOAc): $R_f = 0.50$. **¹H-NMR** (400 MHz, CDCl₃): $\delta = 4.12$ (q, $J = 7.2$ Hz, 2H), 4.08 – 3.99 (m, 1H), 3.74 (d, $J = 1.5$ Hz, 3H), 3.71 (d, $J = 1.6$ Hz, 3H), 2.28 (t, $J = 7.6$ Hz, 2H), 2.01 (d, $J = 6.3$ Hz, 1H), 1.98 – 1.94 (m, 1H), 1.67 – 1.60 (m, 1H), 1.56 – 1.45 (m, 1H), 1.41 – 1.29 (m, 5H), 1.25 (t, $J = 7.1$ Hz, 4H), 0.88 (s, 9H), 0.08 (s, 3H), 0.06 (s, 3H). **¹³C-NMR** (101 MHz, CDCl₃): $\delta = 173.9, 67.6, 60.4, 52.3, 38.0, 34.5, 34.1, 32.7, 29.3, 25.9, 25.1, 24.6, 18.1, 14.4, -4.5$. **IR** (neat): $\tilde{\nu} = 2953, 2931, 2857, 1736, 1254, 1183, 1034, 836, 812, 777$ cm⁻¹. **HRMS** (ESI): calcd for C₁₈H₄₀O₆PSi [(M+H)⁺]: 411.2326; found: 411.2328



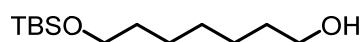
**R10d**

7-((*tert*-Butyldimethylsilyl)oxy)-8-(dimethoxyphosphoryl)octanoic acid (R10d). To a solution of **R20** (120.0 mg, 0.29 mmol, 1.00 equiv.) in EtOH (2 mL) was added 1.0M aqueous NaOH (0.88 mL, 0.88 mmol, 3.00 equiv.) at 0 °C. The cooling bath was removed after 5 min and the yellow solution was stirred at rt for 25 h. The reaction was then quenched by the addition of 2M HCl (0.44 mL, 0.88 mmol, 3.00 equiv.). Subsequently, EtOAc (5 mL) and brine (5 mL) were added, the phases were separated and the aqueous phase was extracted with EtOAc (4 x 5 mL). The combined organic extracts were dried over MgSO₄ and evaporated under reduced pressure. The residue was dried at high vacuum to give crude **R10d** (79.8 mg, 0.21 mmol, 72%) which was used in the next step without further purification.

TLC (EtOAc +1% acetic acid): $R_f = 0.20$. **¹H-NMR** (400 MHz, CDCl₃): $\delta = 4.09 - 3.98$ (m, 1H), 3.74 (d, $J = 2.1$ Hz, 3H), 3.72 (d, $J = 2.1$ Hz, 3H), 2.32 (t, $J = 7.5$ Hz, 2H), 2.02 (dd, $J = 6.3, 3.4$ Hz, 1H), 1.98 (dd, $J = 6.3, 4.5$ Hz, 1H), 1.63 (h, $J = 5.7$ Hz, 3H), 1.57 – 1.45 (m, 1H), 1.43 – 1.27 (m, 4H), 0.88 (s, 9H), 0.07 (s, 3H), 0.05 (s, 3H). **¹³C-NMR** (101 MHz, CDCl₃): $\delta = 178.1, 67.6, 52.5, 37.9, 37.8, 34.3, 33.9, 32.58, 29.1, 25.9, 25.9, 24.9, 24.4, 18.11, -4.5$. **IR** (neat): $\tilde{\nu} = 2952, 2930, 2856, 1725, 1463, 1253, 1214, 1186, 1059, 1034, 836, 813, 776$ cm⁻¹. **HRMS** (ESI): calcd for C₁₆H₃₅NaO₆PSi [(M+Na)⁺]: 405.1833; found: 405.1834



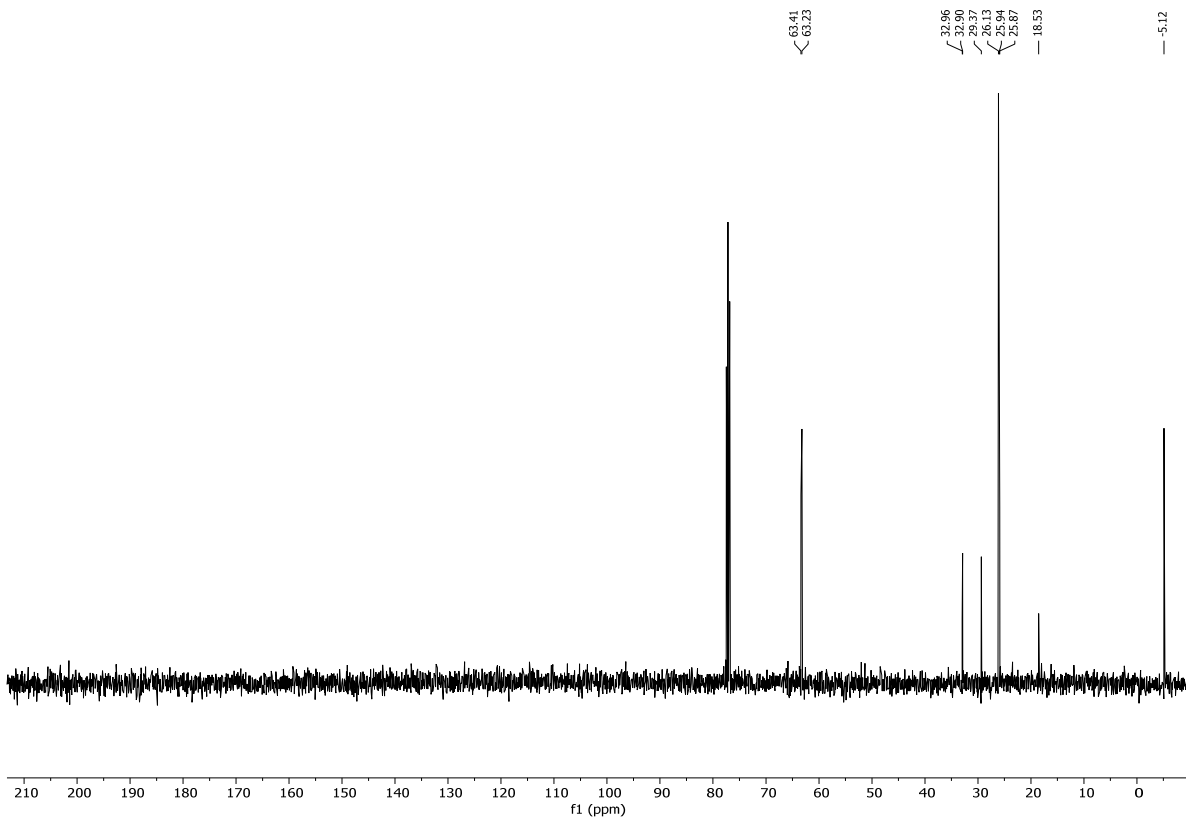
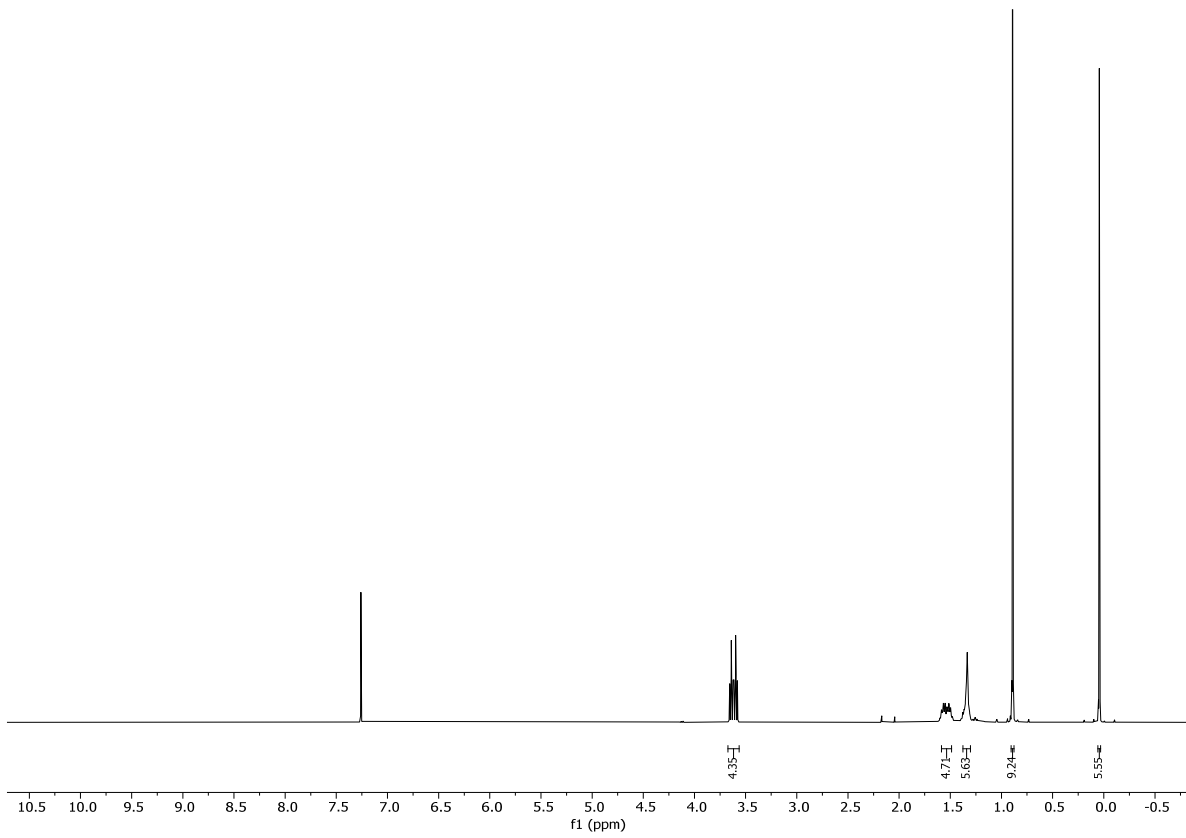
4.2.1.2.2 From heptane-1,7-diol

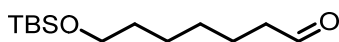
**RS6**

7-((*tert*-Butyldimethylsilyl)oxy)heptan-1-ol (RS6).²² To a solution of heptane-1,7-diol (2.00 mL, 14.39 mmol, 1.00 equiv.) in CH₂Cl₂ (15 mL) was added Et₃N (2.00 mL, 14.39 mmol, 1.00 equiv.) followed by a solution of TBSCl (2.17 g, 14.39 mmol, 1.00 equiv.) in CH₂Cl₂ (7 mL) at 0 °C. After stirring for 18 h at rt, the reaction was quenched with H₂O (20 mL) and the mixture was extracted with CH₂Cl₂ (3 x 20 mL). The combined organic layers were washed with brine (40 mL), dried over MgSO₄ and the solvent was removed under reduced pressure. The residue was purified by FC (EtOAc/hexane 1:4) to afford alcohol intermediate **RS6** (1.90 g, 7.71 mmol, 54%) as a colorless oil.

TLC (EtOAc/hexane 1:5): R_f = 0.20. **¹H-NMR** (400 MHz, CDCl₃): δ = 3.62 (dt, *J* = 16.9, 6.6 Hz, 4H), 1.59 – 1.49 (m, 5H), 1.34 (qd, *J* = 4.8, 3.0 Hz, 6H), 0.89 (s, 9H), 0.04 (s, 6H). **¹³C-NMR** (101 MHz, CDCl₃): δ = 63.4, 63.2, 33.0, 32.9, 29.4, 26.1, 25.9, 25.9, 18.5, -5.1. **IR** (neat): $\tilde{\nu}$ = 2930, 2858, 1472, 1463, 1255, 1097, 1058, 835, 813, 775 cm⁻¹. **HRMS** (ESI): calcd for C₁₃H₃₀NaO₂ Si [(M+Na)⁺]: 269.1907; found: 269.1906.

²² Compound **RS6** was prepared according to Wang *et al.*^[75] Ref.[75] includes ¹H-NMR and ¹³C-NMR data.

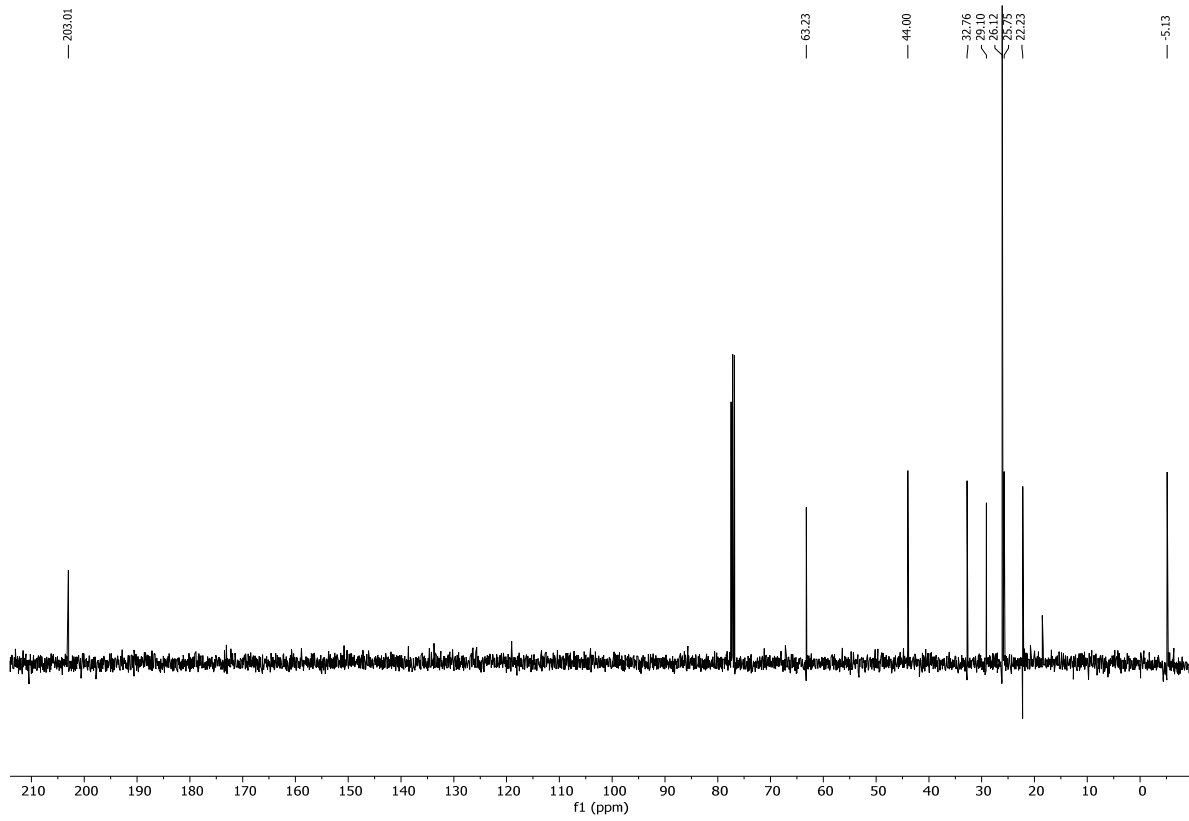
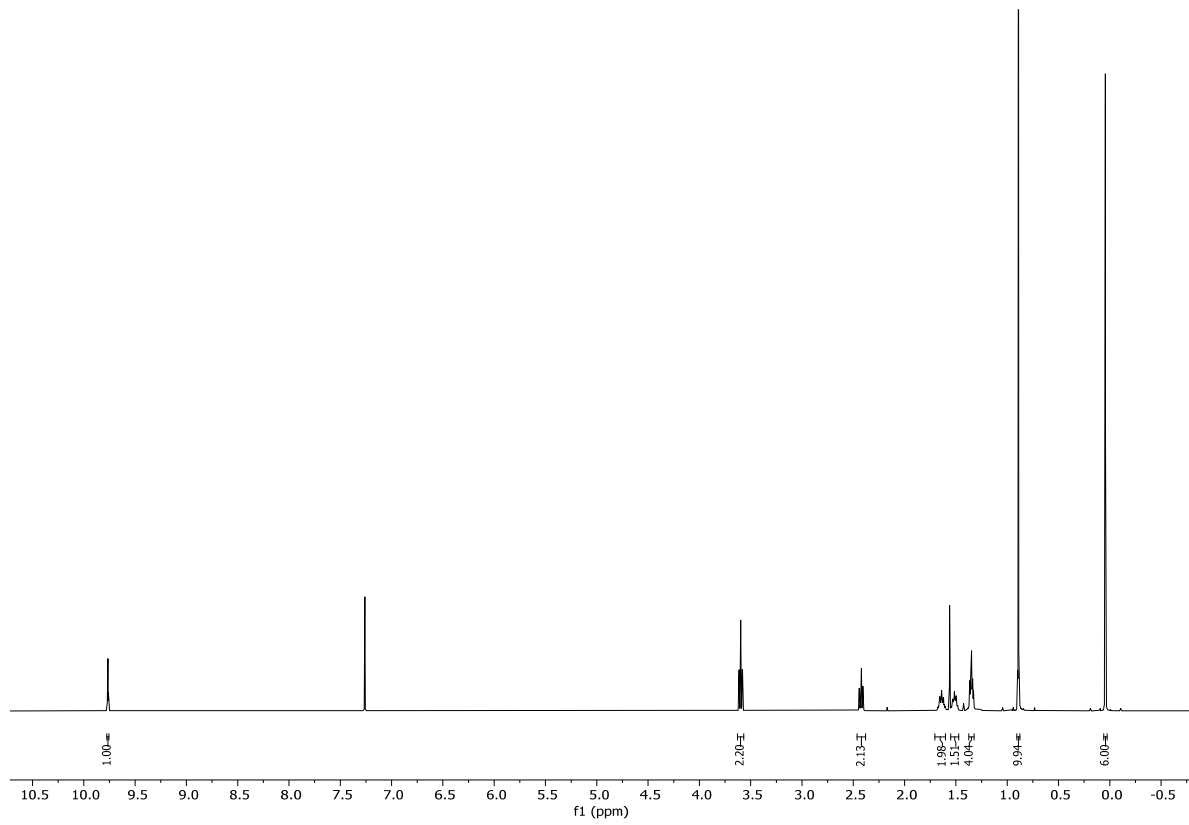


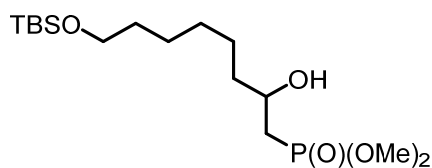
**R22**

7-((tert-Butyldimethylsilyl)oxy)heptanal (R22).²³ To a solution of oxalyl chloride (0.86 mL, 10.02 mmol, 1.30 equiv.) in CH₂Cl₂ (77 mL) was added DMSO (1.21 mL, 16.96 mmol, 2.20 equiv.) dropwise at -78 °C and the reaction mixture was stirred at -78 °C for 10 min. Then a solution of alcohol **RS6** (1.90 g, 7.71 mmol, 1.00 equiv.) in CH₂Cl₂ (4 mL) was added dropwise over a period of 30 min. Immediately following this addition, Et₃N (5.34 mL, 38.54 mmol, 5.00 equiv.) was added and the reaction was stirred at -78 °C for 2 h and then allowed to warm to 0 °C. The reaction was quenched with H₂O (100 mL) and the mixture extracted with CH₂Cl₂ (3 x 90). The combined organic layers were washed with H₂O (100 mL) and brine (100 mL), dried over MgSO₄ and the solvent removed under reduced pressure. The crude material was purified by FC (Et₂O/hexane 1:10) affording aldehyde **R22** (1.67 g, 6.83 mmol, 89%) as a slightly yellow oil.

TLC (EtOAc/hexane 1:5): R_f = 0.40. **¹H-NMR** (400 MHz, CDCl₃): δ = 9.76 (t, *J* = 1.9 Hz, 1H), 3.60 (t, *J* = 6.5 Hz, 2H), 2.42 (td, *J* = 7.3, 1.8 Hz, 2H), 1.64 (tdd, *J* = 7.4, 6.1, 4.1 Hz, 2H), 1.55 – 1.47 (m, 2H), 1.37 – 1.32 (m, 4H), 0.89 (s, 10H), 0.04 (s, 6H). **¹³C-NMR** (101 MHz, CDCl₃): δ = 203.0, 63.2, 44.0, 32.8, 29.1, 26.1, 25.8, 22.2, -5.1. **IR** (neat): $\tilde{\nu}$ = 2930, 2897, 2858, 1723, 1255, 1097, 835, 776 cm⁻¹. **HRMS** (ESI): calcd for C₁₃H₂₈NaO₂Si [(M+Na)⁺]: 267.1751; found: 267.1746.

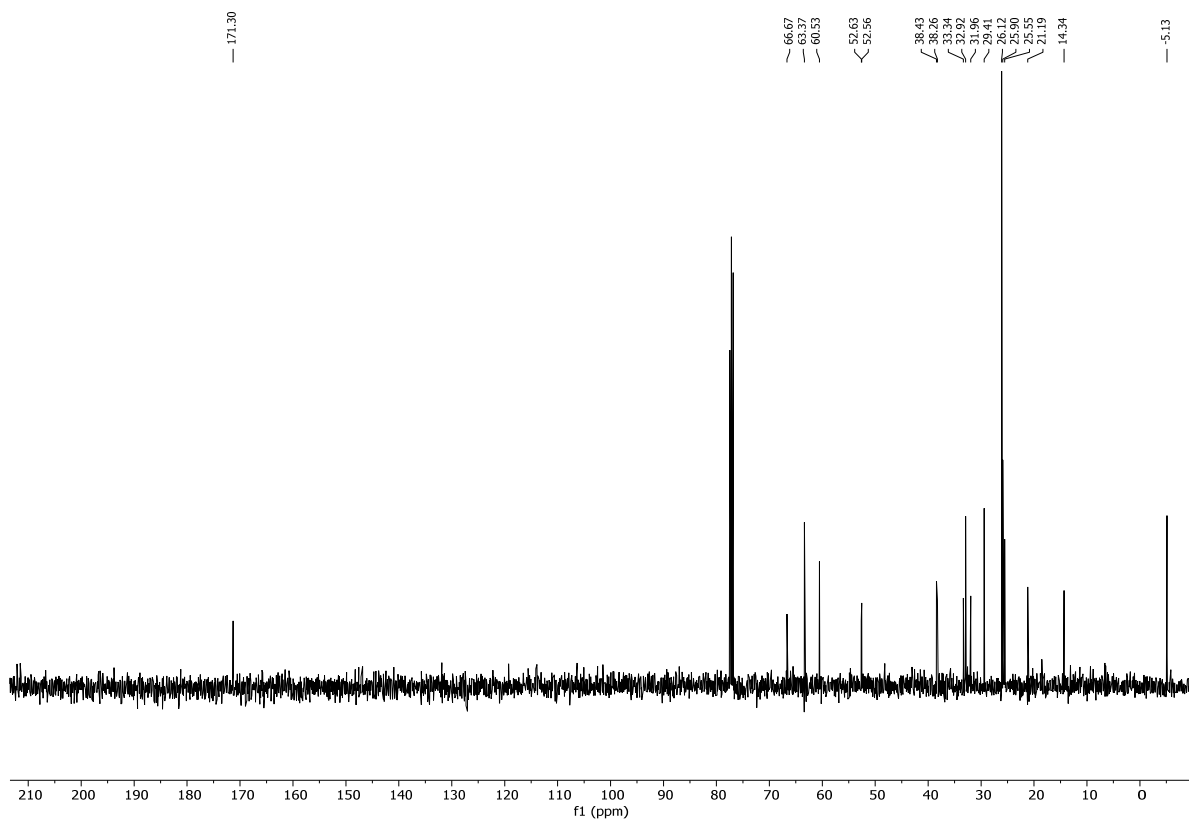
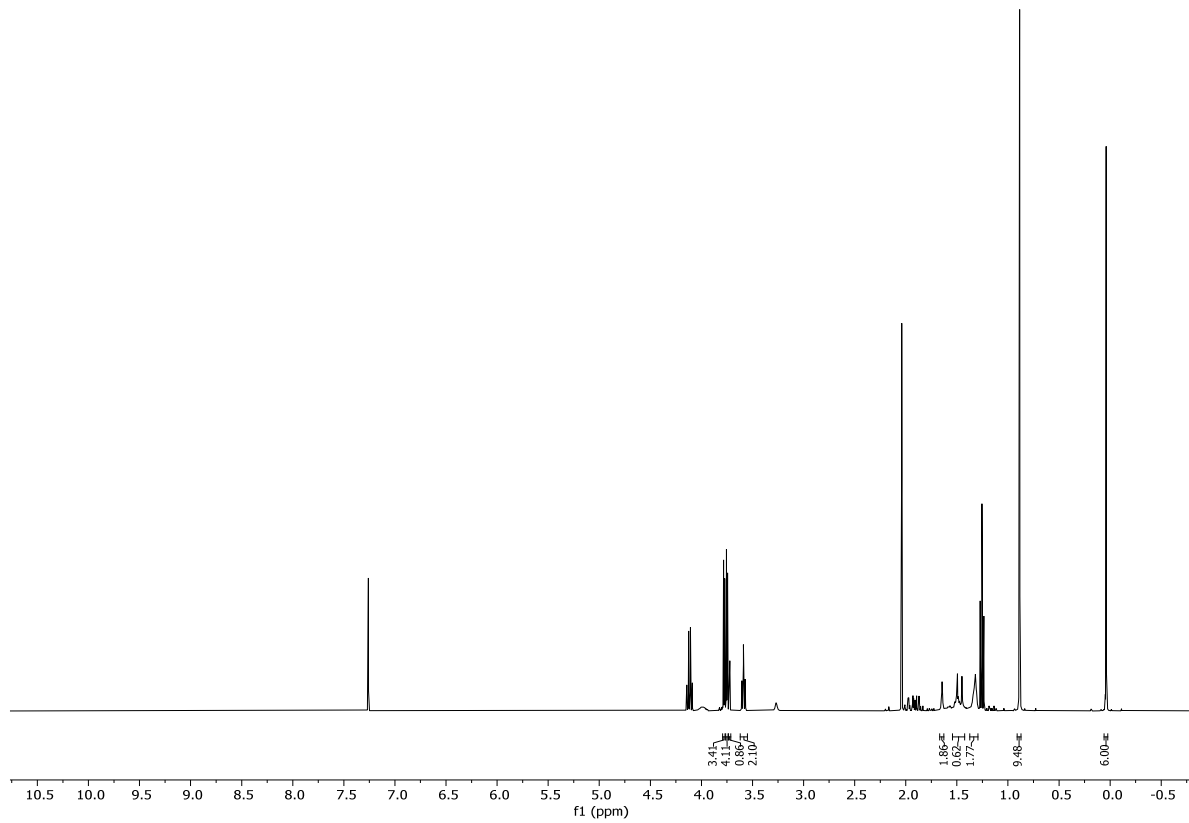
²³ Aldehyde **R22** was prepared according to Boger and Mathvink.^[76] Ref.[76] includes ¹H-NMR data; ¹³C data have not been reported for **R22** (based on the information available in SciFinder).

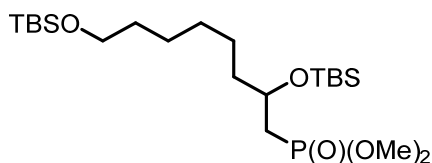


**RS7**

Dimethyl (8-((*tert*-butyldimethylsilyl)oxy)-2-hydroxyoctyl)phosphonate (RS7). To a solution of dimethyl phosphonate (2.70 mL, 25.17 mmol, 3.69 equiv.) in THF (60 mL) was added *n*-BuLi (12.60 mL, 20.15 mmol, 2.95 equiv.) at $-80\text{ }^{\circ}\text{C}$. The resulting yellow solution was stirred for 30 min at $-80\text{ }^{\circ}\text{C}$ and then cooled to $-100\text{ }^{\circ}\text{C}$ (N_2/EtOH). Then, a solution of **R22** (1.67 g, 6.83 mmol, 1.00 equiv.) in THF (40 mL), was added dropwise and the resulting solution was stirred for 1 h at $-100\text{ }^{\circ}\text{C}$. Sat aq. NaHCO_3 (80 mL) was added and the mixture was allowed to warm to rt. After addition of EtOAc (50 mL) and H_2O (50 mL), the layers were separated and the aqueous layer was extracted with EtOAc ($3 \times 80\text{ mL}$). The combined organic layers were dried over MgSO_4 , filtered, and concentrated under reduced pressure. Purification of the residue by FC (EtOAc) afforded alcohol **RS7**. The yield could not be determined because the compound still contained substantial amount of dimethyl methylphosphonate.

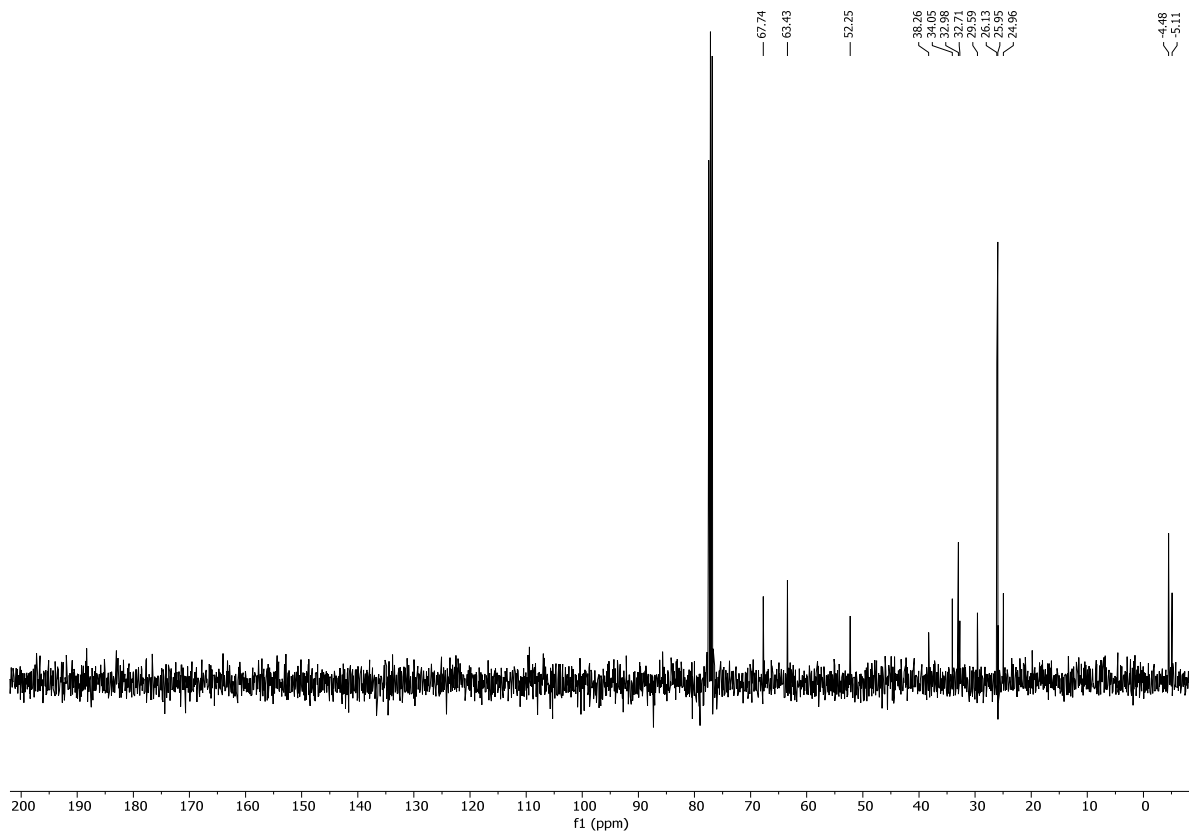
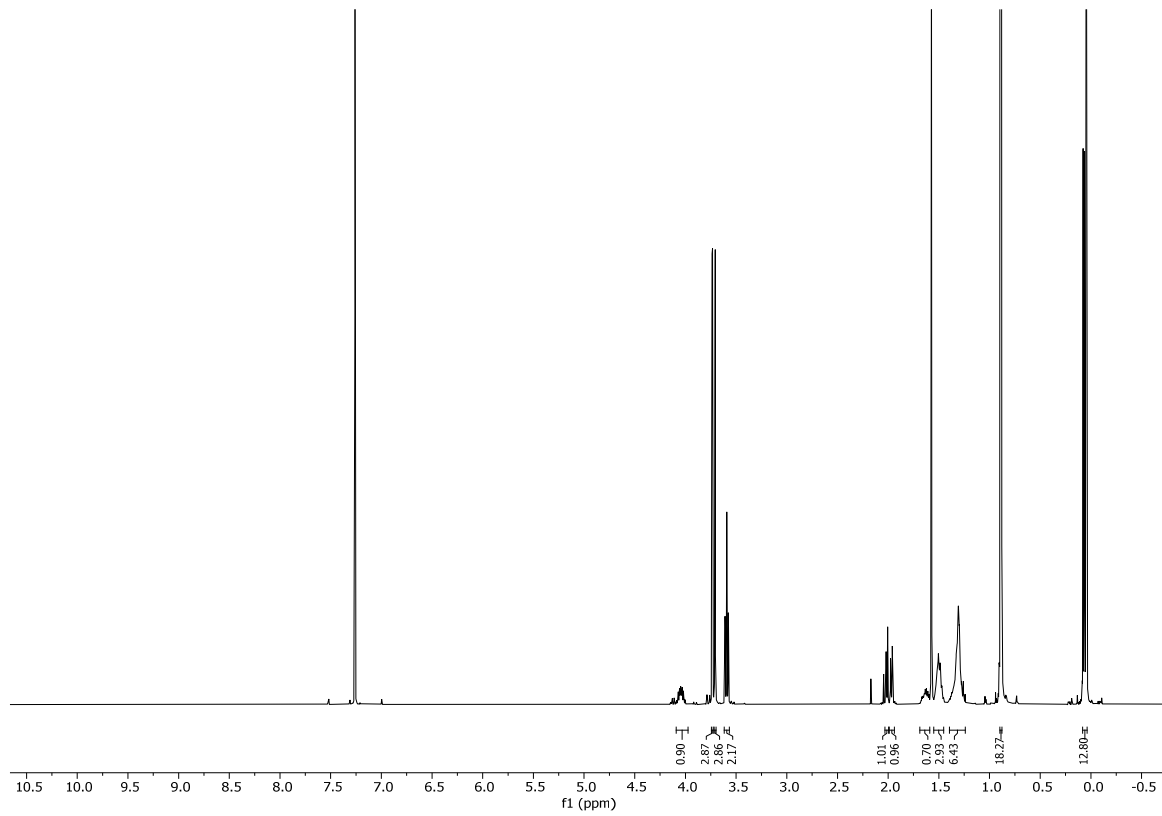
TLC (EtOAc): $R_f = 0.45$. **$^1\text{H-NMR}$** (400 MHz, CDCl_3): $\delta = 3.78$ (d, $J = 4.5\text{ Hz}$, 3H), 3.76 – 3.74 (m, 4H), 3.73 (d, $J = 2.7\text{ Hz}$, 1H), 3.59 (t, $J = 6.6\text{ Hz}$, 2H), 1.64 (s, 2H), 1.47 (d, $J = 17.5\text{ Hz}$, 1H), 1.32 (s, 2H), 0.89 (s, 9H), 0.04 (s, 6H). **$^{13}\text{C-NMR}$** (101 MHz, CDCl_3): $\delta = 171.3, 66.7, 63.4, 60.5, 52.6, 52.6, 38.4, 38.3, 33.3, 32.9, 32.0, 29.4, 26.1, 25.9, 25.6, 21.2, 14.3, -5.1$. **IR** (neat): $\tilde{\nu} = 2952, 2930, 2856, 1252, 1228, 1186, 1098, 1061, 1035, 836, 776\text{ cm}^{-1}$. **HRMS** (ESI): calcd for $\text{C}_{16}\text{H}_{37}\text{NaO}_5\text{PSi}$ [(M+Na) $^+$]: 391.2040; found: 391.2048.

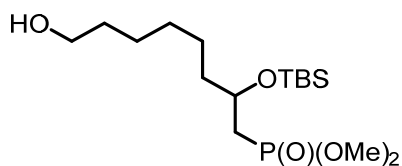


**R23**

Dimethyl (2,8-bis((*tert*-butyldimethylsilyl)oxy)octyl)phosphonate (R23). To a solution of alcohol **RS7** (3.20 g, 10.80 mmol, 1.00 equiv.) in DMF (24 mL) were added sequentially imidazole (4.41 g, 64.80 mmol, 6.00 equiv.), DMAP (1.32 g, 10.80 mmol, 1.00 equiv.) and TBSCl (4.88 g, 32.40 mmol, 3.00 equiv.) at rt. The mixture was stirred for 1 d; H₂O (40 mL) and Et₂O (40 mL) were then added, the phases were separated, and the aqueous phase was extracted with Et₂O (3 x 30 mL). The combined organic extracts were then washed with H₂O (2 x 30 mL), the combined organic phases were dried over MgSO₄ and concentrated under reduced pressure. Purification of the residue by FC (EtOAc/hexane 1:1) afforded **R23** (2.66 g, 5.51 mmol, 85% over two steps) as a colorless oil.

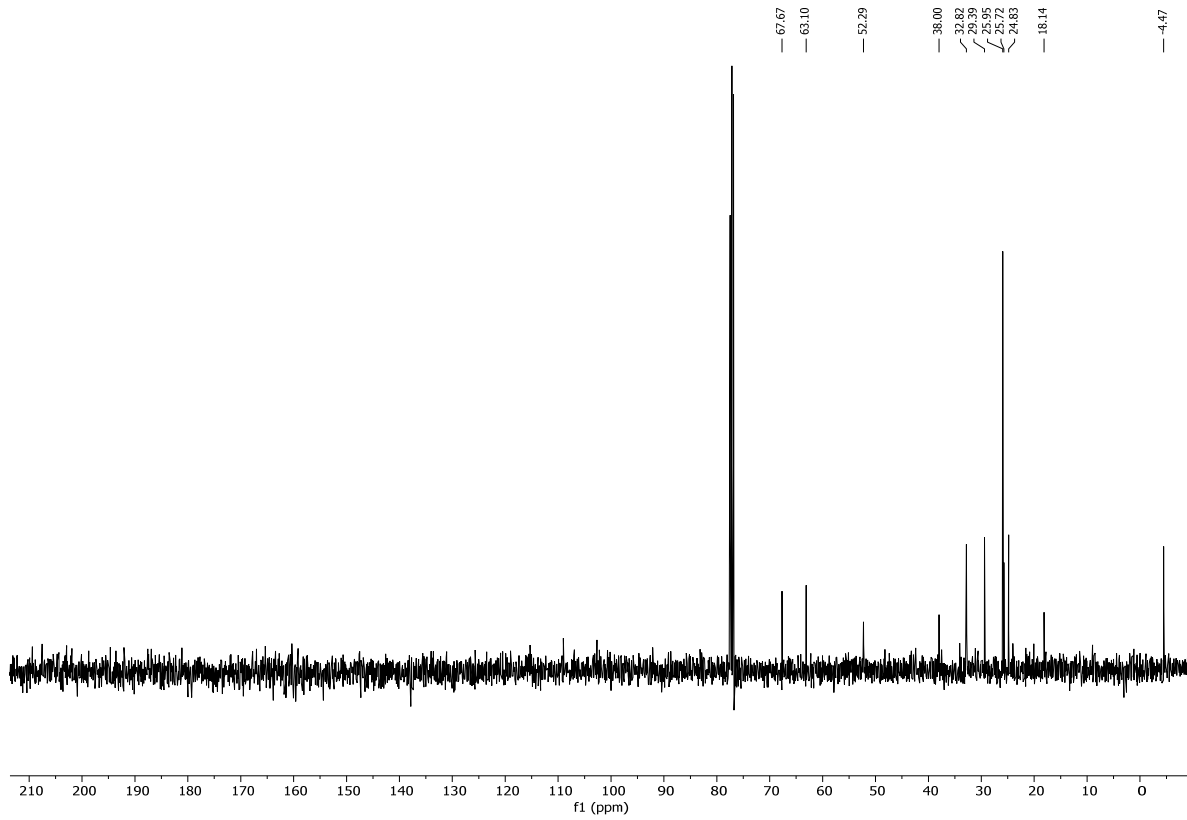
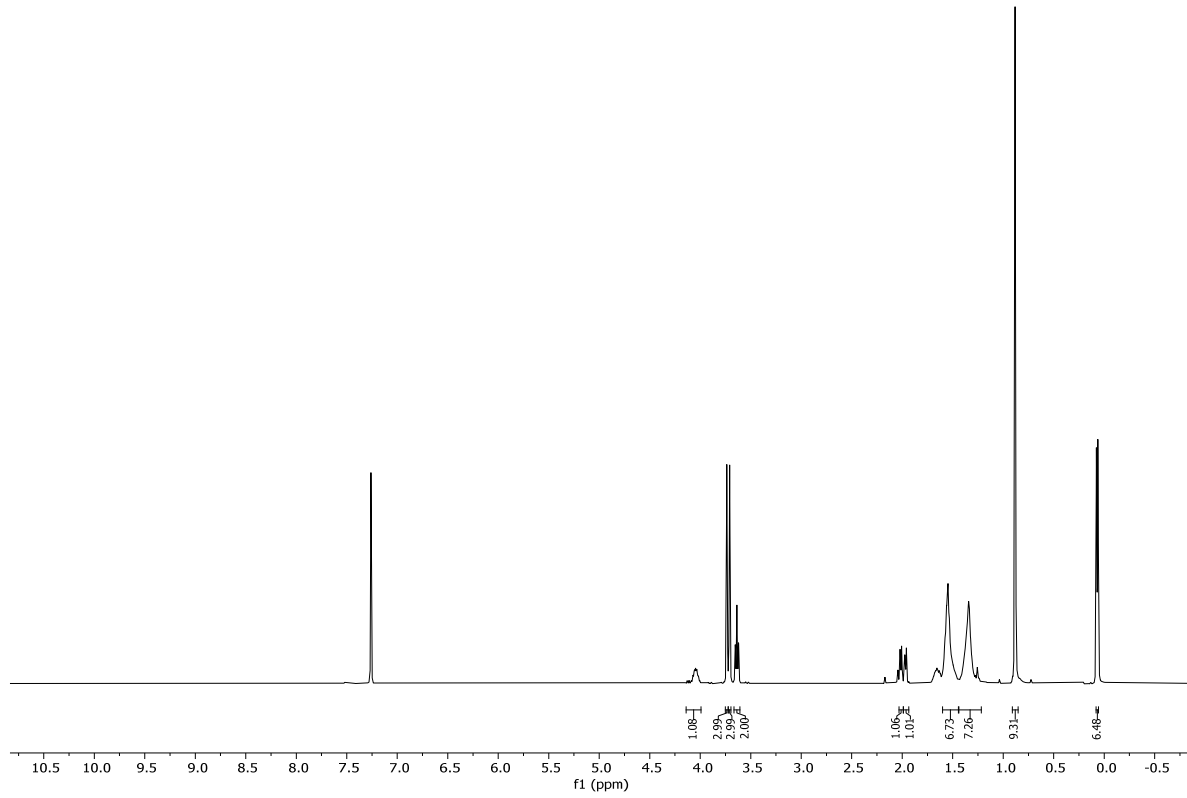
TLC (EtOAc): $R_f = 0.72$. **¹H-NMR** (400 MHz, CDCl₃): $\delta = 4.05$ (ddd, $J = 8.9, 6.2, 4.6$ Hz, 1H), 3.74 (d, $J = 1.5$ Hz, 3H), 3.71 (d, $J = 1.6$ Hz, 3H), 3.59 (t, $J = 6.6$ Hz, 2H), 2.03 – 1.99 (m, 1H), 1.97 (dd, $J = 6.3, 1.2$ Hz, 1H), 1.63 (tt, $J = 10.3, 4.7$ Hz, 1H), 1.50 (t, $J = 7.0$ Hz, 3H), 1.31 (q, $J = 6.6$ Hz, 6H), 0.89 (d, $J = 3.0$ Hz, 18H), 0.08 – 0.04 (m, 13H). **¹³C-NMR** (101 MHz, CDCl₃): $\delta = 67.7, 63.4, 52.3, 38.3, 34.1, 33.0, 32.7, 29.6, 26.1, 26.0, 25.0, -4.5, -5.1$. **IR** (neat): $\tilde{\nu} = 2952, 2929, 2896, 2856, 1472, 1463, 1254, 1098, 1035, 1007, 835, 813, 775$ cm⁻¹. **HRMS** (ESI): calcd for C₂₂H₅₂O₅PSi₂ [(M+H)⁺]: 483.3085; found: 483.3082.

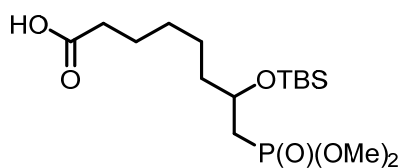


**RS8**

Dimethyl (2-((*tert*-butyldimethylsilyl)oxy)-8-hydroxyoctyl)phosphonate (RS8). CSA (0.25 g, 0.25 mmol, 0.20 equiv.) was added to a solution of **R23** (2.56 g, 5.30 mmol, 1.00 equiv.) in CH₂Cl₂:MeOH 1:1 (106 mL) at 0° C. After 20 min, the mixture was allowed to warm to rt and stirred at rt for 15 min. Sat. aqu. NaHCO₃ (130 mL) was then added and the aqueous layer was extracted with CH₂Cl₂ (3x 150 mL). The combined organic extracts were dried over MgSO₄ and then concentrated. Purification of the residue by FC (EtOAc) afforded primary alcohol **RS8** (1.96 g, 5.30 mmol, quant) as a colorless oil.

TLC (EtOAc): $R_f = 0.23$. **¹H-NMR** (400 MHz, CDCl₃): $\delta = 4.05$ (dt, $J = 10.7, 5.5$ Hz, 1H), 3.74 (s, 3H), 3.71 (s, 3H), 3.64 (t, $J = 6.5$ Hz, 2H), 2.01 (d, $J = 6.2$ Hz, 1H), 1.97 (d, $J = 6.1$ Hz, 1H), 1.56 (q, $J = 7.1$ Hz, 7H), 1.36 (d, $J = 14.8$ Hz, 7H), 0.88 (s, 9H), 0.07 (d, $J = 5.9$ Hz, 6H). **¹³C-NMR** (101 MHz, CDCl₃): $\delta = 67.7, 63.1, 52.3, 38.0, 32.8, 29.4, 26.0, 25.7, 24.8, 18.1, -4.5$. **IR** (neat): $\tilde{\nu} = 2929, 2856, 1254, 1035, 835, 776$ cm⁻¹. **HRMS** (ESI): calcd for C₁₆H₃₇NaO₅PSi [(M+Na)⁺]: 391.2040; found: 391.2040.

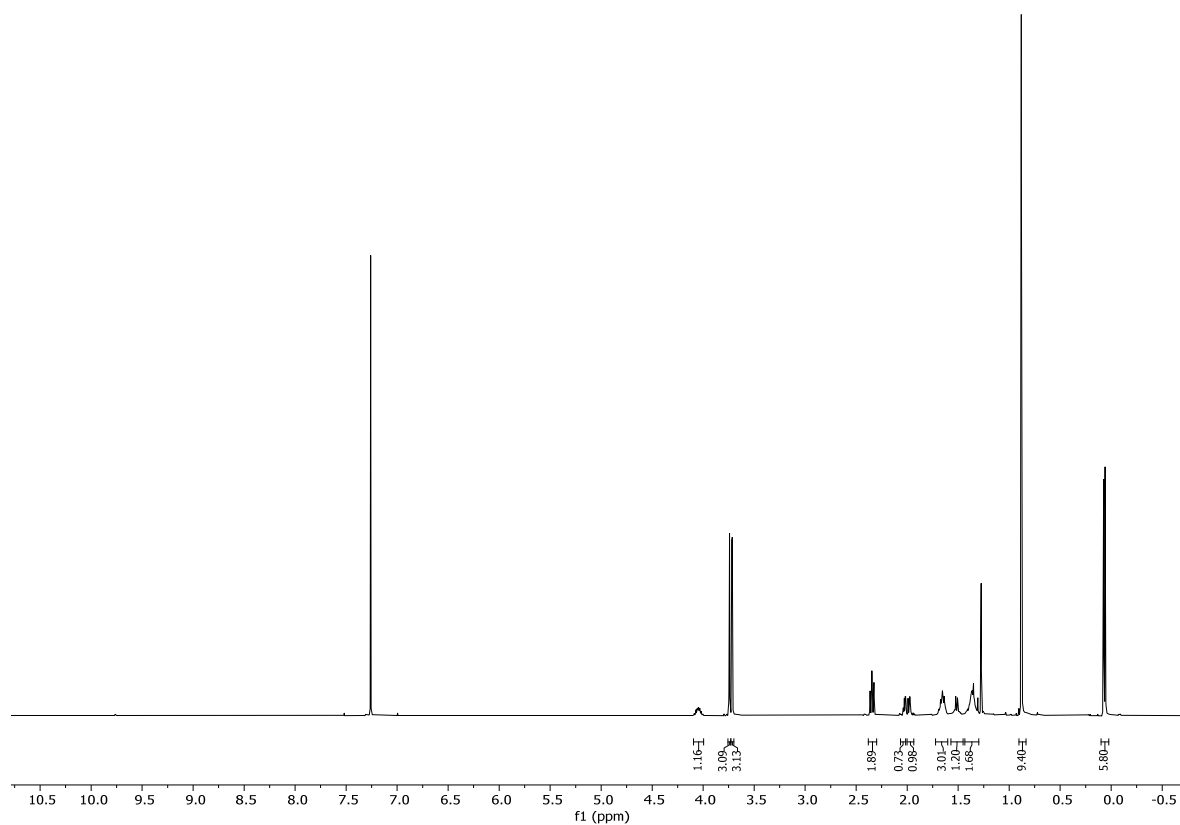


**R10d**

7-((*tert*-Butyldimethylsilyl)oxy)-8-(dimethoxyphosphoryl)octanoic acid (R10d). To a solution of primary alcohol **RS8** (1.00 g, 2.71 mmol, 1.00 equiv.) in CH₂Cl₂ (70 mL) at rt was added NaHCO₃ (0.64 mg, 8.14 mmol, 3.00 equiv.) and Dess-Martin periodinane (1.73 g, 4.07 mmol, 1.50 equiv.). The reaction mixture was stirred at rt for 45 min, when more Dess-Martin periodinane (1.73 g, 4.07 mmol, 1.50 equiv.) was added and the stirring was continued for another 45 min. The reaction mixture was then diluted with CH₂Cl₂ (9 mL) and a mixture of aqu. Na₂S₂O₃ and NaHCO₃ was added (250 mL). The aqueous layer was extracted with CH₂Cl₂ (3 x 250 mL). The combined organic layers were washed with brine (250 mL), dried over MgSO₄ and concentrated under reduced pressure. The crude aldehyde, obtained as a pale yellow oil, was used in the next step without further purification.

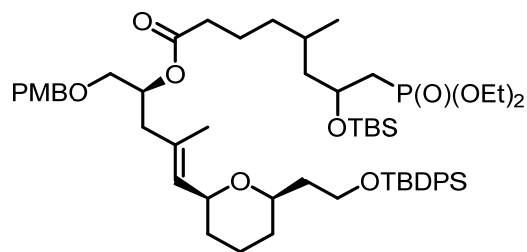
To a solution of the above aldehyde (0.99 g, 2.70 mmol, 1.00 equiv.) in a mixture of *t*-BuOH (35 mL) and 2-methyl-2-butene (35 mL) at 0 °C was added a solution of NaClO₂ (80%, 0.78 g, 8.64 mmol, 3.20 equiv.) and NaH₂PO₄ dihydrate (1.69 g, 10.81 mmol, 4.00 equiv.) in H₂O (100 mL) dropwise. The reaction mixture was stirred at that temperature for 45 min and 2 h at rt before it was diluted with CH₂Cl₂ (100 mL) and brine (100 mL). The layers were separated and the aqueous layer was extracted with CH₂Cl₂ (3 x 150 mL). The combined organic layers were washed with brine (150 mL), dried over MgSO₄ and concentrated under reduced pressure to afford **R10d** (0.96 g (93 % over two steps) as a colorless oil.

¹H-NMR (400 MHz, CDCl₃): δ = 4.09 – 4.00 (m, 1H), 3.74 (d, *J* = 2.0 Hz, 3H), 3.72 (d, *J* = 2.0 Hz, 3H), 2.35 (dd, *J* = 7.9, 7.1 Hz, 2H), 2.07 – 2.02 (m, 1H), 1.98 (dd, *J* = 6.2, 3.7 Hz, 1H), 1.72 – 1.60 (m, 3H), 1.57 – 1.45 (m, 1H), 1.43 – 1.30 (m, 2H), 0.88 (s, 9H), 0.07 (d, *J* = 6.1 Hz, 6H).



4.2.1.3 Assembly of analogs R7 and R8

4.2.1.3.1 Synthesis of analog R7

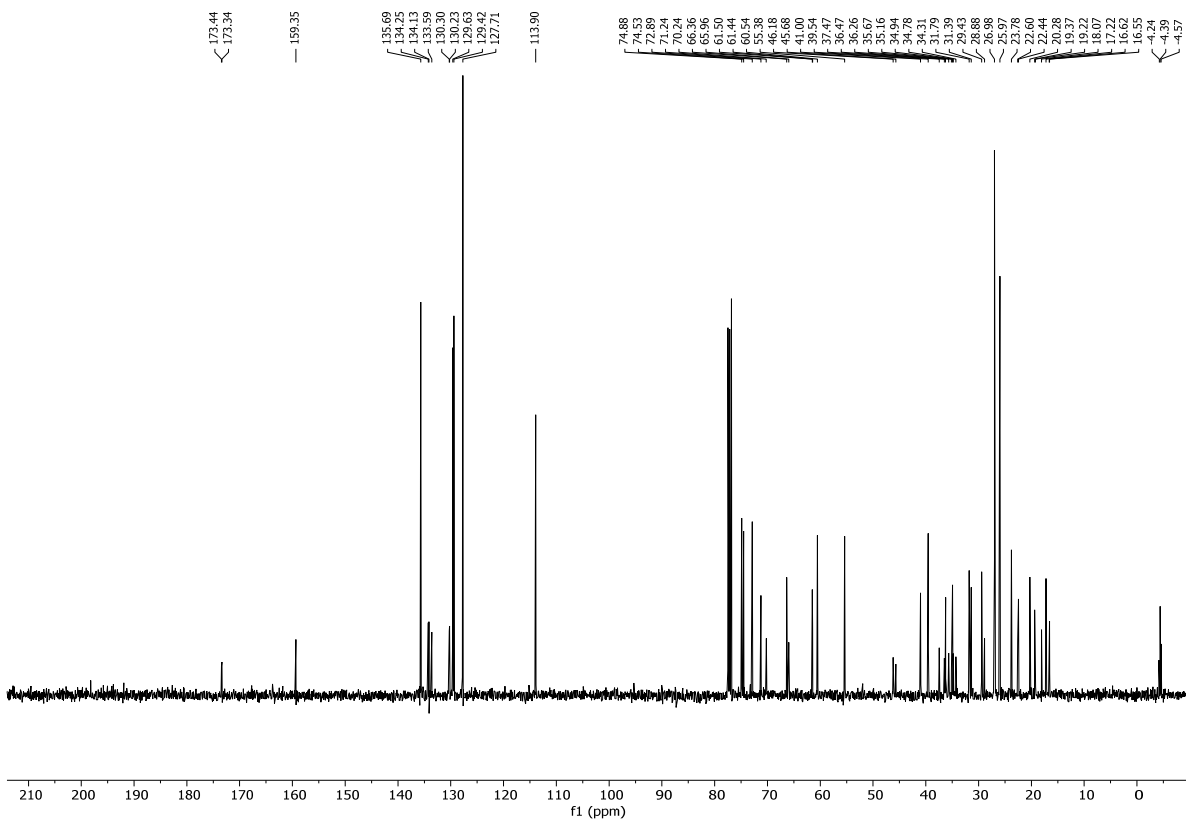
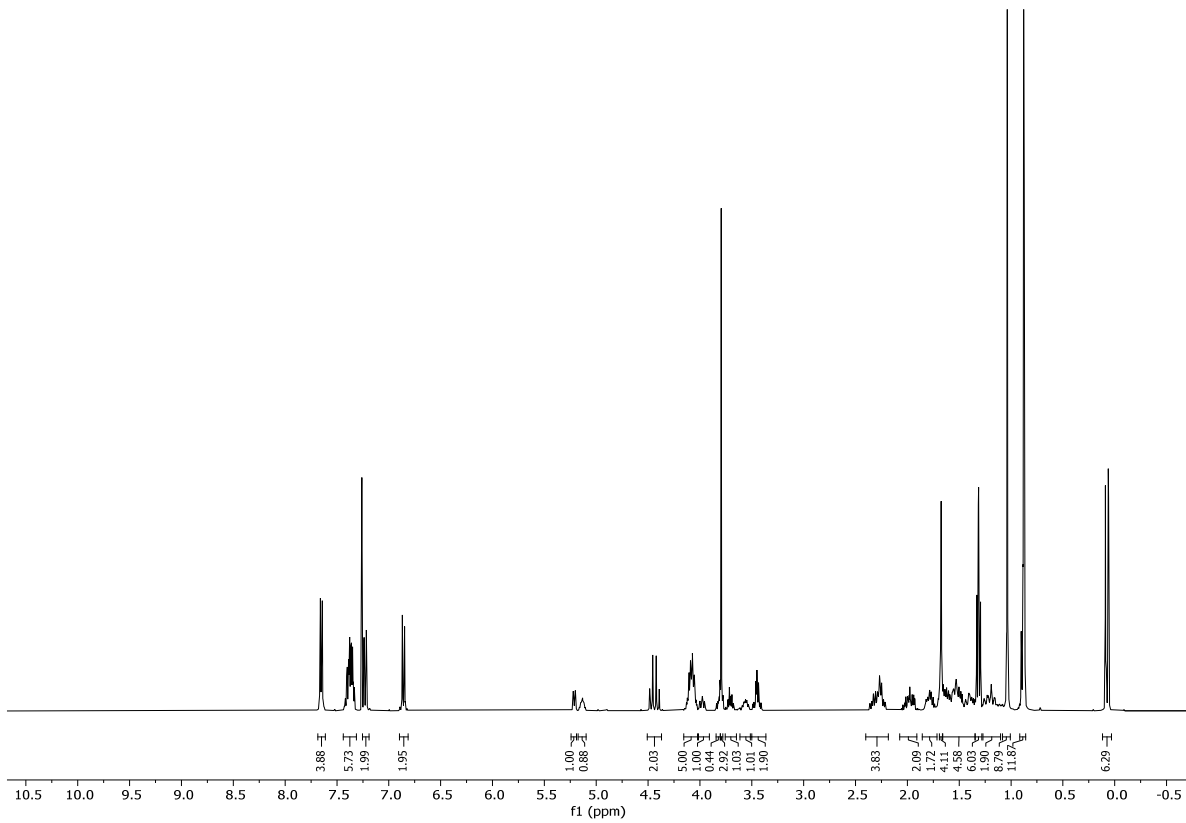


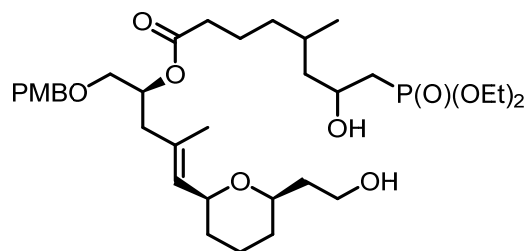
R29ca

(*S,E*)-5-((2*S,6R*)-6-(2-((*tert*-Butyldiphenylsilyl)oxy)ethyl)tetrahydro-2H-pyran-2-yl)-1-((4-methoxybenzyl)oxy)-4-methylpent-4-en-2-yl-7-((*tert*-butyldimethylsilyl)oxy)-8-(diethoxyphosphoryl)-5-methyloctanoate (R29ca). To a solution of **R10c** (1.22 g, 2.43 mmol, 1.20 equiv., co-evaporated twice with 10 mL of toluene immediately before use) in toluene (18 mL) was added Et₃N (0.73 mL, 5.26 mmol, 2.60 equiv.) followed by 2,4,6-trichlorobenzoyl chloride (0.47 mL, 3.04 mmol, 1.50 equiv.). After 2 h at rt, a solution of **R11a** (1.22 g, 2.02 mmol, 1.00 equiv.) and DMAP (0.25g, 2.02 mmol, 1.00 equiv., co-evaporated twice with 10 mL of toluene immediately before use) in toluene (8 mL, plus additional 8 mL from rinsing) was added, immediately leading to a yellow suspension. After stirring at rt for 1.5 h sat. aqu. aqueous NaHCO₃ (35 mL), H₂O (35 mL) and EtOAc (35 mL) were added, the phases were separated and the aqueous phase was extracted with EtOAc (3 x 40 mL). The combined organic extracts were dried over MgSO₄, concentrated under reduced pressure, and the residue was purified by FC (EtOAc/hexane 1:2→1:1) to give **R29ca** (1.55 g, 1.53 mmol, 76%) as a colorless viscous oil.

TLC: R_f = 0.70 (EtOAc). **¹H-NMR** (400 MHz, CDCl₃): δ = 7.68 – 7.61 (m, 4H), 7.37 (dtdd, *J* = 12.7, 8.5, 4.7, 1.7 Hz, 6H), 7.25 – 7.19 (m, 2H), 6.90 – 6.81 (m, 2H), 5.21 (dd, *J* = 7.8, 1.5 Hz, 1H), 5.13 (ddt, *J* = 7.7, 3.8, 1.9 Hz, 1H), 4.51 – 4.37 (m, 2H), 4.16 – 4.01 (m, 5H), 3.98 (ddd, *J* = 10.4, 7.7, 2.3 Hz, 1H), 3.84 – 3.80 (m, 0H), 3.79 (s, 3H), 3.70 (dt, *J* = 10.0, 5.7 Hz, 1H), 3.61 – 3.50 (m, 1H), 3.51 – 3.36 (m, 2H), 2.28 (dddd, *J* = 18.3, 15.2, 13.6, 6.9 Hz, 4H), 2.07 – 1.91 (m, 2H), 1.78 (ddt, *J* = 13.1, 11.0, 4.3 Hz, 2H), 1.68 (d, *J* = 1.3 Hz, 4H), 1.66 – 1.35 (m, 5H), 1.31 (td, *J* = 7.0, 1.2 Hz, 6H), 1.27 – 1.10 (m, 2H), 1.04 (s, 9H), 0.92 – 0.86 (m, 12H), 0.12 – 0.03 (m, 6H). **¹³C-NMR** (101 MHz, CDCl₃) δ = 173.4, 173.3, 159.4, 135.7, 134.3, 134.1, 133.6, 130.3, 130.2, 129.6, 129.4, 127.7, 113.9, 74.9, 74.5, 72.9, 71.2, 70.2, 66.4, 66.0, 61.5, 61.4, 60.5, 55.4, 46.2, 45.7, 41.0, 39.5, 37.5, 36.5, 36.3, 35.7, 35.2, 34.9, 34.8, 34.3, 31.8, 31.4, 29.4, 28.9, 27.0, 26.0, 23.8, 22.6, 22.4, 20.3, 19.4, 19.2, 18.1, 17.2, 16.6, 16.6, -4.2, -4.4, -4.6. **IR** (neat): $\tilde{\nu}$ = 2930, 2856, 1734, 1514, 1472, 1463, 1442,

1428, 1389, 1362, 1302, 1248, 1173, 1109, 1094, 1073, 1031, 957, 912, 835, 823, 808, 775, 741, 703, 688, 614, 546, 505 cm⁻¹. **HRMS** (ESI): calcd for C₅₆H₈₉NO₁₀PSi₂ [(M+Na)⁺]: 1031.5624; found: 1031.5623.

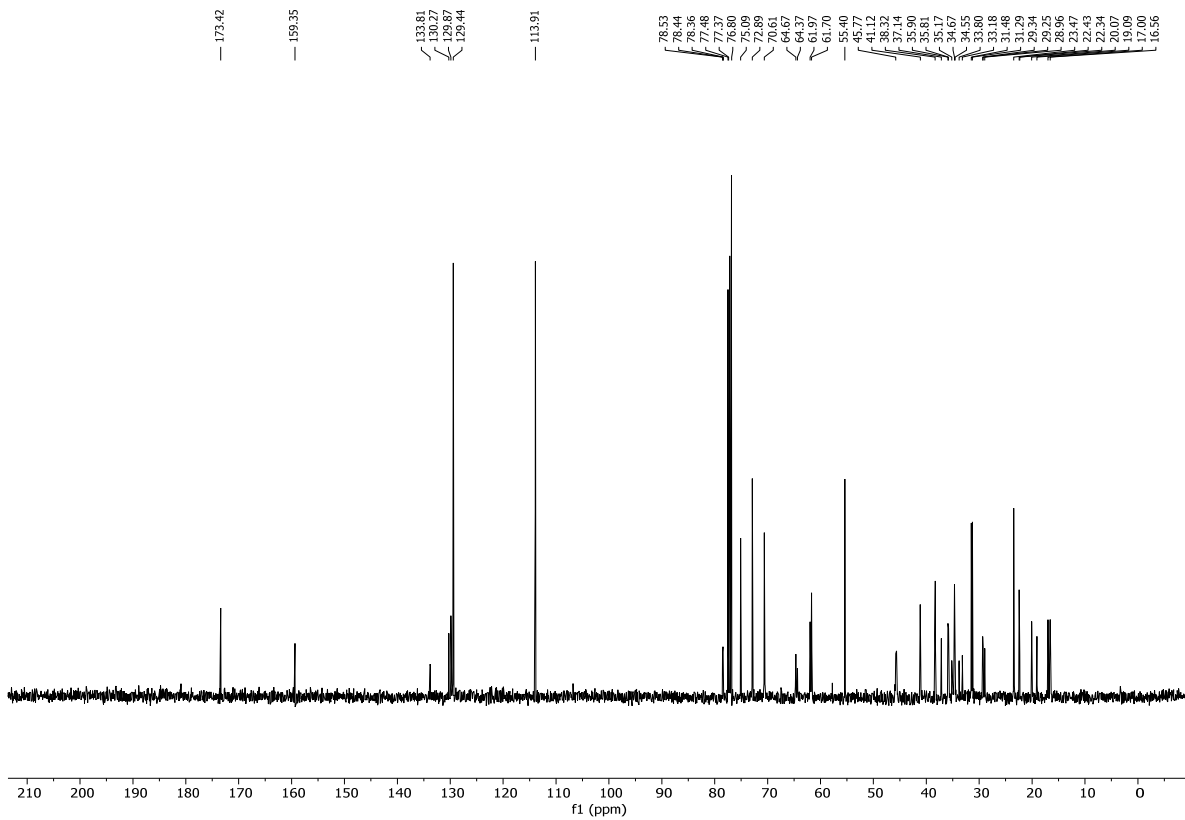
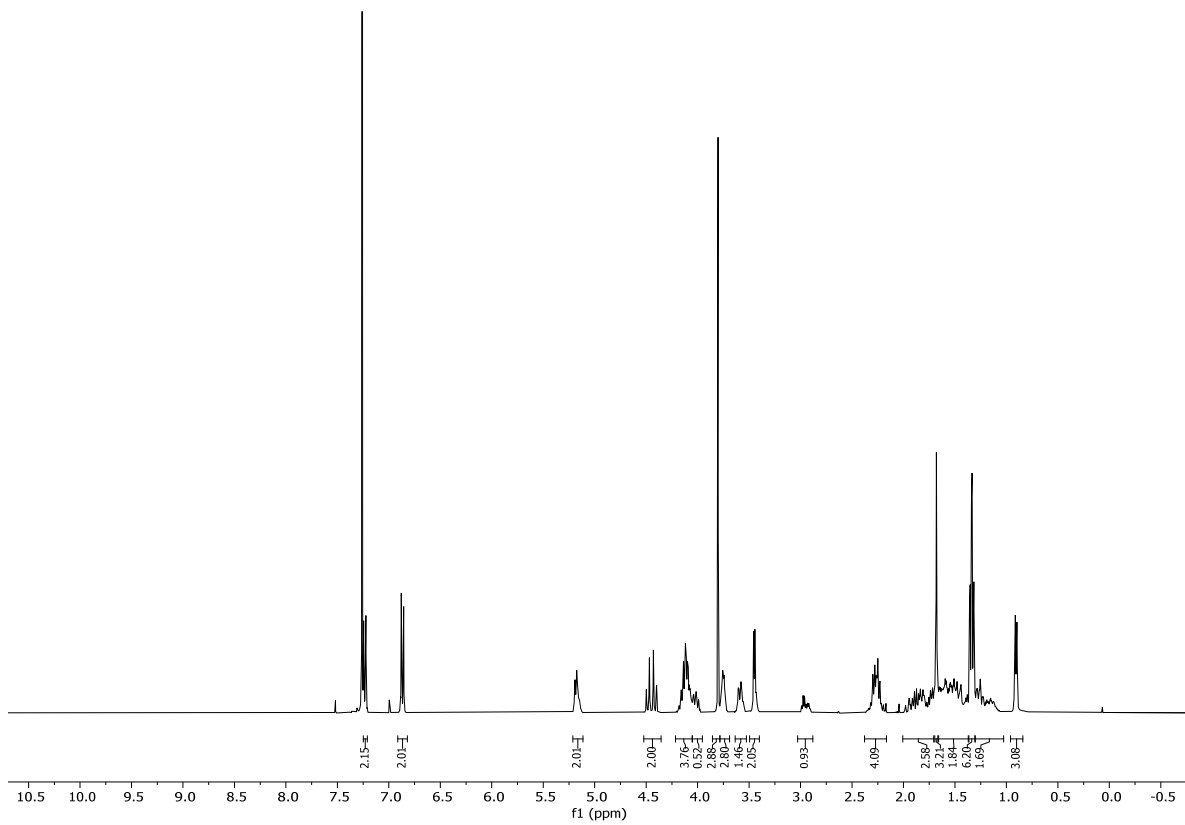


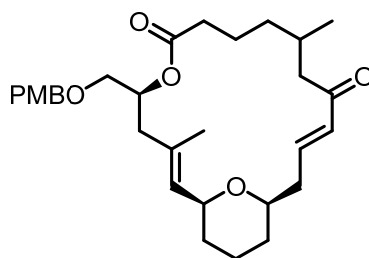


RS18ca

(*S,E*)-5-((*2S,6R*)-6-(2-Hydroxyethyl)tetrahydro-2H-pyran-2-yl)-1-((4-methoxybenzyl)oxy)-4-methylpent-4-en-2-yl 8-(diethoxyphosphoryl)-7-hydroxy-5-methyloctanoate (RS18ca). To a stirred solution of **R29ca** (1.53 g, 1.52 mmol, 1.00 equiv.) in THF (75 mL) in a plastic Erlenmeyer flask was added 70% HF•py (15 mL) along the tube wall at 0 °C. The cooling bath was removed after 5 min and stirring was continued at rt for 20h. The solution was then carefully added to a vigorously stirred mixture of sat. aqu. aqueous NaHCO₃ (700 mL) (check pH) and EtOAc (250 mL) until two clear phases were formed (ca. 15 min). The phases were separated, the aqueous phase was extracted with EtOAc (3 x 250 mL), the combined organic extracts were washed with sat. aqu. NaHCO₃ (200 mL) followed by drying over MgSO₄. Concentration under reduced pressure and purification by FC (acetone/EtOAc 1:1) afforded diol **RS18ca** (0.87 g, 1.33 mmol, 88%) as a pale yellow, viscous oil.

TLC: R_f = 0.50 (acetone/EtOAc 1:1). **¹H-NMR** (400 MHz, CDCl₃): δ = 7.25 – 7.21 (m, 2H), 6.91 – 6.82 (m, 2H), 5.21 – 5.11 (m, 2H), 4.52 – 4.36 (m, 2H), 4.21 – 4.05 (m, 4H), 4.05 – 3.95 (m, 1H), 3.80 (s, 3H), 3.75 (d, *J* = 5.2 Hz, 3H), 3.63 – 3.53 (m, 1H), 3.49 – 3.40 (m, 2H), 2.95 (dt, *J* = 16.8, 5.2 Hz, 1H), 2.38 – 2.17 (m, 4H), 2.01 – 1.71 (m, 3H), 1.68 (d, *J* = 1.3 Hz, 3H), 1.66 – 1.37 (m, 2H), 1.34 (td, *J* = 7.1, 2.5 Hz, 6H), 1.30 – 1.03 (m, 2H), 0.91 (dd, *J* = 6.6, 2.6 Hz, 3H). **¹³C-NMR** (101 MHz, CDCl₃) δ = 173.4, 159.4, 133.8, 130.3, 129.9, 129.4, 113.9, 78.5, 78.4, 78.4, 77.5, 77.4, 76.8, 75.1, 72.9, 70.6, 64.7, 64.4, 62.0, 61.70, 55.40, 45.77, 41.12, 38.32, 37.14, 35.90, 35.81, 35.17, 34.67, 34.55, 33.80, 33.18, 31.48, 31.29, 29.34, 29.25, 28.96, 23.47, 22.43, 22.34, 20.07, 19.09, 17.00, 16.56. **IR** (neat): $\tilde{\nu}$ = 3402, 2931, 2859, 1732, 1613, 1514, 1457, 1442, 1369, 1303, 1247, 1172, 1092, 1054, 1030, 963, 913, 822, 567, 473, 450, 422 cm⁻¹. **HRMS** (ESI): calcd for C₃₄H₅₇O₁₀P [(M+Na)⁺]: 679.3582; found: 679.3577.





R30ca

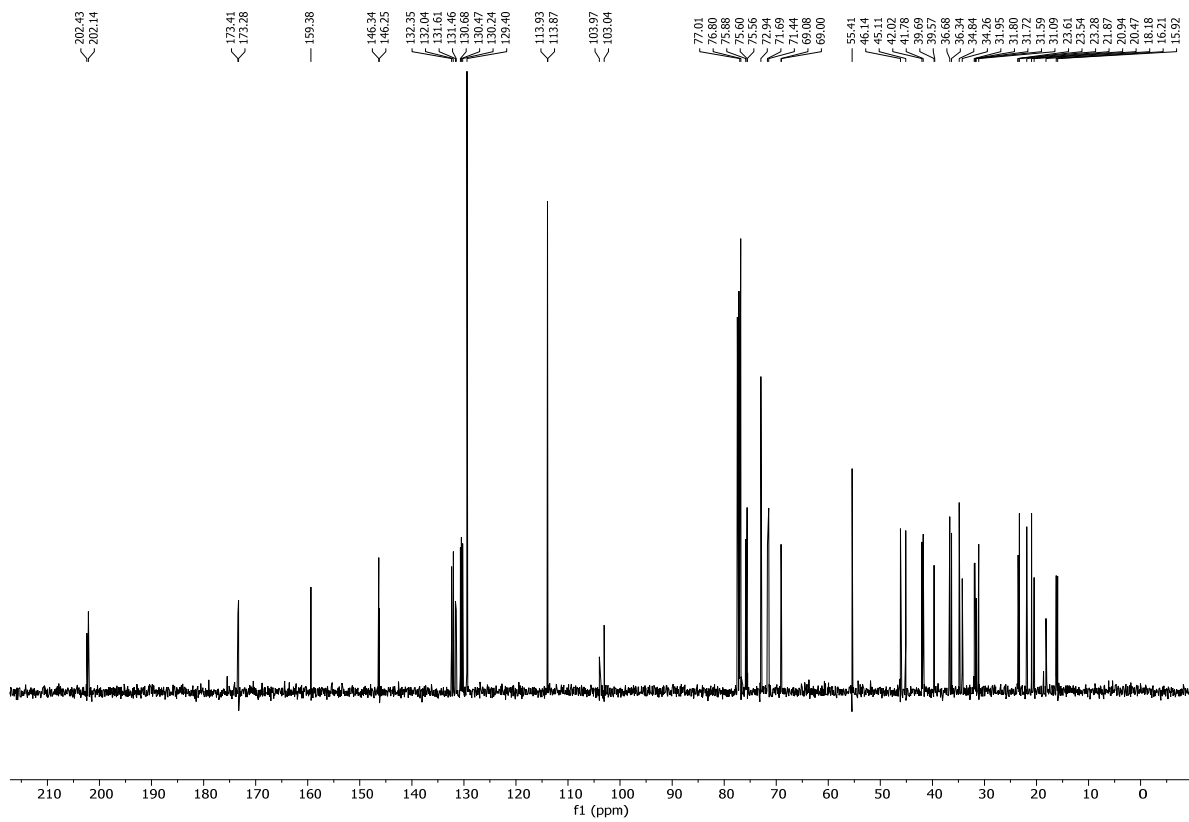
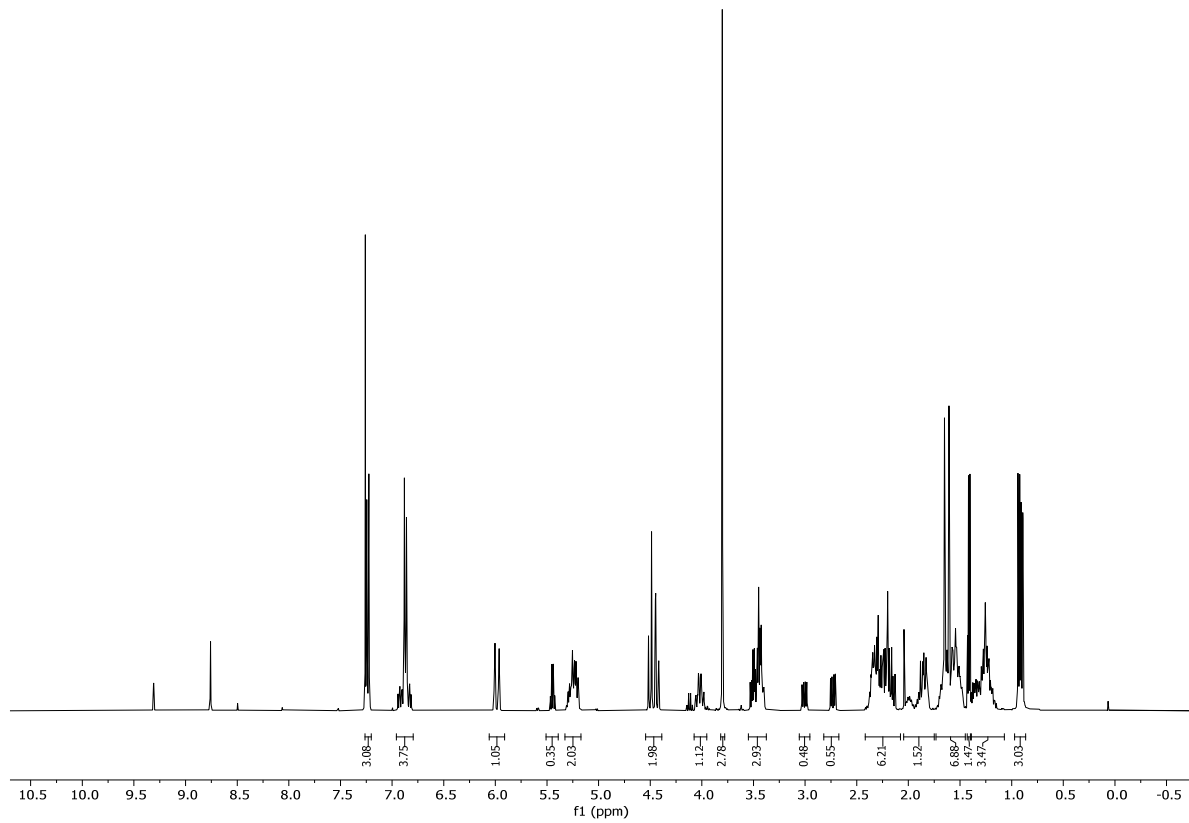
(1S,2E,5S,14E,17R)-5-(((4-Methoxybenzyl)oxy)methyl)-3,11-dimethyl-6,21-

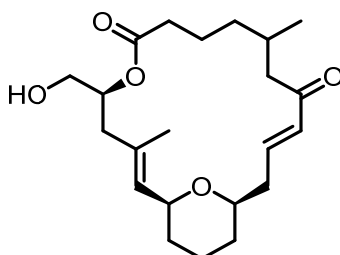
dioxabicyclo[15.3.1]-henicosa-2,14-diene-7,13-dione (R16). To a solution of diol **RS18ca** (0.86 g, 1.31 mmol, 1.00 equiv.) in CH_2Cl_2 (65 mL) was added DMP (1.95 g, 4.60 mmol, 3.50 equiv.) at rt. After 30 min the same amount of DMP was added again (1.95 g, 4.60 mmol, 3.50 equiv.). After 2 h stirring at rt CH_2Cl_2 (130 mL), a mixture of $\text{Na}_2\text{S}_2\text{O}_3$ and NaHCO_3 (500 mL) was added and stirring was continued for 10 min, when two almost clear phases had formed. The phases were separated, the aqueous phase was extracted with CH_2Cl_2 (3 x 250 mL), and the combined organic extracts were dried over MgSO_4 . Concentration of the solution under reduced pressure gave the crude keto aldehyde **R12ca** as a pale-white oil/suspension.

To a stirred solution of the crude aldehyde **R12ca** (0.86 g, 1.31 mmol, 1.00 equiv., co-evaporated with 15 mL of toluene immediately before use) in THF (437 mL) was added H_2O (11 mL) followed by freshly activated $\text{Ba}(\text{OH})_2 \cdot 8\text{H}_2\text{O}$ (0.36 g, 2.10 mmol, 1.6 equiv.) at 0 °C. After 20 min at this temperature, Et_2O (100 mL) and NaHCO_3 (100 mL) were added and stirring was continued for 10 min. The phases were then separated and the aqueous phase was extracted with Et_2O (3 x 100 mL) and then washed first with sat. aqu. aqueous NaHCO_3 (2 x 100 mL) and then with brine (1 x 100 mL). The clear organic phase was dried over MgSO_4 and concentrated. The resulting yellow oil was purified by FC (EtOAc/hexane 1:5→1:2) to afford **R16** (0.48 g, 0.97 mmol, 74% over two steps) as a colorless oil.

TLC: $R_f = 0.35$ (EtOAc/hexane 1:3). **$^1\text{H-NMR}$** (400 MHz, CDCl_3): $\delta = 7.26 - 7.20$ (m, 3H), 6.96 – 6.80 (m, 4H), 5.98 (dt, $J = 16.6, 1.6$ Hz, 1H), 5.45 (q, $J = 5.6$ Hz, 0H), 5.25 (dddd, $J = 16.1, 13.7, 8.4, 6.1$ Hz, 2H), 4.54 – 4.39 (m, 2H), 4.02 (tdd, $J = 11.0, 8.0, 2.3$ Hz, 1H), 3.80 (s, 3H), 3.55 – 3.37 (m, 3H), 3.01 (dd, $J = 12.5, 5.9$ Hz, 0H), 2.73 (dd, $J = 13.1, 5.8$ Hz, 1H), 2.42 – 2.08 (m, 6H), 2.05 – 1.75 (m, 2H), 1.73 – 1.45 (m, 7H), 1.42 (dd, $J = 5.6, 3.5$ Hz, 1H), 1.39 – 1.07 (m, 3H), 0.92 (dd, $J = 12.0, 6.6$ Hz, 3H). **$^{13}\text{C-NMR}$** (101 MHz, CDCl_3): $\delta = 202.4, 202.1, 173.4, 173.3, 159.4, 146.3, 146.3, 132.4, 132.0, 131.6, 131.5, 130.7, 130.5, 130.2, 129.4, 113.9, 113.9, 104.0, 103.4, 77.1, 76.8, 75.9, 75.6, 75.6, 72.9, 71.7, 71.4, 69.1, 69.0, 55.4, 46.1, 45.1, 42.0, 41.8, 39.7, 39.6, 36.7, 36.3, 34.8, 34.3, 32.0, 31.8, 31.7, 31.6, 31.1, 23.6, 23.5, 23.3, 21.9, 20.9, 20.5, 18.2, 16.2, 15.9$. **HRMS** (ESI): calcd for $\text{C}_{30}\text{H}_{46}\text{NO}_6$ [(M+Na) $^+$]: 516.3320; found: 516.3316. **IR** (neat): $\tilde{\nu} = 2932, 2858, 1732, 1663, 1613$,

1586, 1513, 1440, 1373, 1342, 1303, 1247, 1174, 1125, 1087, 1035, 982, 959, 802, 751, 637, 577, 517, 418, 402 cm^{-1} .

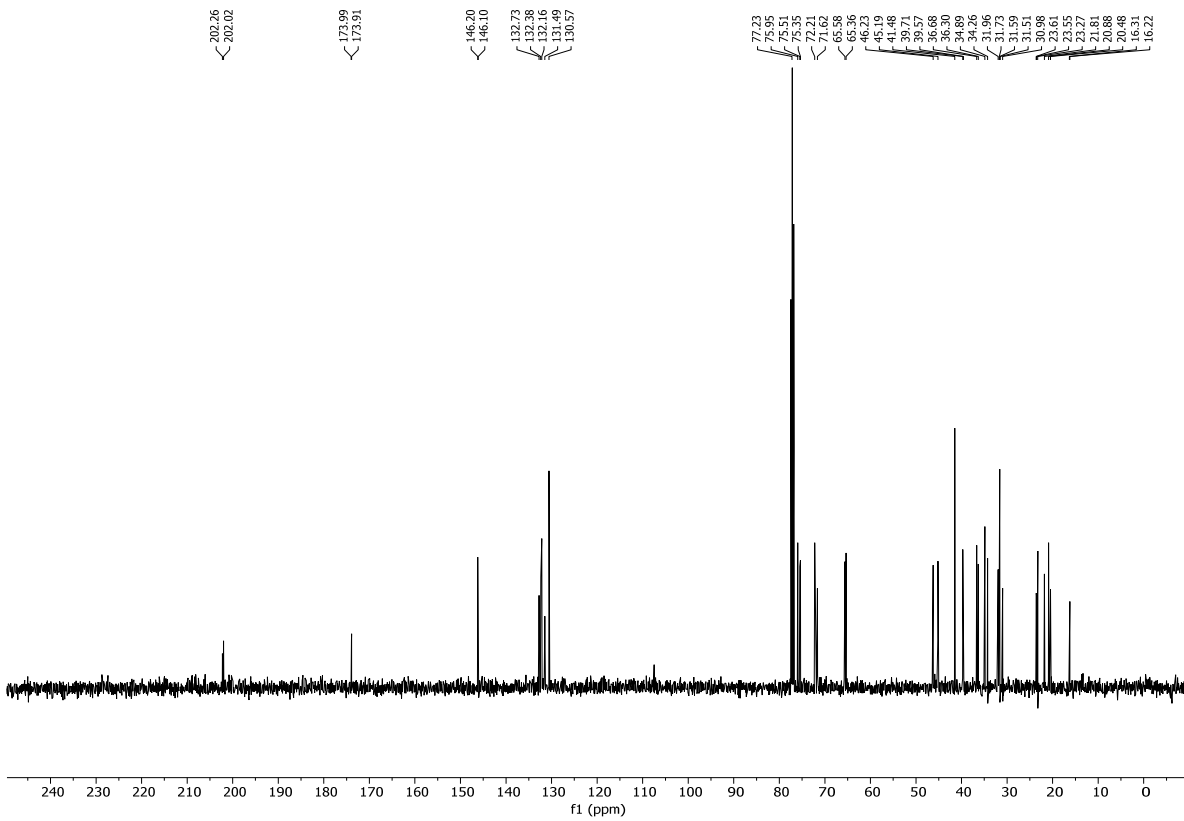
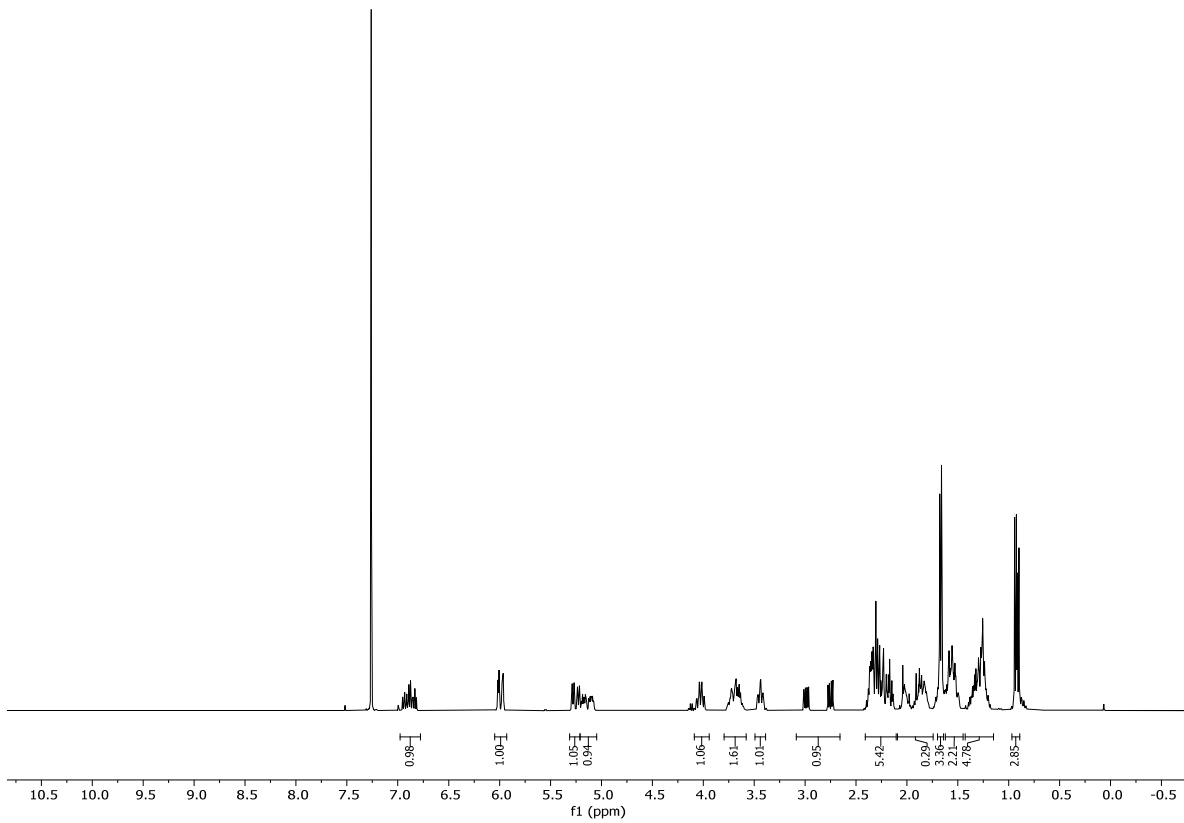


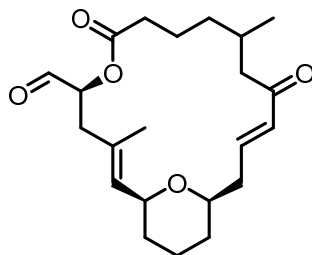


RS19ca

(1*S*,2*E*,5*S*,8*E*,10*Z*,14*E*,17*R*)-5-(Hydroxymethyl)-11-methyl-6,21-dioxabicyclo[15.3.1]henicosa-2,8,10,14-tetraene-7,13-dione (RS19ca). To a solution of **R30ca** (0.20 g, 0.40 mmol, 1.00 equiv.) in CH₂Cl₂ (30 mL) was added phosphate buffer (6 mL, pH=7) followed by DDQ (0.32 mg, 1.40 mmol, 3.50 equiv.) at rt. The mixture was vigorously stirred for 2 h; then, more DDQ (0.18 g, 0.80 mmol, 2.00 equiv.) was added. After a total of 3 h of stirring, sat. aqu. NaHCO₃ (200 mL) and CH₂Cl₂ (150 mL) were added and the phases were separated. The aqueous phase was extracted with CH₂Cl₂ (3 x 150 mL) and the combined organic extracts were dried over MgSO₄ and concentrated under reduced pressure. Purification of the residue by FC (EtOAc/hexane 1:3 → 1:2 → 1:1) gave alcohol **RS19ca** (0.11 g, 0.29 mmol, 73%) as a viscous liquid.

TLC: R_f = 0.35 (EtOAc/hexane 1:1). **¹H-NMR** (400 MHz, CDCl₃): δ = 6.98 – 6.78 (m, 1H), 5.99 (ddt, *J* = 16.2, 4.1, 1.5 Hz, 1H), 5.25 (ddt, *J* = 21.2, 7.7, 1.5 Hz, 1H), 5.21 – 5.05 (m, 1H), 4.09 – 3.94 (m, 1H), 3.79 – 3.58 (m, 2H), 3.44 (dddd, *J* = 11.1, 9.2, 4.1, 2.0 Hz, 1H), 2.87 (ddd, *J* = 95.6, 13.0, 5.9 Hz, 1H), 2.41 – 2.10 (m, 5H), 1.96 (d, *J* = 65.7 Hz, 0H), 1.67 (dd, *J* = 6.6, 1.3 Hz, 3H), 1.56 (ddtd, *J* = 15.2, 9.2, 4.5, 4.0, 1.8 Hz, 2H), 1.43 – 1.15 (m, 5H), 0.92 (dd, *J* = 10.4, 6.7 Hz, 3H). **¹³C-NMR** (101 MHz, CDCl₃): δ = 202.3, 202.0, 174.0, 173.9, 146.2, 146.1, 132.7, 132.4, 132.2, 131.5, 130.6, 77.2, 76.0, 75.5, 75.4, 72.2, 71.6, 65.6, 65.4, 46.2, 45.2, 41.5, 39.7, 39.6, 36.7, 36.3, 34.9, 34.3, 32.0, 31.7, 31.6, 31.5, 31.0, 23.6, 23.6, 23.3, 21.1, 20.9, 20.5, 16.3, 16.2. **IR** (neat): $\tilde{\nu}$ = 3449, 2930, 2859, 1732, 1662, 1457, 1439, 1382, 1342, 1307, 1254, 1194, 1072, 1045, 983, 886, 735 cm⁻¹. **HRMS** (ESI): calcd for C₂₂H₃₅O₅ [(M+H)⁺]: 379.2479; found: 379.2474.

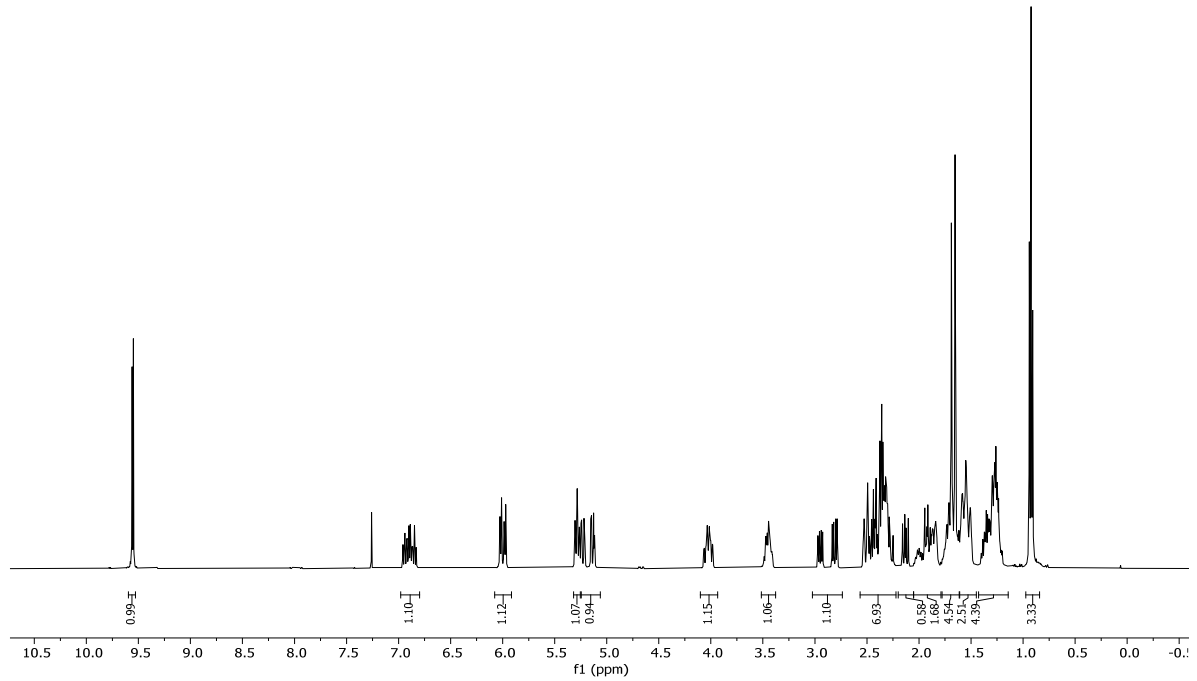




R13ca

(1S,2E,5S,14E,17R)-11-Methyl-7,13-dioxo-6,21-dioxabicyclo[15.3.1]henicosa-2,14-diene-5-carbaldehyde (R13ca). To a stirred solution of alcohol **RS19ca** (45 mg, 0.12 mmol, 1.00 equiv.) in CH_2Cl_2 (12 mL) was added NaHCO_3 (150 mg, 1.78 mmol, 15.00 equiv.) followed by DMP (303 mg, 0.71 mmol, 6.00 equiv.) at rt and stirring was continued for 45 min; then, additional NaHCO_3 (150 mg, 1.78 mmol, 15.00 equiv.) and DMP (303 mg, 0.71 mmol, 6.00 equiv.). After 2 of total reaction time, further portions of NaHCO_3 (150 mg, 1.78 mmol, 15.00 equiv.) and DMP (303 mg, 0.71 mmol, 6.00 equiv.) were added, followed by more DMP (303 mg, 0.71 mmol, 6.00 equiv.) after one further hour. After 4 hours in total, the reaction was quenched with a mixture of $\text{Na}_2\text{S}_2\text{O}_3$ and NaHCO_3 (250 mL) and stirring was continued for 10 min until two clear phases were formed. The phases were separated and the aqueous phase was extracted with CH_2Cl_2 (3 x 200 mL). The combined organic phases were dried over MgSO_4 , concentrated under reduced pressure and the residue was purified by FC (EtOAc/hexane 1:3 \rightarrow 1:1) to afford aldehyde **R13ca** (42 mg, 0.11 mmol, 93%) as a colourless oil.

TLC: $R_f = 0.70$ (EtOAc/hexane 1:1). **$^1\text{H-NMR}$** (400 MHz, Chloroform-*d*): $\delta = 9.55$ (d, $J = 4.9$ Hz, 1H), 6.98 – 6.80 (m, 1H), 6.00 (ddt, $J = 16.3, 5.9, 1.6$ Hz, 1H), 5.28 (tt, $J = 9.1, 1.5$ Hz, 1H), 5.25 – 5.06 (m, 1H), 4.02 (dddd, $J = 13.5, 10.5, 7.7, 2.2$ Hz, 1H), 3.51 – 3.38 (m, 1H), 2.88 (ddd, $J = 55.9, 12.9, 5.6$ Hz, 1H), 2.57 – 2.22 (m, 7H), 2.13 (dd, $J = 13.4, 8.6$ Hz, 1H), 2.05 – 1.79 (m, 2H), 1.78 – 1.61 (m, 5H), 1.54 (dddd, $J = 17.1, 13.6, 6.2, 3.3$ Hz, 3H), 1.43 – 1.14 (m, 4H), 0.92 (t, $J = 6.5$ Hz, 3H). **$^{13}\text{C-NMR}$** (101 MHz, CDCl_3): $\delta = 201.9, 198.8, 198.5, 173.2, 146.2, 146.0, 132.2, 132.0, 131.7, 131.6, 130.5, 130.1, 75.9, 75.6, 75.4, 75.3, 46.1, 45.6, 39.6, 39.5, 39.0, 38.8, 36.8, 36.5, 34.6, 34.2, 31.8, 31.7, 31.6, 31.5, 31.2, 23.6, 23.5, 23.2, 22.1, 20.9, 20.5, 16.0, 15.8$. **IR** (neat): $\tilde{\nu} = 2932, 2856, 1734, 1662, 1457, 1381, 1342, 1307, 1276, 1244, 1194, 1072, 1044, 983, 916, 888, 821, 732, 647, 542, 511, 499$ cm^{-1} **HRMS** (ESI): calcd for $\text{C}_{21}\text{H}_{30}\text{NaO}_5$ [(M+Na) $^+$]: 385.1985; found: 385.1984.



201.90
198.81
196.53

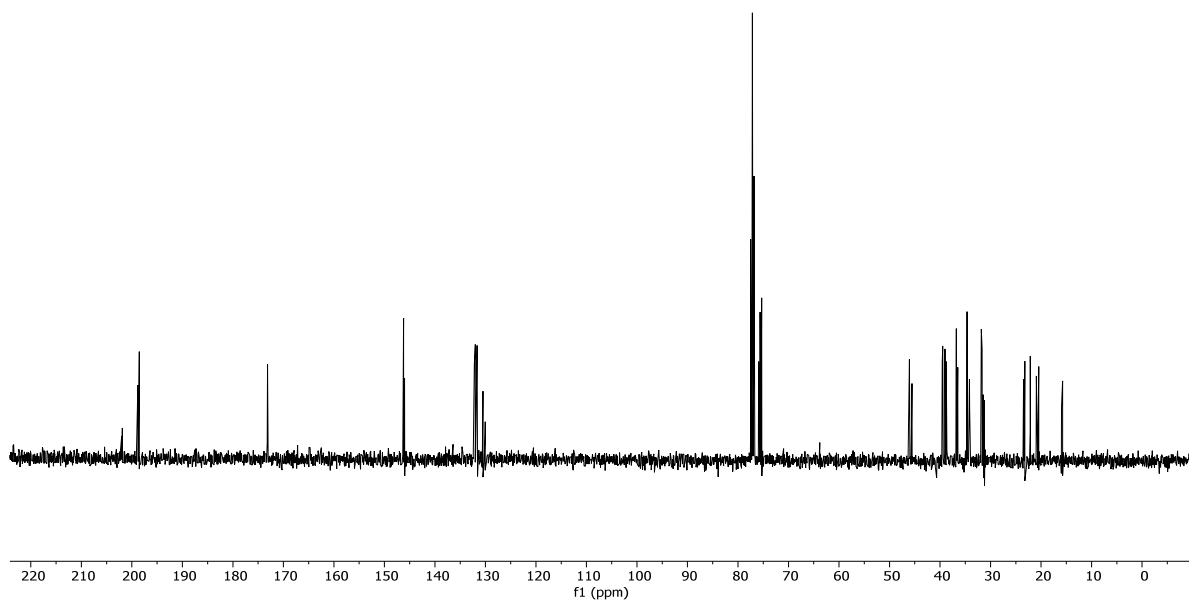
173.15

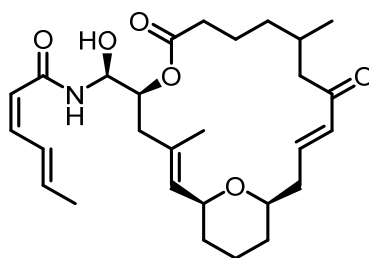
146.21
146.01

132.21
131.67
131.67
131.61
130.49
130.06

75.90
75.63
75.39
75.31

46.07
45.56
39.55
39.45
39.03
38.77
38.66
36.48
34.64
34.16
31.67
31.59
31.23
23.56
23.47
23.22
22.12
20.74
20.46
15.95
15.75





R7

(2Z,4E)-N-((1S)-((1S,2E,5S,14E,17R)-3,11-Dimethyl-7,13-dioxo-6,21-dioxabicyclo[15.3.1]-henicosa-2,14-dien-5-yl)(hydroxy)methyl)hexa-2,4-dienamide (R7). Preparation of a stock solution of (S)-BINAL-sorbamide complex: Reagents and reactants were dried in flasks used to prepare solutions in high vacuum over night. LAH (35.0 mg, 0.96 mmol, 10.00 eq.) was suspended dry THF (2 mL) at rt. Dry EtOH (57 μ L, 0.96 mmol, 10.0 eq.) was diluted with THF (2 mL) and the mixture was added slowly at rt to the LAH suspension. (S)-BINOL (274.0 mg, 0.96 mmol, 10.00 eq.) was added as a solution in THF (2 mL) followed by a solution of (2E,4Z)-sorbamide (106.0 mg, 0.96 mmol, 10.00 eq.) in THF (2 mL) to give a translucent gray solution. NOTE: If the solution turns into a light gray suspension it should not be used for the aza-aldol reaction.

1.6 mL of the stock solution containing the putative amide transfer complex (0.19 mmol, 2.0 eq.) was added immediately to a solution of **R13ca** (36.0 mg, 0.096 mmol, 1.00 eq.) in THF (1 mL). Additional 1.6 mL of the stock solution (0.13 mmol, 2.00 eq.) were added after 22 min, 45 min, and 55 min each. After 75 min, sat. aq. NaHCO₃ (20 mL) was added, the phases were separated and the aqueous phase was extracted with EtOAc (3 x 15 mL). The combined organic phases were dried over MgSO₄, concentrated under reduced pressure and the residue was purified by FC (EtOAc/hexane 1:3, 2% Et₃N) and subsequent normal phase prep HPLC (see details below) to furnish **R7** (19.4 mg, 0.04 mmol, 42%) with >95% purity as a single epimer at C(20) with a dr of 1.4:1 at C(5) as a colourless film.

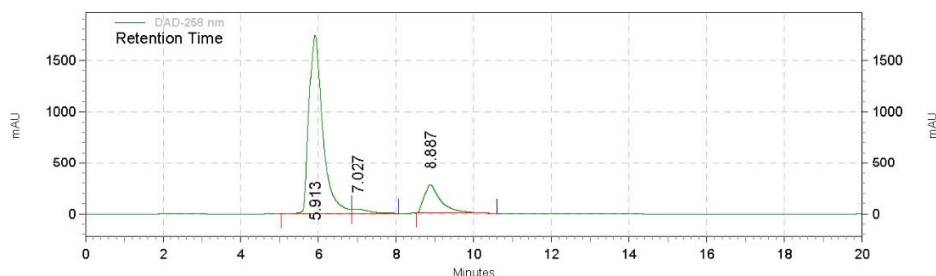
TLC: R_f = 0.4 (EtOAc/hexane 1:1, 2% Et₃N). Analytical data recorded after HPLC purification: **¹H-NMR** (500 Hz, DMSO-*d*₆): δ = 8.17 (t, *J* = 9.6 Hz, 1H), 7.44 (dddt, *J* = 15.7, 11.0, 3.3, 1.5 Hz, 1H), 6.93 – 6.79 (m, 1H), 6.38 (t, *J* = 11.3 Hz, 1H), 6.03 (dd, *J* = 8.0, 5.1 Hz, 1H), 6.02 – 5.91 (m, 2H), 5.66 (d, *J* = 11.3 Hz, 1H), 5.26 (ddt, *J* = 17.2, 8.9, 5.2 Hz, 1H), 5.10 (dd, *J* = 19.7, 7.6 Hz, 1H), 4.92 (dddd, *J* = 13.3, 7.8, 5.3, 2.1 Hz, 1H), 4.05 – 3.93 (m, 1H), 3.46 (dt, *J* = 20.3, 11.0 Hz, 1H), 2.91 – 2.56 (m, 1H), 2.44 – 1.81 (m, 4H), 1.78 (dd, *J* = 6.8, 1.7 Hz, 3H), 1.58 (d, *J* = 1.3 Hz, 1H), 1.55 (d, *J* = 1.2 Hz, 2H), 1.48 – 1.33 (m, 3H), 1.22 (d, *J* = 8.5 Hz, 1H), 1.18 – 1.07 (m, 2H), 0.86 (t, *J* = 6.5 Hz, 3H). **¹³C-NMR** (126 MHz, DMSO-*d*₆) δ = 200.8, 200.7, 172.0, 172.0, 165.2, 146.6, 146.4, 140.7,

137.2, 131.8, 131.5, 130.9, 130.7, 130.3, 130.1, 128.6, 119.1, 76.1, 75.1, 74.7, 74.6, 73.2, 72.9, 71.4, 45.8, 44.2, 39.9, 39.8, 39.6, 35.8, 35.1, 33.8, 33.4, 31.3, 31.2, 31.1, 30.9, 30.2, 22.9, 22.9, 22.6, 21.1, 20.9, 20.3, 18.3, 15.8, 15.7, 15.5. IR (neat): $\tilde{\nu}$ = 3320, 2931, 2856, 1733, 1657, 1604, 1517, 1456, 1435, 1379, 1341, 1306, 1255, 1195, 1070, 1040, 999, 982, 963, 927, 888, 835, 807, 735, 702, 648, 542 cm^{-1} . HRMS (ESI): calcd for $\text{C}_{28}\text{H}_{41}\text{NNaO}_6$ $[(\text{M}+\text{Na})^+]$: 510.2826; found: 510.2826.

Page 1 of 1

Area % Report

Data File: C:\EZChrom Elite\Enterprise\Projects\Etienne\EC-71-1-r4009-chromatogram
 Method: C:\EZChrom Elite\Enterprise\Projects\Default\Method\Etienne C\EC-41_5_80_17Mmin.met
 Acquired: 22.01.2021 15:20:53
 Printed: 22.01.2021 15:29:36



DAD-258 nm

Results

| Retention Time | Area | Area % | Height | Height % |
|----------------|-----------|--------|---------|----------|
| 5.913 | 171408650 | 82.00 | 6962136 | 84.71 |
| 7.027 | 4878838 | 2.33 | 162942 | 1.98 |
| 8.887 | 32749179 | 15.67 | 1093782 | 13.31 |

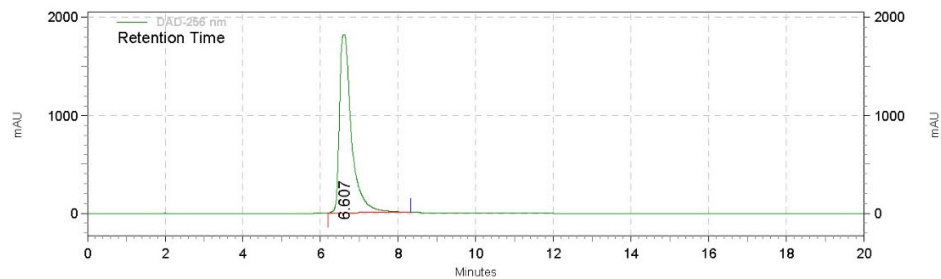
| | | | | |
|--------|-----------|--------|---------|--------|
| Totals | 209036667 | 100.00 | 8218860 | 100.00 |
|--------|-----------|--------|---------|--------|

The analytical HPLC trace (Luna[®] 3 μm u, NH_2 , 100 \AA , 150 x 4.6 mm; hexane/isopropanol gradient from 95:5 to 20:80 in 17 min, 1 mL/min, R_t = 5.9 min, C(20) epimer R_t = 7.0 min, (S)-BINOL R_t = 8.9 min) before purification using prep HPLC is shown above. The diastereomers were separated by prep HPLC (Luna[®] 5 μm u, NH_2 , 100 \AA , 150 x 21.2 mm; hexane/isopropanol 90:10, 15 mL/min, R_t = 7.8 min, C(20) epimer below detection limit, (S)-BINOL R_t = 10.2 min). The reinjection into the analytical HPLC of fraction with R_t = 7.8 min is shown below.

Area % Report

Data File: C:\EZChrom Elite\Enterprise\Projects\Etienne\EC-71-2-prep-rt8-r2030-chromatogram
 Method: C:\EZChrom Elite\Enterprise\Projects\Default\Method\Etienne C\EC-41_5_80_17Mmin.met

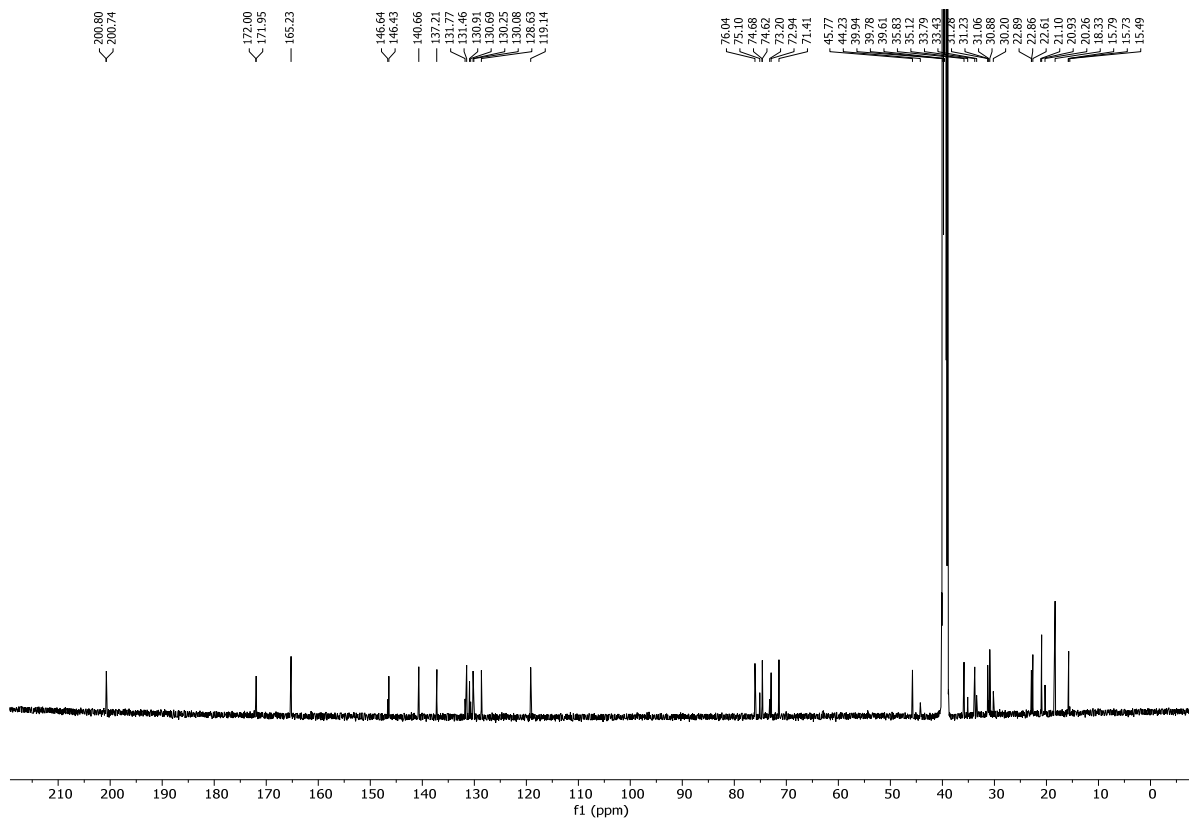
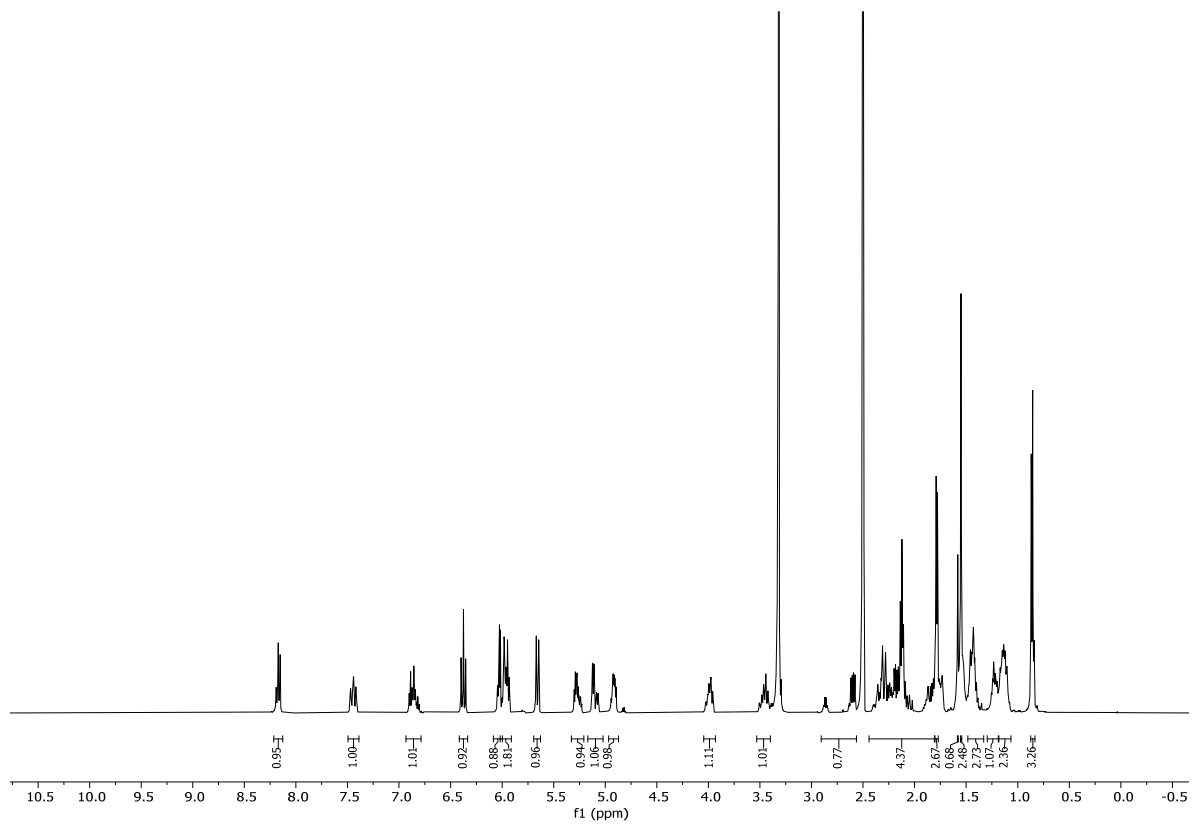
Acquired: 18.02.2021 18:57:34
 Printed: 18.02.2021 18:58:27



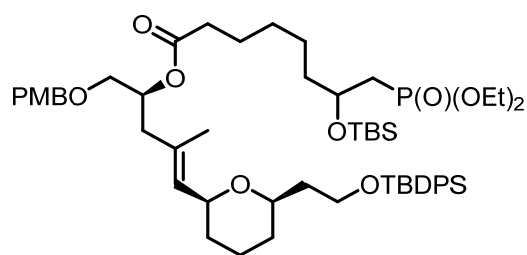
DAD-256 nm
Results

| Retention Time | Area | Area % | Height | Height % |
|----------------|-----------|--------|---------|----------|
| 6.607 | 156029398 | 100.00 | 7274613 | 100.00 |
| Totals | 156029398 | 100.00 | 7274613 | 100.00 |

The analytical HPLC trace (Luna® 3 µm u, NH₂, 100 Å, 150 x 4.6 mm; hexane/isopropanol gradient from 95:5 to 20:80 in 17 min, 1 mL/min, Rt = 6.6 min, no C(20) epimer nor (S)-BINOL were detected) after purification using prep HPLC is shown above. The material thus obtained was used in the biological experiments.



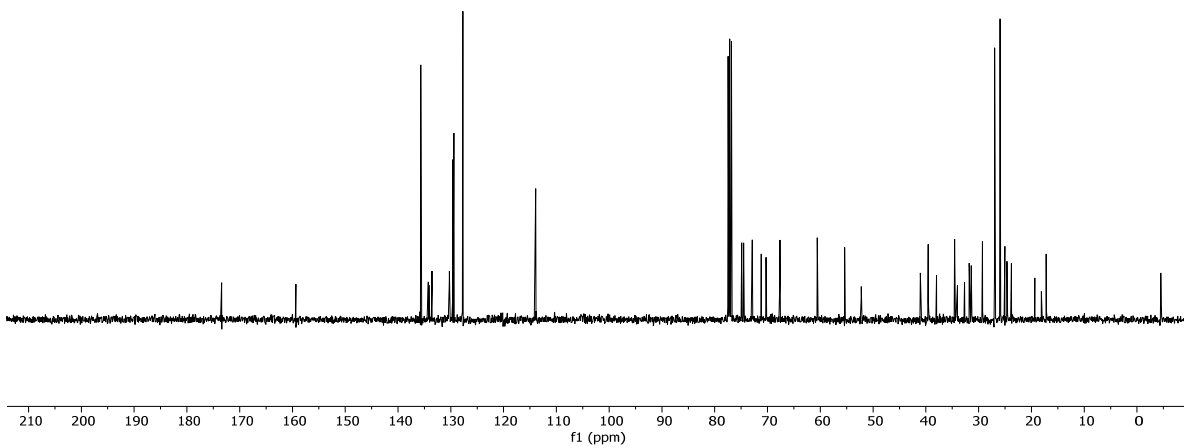
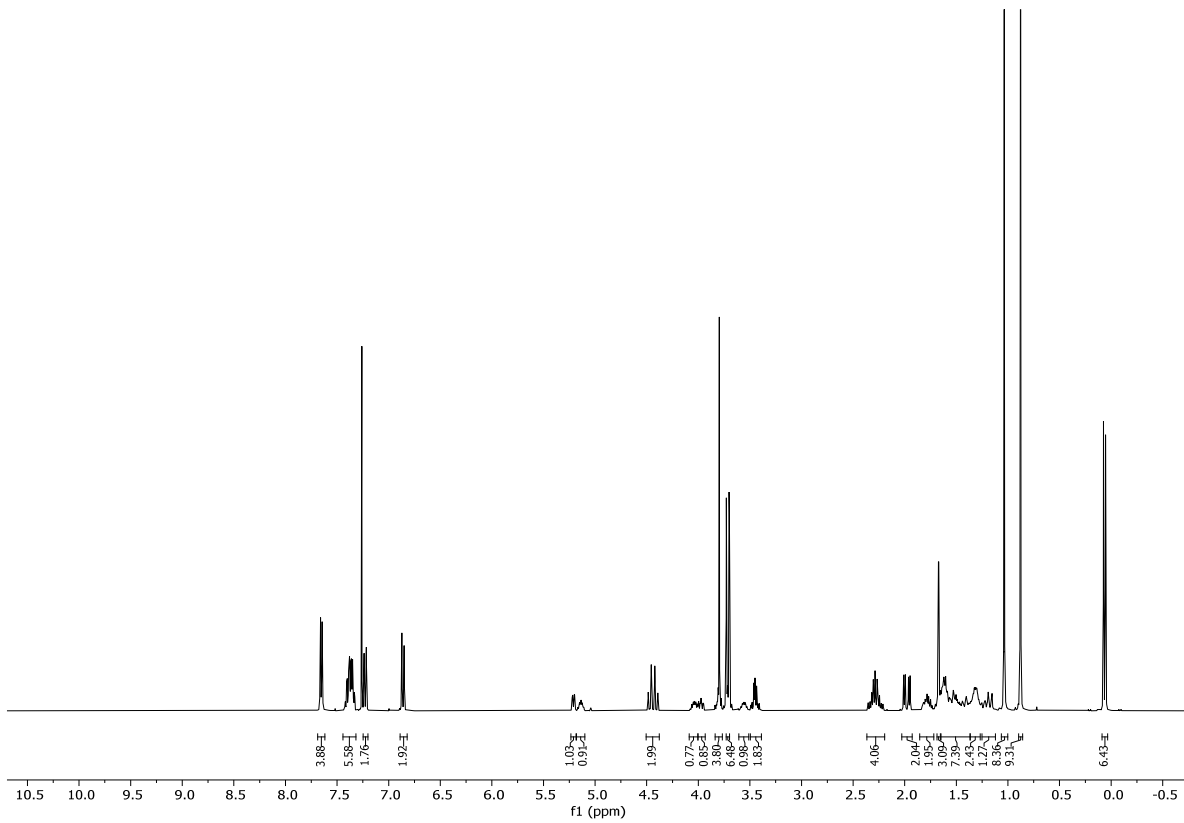
4.2.1.3.2 Synthesis of analog R8

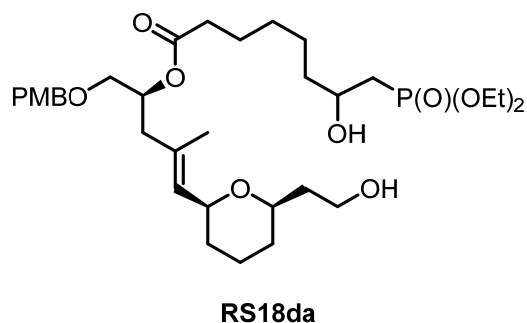


R29da

(*S,E*)-5-((*2S,6R*)-6-(2-((*tert*-Butyldiphenylsilyl)oxy)ethyl)tetrahydro-2H-pyran-2-yl)-1-((4-methoxybenzyl)oxy)-4-methylpent-4-en-2-yl-7-((*tert*-butyldimethylsilyl)oxy)-8-dimethoxyphosphoryl)octanoate (R29da). To a solution of **R10d** (0.15 g, 0.40 mmol, 1.20 equiv., co-evaporated twice with 2 mL of toluene immediately before use) in toluene (3 mL) was added NEt_3 (0.12 mL, 0.86 mmol, 2.60 equiv.) followed by 2,4,6-trichlorobenzoyl chloride (78 μL , 0.50 mmol, 1.50 equiv.) giving a pale yellow mixture. After 2 h at rt, a solution of **R11a** (0.20 g, 0.33 mmol, 1.00 equiv.) and DMAP (40.00 mg, 0.33 mmol, 1.00 equiv. co-evaporated together twice with 2 mL of toluene immediately before use) in toluene (2 mL) was added, immediately leading to a yellow suspension. After stirring at rt for 2.5 h, sat. aq. NaHCO_3 (5 mL), H_2O (5 mL) and EtOAc (5 mL) were added, the phases were separated and the aqueous phase was extracted with EtOAc (3 x 5 mL). The combined organic extracts were dried over MgSO_4 , concentrated under reduced pressure, and the residue was purified by flash chromatography (EtOAc/hexane 1:2 \rightarrow 1:1) to give **R29da** (0.26 g, 0.27 mmol, 82%) as a pale yellow, viscous oil.

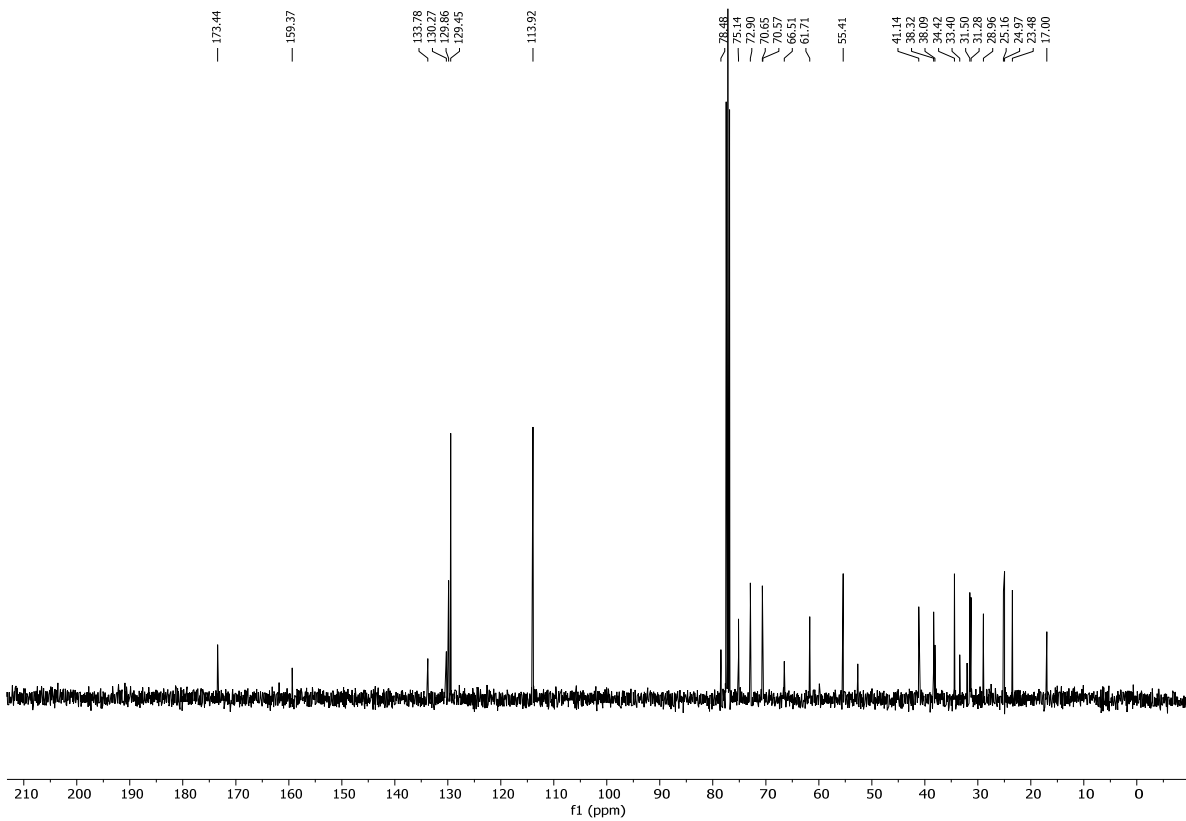
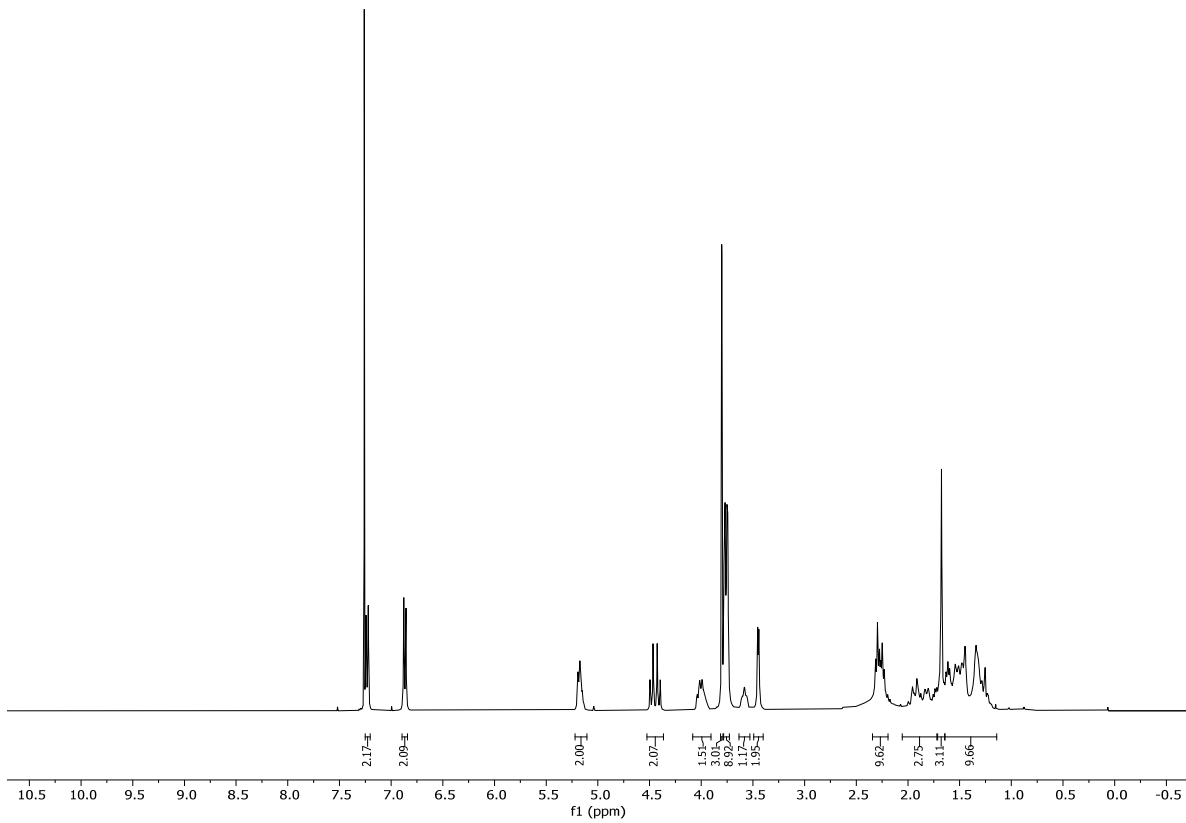
TLC (EtOAc): $R_f = 0.80$. **$^1\text{H-NMR}$** (400 MHz, CDCl_3): $\delta = 7.69 - 7.62$ (m, 4H), 7.44 - 7.32 (m, 6H), 7.25 - 7.20 (m, 2H), 6.89 - 6.82 (m, 2H), 5.21 (dd, $J = 7.8, 1.5$ Hz, 1H), 5.18 - 5.10 (m, 1H), 4.50 - 4.38 (m, 2H), 4.04 (ddt, $J = 8.1, 6.3, 3.2$ Hz, 1H), 3.97 (ddd, $J = 10.3, 7.6, 2.2$ Hz, 1H), 3.80 (s, 4H), 3.71 (dd, $J = 10.9, 1.3$ Hz, 6H), 3.61 - 3.51 (m, 1H), 3.50 - 3.39 (m, 2H), 2.37 - 2.19 (m, 4H), 1.98 (dd, $J = 18.6, 6.3$ Hz, 2H), 1.78 (ddt, $J = 19.1, 7.6, 4.8$ Hz, 2H), 1.67 (d, $J = 1.3$ Hz, 3H), 1.65 - 1.37 (m, 7H), 1.31 (ddt, $J = 10.4, 6.9, 4.4$ Hz, 2H), 1.25 - 1.12 (m, 1H), 1.04 (s, 8H), 0.88 (s, 9H), 0.06 (d, $J = 8.3$ Hz, 6H). **$^{13}\text{C-NMR}$** (101 MHz, CDCl_3): $\delta = 173.4, 159.4, 135.8, 135.7, 135.7, 134.3, 134.2, 133.6, 130.3, 129.6, 129.4, 127.7, 113.9, 74.9, 74.5, 72.9, 71.2, 70.3, 67.7, 60.6, 55.4, 52.3, 41.0, 39.6, 38.1, 38.0, 34.6, 34.0, 32.7, 31.8, 31.4, 29.3, 27.0, 25.9, 25.1, 24.6, 23.8, 19.4, 18.1, 17.2, -4.5$. **IR** (neat): $\tilde{\nu} = 2930, 2856, 1733, 1514, 1471, 1463, 1428, 1362, 1249, 1174, 1108, 1090, 1058, 953, 823, 811, 775, 738, 703, 688, 613, 538, 504, 490$ cm^{-1} . **HRMS** (ESI): calcd for $\text{C}_{53}\text{H}_{87}\text{NO}_{10}\text{PSi}_2$ [($\text{M}+\text{NH}_4$) $^+$]: 984.5601; found: 984.5605.

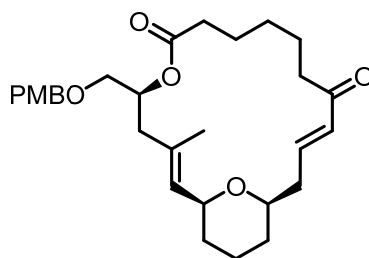




(*S,E*)-5-((*2S,6R*)-6-(2-Hydroxyethyl)tetrahydro-2H-pyran-2-yl)-1-((4-methoxybenzyl)oxy)-4-methylpent-4-en-2-yl 8-(dimethoxyphosphoryl)-7-hydroxyoctanoate (RS18da). To a stirred solution of **R29da** (1.30 g, 1.35 mmol, 1.00 equiv.) in THF (30 mL) in a plastic tube was added 70% HF•py (6.20 mL) at 0 °C. The cooling bath was removed after 5 min and stirring was continued at rt for 16 h. The solution was then carefully added to a vigorously stirred mixture of sat. aqu. NaHCO₃ (500 mL) and EtOAc (250 mL) until two clear phases were formed (ca. 15 min). The phases were separated, the aqueous phase was extracted with EtOAc (3 x 250 mL), and the combined organic extracts were washed with sat. aqu. NaHCO₃ (200 mL) followed by drying over MgSO₄. Concentration under reduced pressure and purification of the residue by FC (acetone/EtOAc 1:1) afforded diol **RS18da** (0.58 g, 0.94 mmol, 73%) as a pale yellow, viscous oil.

TLC (acetone/EtOAc 1:1): $R_f = 0.44$. **¹H-NMR** (400 MHz, CDCl₃): $\delta = 7.25 - 7.20$ (m, 2H), 6.89 – 6.84 (m, 2H), 5.18 (t, $J = 6.0$ Hz, 2H), 4.52 – 4.37 (m, 2H), 4.00 (d, $J = 10.7$ Hz, 2H), 3.80 (s, 3H), 3.76 (dd, $J = 10.8, 3.4$ Hz, 9H), 3.57 (d, $J = 10.8$ Hz, 1H), 3.45 (d, $J = 4.8$ Hz, 2H), 2.27 (dt, $J = 18.5, 7.4$ Hz, 10H), 2.05 – 1.72 (m, 3H), 1.68 (s, 3H), 1.64 – 1.14 (m, 10H). **¹³C-NMR** (101 MHz, CDCl₃): $\delta = 173.4, 159.4, 133.8, 130.3, 129.9, 129.5, 113.9, 78.5, 75.1, 72.9, 70.7, 70.6, 66.5, 61.7, 55.4, 41.1, 38.3, 38.1, 34.4, 33.4, 31.5, 31.3, 29.0, 25.2, 25.0, 23.5, 17.0$. **IR** (neat): $\tilde{\nu} = 3403, 2932, 2856, 1731, 1612, 1514, 1457, 1442, 1370, 1303, 1246, 1174, 1054, 911, 846, 821, 793, 751, 566, 495, 467$ cm⁻¹. **HRMS** (ESI): calcd for C₃₁H₅₂O₁₀P [(M+H)⁺]: 615.3293; found: 615.3291.





R30da

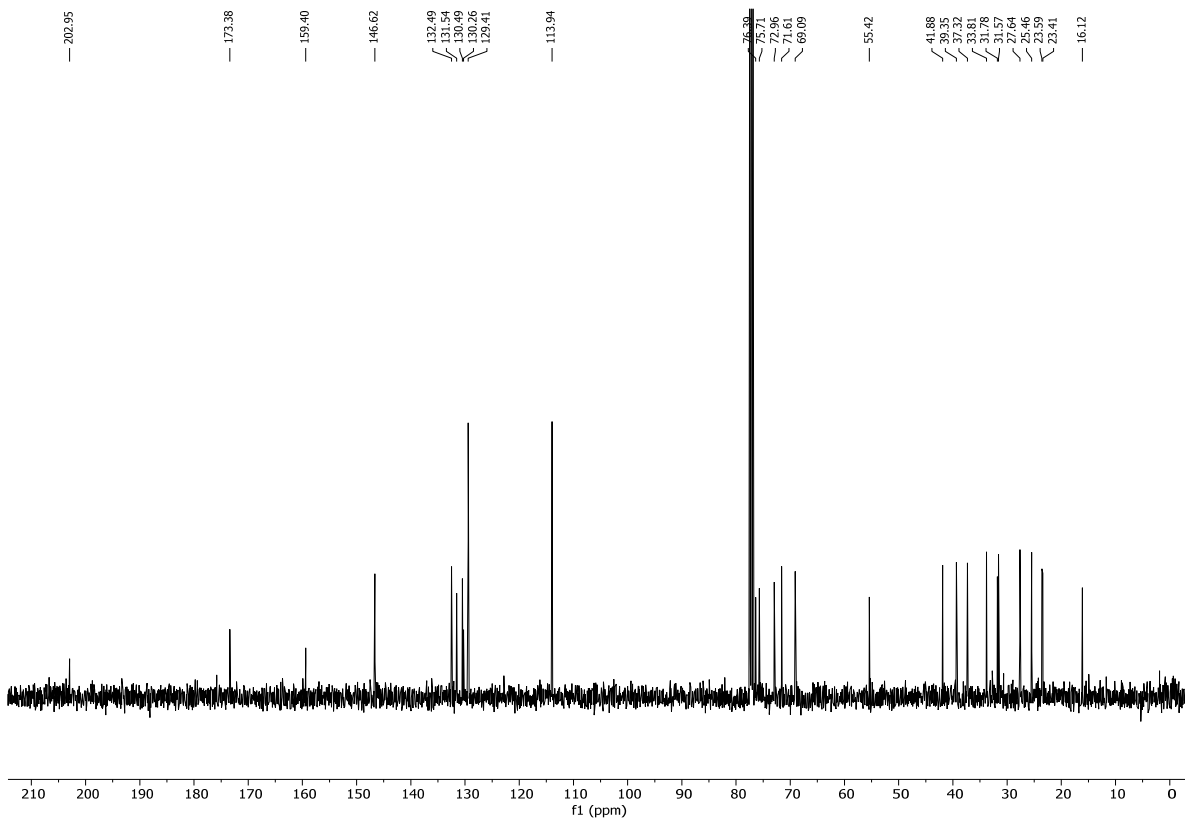
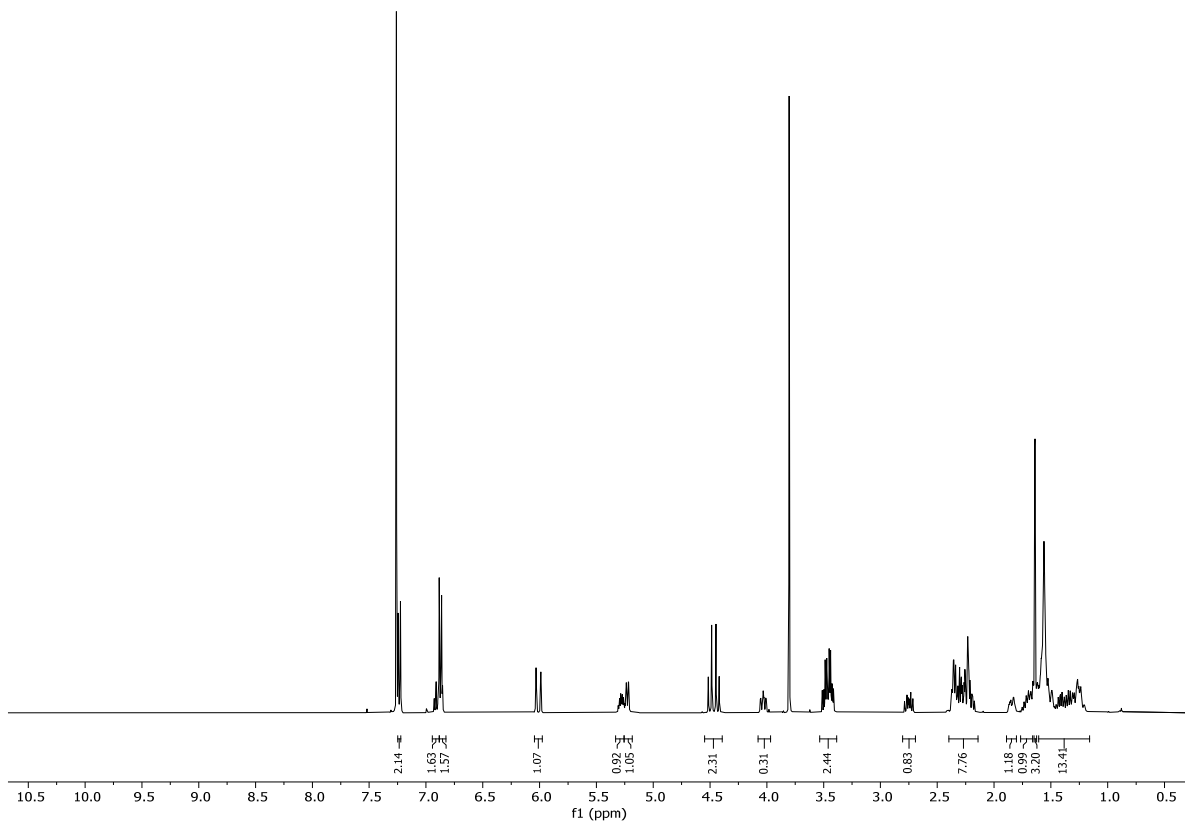
(1*S*,2*E*,5*S*,14*E*,17*R*)-5-(((4-Methoxybenzyl)oxy)methyl)-3-methyl-6,21-

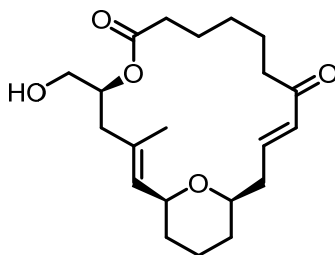
dioxabicyclo[15.3.1]henicosa-2,14-diene-7,13-dione (R30da). To a solution of diol **RS18da** (95.0 mg, 0.15 mmol, 1.00 equiv.) in CH₂Cl₂ (8 mL) was added DMP (0.45 g, 1.08 mmol, 7.00 equiv.) at rt. After 1.5 h of stirring at that temperature, more DMP (0.23 g, 0.54 mmol, 3.50 equiv.) was added to the reaction mixture. After additional 30 min of stirring at rt, CH₂Cl₂ (40 mL) and a mixture of Na₂S₂O₃ and NaHCO₃ (130 mL) was added and stirring was continued for 10 min, resulting in the formation of two almost clear phases. The phases were separated, the aqueous phase was extracted with CH₂Cl₂ (3 x 100 mL), and the combined organic extracts were dried over MgSO₄. Concentration of the solution under reduced pressure gave the crude keto aldehyde **R12da** as a colorless oil.

To a stirred solution of the crude aldehyde **R12da** (94.4 mg, 0.15 mmol, 1.00 equiv., co-evaporated with 3 mL of toluene immediately before use) in THF (52 mL) was added H₂O (1 mL) followed by freshly activated Ba(OH)₂•8H₂O (42.0 mg, 0.12 mmol, 1.60 equiv.) at 0 °C. After 20 min at this temperature Et₂O (15 mL) and NaHCO₃ (15 mL) were added and stirring was continued for 10 min. The phases were then separated and the aqueous phase was extracted with Et₂O (3 x 15 mL). The combined organic phases were washed with sat. aqu. NaHCO₃ (2 x 15 mL) and brine (1 x 15 mL), dried over MgSO₄ and concentrated. The resulting yellow oil was purified by FC (EtOAc/hexane 1:5) to afford macrolactone **R30da** (56.0 mg, 0.12 mmol, 75% over two steps) as a colorless oil.

TLC (EtOAc/hexane 1:3): *R_f* = 0.36. **¹H-NMR** (400 MHz, CDCl₃): δ = 7.25 – 7.22 (m, 2H), 6.90 (d, *J* = 11.0 Hz, 2H), 6.88 – 6.82 (m, 2H), 6.01 (dt, *J* = 16.3, 1.5 Hz, 1H), 5.28 (ddd, *J* = 9.8, 4.9, 3.3 Hz, 1H), 5.26 – 5.18 (m, 1H), 4.55 – 4.39 (m, 2H), 4.03 (s, 0H), 3.53 – 3.38 (m, 2H), 2.80 – 2.69 (m, 1H), 2.40 – 2.14 (m, 8H), 1.84 (ddt, *J* = 11.4, 4.5, 1.6 Hz, 1H), 1.77 – 1.66 (m, 1H), 1.64 (d, *J* = 1.3 Hz, 3H), 1.61 – 1.16 (m, 13H). **¹³C-NMR** (101 MHz, CDCl₃): δ = 203.0, 173.4, 159.4, 146.6, 132.5, 131.5, 130.5, 130.3, 129.4, 113.9, 76.4, 75.7, 73.0, 71.6, 69.1, 55.4, 41.9, 39.4, 37.3, 33.8, 31.8, 31.6,

27.6, 25.5, 23.6, 23.4, 16.1. **HRMS** (ESI): calcd for $C_{29}H_{40}NaO_6$ $[(M+Na)^+]$: 507.2717; found: 507.2715. $[\alpha]_{589}^{20}$: +9.90° (c = 1.00, $CHCl_3$).

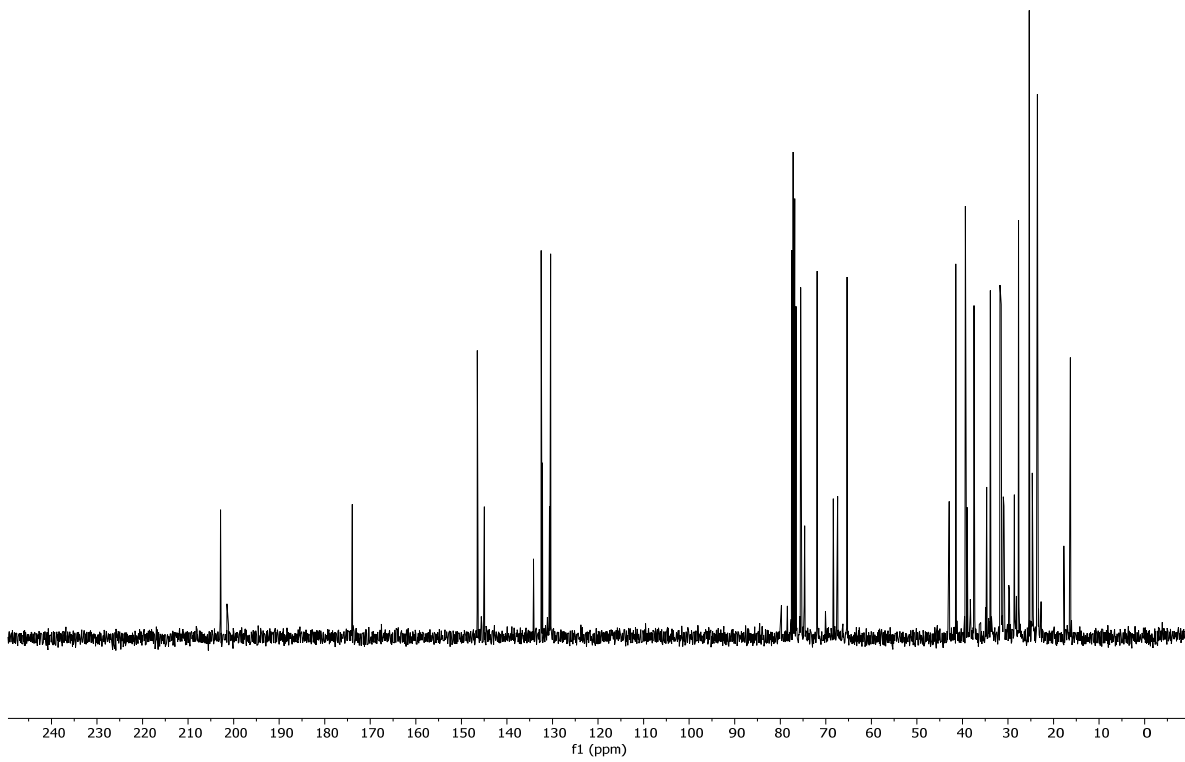
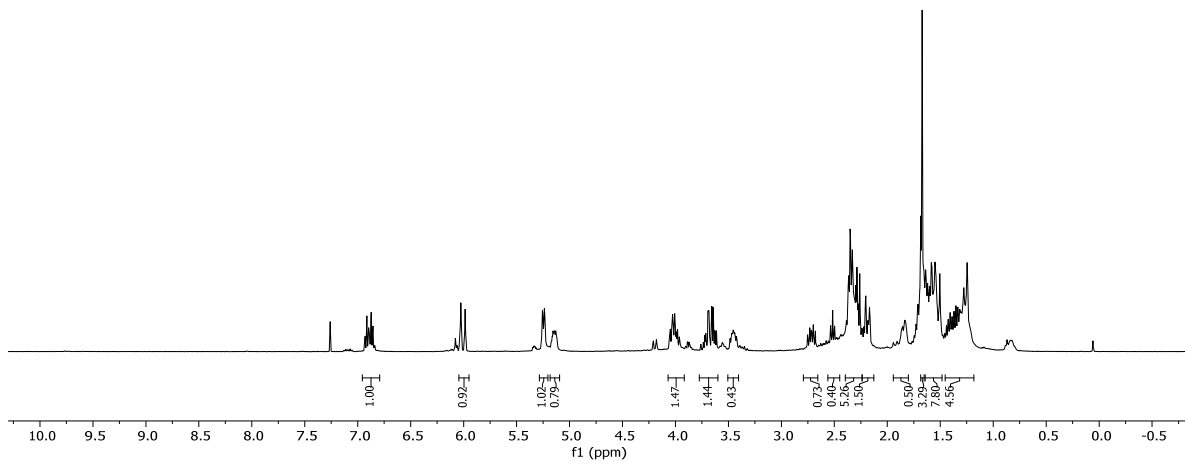


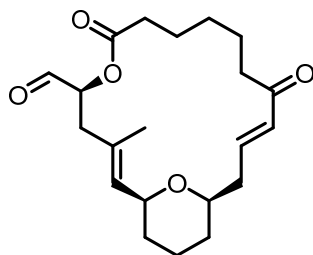


RS19da

(1*S*,2*E*,5*S*,14*E*,17*R*)-5-(Hydroxymethyl)-3-methyl-6,21-dioxabicyclo[15.3.1]henicosa-2,14-diene-7,13-dione (RS19da). To a solution of **R30da** (0.21 g, 0.46 mmol, 1.00 equiv.) in CH₂Cl₂ (30 mL) was added phosphate buffer (6 mL, pH=7) followed by DDQ (0.37 g, 1.63 mmol, 3.50 equiv.) at rt. The mixture was vigorously stirred for 2 h; then, additional DDQ (0.37 g, 1.63 mmol, 3.50 equiv.) was added. After a total of 3.5 h of stirring, sat. aqu. NaHCO₃ (200 mL) and CH₂Cl₂ (150 mL) was added and the phases were separated. The aqueous phase was extracted with CH₂Cl₂ (3 x 150 mL) and the combined organic extracts were dried over MgSO₄ and concentrated under reduced pressure. Purification of the residue by FC (EtOAc/hexane 1:3→1:2→1:1) to afford alcohol **RS19da** (0.14 g, 0.38 mmol, 90%) as a viscous oil.

TLC (EtOAc/hexane 1:1): $R_f = 0.59$. **¹H-NMR** (400 MHz, CDCl₃): $\delta = 6.89$ (dt, $J = 16.3, 6.6$ Hz, 1H), 6.01 (d, $J = 16.3$ Hz, 1H), 5.25 (d, $J = 7.7$ Hz, 1H), 5.14 (ddt, $J = 10.0, 6.2, 2.9$ Hz, 1H), 4.07 – 3.92 (m, 1H), 3.77 – 3.60 (m, 1H), 3.45 (dd, $J = 5.6, 2.8$ Hz, 0H), 2.72 (dt, $J = 13.3, 7.9$ Hz, 1H), 2.52 (t, $J = 7.5$ Hz, 0H), 2.40 – 2.24 (m, 5H), 2.24 – 2.13 (m, 1H), 1.83 (d, $J = 3.7$ Hz, 0H), 1.68 (d, $J = 5.2$ Hz, 3H), 1.64 – 1.48 (m, 8H), 1.45 – 1.18 (m, 5H). **¹³C-NMR** (101 MHz, CDCl₃): $\delta = 202.9, 201.5, 174.0, 146.5, 145.0, 134.2, 132.5, 132.2, 132.1, 130.7, 130.4, 79.7, 78.4, 76.5, 75.5, 75.4, 74.6, 71.9, 70.1, 68.4, 67.4, 65.3, 42.9, 41.5, 39.4, 39.4, 39.0, 38.3, 37.5, 34.9, 34.7, 33.9, 31.8, 31.6, 31.5, 31.0, 30.9, 29.8, 29.7, 28.6, 28.2, 27.7, 25.3, 24.7, 23.6, 23.5, 23.4, 22.7, 17.7, 16.3$. **IR** (neat): $\tilde{\nu} = 3420, 2932, 2859, 1732, 1690, 1662, 1457, 1438, 1380, 1342, 1308, 1286, 1256, 1228, 1196, 1172, 1045, 982$ cm⁻¹. **HRMS** (ESI): calcd for C₂₁H₃₂NaO₅ [(M+Na)⁺]: 387.2142; found: 387.2140. **[α]_D²⁰**: +23.50° ($c = 1.00$, CHCl₃).

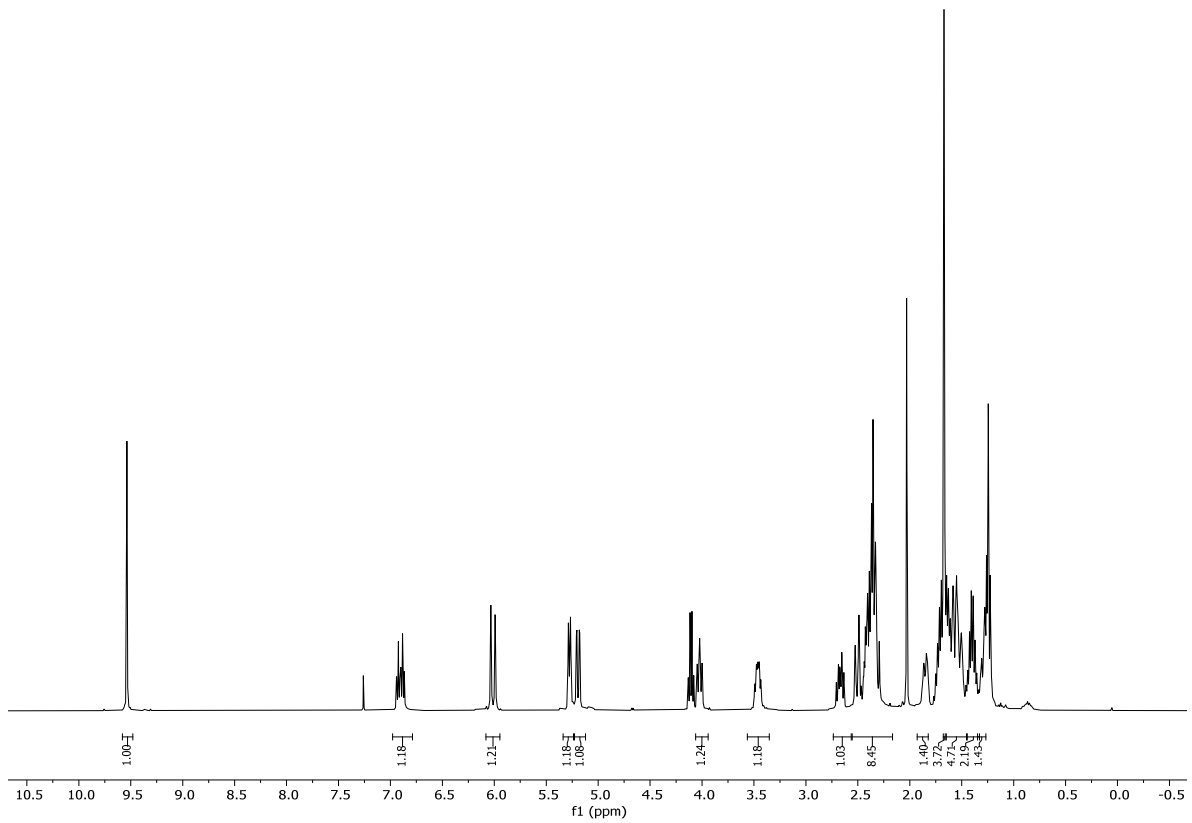




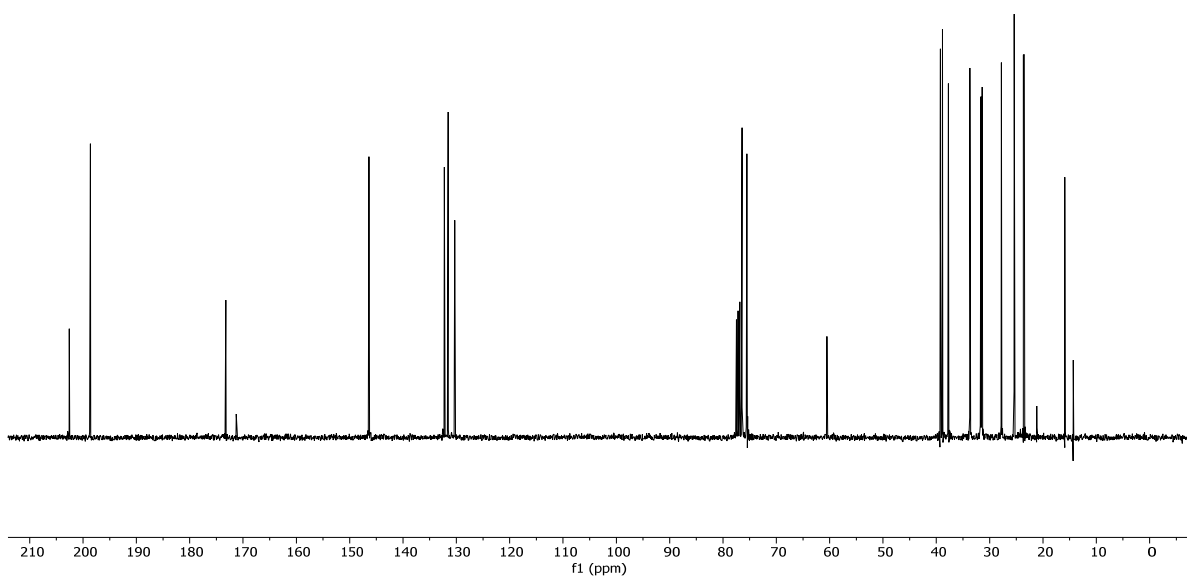
R13da

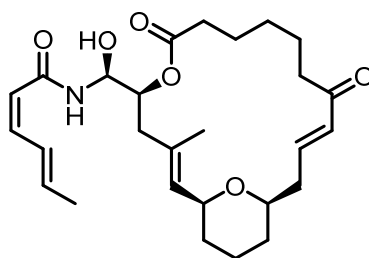
(1*S*,2*E*,5*S*,14*E*,17*R*)-3-Methyl-7,13-dioxo-6,21-dioxabicyclo[15.3.1]henicosa-2,14-diene-5-carbaldehyde (R13da). To a stirred solution of alcohol **RS19da** (20.0 mg, 0.06 mmol, 1.00 equiv.) in CH₂Cl₂ (6 mL) was added NaHCO₃ (69.0 mg, 0.82 mmol, 15.00 equiv.) followed by DMP (0.14 g, 0.33 mmol, 6.00 equiv.) at rt and stirring was continued for 45 min; additional DMP (0.14 g, 0.33 mmol, 6.00 equiv.) was then added to the reaction mixture followed by more DMP after a total reaction time of 2 h (0.14 g, 0.33 mmol, 6.00 equiv.). After additional 2.5 h of stirring the reaction was quenched with a mixture of Na₂S₂O₃ and NaHCO₃ (75 mL) and stirring was continued for 10 min, resulting in the formation of two clear phases. The phases were separated and the aqueous phase was extracted with CH₂Cl₂ (3 x 75 mL). The combined organic phases were dried over MgSO₄, concentrated under reduced pressure and the residue was purified by FC (EtOAc/hexane 1:3→1:2→1:1) to afford aldehyde **R13da** (19.7 mg, 0.05 mmol, 95%) as a colourless oil.

TLC (EtOAc/hexane 1:1): *R_f* = 0.68. **¹H-NMR** (400 MHz, CDCl₃): δ = 9.54 (s, 1H), 6.90 (dt, *J* = 16.4, 6.7 Hz, 1H), 6.01 (d, *J* = 16.3 Hz, 1H), 5.28 (d, *J* = 7.8 Hz, 1H), 5.19 (dd, *J* = 11.1, 2.7 Hz, 1H), 4.02 (ddd, *J* = 10.6, 7.7, 2.2 Hz, 1H), 3.46 (dd, *J* = 11.5, 6.0 Hz, 1H), 2.74 – 2.56 (m, 1H), 2.55 – 2.17 (m, 8H), 1.85 (dt, *J* = 14.5, 3.7 Hz, 1H), 1.67 (s, 4H), 1.65 – 1.45 (m, 5H), 1.40 (h, *J* = 6.8 Hz, 2H), 1.29 (d, *J* = 10.9 Hz, 1H). **¹³C-NMR** (101 MHz, CDCl₃): δ = 202.6, 198.6, 173.2, 171.3, 146.4, 132.2, 131.5, 130.3, 76.4, 75.5, 75.4, 60.5, 39.3, 39.2, 38.8, 38.8, 37.7, 37.7, 33.7, 31.6, 31.4, 27.8, 25.4, 23.7, 23.5, 21.2, 15.9, 14.3. **IR** (neat): $\tilde{\nu}$ = 2931, 2858, 1735, 1690, 1664, 1457, 1439, 1375, 1342, 1307, 1287, 1259, 1241, 1227, 1195, 1147, 1072, 1044, 982, 948, 920, 887, 732 cm⁻¹. **HRMS** (ESI): calcd for C₂₁H₃₀NaO₅ [(M+Na)⁺]: 385.1985; found: 385.1984. [α]₅₈₉²⁰: -18.50° (c = 1.00, CHCl₃).



- 202.58
- 198.63
- 173.22
- 171.29
- 146.39
- 132.24
- 131.54
- 130.31
- 76.44
- 75.52
- 75.44
- 60.51
- 39.34
- 38.74
- 38.63
- 38.79
- 37.73
- 37.68
- 33.71
- 31.56
- 31.58
- 27.79
- 25.40
- 23.67
- 23.50
- 21.17
- 15.33
- 14.32





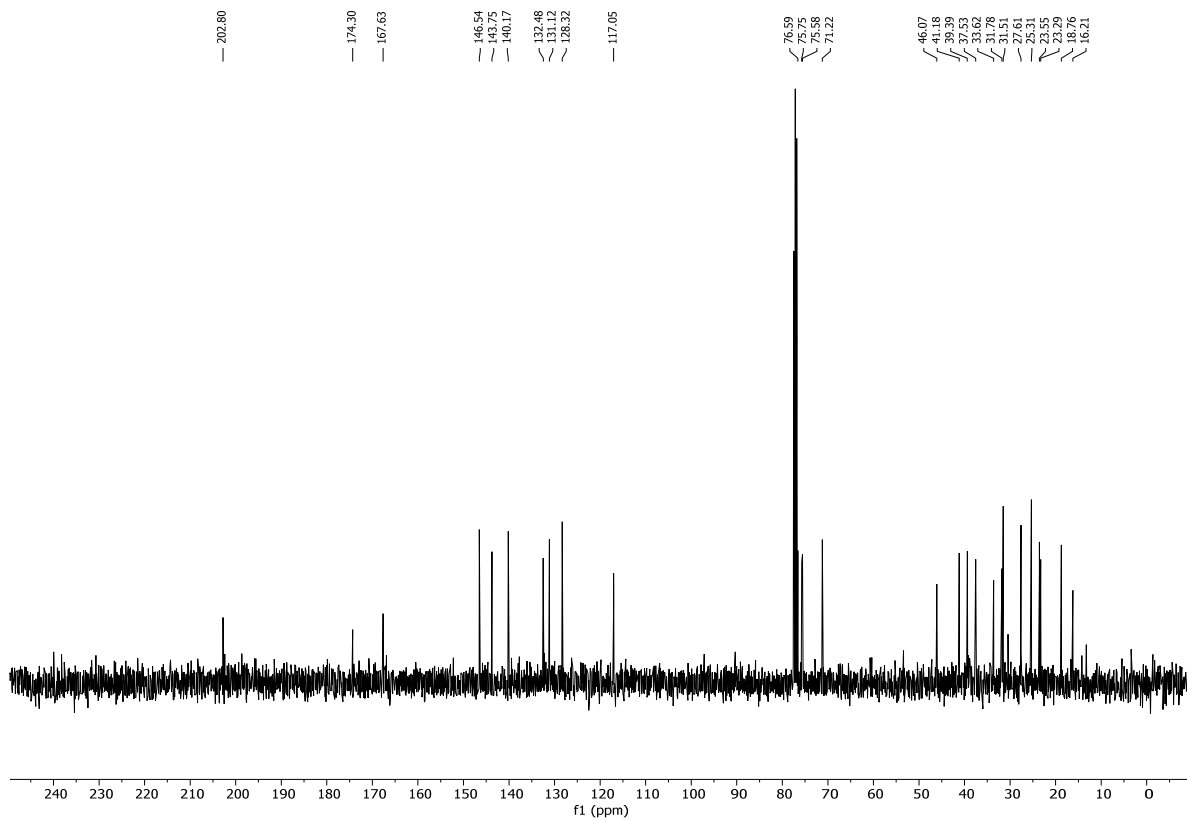
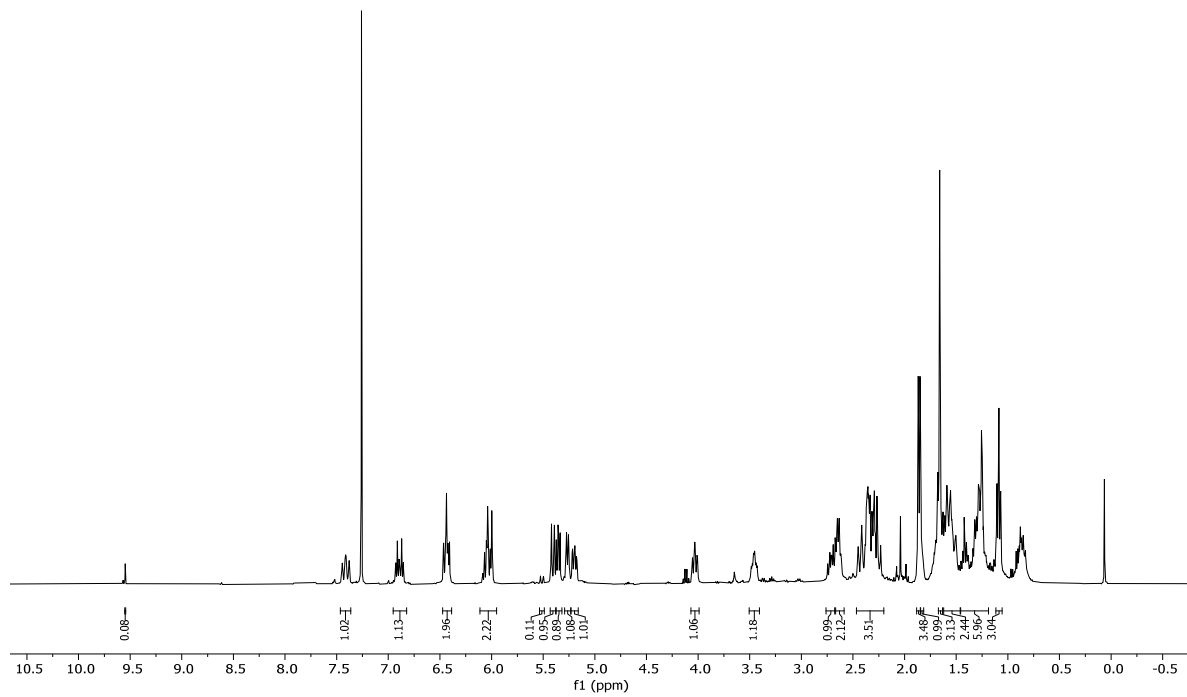
R8

(2Z,4E)-N-((S)-Hydroxy((1S,2E,5S,14E,17R)-3-methyl-7,13-dioxo-6,21-dioxabicyclo[15.3.1]-henicosa-2,14-dien-5-yl)methyl)hexa-2,4-dienamide (R8). Preparation of a stock solution of (S)-BINAL-sorbamide complex: Reagents and reactants were dried in flasks used to prepare solutions in high vacuum over night. LAH (19.10 mg, 0.52 mmol, 10.00 eq.) was suspended dry THF (2 mL) at rt. Dry EtOH (57 μ L, 0.96 mmol, 10.0 eq.) (32 μ L, 0.52 mmol, 10.00 eq.) was diluted with THF (2 mL) and the mixture was added slowly at rt to the LAH suspension. (S)-BINOL (0.15 g, 0.52 mmol, 10.00 eq.) was added as a solution in THF (2 mL) followed by a solution of (2E,4Z)-sorbamide (58.30 mg, 0.52 mmol, 10.00 eq.) in THF (2 mL) to give a translucent gray solution. NOTE: If the solution turns into a light gray suspension it should not be used for the aza-aldol reaction

1.6 mL of the above stock solution of the putative amide transfer complex (0.105 mmol, 2.00 eq.) was added immediately to a solution of **R13da** (19.00 mg, 0.05 mmol, 1.00 eq.) in THF (1 mL). After 6 min, additional 1.6 mL of stock solution (0.11 mmol, 2.0 eq.) were added to the reaction mixture. After 20 min, sat. aqu. NaHCO_3 (4 mL) was added, the phases were separated and the aqueous phase was extracted with EtOAc (3 x 5 mL). The combined organic phases were dried over MgSO_4 , concentrated under reduced pressure and the residue was purified by FC (EtOAc/hexane 1:3 \rightarrow 1:1, 2% Et_3N) to afford zampanolide analog **R8** (5.90 mg, 0.012 mmol, 24%) as a colourless film. The final NMR always showed ca. 8% of aldehyde **R13da**, which we ascribe to facile retro-aza aldol reaction, even if CDCl_3 was filtered over basic Al_2O_3 . Attempts to purify **8** by using normal or reverse phase HPLC only led to decomposition.

TLC (EtOAc): $R_f = 0.52$. **$^1\text{H-NMR}$** (400 MHz, CDCl_3): $\delta = 7.41$ (d, $J = 12.9$ Hz, 1H), 6.89 (dt, $J = 16.3, 6.8$ Hz, 1H), 6.47 – 6.39 (m, 2H), 6.11 – 5.95 (m, 2H), 5.51 (d, $J = 11.3$ Hz, 0H), 5.41 (d, $J = 11.3$ Hz, 1H), 5.35 (dd, $J = 8.2, 6.1$ Hz, 1H), 5.26 (d, $J = 7.9$ Hz, 1H), 5.20 (ddd, $J = 10.7, 6.2, 2.3$ Hz, 1H), 4.03 (td, $J = 8.2, 7.7, 3.9$ Hz, 1H), 3.50 – 3.41 (m, 1H), 2.76 – 2.67 (m, 1H), 2.64 (q, $J = 6.7$ Hz, 2H), 2.47 – 2.20 (m, 4H), 1.86 (dd, $J = 6.9, 1.7$ Hz, 3H), 1.84 (s, 1H), 1.67 – 1.63 (m, 3H), 1.62 – 1.46 (m, 2H), 1.46 – 1.19 (m, 6H), 1.09 (dt, $J = 14.0, 8.0, 6.3$ Hz, 3H). **$^{13}\text{C-NMR}$** (101 MHz, CDCl_3): $\delta = 202.8,$

174.3, 167.6, 146.5, 143.8, 140.2, 132.5, 131.1, 128.3, 117.1, 76.6, 75.8, 75.6, 71.2, 46.1, 41.2, 39.4, 37.5, 33.6, 31.8, 31.5, 27.6, 25.3, 23.6, 23.3, 18.8, 16.2. **IR** (neat): $\tilde{\nu}$ = 3359, 2989, 2932, 2858, 1769, 1759, 1713, 1661, 1648, 1604, 1543, 1523, 1456, 1428, 1376, 1244, 1049 cm^{-1} . **HRMS** (ESI): calcd for $\text{C}_{27}\text{H}_{39}\text{NNaO}_6$ $[(\text{M}+\text{Na})^+]$: 496.2670; found: 496.2664. $[\alpha]_{589}^{20}$: -27.11° ($c = 0.59$, CH_3CN).



4.2.1.4 Cellular and biochemical profiling

4.2.1.4.1 Cell growth inhibition (MTT assay)

A549, A2780, and A2780AD cells: Cells in complete medium (RPMI1640 with 10 % FCS, 1 mM pyruvate, 2 mM glutamine, 100 U/mL penicillin, 100 µg/mL streptomycin and 50 µg/mL gentamicin) were seeded in 96-well culture plates at a density of 10^4 cells/well. After 24 h of incubation (37 °C, 5 % CO₂) compounds were added to cells at different concentrations up to 200 µg/mL and further incubated for 48 h. Then, thiazolyl blue tetrazolium bromide (3-(4,5-dimethylthiazol-2yl)-2,5-diphenyltetrazolium bromide (MTT) solution was added to the plate for 4 h. The MTT reaction was stopped by adding a solution of DMF-SDS. The following day, the plate was gently shaken for 2 h to dissolve formazan crystals prior to measuring 570/690 nm absorbance in an Appliskan (Thermo Scientific) plate reader. Finally, corrected absorbance data were plotted against compound concentration in SigmaPlot and IC₅₀'s were obtained by adjustment of the values to a Four parameter logistic curve using this program. The mean IC₅₀ ± SE of three independent assays was obtained using Excel.

1A9, HT29, and HL60 cells: Cells in 100 µL culture medium were added to each well of a 96-well plate, then serial 2-fold dilutions of test compounds were made in each well to give 200 µL total volume per well and 1×10^4 cells/mL final concentration for adherent cells (1A9 and HT29 cells) and 2.4×10^4 cells per mL for suspension cells (HL-60 cells). After incubation for 48 h (HL-60) or 72 h (1A9 and HT29) at 37 °C, 5% CO₂ in air, MTT responses were determined. Briefly, 20 µL of 5 mg/mL MTT in phosphate-buffered saline (PBS) was added. The plates were incubated for 2 hours at 37 °C, then treated with 100 µL/well MTT solubilizer (10% SDS, 45% DMF, adjusted to pH 4.5 with acetic acid). Plates were incubated overnight to solubilize the blue formazan precipitate before measuring absorbance at 570 nm in an automated microplate reader (EnVision®, PerkinElmer, Waltham, MA). Control wells containing medium without cells were used as blanks. Duplicate wells were measured for each concentration of test compound. The MTT response was expressed as a percentage of the control (untreated) cells. IC₅₀ values were calculated using Graphpad Prism software.

4.2.1.4.2 Microtubule imaging

To assess the effect of zampanolide analogs on cellular microtubules, indirect immunofluorescence images were obtained using A549 cells plated at a density of 10^5 cells onto 12 mm round coverslips, cultured overnight and treated with compounds for 24 h. Vehicle (DMSO; less than 0.5%) and taxol were used as controls. Cells were permeabilized using Triton X-100 and fixed with 37% formaldehyde. Then, cells were incubated with the DM1A monoclonal

antibody reacting against alpha-tubulin. Afterwards, samples were washed, incubated with FITC goat anti-mouse antibody and, finally, the DNA was stained employing 1 µg/ml of Hoechst 33342. The slides were examined with a Zeiss Axioplan epifluorescence microscope and images were obtained using an ORCH-FLASH 4.2 cooled CCD camera.

Images obtained upon treatment with analogs **R5** and **R6** together with those from controls are displayed in **Figure 49**.

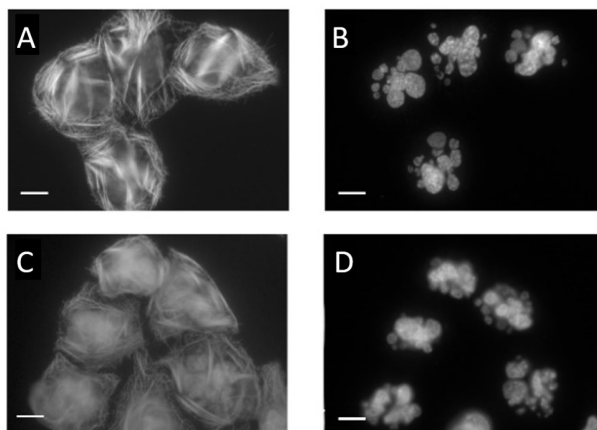


Figure 49: Microtubule bundling in A549 cells induced by 13-desmethylene-17-desmethyl(-)-zampanolide (**R5**) and 13-desmethylene-2,3-dihydro(-)-zampanolide (**R6**). Microtubule (A, C) and DNA (B, D) staining of A549 lung carcinoma cells. Cells were treated with **R5** (100 nM) (A, B); or 50 nM of **R6** (C, D). Microtubules were immunostained with α -tubulin monoclonal antibodies; DNA was stained with Hoechst 33342. Scale bar = 10 µm.

4.2.1.4.3 Cell cycle analysis

Progression through the cell cycle was analyzed in A549 cells by DNA determination with propidium iodide. A549 cells were seeded at a density of 1.5×10^5 in a 24-well plate and cultured in RPMI1640 with 10 % FCS, 1 mM pyruvate, 2 mM glutamine, 100 U/mL penicillin, 100 µg/mL streptomycin and 50 µg/mL gentamicin. Cells were left to attach to the substrate for 24 h at 37 °C and in a 5 % CO₂ air atmosphere. Then, compounds were added to the cells and incubated for further 24 h. Finally, cells were washed in PBS and fixed with 70% EtOH at 4 °C for 1 h, washed twice in phosphate-buffered saline (PBS), and resuspended in 500 µL of PBS containing 60 µg/mL DNase-free RNase A and 50 µg/mL propidium iodide. Samples were incubated at 37 °C for 30 min and analyzed with a Coulter Epics XL flow cytometer.

4.2.1.4.4 Binding to microtubules

Apparent microtubule-binding constants were determined in a Flutax-2 displacement assay.^[60,307,308] Briefly, 50 nM of both cross-linked microtubules and Flutax-2 were incubated with increasing concentrations of each compound up to 25 µM in 96-well plates in the dark for 20 min.

Docetaxel was employed as a control to observe fully displacement of the fluorescent probe. Then, Flutax-2 anisotropy was measured in an Appliskan (ThermoFisher) plate reader with polarized excitation and emission filters (492 and 535 nm, respectively). Finally, anisotropy data were converted to molar saturation fraction and plotted against compound concentration. Apparent binding constants were determined using Equigra v5. Binding constants are expressed as the mean value \pm SE of three independent experiments.

4.2.1.5 Crystallographic data for compound R5

Single crystals of **R5** were analysed on a Bruker Kappa APEX-II Duo diffractometer using microfocus sealed tube Cu-K α radiation and mirror optics ($\lambda = 1.54178 \text{ \AA}$). Measurements were carried out at 100K using an Oxford Cryosystems Cryostream 700 sample cryostat. Data were integrated using SAINT from the Bruker Apex-II program suite and corrected for absorption effects using the multi-scan method (SADABS).^[309] The structure was solved using SHELXT^[310] and refined by full-matrix least-squares analysis (SHELXL),^[311,312] using the program package OLEX2.^[313] All non-hydrogen atoms were refined anisotropically and non-donor hydrogen atoms were constrained to ideal geometries and refined with fixed isotropic displacement parameters (in terms of a riding model). CCDC 1499285 contains the supplementary crystallographic data for this paper, including structure factors and refinement instructions. These data can be obtained free of charge from The Cambridge Crystallographic Data Centre, 12 Union Road, Cambridge CB2 1EZ, UK (fax: +44(1223)-336-033; e-mail: deposit@ccdc.cam.ac.uk), or via <https://www.ccdc.cam.ac.uk/structures>.

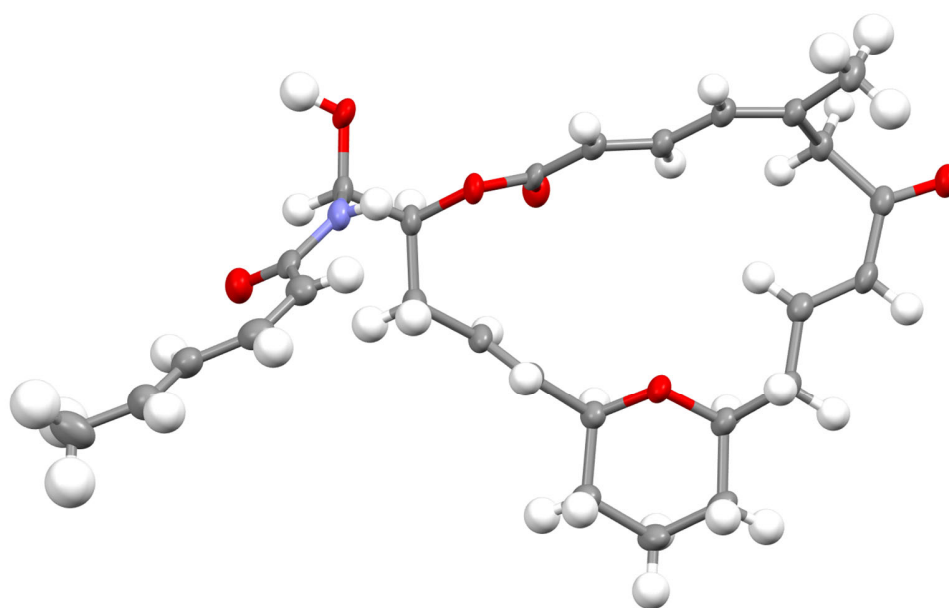


Figure 50: Asymmetric unit of the crystal structure of **R5**. Ellipsoids depicted at 50% probability. Hydrogen atoms shown as sticks for clarity. Absolute configuration was not determined.

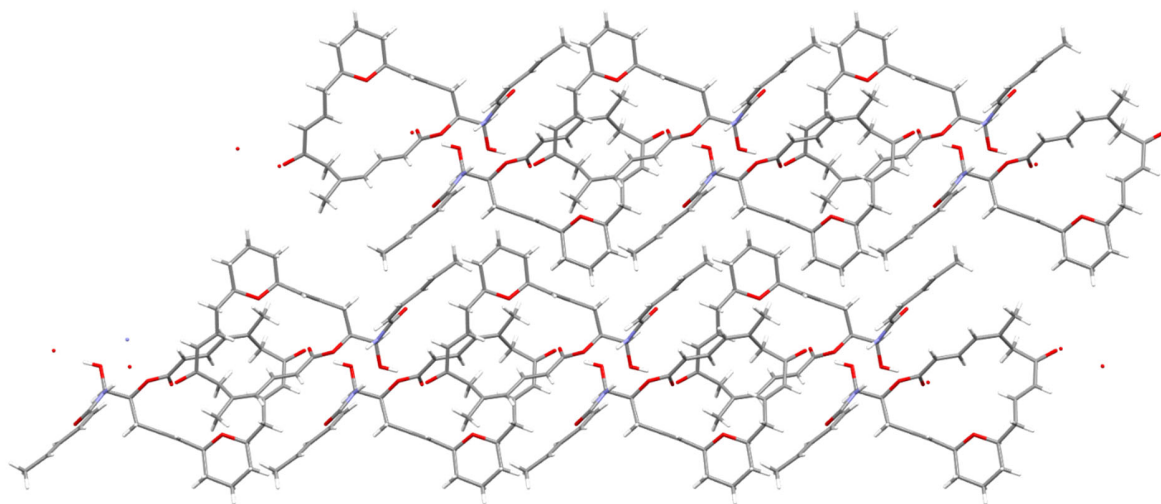


Figure 51: Packing of crystal structure of R5.

Table 19. Crystal and structure refinement data for compound R5.

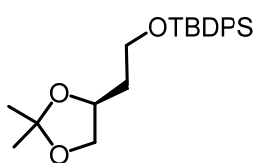
| Compound | R5 |
|---|---|
| CCDC number | 1499285 |
| Empirical formula | C ₂₇ H ₃₅ NO ₆ |
| Formula weight | 469.56 |
| Temperature [K] | 100.0(2) |
| Crystal system | monoclinic |
| Space group (number) | <i>P</i> 2 ₁ (4) |
| <i>a</i> [Å] | 13.2257(7) |
| <i>b</i> [Å] | 7.8567(4) |
| <i>c</i> [Å] | 13.6422(6) |
| α [°] | 90 |
| β [°] | 116.396(3) |
| γ [°] | 90 |
| Volume [Å ³] | 1269.77(11) |
| <i>Z</i> | 2 |
| ρ_{calc} [gcm ⁻³] | 1.228 |
| μ [mm ⁻¹] | 0.700 |
| <i>F</i> (000) | 504 |
| Crystal size [mm ³] | 0.09×0.06×0.03 |
| Crystal colour | clear colourless |
| Crystal shape | block |
| Radiation | CuK α (λ =1.54178 Å) |
| 2 θ range [°] | 7.23 to 133.52 (0.84 Å) |

| | |
|---|--|
| Index ranges | -15 ≤ h ≤ 15 -9 ≤ k ≤ 6 -16 ≤ l ≤ 16 |
| Reflections collected | 16263 |
| Independent reflections | 3594 $R_{\text{int}} = 0.0630$ $R_{\text{sigma}} = 0.0510$ |
| Completeness | 98.9 % |
| Data / Restraints / Parameters | 3594/3/315 |
| Goodness-of-fit on F^2 | 1.062 |
| Final R indexes [$I \geq 2\sigma(I)$] | $R_1 = 0.0534$ $wR_2 = 0.1417$ |
| Final R indexes [all data] | $R_1 = 0.0584$ $wR_2 = 0.1473$ |
| Largest peak/hole [$\text{e}\text{\AA}^{-3}$] | 0.65/-0.20 |
| Flack X parameter | 0.1(2) |

4.2.2 Synthesis and Structure-Activity Relationship Studies of Dioxane- and Oxathiane-Based Analogs of (-)-Zampanolide (Publication 2)

Literature known compounds (*S*)-butane-1,2,4-triol,^[314] (2*Z*,4*E*)-sorbamide (**O14a**),^[68] (2*E*,4*E*)-sorbamide (**O14b**),^[315] **O9**,^[72] **O23**,^[145] **O21**^[118] and (*S,E*)-5-iodo-1-((4-methoxybenzyl)oxy)-4-methylpent-4-en-2-ol^[90] were prepared according to literature procedures.

4.2.2.1 Synthesis of 10



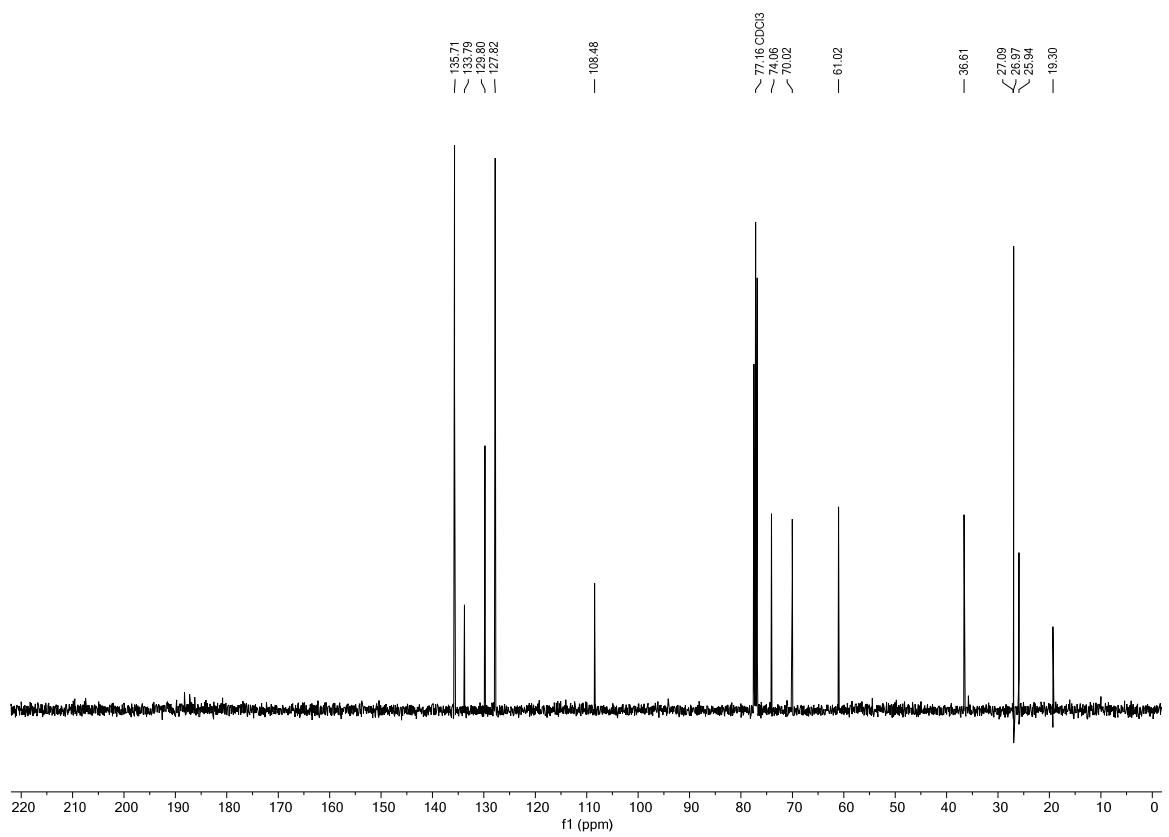
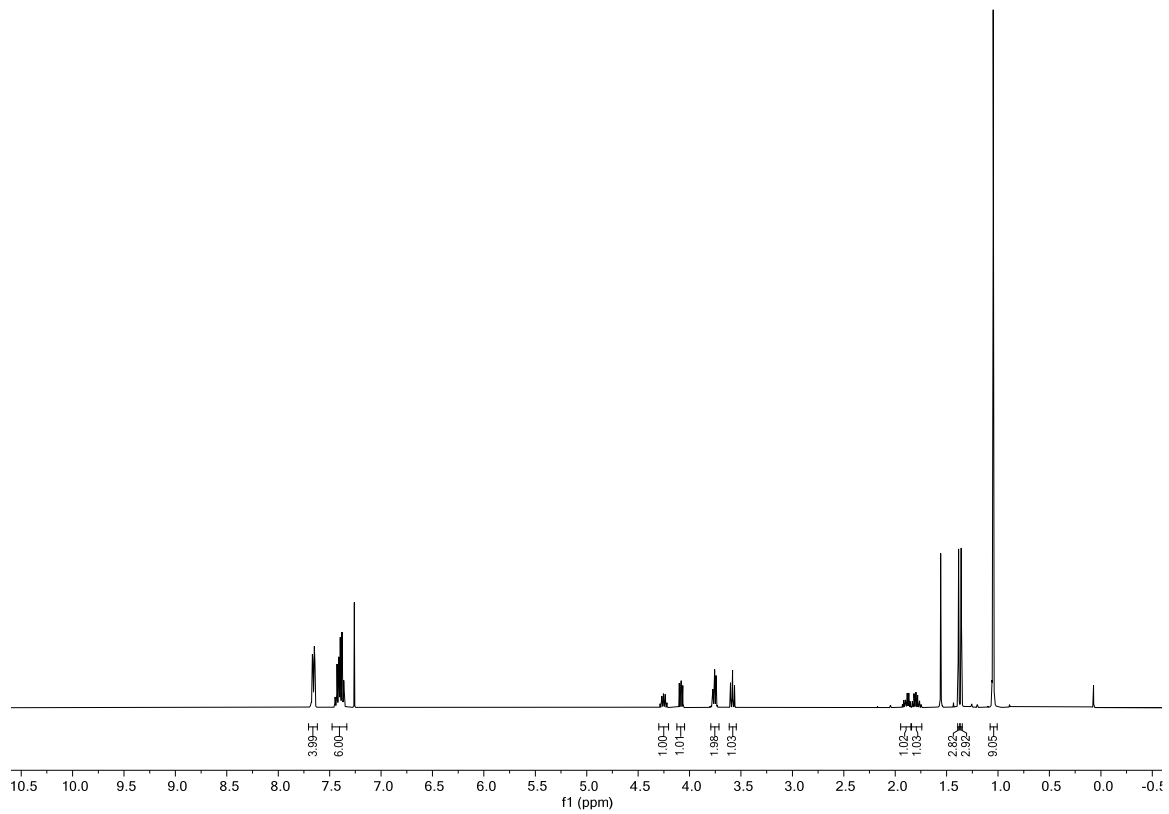
OS1

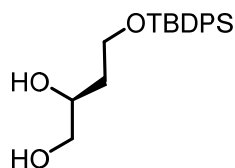
(*S*)-tert-butyl(2-(2,2-dimethyl-1,3-dioxolan-4-yl)ethoxy)diphenylsilane (OS1). To a stirred solution of (*S*)-butane-1,2,4-triol^[314] (5.74 g, 54.09 mmol, 1.00 equiv.) in dry CH₂Cl₂ (60 ml) at 0 °C was added 2,2-dimethoxypropane (13.3 ml, 108.18 mmol, 2.00 equiv.) and a catalytic amount of *p*-TsOH•H₂O (1.03 g, 5.41 mmol, 0.01 equiv.) and the mixture was stirred for 1 h at rt. The reaction was quenched by addition of sat. aqu. NaHCO₃ (60 ml) and the aqueous phase was extracted with CH₂Cl₂ (4 x 180 ml). The combined organic phases were then washed with brine and dried over anhydrous MgSO₄. Removal of the solvent afforded the crude as a colorless oil, which was used without further purification.

To the crude alcohol dissolved in DMF (7.5 ml) were added sequentially imidazole (7.21 g, 105.90 mmol, 2.20 equiv.) and TBDPSCl (13.2 ml, 48.14 mmol, 1.00 equiv.) at 0 °C. The cooling bath was removed and the reaction was stirred for 20 min. The reaction was quenched by addition of methanol (50 ml) and stirred for 15 min at rt. Sequentially, EtOAc (50 ml) and sat. aqu. NaHCO₃ (50 ml) were added, and the aqueous phase was extracted with EtOAc (3x 100 ml). The combined organic phases were washed with water (80 ml) and brine (60 ml), dried over anhydrous MgSO₄, filtered and concentrated under reduced pressure. Purification by flash column chromatography (EtOAc/hexane 1:12) afforded **OS1** (17.17 g, 44.66 mmol, 82% over two steps) as a colorless oil.

TLC: R_f = 0.30 (EtOAc/hexane 1:10). **¹H-NMR** (400 MHz, CDCl₃) δ = 7.71 – 7.62 (m, 4H), 7.48 – 7.33 (m, 6H), 4.30 – 4.20 (m, 1H), 4.12 – 4.05 (m, 1H), 3.79 – 3.71 (m, 2H), 3.58 (t, *J* = 7.8 Hz, 1H), 1.95 – 1.84 (m, 1H), 1.85 – 1.74 (m, 1H), 1.38 (s, 3H), 1.36 (s, 3H), 1.05 (s, 9H). **¹³C-NMR** (101 MHz,

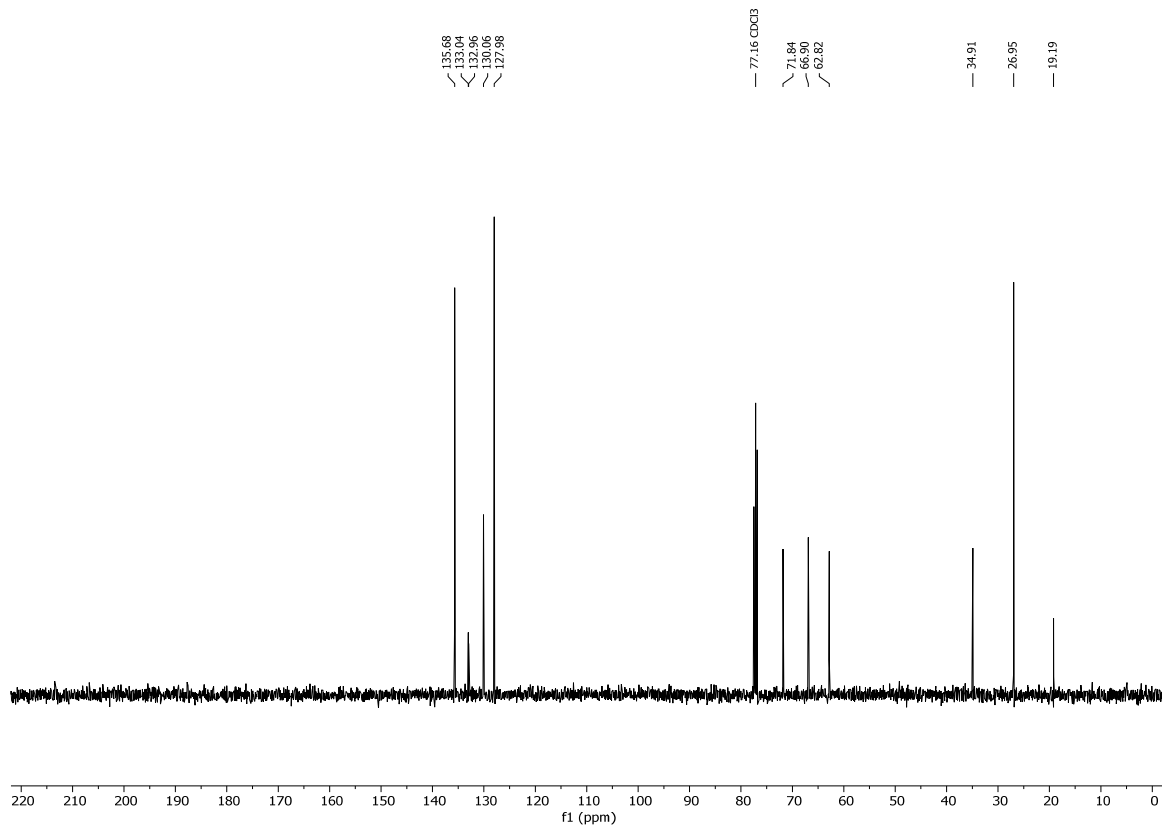
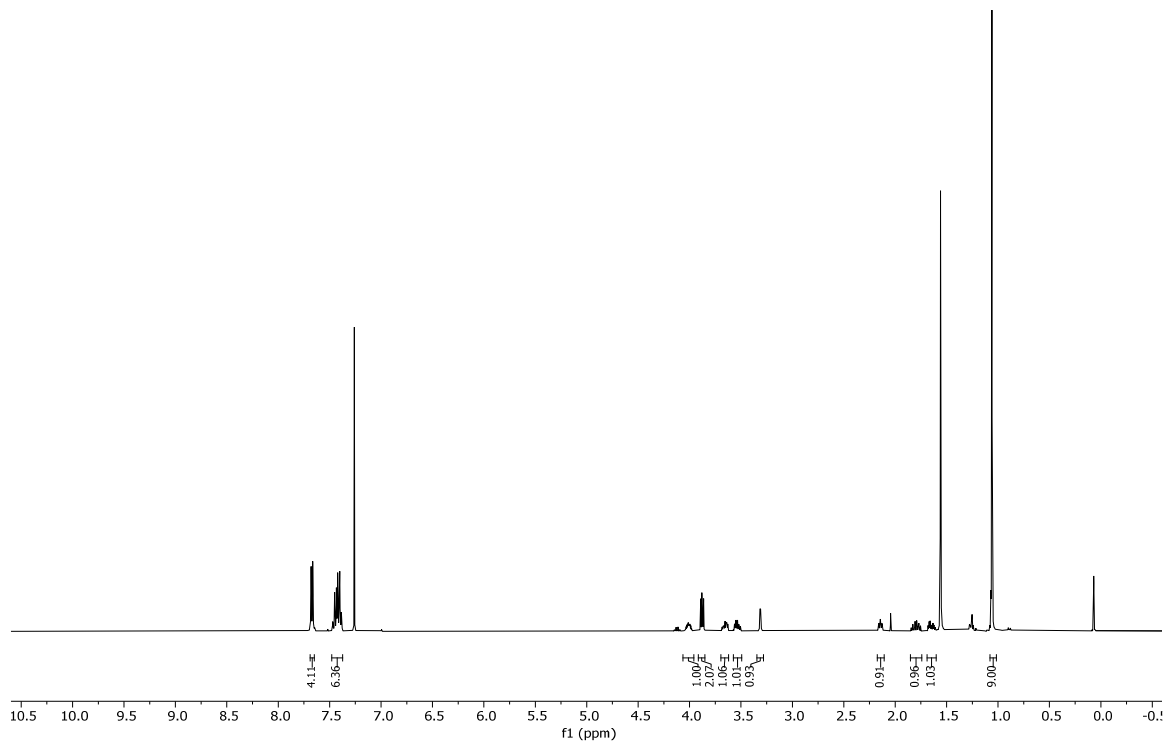
CDCl₃) δ = 135.7, 133.9, 129.8, 127.8, 108.5, 74.1, 70.0, 61.0, 36.6, 27.1, 27.0, 25.9, 19.3. **IR** (film) $\tilde{\nu}$ = 2984, 2932, 2858, 1472, 1428, 1369, 1215, 1160, 1108, 1082, 987, 857, 822, 738, 700. **HRMS** (ESI) calculated for C₂₃H₃₂NaO₃Si [(M+Na)⁺]: 407.2013; found: 407.2010. $[\alpha]_D^{20}$ = 4.29° (0.49 g/100cm³ in CHCl₃).

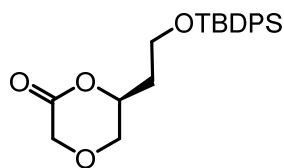


**O15**

(S)-4-((tert-butyldiphenylsilyl)oxy)butane-1,2-diol (O15). A solution of **OS1** (10.4 g, 27.04 mmol, 1.00 equiv.) in 70% aqueous acetic acid (65 ml) was stirred at rt over 16 h. The reaction was quenched by dilution with toluene (80 ml) and the solvents were removed under reduced pressure. Three further co-evaporations with toluene (60 ml) were conducted. Purification by flash column chromatography (EtOAc/hexane 1:1) afforded **O15** (7.48 g, 21.72 mmol, 80%) as white crystals.

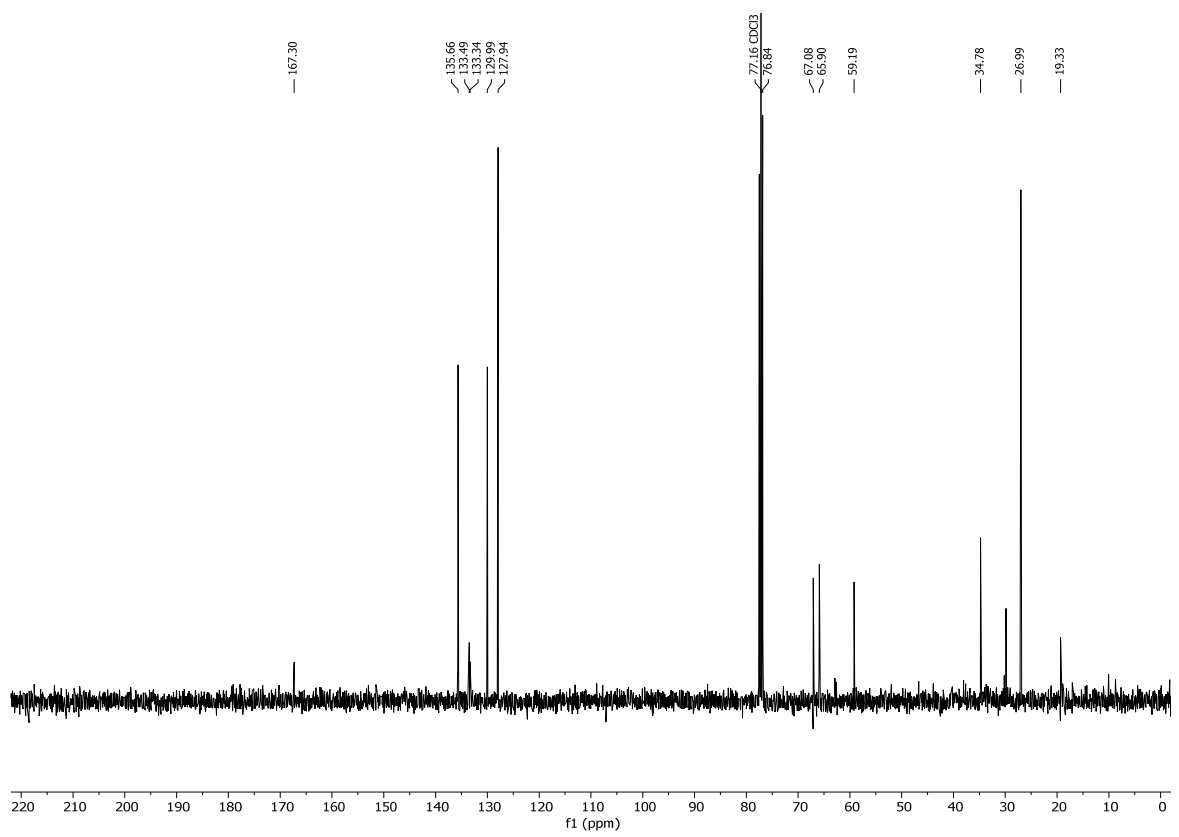
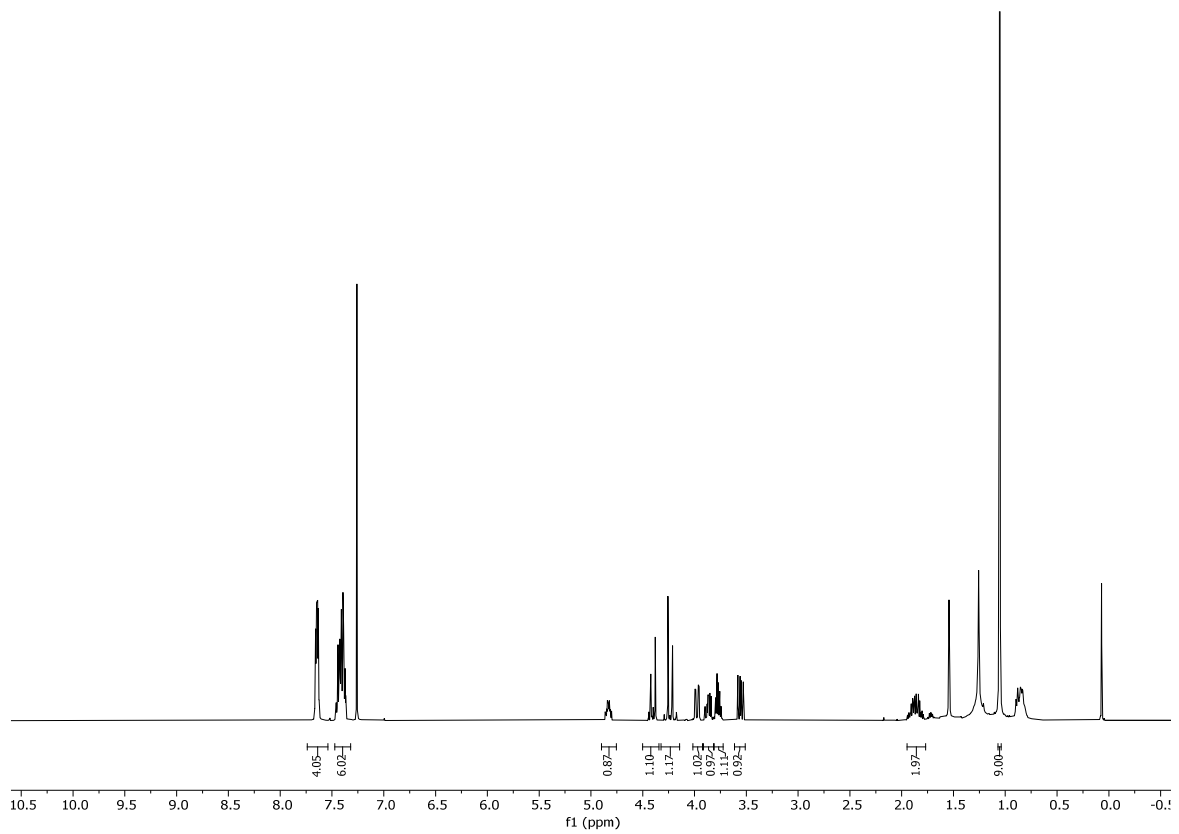
TLC: $R_f = 0.41$ (EtOAc/hexane 1:1). **MP** = 72 °C. **$^1\text{H-NMR}$** (400 MHz, CDCl_3) $\delta = 7.69 - 7.65$ (m, 4H), 7.48 – 7.37 (m, 6H), 4.06 – 3.96 (m, 1H), 3.91 – 3.85 (m, 2H), 3.70 – 3.62 (m, 1H), 3.57 – 3.49 (m, 1H), 3.31 (d, $J = 3.0$ Hz, 1H), 2.14 (t, $J = 6.2$ Hz, 1H), 1.85 – 1.74 (m, 1H), 1.69 – 1.60 (m, 1H), 1.06 (s, 9H). **$^{13}\text{C-NMR}$** (101 MHz, CDCl_3) $\delta = 135.7, 133.0, 133.0, 130.1, 128.0, 71.8, 66.9, 62.8, 34.9, 26.9, 19.2$. **IR** (film) $\tilde{\nu} = 3366, 2929, 2857, 1471, 1427, 1390, 1108, 995, 937, 822, 738$. **HRMS** (ESI) calculated for $\text{C}_{20}\text{H}_{28}\text{NaO}_3\text{Si}$ [(M+Na) $^+$]: 376.1700; found: 376.1699. $[\alpha]_D^{20} = 6.67^\circ$ (0.96 g/100cm 3 in CHCl_3).

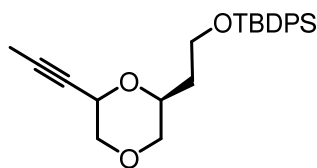


**O17**

(S)-6-(2-((tert-butyldiphenylsilyl)oxy)ethyl)-1,4-dioxan-2-one (O17). A suspension of **O15** (5.00 g, 14.51 mmol, 1.00 equiv.) and dibutyltin oxide (3.79 g, 15.24 mmol, 1.05 equiv.) in methanol (70 ml) was heated at 70 °C for 18 h. The solvent was removed under reduced pressure, the residue was dried under high vacuum for 1 h. The residue was dissolved in toluene (100 ml), tetrabutylammonium iodide (1.07 g, 2.90 mmol, 0.20 equiv.) and ethylbromoacetate (**O16**) (4.8 ml, 43.54 mmol, 3.00 equiv.) were added and the mixture was heated under reflux. After 3 h, the mixture was cooled to rt, diluted with EtOAc (100 ml) and washed with H₂O (500 ml) and brine (300 ml). The organic phase was dried over anhydrous MgSO₄, filtered and concentrated under reduced pressure. The residue was purified by flash column chromatography (EtOAc/hexane 1:8 → 1:3) to afford lactone **O17** (3.73 g, 9.71 mmol, 67%) as a colorless oil.

TLC: R_f = 0.50 (EtOAc/hexane 1:3). **¹H-NMR** (400 MHz, CDCl₃) δ = 7.74 – 7.54 (m, 4H), 7.47 – 7.32 (m, 6H), 4.90 – 4.75 (m, 1H), 4.50 – 4.34 (m, 1H), 4.32 – 4.14 (m, 1H), 3.98 (dd, *J* = 12.6, 0.8 Hz, 1H), 3.91 – 3.82 (m, 1H), 3.81 – 3.72 (m, 1H), 3.56 (dd, *J* = 12.6, 8.4 Hz, 1H), 1.95 – 1.77 (m, 2H), 1.06 (s, 9H). **¹³C-NMR** (101 MHz, CDCl₃) δ = 167.3, 135.7, 133.5, 133.3, 130.0, 127.9, 76.8, 67.1, 65.9, 59.2, 34.78, 27.0, 19.3. **IR** (film) $\tilde{\nu}$ = 2957, 2930, 2857, 1746, 1470, 1427, 1389, 1291, 1255, 1210, 1146, 1107, 1087, 999, 965, 938, 822, 737, 701. **HRMS** (ESI) calculated for C₂₂H₂₈NaO₄Si [(M+Na)⁺]: 407.1649; found: 407.1648. $[\alpha]_D^{20}$ = -26.20° (1.00 g/100cm³ in CHCl₃).

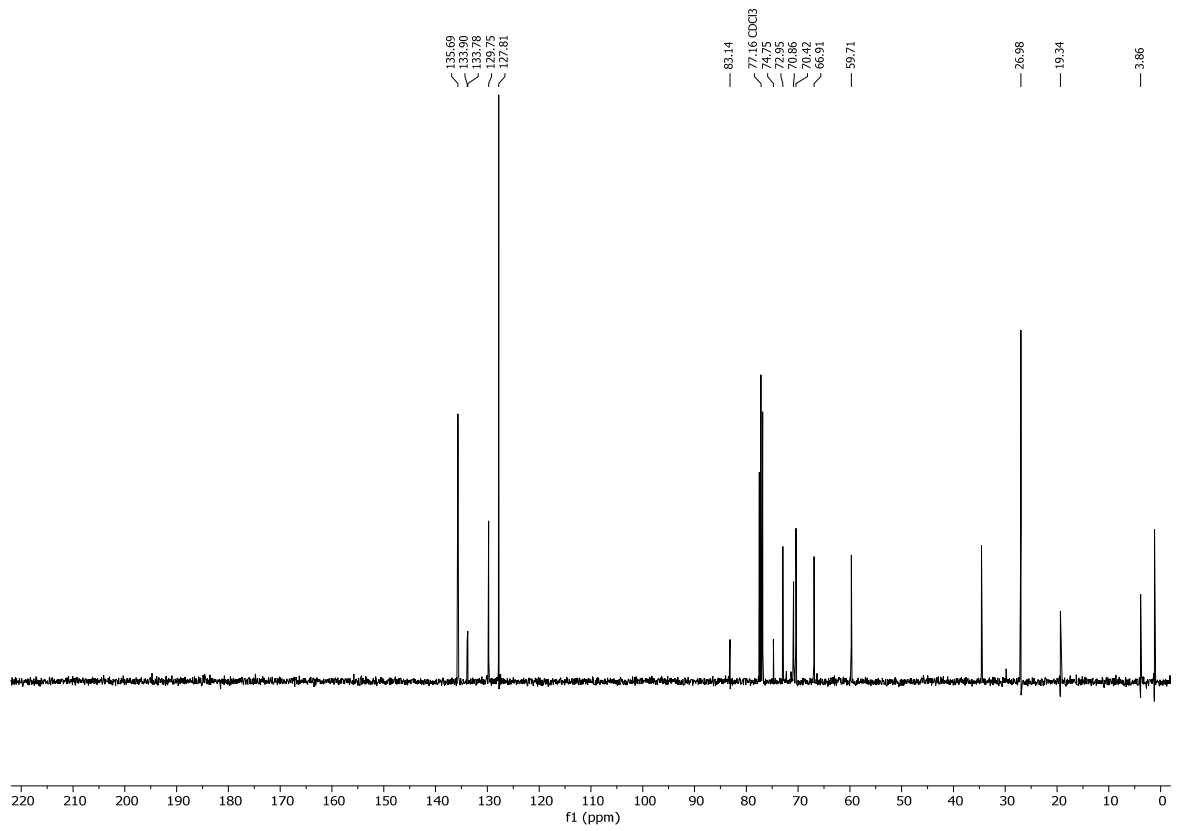
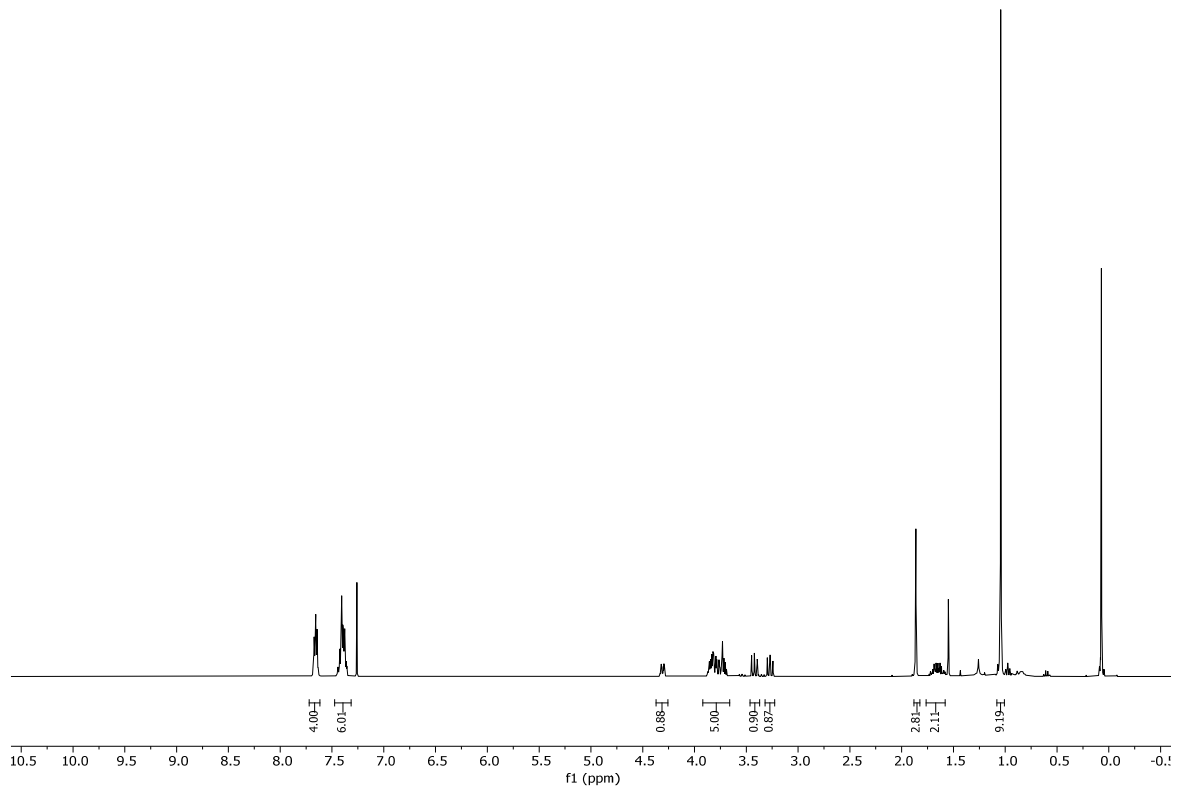


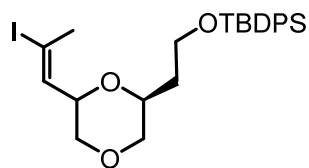
**O19**

tert-butyldiphenyl(2-((2S,6R)-6-(prop-1-yn-1-yl)-1,4-dioxan-2-yl)ethoxy)silane (O19). To a solution of *Z/E*-bromopropene (0.6 ml, 7.02 mmol, 1.50 equiv.) in THF (8 ml) at $-78\text{ }^{\circ}\text{C}$ was added *n*-BuLi (6.4 ml, 1.6M in hexane, 10.30 mmol, 2.20 equiv.) and stirred at $-78\text{ }^{\circ}\text{C}$ for 2 h. Then, **O17** (1.80 g, 4.68 mmol, 1.00 equiv.) dissolved in THF (8 ml) was added dropwise. After stirring at $-78\text{ }^{\circ}\text{C}$ for 1 h, the reaction was quenched by addition of sat. aqu. NaHCO_3 solution (20 ml) and allowed to warm to rt. The aqueous phase was extracted with EtOAc (3 x 20 ml) and the combined organic phases were dried over anhydrous MgSO_4 , filtered and concentrated under reduced pressure to afford the **O18** (1.97 g, 4.64 mmol, 99%). Crude **O18** was used in the next step without further purification.

To a solution crude **O18** (1.97 g, 4.64 mmol, 1.00 equiv.) in dry CH_2Cl_2 (23 ml), was added triethylsilane (7.4 ml, 5.39 g, 46.40 mmol, 10 equiv.), followed by dropwise addition of TFA (5.3 ml, 69.59 mmol, 15 equiv.) at $-78\text{ }^{\circ}\text{C}$. The reaction was slowly warmed to $-40\text{ }^{\circ}\text{C}$. After 2.5 h, the reaction was quenched by addition of sat. aqu. NaHCO_3 solution (125 ml) at $-40\text{ }^{\circ}\text{C}$. After slow warming to rt, the mixture was diluted with H_2O (100 ml) and EtOAc (140 ml) and the aqueous phase was extracted with EtOAc (3 x 125 ml). The combined organic phases were washed with H_2O (100 ml) and sat. aqu. NaCl solution (90 ml), dried over anhydrous MgSO_4 , filtered and concentrated under reduced pressure. Purification by flash column chromatography (EtOAc/hexane 1:10) afforded alkyne **O19** (1.45 g, 3.56 mmol, 76% over two steps) as a colorless oil.

TLC: $R_f = 0.44$ (EtOAc/hexane 1:10). **$^1\text{H-NMR}$** (400 MHz, CDCl_3) $\delta = 7.72 - 7.62$ (m, 4H), 7.47 – 7.31 (m, 6H), 4.37 – 4.26 (m, 1H), 3.92 – 3.66 (m, 5H), 3.46 – 3.37 (m, 1H), 3.32 – 3.23 (m, 1H), 1.86 (d, $J = 2.1$ Hz, 3H), 1.76 – 1.58 (m, 2H), 1.04 (s, 9H). **$^{13}\text{C-NMR}$** (101 MHz, CDCl_3) $\delta = 135.7, 133.9, 133.8, 129.8, 127.8, 83.1, 74.8, 73.0, 70.9, 70.4, 66.9, 59.7, 27.0, 19.3, 3.9$. **IR** (neat): $\tilde{\nu} = 3071., 2958, 2930, 2855, 2365, 2356, 2336, 2170, 1472, 1428, 1389, 1320, 1258, 1219, 1104, 1074, 961, 916, 822, 772, 738, 703, 615, 589, 532, 505, 488, 476, 471, 459, 451, 443, 435, 427, 418, 401\text{ cm}^{-1}$. **$^1\text{HRMS}$** (ESI): calculated for $\text{C}_{25}\text{H}_{32}\text{NaO}_3\text{Si}$ [(M+Na) $^+$]: 431.2013; found: 431.2012. $[\alpha]_D^{20} = -23.00^{\circ}$ (1.00 g/100 cm^3 in CHCl_3).

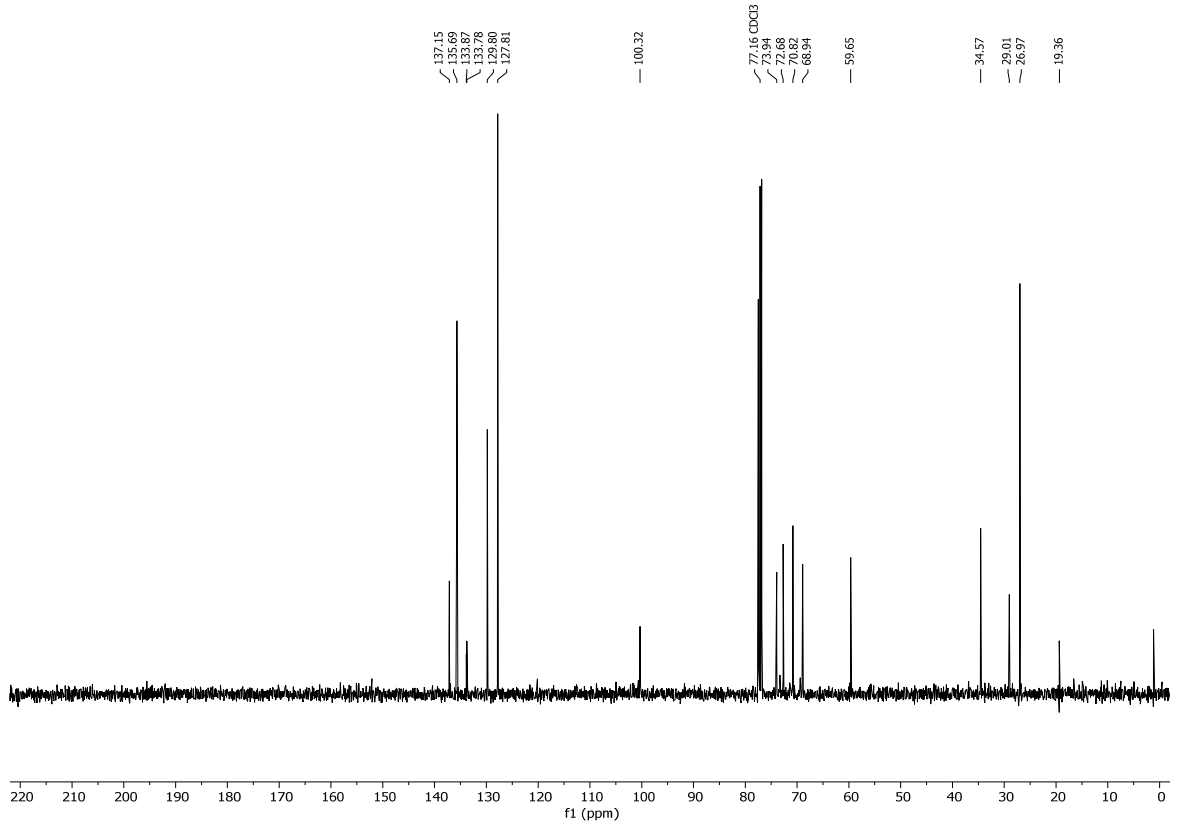
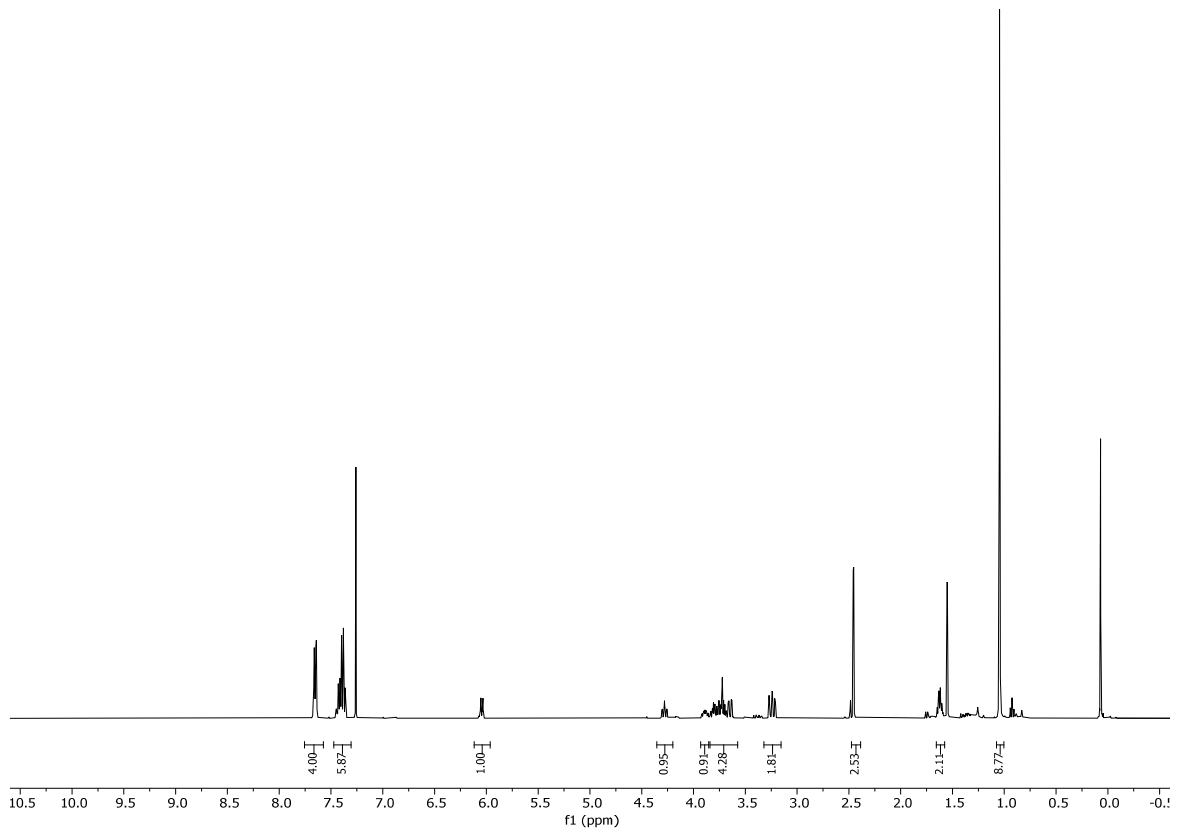


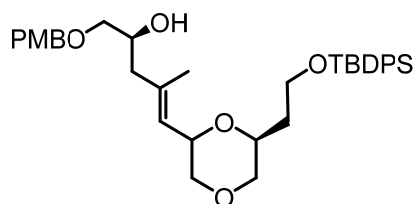
**O20**

tert-butyl(2-((2S)-6-((E)-2-iodoprop-1-en-1-yl)-1,4-dioxan-2-yl)ethoxy)diphenylsilane (O20). To a suspension of CuCN (6.85 g, 76.48 mmol, 5.00 equiv.) in THF (100 ml) at $-78\text{ }^{\circ}\text{C}$ was added a solution of *n*-BuLi (95.6 ml, 1.6M in hexane, 152.96 mmol, 10.00 equiv.). After 5 min, the flask was immersed in a cooling bath at $-40\text{ }^{\circ}\text{C}$, resulting in the formation of a pale-yellow, almost clear solution. The mixture was cooled back to $-78\text{ }^{\circ}\text{C}$ after 10 min, which made it become slightly heterogeneous. Neat Bu_3SnH (41.1 ml, 152.96 mmol, 10.00 equiv.) was then added dropwise, immediately leading to a turbid yellow solution. After 20 min at $-78\text{ }^{\circ}\text{C}$, the mixture was stirred for 5 min at $-40\text{ }^{\circ}\text{C}$, giving an almost clear golden-yellow solution. After 10 min at $-40\text{ }^{\circ}\text{C}$, the solution was cooled back to $-78\text{ }^{\circ}\text{C}$ followed by addition of methanol (68.2 ml, 1682.53 mmol, 110.00 equiv.) under vigorous stirring. After 10 min at $-78\text{ }^{\circ}\text{C}$ the flask was immersed in a cooling bath at $-40\text{ }^{\circ}\text{C}$ giving a clear red solution. After 10 min at $-40\text{ }^{\circ}\text{C}$, the solution was cooled back to $-78\text{ }^{\circ}\text{C}$ and alkyne **O19** (6.25 g, 15.29 mmol, 1.00 equiv.) dissolved in THF (60 ml) was added. The mixture was then stirred over 16 h during which the temperature was allowed to rise to $-15\text{ }^{\circ}\text{C}$. The reaction was quenched by addition of sat. aqu. NH_4Cl (110 ml) and 25% aqu. NH_4OH solution (35 ml), added together with EtOAc (25 ml). Stirring was continued for 30 min, the two phases were separated, and the aqueous phase was extracted with EtOAc (3 x 70 ml). The combined organic phases were dried over anhydrous MgSO_4 and concentrated under reduced pressure. Purification of the residue by flash chromatography on deactivated silica (hexane and 1% (v/v) Et_3N) afforded (*E*)-vinylstannane as a colorless oil which was used in the next step immediately.

A solution of vinylstannane in THF (95 ml) was cooled to $-17\text{ }^{\circ}\text{C}$ followed by addition of NIS (5.16 g, 22.94 mmol, 1.50 equiv.) dissolved in THF (20 ml), to give an almost clear yellow solution. After 20 min, a mixture of sat. aqu. $\text{Na}_2\text{S}_2\text{O}_3$ (45 ml) and sat. aqu. NaHCO_3 (45 ml) was added followed by EtOAc (25 ml). Stirring was continued for 2 min until two clear phases were formed. The phases were separated and the aqueous phase was extracted with EtOAc (3 x 100 ml). The combined organic phases were dried over anhydrous MgSO_4 and concentrated under reduced pressure. The residue was purified by flash chromatography (EtOAc/hexane 1:75 \rightarrow 1:40) to afford **O20** (6.01 g, 11.20 mmol, 73% over two steps) as a pale yellow oil.

TLC: $R_f = 0.27$ (EtOAc/hexane 1:20). **$^1\text{H-NMR}$** (400 MHz, CDCl_3) $\delta = 7.76 - 7.57$ (m, 4H), 7.47 – 7.31 (m, 6H), 6.04 (dq, $J = 8.1, 1.5$ Hz, 1H), 4.28 (ddd, 1H), 3.93 – 3.85 (m, 1H), 3.84 – 3.57 (m, 4H), 3.32 – 3.16 (m, 2H), 2.46 (d, $J = 1.5$ Hz, 3H), 1.66 – 1.58 (m, 2H), 1.05 (s, 9H). **$^{13}\text{C-NMR}$** (101 MHz, CDCl_3) $\delta = 137.2, 135.7, 133.9, 133.8, 129.8, 127.8, 100.3, 73.9, 72.7, 70.8, 68.94, 59.7, 34.6, 29.0, 267.0, 19.4$. **IR** (neat): $\tilde{\nu} = 2956, 2928, 2855, 1472, 1428, 1220, 1112, 1090, 822, 772, 702, 687, 615, 518, 506, 478, 455, 438, 431, 477, 403$ cm^{-1} . **HRMS** (ESI): calculated for $\text{C}_{25}\text{H}_{34}\text{IO}_3\text{Si}$ $[(\text{M}+\text{Na})^+]$: 537.1316; found: 537.1316. $[\alpha]_D^{20} = -20.70^\circ$ ($c = 1.0$ g/100 cm^3 in CHCl_3).

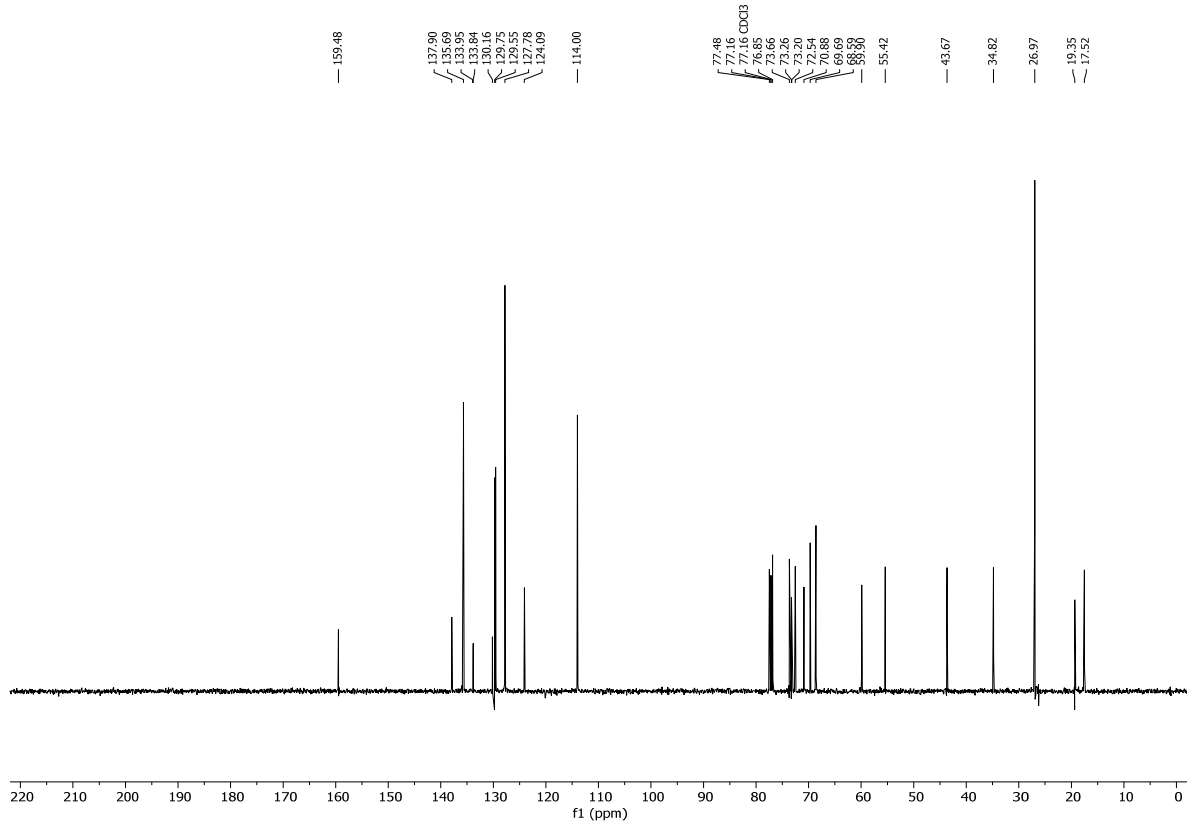
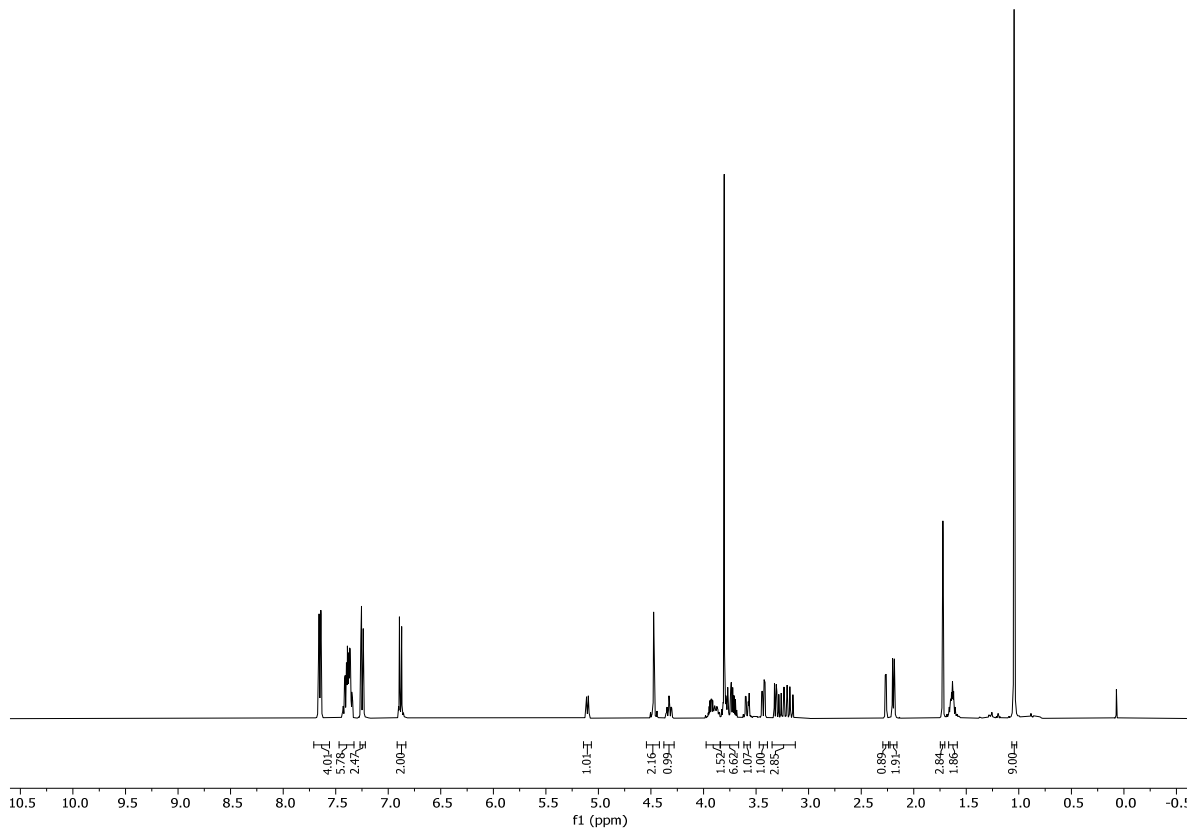


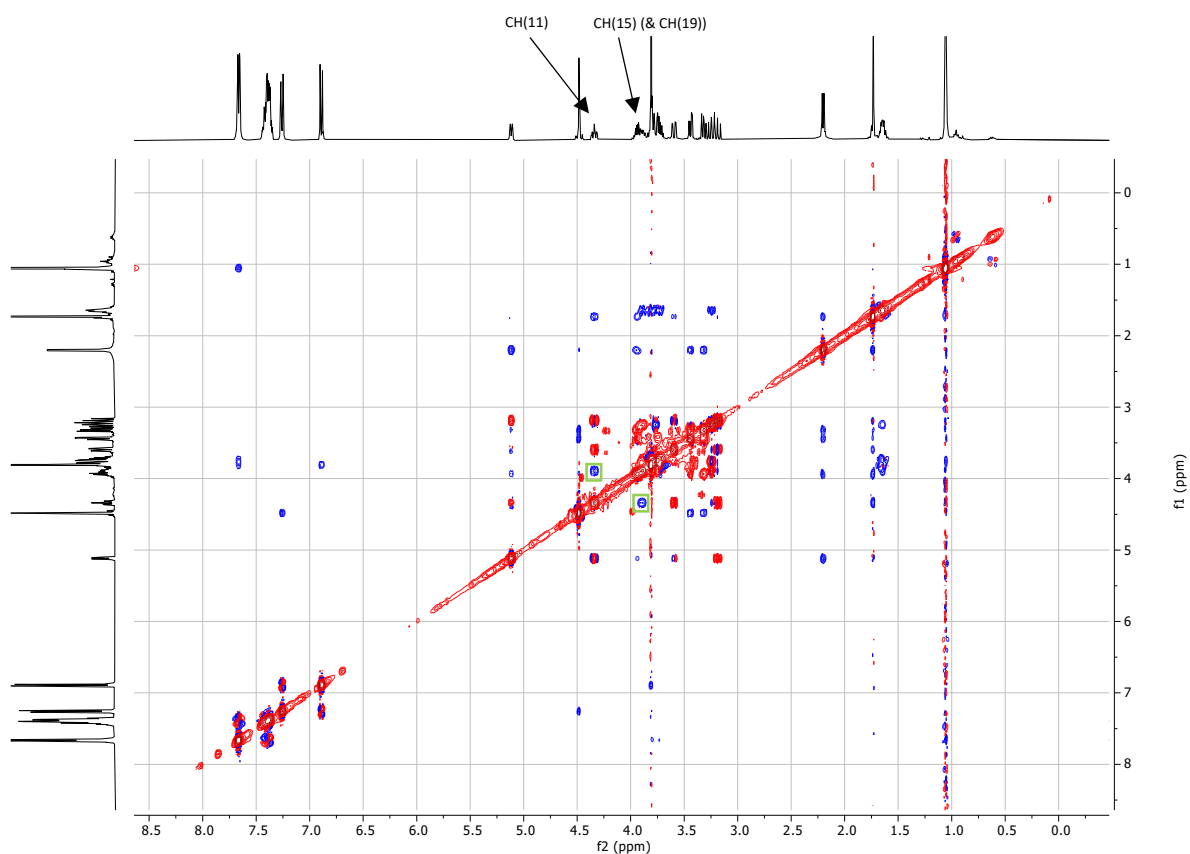


O10

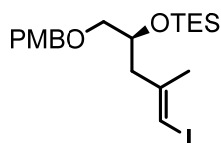
(2*S*,*E*)-5-((6*S*)-6-(2-((*tert*-butyldiphenylsilyl)oxy)ethyl)-1,4-dioxan-2-yl)-1-(4-methoxybenzyl)oxy)-4-methylpent-4-en-2-ol (O10). To a solution of vinyl iodide **O20** (305.0 mg, 0.57 mmol, 1.00 equiv., azeotropically dried twice with 2 ml toluene right before use) dissolved in dry toluene (2 ml), was added dropwise *n*-BuLi (0.4 ml, 1.6M in pentane, 0.63 mmol, 1.10 equiv.) at $-78\text{ }^{\circ}\text{C}$ and the mixture was stirred for 1 h. The reaction mixture was then cooled to $-100\text{ }^{\circ}\text{C}$ (liquid nitrogen/ethanol) and a solution of epoxide **O21**^[118] (280.0 mg, 1.42 mmol, 2.50 equiv., azeotropically dried twice with 2 ml toluene right before use) in dry toluene (1.4 ml) was added dropwise followed by slow addition of $\text{BF}_3 \cdot \text{OEt}_2$ (0.19 ml, 0.75 mmol, 2.70 equiv. distilled over CaH_2 just before use) giving a pale yellow solution. The mixture was allowed to warm up to $-78\text{ }^{\circ}\text{C}$ and stirred for 3 h. The reaction was quenched by addition of sat. aqu. NaHCO_3 solution (7 ml) at $-78\text{ }^{\circ}\text{C}$ and allowed to warm to rt. Then, EtOAc (13 ml) and sat. aqu. NaHCO_3 solution (10 ml) was added and the aqueous phase was extracted with EtOAc (3 x 14 ml). The combined organic phases were dried over anhydrous MgSO_4 and concentrated under reduced pressure. Purification by flash column chromatography (EtOAc/hexane 1:10 \rightarrow 1:2) afforded alcohol **O10** (236.0 mg, 0.39 mmol, 69%) as a colourless oil.

TLC: $R_f = 0.55$ (EtOAc/hexane 1:1). **$^1\text{H-NMR}$** (400 MHz, CDCl_3) $\delta = 7.71 - 7.56$ (m, 4H), 7.47 – 7.33 (m, 6H), 7.27 – 7.22 (m, 2H), 6.88 (d, 2H), 5.10 (d, $J = 1.3$ Hz, 1H), 4.47 (d, $J = 1.5$ Hz, 2H), 4.38 – 4.28 (m, 1H), 3.98 – 3.84 (m, 2H), 3.84 – 3.67 (m, 7H), 3.58 (dd, $J = 11.4, 2.8$ Hz, 1H), 3.43 (dd, $J = 9.5, 3.4$ Hz, 1H), 3.35 – 3.13 (m, 3H), 2.27 (d, $J = 3.7$ Hz, 1H), 2.19 (d, $J = 1.1$ Hz, 2H), 1.72 (d, $J = 1.4$ Hz, 3H), 1.67 – 1.59 (m, 2H), 1.04 (s, 9H). **$^{13}\text{C-NMR}$** (101 MHz, CDCl_3) $\delta = 159.5, 137.9, 135.7, 134.0, 133.8, 130.2, 129.8, 129.6, 127.8, 124.1, 114.0, 77.5, 77.2, 76.9, 73.7, 73.26, 73.2, 72.5, 70.9, 69.7, 68.6, 59.9, 55.4, 43.7, 34.8, 27.0, 19.4, 17.5$. **IR** (film) $\tilde{\nu} = 3445, 2954, 2931, 2856, 1685, 1616, 1588, 1569, 1555, 1540, 1514, 1488, 1473, 1464, 1429, 1398, 1387, 1362, 1303, 1248, 1173, 1111, 1038, 930, 823, 769, 740, 704$. **HRMS** (ESI) calculated for $\text{C}_{36}\text{H}_{48}\text{NaO}_6\text{Si}$ [(M+Na)⁺]: 627.3112, found: 627.3107. $[\alpha]_D^{20} = -8.00^{\circ}$ (1.00 g/100cm³ in CHCl_3).



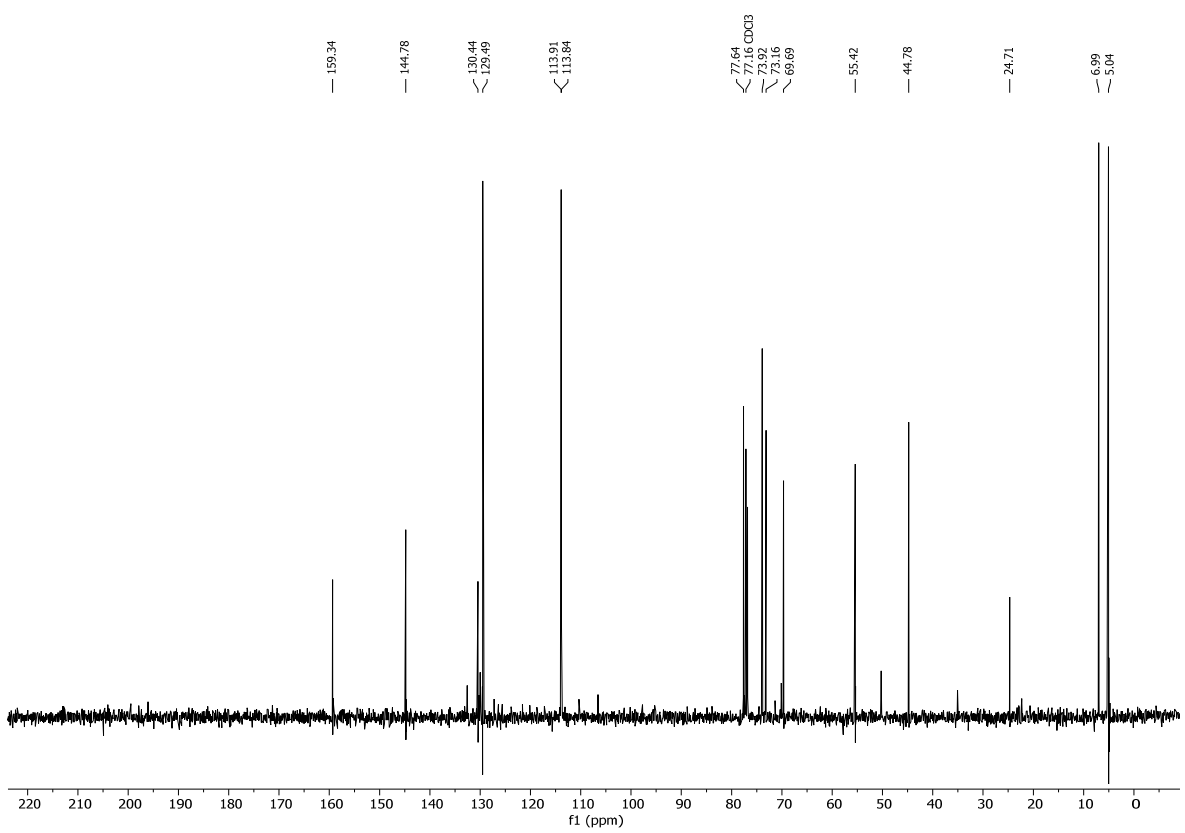
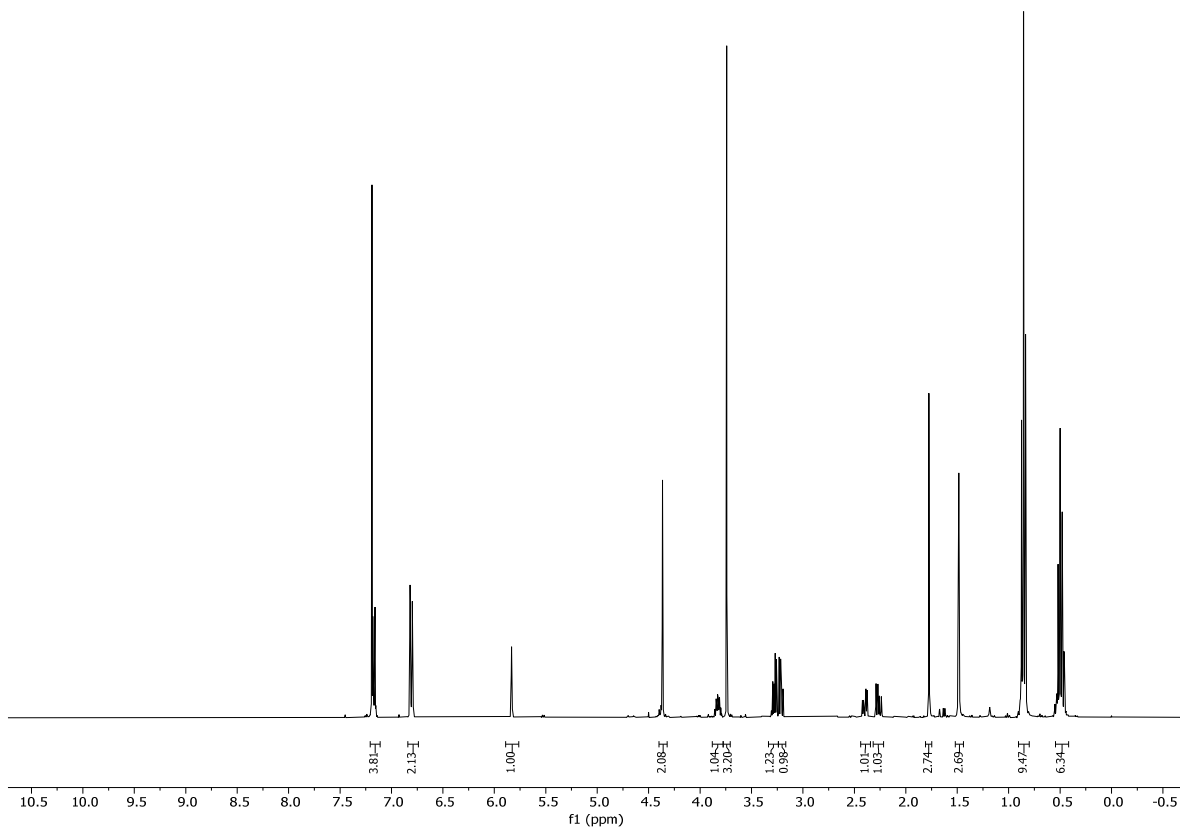


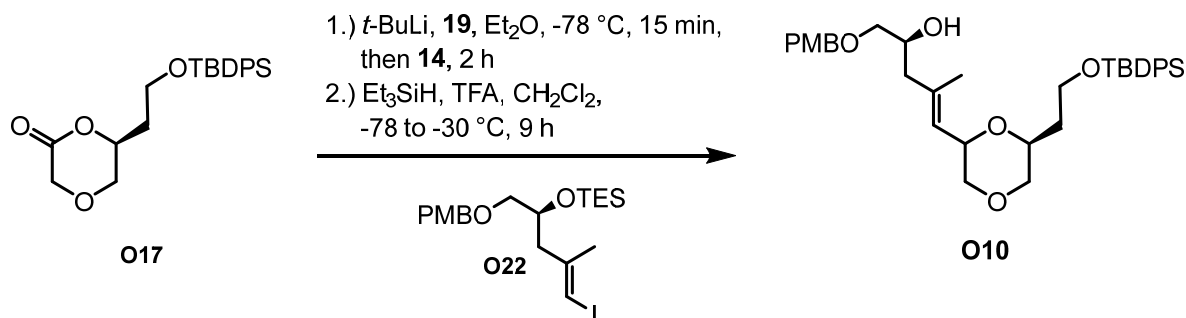
NOE-experiment showing the cross-peaks of CH(11) (4.38 – 4.28 (m, 1H) and CH(15) (3.98 – 3.84 (m, 2H, containing also CH(19))).

**O22**

(S,E)-triethyl((5-iodo-1-((4-methoxybenzyl)oxy)-4-methylpent-4-en-2-yl)oxy)silane (O22). To a solution of (*S,E*)-5-iodo-1-((4-methoxybenzyl)oxy)-4-methylpent-4-en-2-ol^[90] (0.50 g, 1.38 mmol, 1.00 equiv.) in DMF (5 ml) were added imidazole (0.24 mg, 3.45 mmol, 2.50 equiv.) and TESCl (0.35 ml, 2.07 mmol, 1.50 equiv.) at rt. After 45 min of stirring H₂O (40 ml) was added to the reaction, the phases were separated and the aqueous phase was extracted with EtOAc (3 x 50 ml). The combined organic phases were washed with water (2 x 50 ml), dried over MgSO₄, filtered and concentrated under reduced pressure. It was then purified by flash column chromatography (EtOAc/hexane, 1:10) to provide **O22** (0.65 g, 1.37 mmol, 99%) as a colorless oil.

TLC: R_f = 0.49 (EtOAc/hexane 1:10). **¹H-NMR** (400 MHz, CDCl₃) δ = 7.19 – 7.14 (m, 2H), 6.84 – 6.76 (m, 2H), 5.83 (q, *J* = 1.1 Hz, 1H), 4.37 (s, 2H), 3.83 (ddt, *J* = 7.5, 5.8, 4.8 Hz, 1H), 3.74 (s, 3H), 3.28 (dd, *J* = 9.5, 5.1 Hz, 1H), 3.21 (dd, *J* = 9.5, 5.9 Hz, 1H), 2.40 (ddd, *J* = 13.6, 4.6, 1.1 Hz, 1H), 2.26 (ddd, *J* = 13.6, 7.5, 0.9 Hz, 1H), 1.77 (d, *J* = 1.1 Hz, 3H), 1.49 (s, 3H), 0.86 (t, *J* = 7.9 Hz, 10H), 0.49 (q, *J* = 8.2 Hz, 5H). **¹³C-NMR** (101 MHz, CDCl₃) δ = 159.3, 144.8, 130.4, 129.5, 113.9, 113.8, 77.6, 73.9, 73.2, 69.7, 55.4, 44.8, 24.7, 7.0, 5.0. **IR** (film) $\tilde{\nu}$ = 2952, 2909, 2874, 1613, 1513, 1459, 1362, 1302, 1246, 1173, 1087, 1036, 1005, 971, 821, 774, 740, 727, 670. **HRMS** (ESI) calculated for C₂₀H₃₃I NaO₃Si [(M+Na)⁺]: 499.1136; found: 499.1135. $[\alpha]_D^{20}$ = 3.86° (1.00 g/100cm³ in CHCl₃).



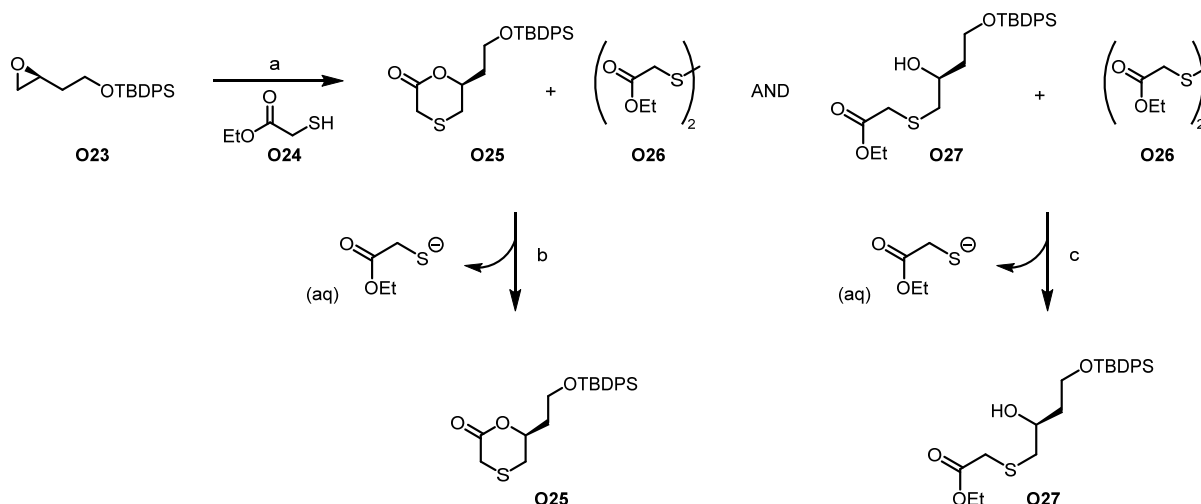


(2*S*,*E*)-5-((6*S*)-6-(2-((*tert*-butyldiphenylsilyl)oxy)ethyl)-1,4-dioxan-2-yl)-1-((4-methoxybenzyl)oxy)-4-methylpent-4-en-2-ol (O10**)**. To a solution of **O22** (1.24 g, 2.60 mmol, 1.00 equiv.) in Et₂O (22 ml) was added *t*-BuLi (1.48 ml, 1.7M in pentane, 2.52 mmol, 0.97 equiv.) at -78 °C. This solution was stirred for 15 min at that temperature before **O17** (1.50 g, 3.90 mmol, 1.50 equiv.) was added dropwise over 5 min as a solution in Et₂O (4 ml). The reaction was stirred for 2 h and was then quenched by the addition of sat. aqu. NaHCO₃ (10 ml) and let warm to rt. The phases were separated and the aqueous layer was extracted with EtOAc (3 x 10 ml). The combined organic phases were dried over MgSO₄, filtered and concentrated under reduced pressure. The crude was submitted to the next step immediately.

To a solution of the crude in CH₂Cl₂ (20 ml) was added triethylsilane (3.3 ml, 20.4 mmol, 10 eq.) and TFA (2.4 ml, 30.6 mmol, 15 eq.) dropwise *via* syringe over 3 min at -78 C. The reaction was stirred at -30 °C and monitored by TLC. After 9 hours the reaction was quenched by the addition of sat. aqu. NaHCO₃ (50 ml), H₂O (40 ml) and was then diluted with EtOAc (60 ml). The phases were separated and the aqueous phase was extracted with EtOAc (3 x 50 ml). The combined organic phases were washed with H₂O (50 ml) and brine (50 ml), dried over MgSO₄, filtered and concentrated under reduced pressure. Purification by flash column chromatography (EtOAc/hexane, 1:3) afforded **O10** (82.1 mg, 0.14 mmol, 5% over two steps) as a colorless oil.

4.2.2.2 Synthesis of O11

4.2.2.2.1 One-pot Synthesis of O25



Scheme 74: One-pot procedure for the formation of **O25** from **O23** and **O24**. a) Triton B, **O24**, 4Å MS, toluene, reflux, 40 h; b) DTT, Et₃N, DCM, rt, 3 h, 56% over two steps. c) DTT, Et₃N, DCM, rt, 3.5 h, 21% over two steps.

(S)-6-(2-((tert-butyldiphenylsilyl)oxy)ethyl)-1,4-oxathian-2-one (O25) and Ethyl (S)-2-((4-((tert-butyldiphenylsilyl)oxy)-2-hydroxybutyl)thio)acetate (O27). To a solution of **O23**^[145] (150.0 mg, 0.46 mmol, 1.00 equiv.) in toluene (1 ml, degassed prior to use), Triton B (54 µl, mmol, 0.30 equiv., 40% solution in methanol) and 4Å molecular sieves (35 mg) was added dropwise ethyl thioglycolate (**O24**) (150.0 µl, 1.38 mmol, 3.00 equiv.) and the mixture was heated under reflux. After 22 h, more ethyl thioglycolate (**O24**) (100 µl, 0.92 mmol, 2.00 equiv.) and Triton B (54 µl, 0.32 mmol, 0.70 equiv., 40 % solution in methanol) were added and the mixture was heated under reflux for 16 h. Then, the reaction mixture was concentrated under reduced pressure and the residue was purified by flash column chromatography (EtOAc/hexane 1:10 → 1:4) to give **O25** and **O27**, each as a mixture with disulfide **O26**.

To a solution of **O25** (114 mg, 0.28 mmol, 1.00 equiv.)²⁴ as a mixture with disulfide **O26** (191.0 mg, 0.80 mmol, 1.00 equiv.) in CH₂Cl₂ (12 ml), DTT (185.0 mg, 1.20 mmol, 1.50 equiv.) and Et₃N (170 µl, 1.20 mmol, 1.50 equiv.) were added and the mixture was stirred at rt. After 3 h, the reaction mixture was quenched by addition of 2M NaOH solution (10 ml). The organic phase was washed with brine solution (7 ml), dried over anhydrous MgSO₄ and concentrated under reduced

²⁴ Amounts of **O25**, **O27** and disulfide **O26** were calculated based on ¹H-NMR spectra of the mixtures.

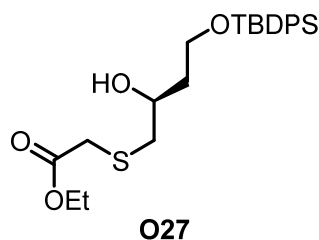
pressure. The residue was purified by flash column chromatography (EtOAc/hexane; 1:6) to afford pure **O25** (115.0 mg, 0.29 mmol, 56% over two steps) as a colorless oil.

To a solution of **O27** (494 mg, 1.11 mmol, 1.00 equiv.) as a mixture with disulfide **O26** (32.0 mg, 0.13 mmol, 1.00 equiv.) in CH₂Cl₂ (4 ml), DTT (31.0 mg, 0.20 mmol, 1.50 equiv.) and Et₃N (20 μl, 0.20 mmol, 1.50 equiv.) were added and the mixture was stirred at rt. After 3.5 h, the reaction mixture was quenched by addition of 2M aq. NaOH solution (4 ml). The two phases were separated and the aqueous phase was extracted with CH₂Cl₂ (3 x 4 ml). The combined organic phases were dried over anhydrous MgSO₄, filtered and concentrated under reduced pressure to afford pure **O27** (503.0 mg, 1.13 mmol, 21% over two steps) as a colorless oil.

Table 20. Conditions investigated for the Triton B-catalyzed opening of epoxide **O23** with ethyl thioglycolate (**O24**).^[a]

| Entry | Scale | Triton B ^[b] | Thiol 24 | Time | Yields ^[c] of O27/O25 | Remarks |
|-------|--------|-------------------------|----------|------|---|----------------------------------|
| 1 | 100 mg | 0.15 eq. | 3.0 eq. | 24 h | 18% / 14% ^[d] | - |
| 2 | 500 mg | 0.35 eq. | 3.5 eq. | 68 h | 45% ^[d] and 32% ^[d] | solvent degassed |
| 3 | 150 mg | 1.0 eq. | 5.0 eq. | 40 h | 21% and 56% | solvent degassed, 4Å MS added |

^[a]For all reactions, a mixture of epoxide **O23**, thiol **O24** and Triton B in toluene was heated under reflux for the specified time period. ^[b]The amount of Triton B present was continuously increased during the reaction by portionwise addition. Indicated is the number of equiv. reached after complete addition. ^[c]Isolated yields after flash column chromatography. ^[d]Compound isolated as a mixture with disulfide **O26**. The yield is based on ¹H-NMR spectroscopic analysis of the mixture.

4.2.2.2 Stepwise Synthesis of **O25**

ethyl (S)-2-((4-((tert-butyldiphenylsilyloxy)-2-hydroxybutyl)thio)acetate (O27**)**. To a solution of ethyl thioglycolate (**O24**) (40 μ l, 0.37 mol, 1.20 equiv.) in THF (0.7 ml) was added DBU (69 μ l, 0.46 mmol, 1.50 equiv.) at -65 $^{\circ}$ C. After 10 min **O23**^[145] (0.10 g, 0.31 mmol, 1.00 equiv.) dissolved in THF (1 ml) and $\text{BF}_3 \cdot \text{OEt}_2$ (57 μ l, 0.46 mmol, 1.50 equiv.) were added and stirring was continued at -65 $^{\circ}$ C for 40 min. Afterwards the cooling bath was removed and sat. aq. NaHCO_3 (10 ml) and EtOAc (10 ml) were added. After the mixture had reached rt the phases were separated and the aqueous phase was extracted with EtOAc (3 x 15 ml) and the combined organic extracts were washed with aq. Sat. NH_4Cl (30 ml). The combined organic extracts were dried over MgSO_4 , concentrated under reduced pressure, and the residue purified by flash chromatography (EtOAc/hexane 1:3 \rightarrow 1:1) to give **O27** (114.5 mg, 0.26 mmol, 84%) as a colorless oil.

The same procedure was followed to create the bulk material of **O27** (13.1 g, 29.33 mmol, 80%) from **O23** (12.0 g, 36.75 mmol, 1.00 equiv.).

TLC: $R_f = 0.55$ (EtOAc/hexane 1:2). **$^1\text{H-NMR}$** (400 MHz, CDCl_3) $\delta = 7.71 - 7.63$ (m, 4H), 7.45 - 7.36 (m, 6H), 4.19 (q, $J = 7.1$ Hz, 2H), 4.10 - 3.98 (m, 1H), 3.94 - 3.79 (m, 2H), 3.53 (d, $J = 2.9$ Hz, 1H), 3.34 - 3.25 (m, 2H), 2.82 (dd, $J = 13.7, 4.3$ Hz, 1H), 2.70 (dd, $J = 13.7, 7.7$ Hz, 1H), 1.84 - 1.71 (m, 2H), 1.28 (t, $J = 7.1$ Hz, 3H), 1.05 (s, 9H). **$^{13}\text{C-NMR}$** (101 MHz, CDCl_3) $\delta = 171.0, 135.7, 133.3, 133.2, 130.0, 127.9, 69.6, 62.5, 61.7, 40.4, 37.9, 34.4, 27.0, 19.2, 14.3$. **IR** (film) $\tilde{\nu} = 3501, 3071, 2956, 2931, 2858, 1732, 1472, 1428, 1390, 1364, 1274, 1175, 1111, 1090, 1030, 1009, 940, 822, 741, 703, 688, 614, 548, 503$. **HRMS** (ESI) calculated for $\text{C}_{24}\text{H}_{34}\text{NaO}_4\text{SSi}$ $[(\text{M}+\text{Na})^+]$: 469.1839, found: 469.1835. $[\alpha]_D^{20} = -9.00^{\circ}$ (1.00 g/100 cm^3 in CHCl_3).

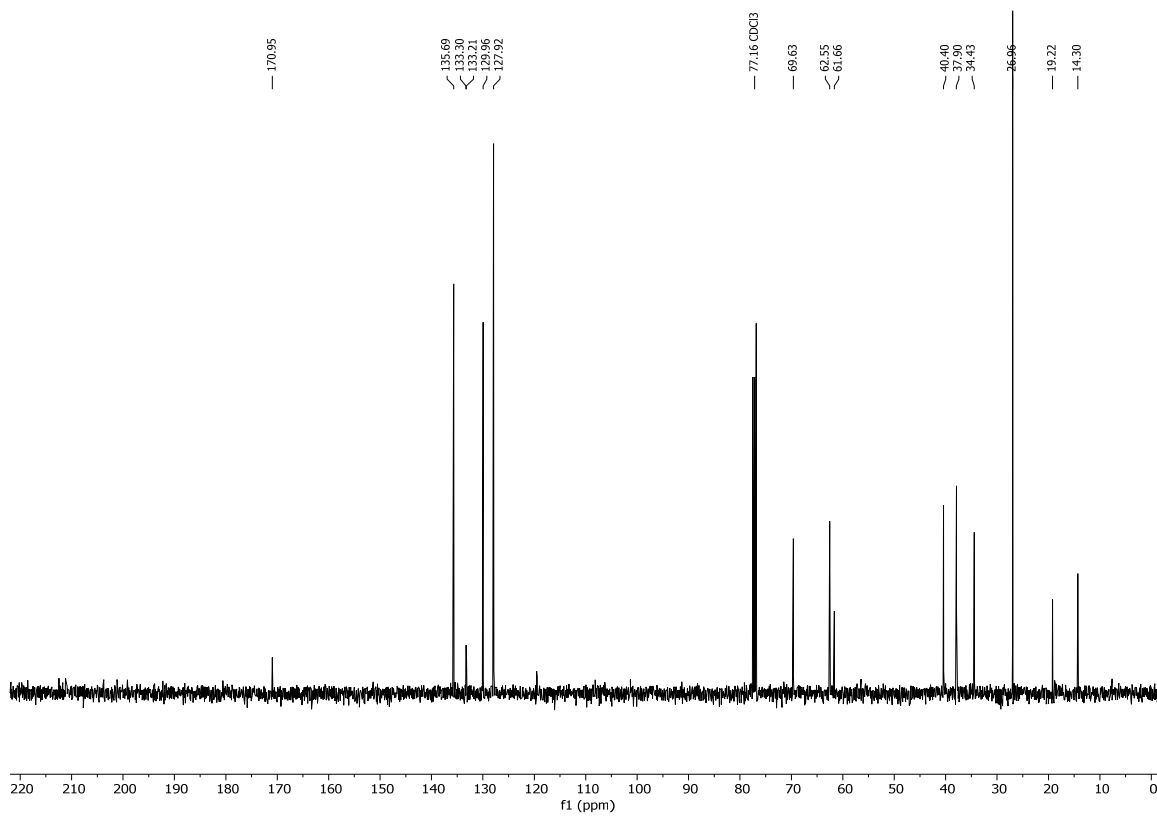
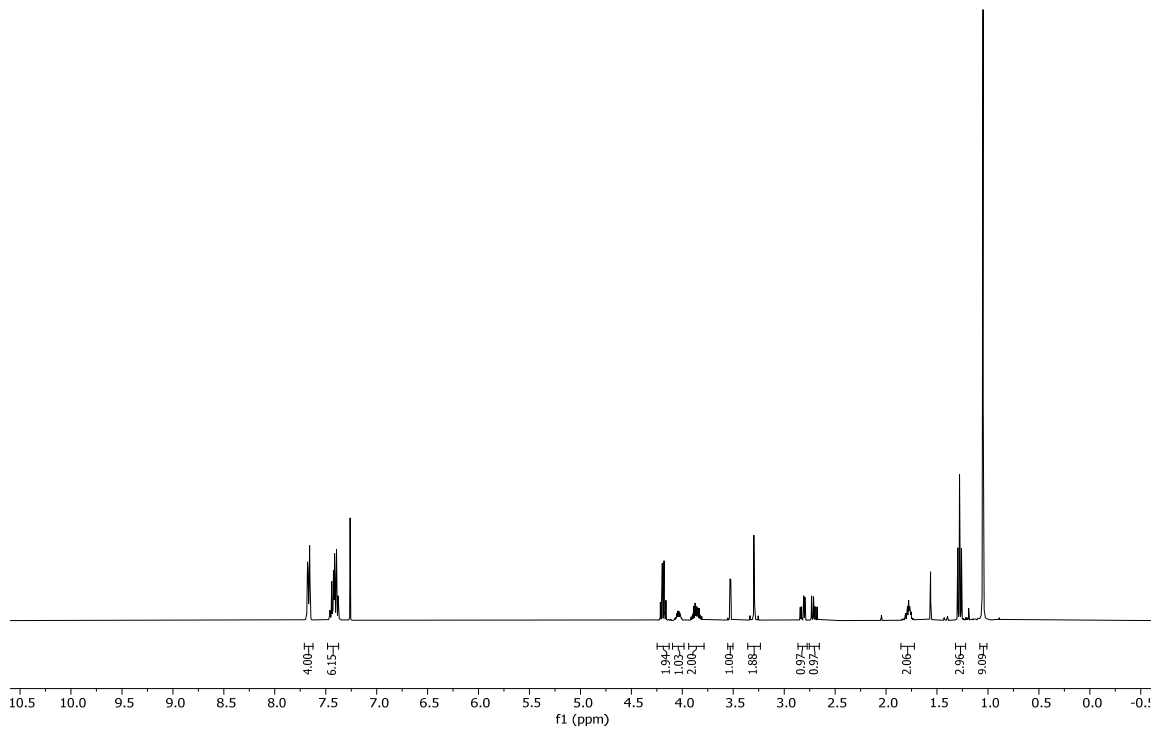
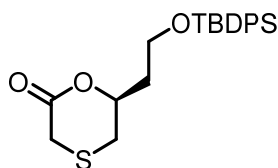


Table 21: Conditions investigated for the opening of epoxide **O23** with ethyl thioglycolate (**O24**).

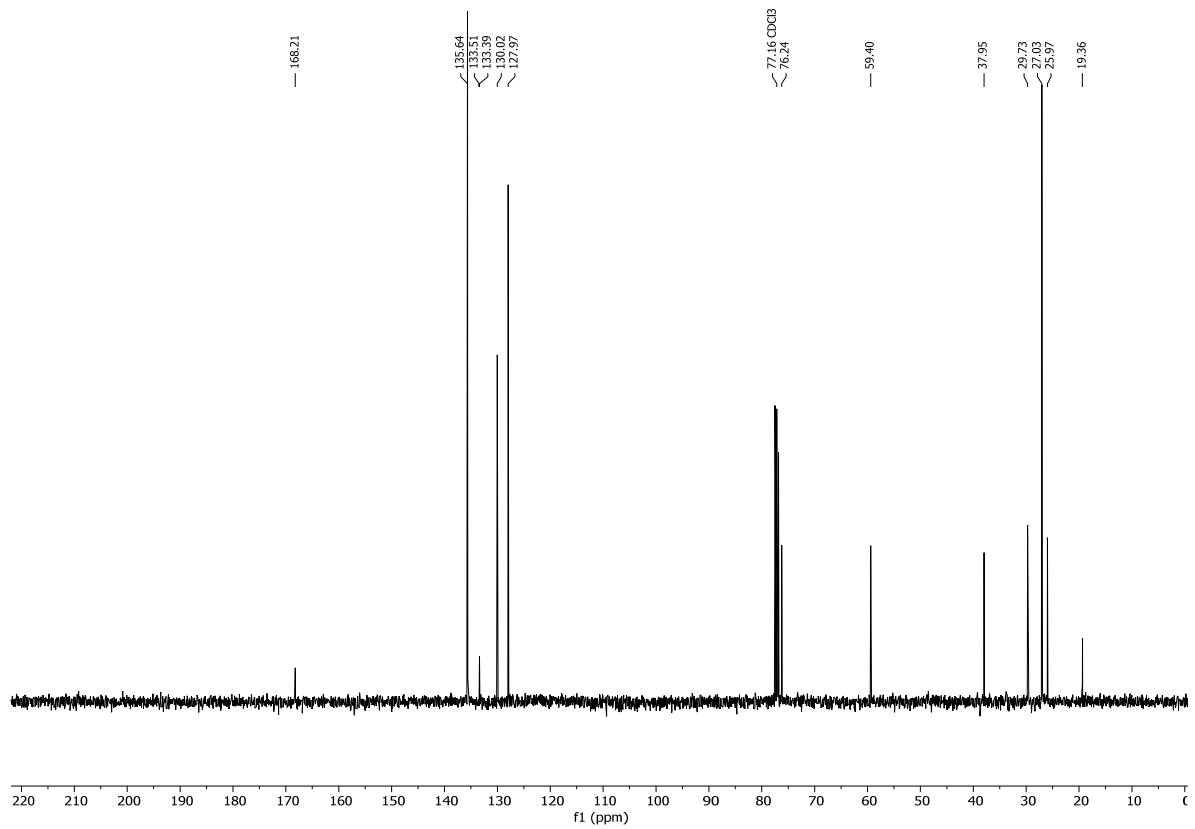
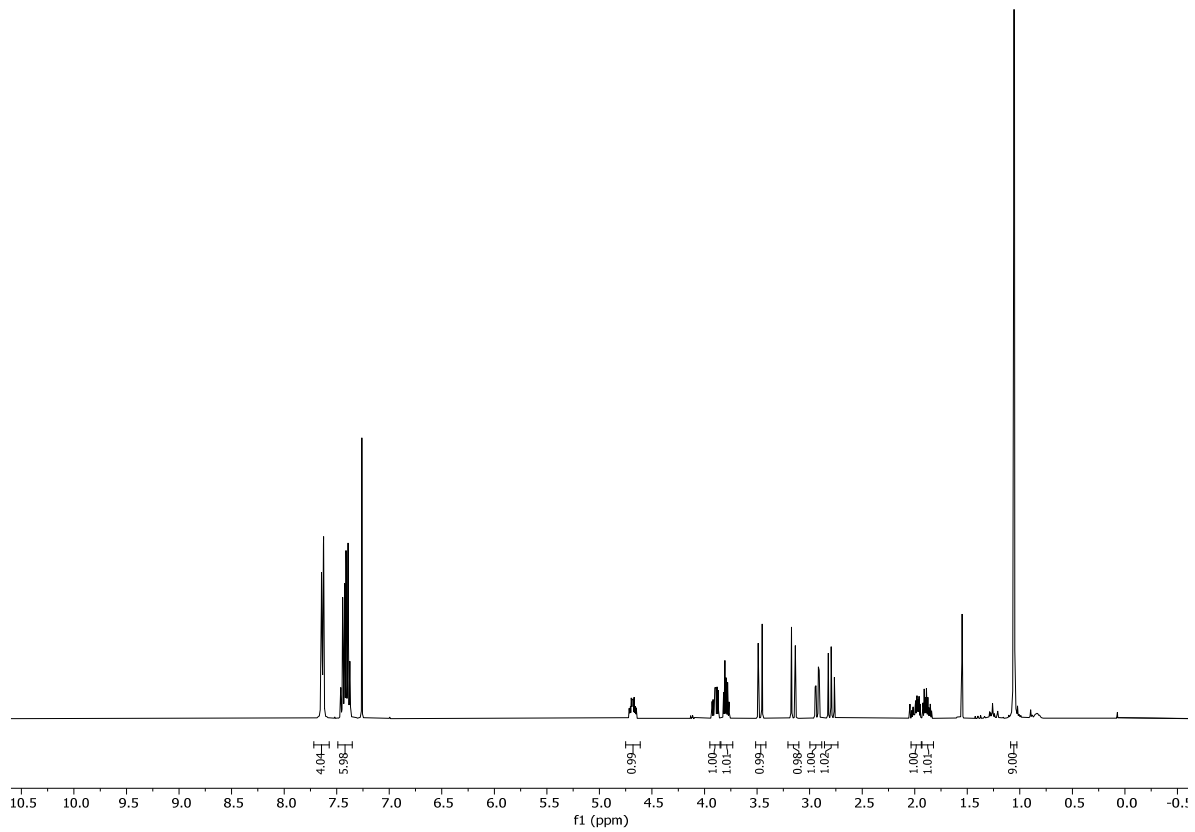
| Entry | Scale | Conditions ^[a] | Yield of O27 ^[b] | Remarks |
|-------|-----------|--|------------------------------------|--|
| 1 | 120 mg | Et₃N (2.5 eq.), O24 (2.0 eq.), toluene, 18 h, reflux | 15% | 70% of O23 reisolated ^[c] |
| 2 | 250 mg | Et₃N (2.5 eq.), O24 (2.0 eq.), toluene, 60 h, reflux | 33% | 53% of O23 reisolated ^[c] |
| 3 | 120 mg | i.) NaH (1.2 eq.), O24 (1.0 eq.), THF, 1 h, 0 °C to rt ii.) O23 , THF, 24 h, rt | n.d. ^[d] | No conversion of O23 ^[e] |
| 4 | 120 mg | i.) NaH (1.2 eq.), O24 (1.0 eq.), THF, 5 min, 0 °C to rt ii.) O23 , THF, 24 h, rt to reflux | n.d. ^[d] | No conversion of O23 ^[e] |
| 5 | 150 mg | i.) NaOEt (1.1 eq.), O24 (1.0 eq.), EtOH, 5 min, rt ii.) O23 , EtOH, 16 h, rt | 0% | Decomposition ^[f] |
| 6 | 100 mg | BF₃•OEt₂ (0.4 eq.), O24 (4.0 eq.), CH ₂ Cl ₂ , 18 h, rt | 0% | 91% TBDPS-OH isolated |
| 7 | 100 mg | i.) <i>t</i> -BuLi (1.1 eq.), BF₃•OEt₂ (1.0 eq.), O24 (1.1 eq.), THF, 10 min, –78 °C ii.) O23 , THF, 35 min, –78 °C | 85% | |
| 8 | 720 mg | i.) <i>t</i> -BuLi (1.1 eq.), BF₃•OEt₂ (1.0 eq.), O24 (1.1 eq.), THF, 10 min, –78 °C ii.) O23 , THF, 6 h, –78 to –10 °C | 71% | |
| 9 | 100 mg | i.) DBU (1.5 eq.), BF₃•OEt₂ (1.5 eq.), O24 (1.2 eq.), THF, 10 min, –65 °C ii.) O23 , THF, 30 min, –65 °C | 84% | |
| 10 | 12'000 mg | i.) DBU (1.5 eq.), BF₃•OEt₂ (1.5 eq.), O24 (1.2 eq.), THF, 10 min, –65 °C ii.) O23 , THF, 30 min, –65 °C | 80% | |

^[a]For all reactions (except for entries 1, 2 and 6) **O24** was pretreated with base under the conditions given in "i.", before **O23** (1.0 eq.) was added under the conditions given in "ii." ^[b]Isolated yield after flash column chromatography. ^[c]Material isolated as a mixture with **O24** and **O26**. ^[d]n.d. = not determined, no purification was conducted, no yield was calculated. ^[e]¹H-NMR spectroscopic analysis of the crude mixture after aqu. workup indicated no conversion of **O23**. ^[f]Reaction monitoring by TLC indicated formation of **O27** and decomposition may have occurred upon aqu. workup.

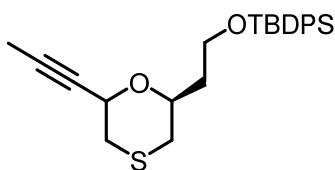
**O25**

(S)-6-(2-((tert-butyldiphenylsilyl)oxy)ethyl)-1,4-oxathian-2-one (O25). A solution of **O27** (0.550 g, 1.24 mmol, 1.00 equiv.), *p*-TsOH•H₂O (36.0 mg, 0.19 mmol, 0.15 equiv.) and 4Å molecular sieves (150 mg) in toluene (110 ml) was heated under reflux over 16 h. Then, more *p*-TsOH•H₂O (36.0 mg, 0.19 mmol, 0.15 equiv.) was added and the mixture was heated under reflux for 3 h, after which again *p*-TsOH•H₂O (36.0 mg, 0.19 mmol, 0.15 equiv.) was added and the mixture was heated under reflux. After additional 18 h, the reaction mixture was filtered, and the solvent was removed under reduced pressure. To the residue was added sat. aqu. NaHCO₃ solution (30 ml) and EtOAc (30 ml), the two phases were separated, and the aqueous phase was extracted with EtOAc (3 x 40 ml). The combined organic phases were dried over anhydrous MgSO₄ and concentrated under reduced pressure. The residue was purified by flash column chromatography (EtOAc/hexane 1:8 → 1:3) to afford **O25** (0.454 mg, 1.13 mmol, 91%) as a colorless oil.

TLC: R_f = 0.54 (EtOAc/hexane 1:3). **¹H-NMR** (400 MHz, CDCl₃) δ = 7.72 – 7.57 (m, 4H), 7.49 – 7.35 (m, 6H), 4.75 – 4.61 (m, 1H), 3.95 – 3.85 (m, 1H), 3.84 – 3.73 (m, 1H), 3.47 (d, *J* = 14.7 Hz, 1H), 3.15 (d, *J* = 0.7 Hz, 1H), 2.93 (dd, *J* = 12.3, 0.7 Hz, 1H), 2.79 (dd, *J* = 12.2, 11.3 Hz, 1H), 2.03 – 1.94 (m, 1H), 1.93 – 1.82 (m, 1H), 1.06 (s, 9H). **¹³C-NMR** (101 MHz, CDCl₃) δ = 168.2, 135.6, 133.5, 133.4, 130.0, 128.0, 76.2, 59.4, 38.0, 29.7, 27.0, 26.0, 19.4. **IR** (film) $\tilde{\nu}$ = 3070, 2957, 2930, 2886, 2857, 1471, 1427, 1391, 1362, 1255, 1206, 1022, 1000, 954, 822, 738, 689, 614, 505. **HRMS** (ESI) calculated for C₂₂H₂₈NaO₃SSi [(M+Na)⁺]: 423.1421, found: 423.1419. $[\alpha]_D^{20}$ = -87.98° (1.00 g/100cm³ in CHCl₃).



4.2.2.2.3 Elaboration of O25 into O11

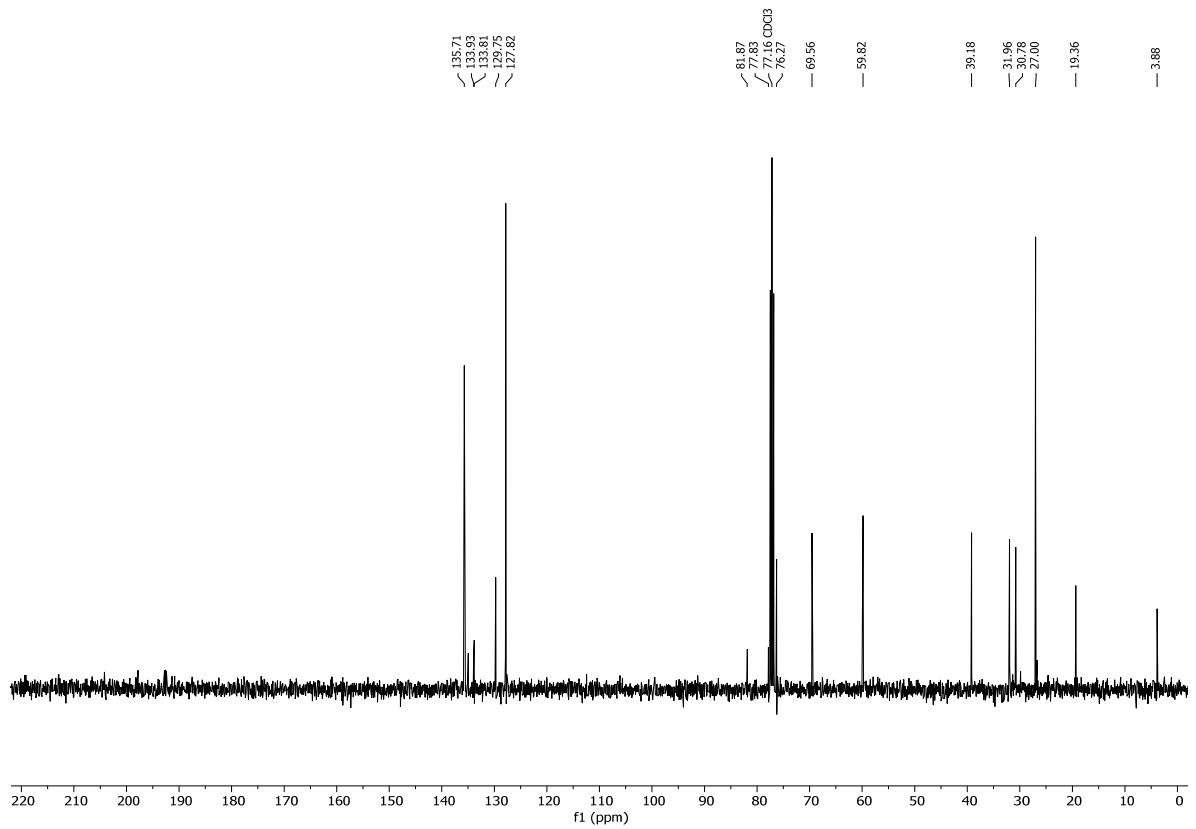
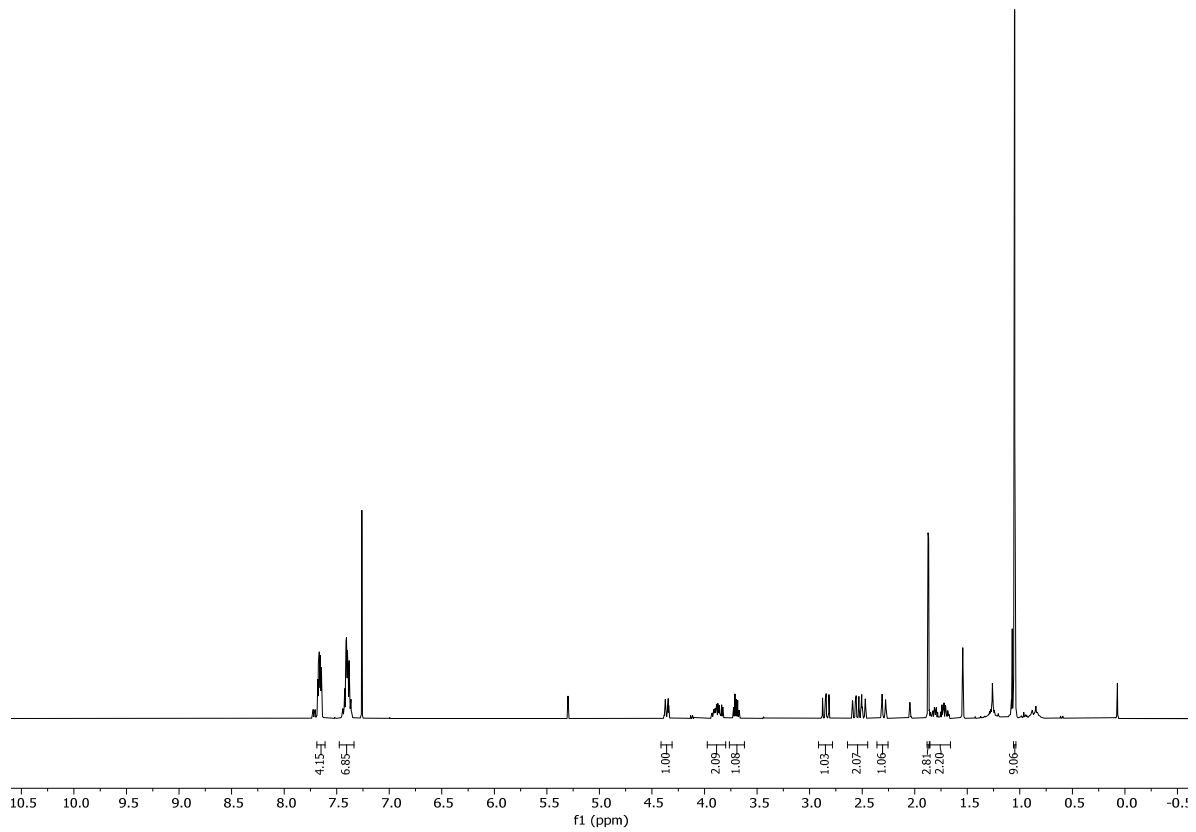


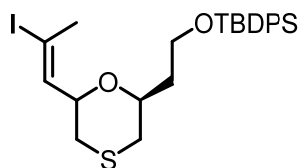
OS2

tert-butyldiphenyl(2-((2S,6R)-6-(prop-1-yn-1-yl)-1,4-oxathian-2-yl)ethoxy)silane (OS2). To a solution of *E*-bromopropene (100 μ l, 1.70 mmol, 1.50 equiv.) in THF (1.4 ml) at -78°C was added *n*-BuLi (1.1 ml, 1.6M in hexane, 10.30 mmol, 2.20 equiv.) and stirred at -78°C for 1 h. Then, **O25** (0.31 g, 0.77 mmol, 1.00 equiv.) dissolved in THF (1.4 ml) was added dropwise. After stirring at -78°C for 2.5 h, the reaction was quenched by addition of sat. aqu. NaHCO_3 solution (3.5 ml) and allowed to warm to rt. The aqueous phase was extracted with EtOAc (3 x 5 ml) and the combined organic phases were dried over anhydrous MgSO_4 , filtered and concentrated under reduced pressure. The crude mixture was used in the next step without further purification.

To a solution of the crude mixture in dry CH_2Cl_2 (5 ml), was added triethylsilane (1.7 ml, 10.44 mmol, 10.00 equiv.), followed by dropwise addition of TFA (1.2 ml, 15.66 mmol, 15.00 equiv.) at -78°C . The reaction was slowly warmed to -40°C . After 3.5 h, the reaction was quenched by addition of sat. aqu. NaHCO_3 solution (30 ml) at -40°C . After slow warming to rt, the mixture was diluted with CH_2Cl_2 (35 ml) and the aqueous phase was extracted with CH_2Cl_2 (3 x 35 ml). The combined organic phases were dried over anhydrous MgSO_4 , filtered and concentrated under reduced pressure. Purification by flash column chromatography (EtOAc/hexane 1:15 \rightarrow 1:3) afforded alkyne **OS2** (0.25 g, 0.59 mmol, 56% over two steps) as a colorless oil.

TLC: $R_f = 0.51$ (EtOAc/hexane 1:10). **$^1\text{H-NMR}$** (400 MHz, CDCl_3) $\delta = 7.69 - 7.61$ (m, 4H), 7.48 – 7.33 (m, 7H), 4.41 – 4.31 (m, 1H), 3.97 – 3.80 (m, 2H), 3.76 – 3.62 (m, 1H), 2.85 (dd, $J = 13.5, 10.8$ Hz, 1H), 2.64 – 2.45 (m, 2H), 2.36 – 2.25 (m, 1H), 1.87 (d, $J = 2.1$ Hz, 3H), 1.85 – 1.66 (m, 2H), 1.05 (s, 9H). **$^{13}\text{C-NMR}$** (101 MHz, CDCl_3) $\delta = 135.7, 133.9, 133.8, 129.8, 127.8, 81.9, 77.8, 76.3, 69.6, 59.8, 39.2, 32.0, 30.8, 27.0, 19.4, 3.9$. **IR** (film) $\tilde{\nu} = 3069, 2987, 2959, 2928, 2901, 2858, 2360, 1472, 1427, 1410, 1392, 1330, 1315, 1251, 1231, 1188, 1167, 1110, 1081, 1057, 998, 981, 952, 893, 879, 822, 738, 702, 688, 614, 504$. **HRMS** (ESI) calculated for $\text{C}_{25}\text{H}_{32}\text{NaO}_2\text{Si}$ [(M+Na) $^+$]: 447.1784, found: 447.1783. $[\alpha]_D^{20} = -77.98^\circ$ (1.00 g/100cm 3 in CHCl_3).





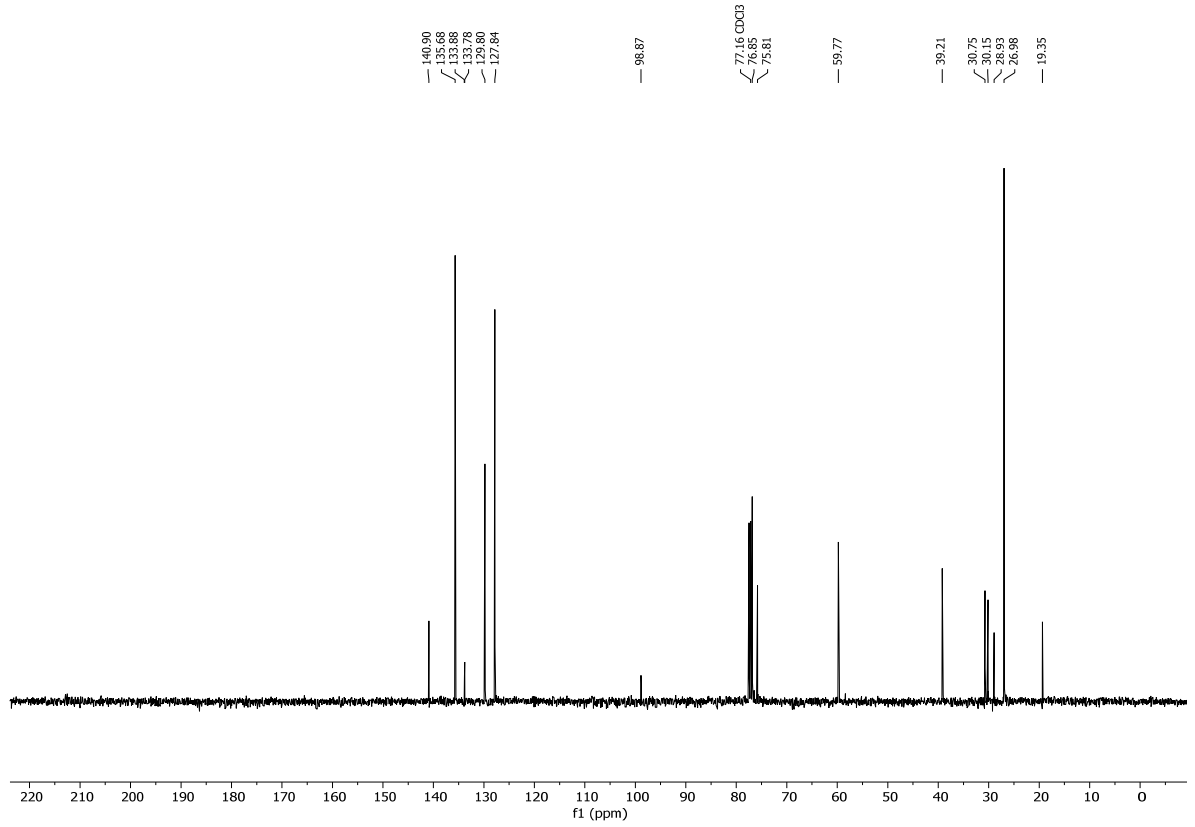
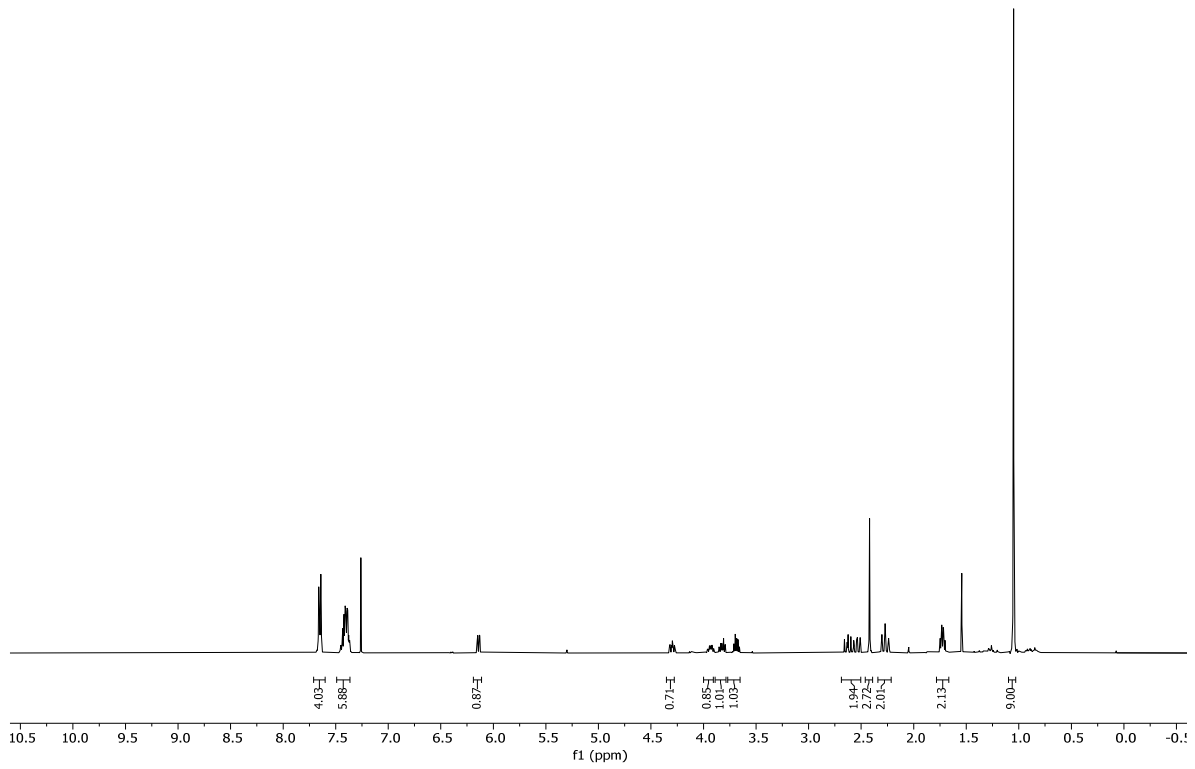
O28

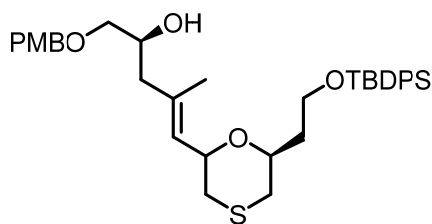
tert-butyl(2-((2S,6R)-6-((E)-2-iodoprop-1-en-1-yl)-1,4-oxathian-2-yl)ethoxy)diphenylsilane

(O28). To a suspension of CuCN (10.23 g, 114.21 mmol, 10.00 equiv.) in THF (140 ml) at $-78\text{ }^{\circ}\text{C}$ was added a solution of *n*-BuLi (142.8 ml, 1.6M in hexane, 228.41 mmol, 20.00 equiv.). After 5 min, the flask was immersed in a cooling bath at $-40\text{ }^{\circ}\text{C}$, resulting in the formation of a pale-yellow, almost clear solution. The mixture was cooled back to $-78\text{ }^{\circ}\text{C}$ after 10 min, which made it become slightly heterogeneous. Neat Bu₃SnH (61.4 mL, 228.41 mmol, 20.00 equiv.) was then added dropwise, immediately leading to a turbid yellow solution. After 20 min at $-78\text{ }^{\circ}\text{C}$, the mixture was stirred for 5 min at $-40\text{ }^{\circ}\text{C}$, giving an almost clear golden-yellow solution. After 10 min at $-40\text{ }^{\circ}\text{C}$, the solution was cooled back to $-78\text{ }^{\circ}\text{C}$ followed by addition of methanol (101.9 ml, 2512.54 mmol, 220.00 equiv.) under vigorous stirring. After 10 min at $-78\text{ }^{\circ}\text{C}$ the flask was immersed in a cooling bath at $-40\text{ }^{\circ}\text{C}$ giving a clear red solution. After 10 min at $-40\text{ }^{\circ}\text{C}$, the solution was cooled back to $-78\text{ }^{\circ}\text{C}$ and alkyne **OS2** (4.85 g, 11.42 mmol, 1.00 equiv.) dissolved in THF (114 ml) was added. The mixture was then stirred over 16 h during which the temperature was allowed to rise to $-15\text{ }^{\circ}\text{C}$. The reaction was quenched by addition of sat. aq. NH₄Cl (800 ml) and 25% aqueous NH₄OH solution (200 ml), added together with EtOAc (800 ml). Stirring was continued for 30 min, the two phases were separated, and the aqueous phase was extracted with EtOAc (3 x 500 ml). The combined organic phases were dried over anhydrous MgSO₄ and concentrated under reduced pressure. Purification of the residue by flash chromatography on deactivated silica (hexane and 1% (v/v) Et₃N) afforded the (*E*)-vinylstannane as a colorless oil which was used in the next step immediately.

A solution of the above vinylstannane in THF (80 ml) was cooled to $-17\text{ }^{\circ}\text{C}$ followed by addition of NIS (3.85 g, 17.13 mmol, 1.50 equiv.) dissolved in THF (15 ml), to give an almost clear yellow solution. After 20 min, a mixture of sat. aqu. Na₂S₂O₃ (150 ml) and sat. aqu. NaHCO₃ (150 ml) was added followed by EtOAc (300 ml). Stirring was continued for 2 min until two clear phases were formed. The phases were separated and the aqueous phase was extracted with EtOAc (3 x 300ml). The combined organic phases were dried over anhydrous MgSO₄ and concentrated under reduced pressure. The residue was purified by flash chromatography (EtOAc/hexane 1:75) to afford vinyl iodide **O28** (5.83 g, 10.55 mmol, 92 % over two steps) as a pale yellow oil.

TLC: $R_f = 0.14$ (EtOAc/hexane 1:20). **$^1\text{H-NMR}$** (400 MHz, CDCl_3) $\delta = 7.70 - 7.60$ (m, 4H), 7.47 – 7.34 (m, 6H), 6.14 (dq, $J = 7.8, 1.4$ Hz, 1H), 4.30 (ddd, $J = 10.3, 7.8, 2.0$ Hz, 1H), 3.99 – 3.86 (m, 1H), 3.88 – 3.77 (m, 1H), 3.74 – 3.64 (m, 1H), 2.68 – 2.48 (m, 2H), 2.42 (d, $J = 1.5$ Hz, 3H), 2.33 – 2.20 (m, 1H), 1.78 – 1.68 (m, 2H), 1.05 (s, 9H). **$^{13}\text{C-NMR}$** (101 MHz, CDCl_3) $\delta = 140.9, 135.7, 133.9, 133.8, 129.8, 127.8, 98.9, 76.9, 75.8, 59.8, 39.2, 30.7, 30.1, 28.9, 27.0, 19.3$. **IR** (film) $\tilde{\nu} = 2987, 2972, 2901, 1472, 1452, 1426, 1407, 1393, 1382, 1251, 1242, 1229, 1076, 1066, 1056, 893, 880, 870, 702$. **HRMS** (ESI) calculated for $\text{C}_{25}\text{H}_{33}\text{INaO}_2\text{SSi}$ $[(\text{M}+\text{Na})^+]$: 575.0907, found: 575.0902. $[\alpha]_D^{20} = -22.00^\circ$ (1.00 g/100cm³ in CHCl_3).

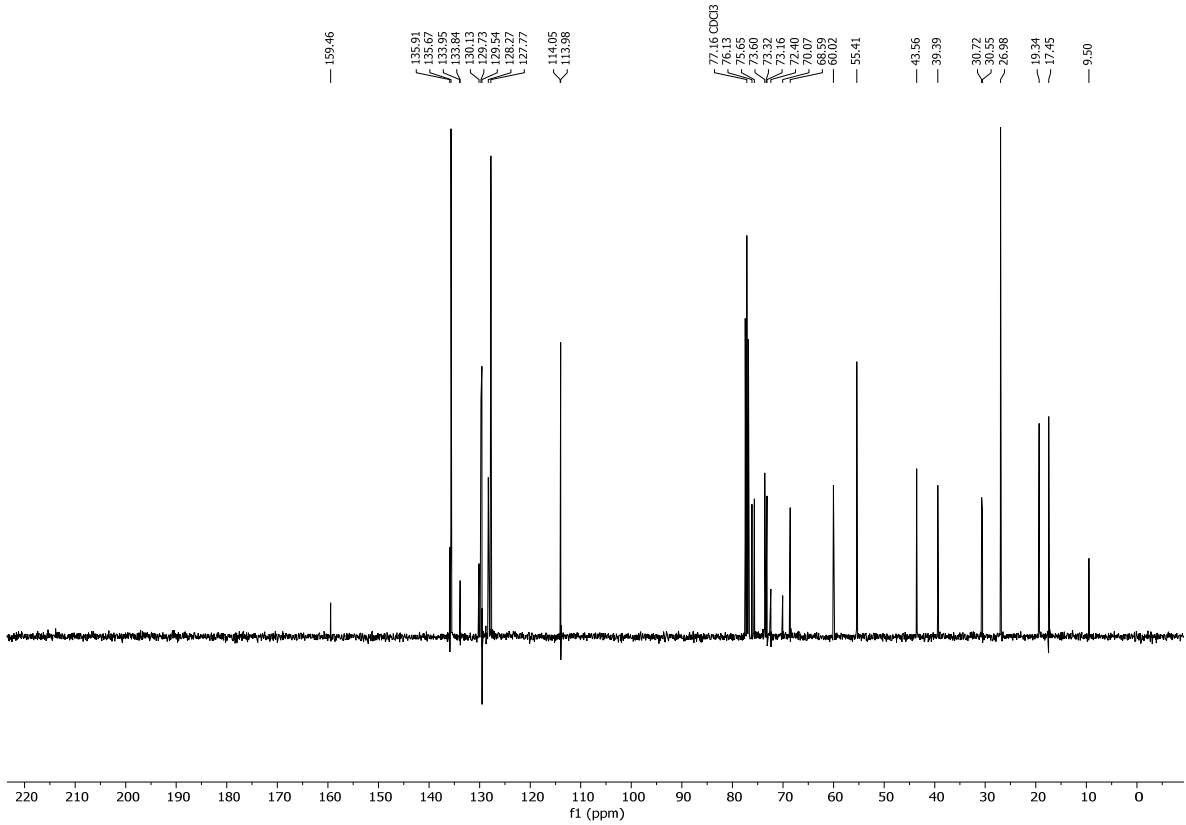
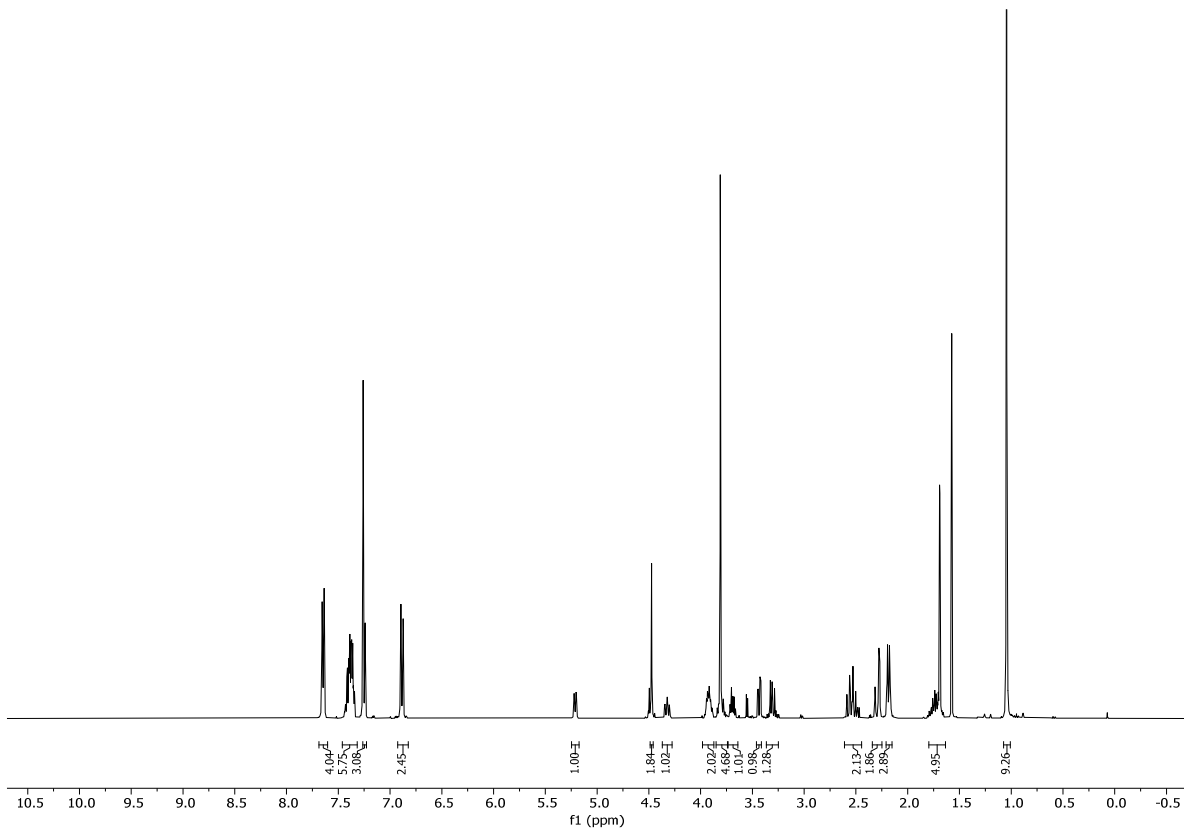


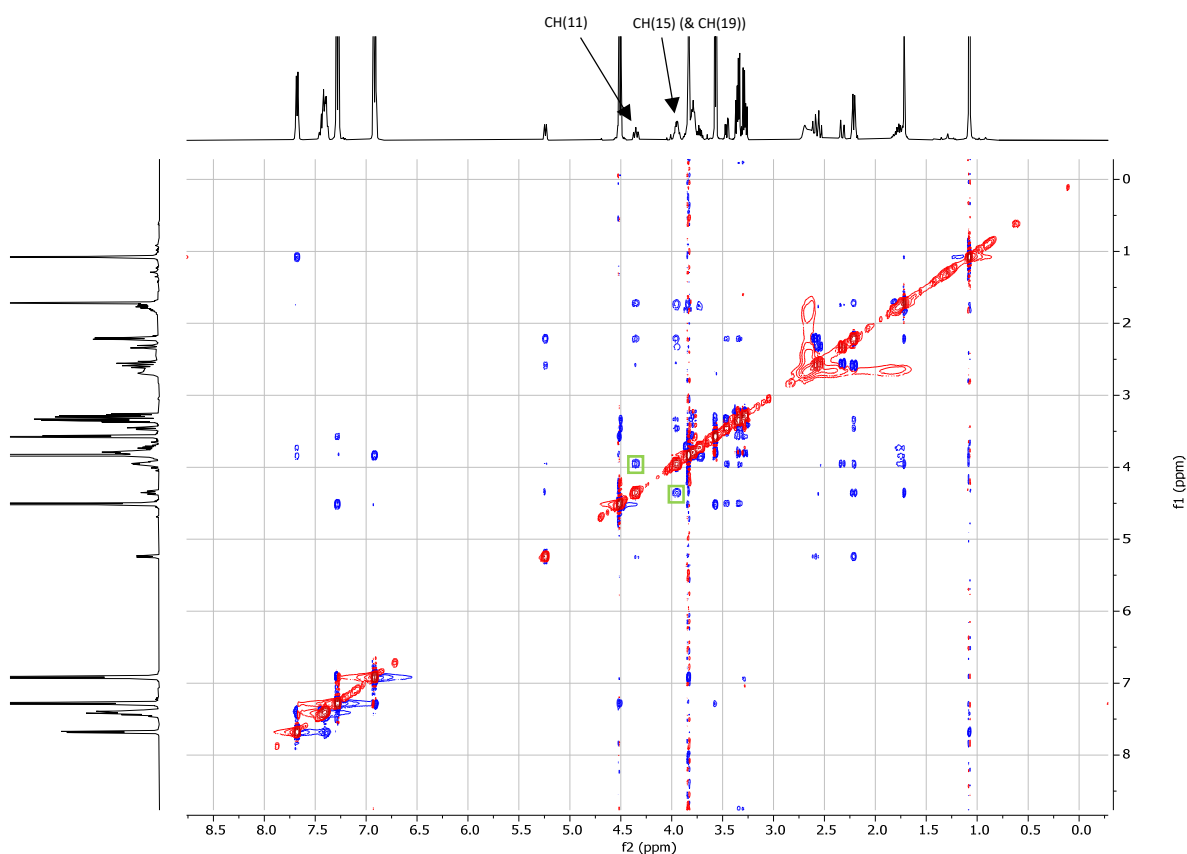


O11

(2*S*,*E*)-5-((6*S*)-6-(2-((*tert*-butyldiphenylsilyl)oxy)ethyl)-1,4-oxathian-2-yl)-1-((4-methoxybenzyl)oxy)-4-methylpent-4-en-2-ol (O11). Vinyl iodide **O28** (3.25 g, 5.88 mmol, 1.00 equiv., azeotropically dried once with 15 ml of toluene right before use) was dissolved in dry toluene (60 ml) and the solution was cooled to -78 °C. *t*-BuLi (1.7 M in pentane, 5.9 ml, 10.00 mmol, 1.70 equiv.) was then added and the near colorless solution was stirred for 20 min at -45 °C; it was then cooled back to -78 and Li(2-th)CuCN (0.25M solution in THF, 25.9 ml, 6.47 mmol, 1.10 equiv.) was added. Stirring at -45 °C was then continued for 30 min, before a solution of **O21**^[49] (1.71 g, 8.82 mmol, 1.50 equiv., azeotropically dried once with 4 ml of toluene right before use) in dry toluene (12 ml) was added. The reaction mixture was allowed to warm up to 0 °C over 45 min and stirring was continued at that temperature for 1 h. Afterwards the cooling bath was removed and sat. aqu. NaHCO₃ (150 ml) and EtOAc (250 ml) were added. After the mixture had reached rt, the phases were separated and the aqueous phase was extracted with EtOAc (3 x 250 ml). The combined organic extracts were dried over MgSO₄, concentrated under reduced pressure, and the residue purified by flash chromatography (EtOAc/hexane 1:3) to give **O11** (2.31g, 3.71 mmol, 63%) as a colorless oil.

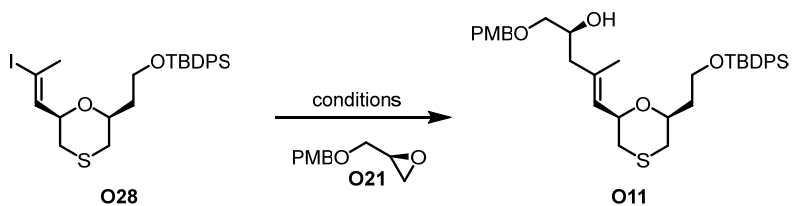
TLC: *R*_f = 0.75 (EtOAc/hexane 1:1). **¹H-NMR** (400 MHz, CDCl₃) δ = 7.65 (dq, *J* = 6.4, 1.4 Hz, 4H), 7.38 (ddtd, *J* = 15.8, 8.4, 4.3, 1.6 Hz, 6H), 7.25 (d, *J* = 8.0 Hz, 3H), 6.93 – 6.82 (m, 2H), 5.21 (dq, *J* = 7.6, 1.3 Hz, 1H), 4.47 (s, 2H), 4.32 (ddd, *J* = 10.2, 7.7, 2.1 Hz, 1H), 3.92 (dtd, *J* = 10.7, 5.5, 3.1 Hz, 2H), 3.81 (d, *J* = 1.3 Hz, 5H), 3.69 (dt, *J* = 10.5, 5.5 Hz, 1H), 3.43 (dd, *J* = 9.5, 3.4 Hz, 1H), 3.37 – 3.25 (m, 1H), 2.61 – 2.45 (m, 2H), 2.34 – 2.25 (m, 2H), 2.21 – 2.15 (m, 3H), 1.80 – 1.64 (m, 5H), 1.04 (s, 9H). **¹³C-NMR** (101 MHz, CDCl₃) δ = 159.5, 135.9, 135.7, 134.0, 133.8, 130.1, 129.7, 129.5, 128.3, 127.8, 114.1, 114.0, 76.1, 75.7, 73.6, 73.3, 73.16, 7.4, 70.1, 68.6, 60.0, 55.4, 43.6, 39.4, 30.7, 30.6, 27.0, 19.3, 17.5, 9.5. **IR** (film) $\tilde{\nu}$ = 3439, 3070, 2930, 2856, 1612, 1587, 1513, 1463, 1427, 1389, 1361, 1303, 1478, 1209, 1174, 1154, 1111, 1092, 1035, 997, 948, 822, 741, 703, 688, 613, 505. **HRMS** (ESI) calculated for C₃₆H₄₈NaO₅SSi [(M+Na)⁺]: 643.2884, found: 643.2877. $[\alpha]_D^{20}$ = -4.00° (1.00 g/100cm³ in CHCl₃).





NOE-experiment showing the cross-peaks of CH(11) (4.32 (ddd, $J = 10.2, 7.7, 2.1$ Hz, 1H) and CH(15) (3.92 (dtd, $J = 10.7, 5.5, 3.1$ Hz, 2H, containing also CH(19))).

Table 22. Conditions investigated for the opening of epoxide **O21** with vinyl iodide **O28**.

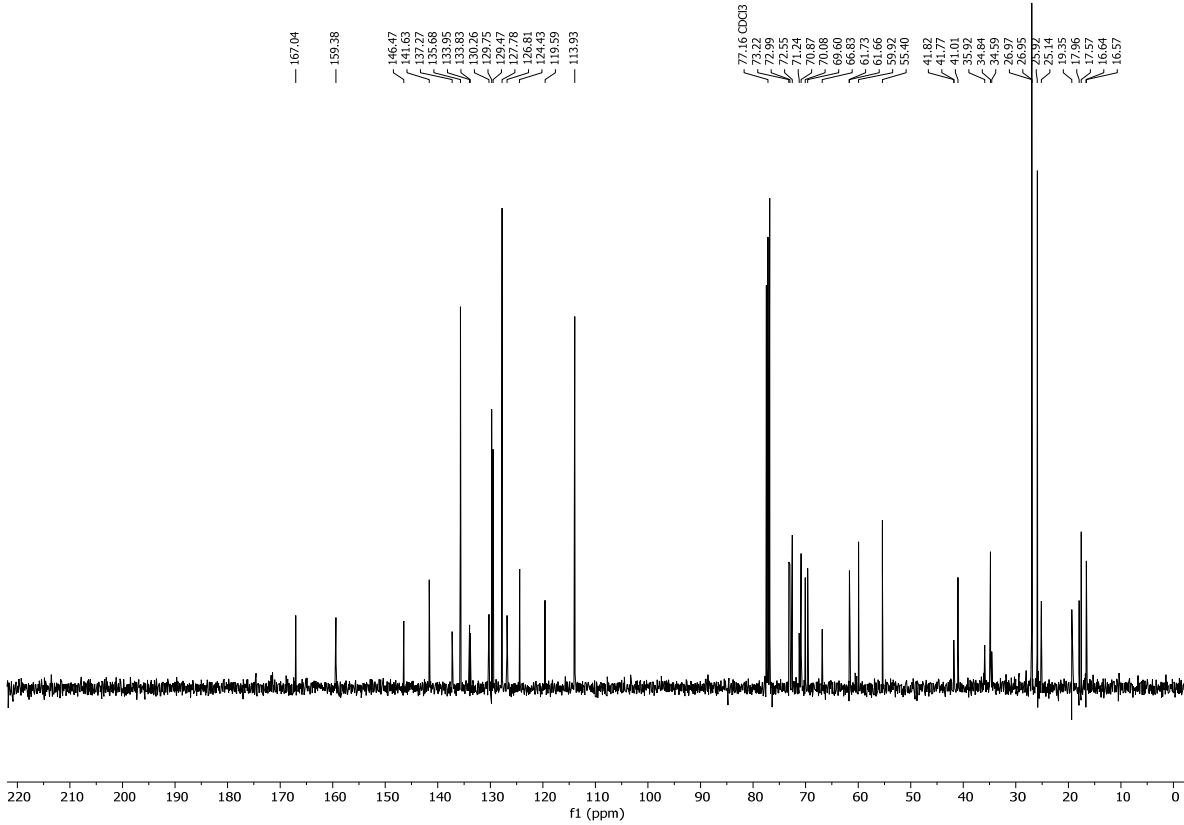
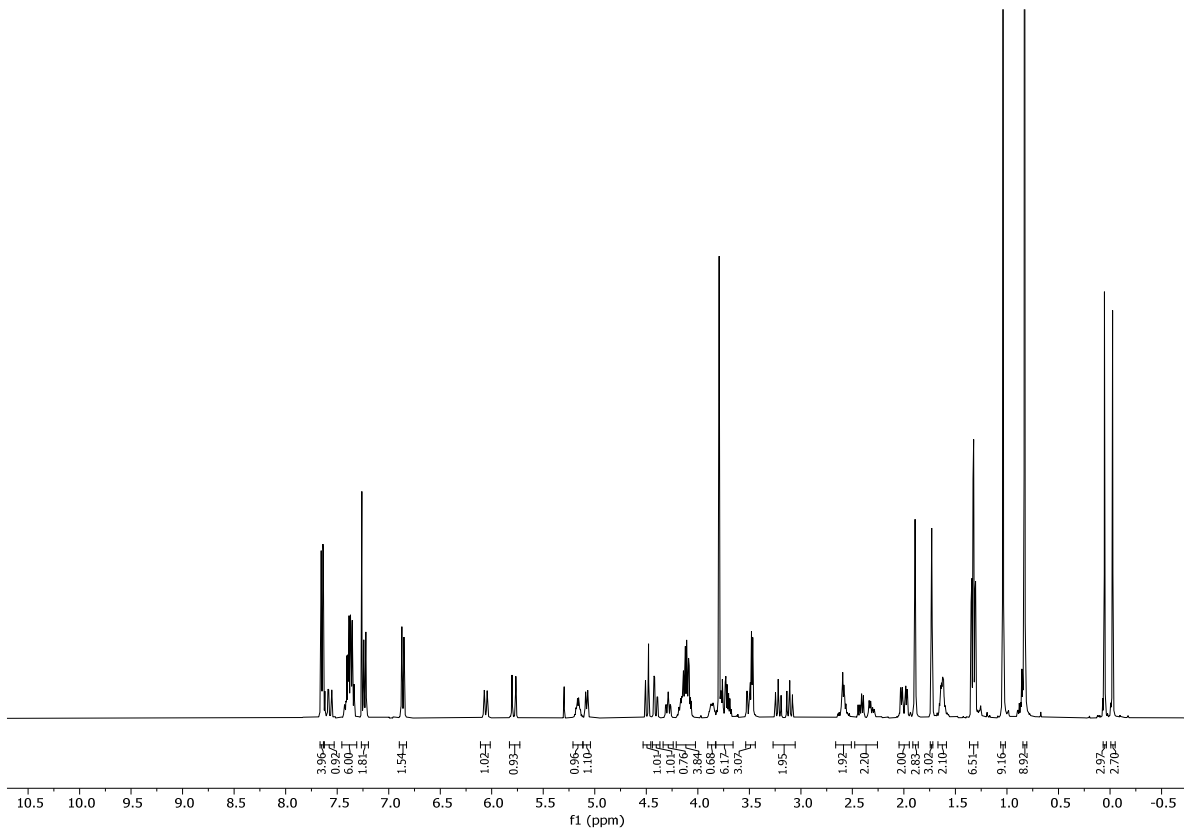


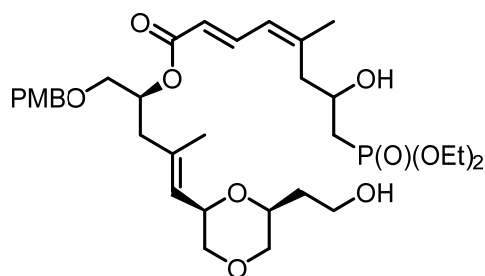
| Entry | Scale | Conditions ^[a] | Yield of O11 ^[b] |
|-------|--------|--|------------------------------------|
| 1 | 138 mg | i.) <i>n</i> -BuLi (1.1 eq.), BF ₃ •OEt ₂ (2.5 eq.), toluene, -78 °C, 1 h ii.) O21 (2.5 eq.), -100 to -78 °C, 3 h | traces |
| 2 | 50 mg | i.) <i>n</i> -BuLi (1.1 eq.), BF ₃ •OEt ₂ (2.5 eq.), toluene, -78 °C, 1 h ii.) O21 (1.2 eq.), -90 to -78 °C, 1 h | traces |
| 3 | 77 mg | i.) <i>n</i> -BuLi (1.1 eq.), BF ₃ •OEt ₂ (2.5 eq.), toluene, -78 °C, 1 h ii.) CuCN (1.5 eq.), -60 to -40 °C, 30 min iii.) O21 (2.5 eq.) toluene, -78 to -40 °C, 18 h | traces |

| | | | |
|----|---------|---|-----|
| 4 | 50 mg | i.) <i>t</i> -BuLi (2.0 eq.), BF ₃ •OEt ₂ (2.5 eq.), toluene, -78 °C, 30 min ii.) O21 (2.5 eq.), -90 to -78 °C, 4 h | 18% |
| 5 | 500 mg | i.) <i>t</i> -BuLi (2.0 eq.), BF ₃ •OEt ₂ (2.5 eq.), toluene, -78 °C, 30 min ii.) O21 (2.5 eq.), -90 to -78 °C, 4 h | 13% |
| 6 | 100 mg | i.) <i>t</i> -BuLi (2.5 eq.), BF ₃ •OEt ₂ (3.5 eq.), toluene, -78 °C, 30 min ii.) O21 (3.5 eq.), -90 to -78 °C, 4 h | 11% |
| 7 | 50 mg | i.) <i>t</i> -BuLi (2.0 eq.), BF ₃ •OEt ₂ (2.5 eq.), THF, -78 °C, 30 min ii.) O21 (2.5 eq.), -90 to -78 °C, 4 h | - |
| 8 | 50 mg | i.) <i>t</i> -BuLi (2.0 eq.), BF ₃ •OEt ₂ (2.5 eq.), Et ₂ O, -78 °C, 30 min ii.) O21 (2.5 eq.), -90 to -78 °C, 4 h | - |
| 9 | 50 mg | i.) <i>t</i> -BuLi (1.6 eq.), BF ₃ •OEt ₂ (1.6 eq.), toluene, -78 °C, 30 min ii.) O21 (1.6 eq.), -90 to -78 °C, 8 h | 12% |
| 10 | 50 mg | i.) <i>t</i> -BuLi (1.6 eq.), BF ₃ •OEt ₂ (1.6 eq.), toluene, -78 °C, 30 min ii.) O21 (1.6 eq.), -90 to -40 °C, 5 h | 30% |
| 11 | 50 mg | i.) <i>t</i> -BuLi (1.6 eq.), BF ₃ •OEt ₂ (1.6 eq.), toluene, -78 °C, 30 min ii.) O21 (1.6 eq.), -90 to -10 °C, 4 h | 7% |
| 12 | 500 mg | i.) <i>t</i> -BuLi (1.6 eq.), BF ₃ •OEt ₂ (1.6 eq.), toluene, -78 °C, 30 min ii.) O21 (1.6 eq.), -40 °C, 2 h | 28% |
| 13 | 50 mg | i.) <i>t</i> -BuLi (1.7 eq.), toluene, -78 to -45 °C, 20 min ii.) Li(2-th)CuCN (0.07 eq.), -78 to -45 °C, 30 min iii.) O21 (1.5 eq.), -78 to 0 °C, 3 h | 47% |
| 14 | 1000 mg | i.) <i>t</i> -BuLi (1.7 eq.), -78 to -45 °C, 20 min ii.) Li(2-th)CuCN (1.1 eq.), -78 to -45 °C, 30 min iii.) O21 (1.5 eq.), -78 to 0 °C, 3 h | 59% |
| 15 | 3250 mg | i.) <i>t</i> -BuLi (1.7 eq.), -78 to -45 °C, 20 min ii.) Li(2-th)CuCN (1.1 eq.), -78 to -45 °C, 30 min iii.) O21 (1.5 eq.), -78 to 0 °C, 3 h | 63% |

^[a]For all reactions **O28** was pretreated with base under the conditions given in "i.", before **O21** was added under the conditions given in "ii.". For entries 3 and 13-15, additional treatment with conditions given in "ii" preceded addition of **O21** under conditions given in "iii."; ^[b]Isolated yield after flash column chromatography. "-" refers to unidentifiable product(s).

59.9, 55.4, 41.8, 41.8, 41.0, 35.9, 34.8, 34.6, 27.0, 27.0, 25.9, 25.1, 19.4, 18.0, 17.6, 16.6, 16.6, -4.6, -4.7. **IR** (film) $\tilde{\nu}$ = 2954, 2930, 2903, 2857, 1772, 1762, 1712, 1685, 1669, 1640, 1631, 1616, 1569, 1555, 1540, 1530, 1514, 1488, 1473, 1464, 1444, 1429, 1388, 1363, 1304, 1250, 1146, 1111, 1072, 1049, 1028, 960, 935, 824, 810, 775, 741, 705. **HRMS** (ESI) calculated for $C_{55}H_{83}NaO_{11}PSi_2$ [(M+Na)⁺]: 1029.5104, found: 1029.5087.

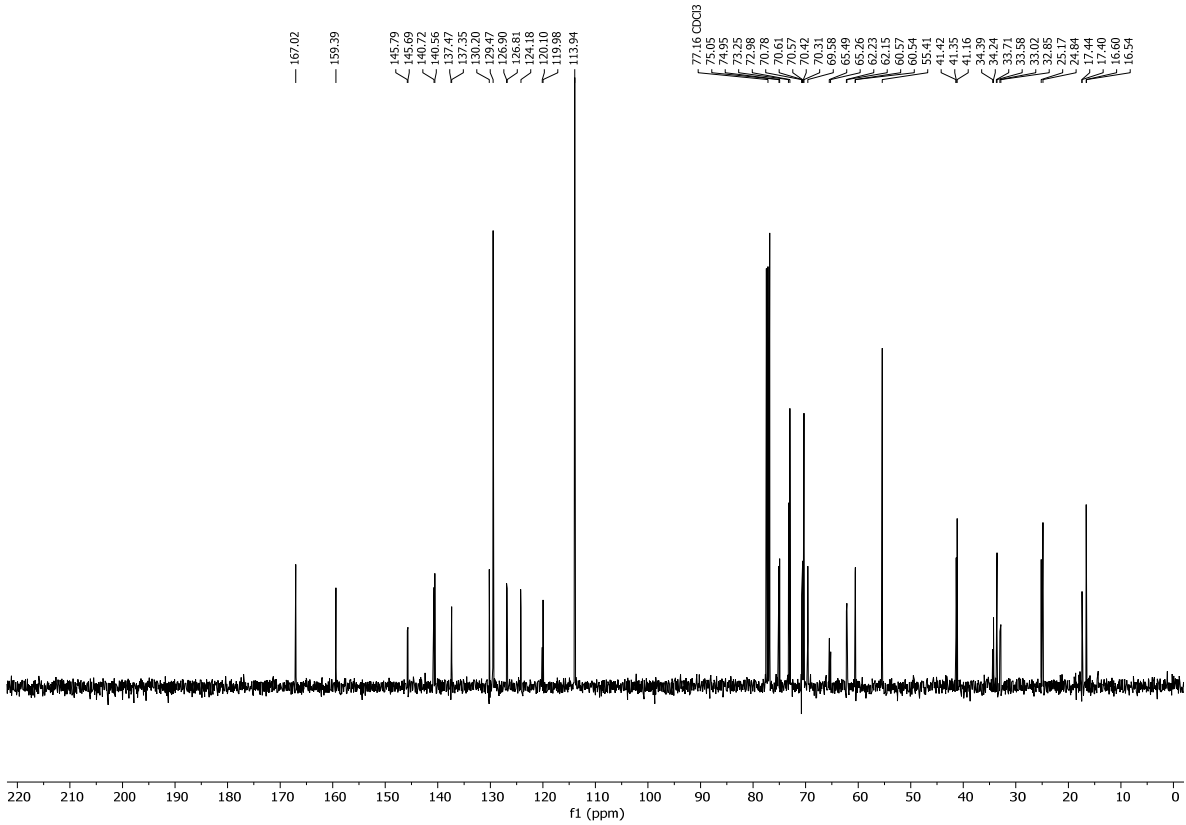
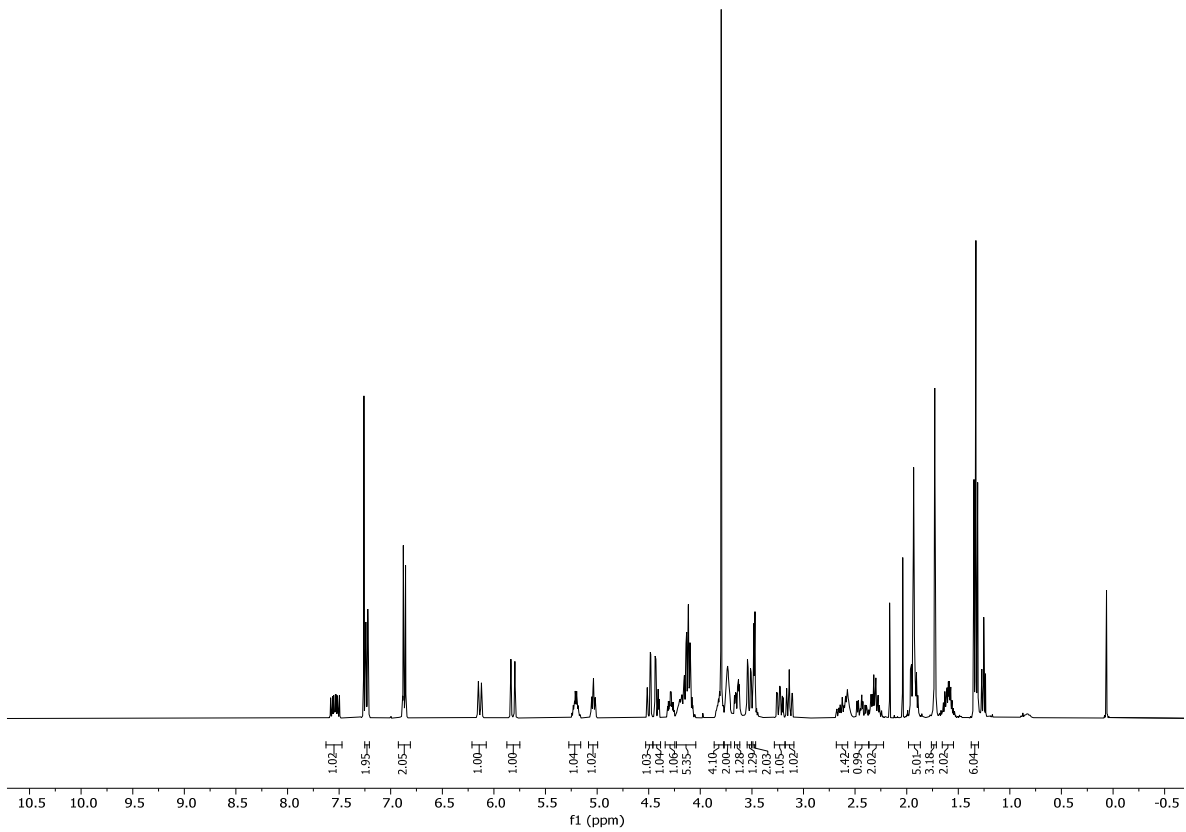


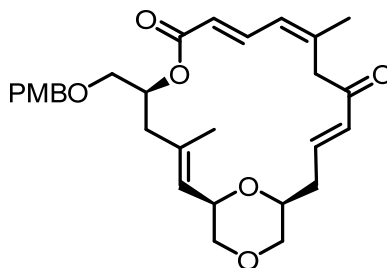


O29

(*S,E*)-5-((*2R,6S*)-6-(2-hydroxyethyl)-1,4-dioxan-2-yl)-1-((4-methoxybenzyl)oxy)-4-methylpent-4-en-2-yl (2*E,4Z*)-8-(diethoxyphosphoryl)-7-hydroxy-5-methylocta-2,4-dienoate (O29). To a solution of **OS3** (0.50 g, 0.50 mmol, 1.00 equiv.) in THF (15 ml) in a plastic tube was carefully added 70% HF•pyridine (3.2 ml) at 0 °C. The cooling bath was removed after 5 min and stirring was continued at rt for 16 h. The solution was then carefully added to a vigorously stirred mixture of sat. aq. NaHCO₃ (195 ml) and EtOAc (160 ml) until two clear phases had formed (ca. 15 min). The phases were separated and the aqueous phase was extracted with EtOAc (3 x 35 ml). The combined organic phases were washed with sat. aq. NaHCO₃ solution (64 ml) and dried over anhydrous MgSO₄. Concentration under reduced pressure and purification using flash column chromatography (EtOAc/acetone 1:0 → 3:1) afforded diol **O29** (0.26 g, 0.39 mmol, 78%) as a slightly yellow oil.

TLC: R_f = 0.19 (EtOAc/acetone 2:1). **¹H-NMR** (400 MHz, CDCl₃) δ = 7.63 – 7.47 (m, 1H), 7.23 (d, 2H), 6.87 (d, *J* = 8.7 Hz, 2H), 6.14 (d, *J* = 11.7 Hz, 1H), 5.82 (d, *J* = 1.0 Hz, 1H), 5.27 – 5.16 (m, 1H), 5.08 – 4.99 (m, 1H), 4.50 (dd, 1H), 4.42 (dd, 1H), 4.34 – 4.25 (m, 1H), 4.23 – 4.04 (m, 5H), 3.87 – 3.77 (m, 4H), 3.77 – 3.70 (m, 2H), 3.65 (ddd, *J* = 11.4, 4.3, 2.5 Hz, 1H), 3.52 (dd, *J* = 11.6, 2.8 Hz, 1H), 3.49 – 3.46 (m, 2H), 3.28 – 3.18 (m, 1H), 3.18 – 3.09 (m, 1H), 2.68 – 2.57 (m, 1H), 2.50 – 2.37 (m, 1H), 2.37 – 2.22 (m, 2H), 1.98 – 1.87 (m, 5H), 1.73 (t, *J* = 1.5 Hz, 3H), 1.66 – 1.55 (m, 2H), 1.33 (td, *J* = 7.0, 1.8 Hz, 6H). **¹³C-NMR** (101 MHz, CDCl₃) δ = 167.0, 159.4, 145.8, 145.7, 140.7, 140.6, 137.5, 137.35, 130.2, 129.5, 126.9, 126.8, 124.2, 120.1, 120.0, 113.9, 75.1, 75.0, 73.3, 73.0, 70.8, 70.6, 70.6, 70.4, 70.3, 69.6, 65.5, 65.3, 62.2, 62.2, 60.6, 60.5, 55.4, 41.4, 41.4, 41.2, 34.4, 34.2, 33.7, 33.6, 33.0, 32.9, 25.2, 24.8, 17.4, 17.4, 16.6, 16.5. **IR** (film) $\tilde{\nu}$ = 3383, 2956, 2908, 1761, 1710, 1687, 1670, 1631, 1612, 1569, 1555, 1514, 1488, 1474, 1464, 1444, 1431, 1420, 1387, 1366, 1303, 1276, 1248, 1223, 1148, 1122, 1100, 1049, 1028, 975, 903, 820, 770. **HRMS** (ESI) calculated for C₃₃H₅₁NaO₁₁P [(M+Na)⁺]: 677.3061, found: 677.3062.



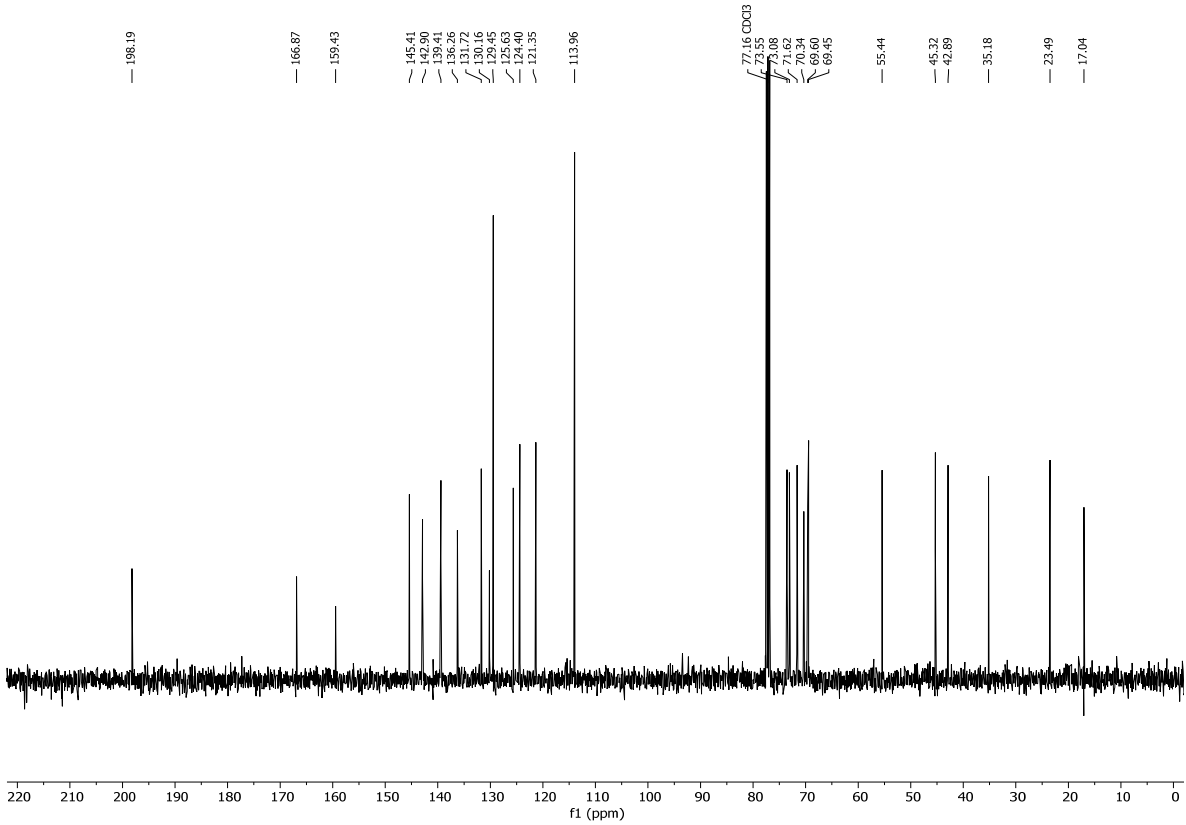
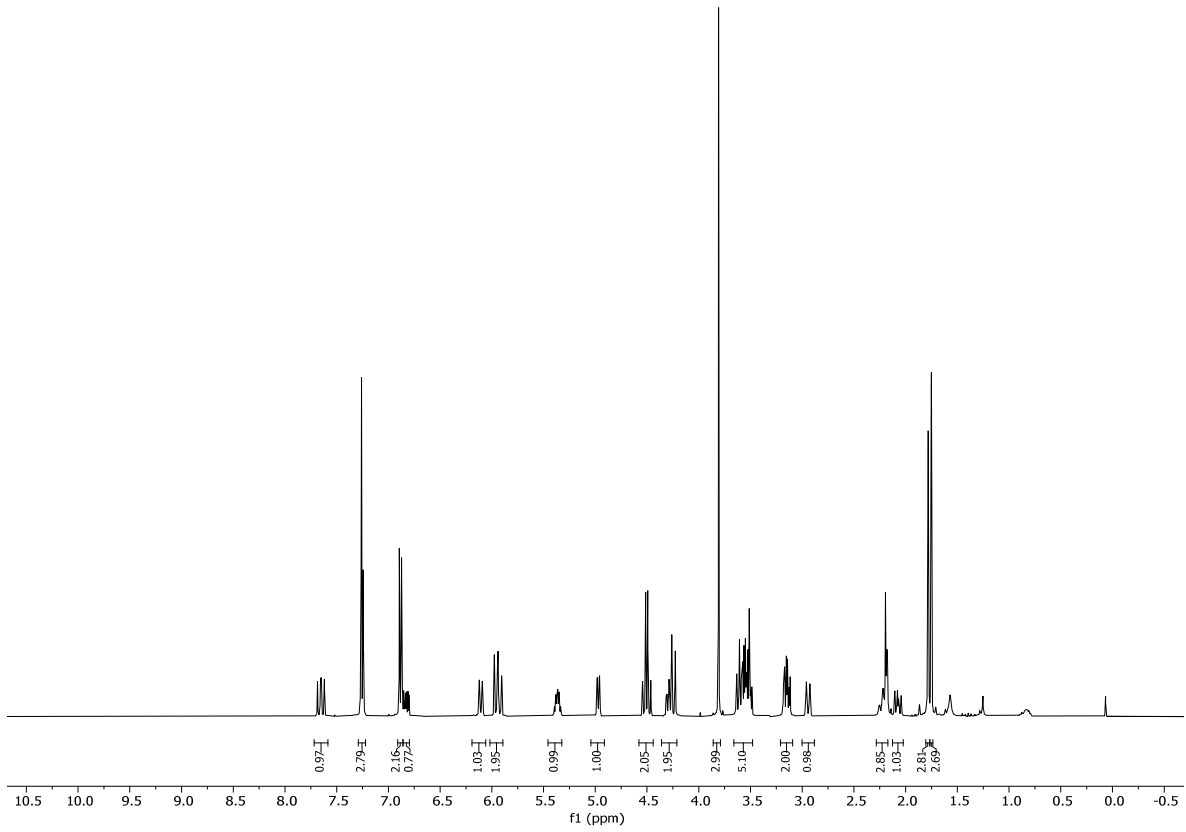


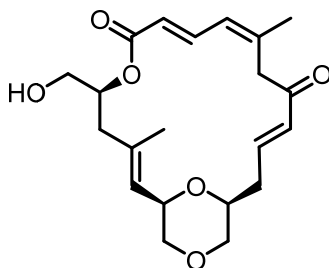
O31

(1R,2E,5S,8E,10Z,14E,17S)-5-(((4-methoxybenzyl)oxy)methyl)-3,11-dimethyl-6,19,21-trioxabicyclo[15.3.1]henicosa-2,8,10,14-tetraene-7,13-dione (O31). To a stirred solution of diol **26** (100.0 mg, 0.15 mmol, 1.00 equiv.) in CH₂Cl₂ (14.5 ml) under argon was added a suspension of DMP (259.0 mg, 0.61 mmol, 4.00 equiv.) in CH₂Cl₂ (1.6 ml) and stirred at rt for 1 h. The reaction mixture was quenched by addition of sat. aqu. Na₂S₂O₃ solution (3.3 ml), sat. aqu. NaHCO₃ solution (10 ml) and H₂O (16 ml) and stirred at rt until two clear phases have formed. The phases were separated and the aqueous phase was extracted with CH₂Cl₂ (3 x 17 ml). The combined organic phases were dried over anhydrous MgSO₄, filtered and concentrated under reduced pressure to obtain the crude aldehyde mixture.

To a stirred solution of the crude aldehyde mixture in THF (50 ml) under argon was added H₂O (1.2 ml), the solution was cooled to 0 °C and Ba(OH)₂•8H₂O (39.3 mg, 0.23 mmol, 1.50 equiv.) was added. After 20 min, sat. aqu. NaHCO₃ solution (45 ml) was added, the phases were separated and the aqueous phase was extracted with EtOAc (3 x 35 ml). The combined organic phases were dried over anhydrous MgSO₄, filtered and concentrated under reduced pressure. Purification of the residue by flash column chromatography (EtOAc/hexane 1:2) afforded **O31** (51.2 mg, 0.10 mmol, 68% over two steps) as a colourless oil.

TLC: R_f = 0.18 (EtOAc/hexane 1:2). **¹H-NMR** (400 MHz, CDCl₃) δ = 7.65 (dd, *J* = 15.0, 11.6 Hz, 1H), 7.29 – 7.22 (m, 3H), 6.88 (d, *J* = 8.6 Hz, 2H), 6.86 – 6.80 (m, 1H), 6.11 (d, 1H), 6.02 – 5.89 (m, 2H), 5.46 – 5.32 (m, 1H), 4.97 (d, *J* = 1.3 Hz, 1H), 4.58 – 4.44 (m, 2H), 4.36 – 4.21 (m, 2H), 3.81 (s, 3H), 3.66 – 3.48 (m, 5H), 3.21 – 3.09 (m, 2H), 2.94 (d, 1H), 2.28 – 2.17 (m, 3H), 2.13 – 2.02 (m, 1H), 1.78 (s, 3H), 1.75 (d, *J* = 1.4 Hz, 3H). **¹³C-NMR** (101 MHz, CDCl₃) δ = 198.2, 166.9, 159.4, 145.4, 142.9, 139.4, 136.3, 131.7, 130.2, 129.5, 125.6, 124.4, 121.4, 114.0, 73.6, 73.1, 71.6, 70.3, 69.6, 69.5, 55.4, 45.3, 42.9, 35.2, 23.5, 17.0. **IR** (film) $\tilde{\nu}$ = 2846, 1715, 1669, 1634, 1613, 1586, 1513, 1441, 1360, 1301, 1281, 1248, 1209, 1175, 1149, 1119, 1102, 1032, 980, 932, 875, 822, 758, 576, 539, 523. **HRMS** (ESI) calculated for C₂₉H₃₇O₇ [(M+H)⁺]: 497.2534, found: 497.2533. $[\alpha]_D^{20}$ = –192.96° (1.00 g/100cm³ in CHCl₃).

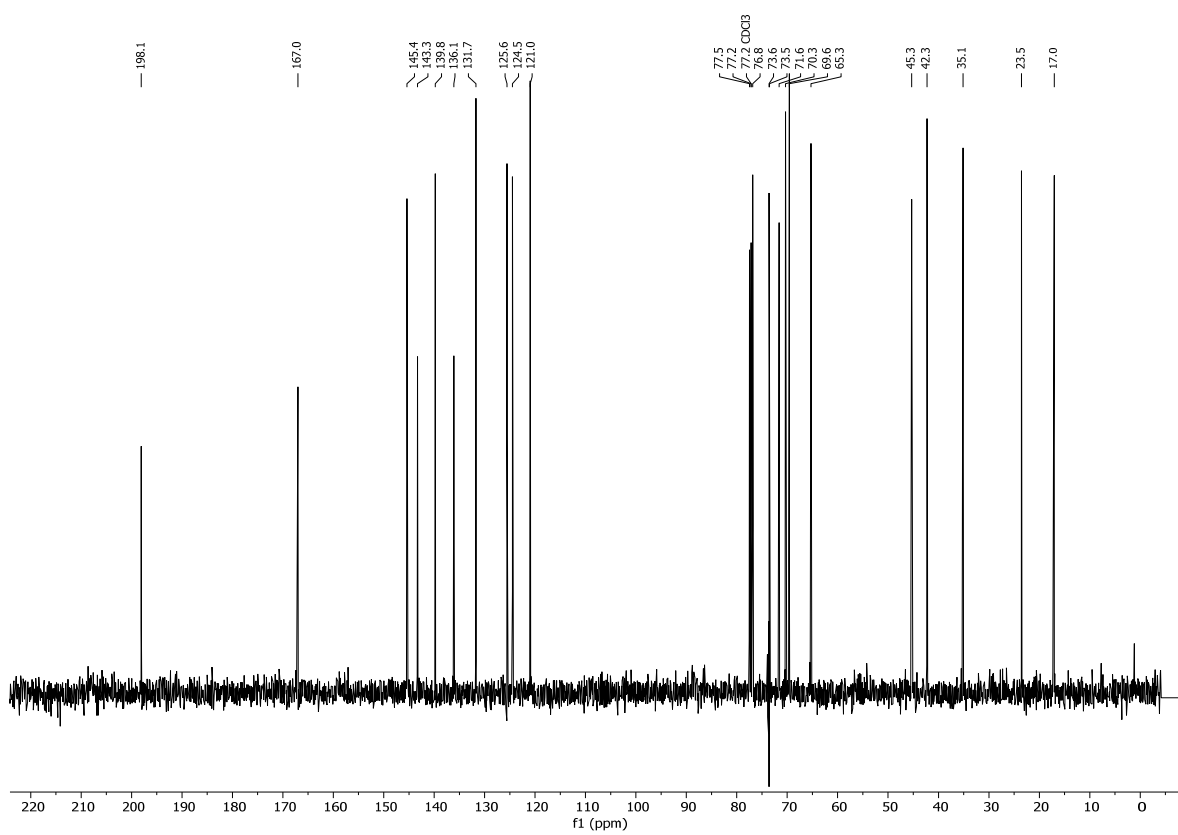
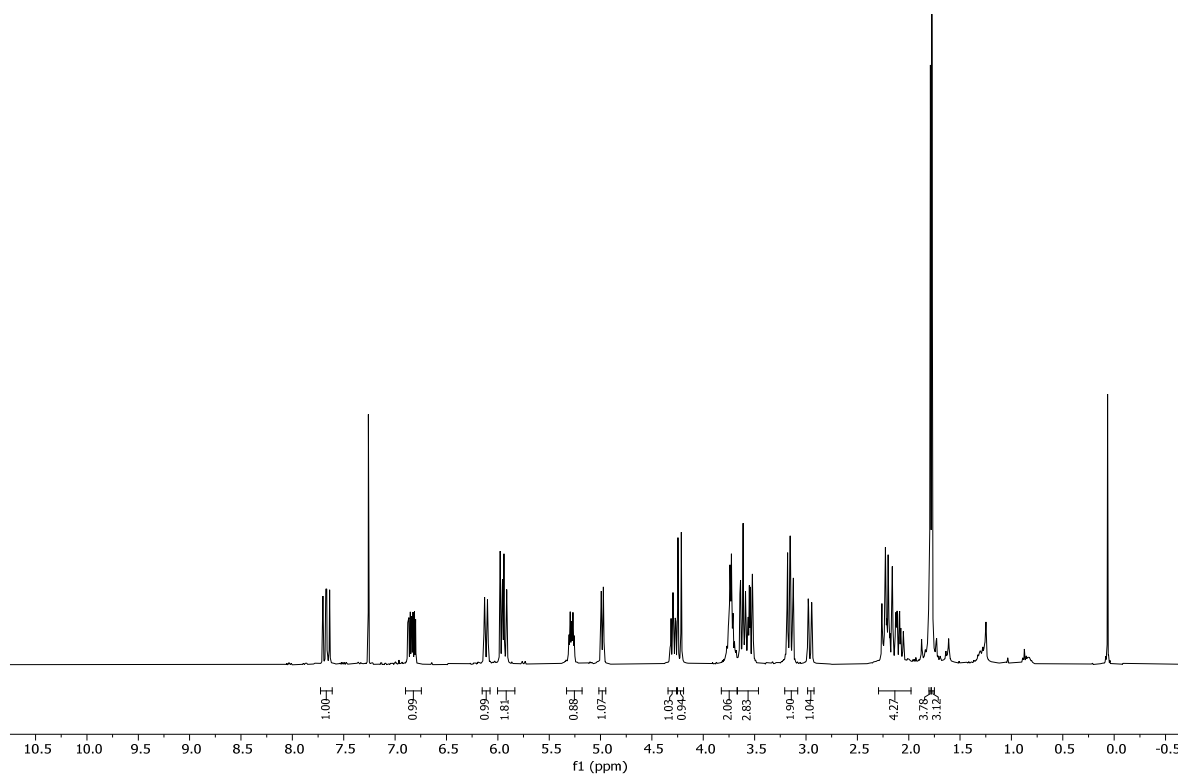


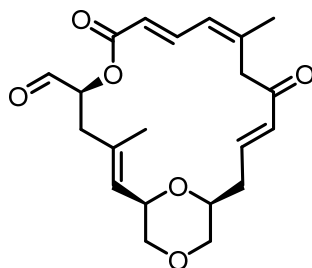


OS4

(1R,2E,5S,8E,10Z,14E,17S)-5-(hydroxymethyl)-3,11-dimethyl-6,19,21-trioxabicyclo[15.3.1]henicosa-2,8,10,14-tetraene-7,13-dione (OS4). To a solution of **O31** (134.0 mg, 0.28 mmol, 1.00 equiv.) in CH_2Cl_2 (17 ml) was added phosphate buffer (3.6 ml, pH = 7.2) followed by DDQ (220.0 mg, 0.97 mmol, 3.50 equiv.) at rt and the mixture was vigorously stirred for at rt 2 h. Then, DDQ (63.0 mg, 0.28 mmol, 1.00 equiv.) was added and stirring was continued at rt for an additional hour. The reaction was quenched by addition of sat. aqu. NaHCO_3 (150 ml) and CH_2Cl_2 (150 ml). The two phases were separated, the aqueous phase was extracted with CH_2Cl_2 (3 x 150 ml) and the combined organic extracts were dried over anhydrous MgSO_4 and concentrated under reduced pressure. Purification of the residue by flash column chromatography (EtOAc/hexane 1:2 \rightarrow 1.5:1) afforded **OS4** (87.6 mg, 0.23 mmol, 84%) as a colorless oil.

TLC: R_f = 0.13 (EtOAc/hexane 1:1). **$^1\text{H-NMR}$** (400 MHz, CDCl_3) δ = 7.67 (dd, J = 15.0, 11.5 Hz, 1H), 6.84 (ddd, J = 16.4, 9.8, 4.1 Hz, 1H), 6.11 (d, J = 11.6 Hz, 1H), 6.00 – 5.83 (m, 2H), 5.28 (dtd, J = 8.9, 4.1, 2.0 Hz, 1H), 4.98 (d, J = 8.4 Hz, 1H), 4.29 (ddd, J = 10.5, 8.4, 2.9 Hz, 1H), 4.23 (d, J = 13.3 Hz, 1H), 3.73 (q, J = 5.6 Hz, 2H), 3.67 – 3.46 (m, 3H), 3.21 – 3.08 (m, 2H), 2.96 (d, J = 13.3 Hz, 1H), 2.29 – 1.98 (m, 4H), 1.79 (s, 4H), 1.77 (d, J = 1.3 Hz, 3H). **$^{13}\text{C-NMR}$** (101 MHz, CDCl_3) δ = 198.1, 167.0, 145.4, 143.3, 139.8, 136.1, 131.7, 125.6, 124.5, 121.0, 77.5, 77.2, 76.8, 73.6, 73.5, 71.6, 70.3, 69.6, 65.3, 45.3, 42.3, 35.1, 23.5, 17.0. **IR** (film) $\tilde{\nu}$ = 3462, 2957, 2910, 2850, 1715, 1669, 1634, 1437, 1360, 1281, 1210, 1177, 1150, 1118, 1104, 1066, 1051, 980, 931, 894, 876, 756, 538, 501. **HRMS** (ESI) calculated for $\text{C}_{21}\text{H}_{29}\text{O}_6$ [(M+H) $^+$]: 377.1959, found: 377.1955. $[\alpha]_D^{20}$ = -255.95° (1.00 g/100cm 3 in CHCl_3).

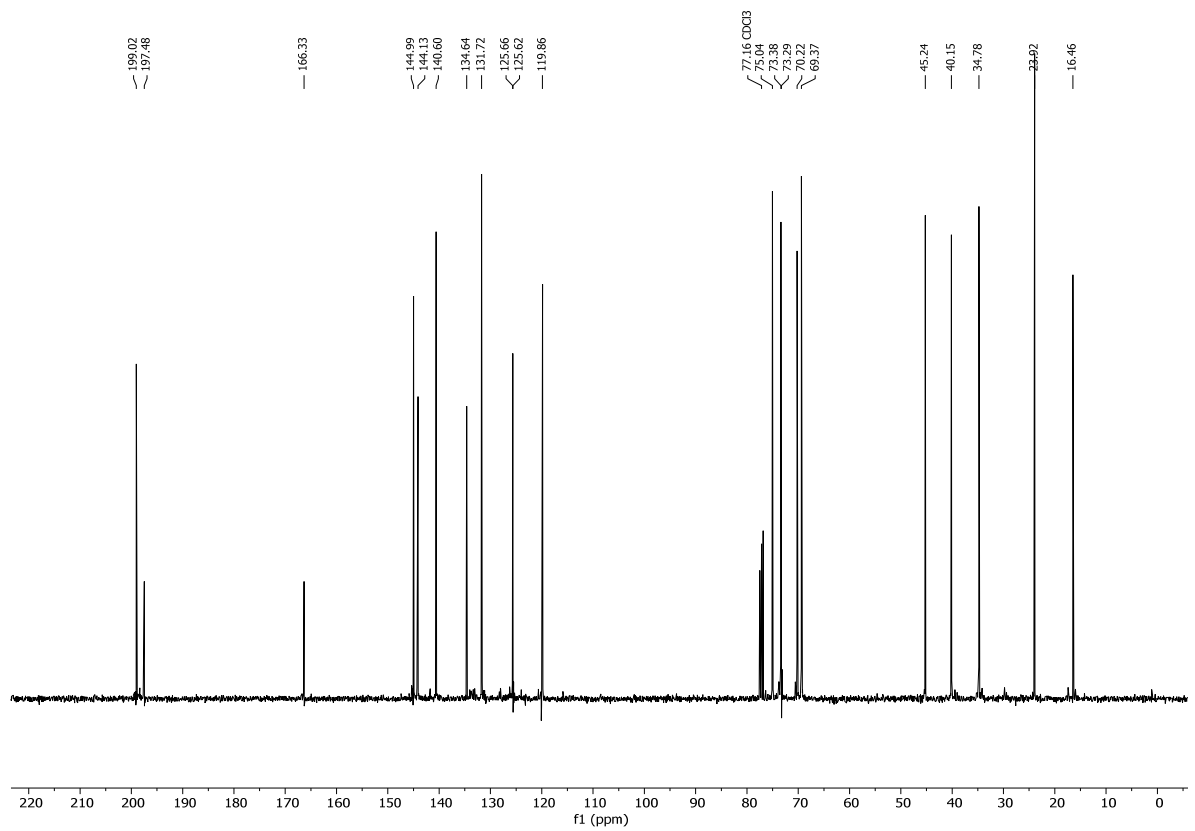
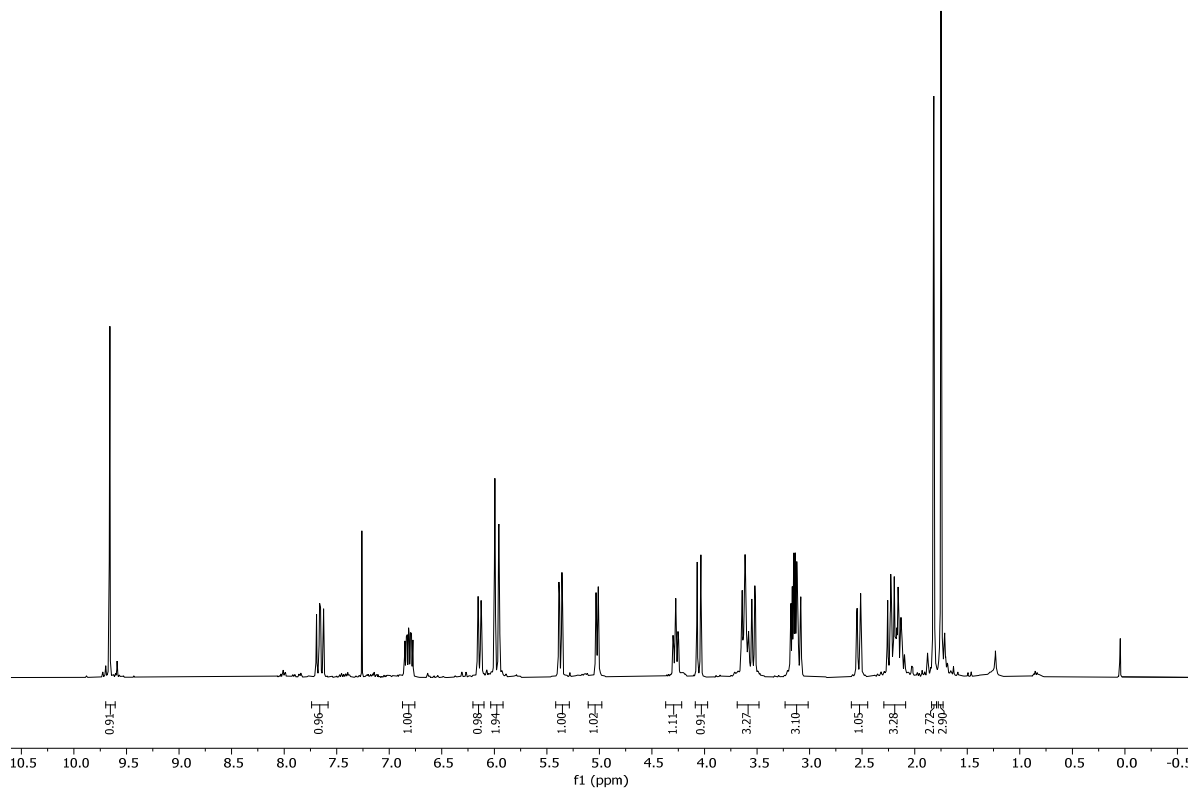


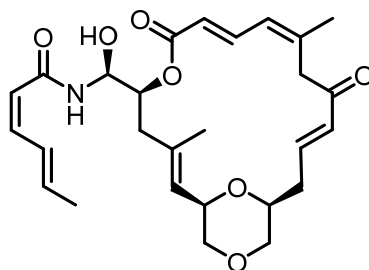


O33

(1*R*,2*E*,5*S*,8*E*,10*Z*,14*E*,17*S*)-3,11-dimethyl-7,13-dioxo-6,19,21-trioxabicyclo[15.3.1]henicosa-2,8,10,14-tetraene-5-carbaldehyde (O33). To a stirred solution of **OS4** (43.2 mg, 0.12 mmol, 1.00 equiv.) in CH₂Cl₂ (11 ml) was added NaHCO₃ (77.2 mg, 0.92 mmol, 8.00 equiv.) followed by DMP (194.8 mg, 0.46 mmol, 4.00 equiv.) at rt and the reaction mixture was stirred at rt. After 1.5 h NaHCO₃ (38.6 mg, 0.46 mmol, 4.00 equiv.) and DMP (97.4 mg, 0.23 mmol, 2.00 equiv.) were added and the mixture was stirred at rt. After 3.5 h and 4.5 h DMP (97.4 mg, 0.23 mmol, 2.00 equiv. and 48.2 mg, 0.12 mmol, 1.00 equiv., respectively) was added and stirring was continued for 1 h. The reaction was quenched by addition by addition of a mixture of aqueous Na₂S₂O₃ and NaHCO₃ (60 ml) and stirring was continued for 10 min until two clear phases were formed. The phases were separated the aqueous phase was extracted with CH₂Cl₂ (3 x 60 ml), the combined organic phases were dried over anhydrous MgSO₄ and concentrated under reduced pressure. The residue was purified by flash column chromatography (EtOAc/hexane 1:1) affording **O33** (36.5 mg, 0.10 mmol, 85%) as a colorless oil.

TLC: R_f = 0.53 (EtOAc/hexane 1:2). **¹H-NMR** (400 MHz, CDCl₃) δ = 9.66 (s, 1H), 7.66 (dd, *J* = 15.0, 11.7 Hz, 1H), 6.87 – 6.76 (m, 1H), 6.14 (d, *J* = 11.7 Hz, 1H), 5.98 (d, *J* = 15.1 Hz, 2H), 5.37 (dd, *J* = 11.5, 2.1 Hz, 1H), 5.02 (d, *J* = 8.4 Hz, 1H), 4.37 – 4.22 (m, 1H), 4.05 (d, *J* = 13.8 Hz, 1H), 3.69 – 3.48 (m, 3H), 3.23 – 3.01 (m, 3H), 2.53 (d, *J* = 13.8 Hz, 1H), 2.29 – 2.09 (m, 3H), 1.82 (s, 3H), 1.75 (s, 3H). **¹³C-NMR** (101 MHz, CDCl₃) δ = 199.0, 197.5, 166.3, 145.0, 144.1, 140.6, 134.6, 131.7, 125.7, 125.6, 119.9, 75.0, 73.4, 73.3, 70.2, 69.4, 45.2, 40.1, 34.8, 23.9, 16.5. **IR** (film) $\tilde{\nu}$ = 3449, 3023, 2952, 2915, 2849, 1720, 1668, 1633, 1436, 1382, 1356, 1301, 1279, 1258, 1207, 1176, 1145, 1117, 1068, 1051, 979, 931, 906, 876, 822, 753, 712, 665, 642, 590, 534, 525, 516. **HRMS** (ESI) calculated for C₂₁H₂₇O₆ [(M+H)⁺]: 375.1802, found: 375.1812. [α]_D²⁰ = -268.95° (1.00 g/100cm³ in CHCl₃).





O4

(2Z,4E)-N-((S)-((1R,2E,5S,8E,10Z,14E,17S)-3,11-dimethyl-7,13-dioxo-6,19,21-trioxabicyclo[15.3.1]henicosa-2,8,10,14-tetraen-5-yl)(hydroxy)methyl)hexa-2,4-dienamide

(O4). Preparation of stock solution of (S)-BINAL-sorbamide complex: Reagents and reactants were dried in flasks used to prepare solutions in high vacuum over night. LAH (32.2 mg, 0.86 mmol, 10.00 equiv.) was suspended in dry THF (2 ml) at rt. Dry EtOH (51 μ L, 0.86 mmol, 10.00 equiv.) was diluted with THF (2 ml) and the mixture was added slowly at rt to the LAH suspension. (S)-BINOL (244.7 mg, 0.86 mmol, 10.00 equiv.) was added as a solution in THF (2 ml) followed by (2E,4Z)-sorbamide **O14a**^[68] (95.0 mg, 0.86 mmol, 10.00 equiv.) in THF (2 ml) to give a gray mixture.

1.6 ml of the stock solution containing the putative amide transfer complex (0.17 mmol, 2.00 equiv.) was added immediately to a solution of aldehyde **O33** (32.0 mg, 0.09 mmol, 1.00 equiv.) in THF (1.2 ml) and the mixture was stirred at rt. Additional 1.6 ml of stock solution (0.17 mmol, 2.00 equiv.) were added after 5 min. After 15 min another 0.8 mL of stock solution (0.09 mmol, 1.00 equiv.) were added and stirring was continued. The reaction mixture was quenched by addition of sat. aqu. NaHCO₃ solution (7 ml) after 40 min and the mixture was stirred until two clear phases have formed (approx. 10 min). The phases were separated and the aqueous phase was extracted with EtOAc (3 x 9 ml), the combined organic phases were dried over anhydrous MgSO₄ and concentrated under reduced pressure. The residue was purified by flash column chromatography (EtOAc/Hex 1:2 \rightarrow 1:1, 2% Et₃N) and subsequent reverse-phase preparative HPLC (35% \rightarrow 65% acetonitrile in H₂O in 15 min, 25 ml/min) affording **O4** (19.2 mg, 0.04 mmol, 46%) as a colourless film.

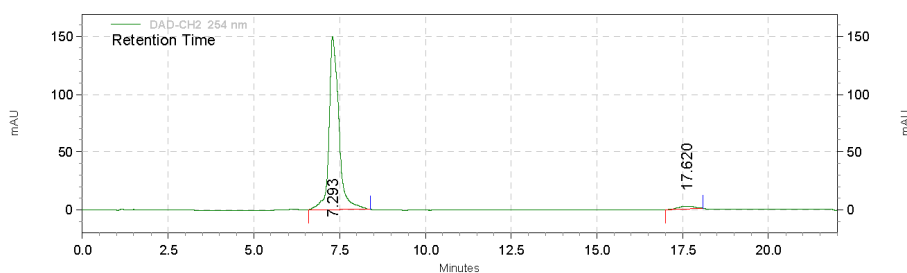
TLC: R_f = 0.54 (EtOAc/hexane 2:1). **¹H-NMR** (500 MHz, DMSO-*d*₆) δ = 8.35 (d, *J* = 8.9 Hz, 1H), 7.55 (dd, *J* = 15.0, 11.6 Hz, 1H), 7.50 – 7.34 (m, 1H), 6.82 – 6.68 (m, 1H), 6.38 (t, *J* = 11.3 Hz, 1H), 6.23 – 6.17 (m, 1H), 6.14 (d, *J* = 5.1 Hz, 1H), 5.99 – 5.91 (m, 4H), 5.65 (d, *J* = 11.4 Hz, 2H), 5.31 (dd, *J* = 9.9, 4.9 Hz, 1H), 5.03 – 4.96 (m, 1H), 4.89 (d, *J* = 8.3 Hz, 1H), 4.25 (d, *J* = 13.8 Hz, 1H), 4.19 – 4.10 (m, 1H), 3.61 (dd, *J* = 11.2, 2.6 Hz, 1H), 3.57 – 3.50 (m, 1H), 3.45 (dd, *J* = 11.5, 2.9 Hz, 1H), 3.06 – 2.99 (m, 2H), 2.86 (d, *J* = 13.6 Hz, 1H), 2.39 – 2.30 (m, 1H), 2.22 – 1.98 (m, 3H), 1.79 (dd, *J* = 6.9,

1.8 Hz, 5H), 1.72 (s, 3H), 1.67 (d, $J = 1.2$ Hz, 3H). $^{13}\text{C-NMR}$ (126 MHz, $\text{DMSO-}d_6$) $\delta = 197.3, 165.6, 165.3, 145.3, 142.9, 140.7, 139.4, 137.3, 135.6, 130.9, 128.6, 125.2, 124.1, 120.9, 119.1, 73.0, 72.9, 72.7, 71.8, 69.4, 68.7, 45.0, 41.1, 34.1, 23.4, 18.3, 16.7$. IR (film) $\tilde{\nu} = 3325, 2848, 2359, 1718, 1667, 1634, 1604, 1519, 1435, 1356, 1281, 1208, 1148, 1118, 980, 931, 834, 805, 752$. HRMS (ESI) calculated for $\text{C}_{27}\text{H}_{35}\text{NNaO}_7$ $[(\text{M}+\text{Na})^+]$: 508.2306, found: 508.2303. $[\alpha]_D^{20} = -295.94^\circ$ (1.00 g/100cm³ in CHCl_3).

Page 1 of 1

Area % Report

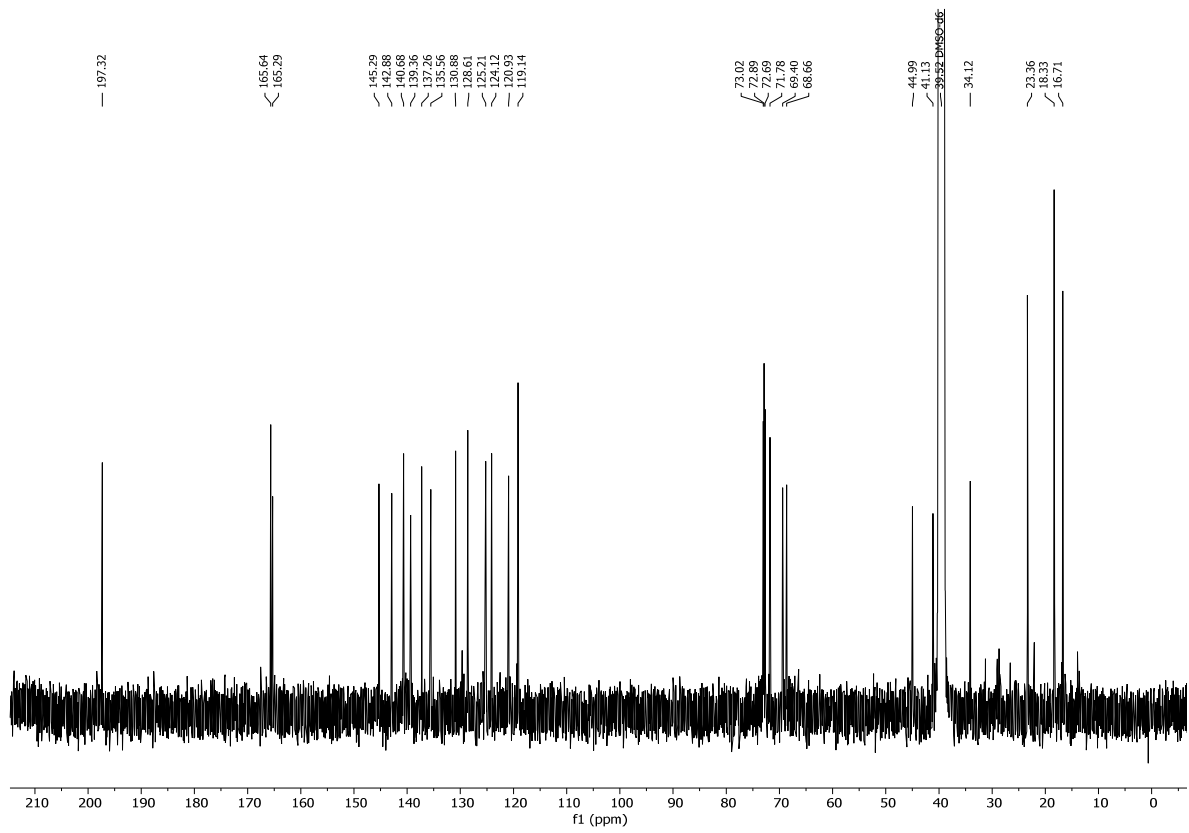
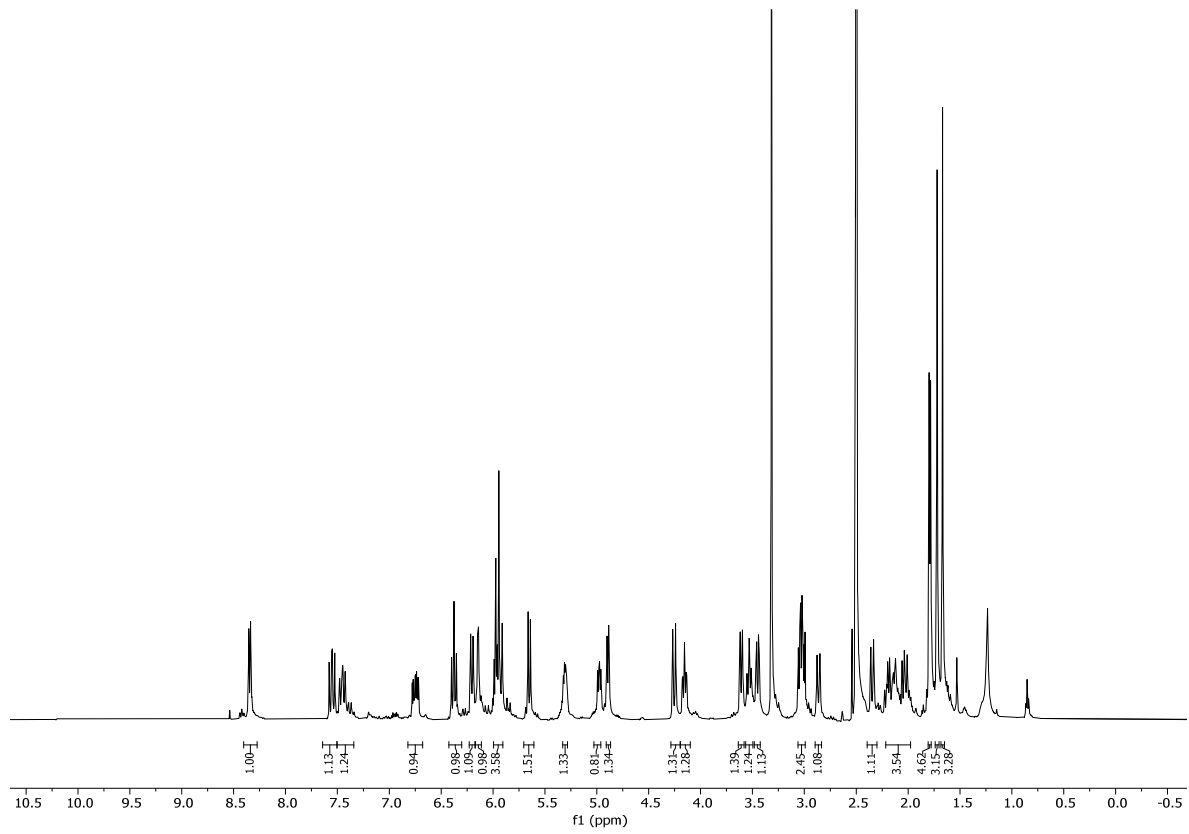
Data File: C:\EZChrom Elite\Enterprise\Projects\Etienne\Alina\LZ-22-4-hplc-r2-f11-trace
 Method: C:\EZChrom Elite\Enterprise\Projects\Etienne\Alina\LZ-35_65_15min.met
 Acquired: 01.03.2022 18:25:51
 Printed: 01.03.2022 18:29:26



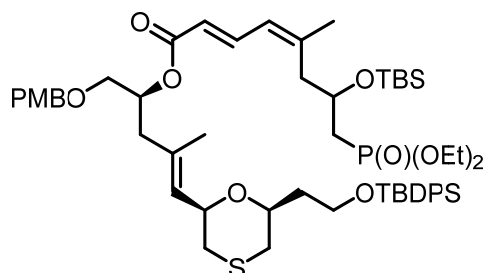
DAD-CH2 254 nm Results

| Retention Time | Area | Area % | Height | Height % |
|----------------|----------|--------|--------|----------|
| 7.293 | 11818666 | 97.36 | 599191 | 98.41 |
| 17.620 | 320304 | 2.64 | 9701 | 1.59 |
| Totals | 12138970 | 100.00 | 608892 | 100.00 |

The reversed phase analytical HPLC trace shown above was measured with the Elite LaChrom device mentioned in the general part. A gradient of 35% → 65% acetonitrile in H_2O in 15 min, with a flow rate of 1 mL/min was used. The material thus obtained was used in the biological experiments.



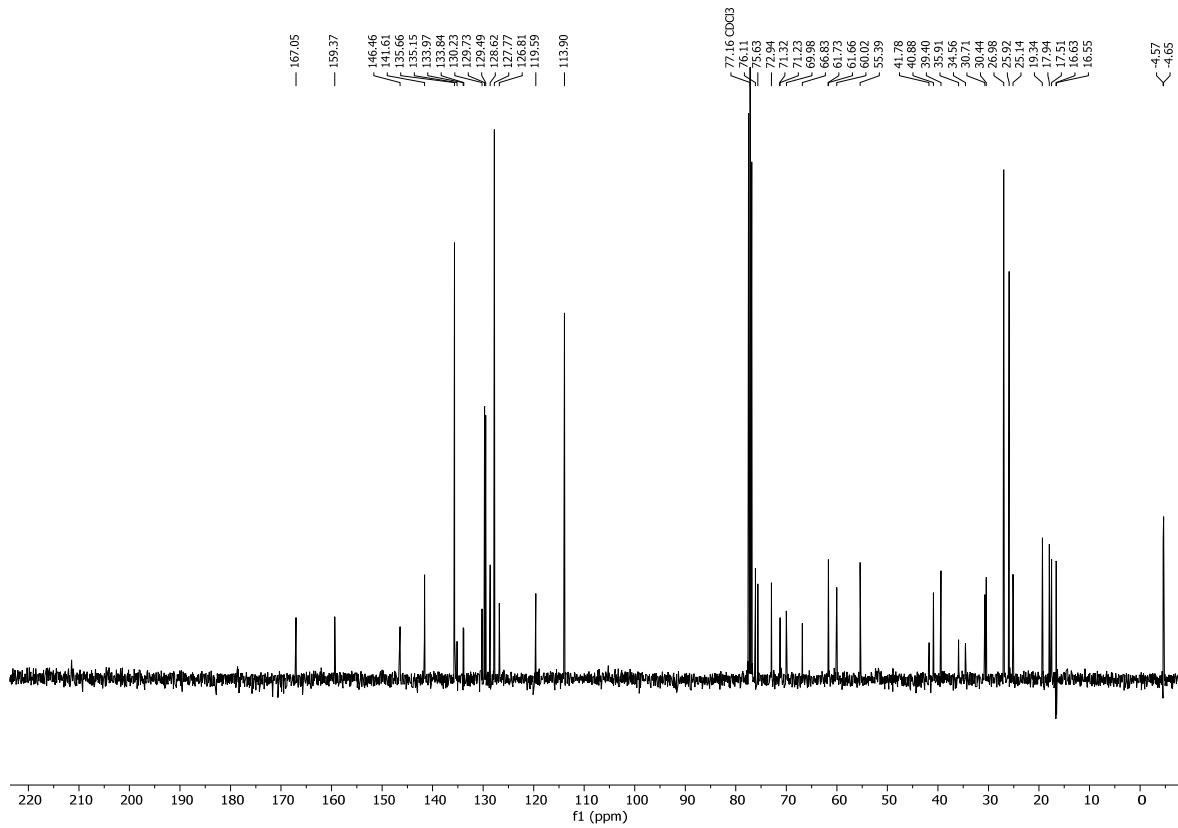
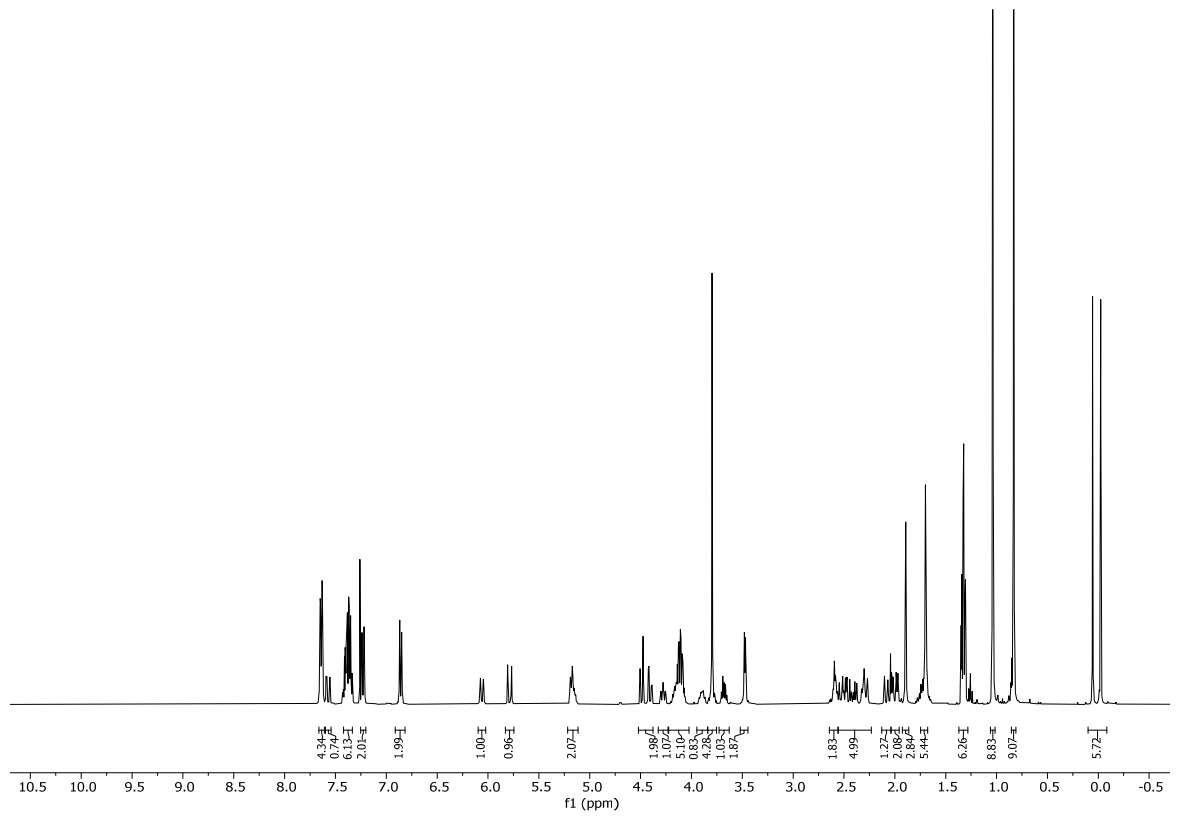
4.2.2.4 Synthesis of Analog O5 and O7

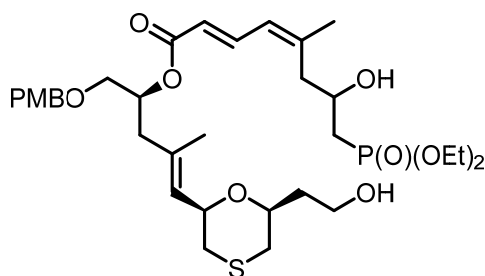


OS5

(S,E)-5-((2R,6S)-6-(2-((tert-butylidiphenylsilyl)oxy)ethyl)-1,4-oxathian-2-yl)-1-((4-methoxybenzyl)oxy)-4-methylpent-4-en-2-yl (2E,4Z)-7-((tert-butyl dimethylsilyl)oxy)-8-(diethoxyphosphoryl)-5-methylocta-2,4-dienoate (OS5). To a solution of **O9**^[72] (0.33 g, 0.79 mmol, 1.20 equiv., co-evaporated twice with 2 ml of toluene immediately before use) in toluene (6 ml) was added Et₃N (0.24 ml, 1.71 mmol, 2.60 equiv.) followed by 2,4,6-trichlorobenzoyl chloride (0.15 ml, 0.99 mmol, 1.50 equiv.). After 1.5 h at rt, a solution of **O11** (0.41 g, 0.66 mmol, 1.00 equiv. co-evaporated together twice with 2 ml of toluene immediately before use) in toluene (4 ml) and DMAP (0.09 g, 0.72 mmol, 1.10 equiv.) were added, immediately leading to a yellow suspension. After stirring at room temperature for 2.5 h sat. aqu. NaHCO₃ (20 ml), H₂O (20 ml) and EtOAc (20 ml) were added, the phases were separated and the aqueous phase was extracted with EtOAc (3 x 25 ml). The combined organic extracts were dried over MgSO₄, concentrated under reduced pressure, and the residue was purified by flash chromatography (EtOAc/Hex 1:1) to give **OS5** (0.65 g, 0.64 mmol, 97%) as colorless viscous oil.

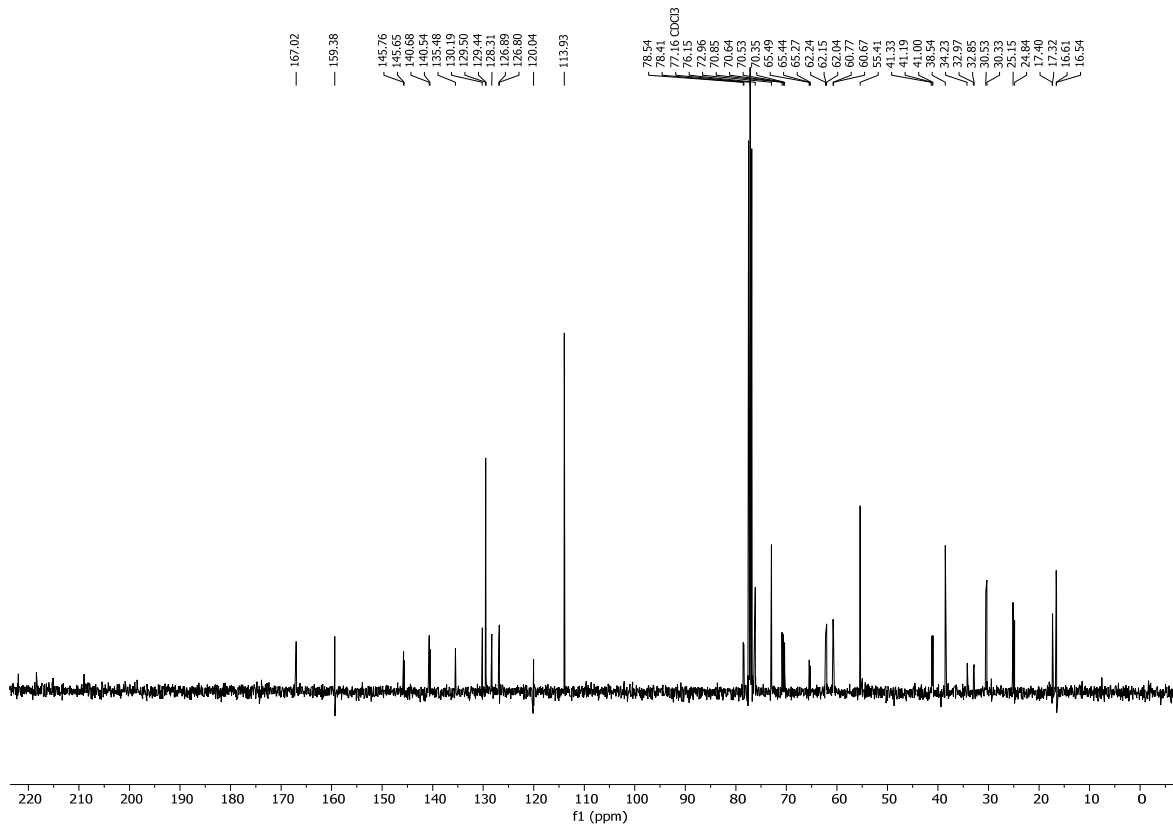
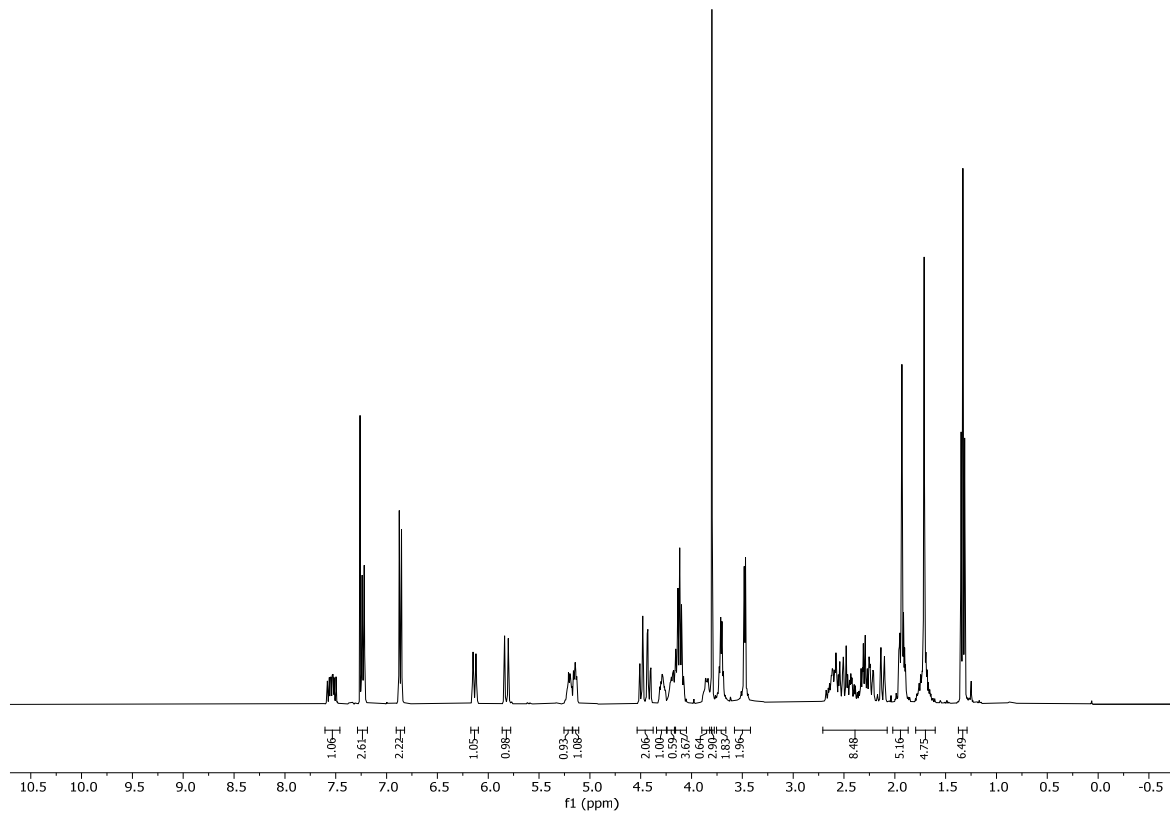
TLC: R_f = 0.50 (EtOAc/hexane 1:1). **¹H-NMR** (400 MHz, CDCl₃) δ = 7.64 (dp, *J* = 8.3, 2.0 Hz, 4H), 7.60 – 7.54 (m, 1H), 7.42 – 7.33 (m, 6H), 7.25 – 7.20 (m, 2H), 6.91 – 6.82 (m, 2H), 6.06 (d, *J* = 11.5 Hz, 1H), 5.79 (d, *J* = 15.2 Hz, 1H), 5.17 (ddt, *J* = 9.1, 5.8, 2.0 Hz, 2H), 4.52 – 4.38 (m, 2H), 4.28 (ddd, *J* = 10.2, 7.7, 2.1 Hz, 1H), 4.22 – 4.02 (m, 5H), 3.95 – 3.84 (m, 1H), 3.80 (s, 4H), 3.68 (dt, *J* = 10.6, 5.5 Hz, 1H), 3.52 – 3.45 (m, 2H), 2.59 (q, *J* = 3.8 Hz, 2H), 2.56 – 2.23 (m, 5H), 2.13 – 2.04 (m, 1H), 2.04 – 1.96 (m, 2H), 1.89 (s, 3H), 1.75 – 1.68 (m, 5H), 1.33 (td, *J* = 7.1, 2.8 Hz, 6H), 1.04 (s, 9H), 0.83 (s, 9H), 0.02 (d, *J* = 31.7 Hz, 6H). **¹³C-NMR** (101 MHz, CDCl₃) δ = 167.1, 159.4, 146.5, 141.6, 135.7, 135.2, 134.0, 133.8, 130.2, 129.7, 129.5, 128.6, 127.8, 126.8, 119.6, 113.9, 76.1, 75.6, 72.9, 71.3, 71.2, 70.0, 66.8, 61.7, 61.7, 60.0, 55.4, 41.8, 40.9, 39.4, 35.9, 34.6, 30.7, 30.4, 27.0, 25.9, 25.1, 19.3, 17.9, 17.5, 16.6, 16.6, -4.6, -4.7. **IR** (film) $\tilde{\nu}$ = 2955, 2929, 2902, 2857, 1709, 1636, 1612, 1514, 1471, 1463, 1428, 1389, 1364, 1303, 1249, 1208, 1147, 1111, 1085, 1050, 1026, 980, 959, 937, 824, 809, 776, 740, 704, 688, 614, 543, 505. **HRMS** (ESI) calculated for C₅₅H₈₃NaO₁₀PSSi₂ [(M+Na)⁺]: 1045.4875, found: 1045.4851.

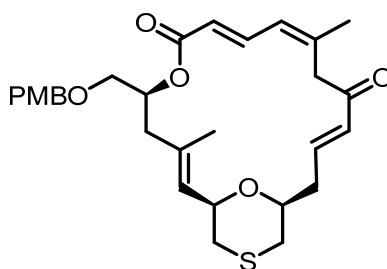


**O30**

(*S,E*)-5-((*2R,6S*)-6-(2-hydroxyethyl)-1,4-oxathian-2-yl)-1-((4-methoxybenzyl)oxy)-4-methylpent-4-en-2-yl (2*E,4Z*)-8-(diethoxyphosphoryl)-7-hydroxy-5-methylocta-2,4-dienoate (O30**).** To a stirred solution of **OS5** (0.80 g, 0.78 mmol, 1.00 equiv.) in THF (39 ml) in a plastic Erlenmeyer flask was added 70% HF•py (7.7 ml) along the tube wall at 0 °C. The cooling bath was removed after 5 min and stirring was continued at rt for 18 h. The solution was then carefully added to a vigorously stirred mixture of sat. aqu. NaHCO₃ (250 ml) and EtOAc (100 ml) until two clear phases were formed (ca. 15 min). The phases were separated, the aqueous phase was extracted with EtOAc (3 x 250 ml), the combined organic extracts were washed with sat. aqu. NaHCO₃ (200 ml) followed by drying over MgSO₄. Concentration under reduced pressure and purification using flash chromatography (acetone/EtOAc 1:1) afforded **O30** (0.50 g, 0.75 mmol, 96%) as a pale yellow, viscous oil.

TLC: R_f = 0.65 (acetone/EtOAc 1:1). **¹H-NMR** (400 MHz, CDCl₃) δ = 7.54 (ddd, *J* = 15.1, 11.7, 7.6 Hz, 1H), 7.29 – 7.19 (m, 3H), 6.91 – 6.82 (m, 2H), 6.13 (d, *J* = 11.6 Hz, 1H), 5.82 (d, *J* = 15.0 Hz, 1H), 5.21 (tdd, *J* = 8.0, 6.9, 3.6 Hz, 1H), 5.15 (t, *J* = 6.2 Hz, 1H), 4.54 – 4.38 (m, 2H), 4.34 – 4.25 (m, 1H), 4.24 – 4.16 (m, 1H), 4.12 (pd, *J* = 7.1, 1.6 Hz, 4H), 3.86 (dq, *J* = 8.6, 4.2, 2.2 Hz, 1H), 3.80 (s, 3H), 3.71 (qd, *J* = 6.7, 4.0 Hz, 2H), 3.58 – 3.42 (m, 2H), 2.71 – 2.08 (m, 8H), 2.02 – 1.87 (m, 5H), 1.79 – 1.60 (m, 5H), 1.33 (t, *J* = 1.7 Hz, 6H). **¹³C-NMR** (101 MHz, CDCl₃) δ = 167.0, 159.4, 145.8, 145.7, 140.7, 140.5, 135.5, 130.2, 129.5, 129.4, 128.3, 126.9, 126.8, 120.0, 113.9, 78.5, 78.4, 76.2, 73.0, 70.9, 70.6, 70.5, 70.4, 65.5, 65.4, 65.3, 62.2, 62.2, 62.0, 60.8, 60.7, 55.4, 41.3, 41.2, 41.0, 38.5, 34.2, 33.0, 32.9, 30.5, 30.3, 25.2, 24.8, 17.4, 17.3, 16.6, 16.5. **IR** (film) $\tilde{\nu}$ = 3390, 2979, 2933, 2908, 2869, 1737, 1709, 1633, 1611, 1514, 1443, 1371, 1302, 1242, 1147, 1082, 1024, 976, 894, 819, 721, 634, 606, 545. **HRMS** (ESI) calculated for C₃₃H₅₂O₁₀PS [(M+H)⁺]: 671.3013, found: 671.3014.



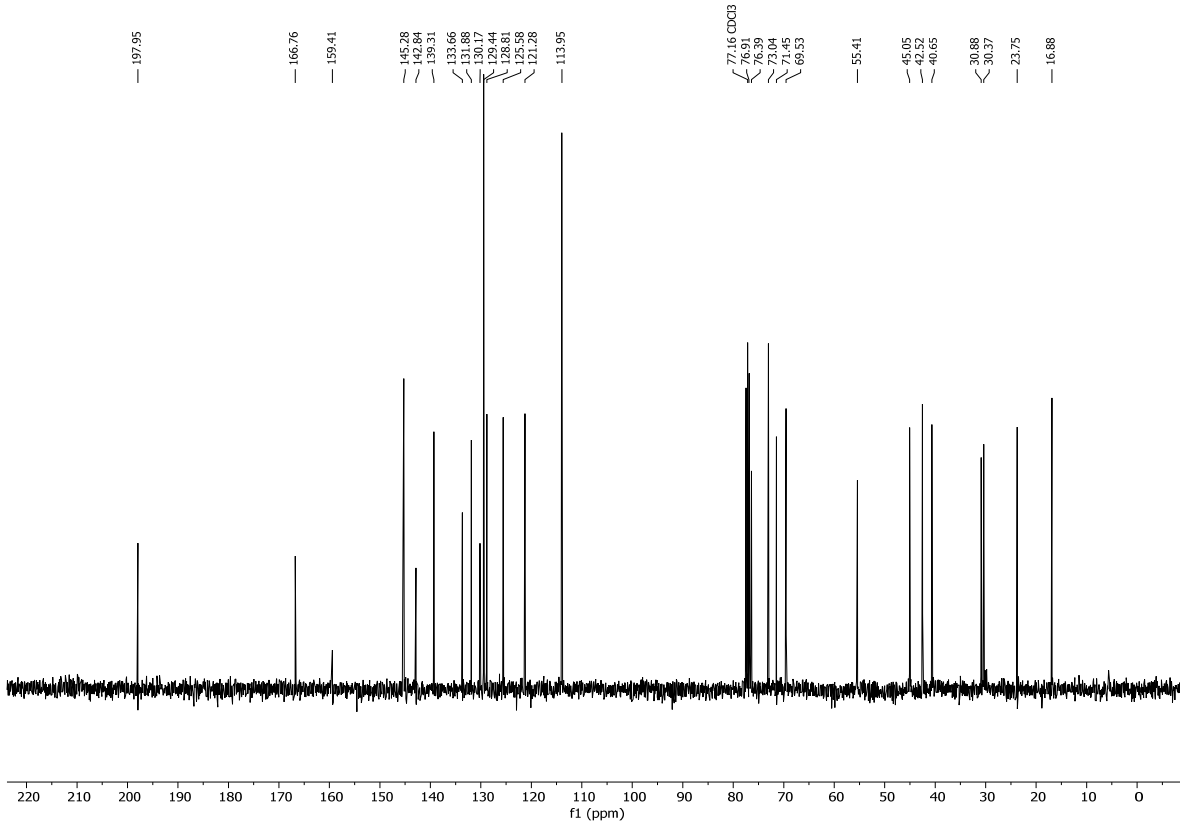
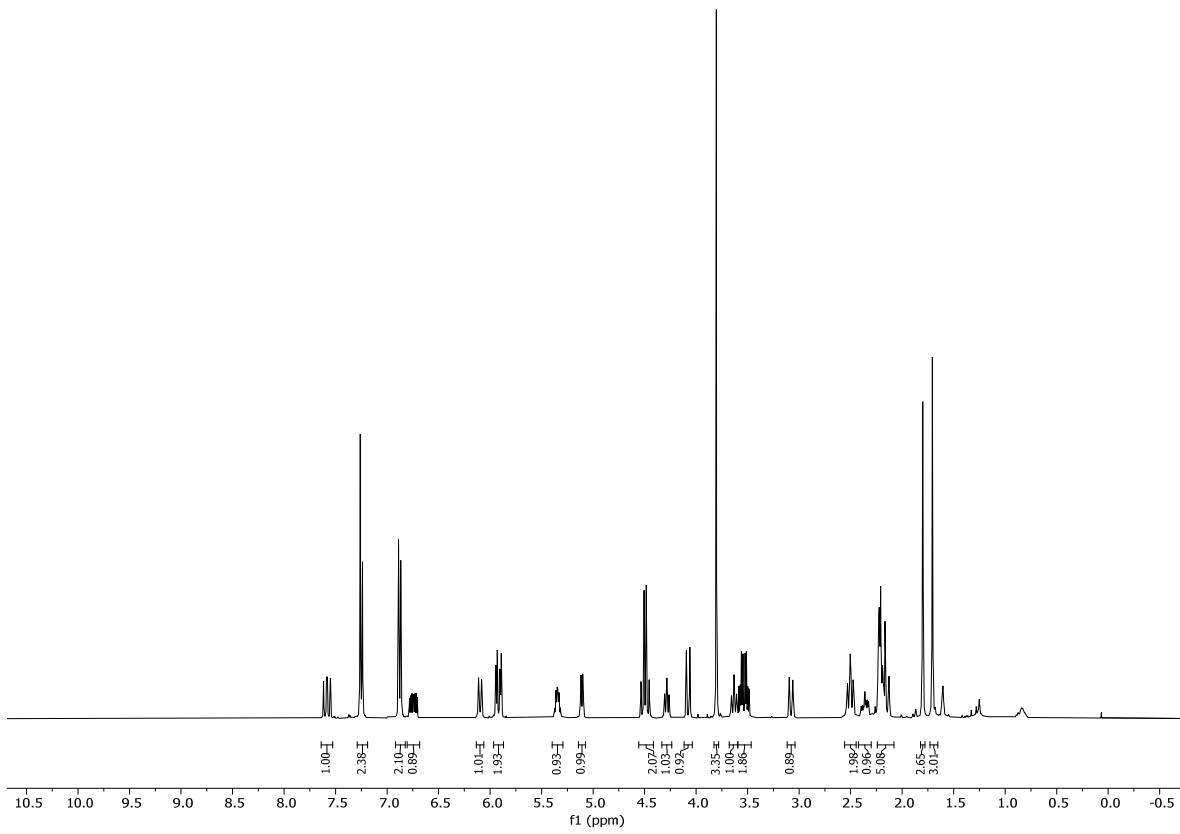


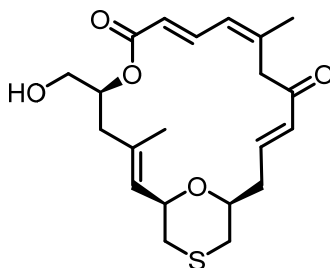
O32

(1R,2E,5S,8E,10Z,14E,17S)-5-(((4-methoxybenzyl)oxy)methyl)-3,11-dimethyl-6,21-dioxa-19-thiabicyclo[15.3.1]henicosa-2,8,10,14-tetraene-7,13-dione (O32). To a stirred solution of diol **O30** (0.49 g, 0.73 mmol, 1.00 equiv.) in CH₂Cl₂ (37 ml) was added DMP (0.68 g, 1.61 mmol, 2.20 equiv.) at rt. After 1 h the reaction mixture was quenched by addition of a mixture of an aqu. solution of Na₂S₂O₃ and NaHCO₃ (400 ml) and H₂O (16 ml) and stirring was continued for 10 min. The phases were separated and the aqueous phase was extracted with CH₂Cl₂ (3 x 200 ml). The combined organic phases were dried over anhydrous MgSO₄, filtered and concentrated under reduced pressure to obtain the crude aldehyde mixture.

To a stirred solution of the crude aldehyde mixture in THF (243 ml) was added H₂O (6 ml), the solution was cooled to 0 °C and Ba(OH)₂•8H₂O (0.20 g, 1.17 mmol, 1.60 equiv.) was added. After 20 min Et₂O (70 ml) and sat. aqu. NaHCO₃ (70 ml) were added, the phases were separated, the aqueous phase was extracted with Et₂O (3 x 75 ml), the combined organic layers were washed with NaHCO₃ (2 x 100 ml) and brine (100 ml). The clear organic phase was dried over anhydrous MgSO₄, filtered and concentrated under reduced pressure. Purification of the residue by flash column chromatography (EtOAc/hexane 1:5 → 1:2) afforded **O32** (0.24 mg, 0.46 mmol, 63% over two steps) as a colourless oil.

TLC: R_f = 0.20 (EtOAc/hexane 1:3). **¹H-NMR** (400 MHz, CDCl₃) δ = 7.58 (dd, *J* = 15.1, 11.5 Hz, 1H), 7.25 (d, *J* = 8.6 Hz, 2H), 6.92 – 6.82 (m, 2H), 6.74 (ddd, *J* = 16.2, 9.4, 4.8 Hz, 1H), 6.10 (d, *J* = 11.5 Hz, 1H), 5.92 (dd, *J* = 15.3, 5.8 Hz, 2H), 5.35 (dq, *J* = 7.9, 5.1 Hz, 1H), 5.11 (dd, *J* = 7.6, 1.4 Hz, 1H), 4.56 – 4.41 (m, 2H), 4.28 (ddd, *J* = 10.3, 7.8, 2.2 Hz, 1H), 4.08 (d, *J* = 13.7 Hz, 1H), 3.80 (s, 3H), 3.63 (ddt, *J* = 10.4, 8.3, 1.9 Hz, 1H), 3.59 – 3.47 (m, 2H), 3.08 (d, *J* = 13.7 Hz, 1H), 2.50 (ddd, *J* = 13.4, 10.7, 2.4 Hz, 2H), 2.36 (dddd, *J* = 14.8, 10.0, 4.8, 1.9 Hz, 1H), 2.24 – 2.08 (m, 5H), 1.80 (s, 3H), 1.71 (d, *J* = 1.3 Hz, 3H). **¹³C-NMR** (101 MHz, CDCl₃) δ = 198.0, 166.8, 159.4, 145.3, 142.8, 139.3, 133.7, 131.9, 130.2, 129.4, 128.8, 125.6, 121.3, 114.0, 76.9, 76.4, 73.0, 71.5, 69.5, 55.4, 45.1, 42.5, 40.7, 30.7, 30.4, 23.8, 16.9. **IR** (film) $\tilde{\nu}$ = 3003, 2956, 2906, 2858, 1710, 1667, 1634, 1613, 1513, 1463, 1440, 1361, 1318, 1280, 1248, 1209, 1172, 1152, 1117, 1080, 1035, 977, 888, 847, 818, 753, 711, 665, 580, 514. **HRMS** (ESI) calculated for C₂₉H₃₇O₆S [(M+H)⁺]: 513.2305, found: 513.2301. $[\alpha]_D^{20}$ = –191.00° (1.00 g/100cm³ in CHCl₃).

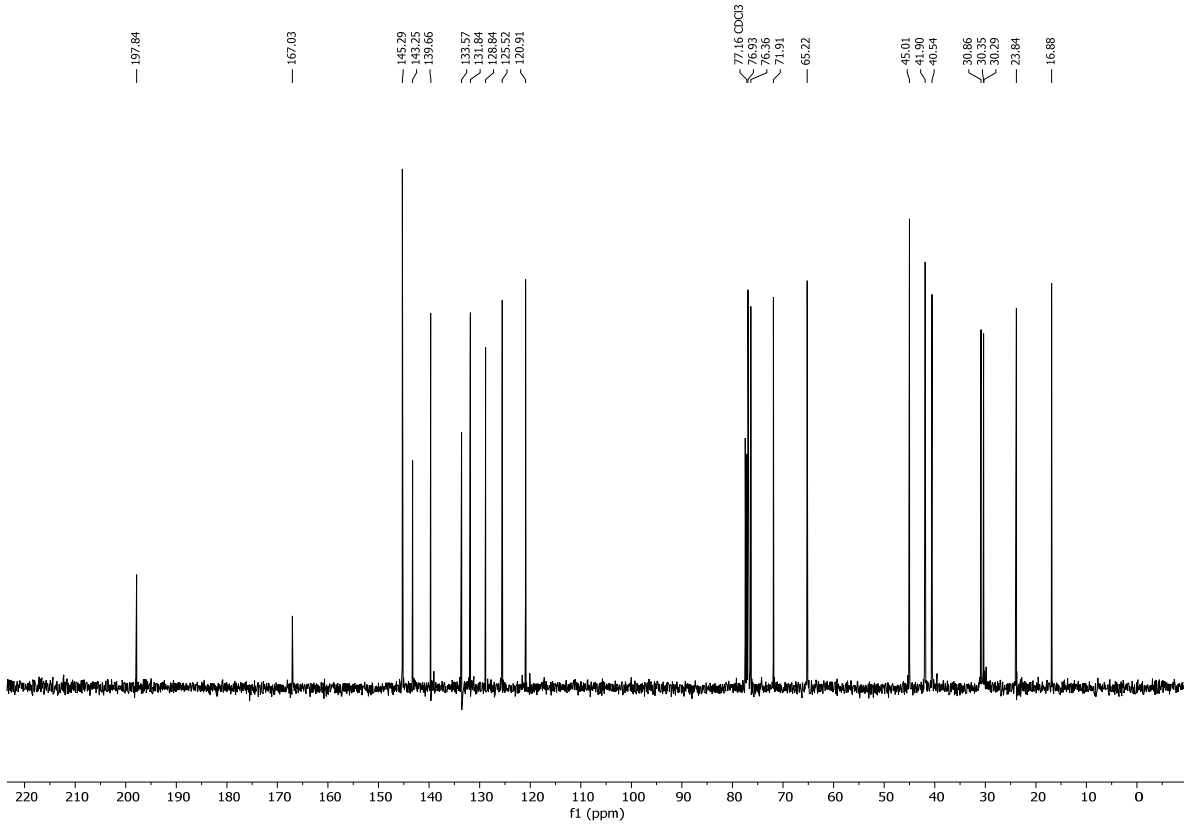
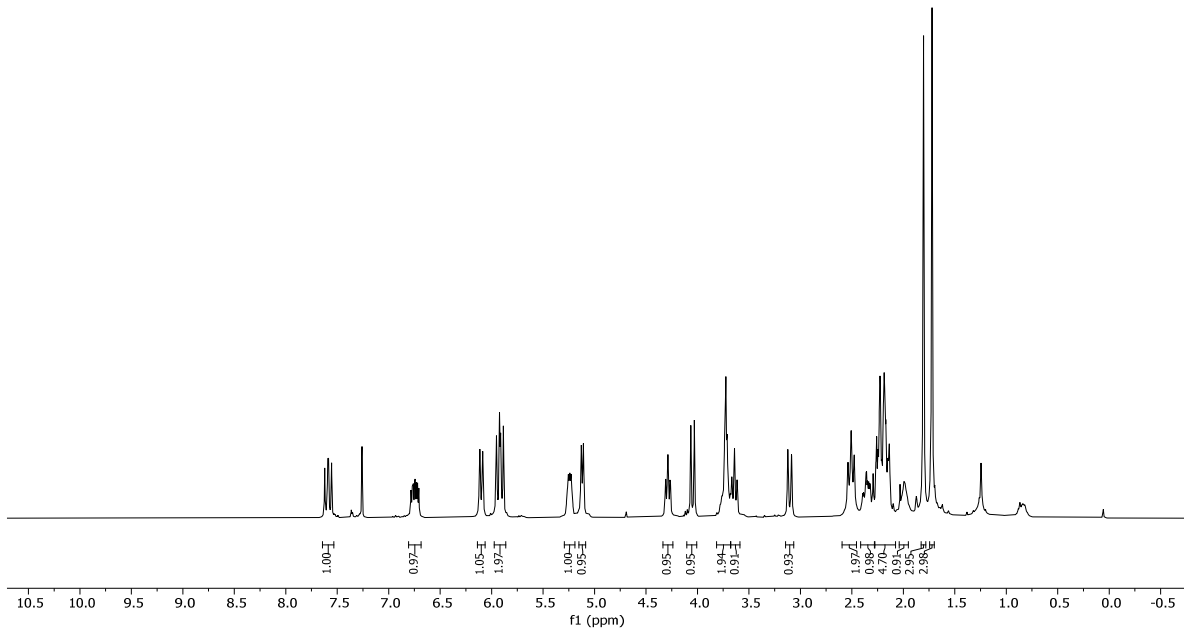


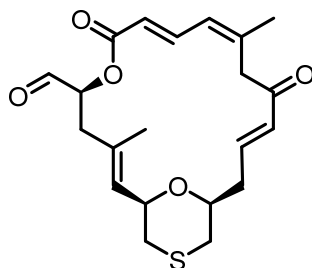


OS6

(1R,2E,5S,8E,10Z,14E,17S)-5-(hydroxymethyl)-3,11-dimethyl-6,21-dioxa-19-thiabicyclo[15.3.1]henicosa-2,8,10,14-tetraene-7,13-dione (OS6). To a solution of **O32** (40.0 mg, 0.08 mmol, 1.00 equiv.) in CH₂Cl₂ (6 mL) was added phosphate buffer (0.4 mL, pH=7) followed by DDQ (21.0 mg, 0.09 mmol, 1.20 equiv.) at room temperature. The mixture was vigorously stirred for 2 h, before again DDQ (21.0 mg, 0.09 mmol, 1.20 equiv.) was added. After a total of 5 h of stirring at rt sat. aq. NaHCO₃ (30 mL) and CH₂Cl₂ (30 mL) were added and the phases were separated. The aqueous phase was extracted with CH₂Cl₂ (3 x 30 mL), the combined organic extracts were dried over MgSO₄ and concentrated under reduced pressure. Purification of the residue by flash chromatography (EtOAc/Hex 1:3→1:2→1:1) led to **OS6** (22.0 mg, 0.06 mmol, 72%) as a viscous liquid.

TLC: R_f = 0.30 (EtOAc/hexane 1:1). **¹H-NMR** (400 MHz, CDCl₃) δ = 7.59 (dd, *J* = 15.1, 11.5 Hz, 1H), 6.75 (ddd, *J* = 16.3, 9.3, 5.0 Hz, 1H), 6.10 (d, *J* = 11.5 Hz, 1H), 5.92 (dd, *J* = 15.7, 11.2 Hz, 2H), 5.24 (dddd, *J* = 10.5, 6.3, 4.3, 2.2 Hz, 1H), 5.12 (d, *J* = 7.8 Hz, 1H), 4.29 (ddd, *J* = 10.3, 7.8, 2.2 Hz, 1H), 4.05 (d, *J* = 13.8 Hz, 1H), 3.81 – 3.68 (m, 2H), 3.68 – 3.59 (m, 1H), 3.10 (d, *J* = 13.8 Hz, 1H), 2.59 – 2.46 (m, 2H), 2.42 – 2.28 (m, 1H), 2.28 – 2.08 (m, 5H), 2.01 (d, *J* = 16.7 Hz, 1H), 1.80 (s, 3H), 1.72 (s, 3H). **¹³C-NMR** (101 MHz, CDCl₃) δ = 197.8, 167.0, 145.3, 143.3, 139.7, 133.6, 131.8, 128.8, 125.5, 120.9, 76.9, 76.4, 71.9, 65.2, 45.0, 41.9, 40.5, 30.9, 30.4, 30.3, 23.8, 16.9. **IR** (film) $\tilde{\nu}$ = 3441, 2957, 2907, 1705, 1667, 1633, 1434, 1417, 1382, 1360, 1319, 1281, 1209, 1170, 1153, 1116, 1078, 1047, 977, 913, 888, 648, 591. **HRMS** (ESI) calculated for C₂₁H₂₈NaO₅S [(M+Na)⁺]: 415.1550, found: 415.1546. $[\alpha]_D^{20}$ = -248.80° (1.00 g/100cm³ in CHCl₃).

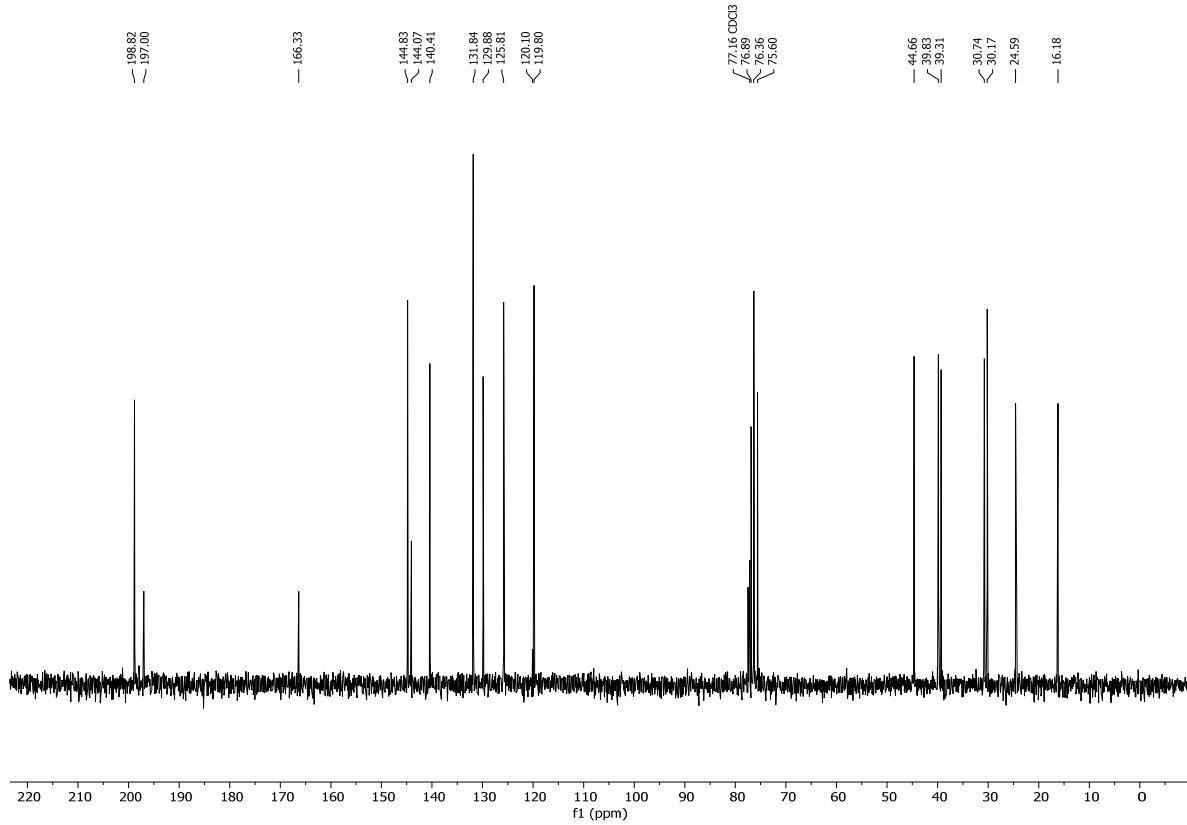
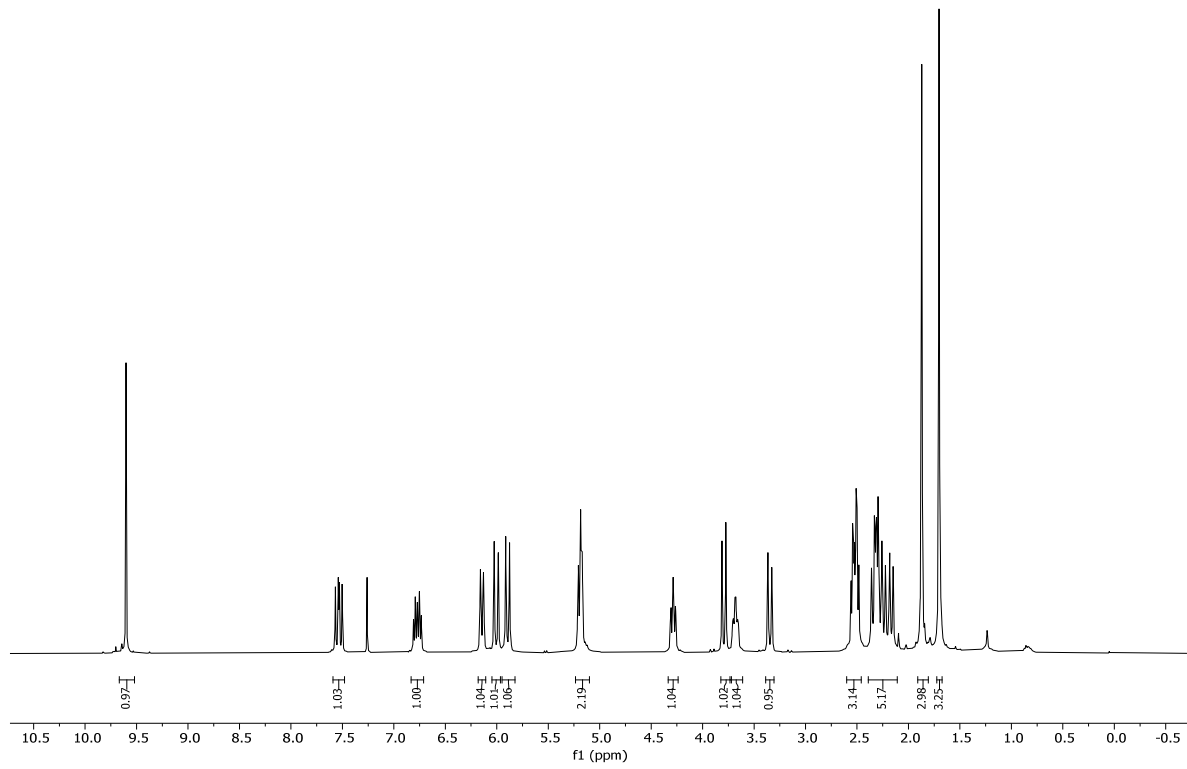


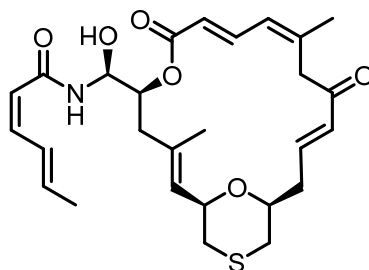


O34

(1*R*,2*E*,5*S*,8*E*,10*Z*,14*E*,17*S*)-3,11-dimethyl-7,13-dioxo-6,21-dioxa-19-thiabicyclo[15.3.1]henicosa-2,8,10,14-tetraene-5-carbaldehyde (O34). To a stirred solution of **O56** (30.0 mg, 0.08 mmol, 1.00 equiv.) in CH₂Cl₂ (7 mL) was added NaHCO₃ (19.0 mg, 0.21 mmol, 3.00 equiv.) followed by DMP (36.0 mg, 0.08 mmol, 1.10 equiv.) at rt and stirring was continued for 2 h. The reaction was quenched with a mixture of Na₂S₂O₃ and NaHCO₃ (20 mL) and stirring was continued for 10 min until two clear phases were formed. The phases were separated then the aqueous phase was extracted with CH₂Cl₂ (3 x 40 mL), the combined organic phases were dried over MgSO₄, concentrated under reduced pressure then purified using flash chromatography (EtOAc/Hex 1:1) affording **O34** (29.0 mg, 0.74 mmol, 91%) as a colourless oil.

TLC: R_f = 0.40 (EtOAc/hexane 1:1). **¹H-NMR** (400 MHz, CDCl₃) δ = 9.60 (s, 1H), 7.54 (dd, *J* = 15.2, 11.6 Hz, 1H), 6.77 (dt, *J* = 16.1, 7.3 Hz, 1H), 6.14 (d, *J* = 11.6 Hz, 1H), 6.01 (d, *J* = 16.1 Hz, 1H), 5.89 (d, *J* = 15.2 Hz, 1H), 5.24 – 5.10 (m, 2H), 4.29 (ddd, *J* = 10.3, 7.8, 2.2 Hz, 1H), 3.79 (d, *J* = 15.0 Hz, 1H), 3.68 (tdd, *J* = 10.5, 4.0, 1.9 Hz, 1H), 3.35 (d, *J* = 14.9 Hz, 1H), 2.52 (ddd, *J* = 13.6, 10.4, 6.4 Hz, 3H), 2.39 – 2.11 (m, 5H), 1.87 (s, 3H), 1.70 (s, 3H). **¹³C-NMR** (101 MHz, CDCl₃) δ = 198.8, 197.0, 166.3, 144.8, 144.1, 140.4, 131.8, 129.9, 125.8, 120.1, 119.8, 76.9, 76.4, 75.6, 44.7, 39.8, 39.3, 30.7, 30.2, 24.6, 16.2. **IR** (film) $\tilde{\nu}$ = 3017, 2908, 2856, 1734, 1703, 1669, 1634, 1433, 1379, 1356, 1324, 1253, 1207, 1170, 1150, 1115, 1081, 1048, 977, 888, 811, 755, 713, 664, 531. **HRMS** (ESI) calculated for C₂₁H₂₆NaO₅S [(M+Na)⁺]: 413.1393, found: 413.1399. $[\alpha]_D^{20}$ = -179.96° (1.00 g/100cm³ in CHCl₃).





O5

(2Z,4E)-N-((S)-((1R,2E,5S,8E,10Z,14E,17S)-3,11-dimethyl-7,13-dioxo-6,21-dioxa-19-thiabiacyclo[15.3.1]henicosa-2,8,10,14-tetraen-5-yl)(hydroxy)methyl)hexa-2,4-dienamide (O5).

Preparation of stock solution of (S)-BINAL-sorbamide complex: Reagents and reactants were dried in flasks used to prepare solutions in high vacuum over night. LAH (25.0 mg, 0.69 mmol, 10.00 equiv.) was suspended in dry THF (2 ml) at rt. Dry EtOH (41 μ L, 0.69 mmol, 10.00 equiv.) was diluted with THF (2 ml) and the mixture was added slowly at rt to the LAH suspension. (S)-BINOL (198.0 mg, 0.69 mmol, 10.00 equiv.) was added as a solution in THF (2 ml) followed by (2E,4Z)-sorbamide **O14a**^[68] (77.0 mg, 0.69 mmol, 10.00 equiv.) in THF (2 ml) to give a gray mixture.

1.6 ml of the stock solution containing the putative amide transfer complex (0.14 mmol, 2.00 equiv.) was added immediately to a solution of aldehyde **O34** (27.0 mg, 0.07 mmol, 1.00 equiv.) in THF (1 ml) and the mixture was stirred at rt. Additional 1.6 ml of stock solution (0.17 mmol, 2.00 equiv.) were added after 20 min. After 40 min another 0.8 mL of stock solution (0.07 mmol, 1.00 equiv.) were added and stirring was continued. The reaction mixture was quenched by addition of sat. aqu. NaHCO₃ solution (7 ml) after 75 min and the mixture was stirred until two clear phases have formed (approx. 10 min). The phases were separated and the aqueous phase was extracted with EtOAc (3 x 10 ml), the combined organic phases were dried over anhydrous MgSO₄ and concentrated under reduced pressure. The residue was purified by flash column chromatography (EtOAc/Hex 1:3 \rightarrow 1:2, 2% Et₃N) and subsequent normal phase preparative HPLC (10% \rightarrow 80% propan-2-ol in hexane in 15 min, 15 ml/min) affording **O5** (14.0 mg, 0.03 mmol, 40%) as a colourless film.

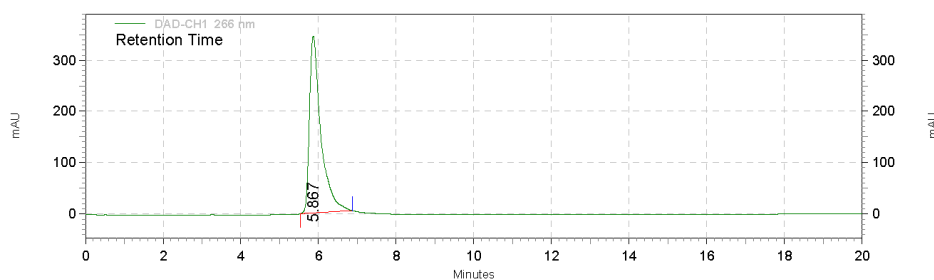
TLC: R_f = 0.40 (EtOAc/hexane 1:1.3). **¹H-NMR** (400 MHz, DMSO-*d*₆) δ = 8.28 (d, *J* = 8.9 Hz, 1H), 7.54 – 7.37 (m, 2H), 6.70 (ddd, *J* = 16.0, 8.3, 5.8 Hz, 1H), 6.36 (t, *J* = 11.3 Hz, 1H), 6.18 (d, *J* = 11.6 Hz, 1H), 6.12 (s, 1H), 6.02 – 5.84 (m, 3H), 5.63 (d, *J* = 11.4 Hz, 1H), 5.37 – 5.28 (m, 1H), 5.07 (d, *J* = 7.5 Hz, 1H), 4.93 (ddd, *J* = 8.7, 6.2, 2.2 Hz, 1H), 4.16 (ddd, *J* = 10.2, 7.6, 2.2 Hz, 1H), 4.03 (d, *J* = 14.6 Hz, 1H), 3.60 (tt, *J* = 9.4, 2.8 Hz, 1H), 3.14 (d, *J* = 14.6 Hz, 1H), 2.47 – 2.18 (m, 7H), 2.11 (dd, *J* = 13.7, 9.6 Hz, 1H), 1.78 (dd, *J* = 6.8, 1.7 Hz, 3H), 1.75 (s, 3H), 1.62 (s, 3H). **¹³C-NMR** (101 MHz,

DMSO- d_6) δ = 197.1, 165.5, 165.2, 145.1, 143.1, 140.6, 139.7, 137.2, 133.5, 131.0, 128.6, 128.5, 125.1, 120.4, 119.2, 76.6, 75.7, 72.7, 72.0, 44.7, 40.5, 40.2, 29.7, 29.4, 23.9, 18.3, 16.9. IR (film) $\tilde{\nu}$ = 3324, 2910, 2852, 1709, 1665, 1636, 1604, 1523, 1432, 1358, 1281, 1258, 1209, 1153, 1078, 1050, 1026, 1001, 979, 927, 887, 836, 753, 711, 663, 612, 548, 512. HRMS (ESI) calculated for $C_{27}H_{35}NNaO_6S$ $[(M+Na)^+]$: 524.2077, found: 524.2067. $[\alpha]_D^{20} = -171.97^\circ$ (1.00 g/100cm³ in CHCl₃).

Page 1 of 1

Area % Report

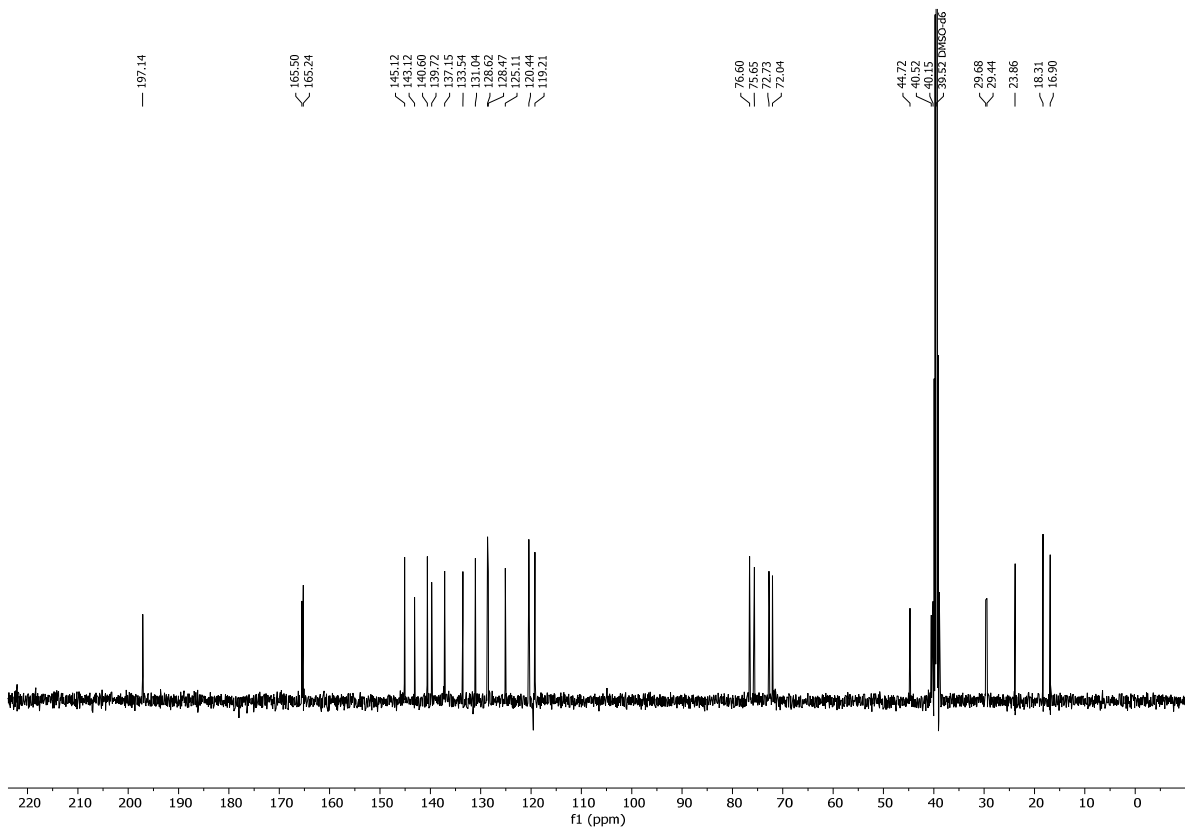
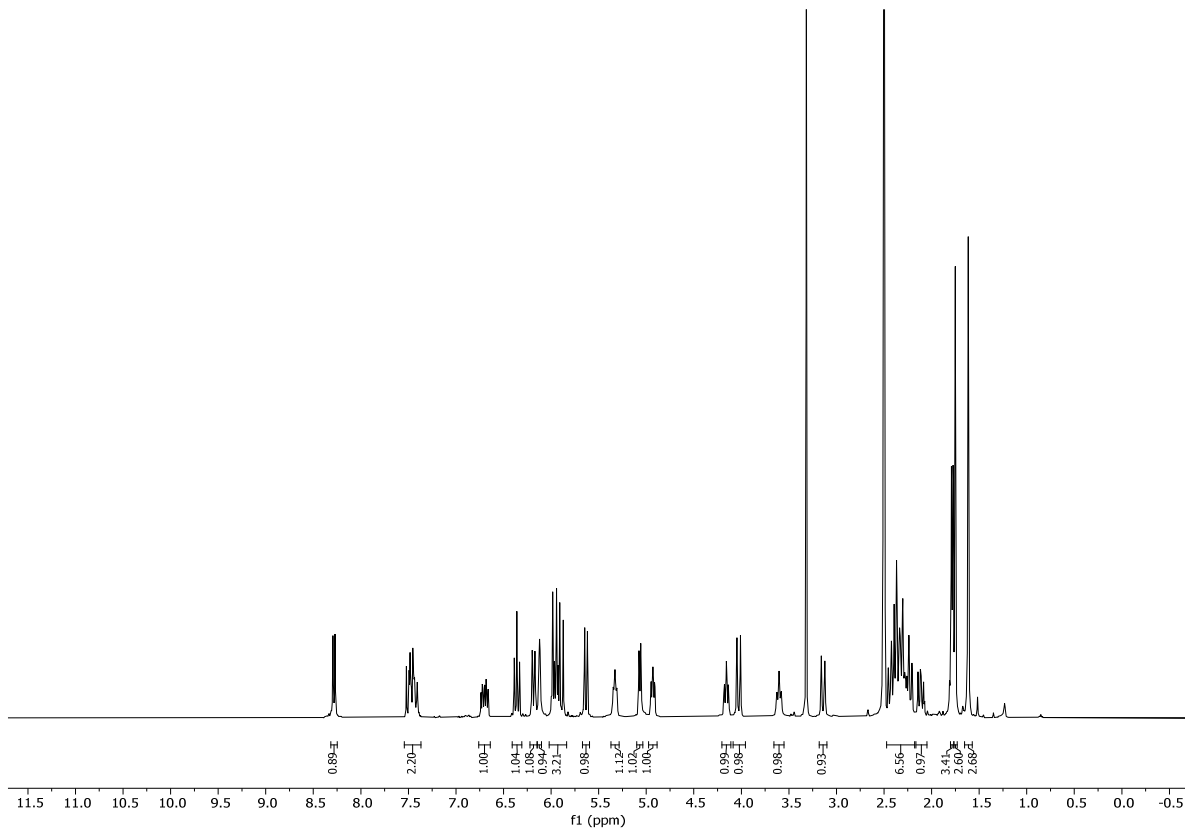
Data File: C:\EZChrom Elite\Enterprise\Projects\Etienne\EC-152-2-after-prep-trace
 Method: C:\EZChrom Elite\Enterprise\Projects\Default\Method\Etienne C\EC-10-80_15min.met
 Acquired: 04.04.2023 12:25:59
 Printed: 04.04.2023 12:35:08

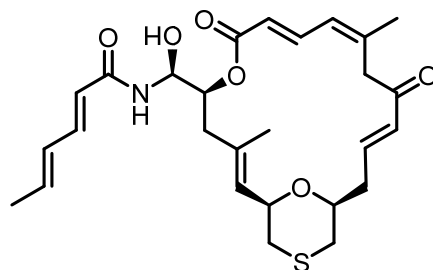


**DAD-CH1 266
nm Results**

| Retention Time | Area | Area % | Height | Height % |
|----------------|----------|--------|---------|----------|
| 5.867 | 27992908 | 100.00 | 1378406 | 100.00 |
| Totals | 27992908 | 100.00 | 1378406 | 100.00 |

The normal phase analytical HPLC trace shown above was measured with the Elite LaChrom device mentioned in the general part. A gradient of 10% → 80% propan-2-ol in hexane in 15 min, with a flow rate of 1 mL/min was used. The material thus obtained was used in the biological experiments.





07

(2E,4E)-N-((S)-((1R,2E,5S,8E,10Z,14E,17S)-3,11-dimethyl-7,13-dioxo-6,21-dioxa-19-thiabiacyclo[15.3.1]henicosa-2,8,10,14-tetraen-5-yl)(hydroxy)methyl)hexa-2,4-dienamide (07).

Preparation of stock solution of (S)-BINAL-sorbamide complex: Reagents and reactants were dried in flasks used to prepare solutions in high vacuum over night. LAH (20.0 mg, 0.54 mmol, 10.00 equiv.) was suspended in dry THF (2 ml) at rt. Dry EtOH (32 μ L, 0.54 mmol, 10.00 equiv.) was diluted with THF (2 ml) and the mixture was added slowly at rt to the LAH suspension. (S)-BINOL (154.0 mg, 0.54 mmol, 10.00 equiv.) was added as a solution in THF (2 ml) followed by (2E,4E)-sorbamide **O14b**^[315] (60.0 mg, 0.54 mmol, 10.00 equiv.) in THF (2 ml) to give a gray mixture.

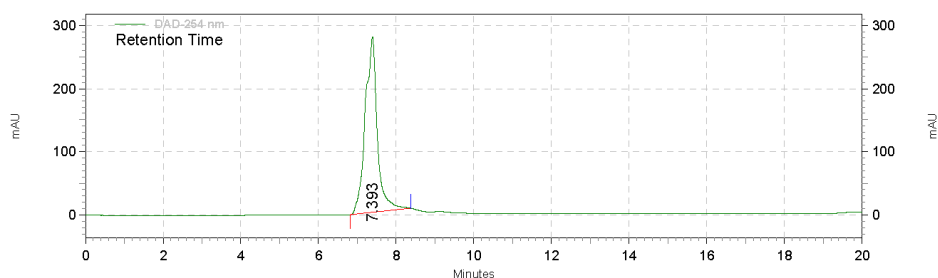
1.6 ml of the stock solution containing the putative amide transfer complex (0.11 mmol, 2.00 equiv.) was added immediately to a solution of aldehyde **O34** (21.0 mg, 0.05 mmol, 1.00 equiv.) in THF (1 ml) and the mixture was stirred at rt. Additional 1.6 ml of stock solution (0.11 mmol, 2.00 equiv.) were added after 20 min. After 40 min another 0.8 mL of stock solution (0.05 mmol, 1.00 equiv.) were added and stirring was continued. The reaction mixture was quenched by addition of sat. aq. NaHCO₃ solution (10 ml) after 75 min and the mixture was stirred until two clear phases have formed (approx. 10 min). The phases were separated and the aqueous phase was extracted with EtOAc (3 x 10 ml), the combined organic phases were dried over anhydrous MgSO₄ and concentrated under reduced pressure. The residue was purified by flash column chromatography (EtOAc/Hex 1:3 \rightarrow 1:1 \rightarrow 1:2, 2% Et₃N) and subsequent normal phase preparative HPLC (10% \rightarrow 80% propan-2-ol in hexane in 15 min, 15 ml/min) affording **O7** (9.9 mg, 0.02 mmol, 38% calculated yield) as a colourless film. This material contained additional 13 mol% of **O5** and 22 mol% of (2E,4E)-sorbamide. The presence of **O5** is due to minor contamination of **O14b** with **O14a**. In order to remove these impurities further purifications were done: second normal phase prep HPLC (5% \rightarrow 40% propan-2-ol in hexane in 30 min, 15 ml/min), second column (EtOAc/Hex 1:5 \rightarrow 1:2, 2% Et₃N), third column (EtOAc/Hex 1:6 \rightarrow 1:3, 2% Et₃N), third HPLC (10% \rightarrow 80% propan-2-ol in hexane in 15 min, 15 ml/min). After this extensive purification steps **O7** (1.2 mg, 0.0024 mmol, 5%) was isolated with no detectable impurities of **O5** or (2E,4E)-sorbamide.

In order to prove that the double bond isomerization did not happen during the reaction itself, a stock solution was prepared using the same procedure as above, but using (2*Z*,4*E*)-sorbamide with no contamination of (2*E*,4*E*)-sorbamide (according to ¹H-NMR spectroscopy). This stock solution was quenched after 3 hours at rt, the crude was purified using normal phase HPLC and analyzed by ¹H-NMR spectroscopy. No isomerization of the double bond was observed.

TLC: R_f = 0.40 (EtOAc/hexane 1:1.3). **¹H-NMR** (400 MHz, DMSO-*d*₆) δ = 8.31 (d, *J* = 8.9 Hz, 1H), 7.48 (dd, *J* = 15.1, 11.5 Hz, 1H), 7.02 (dd, *J* = 15.2, 10.5 Hz, 1H), 6.70 (dt, *J* = 14.7, 7.2 Hz, 1H), 6.24 – 6.10 (m, 3H), 5.95 (d, *J* = 15.5 Hz, 2H), 5.89 (d, *J* = 15.0 Hz, 1H), 5.36 (t, *J* = 7.7 Hz, 1H), 5.05 (d, *J* = 7.5 Hz, 1H), 4.94 (t, *J* = 8.0 Hz, 1H), 4.16 (t, *J* = 9.2 Hz, 1H), 4.06 (d, *J* = 14.5 Hz, 1H), 3.59 (s, 1H), 3.10 (d, *J* = 14.7 Hz, 1H), 2.45 – 2.16 (m, 7H), 2.15 – 2.05 (m, 1H), 1.79 (d, *J* = 6.4 Hz, 4H), 1.75 (s, 3H), 1.61 (s, 3H). **¹³C-NMR** (126 MHz, DMSO-*d*₆) δ = 197.2, 197.1, 167.5, 165.5, 165.5, 165.2, 165.0, 145.1, 145.1, 143.1, 143.1, 140.6, 140.2, 139.9, 139.7, 139.6, 139.6, 137.1, 137.0, 136.7, 133.5, 133.4, 131.1, 131.0, 129.9, 128.6, 128.5, 128.5, 125.1, 122.9, 122.8, 120.5, 120.4, 119.3, 119.2, 76.6, 75.6, 73.0, 72.0, 44.7, 44.7, 40.6, 39.8, 29.7, 29.4, 23.8, 18.3, 18.2, 16.8. **IR** (film) $\tilde{\nu}$ = 3338, 3324, 2965, 2909, 1711, 1665, 1634, 1527, 1435, 1357, 1320, 1281, 1257, 1209, 1152, 1119, 1077, 1047, 998, 978, 888, 866, 764, 750, 719, 664, 621, 583, 543. **HRMS** (ESI) calculated for C₂₇H₃₅NNaO₆S [(M+Na)⁺]: 524.2077, found: 524.2070. $[\alpha]_D^{20}$ = -178.96° (1.00 g/100cm³ in CHCl₃).

Area % Report

Data File: C:\EZChrom Elite\Enterprise\Projects\Etienne\EC-152-1-after-prep-trace4
 Method: C:\EZChrom Elite\Enterprise\Projects\Default\Method\Etienne
 C\EC-10-80_15min-EC-152-1-report.met
 Acquired: 17.03.2023 15:51:07
 Printed: 17.03.2023 15:54:19

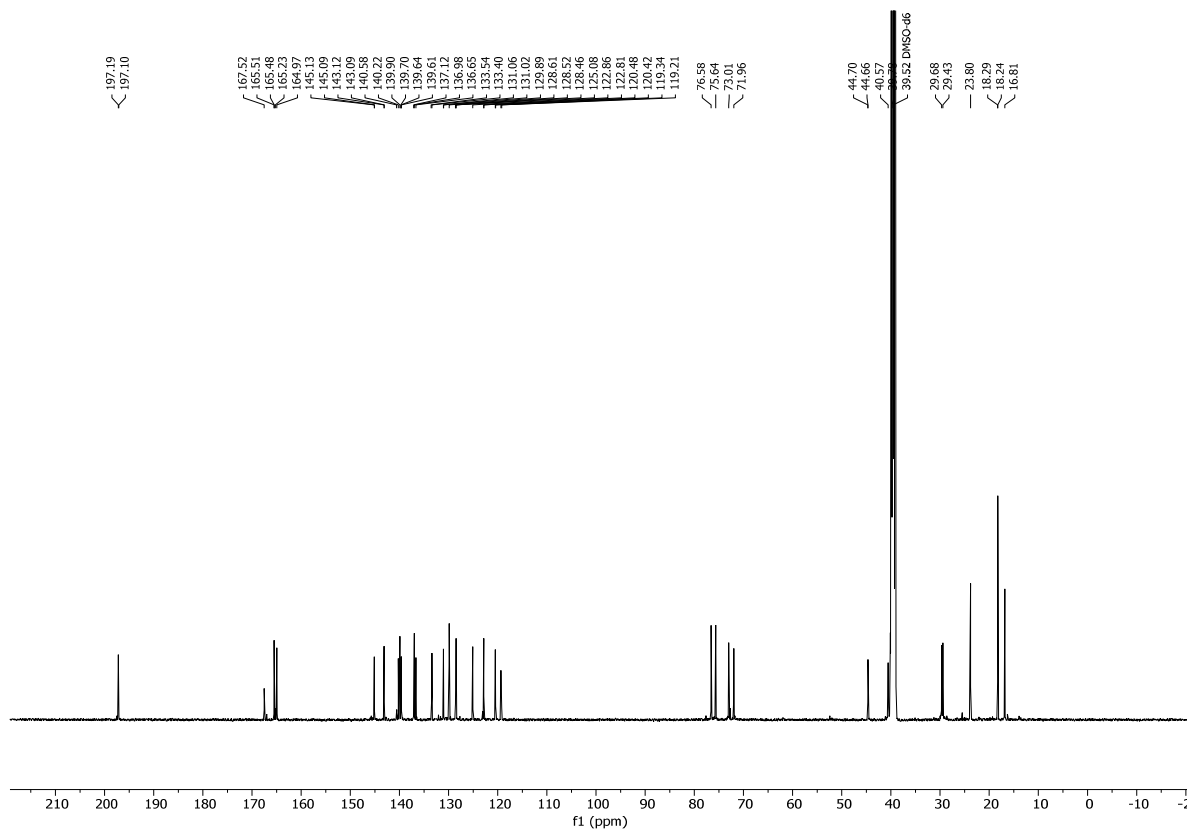
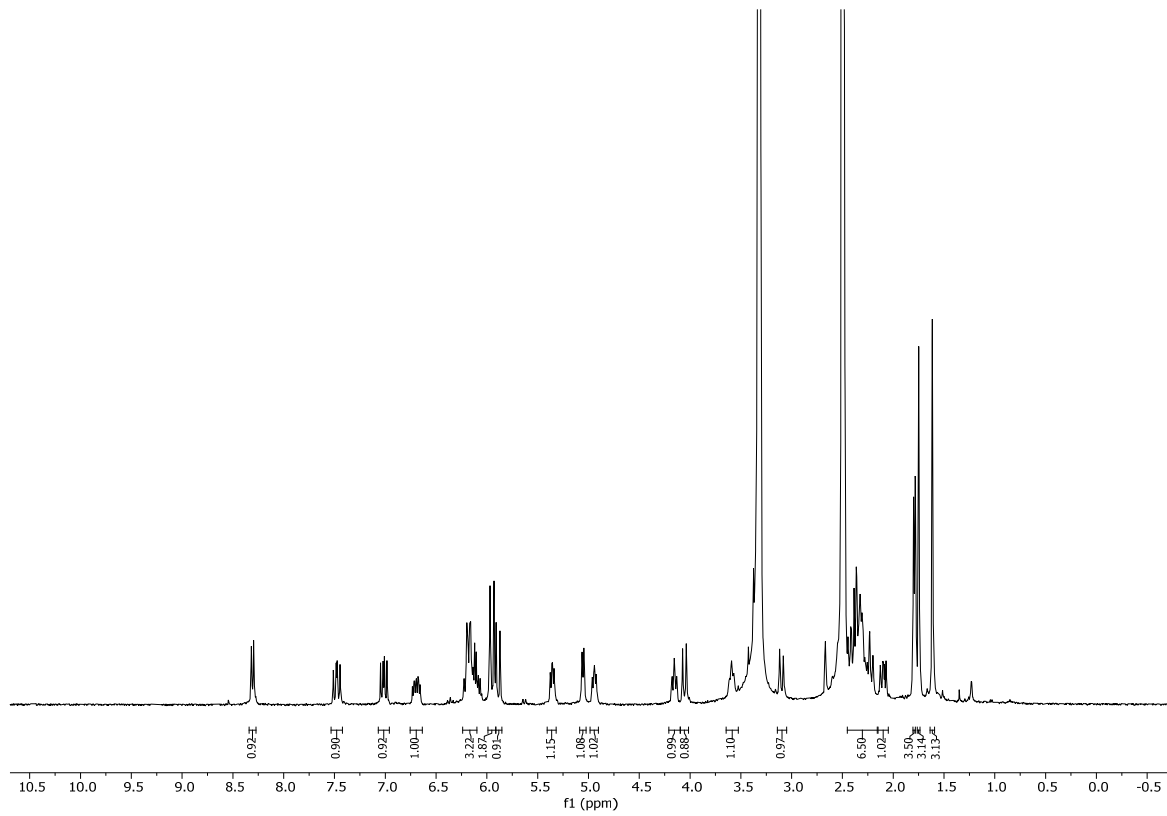


DAD-254 nm

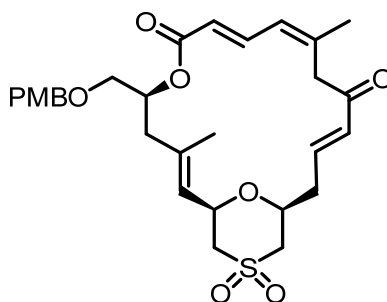
Results

| Retention Time | Area | Area % | Height | Height % |
|----------------|----------|--------|---------|----------|
| 7.393 | 23916150 | 100.00 | 1111496 | 100.00 |
| Totals | 23916150 | 100.00 | 1111496 | 100.00 |

The normal phase analytical HPLC trace shown above was measured with the Elite LaChrom device mentioned in the general part. A gradient of 10% → 80% propan-2-ol in hexane in 15 min, with a flow rate of 1 mL/min was used. The material thus obtained was used in the biological experiments.



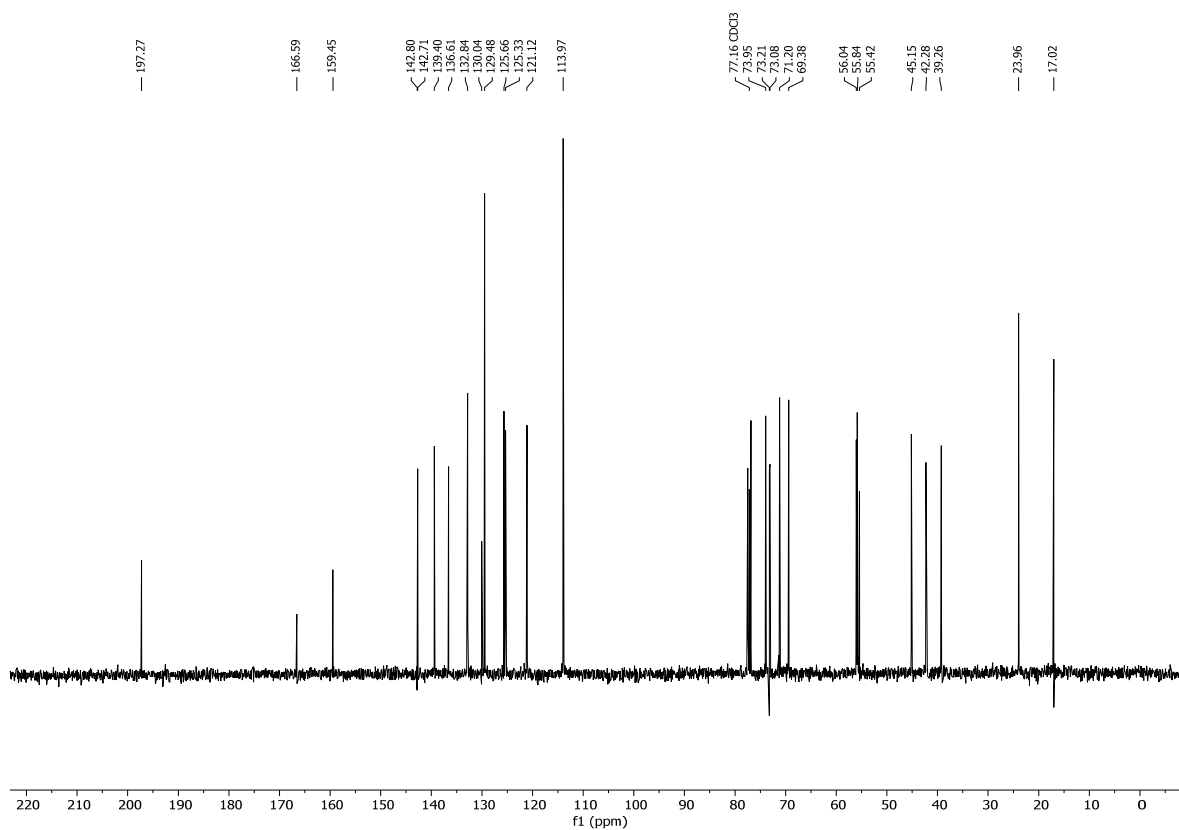
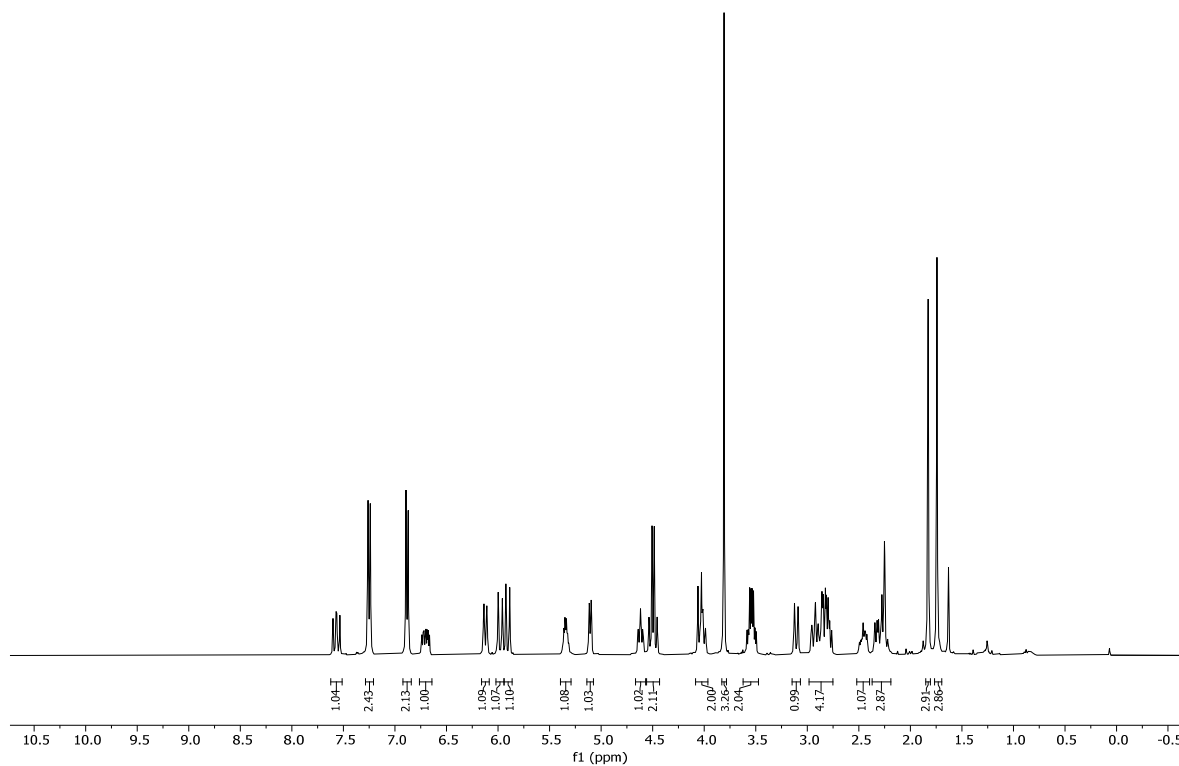
4.2.2.5 Synthesis of Analog 6 and 8

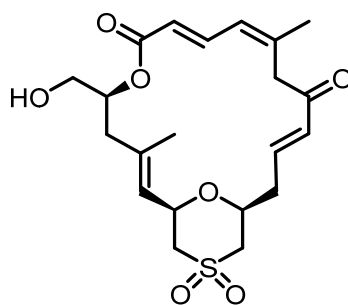


OS7

(1*R*,2*E*,5*S*,8*E*,10*Z*,14*E*,17*S*)-5-(((4-methoxybenzyl)oxy)methyl)-3,11-dimethyl-6,21-dioxo-19-thiabiacyclo[15.3.1]hencosa-2,8,10,14-tetraene-7,13-dione 19,19-dioxide (OS7). **O32** (195.0 mg, 0.38 mmol, 1.00 equiv.) was dissolved in CH₂Cl₂ (0.8 mL) and the solution was cooled to –35 °C, before a solution of *m*-CPBA (144.0 mg, of pure reagent, 0.84 mmol, 2.20 equiv.) in CH₂Cl₂ (1.7 mL) was added over 5 minutes. The reaction mixture was stirred for 2 h at that temperature before the cooling bath was removed, CH₂Cl₂ (4 mL) and 3M NaOH (4 mL) were added, the phases were separated, the organic phase was washed with 3M NaOH (2 x 5 mL), the combined aqueous phase was extracted with CH₂Cl₂ (3 x 15 mL), the combined organic phase was washed with H₂O (15 mL) and brine (15 mL), the organic extracts were dried over MgSO₄, concentrated under reduced pressure, and the residue purified by flash chromatography (EtOAc/hexane 1:2 → 1:1) to give **OS7** (162.0 mg, 0.30 mmol, 78%) as a colorless oil.

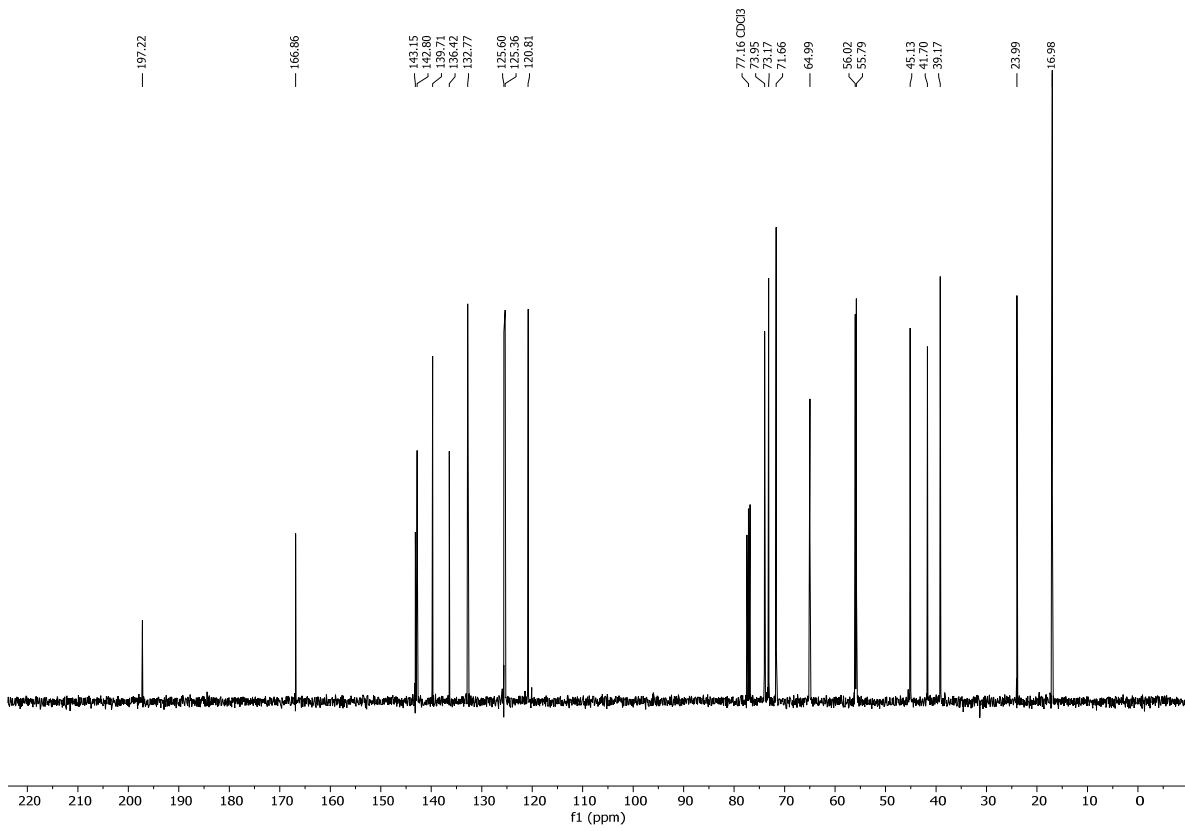
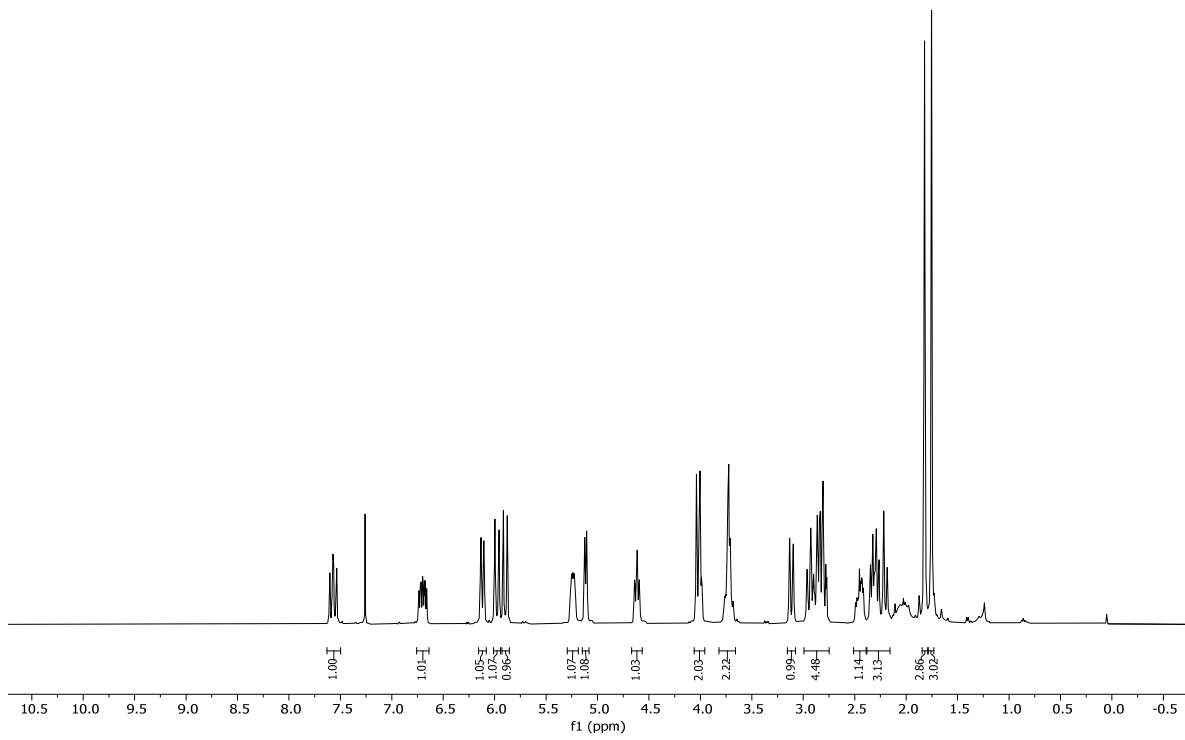
TLC: *R*_f = 0.40 (EtOAc/hexane 1:1). **¹H-NMR** (400 MHz, CDCl₃) δ = 7.57 (dd, *J* = 15.1, 11.5 Hz, 1H), 7.29 – 7.21 (m, 2H), 6.92 – 6.84 (m, 2H), 6.70 (ddd, *J* = 16.1, 8.9, 5.2 Hz, 1H), 6.12 (d, *J* = 11.5 Hz, 1H), 5.98 (d, *J* = 16.2 Hz, 1H), 5.90 (d, *J* = 15.0 Hz, 1H), 5.35 (dt, *J* = 9.5, 4.6 Hz, 1H), 5.11 (d, *J* = 7.8 Hz, 1H), 4.62 (ddd, *J* = 10.6, 7.8, 2.5 Hz, 1H), 4.56 – 4.43 (m, 2H), 4.08 – 3.96 (m, 2H), 3.81 (s, 3H), 3.54 (qd, *J* = 10.3, 5.3 Hz, 2H), 3.11 (d, *J* = 13.8 Hz, 1H), 2.98 – 2.75 (m, 4H), 2.52 – 2.40 (m, 1H), 2.37 – 2.19 (m, 3H), 1.83 (s, 3H), 1.74 (s, 3H). **¹³C-NMR** (101 MHz, CDCl₃) δ = 197.3, 166.6, 159.5, 142.8, 142.7, 139.4, 136.6, 132.8, 130.0, 129.5, 125.7, 125.3, 121.1, 114.0, 74.0, 73.2, 73.1, 71.2, 69.4, 56.0, 55.8, 55.4, 45.2, 42.3, 39.3, 24.0, 17.0. **IR** (film) $\tilde{\nu}$ = 2928, 2911, 2867, 1708, 1669, 1634, 1613, 1513, 1456, 1440, 1361, 1331, 1300, 1281, 1247, 1211, 1176, 1151, 1136, 1122, 1087, 1033, 978, 913, 885, 821, 781, 731, 648, 578, 543, 521, 496, 459. **HRMS** (ESI) calculated for C₂₉H₃₆NaO₈S [(M+Na)⁺]: 567.2023, found: 567.2016. $[\alpha]_D^{20}$ = –155.97° (1.00 g/100cm³ in CHCl₃).

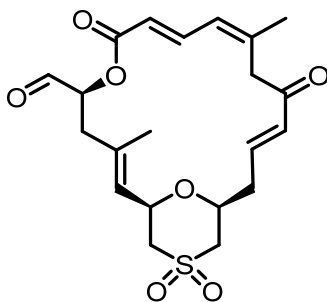


**OS8**

(1R,2E,5S,8E,10Z,14E,17S)-5-(hydroxymethyl)-3,11-dimethyl-6,21-dioxa-19-thiabicyclo[15.3.1]henicosa-2,8,10,14-tetraene-7,13-dione 19,19-dioxide (OS8). To a solution of **OS7** (50.0 mg, 0.09 mmol, 1.00 equiv.) in CH₂Cl₂ (7 mL) was added phosphate buffer (0.5 mL, pH=7) followed by DDQ (63.0 mg, 0.28 mmol, 3.00 equiv.) at rt. The mixture was vigorously stirred for 1 h, before again DDQ (63 mg, 0.28 mmol, 3.00 equiv.) was added. After a total of 3 h of stirring at rt sat. aqu. NaHCO₃ (35 mL) and CH₂Cl₂ (35 mL) were added and the phases were separated. The aqueous phase was extracted with CH₂Cl₂ (3 x 35 mL), the combined organic extracts were dried over MgSO₄ and concentrated under reduced pressure. Purification of the residue by flash chromatography (EtOAc/Hex 1:1→ EtOAc) led to **OS8** (34.0 mg, 0.08 mmol, 87%) as a viscous liquid.

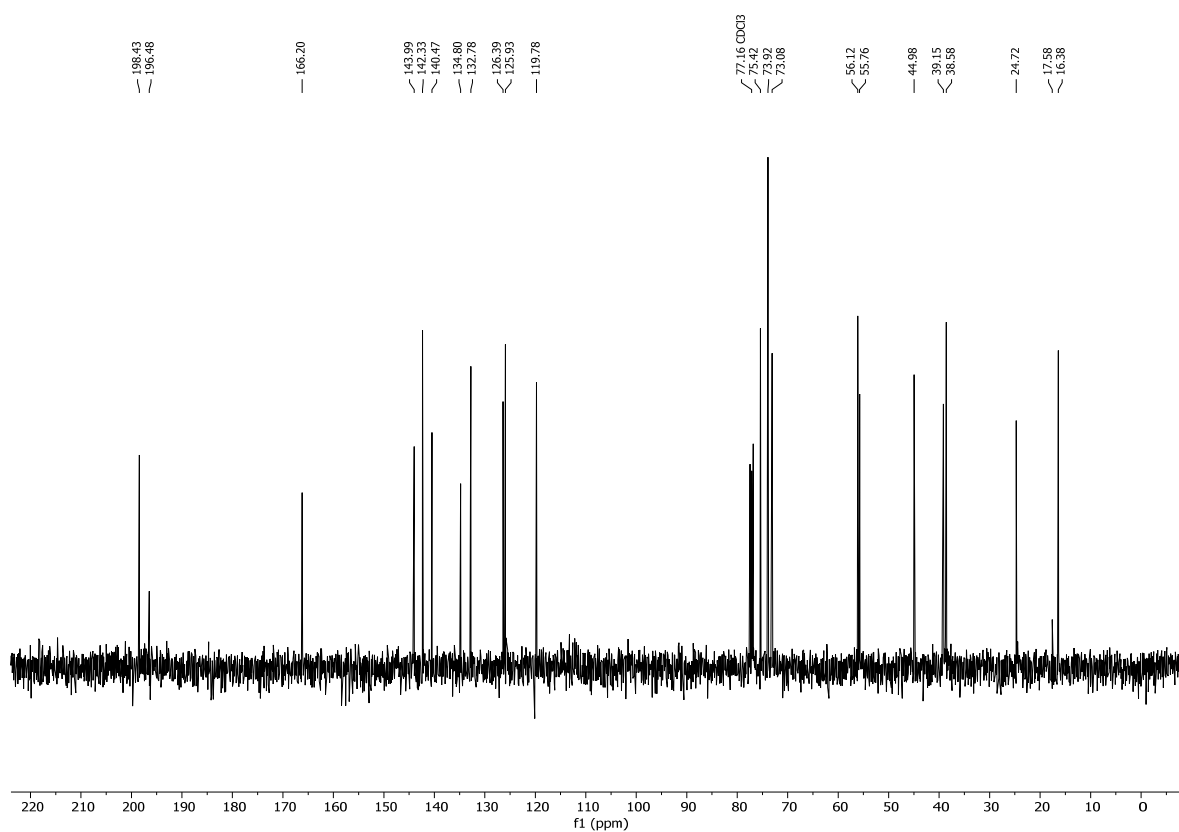
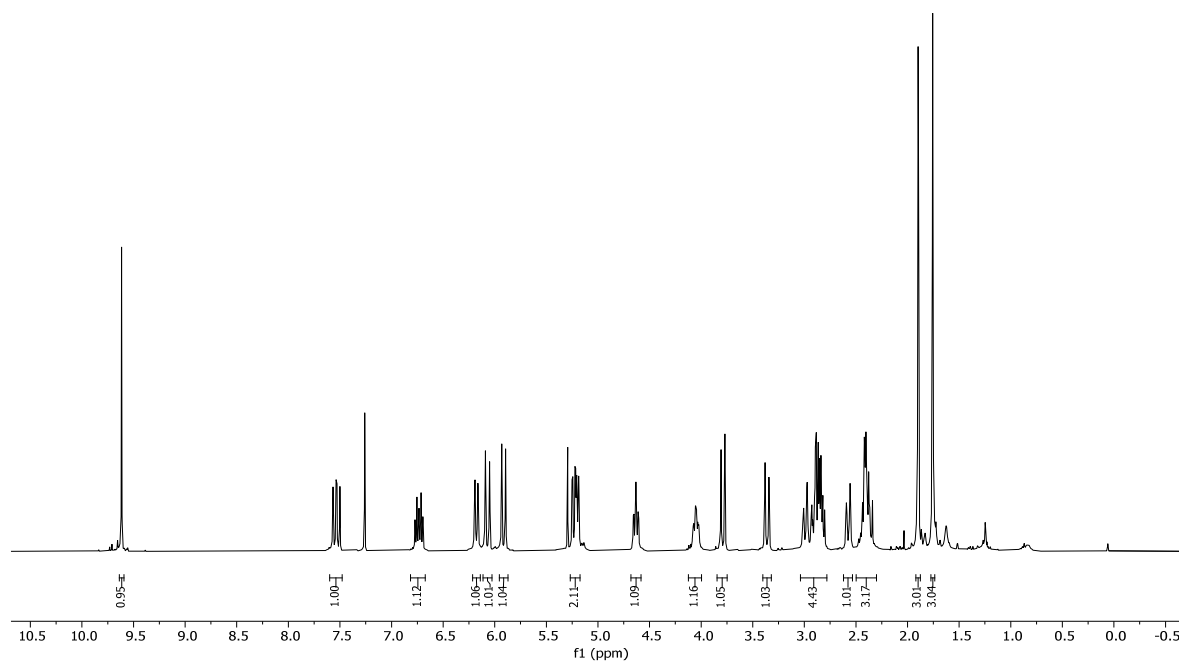
TLC: R_f = 0.65 (EtOAc). **¹H-NMR** (400 MHz, CDCl₃) δ = 7.57 (ddd, *J* = 14.9, 11.5, 2.2 Hz, 1H), 6.70 (ddd, *J* = 15.7, 8.7, 5.3 Hz, 1H), 6.12 (d, *J* = 11.5 Hz, 1H), 5.98 (d, *J* = 16.2 Hz, 1H), 5.90 (d, *J* = 15.0 Hz, 1H), 5.24 (dtt, *J* = 10.6, 4.3, 2.3 Hz, 1H), 5.12 (d, *J* = 7.7 Hz, 1H), 4.61 (ddd, *J* = 10.3, 7.8, 2.4 Hz, 1H), 4.06 – 3.96 (m, 2H), 3.82 – 3.66 (m, 2H), 3.12 (d, *J* = 13.8 Hz, 1H), 2.99 – 2.75 (m, 4H), 2.51 – 2.39 (m, 1H), 2.38 – 2.16 (m, 3H), 1.82 (s, 3H), 1.75 (s, 3H). **¹³C-NMR** (101 MHz, CDCl₃) δ = 197.2, 166.9, 143.2, 142.8, 139.7, 136.4, 132.8, 125.6, 125.4, 120.8, 74.0, 73.2, 71.7, 65.0, 56.0, 55.8, 45.1, 41.7, 39.2, 24.0, 17. **IR** (film) $\tilde{\nu}$ = 3511, 3020, 2925, 1705, 1669, 1633, 1433, 1359, 1331, 1297, 1283, 1259, 1212, 1179, 1152, 1137, 1121, 1087, 1045, 978, 885, 755, 713, 664, 599, 547, 520. **HRMS** (ESI) calculated for C₂₁H₂₈NaO₇S [(M+Na)⁺]: 447.1448, found: 447.1441. $[\alpha]_D^{20}$ = –120.98° (1.00 g/100cm³ in CHCl₃).

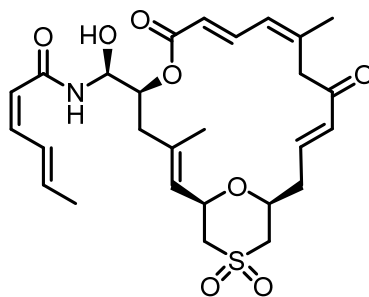


**O35**

(1R,2E,5S,8E,10Z,14E,17S)-3,11-dimethyl-7,13-dioxo-6,21-dioxa-19-thiabicyclo[15.3.1]henicosa-2,8,10,14-tetraene-5-carbaldehyde 19,19-dioxide (O35). To a stirred solution of **OS8** (30.0 mg, 0.07 mmol, 1.00 equiv.) in CH₂Cl₂ (7 mL) was added NaHCO₃ (89.0 mg, 1.06 mmol, 15.00 equiv.) followed by DMP (180.0 mg, 0.42 mmol, 6.00 equiv.) at rt and stirring was continued for 1 h; then NaHCO₃ (89.0 mg, 1.06 mmol, 15.00 equiv.) and DMP (180.0 mg, 0.42 mmol, 6.00 equiv.) were added to the reaction mixture. The reaction was quenched after 2 h with a mixture of Na₂S₂O₃ and NaHCO₃ (70 mL) and stirring was continued for 10 min until two clear phases were formed. The phases were separated, the aqueous phase was extracted with CH₂Cl₂ (3 x 70 mL), the combined organic phases were dried over MgSO₄, concentrated under reduced pressure then purified using flash chromatography (EtOAc/Hex 1:1) affording **O35** (23.0 mg, 0.07 mmol, 77%) of a colourless oil.

TLC: R_f = 0.60 (EtOAc/hexane 5:1). **¹H-NMR** (400 MHz, CDCl₃) δ = 9.62 (s, 1H), 7.53 (dd, *J* = 15.1, 11.5 Hz, 1H), 6.73 (dt, *J* = 16.0, 7.3 Hz, 1H), 6.18 (d, *J* = 11.5 Hz, 1H), 6.07 (d, *J* = 16.2 Hz, 1H), 5.91 (d, *J* = 15.1 Hz, 1H), 5.27 – 5.17 (m, 2H), 4.63 (ddd, *J* = 10.5, 7.8, 2.6 Hz, 1H), 4.12 – 4.00 (m, 1H), 3.79 (d, *J* = 14.9 Hz, 1H), 3.36 (d, *J* = 15.0 Hz, 1H), 3.04 – 2.78 (m, 4H), 2.62 – 2.53 (m, 1H), 2.50 – 2.30 (m, 3H), 1.90 (d, *J* = 1.3 Hz, 3H), 1.76 (d, *J* = 1.3 Hz, 3H). **¹³C-NMR** (101 MHz, CDCl₃) δ = 198.4, 196.5, 166.2, 144.0, 142.3, 140.5, 134.8, 132.8, 126.4, 125.9, 119.8, 75.4, 73.9, 73.1, 56.1, 55.8, 45.0, 39.2, 38.6, 24.7, 17.6, 16.4. **IR** (film) $\tilde{\nu}$ = 3021, 2925, 2853, 1734, 1703, 1671, 1634, 1435, 1357, 1330, 1300, 1277, 1247, 1208, 1181, 1137, 1122, 1087, 1047, 978, 885, 753, 714, 664, 542, 521, 505. **HRMS** (ESI) calculated for C₂₁H₂₇O₇S [(M+H)⁺]: 423.1472, found: 423.1465. $[\alpha]_D^{20}$ = –60.00° (1.00 g/100cm³ in CHCl₃).





O6

(2Z,4E)-N-((S)-((1R,2E,5S,8E,10Z,14E,17S)-3,11-dimethyl-19,19-dioxido-7,13-dioxo-6,21-dioxo-19-thiabicyclo[15.3.1]heneicosa-2,8,10,14-tetraen-5-yl)(hydroxy)methyl)hexa-2,4-dienamide

(O6). Preparation of stock solution of (S)-BINAL-sorbamide complex: Reagents and reactants were dried in flasks used to prepare solutions in high vacuum over night. LAH (48.0 mg, 1.30 mmol, 10.00 equiv.) was suspended in dry THF (2.5 ml) at rt. Dry EtOH (78 μ L, 1.30 mmol, 10.00 equiv.) was diluted with THF (2.5 ml) and the mixture was added slowly at rt to the LAH suspension. (S)-BINOL (373.0 mg, 1.30 mmol, 10.00 equiv.) was added as a solution in THF (2.5 ml) followed by (2E,4Z)-sorbamide **O14a**^[68] (77.0 mg, 1.30 mmol, 10.00 equiv.) in THF (2.5 ml) to give a gray mixture.

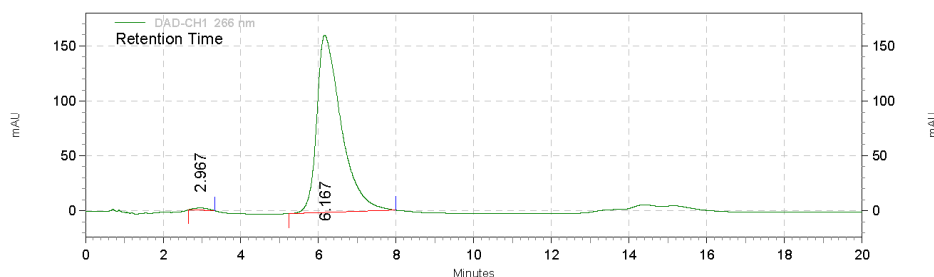
2.0 ml of the stock solution containing the putative amide transfer complex (0.26 mmol, 2.00 equiv.) was added immediately to a solution of aldehyde **O35** (55.0 mg, 0.13 mmol, 1.00 equiv.) in THF (2 ml) and the mixture was stirred at rt. Additional 2.0 ml of stock solution (0.26 mmol, 2.00 equiv.) were added after 20 min. The reaction mixture was quenched by addition of sat. aqu. NaHCO₃ solution (40 ml) after 45 min and the mixture was stirred until two clear phases have formed (approx. 10 min). The phases were separated and the aqueous phase was extracted with EtOAc (3 x 40 ml), the combined organic phases were dried over anhydrous MgSO₄ and concentrated under reduced pressure. The residue was purified by flash column chromatography (EtOAc/Hex 1:1 \rightarrow 2:1 \rightarrow 4:1, 2% Et₃N) and subsequent normal phase preparative HPLC (30% \rightarrow 90% propan-2-ol in hexane in 15 min, 15 ml/min) affording **O6** (40.1 mg, 0.08 mmol, 58%) as a colourless film.

TLC: R_f = 0.45 (EtOAc/hexane 6:1). **¹H-NMR** (400 MHz, DMSO-*d*₆) δ = 8.27 (d, *J* = 9.0 Hz, 1H), 7.52 – 7.38 (m, 2H), 6.73 (dt, *J* = 16.1, 7.0 Hz, 1H), 6.36 (t, *J* = 11.3 Hz, 1H), 6.17 (s, 1H), 6.12 (d, *J* = 4.8 Hz, 1H), 6.02 (d, *J* = 16.1 Hz, 1H), 5.95 (dd, *J* = 15.2, 6.8 Hz, 1H), 5.86 (d, *J* = 15.0 Hz, 1H), 5.63 (d, *J* = 11.3 Hz, 1H), 5.39 – 5.29 (m, 1H), 5.12 (d, *J* = 7.6 Hz, 1H), 4.93 (ddd, *J* = 8.9, 6.2, 2.4 Hz, 1H), 4.42 (ddd, *J* = 9.9, 7.6, 2.0 Hz, 1H), 3.99 – 3.87 (m, 2H), 3.31 – 3.21 (m, 2H), 3.18 – 2.84 (m, 3H),

2.45 – 2.27 (m, 3H), 2.17 (dd, $J = 13.7, 9.1$ Hz, 1H), 1.78 (d, $J = 5.1$ Hz, 6H), 1.62 (s, 3H). $^{13}\text{C-NMR}$ (101 MHz, $\text{DMSO-}d_6$) $\delta = 197.0, 165.4, 165.2, 144.0, 143.2, 140.6, 140.1, 137.2, 135.8, 131.2, 128.6, 125.6, 125.3, 120.1, 119.2, 73.9, 72.7, 72.5, 72.1, 55.0, 54.8, 44.8, 40.2, 37.9, 24.3, 18.3, 17.1$. IR (film) $\tilde{\nu} = 3358, 2968, 2924, 1705, 1669, 1629, 1626, 1603, 1525, 1431, 1362, 1332, 1297, 1283, 1212, 1199, 1181, 1152, 1134, 1121, 1086, 1005, 981, 924, 883, 832, 754, 749, 715$. HRMS (ESI) calculated for $\text{C}_{27}\text{H}_{35}\text{NNaO}_8\text{S}$ $[(\text{M}+\text{Na})^+]$: 556.1976, found: 556.1977. $[\alpha]_D^{20} = -133.97^\circ$ (1.00 g/100cm³ in CHCl_3).

Area % Report

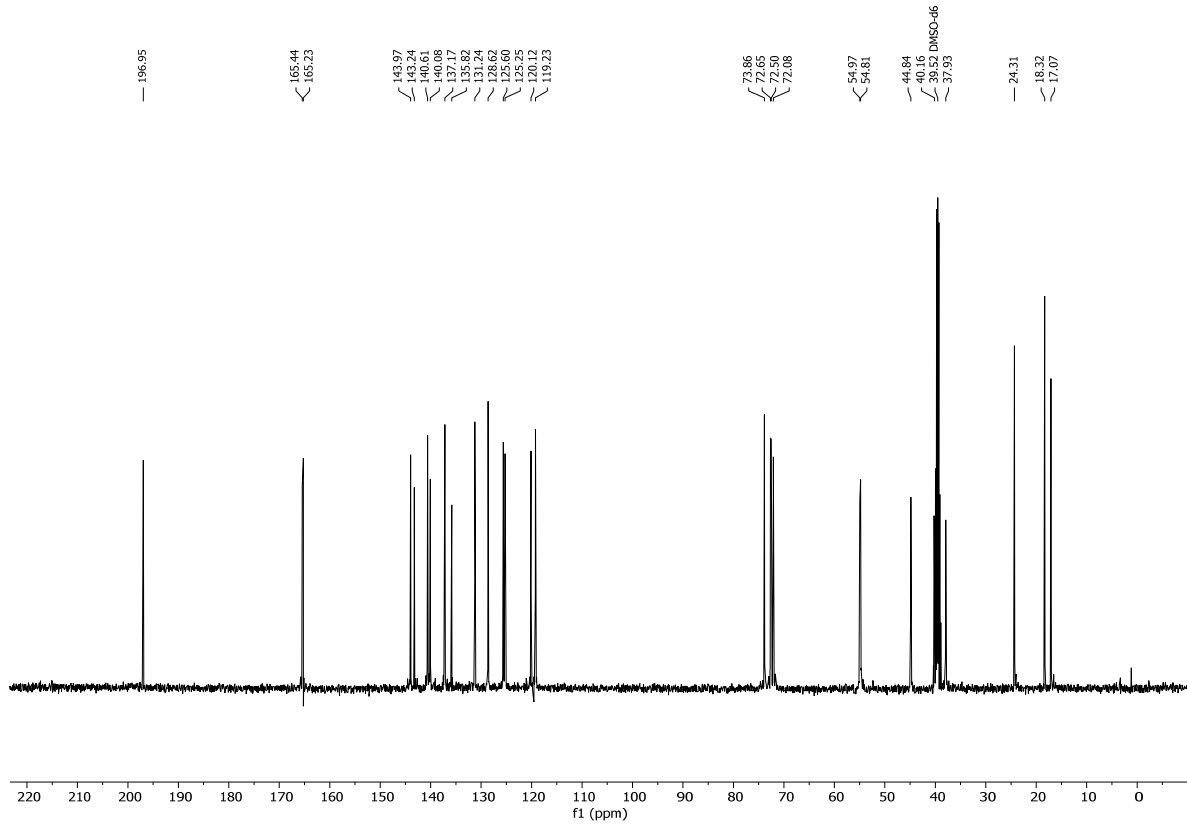
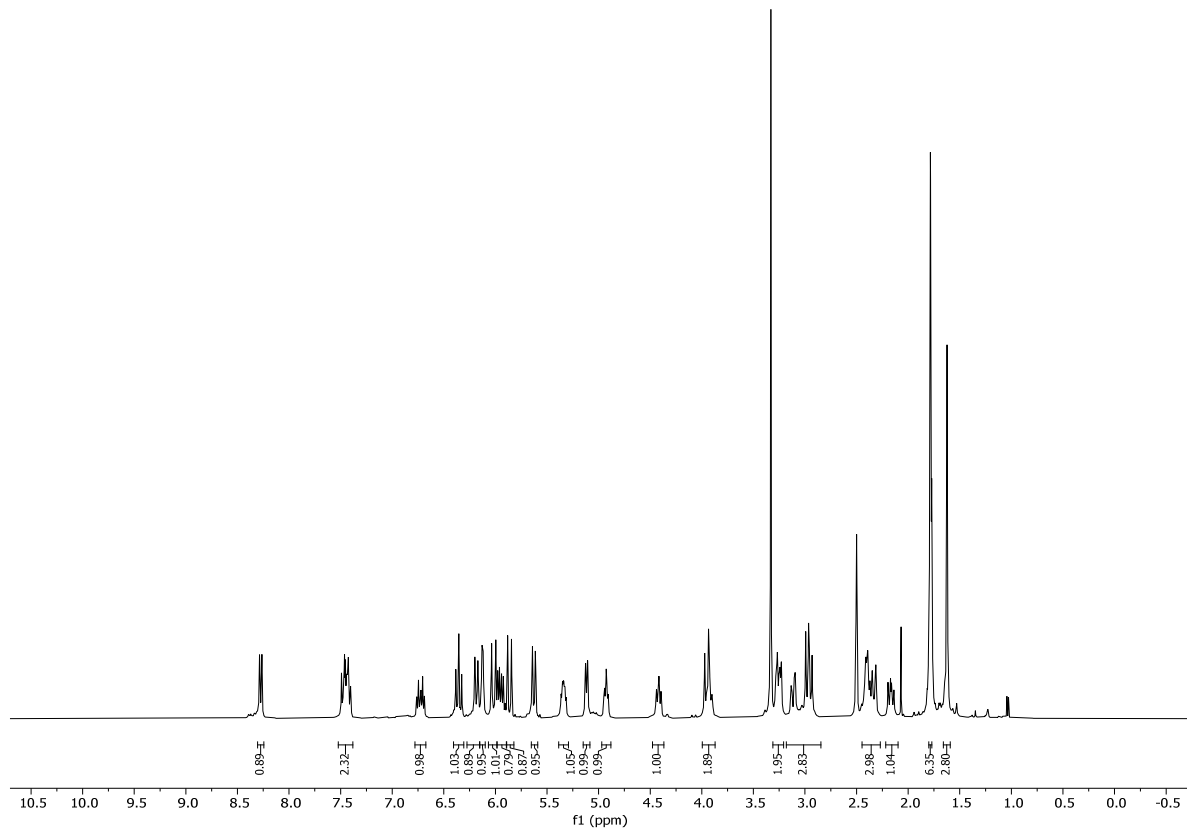
Data File: C:\EZChrom Elite\Enterprise\Projects\Etienne\EC-158-after-HPLC-r2
 Method: C:\EZChrom Elite\Enterprise\Projects\Default\Method\Etienne C\EC-30-90_15min.met
 Acquired: 01.05.2023 17:53:16
 Printed: 01.05.2023 17:57:32

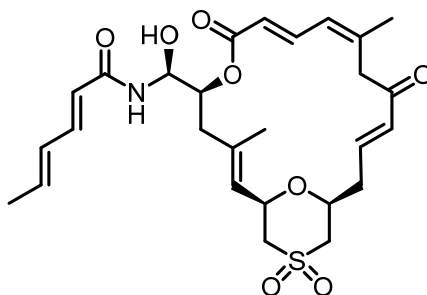
DAD-CH1 266
nm Results

| Retention Time | Area | Area % | Height | Height % |
|----------------|----------|--------|--------|----------|
| 2.967 | 211583 | 0.75 | 8303 | 1.27 |
| 6.167 | 28008545 | 99.25 | 643851 | 98.73 |

| | | | | |
|--------|----------|--------|--------|--------|
| Totals | 28220128 | 100.00 | 652154 | 100.00 |
|--------|----------|--------|--------|--------|

The normal phase analytical HPLC trace shown above was measured with the Elite LaChrom device mentioned in the general part. A gradient of 30% → 90% propan-2-ol in hexane 15 min, with a flow rate of 1 mL/min was used. The material thus obtained was used in the biological experiments.



**O8**

(2E,4E)-N-((S)-((1R,2E,5S,8E,10Z,14E,17S)-3,11-dimethyl-19,19-dioxido-7,13-dioxo-6,21-dioxo-19-thiabicyclo[15.3.1]henicosa-2,8,10,14-tetraen-5-yl)(hydroxy)methyl)hexa-2,4-dienamide

(O8). Preparation of stock solution of (S)-BINAL-sorbamide complex: Reagents and reactants were dried in flasks used to prepare solutions in high vacuum over night. LAH (14.0 mg, 0.38 mmol, 10.00 equiv.) was suspended in dry THF (1 ml) at rt. Dry EtOH (23 μ L, 0.38 mmol, 10.00 equiv.) was diluted with THF (1 ml) and the mixture was added slowly at rt to the LAH suspension. (S)-BINOL (108.0 mg, 0.38 mmol, 10.00 equiv.) was added as a solution in THF (1 ml) followed by (2E,4E)-sorbamide **O14b**^[315] (42.0 mg, 0.38 mmol, 10.00 equiv.) in THF (1 ml) to give a gray mixture.

0.8 ml of the stock solution containing the putative amide transfer complex (0.076 mmol, 2.00 equiv.) was added immediately to a solution of aldehyde **O35** (16.0 mg, 0.038 mmol, 1.00 equiv.) in THF (1 ml) and the mixture was stirred at rt. Additional 0.8 ml of stock solution (0.076 mmol, 2.00 equiv.) were added after 20 min. The reaction mixture was quenched by addition of sat. aqu. NaHCO₃ solution (10 ml) after 45 min and the mixture was stirred until two clear phases have formed (approx. 10 min). The phases were separated and the aqueous phase was extracted with EtOAc (3 x 10 ml), the combined organic phases were dried over anhydrous MgSO₄ and concentrated under reduced pressure. The residue was purified by flash column chromatography (EtOAc/Hex 1:1 \rightarrow 2:1 \rightarrow 4:1, 2% Et₃N) and subsequent normal phase preparative HPLC (30% \rightarrow 80% propan-2-ol in hexane in 15 min, 15 ml/min) affording **O8** (6.8 mg, 0.013 mmol, 34%) as a colourless film.

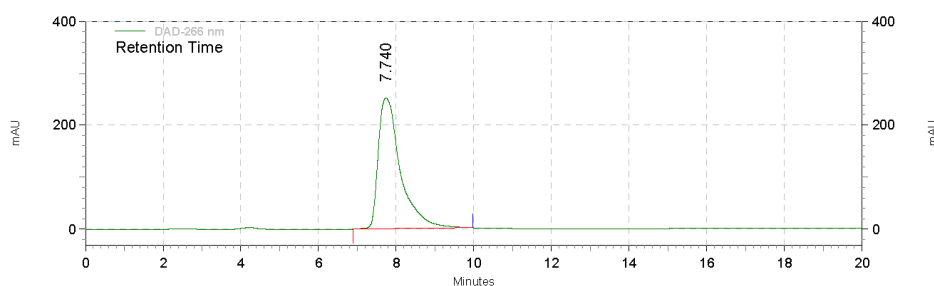
TLC: R_f = 0.45 (EtOAc/hexane 6:1). **¹H-NMR** (500 MHz, DMSO-*d*₆) δ = 8.30 (dd, *J* = 9.1, 1.7 Hz, 1H), 7.44 (ddd, *J* = 15.1, 11.6, 1.9 Hz, 1H), 7.01 (ddd, *J* = 15.2, 10.7, 1.9 Hz, 1H), 6.72 (dtd, *J* = 16.0, 7.1, 1.8 Hz, 1H), 6.23 – 6.14 (m, 3H), 6.14 – 6.04 (m, 1H), 6.00 (d, *J* = 15.8 Hz, 1H), 5.94 (d, *J* = 15.4 Hz, 1H), 5.87 (dd, *J* = 14.7, 7.0 Hz, 1H), 5.37 (t, *J* = 7.7 Hz, 1H), 5.10 (d, *J* = 7.7 Hz, 1H), 4.94 (ddt, *J* = 9.5, 6.4, 2.0 Hz, 1H), 4.42 (ddt, *J* = 11.1, 7.7, 2.0 Hz, 1H), 3.99 (dd, *J* = 15.0, 1.8 Hz, 1H), 3.91 (ddd, *J* = 11.2, 9.1, 2.3 Hz, 1H), 3.35 – 3.04 (m, 3H), 2.96 (dd, *J* = 13.9, 11.1 Hz, 2H), 2.46 – 2.27 (m, 3H),

2.14 (dd, $J = 13.9, 9.7$ Hz, 1H), 1.79 (d, $J = 7.2$ Hz, 6H), 1.62 (d, $J = 1.5$ Hz, 3H). $^{13}\text{C-NMR}$ (126 MHz, DMSO- d_6) $\delta = 197.1, 165.5, 165.0, 144.1, 143.3, 140.0, 137.1, 135.6, 131.3, 129.9, 125.6, 125.3, 122.9, 120.2, 73.9, 73.0, 72.6, 72.0, 55.0, 54.8, 44.8, 40.4, 38.0, 24.3, 18.3, 17.0$. IR (film) $\tilde{\nu} = 3357, 2925, 1709, 1668, 1634, 1522, 1435, 1356, 1332, 1299, 1282, 1254, 1210, 1150, 1122, 1087, 1045, 999, 979, 884, 714, 522$. HRMS (ESI) calculated for $\text{C}_{27}\text{H}_{35}\text{NNaO}_8\text{S}$ $[(\text{M}+\text{Na})^+]$: 556.1976, found: 556.1972. $[\alpha]_D^{20} = -67.99^\circ$ (1.00 g/100cm 3 in CHCl_3).

Page 1 of 1

Area % Report

Data File: C:\EZChrom Elite\Enterprise\Projects\Etienne\EC-158-1-afterPrep-30-90_15min-trace
 Method: C:\EZChrom Elite\Enterprise\Projects\Default\Method\Etienne C\EC-30-90_15min.met
 Acquired: 07.03.2023 11:45:46
 Printed: 07.03.2023 12:58:07

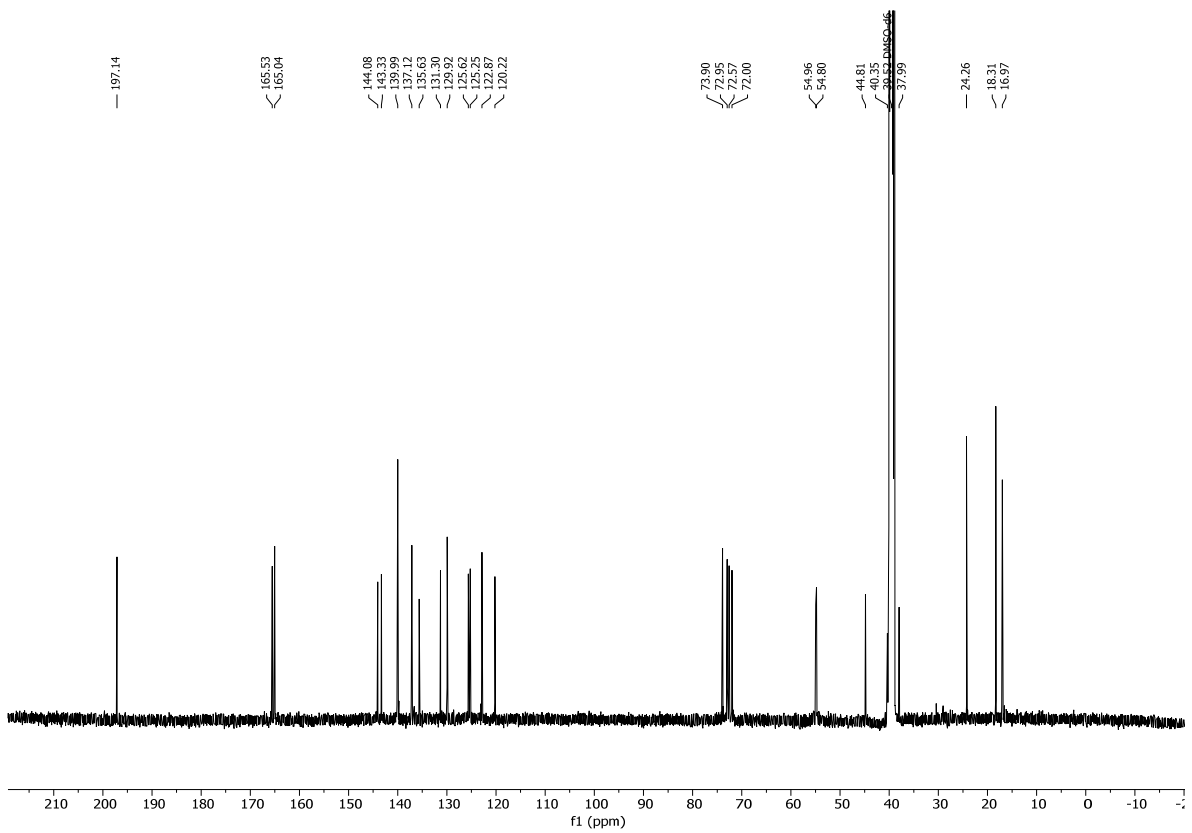
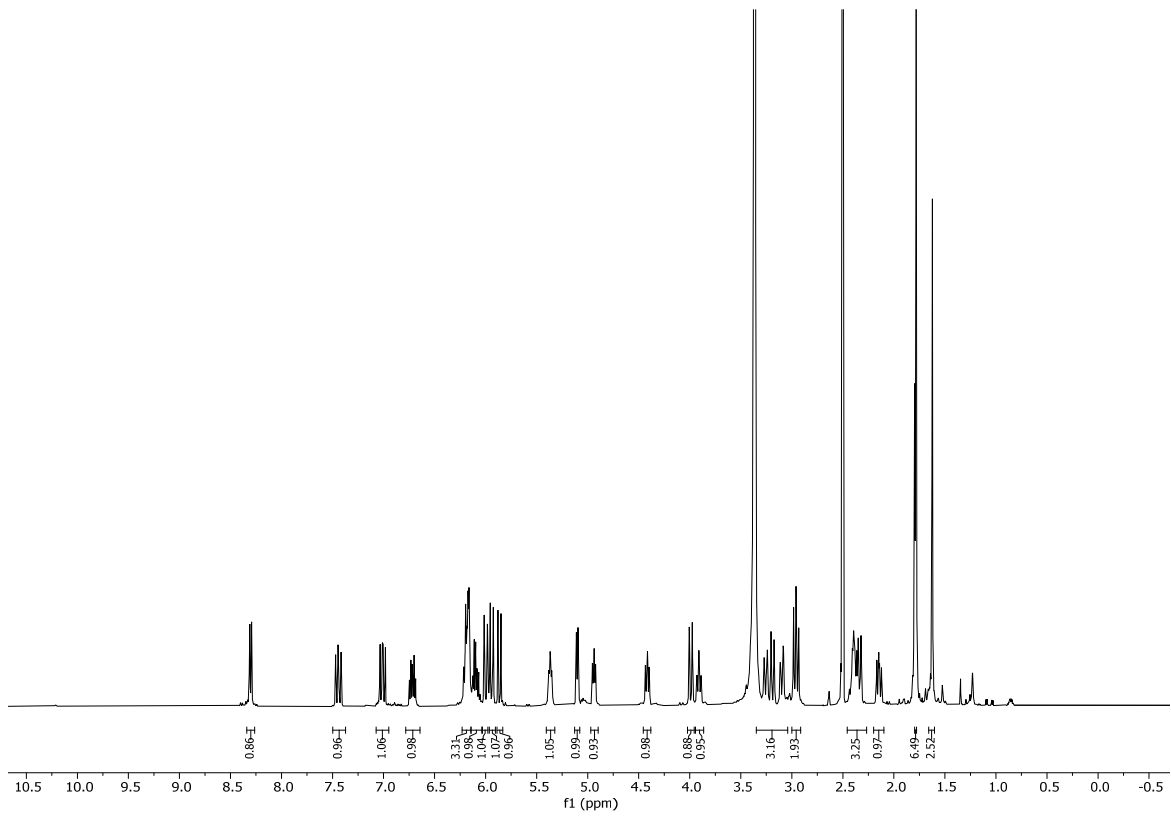


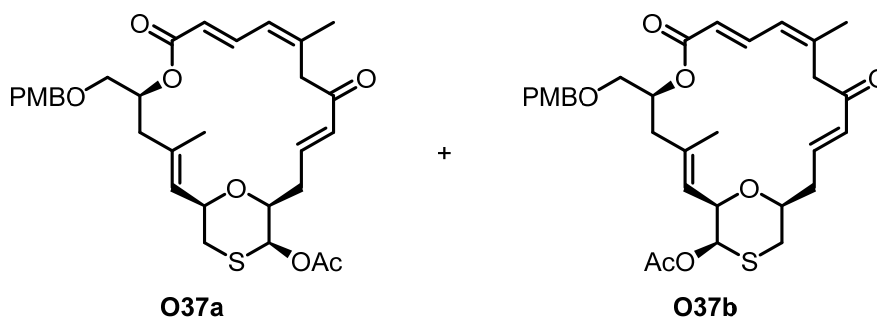
DAD-266 nm

Results

| Retention Time | Area | Area % | Height | Height % |
|----------------|----------|--------|---------|----------|
| 7.740 | 39812971 | 100.00 | 1009632 | 100.00 |
| Totals | 39812971 | 100.00 | 1009632 | 100.00 |

The normal phase analytical HPLC trace shown above was measured with the Elite LaChrom device mentioned in the general part. A gradient of 30% \rightarrow 90% in propan-2-ol in hexane 15 min, with a flow rate of 1 mL/min was used. The material thus obtained was used in the biological experiments.



4.2.2.5.1 α -Acyloxylation of **O30** to Give **O37a** and **O37b** and Their Reduction to Give **O32**

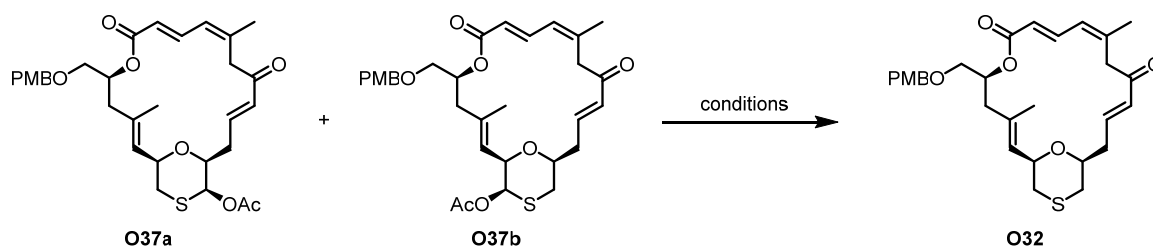
(1R,2E,5S,8E,10Z,14E,17S,18S)-5-formyl-3,11-dimethyl-7,13-dioxo-6,21-dioxa-19-thiabiacyclo[15.3.1]henicosa-2,8,10,14-tetraen-18-yl acetate (O37a) and

(1R,2E,5S,8E,10Z,14E,17S,20R)-5-formyl-3,11-dimethyl-7,13-dioxo-6,21-dioxa-19-thiabiacyclo[15.3.1]henicosa-2,8,10,14-tetraen-20-yl acetate (O37b). To a solution of **O30** (1.47

g, 2.19 mmol, 1.00 equiv.) in CH_2Cl_2 (110 mL) was added DMP (2.05 g, 4.82 mmol, 2.20 equiv.) at rt. After 2 h DMP (1.03 g, 2.41 mmol, 1.10 equiv.) was added again and stirring at rt was continued for another hour. After 3 hours in total CH_2Cl_2 (250 mL) and a mixture of $\text{Na}_2\text{S}_2\text{O}_3$ and NaHCO_3 (350 mL) were added and stirring at rt was continued for 10 min, when two almost clear phases had formed. The phases were separated, the aqueous phase was extracted with CH_2Cl_2 (3 x 250 mL), and the combined organic extracts were dried over MgSO_4 . Concentration of the solution under reduced pressure gave **O32** (0.22 mg, 0.42 mmol, 20%) as colorless oil and an inseparable mixture of **O37a** and **O37b** (0.32 g, 0.56 mmol, 27%, 1.8:1) as colorless oil.

Analytical data of the 1:1.8 mixture of **O37a** and **O37b**:

TLC: $R_f = 0.10$ (EtOAc/hexane 1:3). **$^1\text{H-NMR}$** (400 MHz, CDCl_3) $\delta = 7.56$ (dt, $J = 15.1, 11.6$ Hz, 3H), 7.28 – 7.19 (m, 8H), 6.92 – 6.82 (m, 6H), 6.70 (dddd, $J = 16.1, 8.7, 5.2, 3.7$ Hz, 3H), 6.11 (d, $J = 11.6$ Hz, 3H), 6.00 – 5.85 (m, 7H), 5.52 (d, $J = 8.8$ Hz, 1H), 5.49 (d, $J = 8.9$ Hz, 1H), 5.33 (tdd, $J = 9.2, 5.6, 3.4$ Hz, 3H), 5.15 – 5.09 (m, 2H), 4.98 (d, $J = 8.4$ Hz, 1H), 4.56 – 4.41 (m, 6H), 4.39 – 4.25 (m, 3H), 4.05 (d, $J = 13.8$ Hz, 1H), 3.96 (d, $J = 14.0$ Hz, 2H), 3.80 (s, 9H), 3.75 – 3.61 (m, 3H), 3.61 – 3.43 (m, 6H), 3.16 (d, $J = 14.1$ Hz, 2H), 3.11 (d, $J = 13.8$ Hz, 1H), 2.81 (ddd, $J = 13.7, 10.2, 2.0$ Hz, 3H), 2.56 – 2.33 (m, 6H), 2.30 – 2.19 (m, 8H), 2.10 (s, 5H), 1.99 (s, 3H), 1.84 – 1.68 (m, 16H). **$^{13}\text{C-NMR}$** (101 MHz, CDCl_3) $\delta = 197.6, 169.3, 169.0, 166.7, 159.4, 144.7, 144.1, 142.9, 142.8, 139.4, 139.3, 137.6, 134.8, 132.4, 132.1, 130.1, 129.5, 127.5, 125.7, 125.6, 125.0, 121.3, 121.2, 114.0, 79.2, 78.4, 76.1, 75.7, 73.1, 71.4, 71.3, 71.1, 70.8, 69.5, 69.4, 55.4, 45.1, 42.8, 42.3, 39.7, 35.9, 33.7, 33.1, 24.0, 23.8, 21.0, 20.9, 17.5, 16.9$. **IR** (film) $\tilde{\nu} = 2910, 2862, 1752, 1710, 1668, 1635, 1613, 1586, 1513, 1439, 1365, 1281, 1249, 1209, 1175, 1149, 1088, 1036, 978, 890, 821, 732, 648, 575, 509$. **HRMS** (ESI) calculated for $\text{C}_{31}\text{H}_{38}\text{NaO}_8\text{S}$ [(M+Na) $^+$]: 593.2180, found: 593.2166.

Table 23: Conditions investigated for the reduction of **O37a/O37b** to **O32**.

| Entry | Scale | Reagents | Conditions | Yield of O32 ^[a] |
|-------|-------|--|--|-----------------------------|
| 1 | 30 mg | TMSOTf, Et ₃ SiH | MeCN, rt, 24 h | - |
| 2 | 20 mg | AcOH, Et ₃ SiH | CH ₂ Cl ₂ , rt, 24 h | - |
| 3 | 20 mg | H ₂ N-NH ₂ ·AcOH | DMF, rt, 3h | - |
| 4 | 15 mg | TFA, Et ₃ SiH | CH ₂ Cl ₂ , rt, 1 h | - |
| 5 | 20 mg | TFA (15 eq.), Et ₃ SiH (10 eq.) | CH ₂ Cl ₂ , -78 to -40 °C, 6 h | 11% |
| 6 | 15 mg | TFA (15 eq.), Et ₃ SiH (30 eq.) | CH ₂ Cl ₂ , -40 °C, 3 h | 9% |

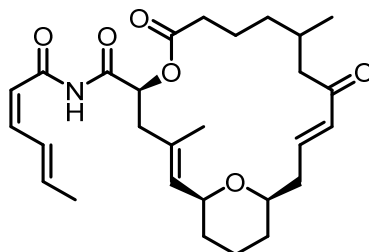
^[a] "-" refers to unidentifiable product(s).

4.2.2.5.2 Induction of Microtubule Polymerization

Tubulin (25 μM) was polymerized in GAB buffer (10 mM NaPi pH 6.7, 30% glycerol, 1 mM EGTA, 6 mM MgCl_2 and 1 mM GTP) in presence of **O5-O8** at 37 °C for *ca.* 60 min. DMSO was used as blank and (–)-zampanolide (**O1**) was used as reference compound. The samples were prepared on ice to prevent polymerization before the actual measurement. All samples were measured in duplicates and the polymerization was monitored with a Multiskan plate reader measuring the absorbance at 350 nm in a 30-second interval.

4.2.3 Side chain-modified analogs

4.2.3.1 Imide-based analogs of R7, O4 and O6



IM-4

(1*S*,2*E*,5*S*,14*E*,17*R*)-*N*-((2*Z*,4*E*)-hexa-2,4-dienoyl)-3,11-dimethyl-7,13-dioxo-6,21-dioxabicyclo[15.3.1]henicosa-2,14-diene-5-carboxamide (IM-4). To a stirred solution of **R7** (8.2 mg, 0.017 mmol, 1.00 equiv.) in CH₂Cl₂ (1.7 mL) was added NaHCO₃ (4.2 mg, 0.050 mmol, 3.00 equiv.) followed by DMP (10.7 mg, 0.025 mmol, 1.50 equiv.) at rt. The reaction was checked by TLC every hour and the same amount of NaHCO₃ and DMP were added until complete conversion of the starting material was observed, which, was the case after 18h using a total of 24 equivalents of DMP and 48 equivalents of NaHCO₃. The reaction was quenched with a mixture of Na₂S₂O₃ and NaHCO₃ (10 mL) and stirring was continued for 10 min until two clear phases were formed. The phases were separated then the aqueous phase was extracted with CH₂Cl₂ (3 x 10 mL), the combined organic phases were dried over MgSO₄, concentrated under reduced pressure then purified using flash chromatography (EtOAc/Hex 1:3) and subsequent normal phase prep HPLC (1 → 30% *i*-PrOH in hexane in 20 min) affording **IM-4** (4.5 mg, 0.009 mmol, 55%) as a colorless film.

TLC: *R*_f = 0.70 (EtOAc/hexane 1:1, 2% Et₃N). Analytical data recorded after HPLC purification: **¹H-NMR** (500 Hz, DMSO-*d*₆): δ = 10.94 (s, 1H), 7.34 (ddtd, *J* = 14.5, 11.3, 2.1, 1.2 Hz, 1H), 6.96 – 6.82 (m, 1H), 6.69 (td, *J* = 11.4, 2.3 Hz, 1H), 6.28 – 6.18 (m, 1H), 6.01 (dd, *J* = 11.2, 7.6 Hz, 1H), 5.98 – 5.89 (m, 1H), 5.55 – 5.44 (m, 1H), 5.25 – 5.18 (m, 1H), 4.11 – 3.97 (m, 1H), 3.47 (dt, *J* = 43.6, 10.9 Hz, 1H), 2.79 (ddd, *J* = 15.6, 13.1, 5.6 Hz, 1H), 2.49 – 2.38 (m, 1H), 2.37 – 2.15 (m, 3H), 2.07 (dd, *J* = 13.5, 8.7 Hz, 1H), 2.00 – 1.87 (m, 0H), 1.85 (dd, *J* = 6.9, 1.5 Hz, 3H), 1.84 – 1.72 (m, 1H), 1.72 – 1.66 (m, 3H), 1.65 – 1.39 (m, 4H), 1.32 – 1.07 (m, 5H), 0.83 (dd, *J* = 6.6, 3.2 Hz, 3H). **¹³C-NMR** (126 MHz, DMSO-*d*₆): δ = 200.9, 200.6, 172.3, 172.3, 171.1, 165.4, 165.3, 146.9, 146.3, 145.9, 145.9, 142.0, 131.4, 131.3, 131.1, 131.0, 130.5, 130.3, 128.4, 116.8, 116.8, 76.8, 75.0, 74.3, 74.3, 71.0, 70.9, 45.6, 45.3, 39.9, 39.8, 38.8, 38.5, 36.1, 35.81, 34.1, 33.7, 31.3, 31.2, 31.1, 30.8, 30.6, 22.9, 22.9, 22.8, 21.7, 20.6, 20.1, 18.6, 15.4, 14.9. **IR** (neat): $\tilde{\nu}$ = 2932, 2852, 1725, 1688, 1666, 1634,

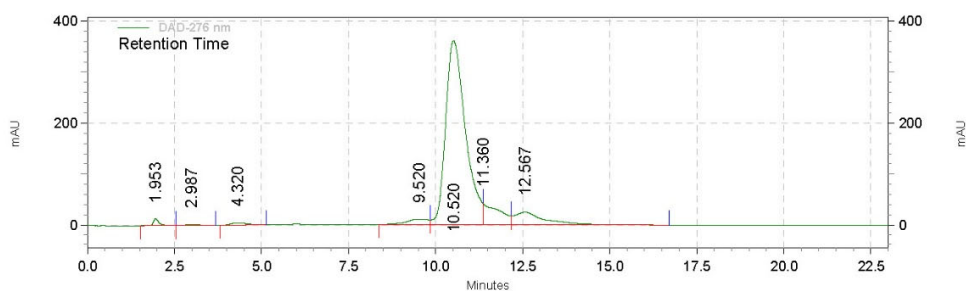
1592, 1489, 1427, 1376, 1308, 1197, 1150, 1124, 1073, 1048, 984, 936, 837, 803 cm^{-1} HRMS (ESI):
calcd for $\text{C}_{28}\text{H}_{40}\text{NO}_6$ [(M+H)⁺]: 486.2850; found: 486.2850.

Page 1 of 1

Area % Report

Data File: C:\EZChrom Elite\Enterprise\Projects\Etienne\EC-73-1-r3017-chromatogram
Method: C:\EZChrom Elite\Enterprise\Projects\Default\Method\Etienne C\EC-41_1_30_20Mmin.met

Acquired: 04.02.2021 17:03:29
Printed: 04.02.2021 17:18:48

**DAD-276 nm****Results**

| Retention Time | Area | Area % | Height | Height % |
|----------------|----------|--------|---------|----------|
| 1.953 | 601837 | 0.83 | 51928 | 2.84 |
| 2.987 | 237302 | 0.33 | 8660 | 0.47 |
| 4.320 | 590933 | 0.82 | 17613 | 0.96 |
| 9.520 | 1889584 | 2.62 | 41580 | 2.27 |
| 10.520 | 57140711 | 79.13 | 1443340 | 78.87 |
| 11.360 | 5544346 | 7.68 | 167692 | 9.16 |
| 12.567 | 6203359 | 8.59 | 99126 | 5.42 |

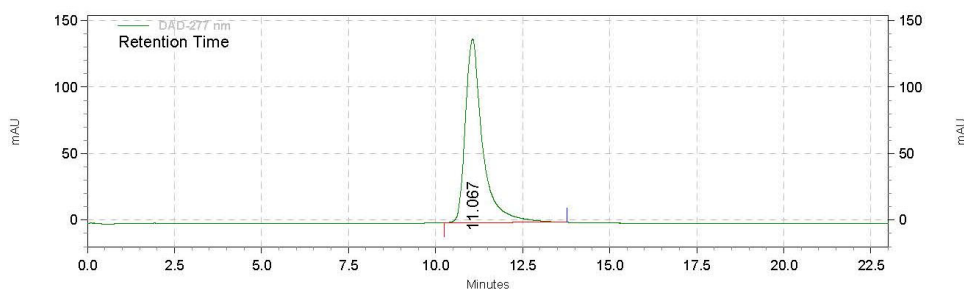
| | | | | |
|--------|----------|--------|---------|--------|
| Totals | 72208072 | 100.00 | 1829939 | 100.00 |
|--------|----------|--------|---------|--------|

The analytical HPLC trace (Luna[®] 3 μm u, NH_2 , 100 \AA , 150 x 4.6 mm; hexane/*i*-PrOH gradient from 1:99 to 30:70 in 20 min, 1 mL/min, R_t = 10.5 min, others species of other peaks were not identified) before purification using prep HPLC is shown above. Imide **IM-4** was purified by prep HPLC (Luna[®] 5 μm u, NH_2 , 100 \AA , 150 x 21.2 mm; hexane/*i*-PrOH 99:1 to 70:30, 20 mL/min, R_t = 15.0 min). The reinjection into the analytical HPLC of fraction with R_t = 15.0 min is shown below.

Area % Report

Data File: C:\EZChrom Elite\Enterprise\Projects\Etienne\EC-73-2-r2032-chromatogram
 Method: C:\EZChrom Elite\Enterprise\Projects\Default\Method\Etienne C\EC-41_1_30_20Mmin.met

Acquired: 24.02.2021 17:44:23
 Printed: 24.02.2021 17:46:49

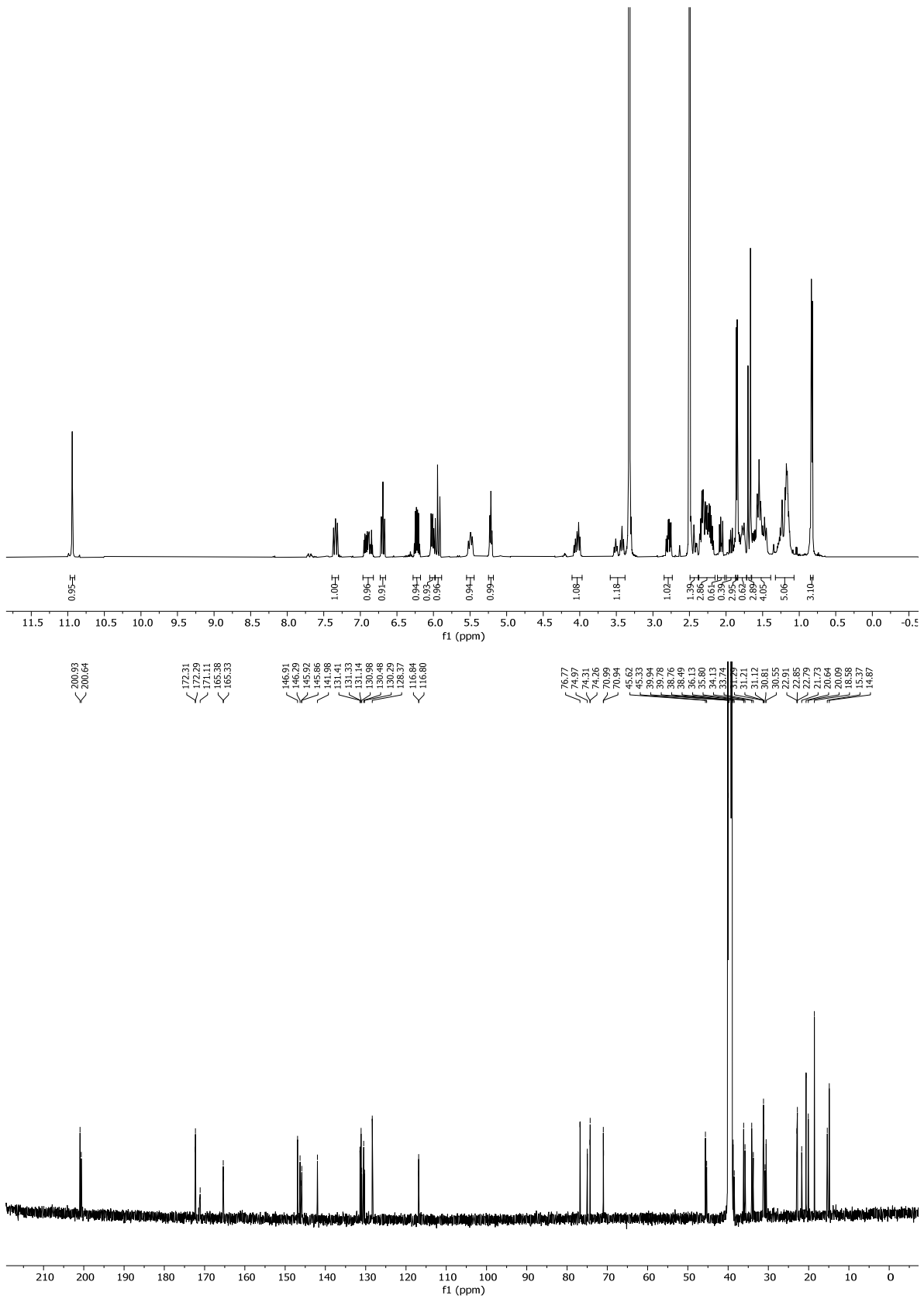


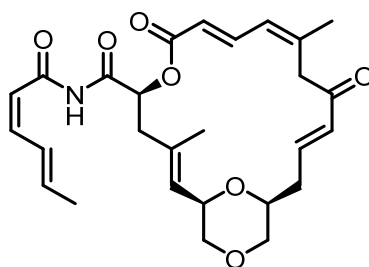
DAD-277 nm

Results

| Retention Time | Area | Area % | Height | Height % |
|----------------|----------|--------|--------|----------|
| 11.067 | 18982787 | 100.00 | 553178 | 100.00 |
| Totals | 18982787 | 100.00 | 553178 | 100.00 |

The analytical HPLC trace (Luna® 3 µm u, NH₂, 100 Å, 150 x 4.6 mm; hexane/*i*-PrOH gradient from 99:1 to 70:30 in 20 min, 1 mL/min, Rt = 11.1 min, no other peaks detected) after purification using prep HPLC is shown above. The material thus obtained was used in the biological experiments.





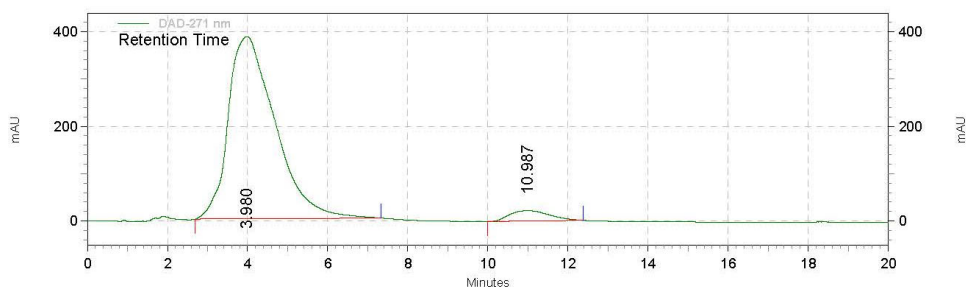
IM-5

(1R,2E,5S,8E,10Z,14E,17S)-N-((2Z,4E)-hexa-2,4-dienoyl)-3,11-dimethyl-7,13-dioxo-6,19,21-trioxabicyclo[15.3.1]henicosa-2,8,10,14-tetraene-5-carboxamide (IM-5). To a stirred solution of **3** (8.8 mg, 0.018 mmol, 1.00 eq.) in CH₂Cl₂ (1.8 ml) was added NaHCO₃ (4.5 mg, 0.054 mmol, 3.00 eq.) followed by DMP (11.5 mg, 0.027 mmol, 1.50 eq.) at rt. The reaction was monitored by TLC every 30 min and NaHCO₃ and DMP were added until complete conversion of hemiaminal **3** was observed, which, was the case after 4 h using in total 13.50 eq. NaHCO₃ and 6.00 eq. DMP. The reaction was quenched by addition of aqueous Na₂S₂O₃ and NaHCO₃ solution (10 ml) and stirring was continued for 10 min until two clear phases were formed. The phases were separated and the aqueous phase was extracted with CH₂Cl₂ (3 x 10 ml), the combined organic phases were dried over anhydrous MgSO₄ and concentrated under reduced pressure. The residue was purified by flash column chromatography (EtOAc/Hex 1:1) and normal phase HPLC (15 → 55% *i*-PrOH in *n*-hexane in 20 min) affording **IM-5** (1.5 mg, 0.003 mmol, 17%) as a colourless film.

TLC: *R*_f = 0.31 (EtOAc/hexane 1:1). Analytical data recorded after HPLC purification: **¹H-NMR** (500 Hz, CDCl₃): δ = 8.31 (s, 1H), 7.73 (dd, *J* = 14.9, 11.7 Hz, 1H), 7.44 – 7.32 (m, 1H), 6.90 – 6.78 (m, 1H), 6.70 (t, *J* = 11.3 Hz, 1H), 6.56 – 6.48 (m, 1H), 6.29 – 6.12 (m, 2H), 6.05 – 5.94 (m, 2H), 5.68 (d, 1H), 5.03 (d, *J* = 8.8 Hz, 1H), 4.33 – 4.25 (m, 1H), 4.17 (d, *J* = 13.6 Hz, 1H), 3.66 – 3.52 (m, 4H), 3.16 (ddd, *J* = 11.7, 10.4, 5.2 Hz, 2H), 3.06 (d, *J* = 13.6 Hz, 1H), 2.74 – 2.68 (m, 1H), 2.31 – 2.19 (m, 2H), 2.17 – 2.07 (m, 1H), 1.92 (d, *J* = 7.0 Hz, 3H), 1.85 (s, 3H), 1.81 (d, *J* = 1.3 Hz, 3H). **¹³C-NMR** (126 MHz, CDCl₃) δ = 197.6, 169.0, 165.7, 165.3, 148.1, 145.2, 145.1, 143.4, 141.5, 135.3, 131.8, 129.3, 125.8, 125.4, 119.3, 115.7, 73.6, 73.5, 73.4, 70.7, 70.3, 69.5, 45.4, 43.4, 35.0, 32.1, 30.5, 29.9, 29.8, 29.5, 23.9, 22.8, 19.0, 16.6, 14.3, 1.2. **IR** (film): *ν* = 2923, 2852, 1714, 1672, 1633, 1592, 1486, 1428, 1357, 1280, 1205, 1144, 1119, 978, 772, 756. **HRMS** (ESI) calculated for C₂₇H₃₄NO₇ [(M+H)⁺]: 484.2330, found: 484.2328. [*α*]_D²⁰ = -279.94° (0.30 g/100cm³ in CHCl₃).

Area % Report

Data File: C:\EZChrom
 Elite\Enterprise\Projects\Etienne\Alina\LZ-24-1_after_column_15-55_20min035-tr
 Method: C:\EZChrom Elite\Enterprise\Projects\Default\Method\Etienne CLZ_15-55_20min.met
 Acquired: 29.03.2024 11:30:37
 Printed: 29.03.2024 11:31:53



DAD-271 nm

Results

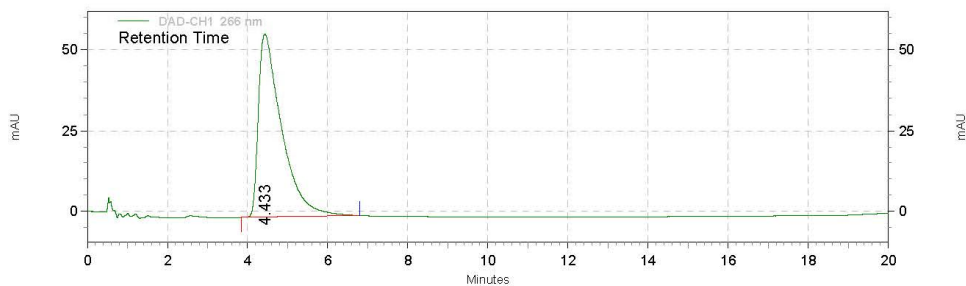
| Retention Time | Area | Area % | Height | Height % |
|----------------|-----------|--------|---------|----------|
| 3.980 | 125199253 | 95.39 | 1540372 | 94.61 |
| 10.987 | 6046172 | 4.61 | 87674 | 5.39 |

| Totals | Area | Area % | Height | Height % |
|--------|-----------|--------|---------|----------|
| | 131245425 | 100.00 | 1628046 | 100.00 |

The analytical HPLC trace (Luna® 3 µm u, NH₂, 100 Å, 150 x 4.6 mm; hexane/*i*-PrOH gradient from 15:85 to 55:45 in 20 min, 1 mL/min, Rt = 4.0 min, others species of other peaks were not identified) before purification using prep HPLC is shown above. Imide **IM-5** was purified by prep HPLC (Luna® 5 µm u, NH₂, 100 Å, 150 x 21.2 mm; hexane/isopropanol 15:85 to 55:45, 20 mL/min, Rt = 8.1 min). The reinjection into the analytical HPLC of fraction with Rt = 8.1 min is shown below.

Area % Report

Data File: C:\EZChrom Elite\Enterprise\Projects\Etienne\Alina\LZ-24-1-after-prep
 Method: C:\EZChrom Elite\Enterprise\Projects\Default\Method\Etienne CLZ_15-55_20min.met
 Acquired: 29.03.2024 11:35:01
 Printed: 29.03.2024 11:36:13

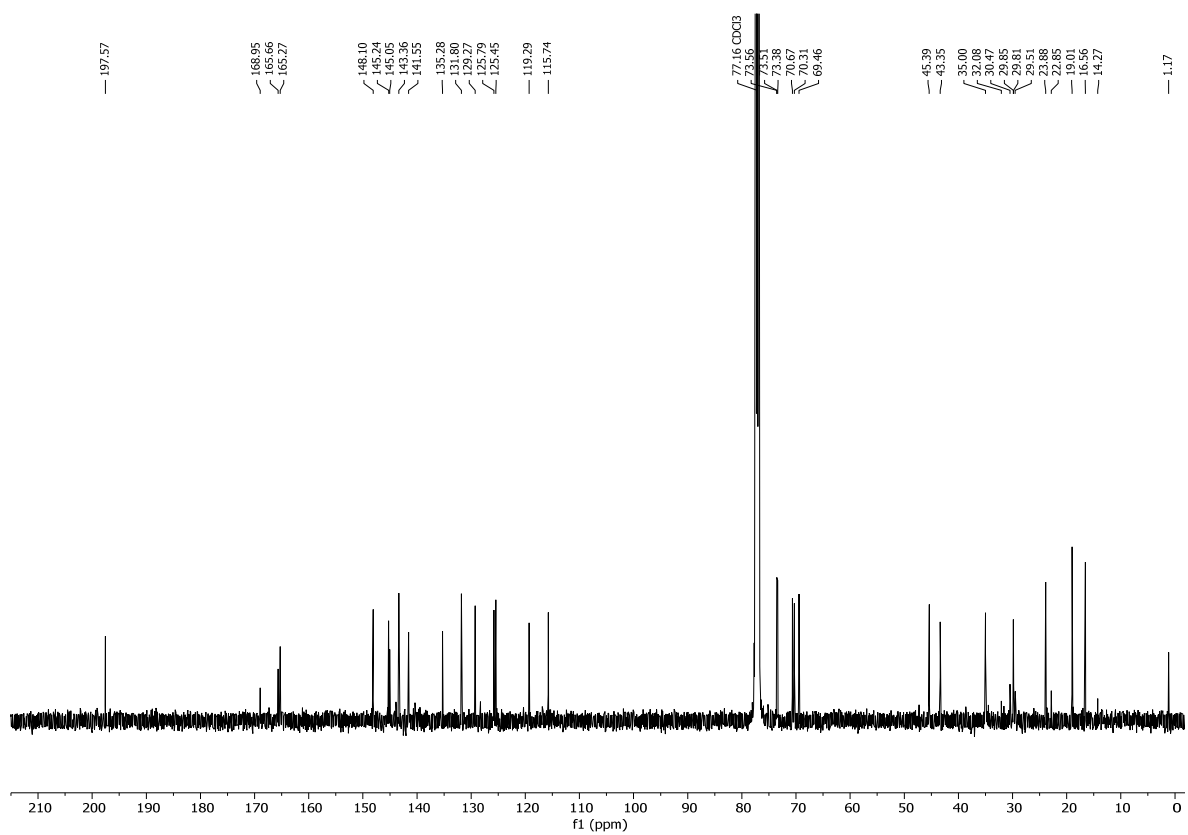
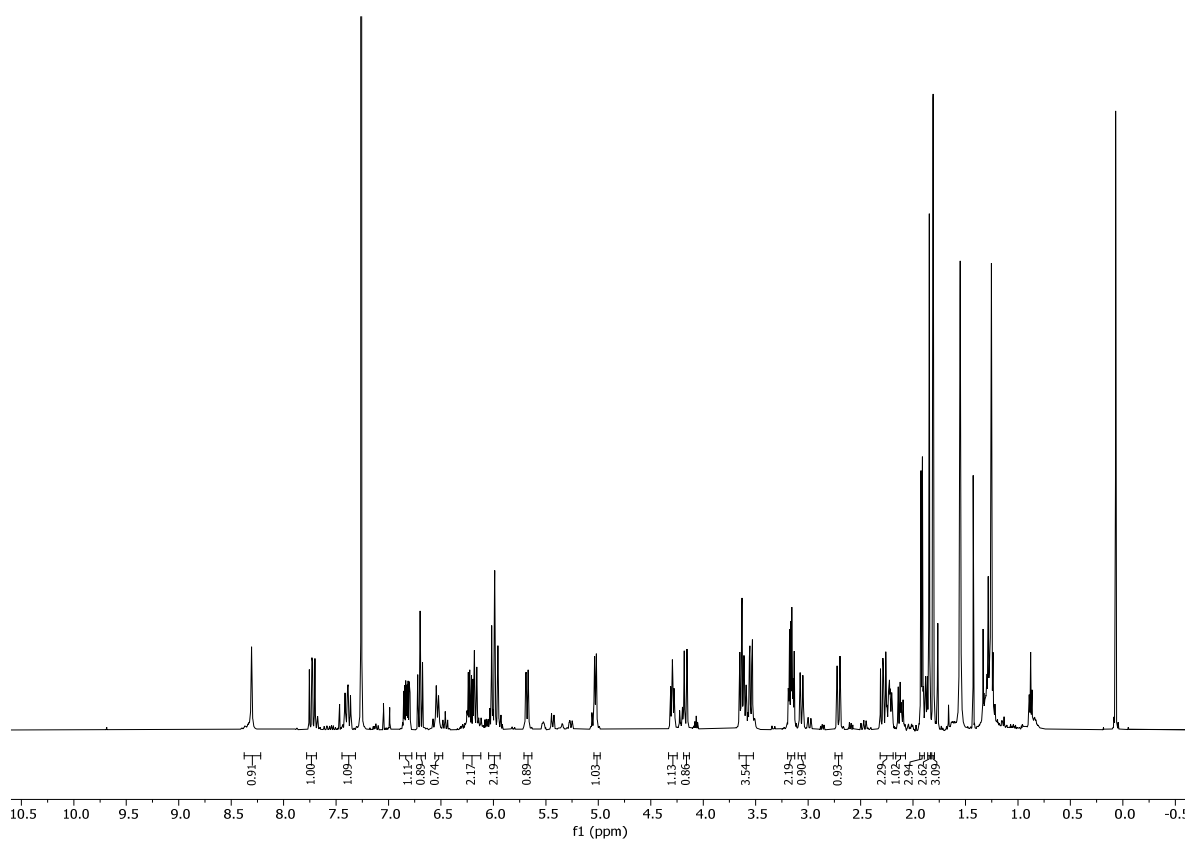


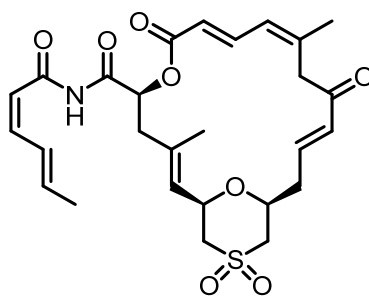
DAD-CH1 266 nm Results

| Retention Time | Area | Area % | Height | Height % |
|----------------|---------|--------|--------|----------|
| 4.433 | 9086811 | 100.00 | 226145 | 100.00 |

| | | | | |
|--------|---------|--------|--------|--------|
| Totals | 9086811 | 100.00 | 226145 | 100.00 |
|--------|---------|--------|--------|--------|

The analytical HPLC trace (Luna® 3 µm u, NH₂, 100 Å, 150 x 4.6 mm; hexane/*i*-PrOH gradient from 15:85 to 55:45 in 20 min, 1 mL/min, Rt = 4.4 min, no other peaks detected) after purification using prep HPLC is shown above. The material thus obtained was used in the biological experiments.





IM-5

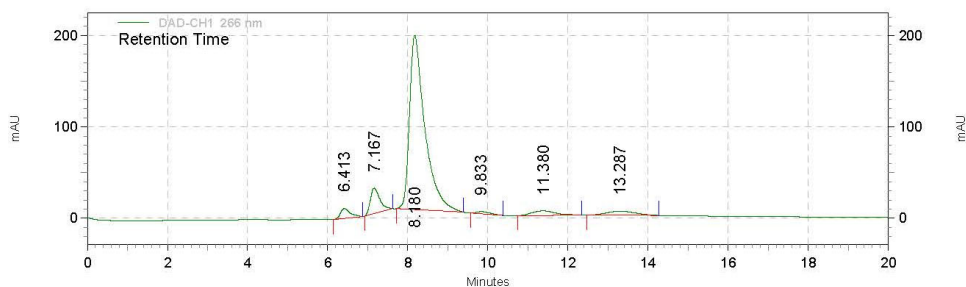
(1R,2E,5S,8E,10Z,14E,17S)-N-((2Z,4E)-hexa-2,4-dienoyl)-3,11-dimethyl-7,13-dioxo-6,21-dioxo-19-thiabicyclo[15.3.1]henicosa-2,8,10,14-tetraene-5-carboxamide 19,19-dioxide (IM-6). To a stirred solution of **5** (8.0 mg, 0.015 mmol, 1.00 equiv.) in CH₂Cl₂ (2 mL) was added NaHCO₃ (2.8 mg, 0.033 mmol, 2.20 equiv.) followed by DMP (7.0 mg, 0.017 mmol, 1.10 equiv.) at rt. The reaction was checked by TLC every hour and the same amount of NaHCO₃ and DMP were added until complete conversion of the starting material was observed, which, was the case after 5 h using in total 5.5 equivalents of DMP and 11.0 equivalents of NaHCO₃. The reaction was quenched with a mixture of Na₂S₂O₃ and NaHCO₃ (25 mL) and stirring was continued for 10 min until two clear phases were formed. The phases were separated then the aqueous phase was extracted with CH₂Cl₂ (3 x 20 mL), the combined organic phases were dried over MgSO₄, concentrated under reduced pressure then purified using flash chromatography (EtOAc/Hex 1:1) and subsequent normal phase prep HPLC (30 → 90% *i*-PrOH in hexane in 15 min) affording **IM-6** (3.0 mg, 0.005 mmol, 38%) as a colourless film.

TLC: R_f = 0.66 (EtOAc/hexane 4:1). Analytical data recorded after HPLC purification: **¹H-NMR** (500 MHz, DMSO-*d*₆) δ = 10.96 (s, 1H), 7.36 (dddd, *J* = 12.7, 10.0, 5.8, 1.5 Hz, 1H), 7.20 (dd, *J* = 15.1, 11.4 Hz, 1H), 6.87 – 6.80 (m, 1H), 6.70 (dd, *J* = 12.9, 9.8 Hz, 1H), 6.26 – 6.20 (m, 2H), 6.13 – 6.08 (m, 1H), 6.00 (d, *J* = 11.3 Hz, 1H), 5.83 (d, *J* = 15.1 Hz, 1H), 5.56 (d, *J* = 11.6 Hz, 1H), 5.32 – 5.30 (m, 1H), 4.57 – 4.53 (m, 1H), 4.04 (ddt, *J* = 10.2, 7.5, 2.4 Hz, 1H), 3.73 – 3.57 (m, 2H), 3.28 – 2.87 (m, 4H), 2.54 (s, 2H), 2.42 – 2.28 (m, 2H), 1.89 (d, *J* = 1.4 Hz, 3H), 1.87 – 1.85 (m, 3H), 1.71 (s, 3H).

¹³C-NMR (126 MHz, DMSO-*d*₆) δ = 196.6, 165.9, 165.8, 146.5, 144.5, 144.4, 142.6, 139.9, 133.5, 132.3, 128.8, 126.9, 126.1, 120.3, 117.2, 73.7, 73.0, 71.4, 55.5, 55.2, 44.1, 37.6, 25.8, 19.1, 15.3. **IR** (film): ν = 2926, 1745, 1687, 1634, 1594, 1541, 1509, 1501, 1428, 1375, 1330, 1299, 1247, 1203, 1151, 1124, 1051, 1026, 1006, 979, 936, 882, 822, 759. **HRMS** (ESI) calculated for C₂₇H₃₄NO₈S [(M+H)⁺]: 532.2000, found: 531.1996. $[\alpha]_D^{20}$ = -18.00° (1.00 g/100cm³ in CHCl₃).

Area % Report

Data File: C:\EZChrom Elite\Enterprise\Projects\Etienne\EC-159-1-column-r2074.dat
 Method: C:\EZChrom Elite\Enterprise\Projects\Default\Method\Etienne C\EC-30-90_15min.met
 Acquired: 03.05.2023 14:53:30
 Printed: 04.01.2024 14:51:28


**DAD-CH1 266
 nm Results**

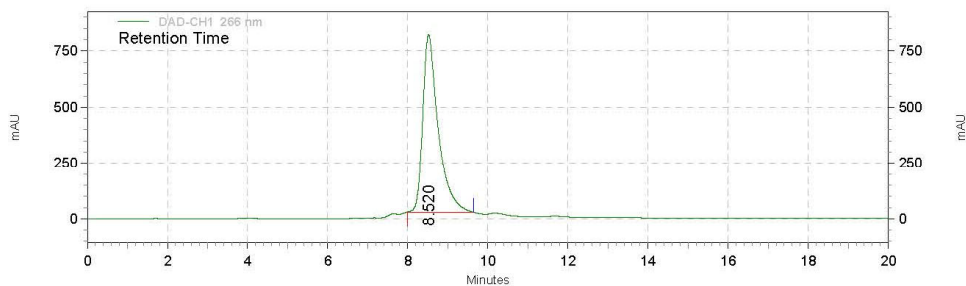
| Retention Time | Area | Area % | Height | Height % |
|----------------|----------|--------|--------|----------|
| 6.413 | 749215 | 3.01 | 43818 | 4.53 |
| 7.167 | 1870688 | 7.51 | 112195 | 11.61 |
| 8.180 | 20305880 | 81.47 | 761857 | 78.83 |
| 9.833 | 243230 | 0.98 | 10182 | 1.05 |
| 11.380 | 833829 | 3.35 | 20327 | 2.10 |
| 13.287 | 921581 | 3.70 | 18123 | 1.88 |

| | | | | |
|--------|----------|--------|--------|--------|
| Totals | 24924423 | 100.00 | 966502 | 100.00 |
|--------|----------|--------|--------|--------|

The analytical HPLC trace (Luna® 3 µm u, NH₂, 100 Å, 150 x 4.6 mm; hexane/*i*-PrOH gradient from 30:70 to 90:10 in 20 min, 1 mL/min, Rt = 8.2 min, others species of other peaks were not identified) before purification using prep HPLC is shown above. Imide **IM-6** was purified by prep HPLC (Luna® 5 µm u, NH₂, 100 Å, 150 x 21.2 mm; hexane/isopropanol 30:70 to 90:10, 15 mL/min, Rt = 8.9 min). The reinjection into the analytical HPLC of fraction with Rt = 8.9 min is shown below.

Area % Report

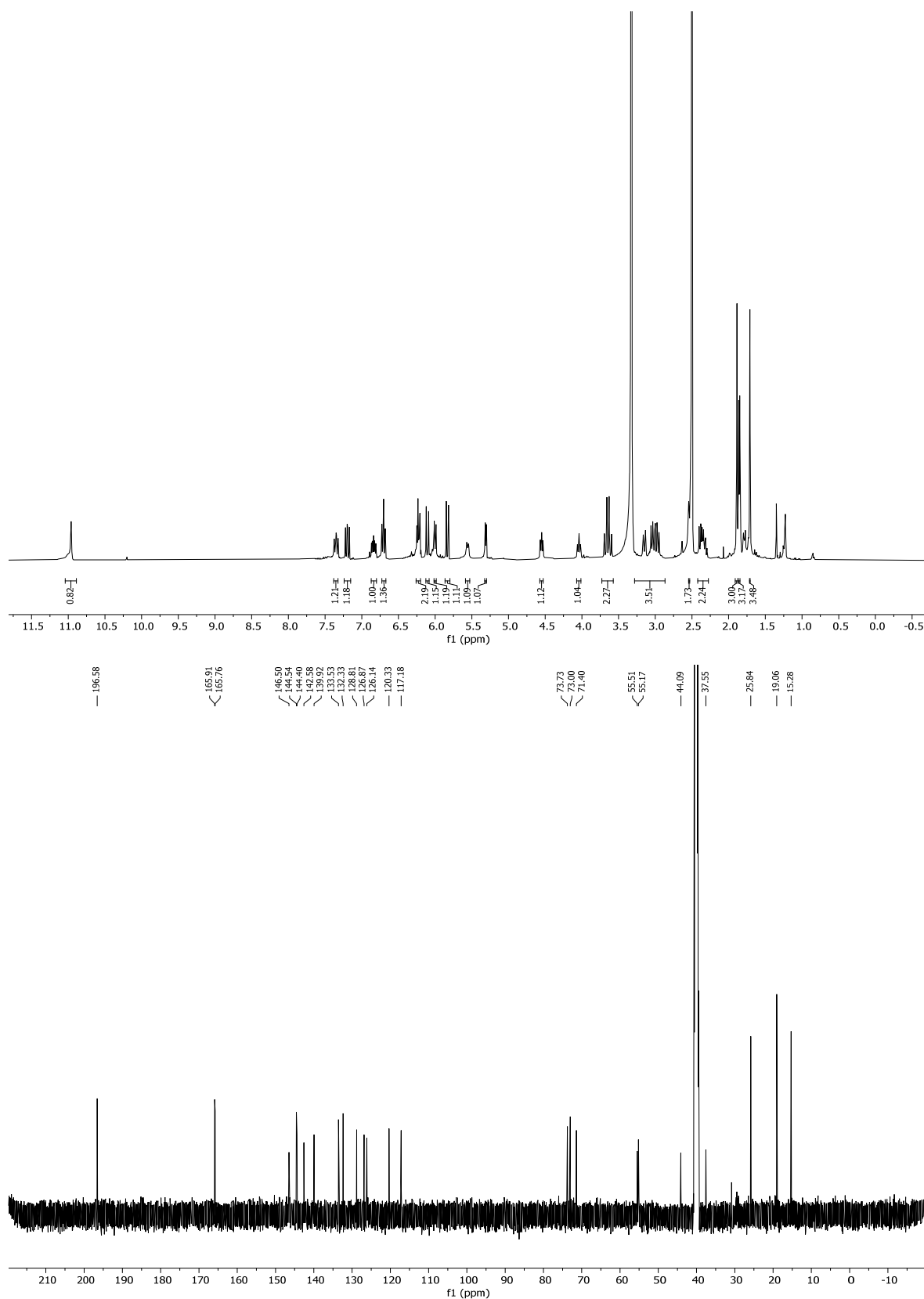
Data File: C:\EZChrom Elite\Enterprise\Projects\Etienne\EC-159-1-after-prep-HPLC075.dat
 Method: C:\EZChrom Elite\Enterprise\Projects\Default\Method\Etienne C\EC-30-90_15min.met
 Acquired: 03.05.2023 16:39:18
 Printed: 04.01.2024 14:52:45



**DAD-CH1 266
nm Results**

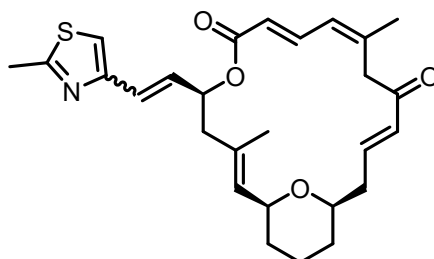
| Retention Time | Area | Area % | Height | Height % |
|----------------|----------|--------|---------|----------|
| 8.520 | 84881702 | 100.00 | 3173878 | 100.00 |
| Totals | 84881702 | 100.00 | 3173878 | 100.00 |

The analytical HPLC trace (Luna® 3 µm u, NH₂, 100 Å, 150 x 4.6 mm; hexane/*i*-PrOH gradient from 30:70 to 90:10 in 20 min, 1 mL/min, Rt = 8.5 min, no other peaks detected) after purification using prep HPLC is shown above. The material thus obtained was used in the biological experiments.



4.2.3.2 Zampanolide-Epothilone Hybrids

Literature known compounds 13-desmethylene(-)-dactyloide (**3**),^[68] **H16** (thiazole Wittig salt)^[161] and **H17** (isoxazole Wittig salt),^[162] were prepared according to literature procedures.



H1

(1*S*,2*E*,5*S*,8*E*,10*Z*,14*E*,17*R*)-3,11-dimethyl-5-((*E*)-2-(2-methylthiazol-4-yl)vinyl)-6,21-dioxabicyclo[15.3.1]henicosa-2,8,10,14-tetraene-7,13-dione (H1**):** To a solution of **H16**^[161] (75.0 mg, 0.22 mmol, 4.00 equiv.) in THF (2 mL) was added *t*-BuOK (24.0 mg, 0.22 mmol, 4.00 equiv.) at 0 °C and stirred for 30 min. The reaction mixture was cooled to -78 °C and crude mixture of **3**^[68] (20.0 mg, 0.54 mmol, 1.00 equiv.) was added dropwise in THF (0.5 mL). The reaction mixture was allowed to warm to -20 °C over a period of 2 h. The reaction was then quenched by addition of sat. aqu. NH₄Cl (4 mL), the phases were separated and the aqueous phase was extracted with Et₂O (3 x 6 mL). The combined organic phases were dried over MgSO₄, concentrated under reduced pressure and the residue was purified by flash column chromatography (Hexane/EtOAc 5:1 → 4:1) and reverse-phase preparative HPLC (for each isomer separately) (25% → 95% acetonitrile in H₂O in 20 min, 25 ml/min) giving **H1-Z** (0.7 mg, 0.002 mmol, 3%) and **H1-E** (12.0 mg, 0.026 mmol, 48%) as pale yellow oils.

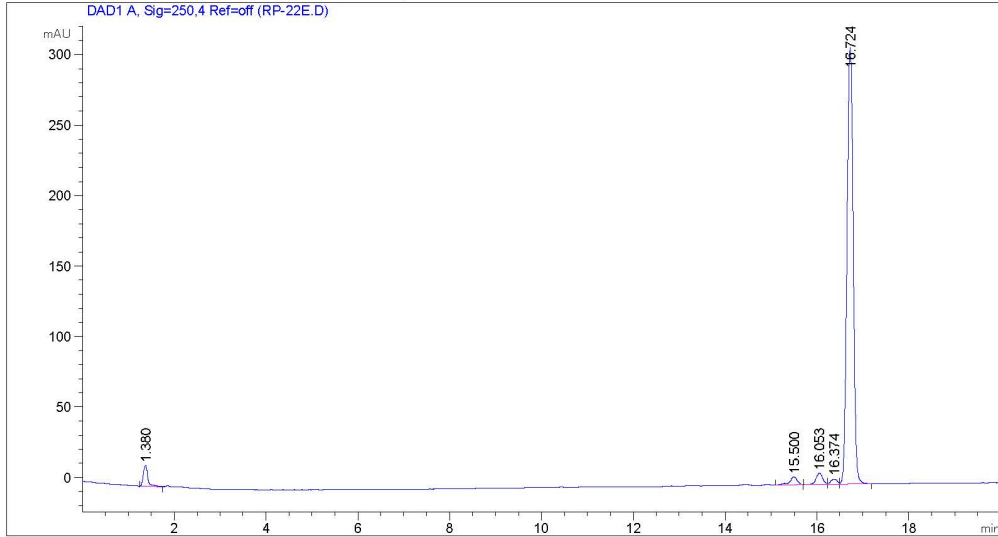
Analytcs of H1-Z:

TLC: R_f = 0.26 (EtOAc/Hexane 1:4). **¹H-NMR** (400 MHz, CDCl₃) δ = 7.63 (dd, *J* = 15.0, 11.6 Hz, 1H), 7.02 (s, 1H), 6.96 – 6.81 (m, 2H), 6.34 (dd, *J* = 11.9, 1.4 Hz, 1H), 6.13 – 6.05 (m, 1H), 5.98 – 5.86 (m, 2H), 5.75 (dd, *J* = 11.8, 7.9 Hz, 1H), 5.17 (dt, *J* = 7.8, 1.4 Hz, 1H), 4.17 (d, *J* = 13.5 Hz, 1H), 4.05 (ddd, *J* = 10.8, 8.0, 2.3 Hz, 1H), 3.31 (tt, *J* = 10.6, 2.0 Hz, 1H), 3.01 (d, *J* = 13.5 Hz, 1H), 2.72 (s, 3H), 2.45 – 2.11 (m, 4H), 1.88 (d, *J* = 1.3 Hz, 3H), 1.78 (s, 3H), 1.54 – 1.35 (m, 3H), 1.23 (dddd, *J* = 17.4, 15.4, 11.1, 4.2 Hz, 3H). **¹³C-NMR** (151 MHz, CDCl₃) δ = 198.6, 166.7, 165.5, 152.4, 147.2, 142.5, 138.9, 132.6, 131.4, 129.9, 125.7, 122.0, 121.9, 117.7, 76.2, 75.5, 69.7, 46.1, 45.11, 40.7, 32.0, 31.8, 23.6, 19.4, 16.4. **IR** (neat): $\tilde{\nu}$ = 2923, 2854, 1709, 1669, 1635, 1503, 1437, 1378, 1353, 1277, 1257, 1208, 1177, 1121, 1077, 1012, 976, 884, 865, 782, 754, 673 cm⁻¹. **HRMS** (ESI): calcd for C₂₇H₃₄NO₄S [M+H]⁺ 468.2203, found 468.2192. $[\alpha]_D^{20}$: -413.25° (c = 0.15, CHCl₃).

Data File C:\CHEM32\1\DATA\DEF_LC 2023-11-16 13-17-01\RP-22E.D
 Sample Name: RP22Z

```

=====
Acq. Operator   : SYSTEM                      Seq. Line :    1
Acq. Instrument : LCMS309                    Location  : Vial 1
Injection Date  : 11/16/2023 1:17:57 PM      Inj       :    1
                                           Inj Volume: 4.000 µl
Sequence File   : C:\Chem32\1\DATA\DEF_LC 2023-11-16 13-17-01\DEF_LC.S
Method          : C:\CHEM32\1\DATA\DEF_LC 2023-11-16 13-17-01\RP_40A100EN16_20TOTAL.M (
                  Sequence Method)
Last changed    : 11/16/2023 1:17:01 PM by SYSTEM
    
```



Area Percent Report

```

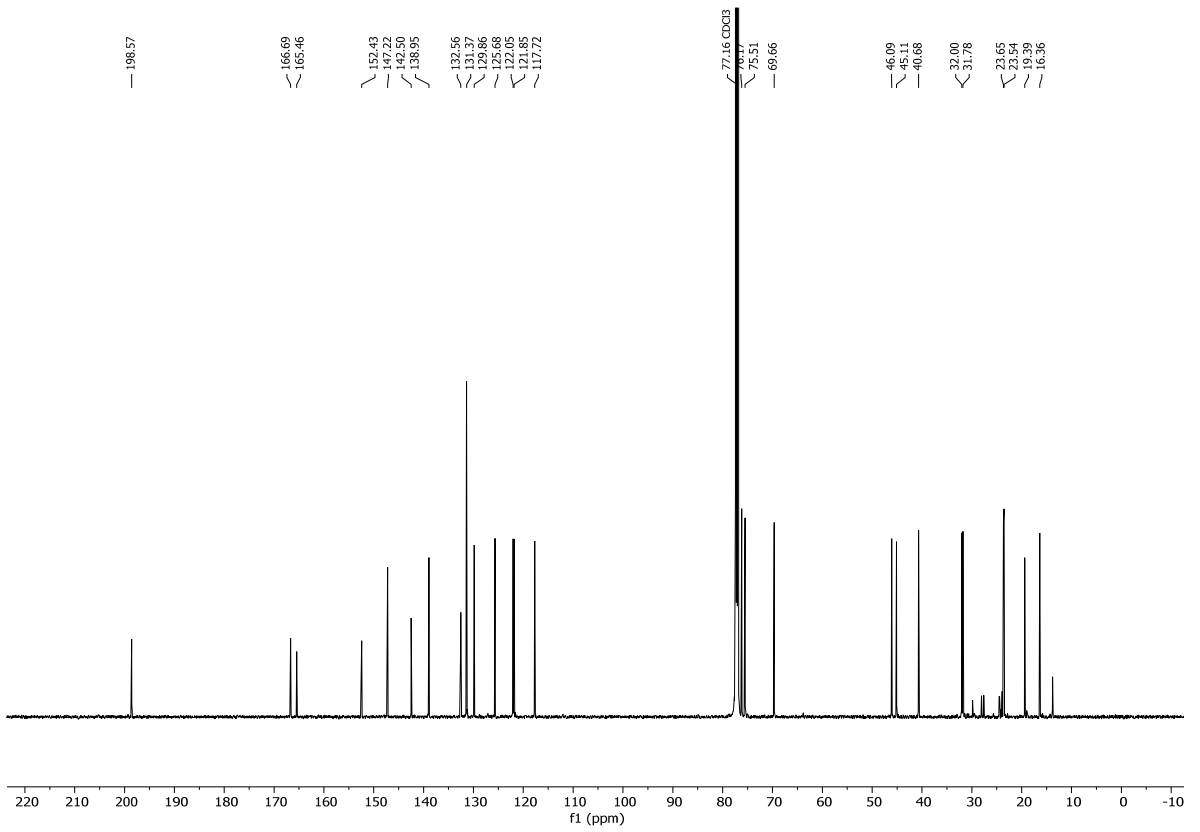
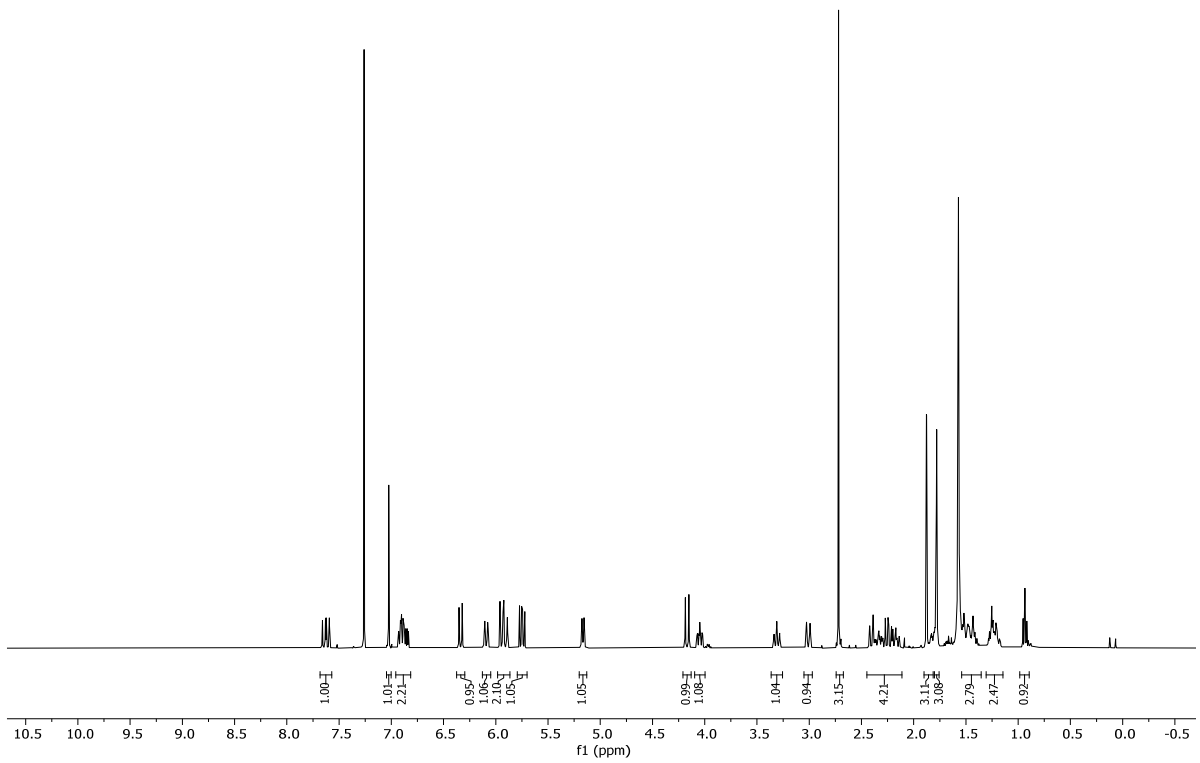
Sorted By      :      Signal
Multiplier     :      1.0000
Dilution       :      1.0000
Use Multiplier & Dilution Factor with ISTDs
    
```

Signal 1: DAD1 A, Sig=250,4 Ref=off

| Peak # | RetTime [min] | Type | Width [min] | Area [mAU*s] | Height [mAU] | Area % |
|--------|---------------|------|-------------|--------------|--------------|---------|
| 1 | 1.380 | BB | 0.1095 | 100.19541 | 14.69879 | 3.1330 |
| 2 | 15.500 | BB | 0.1707 | 60.52794 | 5.40274 | 1.8927 |
| 3 | 16.053 | BV | 0.1554 | 78.37458 | 7.92104 | 2.4507 |
| 4 | 16.374 | VV | 0.1503 | 35.63248 | 3.76794 | 1.1142 |
| 5 | 16.724 | VB | 0.1521 | 2923.31396 | 309.87878 | 91.4094 |

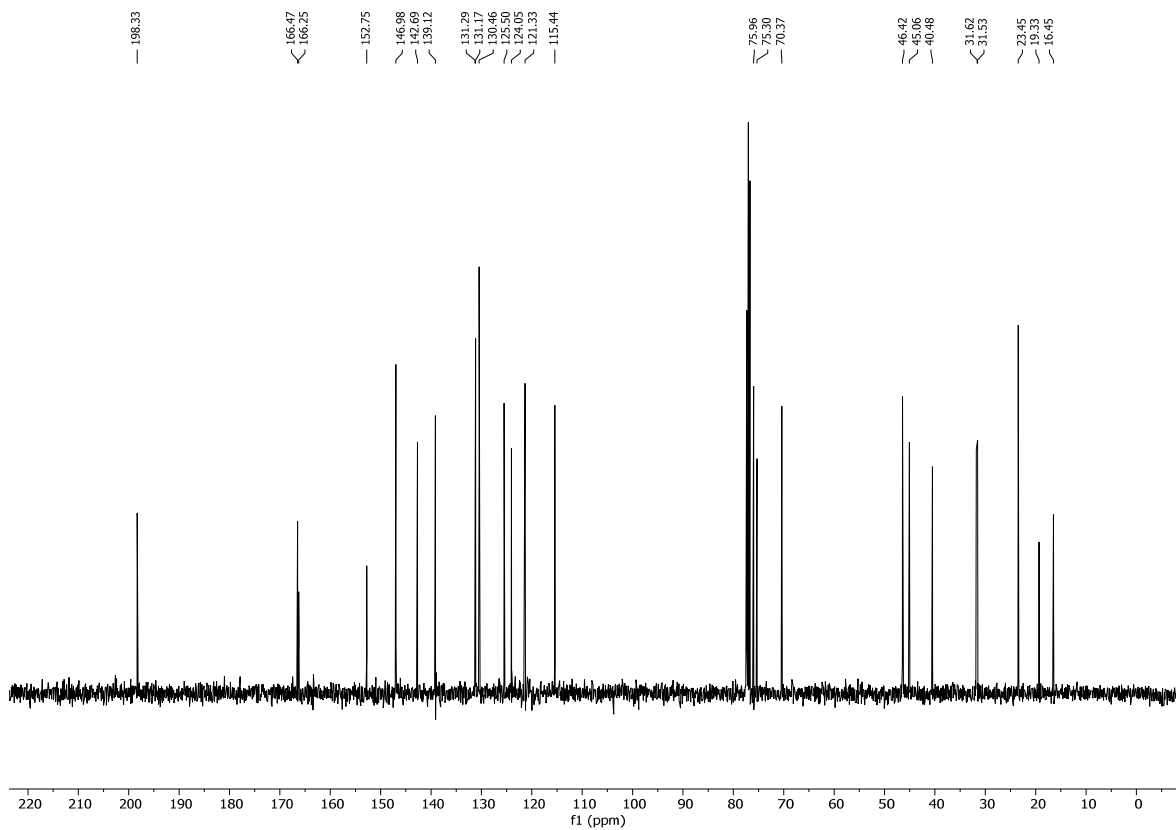
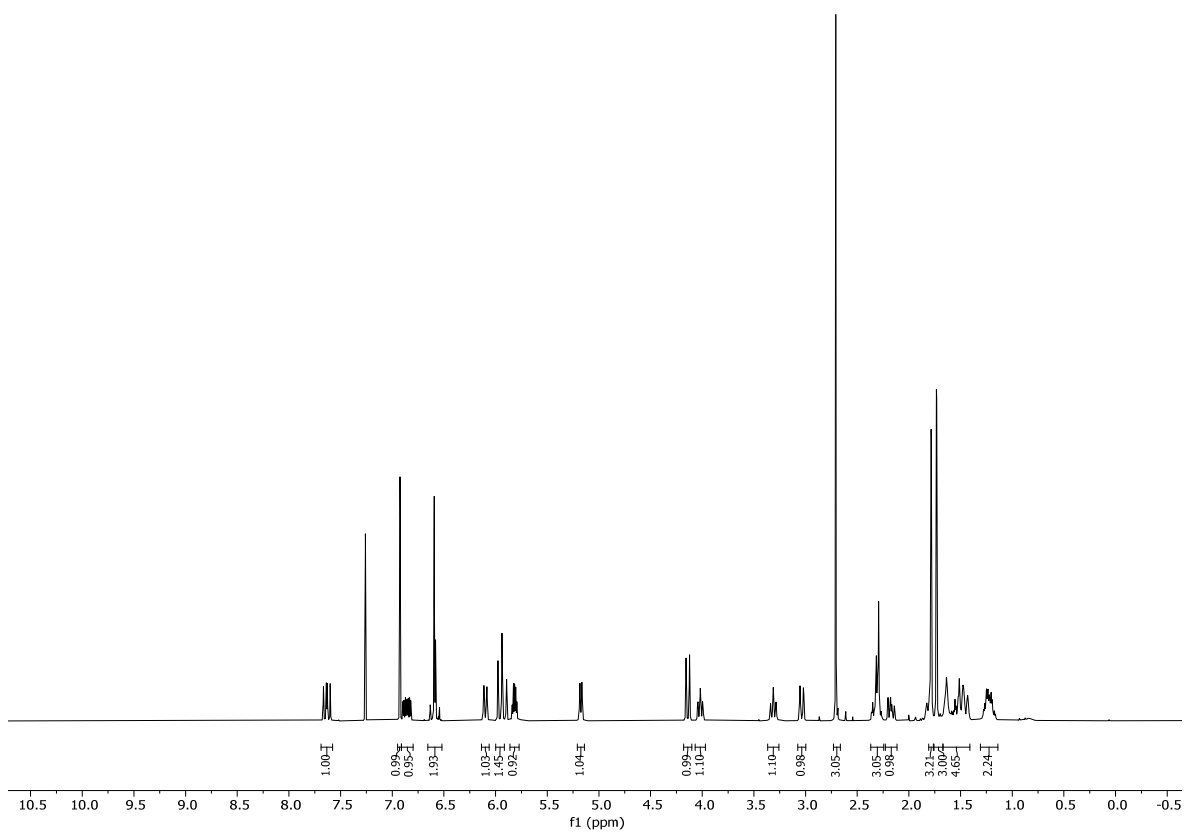
Totals : 3198.04437 341.66930

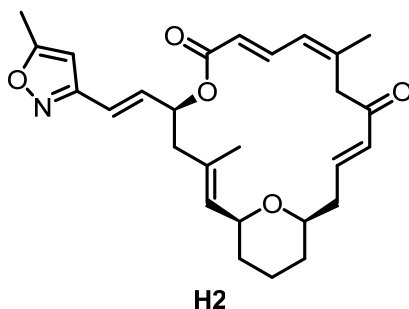
The reversed phase analytical HPLC trace shown above was measured with the Agilent 1100 device mentioned in the general part. A gradient of 40% → 100% acetonitrile in H₂O in 16 min, with a flow rate of 1 mL/min was used. Peak 1 is the injection peak (DMSO), therefore the purity of compound is 94% (areas of peak 2-4 vs. area of peak 5). Thus, the material obtained was used in the biological experiments.



Analytics of H1-E:

TLC: $R_f = 0.19$ (EtOAc/Hexane 1:4). **$^1\text{H-NMR}$** (400 MHz, CDCl_3) $\delta = 7.63$ (dd, $J = 15.0, 11.5$ Hz, 1H), 6.93 (s, 1H), 6.86 (ddd, $J = 16.3, 9.8, 4.5$ Hz, 1H), 6.59 (d, $J = 5.1$ Hz, 2H), 6.10 (d, $J = 11.5$ Hz, 1H), 6.00 – 5.91 (m, 2H), 5.82 (dt, $J = 8.8, 4.3$ Hz, 1H), 5.17 (dd, $J = 7.8, 1.5$ Hz, 1H), 4.14 (d, $J = 13.6$ Hz, 1H), 4.02 (ddd, $J = 10.8, 8.1, 2.4$ Hz, 1H), 3.37 – 3.26 (m, 1H), 3.04 (d, $J = 13.5$ Hz, 1H), 2.71 (s, 3H), 2.37 – 2.24 (m, 3H), 2.23 – 2.11 (m, 1H), 1.79 (s, 3H), 1.73 (d, $J = 1.3$ Hz, 3H), 1.67 – 1.41 (m, 4H), 1.31 – 1.14 (m, 2H). **$^{13}\text{C-NMR}$** (101 MHz, CDCl_3) = δ 198.3, 166.5, 166.2, 152.6, 147.0, 142.7, 139.1, 131.23, 131.2, 130.5, 125.5, 124.0, 121.3, 115.4, 76.0, 75.3, 70.4, 46.4, 45.1, 40.5, 31.6, 31.5, 23.5, 19.3, 16.5. **IR** (neat): $\tilde{\nu} = 3106, 2930, 2855, 1712, 1668, 1634, 1508, 1436, 1379, 1355, 1279, 1256, 1208, 1177, 1120, 1077, 1042, 1015, 975, 884, 861, 814, 754, 666, 592$ cm^{-1} . **HRMS** (ESI): calcd for $\text{C}_{27}\text{H}_{34}\text{NO}_4\text{S}$ $[\text{M}+\text{H}]^+$ 468.2203, found 468.2193. $[\alpha]_D^{20}$: -293.79° ($c = 1.2, \text{CHCl}_3$).





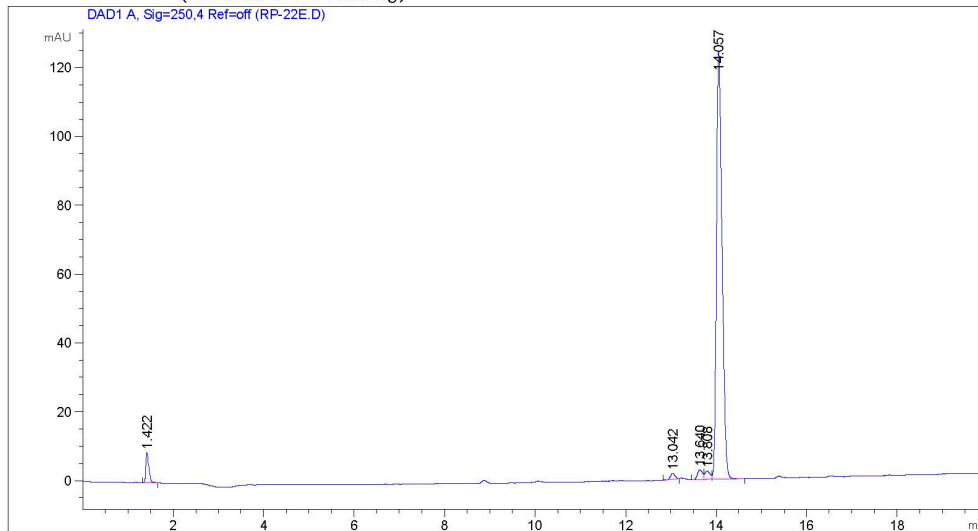
(1*S*,2*E*,5*S*,8*E*,10*Z*,14*E*,17*R*)-3,11-dimethyl-5-((*E*)-2-(5-methylisoxazol-3-yl)vinyl)-6,21-dioxabicyclo[15.3.1]henicosa-2,8,10,14-tetraene-7,13-dione (H2**):** To a solution of **H17**^[162] (72.0 mg, 0.22 mmol, 4.00 equiv.) in THF (2 mL) was added *t*-BuOK (24.0 mg, 0.22 mmol, 4.00 equiv.) at 0 °C and stirred for 30 min. The reaction mixture was cooled to -78 °C and crude mixture of **3**^[68] (20.0 mg, 0.08 mmol, 1.00 equiv.) was added dropwise in THF (1 mL). The reaction mixture was allowed to warm to -20 °C over a period of 2 h. The reaction was then quenched by addition of sat. aqu. NH₄Cl (4 mL), the phases were separated and the aqueous phase was extracted with Et₂O (3 x 6 mL). The combined organic phases were dried over MgSO₄, concentrated under reduced pressure and the residue was purified by flash column chromatography (Hexane/EtOAc 5:1 → 4:1) to afford **H2** (12.0 mg, 0.03 mmol, 50%) as a pale yellow oil.

TLC: *R*_f = 0.18 (EtOAc/Hexane 1:4). **¹H-NMR** (400 MHz, CDCl₃) δ = 7.64 (dd, *J* = 15.0, 11.5 Hz, 1H), 6.85 (ddd, *J* = 16.3, 9.6, 4.5 Hz, 1H), 6.66 (dd, *J* = 16.2, 1.5 Hz, 1H), 6.33 (dd, *J* = 16.2, 5.5 Hz, 1H), 6.14 – 6.05 (m, 2H), 5.94 (t, *J* = 15.3 Hz, 2H), 5.81 (dtd, *J* = 10.2, 5.1, 1.6 Hz, 1H), 5.18 (dd, *J* = 8.1, 1.5 Hz, 1H), 4.17 – 4.09 (m, 1H), 4.01 (ddd, *J* = 10.6, 8.0, 2.3 Hz, 1H), 3.37 – 3.26 (m, 1H), 3.05 (d, *J* = 13.5 Hz, 1H), 2.41 (s, 3H), 2.36 – 2.25 (m, 3H), 2.18 (ddd, *J* = 15.3, 9.6, 2.0 Hz, 1H), 1.79 (s, 3H), 1.73 (d, *J* = 1.3 Hz, 3H), 1.60 – 1.39 (m, 3H), 1.32 – 1.14 (m, 3H). **¹³C-NMR** (101 MHz, CDCl₃) δ = 198.3, 169.5, 166.4, 161.1, 147.1, 143.2, 139.7, 135.5, 131.3, 130.9, 125.6, 121.0, 119.3, 98.9, 76.1, 75.4, 69.8, 46.0, 45.2, 40.5, 31.9, 31.6, 23.6, 23.5, 16.6, 12.4. **IR** (neat): $\tilde{\nu}$ = 2961, 2928, 2855, 1712, 1668, 1634, 1604, 1436, 1356, 1279, 1260, 1207, 1176, 1147, 1078, 1016, 928, 903, 884, 800, 753, 710 666, 591 cm⁻¹. **HRMS** (ESI): calcd for C₂₇H₃₃NNaO₅ [M+Na]⁺ 474.2251, found 474.2246. [α]_D²⁰: -255.40° (c = 1.1, CHCl₃).

Data File C:\CHEM32\1\DATA\DEF_LC 2023-11-16 14-14-22\RP-22E.D
 Sample Name: RP-20

```

=====
Acq. Operator   : SYSTEM                      Seq. Line :    1
Acq. Instrument : LCMS309                     Location  : Vial 1
Injection Date  : 11/16/2023 2:15:17 PM      Inj       :    1
                                           Inj Volume: 4.000 µl
Sequence File   : C:\Chem32\1\DATA\DEF_LC 2023-11-16 14-14-22\DEF_LC.S
Method          : C:\CHEM32\1\DATA\DEF_LC 2023-11-16 14-14-22\RP_40A100EN16_20TOTAL.M (
                  Sequence Method)
Last changed    : 11/16/2023 2:34:41 PM by SYSTEM
                  (modified after loading)
    
```



Area Percent Report

```

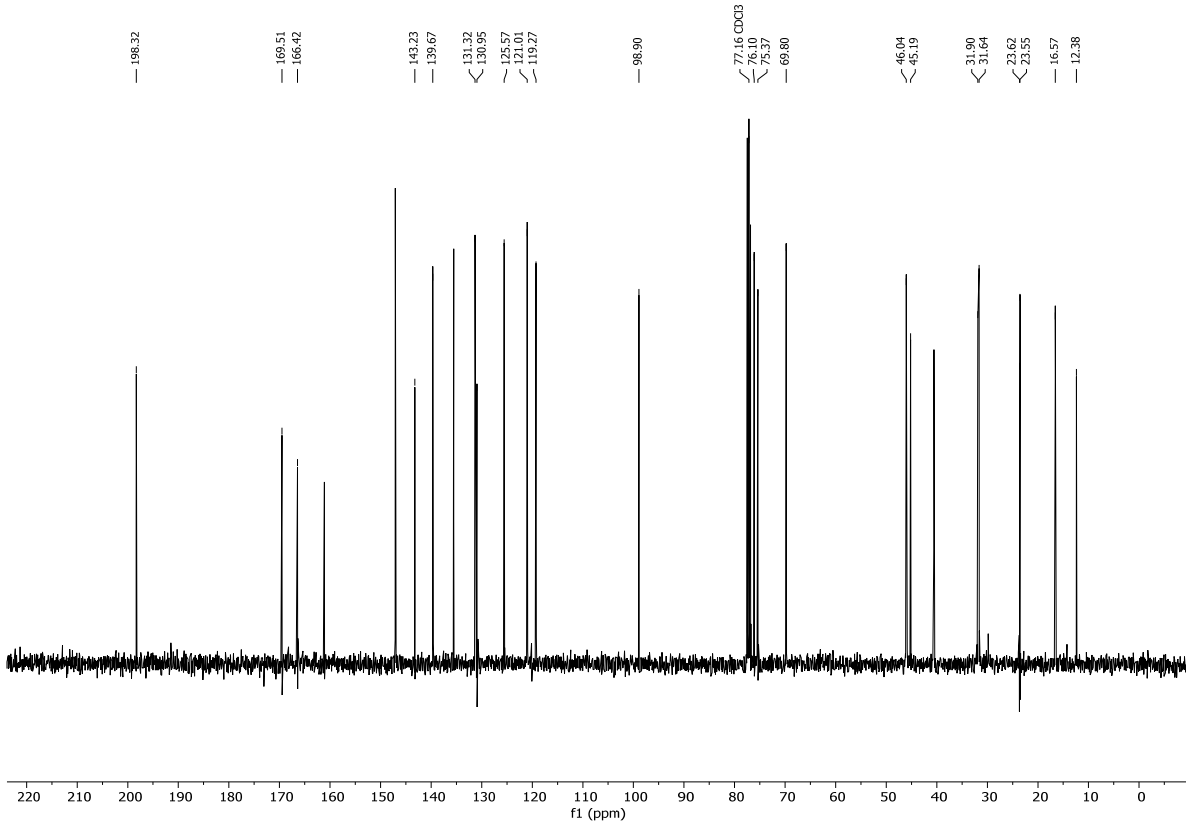
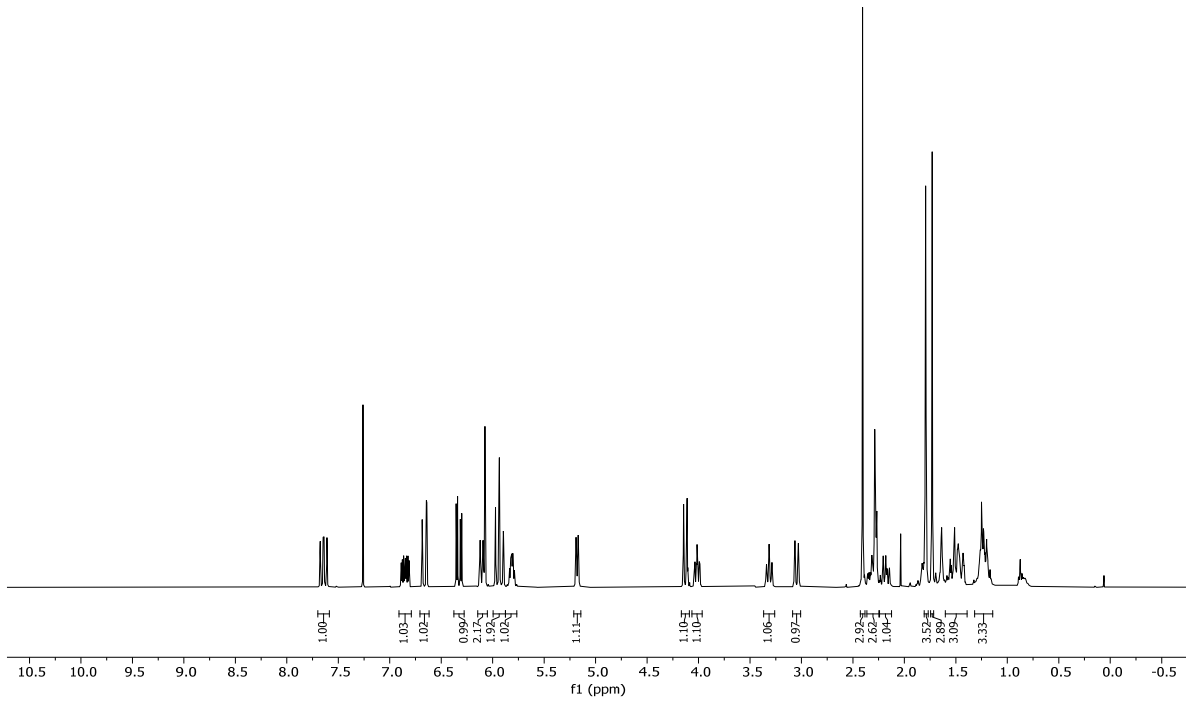
Sorted By      : Signal
Multiplier     : 1.0000
Dilution       : 1.0000
Use Multiplier & Dilution Factor with ISTDs
    
```

Signal 1: DAD1 A, Sig=250,4 Ref=off

| Peak # | RetTime [min] | Type | Width [min] | Area [mAU*s] | Height [mAU] | Area % |
|--------|---------------|------|-------------|--------------|--------------|---------|
| 1 | 1.422 | BB | 0.0640 | 39.31610 | 8.81457 | 3.3746 |
| 2 | 13.042 | BB | 0.1133 | 12.19326 | 1.70868 | 1.0466 |
| 3 | 13.640 | BV | 0.1148 | 21.69508 | 2.85145 | 1.8622 |
| 4 | 13.808 | VV | 0.1173 | 19.31392 | 2.41639 | 1.6578 |
| 5 | 14.057 | VB | 0.1266 | 1072.53442 | 124.34931 | 92.0589 |

Totals : 1165.05279 140.14040

The reversed phase analytical HPLC trace shown above was measured with the Agilent 1100 device mentioned in the general part. A gradient of 40% → 100% acetonitrile in H₂O in 16 min, with a flow rate of 1 mL/min was used. Peak 1 is the injection peak (DMSO), therefore the purity of compound is 95% (areas of peak 2-4 vs. area of peak 5). Thus, the material obtained was used in the biological experiments.

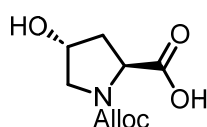


4.3 Studies Towards the Synthesis of Core-Modified Analogs of β -lactam Antibiotics

4.3.1 Studies Towards the Synthesis of 1,3-Diazetidione-Based Analogs of β -Lactam Antibiotics

Literature known compounds **D6**,^[232] **D8**,^[229] **D9**•HCl,^[231,316] **D18**,^[234] **D22**,^[233] and **DS7**^[235] were prepared according to literature procedures.

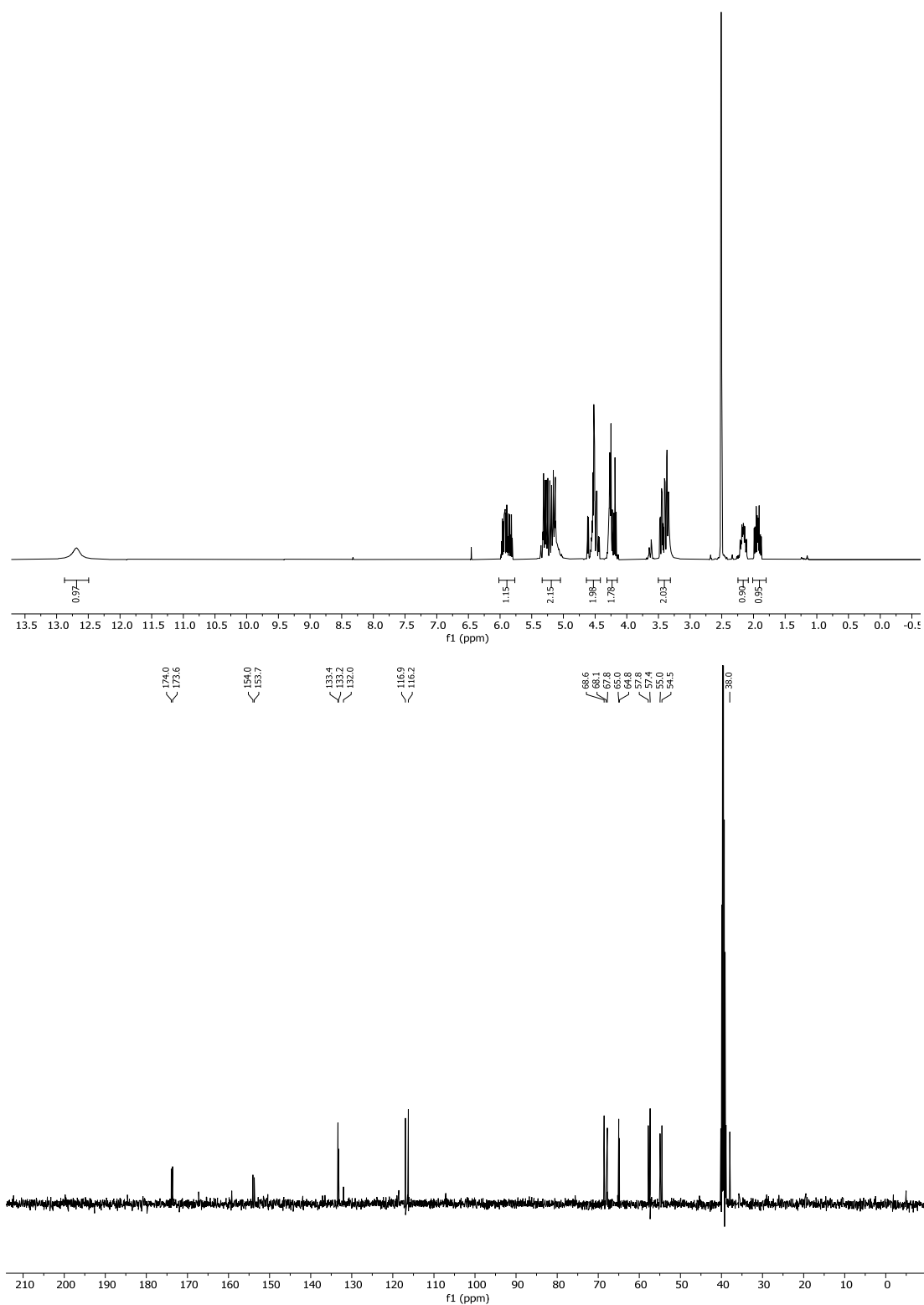
4.3.1.1 Synthesis of D5a



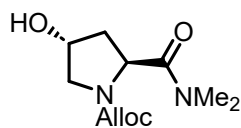
DS1

(2S,4R)-1-((Allyloxy)carbonyl)-4-hydroxyproline-2-carboxylic acid (DS1).^[317] A solution of allyl chloroformate (5.9 mL, 54.91 mmol, 1.20 equiv.) in THF (6.1 mL) was added dropwise to a suspension of trans-4-hydroxy-L-proline (6.00 g, 45.76 mmol, 1.00 equiv.) in a mixture of THF (30 mL) and H₂O (30 mL) at 0 °C, while maintaining the pH at 9 with 4M NaOH. After being stirred at 0 °C for 1 h, the mixture was saturated with solid NaCl and extracted with EtOAc (60 mL). The aqueous phase was separated, washed with further EtOAc (60 mL) and then adjusted to pH 2 with 12M HCl. The resulting milky emulsion was extracted with EtOAc (2 x 60 mL), and the combined organic extracts were washed with brine (120 mL), dried over MgSO₄ and concentrated to give **DS1** (8.51 g, 39.54 mmol, 86%) as a viscous oil that was used in the next step without further purification.

TLC: R_f = 0.45 (acetone/EtOAc 1:1, + 1% acetic acid). **¹H-NMR** (400 MHz, DMSO): δ 12.69 (s, 1H), 5.89 (dddt, J = 29.4, 17.3, 10.7, 5.0 Hz, 1H), 5.34 – 5.05 (m, 2H), 4.64 – 4.42 (m, 2H), 4.31 – 4.15 (m, 2H), 3.50 – 3.31 (m, 2H), 2.24 – 2.08 (m, 1H), 1.93 (dddd, J = 18.2, 12.9, 7.9, 4.8 Hz, 1H). **¹³C-NMR** (101 MHz, DMSO): δ = 174.0, 173.6, 154.0, 153.8, 133.4, 133.2, 132.0, 116.9, 116.2, 68.6, 68.1, 67.8, 65.0, 64.9, 57.8, 57.4, 55.0, 54.5, 38.0. **HRMS** (ESI): calcd for C₉H₁₃NNaO₅ [(M+Na)⁺]: 238.0686; found: 238.0691.

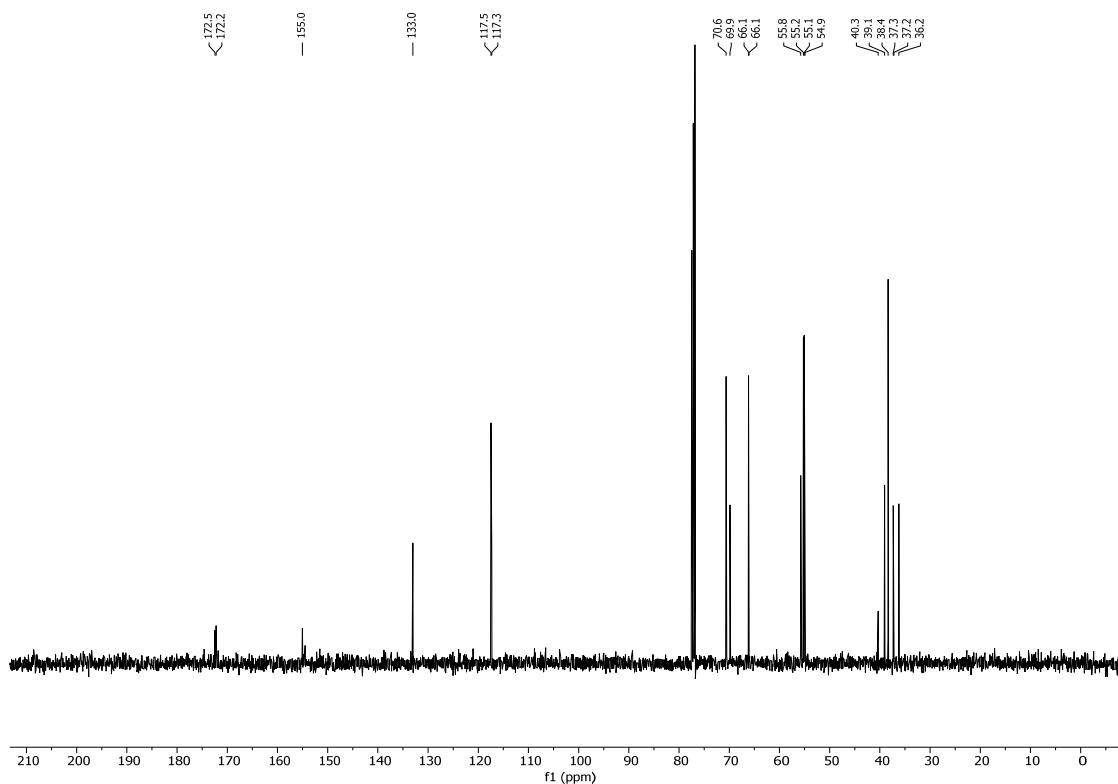
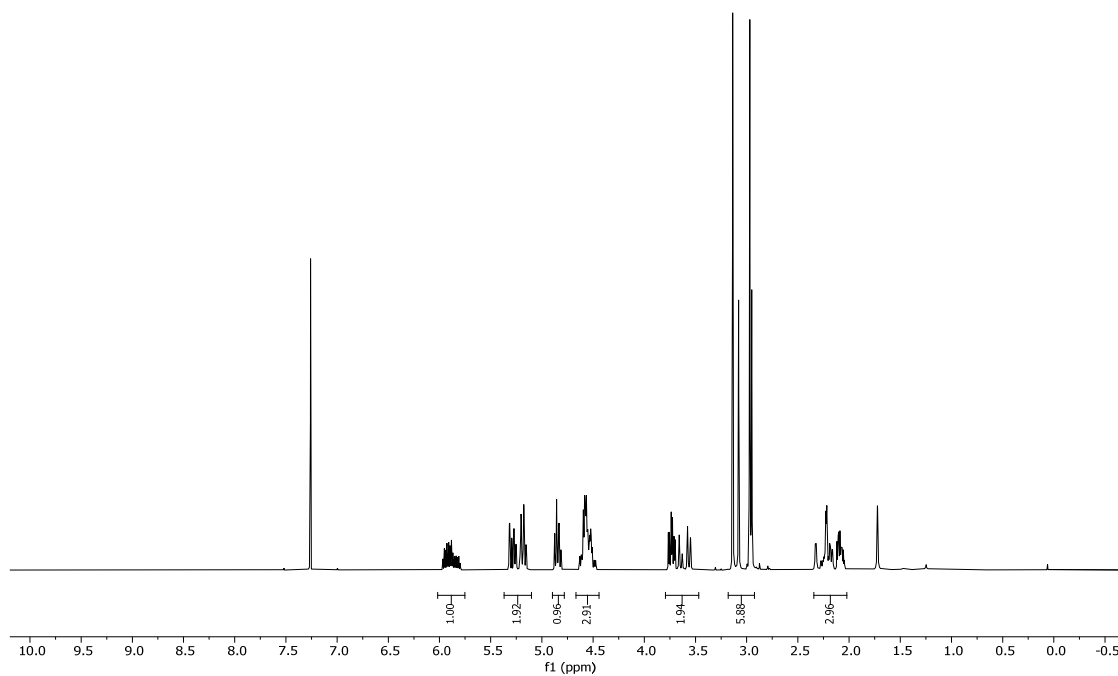


Remark: Peaks in ^1H and ^{13}C -NMR spectra broad and split due to the presence of *N*-Alloc rotamers

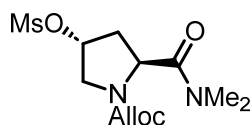
**DS2**

Allyl (2*S*,4*R*)-2-(dimethylcarbamoyl)-4-hydroxypyrrolidine-1-carboxylate (DS2). A solution of **DS1** (0.50 g, 2.32 mmol, 1.00 equiv.) and HBTU (3.52 g, 9.29 mmol, 4.00 equiv.) in DMF (16 mL) was stirred for 5 min before DIPEA (3.16 mL, 18.59 mmol, 8.00 equiv.) was added and stirring was continued for 10 more minutes. Me₂NH•HCl (0.76 g, 9.29 mmol, 4.00 equiv.) was then added. The mixture was stirred for 5 h. The solvent was evaporated under reduced pressure and the residue was dissolved in EtOAc (100 mL). The solution was washed with H₂O (40 mL), sat. aq. NaHCO₃ (40 mL) and brine (40 mL). The combined aqueous layers were re-extracted with CH₂Cl₂ (3 x 150) and the combined organic extracts were dried over MgSO₄, concentrated in vacuo and the residue was purified by FC (CH₂Cl₂/MeOH 20:1) to give **DS2** (0.41 g, 1.92 mmol, 85%) as a colorless oil.

TLC: R_f = 0.35 (acetone/EtOAc 1:1, + 1% acetic acid). **¹H-NMR** (400 MHz, CDCl₃): δ = 5.88 (dddt, *J* = 29.1, 17.1, 10.7, 5.4 Hz, 1H), 5.37 – 5.10 (m, 2H), 4.84 (dt, *J* = 9.6, 7.5 Hz, 1H), 4.67 – 4.44 (m, 3H), 3.79 – 3.47 (m, 2H), 3.18 – 2.92 (m, 6H), 2.34 – 2.02 (m, 3H). **¹³C-NMR** (101 MHz, CDCl₃): δ = 172.5, 172.2, 155.1, 133.0, 117.5, 117.3, 70.6, 7.86, 66.2, 66.1, 55.8, 55.2, 55.1, 54.9, 40.4, 39.1, 38.4, 37.3, 37.2, 36.2. **IR** (neat): $\tilde{\nu}$ = 3398, 2940, 2879, 1690, 1638, 1501, 1410, 1343, 1274, 1260, 1202, 1178, 1145, 1086, 1051, 992, 972, 930, 845, 769, 617 cm⁻¹. **HRMS** (ESI): calcd for C₁₁H₁₉N₂O₄ [(M+H)⁺]: 243.1339; found: 243.1336. $[\alpha]_D^{20}$: -18.30 (c = 1.00 in CHCl₃).

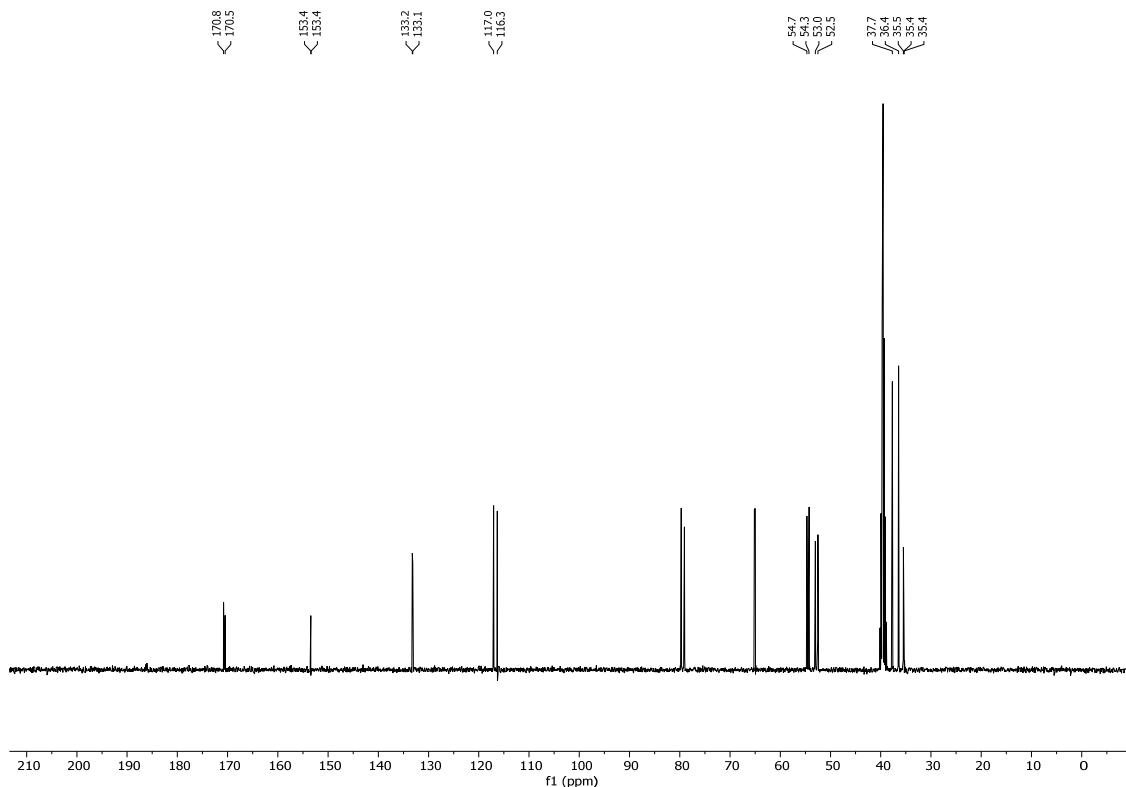
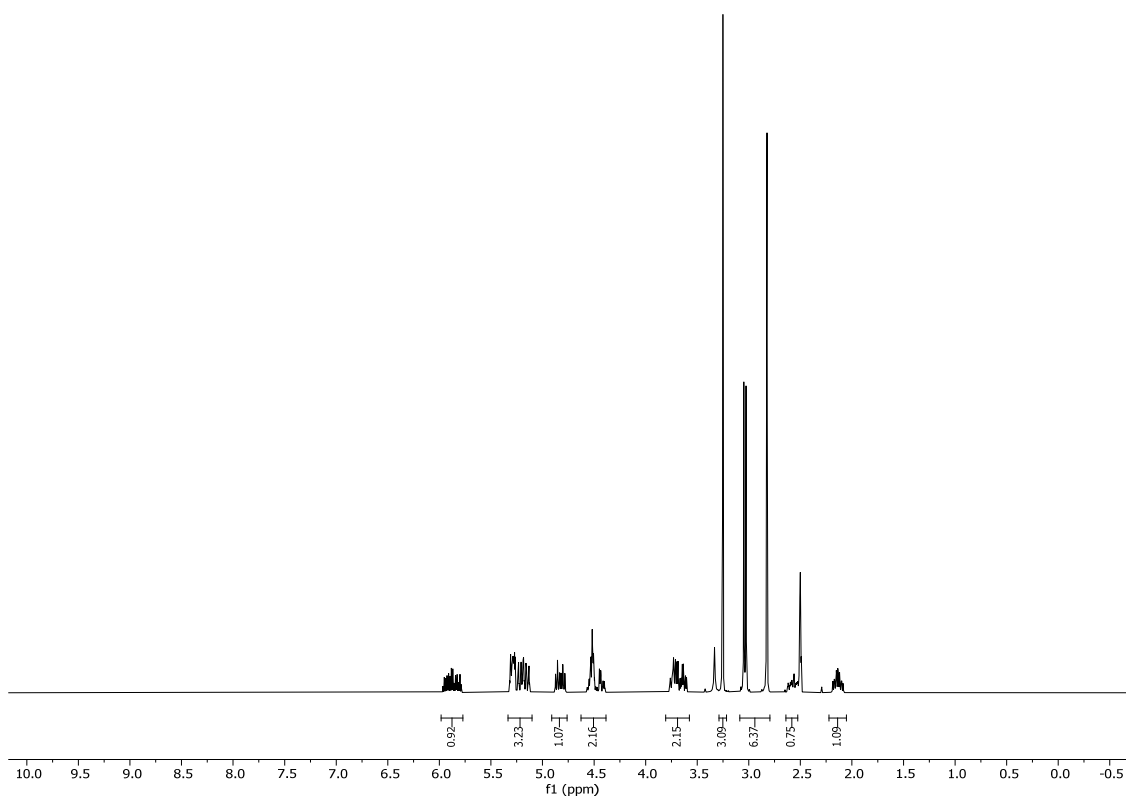


Remark: Peaks in ^1H and ^{13}C -NMR spectra broad and split due to the presence of *N*-Alloc and *N*-Me₂ rotamers.

**DS3****Allyl (2S,4R)-2-(dimethylcarbamoyl)-4-((methylsulfonyl)oxy)pyrrolidine-1-carboxylate (DS3).**

To a suspension of **DS2** (0.5 g, 2.06 mmol, 1.00 equiv.) in CH_2Cl_2 (4 mL) were added Et_3N (0.35 mL, 2.45 mmol, 1.20 equiv.) and MsCl (0.19 mL, 2.45 mmol, 1.20 equiv.) dropwise at 0° . After stirring for 1 h at that temperature the mixture was successively washed with brine (5 mL), sat. aq. NaHCO_3 (5 mL) and brine (5 mL) again and the two brine washings were re-extracted with CH_2Cl_2 (3 x 20 mL). The combined organic layers were dried over MgSO_4 , concentrated in vacuo and purified by FC (EtOAc/hexane 1:1 \rightarrow EtOAc) to give **DS3** (0.57 g, 1.78 mmol, 86%) as a colorless oil.

TLC: R_f = 0.50 (acetone/EtOAc 1:1). **$^1\text{H-NMR}$** (400 MHz, DMSO): δ = 5.98 – 5.77 (m, 1H), 5.33 – 5.10 (m, 3H), 4.91 – 4.76 (m, 1H), 4.63 – 4.38 (m, 2H), 3.81 – 3.58 (m, 2H), 3.25 (s, 3H), 3.09 – 2.80 (m, 6H), 2.64 – 2.53 (m, 1H), 2.14 (tdd, J = 14.0, 7.1, 5.2 Hz, 1H). **$^{13}\text{C-NMR}$** (101 MHz, DMSO): δ = 170.8, 170.5, 153.4, 153.4, 133.2, 133.2, 117.1, 116.3, 54.7, 54.3, 53.0, 52.5, 37.7, 36.5, 35.5, 35.4, 35.4. **IR** (neat): $\tilde{\nu}$ = 2937, 1703, 1651, 1500, 1411, 1354, 1264, 1205, 1172, 1145, 1050, 959, 901, 845, 796, 769, 527 cm^{-1} . **HRMS** (ESI): calcd for $\text{C}_{12}\text{H}_{20}\text{N}_2\text{NaO}_6\text{S}$ [(M+Na) $^+$]: 343.0934; found: 343.0934. $[\alpha]_D^{20}$: -11.10 (c = 1.00 in CHCl_3).

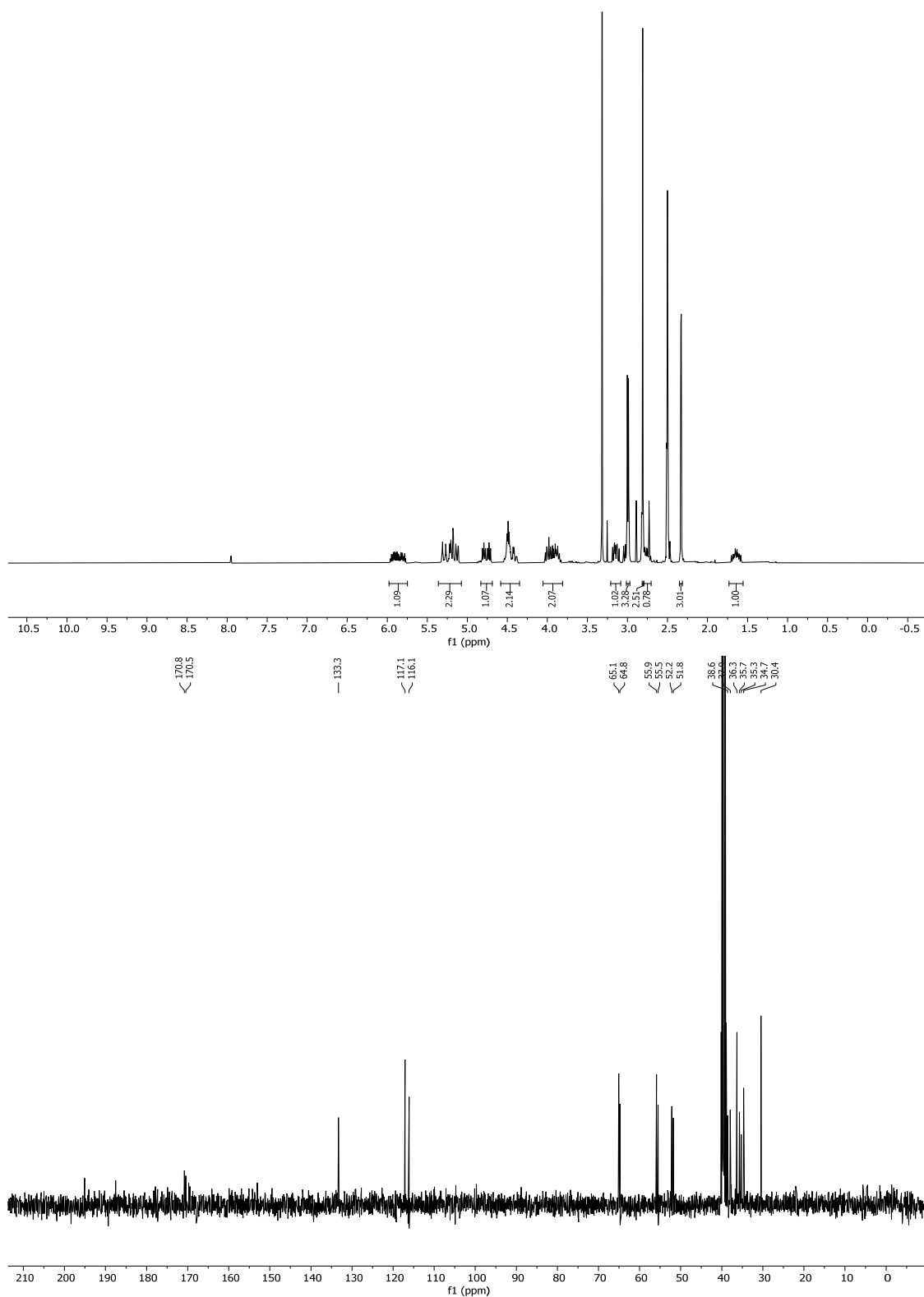


Remark: Peaks in ^1H and ^{13}C -NMR spectra broad and split due to the presence of *N*-Alloc and *N*-Me₂ rotamers.

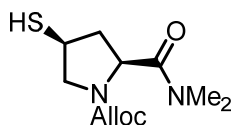
**DS4**

Allyl (2S,4S)-4-(acetylthio)-2-(dimethylcarbamoyl)pyrrolidine-1-carboxylate (DS4). A mixture of **DS3** (0.56 g, 1.75 mmol, 1.00 equiv.) and AcSK (0.30 g, 2.62 mmol, 1.50 equiv.) in DMF/toluene (5 mL, 1:1) was stirred for 7 h at 60-70 °C. After the reaction mixture was cooled to rt toluene (15 mL) and H₂O (5 mL) were added, the layers were separated and the aqueous layer was extracted with toluene (3x 20 mL). The combined organic extracts were washed with H₂O (2x 10 mL) and with brine (10 mL), dried over MgSO₄ and then concentrated affording **DS4** (0.44 g, 1.46, 84%) as a red oil, which was used for the next step without further purification.

TLC: R_f = 0.50 (acetone/EtOAc 1:1). **MP** = 51 °C. **¹H-NMR³** (400 MHz, DMSO): δ = 5.98 – 5.75 (m, 1H), 5.36 – 5.07 (m, 2H), 4.83 – 4.69 (m, 1H), 4.58 – 4.35 (m, 2H), 4.05 – 3.81 (m, 2H), 3.14 (ddd, J = 13.8, 10.3, 8.5 Hz, 1H), 2.99 (d, J = 6.1 Hz, 3H), 2.81 (s, 3H), 2.79 – 2.70 (m, 1H), 2.33 (d, J = 2.3 Hz, 3H), 1.64 (dddd, J = 19.0, 12.8, 8.9, 6.7 Hz, 1H). **¹³C-NMR** (101 MHz, DMSO): δ = 170.8, 170.5, 133.3, 117.1, 116.1, 65.1, 64.8, 55.9, 55.5, 52.2, 51.8, 38.6, 37.9, 36.3, 35.7, 35.3, 34.7, 30.4. **IR** (neat): $\tilde{\nu}$ = 2939, 2878, 1698, 1654, 1498, 1405, 1353, 1285, 1265, 1218, 1197, 1117, 1057, 999, 979, 954, 921, 768, 630 cm⁻¹. **HRMS** (ESI): calcd for C₁₃H₂₁N₂O₄S [(M+H)⁺]: 301.1217; found: 301.1214. $[\alpha]_D^{20}$: -9.50 (c = 1.00 in CHCl₃).

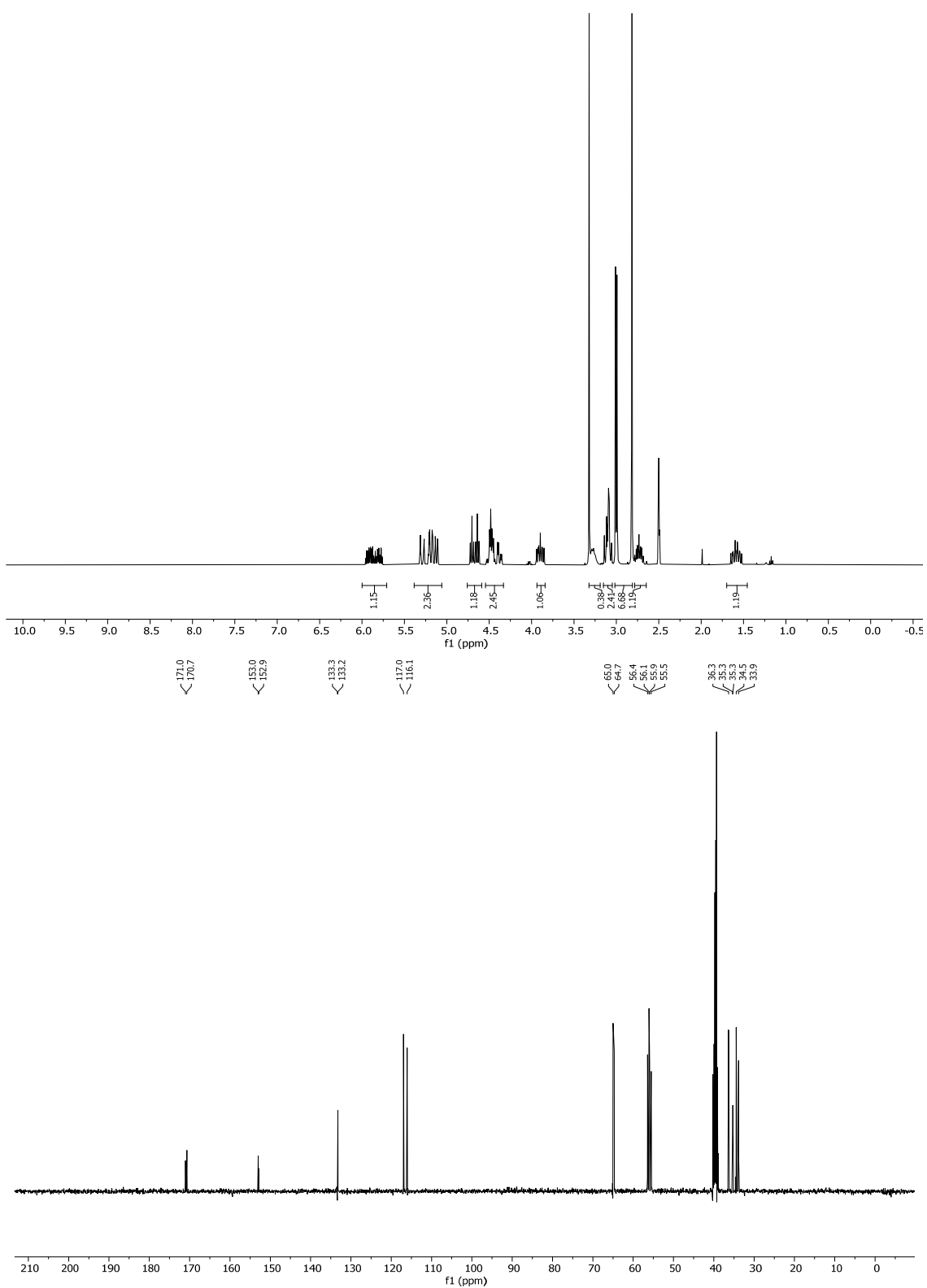


Remark: Spectra contain traces of DMF and Peaks in ^1H and ^{13}C -NMR spectra broad and split due to the presence of *N*-Alloc and *N*-Me₂ rotamers.

**D5a**

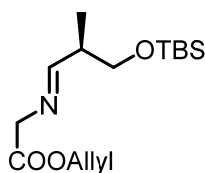
Allyl (2*S*,4*S*)-2-(dimethylcarbamoyl)-4-mercaptopyrrolidine-1-carboxylate (D5a). To a solution of **DS4** (0.53 g, 1.75 mmol, 1.00 equiv.) in MeOH (5 mL) was added 4M NaOH (0.46 mL, 1.84 mmol, 1.05 equiv.) dropwise at 0 °C and the mixture was stirred for 15 min at that temperature. 4M HCl (0.48 mL, 1.92 mmol, 1.10 equiv.), H₂O (20 mL) and EtOAc (30 mL) were then added. The layers were separated and the aqueous layer was extracted with EtOAc (3x 25 mL). The combined organic extracts were washed with brine (40 mL) dried over MgSO₄ and then concentrated. Purification of the residue by FC (EtOAc) afforded **D5a** (0.29 g, 1.11 mmol, 63% over two steps from **DS3**) as a red oil.

TLC: R_f = 0.65 (acetone/EtOAc 1:1). **¹H-NMR** (400 MHz, DMSO): δ = 6.00 – 5.71 (m, 1H), 5.38 – 5.06 (m, 2H), 4.67 (dt, *J* = 25.5, 8.0 Hz, 1H), 4.54 – 4.33 (m, 2H), 3.94 – 3.84 (m, 1H), 3.32 – 3.19 (m, 0H), 3.15 – 3.05 (m, 2H), 3.02 – 2.81 (m, 7H), 2.73 (tt, *J* = 12.9, 7.2 Hz, 1H), 1.59 (dddd, *J* = 20.3, 12.5, 10.3, 8.1 Hz, 1H). **¹³C-NMR** (101 MHz, DMSO): δ = 171.0, 170.7, 153.0, 152.9, 133.4, 133.2, 117.0, 116.1, 65.0, 64.7, 56.4, 56.1, 55.9, 55.5, 36.3, 35.4, 35.3, 34.5, 33.9. **IR** (neat): $\tilde{\nu}$ = 3726, 3626, 3599, 3568, 3549, 3525, 2938, 2872, 2342, 1500, 1651, 1289, 1265, 1198, 1174, 1146, 1122, 999, 980, 922, 768, 677, 656 cm⁻¹. **HRMS** (ESI): calcd for C₁₁H₁₉N₂O₃S [(M+H)⁺]: 259.1111; found: 259.1108. $[\alpha]_D^{20}$: -4.00 (c = 1.00 in CHCl₃).



Remark: Remark: Peaks in ^1H and ^{13}C -NMR spectra broad and split due to the presence of *N*-Alloc and *N*-Me₂ rotamers.

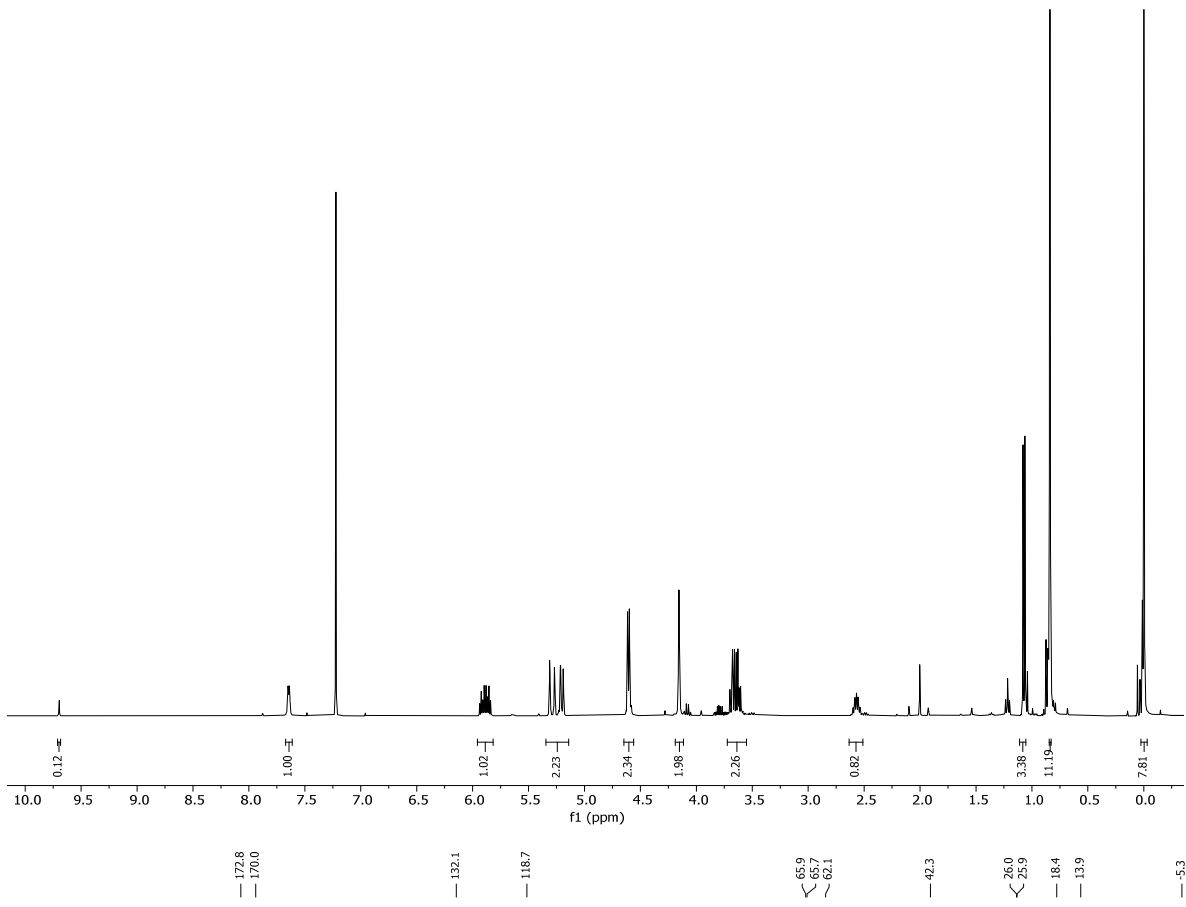
4.3.1.2 Synthesis of D12-D15



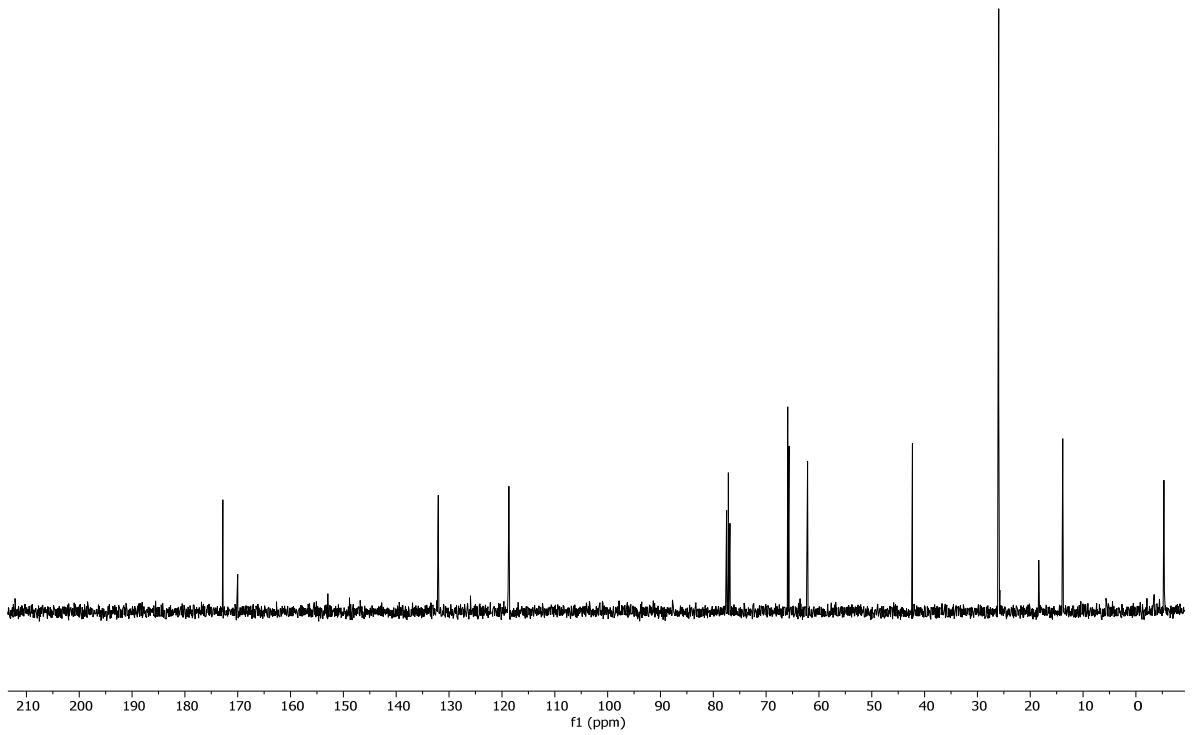
D7

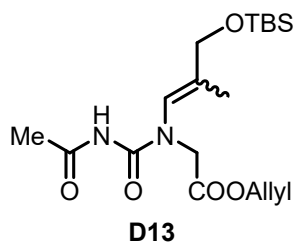
Allyl (*R,E*)-2-((3-((*tert*-butyldimethylsilyl)oxy)-2-methylpropylidene)amino)acetate (D7). Allyl glycinate hydrochloride (**D9**•HCl)^[231,316] (72.0 mg, 0.48 mmol, 1.00 equiv.) was dissolved in CH₂Cl₂ (5 mL) and Et₃N (1 mL). The solution was stirred for 20 min. (*S*)-3-((*tert*-Butyldimethylsilyl)oxy)-2-methylpropanal (**D8**)^[229] (82.0 mg, 0.34 mmol, 0.70 equiv.) in CH₂Cl₂ (5 mL) and MgSO₄ (200 mg) were added to the solution. The reaction mixture was stirred for 2 h. The MgSO₄ was removed by filtration, the filtrate was diluted with EtOAc (15 mL) and H₂O (15 mL), the layers were separated and the aqueous layer was extracted with EtOAc (3 x 15 mL). The organic layer was washed with H₂O (25 mL) and brine (2 x 25 mL). The organic layer was dried over MgSO₄ and the solvent was removed under reduced pressure to afford **D7** (106.7 mg, 0.39 mmol, 88%, as an 8.3:1 mixture with **D8** (11%), calculated based on NMR spectroscopy).

TLC: R_f = 0.48 (EtOAc/hexane 1:9). **¹H-NMR** (400 MHz, CDCl₃): δ = 5.98 – 5.82 (m, 1H), 5.40 – 5.20 (m, 2H), 4.68 – 4.54 (m, 3H), 0.14 – -0.01 (m, 1H). **¹³C-NMR** (101 MHz, CDCl₃): δ = 172.8, 170.0, 132.1, 118.7, 65.9, 65.7, 62.1, 42.3, 26.0, 25.9, 18.4, 13.9, -5.3. **IR** (neat): $\tilde{\nu}$ = 2954, 2929, 2884, 2857, 1747, 1671, 1472, 1463, 1389, 1362, 1254, 1220, 1177, 1093, 1032, 1007, 987, 935, 835, 815, 774 cm⁻¹. **HRMS** (ESI): calcd for C₁₅H₃₀NO₃Si [(M+H)⁺]: 300.1989; found: 300.1993. **[α]_D²⁰**: +4.00° (c = 1.00, CHCl₃).



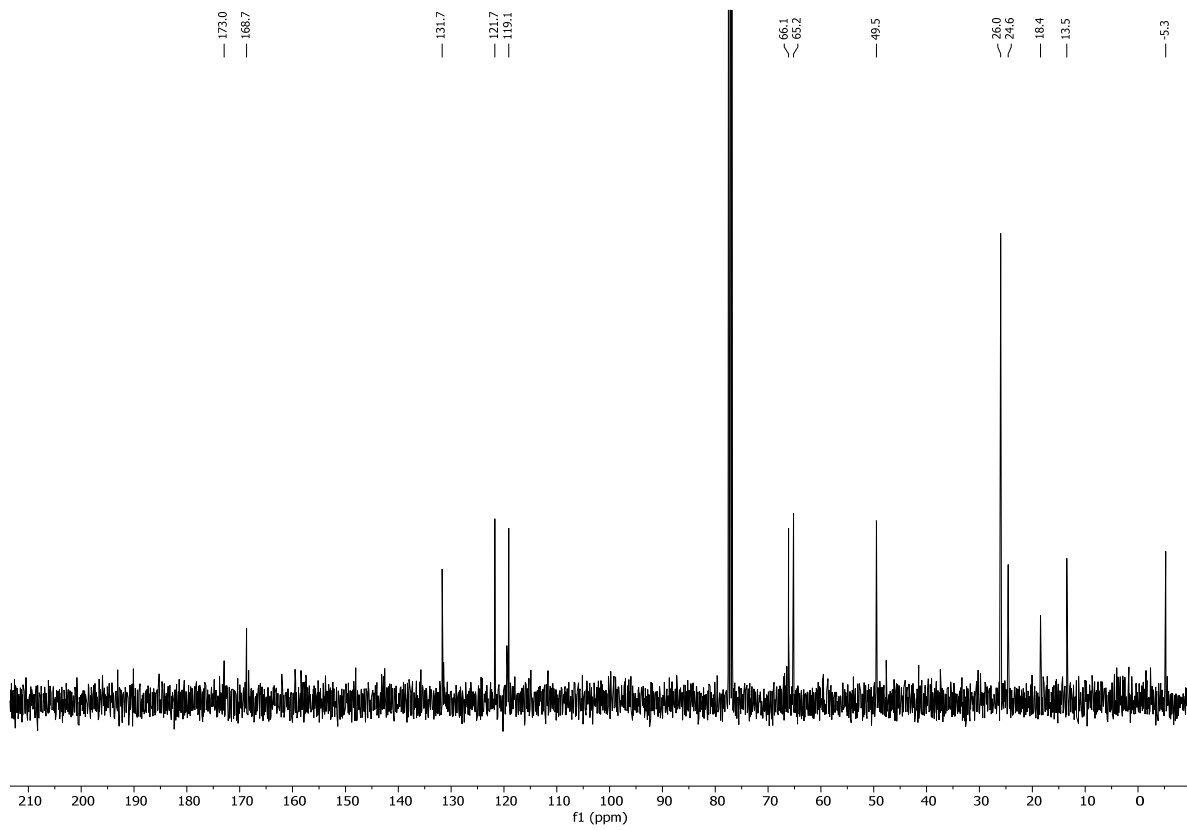
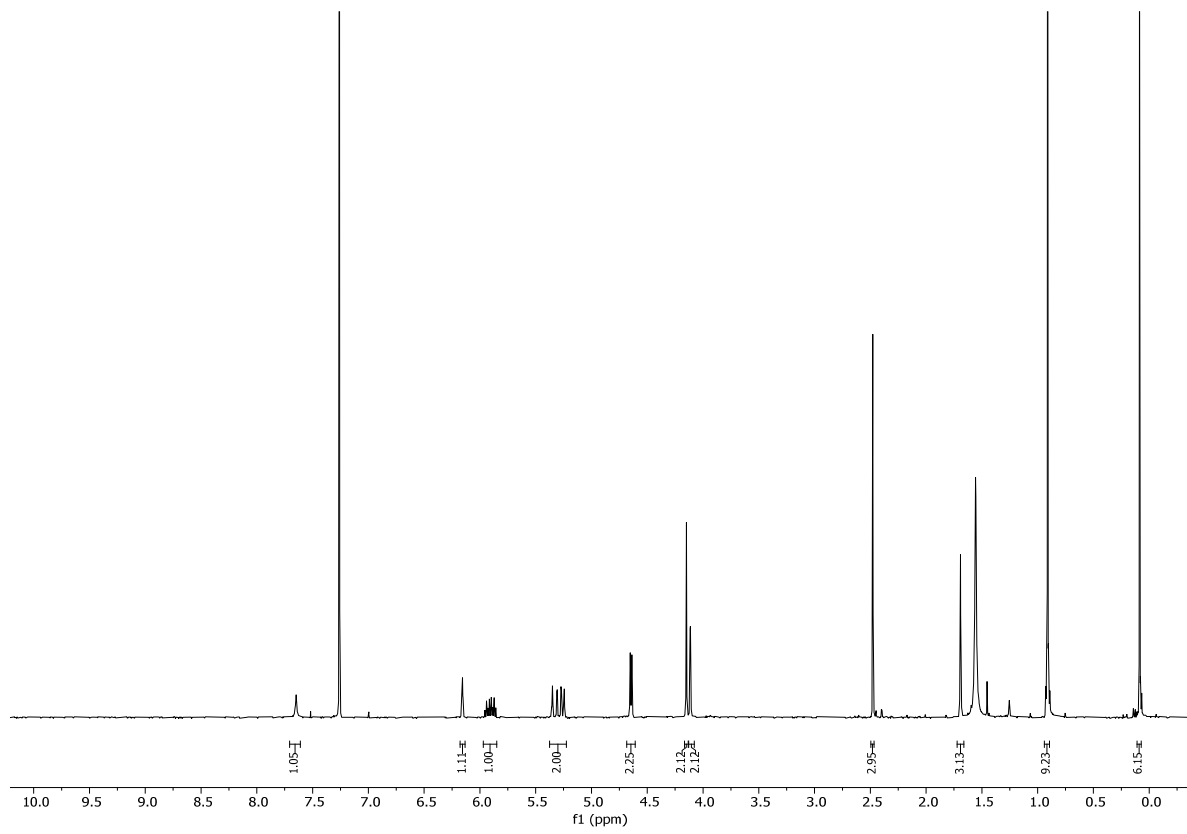
172.8
170.0
132.1
118.7
65.9
65.7
62.1
42.3
26.0
25.9
18.4
13.9
5.3

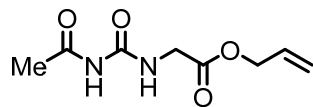




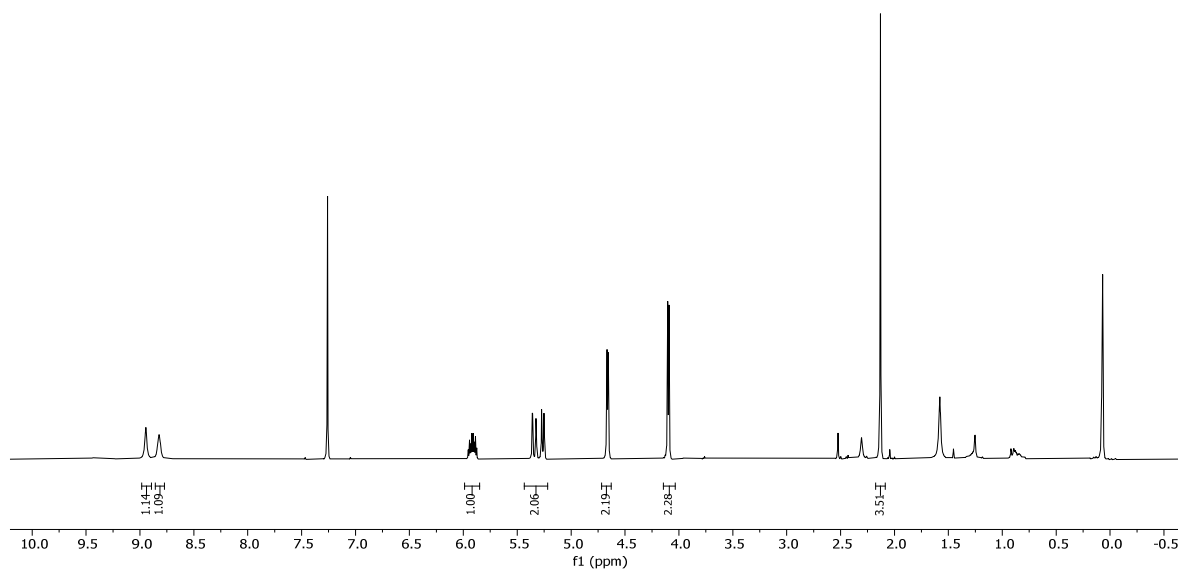
Allyl N-(acetylcabamoyl)-N-(3-((tert-butyldimethylsilyl)oxy)-2-methylprop-1-en-1-yl)glycinate (D13). *In situ* preparation of **D6**.^[232] Acetamide (74.00 mg, 1.25 mmol, 2.50 eq.) was suspended in 1,2-DCE (0.74 mL) in a flame-dried necked round bottom flask and attached to a reflux condenser under argon. Addition of oxalyl chloride (0.12 mL, 1.40 mmol, 2.80 eq.) caused the development of a gas. The reaction was refluxed for 3 h. During that time the yellow solution turned light brown and developed small white particles. The solvent was not removed under reduced pressure as acetylisocyanate¹ has a similar boiling ppoint as DCE (80°C vs. 84°C for DCE). Et₂O (6.3 mL) was added and the solution was transferred dropwise to a solution of **D7** (150 mg, 0.50 mmol, 1.00 equiv.) in Et₂O (10 mL) at -78 °C. The mixture was stirred at that temperature for 6 h. H₂O (15 mL) was then added, the phases were separated and the aqueous phase was extracted with CH₂Cl₂ (3 x 15 mL), the combined organic phases were washed with H₂O (25 mL), dried over MgSO₄. The crude residue was purified by FC (EtOAc/hexane 1:5 → 1:2 → pure EtOAc) to afford **D13** (9.0 mg, 0.02 mmol, 5%, unknown E/Z ratio) as a pale yellow oil. In addition, Allyl (acetylcabamoyl)glycinate (**D12**) (31.0 mg, 0.14 mmol, 30%) was isolated as colorless powder.

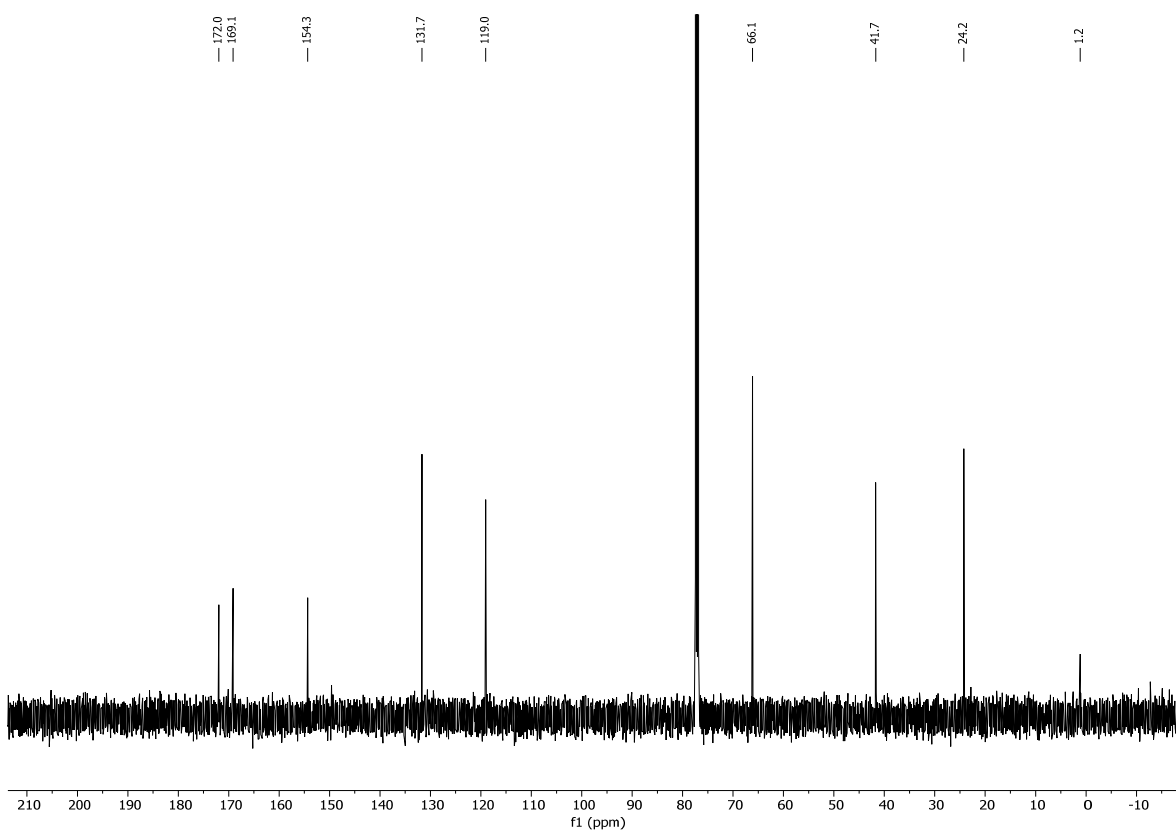
TLC: R_f = 0.45 (EtOAc/hexane 1:2). **¹H-NMR** (400 MHz, CDCl₃): δ = 7.65 (s, 1H), 6.16 (q, J = 1.5 Hz, 1H), 5.91 (ddt, J = 17.2, 10.4, 5.8 Hz, 1H), 5.38 – 5.22 (m, 2H), 4.65 (dt, J = 5.8, 1.4 Hz, 2H), 4.15 (s, 2H), 4.11 (d, J = 1.7 Hz, 2H), 2.48 (s, 3H), 1.69 (d, J = 1.5 Hz, 3H), 0.91 (s, 9H), 0.09 (s, 6H). **¹³C-NMR** (101 MHz, CDCl₃): δ = 173.0, 168.7, 131.7, 121.7, 119.1, 66.1, 65.2, 49.5, 26.0, 24.6, 18.4, 13.5, -5.3. **IR** (neat): $\tilde{\nu}$ = 3297, 2950, 1690, 1543, 1494, 1448, 1413, 1378, 1250, 1092, 986, 839, 779, 761, 668, 603 cm⁻¹. **HRMS** (ESI): calcd for C₁₈H₃₂N₂NaO₅Si [(M+Na)⁺]: 407.1973; found: 407.1972.

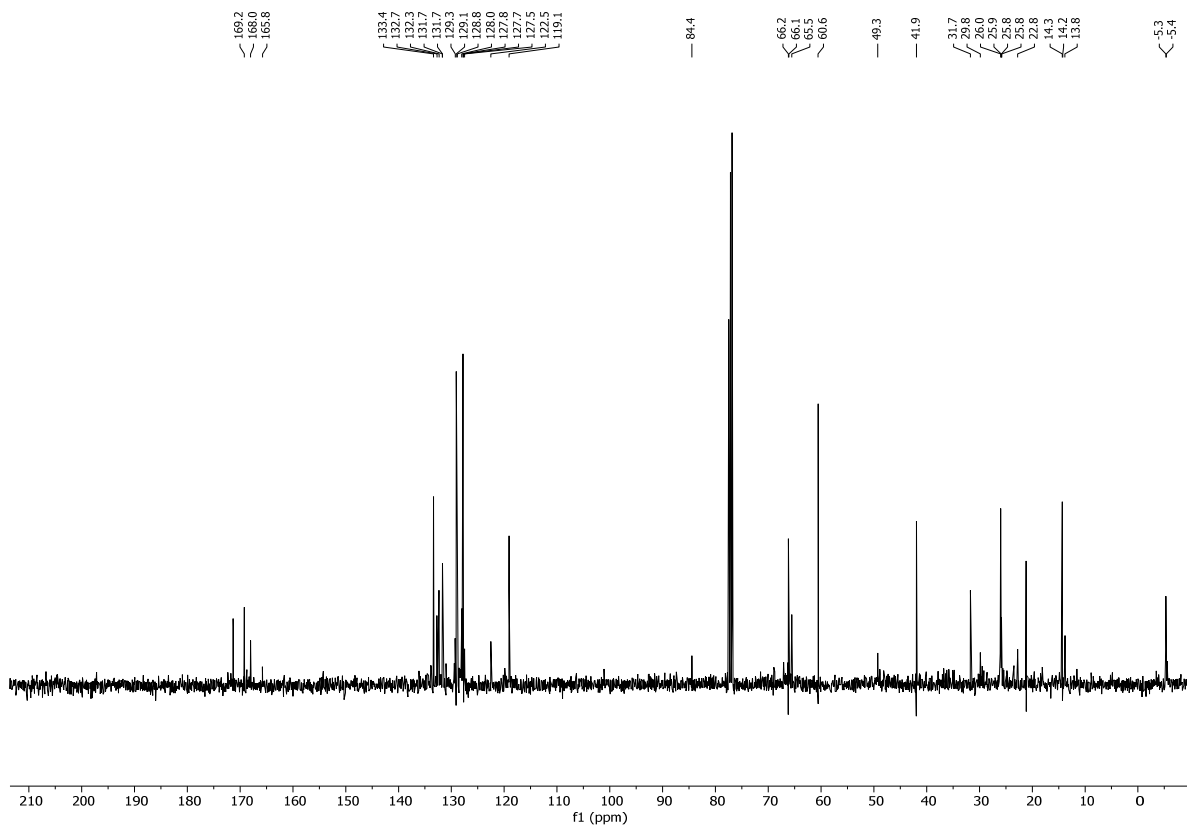
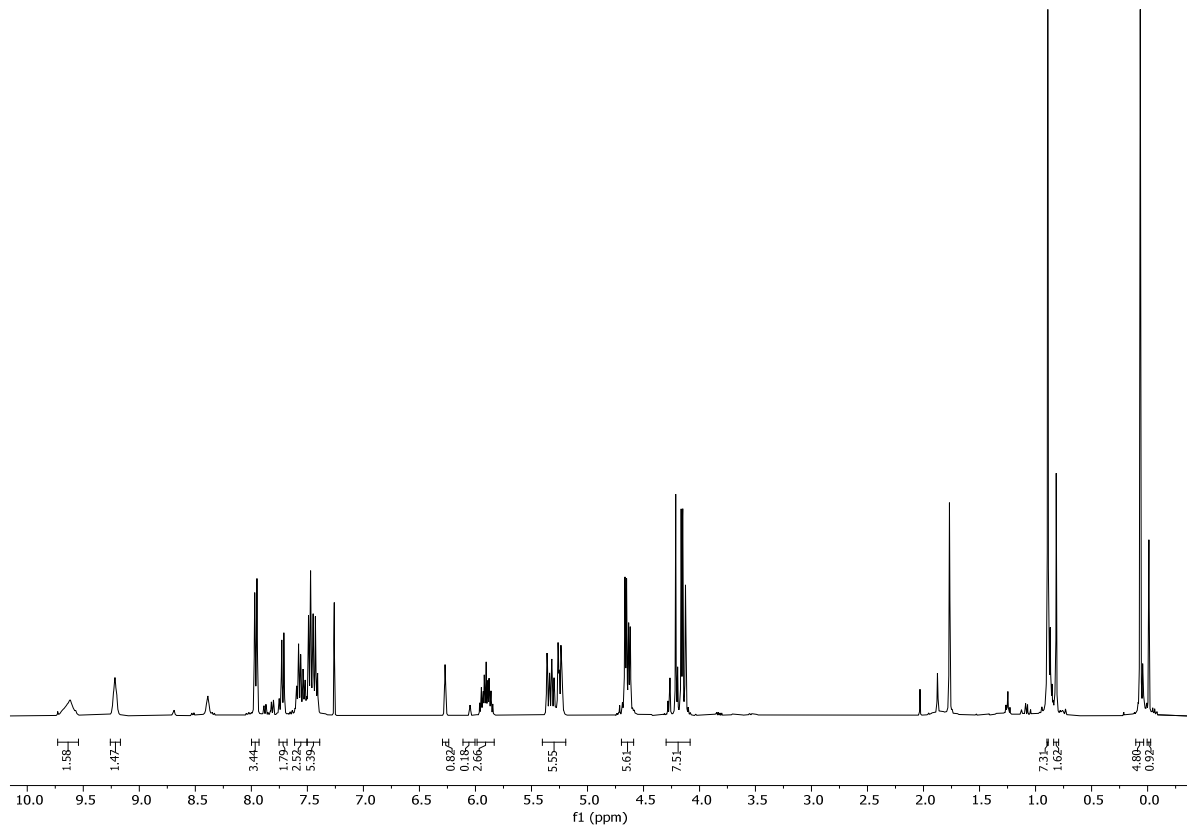


**D12**

TLC: $R_f = 0.15$ (EtOAc/hexane 1:2). **MP** = 115 °C. **$^1\text{H-NMR}$** (500 MHz, CDCl_3): $\delta = 8.95$ (s, 1H), 8.82 (s, 1H), 5.92 (ddt, $J = 16.5, 10.4, 5.8$ Hz, 1H), 5.43 – 5.22 (m, 2H), 4.66 (dt, $J = 5.7, 1.4$ Hz, 2H), 4.10 (d, $J = 5.7$ Hz, 2H), 2.13 (s, 4H). **$^{13}\text{C-NMR}$** (126 MHz, CDCl_3): $\delta = 171.96, 169.15, 154.33, 131.67, 119.04, 66.13, 41.71, 24.22, 1.18$. **IR** (neat): $\tilde{\nu} = 3369, 3320, 3244, 3185, 1693, 1617, 1525, 1383, 1354, 1272, 1201, 1109, 985, 929, 832, 751, 671, 649, 618$ cm^{-1} . **HRMS** (ESI): calcd for $\text{C}_8\text{H}_{12}\text{N}_2\text{NaO}_4$ [(M+Na) $^+$]: 223.0690; found: 223.0689.

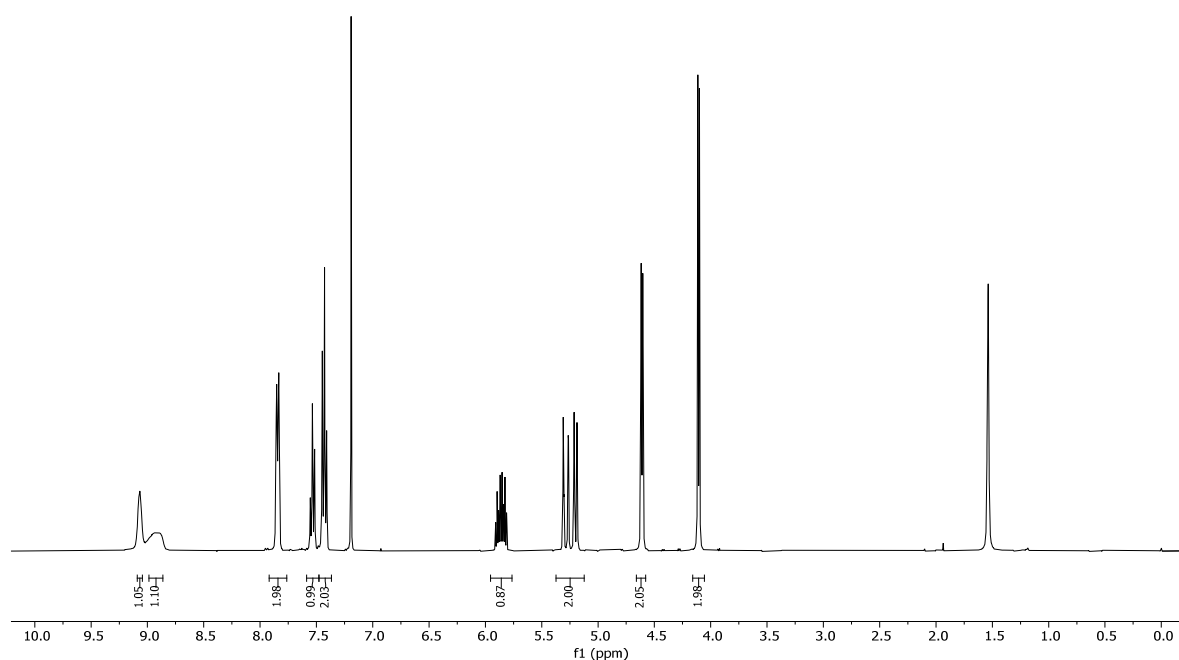


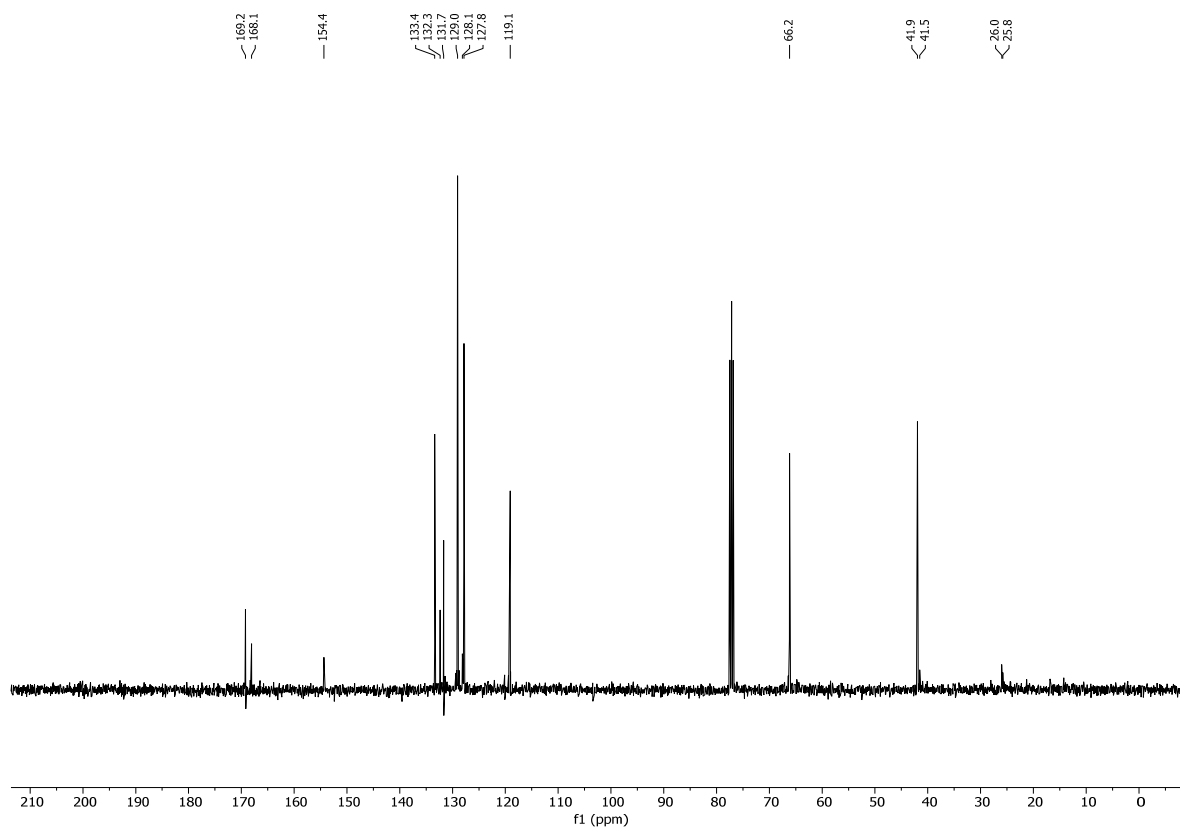




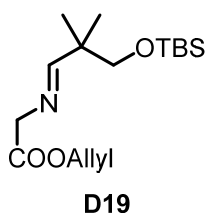
Analytcs of pure **D14**:

TLC: $R_f = 0.35$ (EtOAc/hexane 1:2). **MP** = 95 °C. **$^1\text{H-NMR}$** (400 MHz, CDCl_3): $\delta = 9.07$ (s, 1H), 8.93 (s, 1H), 7.84 (d, $J = 7.6$ Hz, 2H), 7.59 – 7.48 (m, 1H), 7.43 (t, $J = 7.7$ Hz, 2H), 5.86 (ddt, $J = 16.2, 10.4, 5.8$ Hz, 1H), 5.37 – 5.12 (m, 2H), 4.61 (dt, $J = 5.9, 1.4$ Hz, 2H), 4.11 (d, $J = 5.6$ Hz, 2H). **$^{13}\text{C-NMR}$** (101 MHz, CDCl_3): $\delta = 169.2, 168.1, 154.4, 133.4, 132.4, 131.7, 129.0, 128.1, 127.8, 119.1, 66.2, 41.9, 41.51, 26.0, 25.8$. **IR** (neat): $\tilde{\nu} = 3290, 3066, 1748, 1687, 1602, 1504, 1473, 1447, 1411, 1381, 1361, 1268, 1220, 1198, 1161, 1120, 984, 932, 705, 660, 611$ cm^{-1} . **HRMS** (ESI): calcd for $\text{C}_{13}\text{H}_{14}\text{N}_2\text{NaO}_4$ [(M+Na) $^+$]: 285.0846; found: 285.0845.





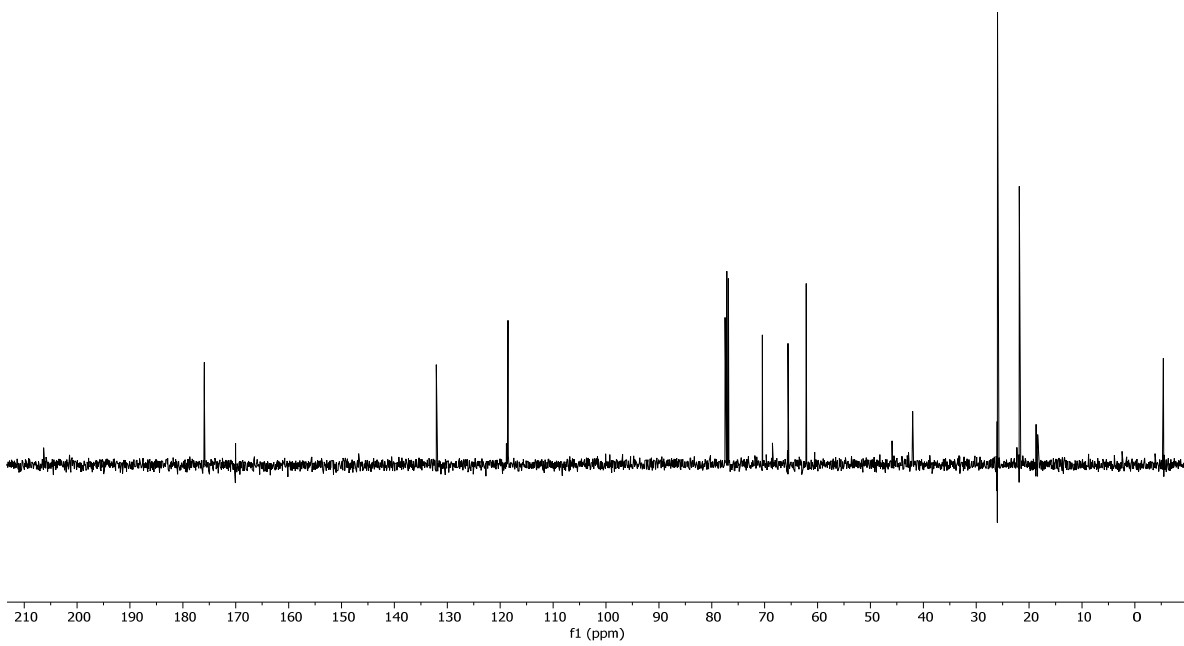
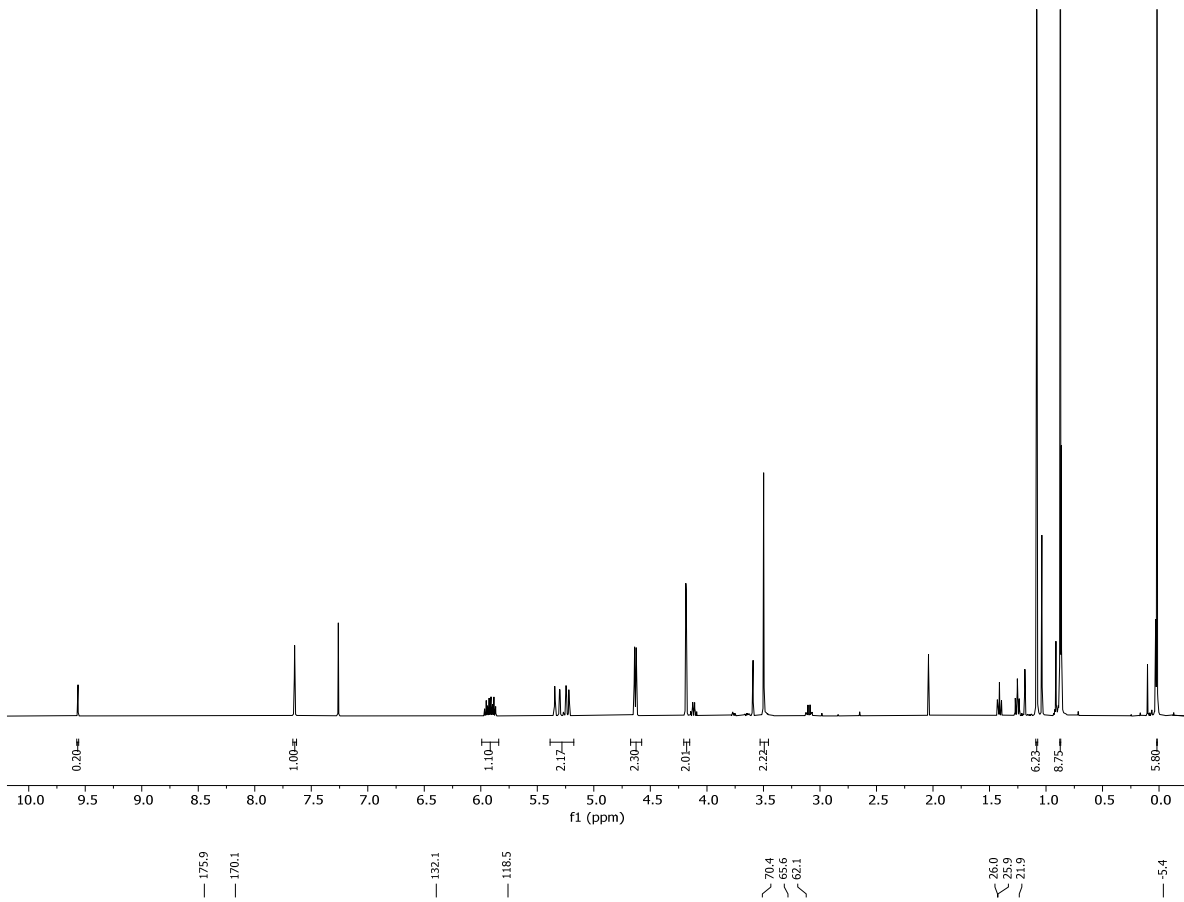
4.3.1.3 Synthesis of DS5

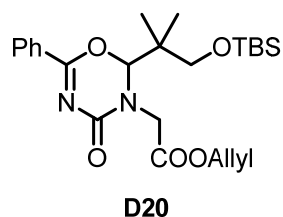


Allyl (E)-2-((3-((tert-butyldimethylsilyl)oxy)-2,2-dimethylpropylidene)amino)acetate (D19).

Allyl glycinate hydrochloride (**D9**•HCl)^[231,316] (0.21 g, 1.39 mmol, 1.00 equiv.) was dissolved in CH₂Cl₂ (14 mL) and Et₃N (2 mL). The solution was stirred for 20 min at rt before a solution of **D18**^[234] (0.27 g, 1.25 mmol, 0.90 equiv.) in CH₂Cl₂ (14 mL) and MgSO₄ (0.60 g) were added and the mixture was stirred for 2.5 h at rt. Afterwards the MgSO₄ was removed *via* filtration, the filtrate was diluted with EtOAc (20 mL) and H₂O (20 mL), the layers were separated and the aqueous layer was extracted with EtOAc (3 x 20 mL). The organic layer was washed with H₂O (20 mL) and brine (20 mL). The organic layer was dried over MgSO₄ and the solvent was removed under reduced pressure to afford crude **D19** (247.8 mg, 0.79 mmol, 63%, as a 5:1 mixture with **D18** (13%), calculated based on NMR spectroscopy) as a pale yellow oil.

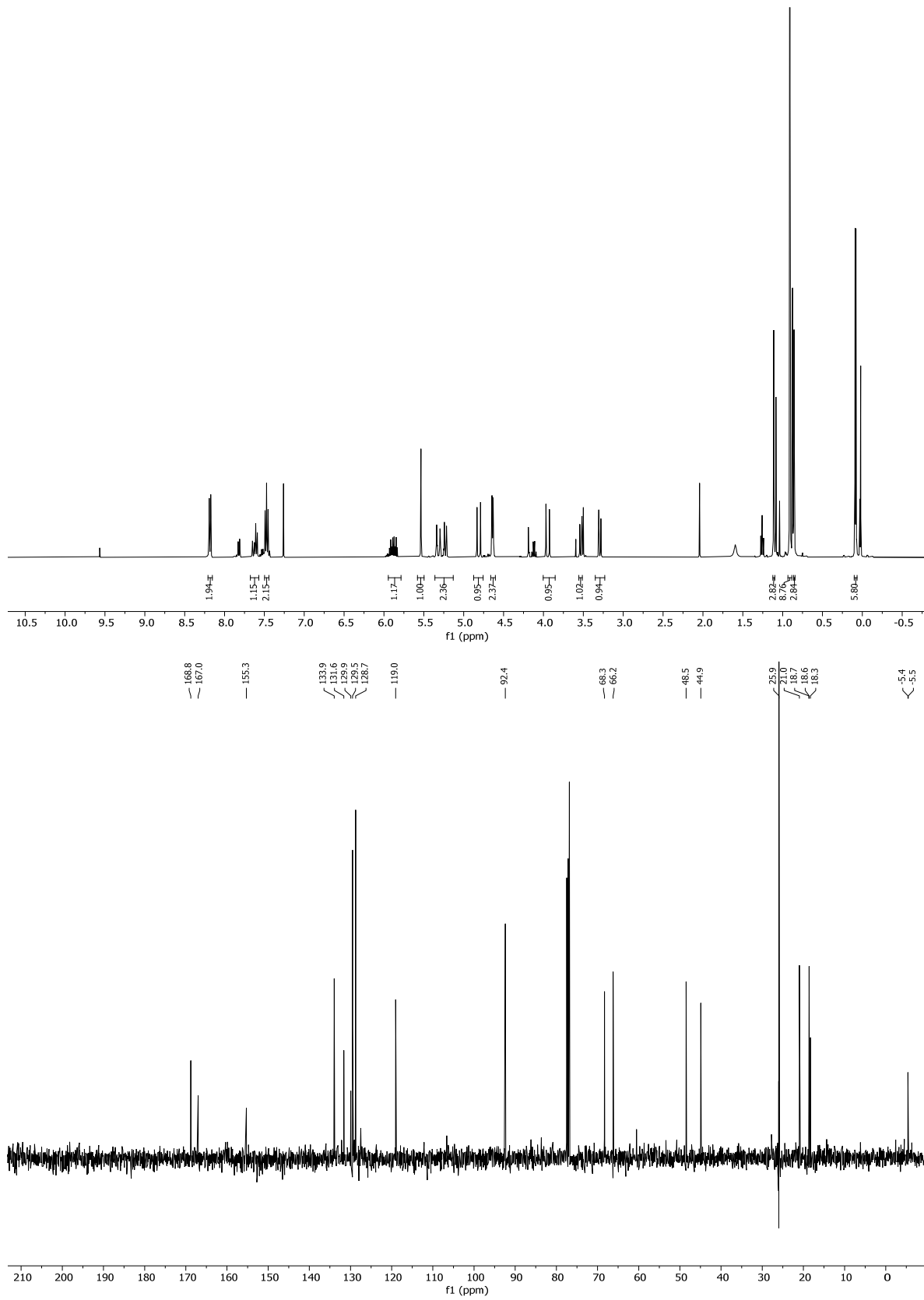
TLC: R_f = 0.70 (EtOAc/hexane 1:4). **¹H-NMR** (400 MHz, CDCl₃): δ = 9.56 (s, 0H), 7.65 (t, *J* = 1.3 Hz, 1H), 5.92 (ddt, *J* = 17.2, 10.4, 5.7 Hz, 1H), 5.39 – 5.18 (m, 2H), 4.63 (dt, *J* = 5.6, 1.4 Hz, 2H), 4.18 (d, *J* = 1.2 Hz, 2H), 3.50 (s, 2H), 1.08 (s, 6H), 0.87 (s, 9H), 0.02 (s, 6H). **¹³C-NMR** (101 MHz, CDCl₃): δ = 175.9, 170.1, 132.1, 118.5, 70.4, 65.6, 62.1, 26.0, 25.9, 21.9, -5.4. **IR** (neat): $\tilde{\nu}$ = 2955, 2929, 2857, 1749, 1668, 1472, 1464, 1362, 1253, 1174, 1096, 1006, 987, 936, 835, 816, 774, 671 cm⁻¹. **HRMS** (ESI): calcd for C₁₆H₃₂NO₃Si [(M+H)⁺]: 314.2146; found: 314.2145.

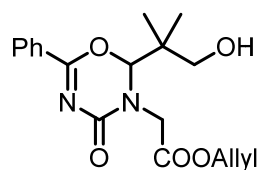




Allyl 2-(2-(1-((tert-butyl dimethylsilyl)oxy)-2-methylpropan-2-yl)-4-oxo-6-phenyl-2H-1,3,5-oxadiazin-3(4H)-yl)acetate (D20). To a solution of **D19** (80.0 mg, 0.26 mmol, 1.00 equiv.) in CH₂Cl₂ (2.5 mL) was added a solution of benzoyl isocyanate (0.16 mL, 1.28 mmol, 5.00 equiv.) in CH₂Cl₂ (13.0 mL) dropwise at rt. The mixture was stirred at that temperature for 2 h. Afterwards H₂O (10 mL) was added, the phases were separated and the aqueous phase was extracted with CH₂Cl₂ (3 x 10 mL), washed with brine (20 mL), the combined organic phases were dried over MgSO₄, concentrated under reduced pressure and purified by FC (EtOAc/hexane 1:6 → 1:5 → 1:4) to afford **D20** (85.4 mg, 0.19 mmol, 73%) as white solid.

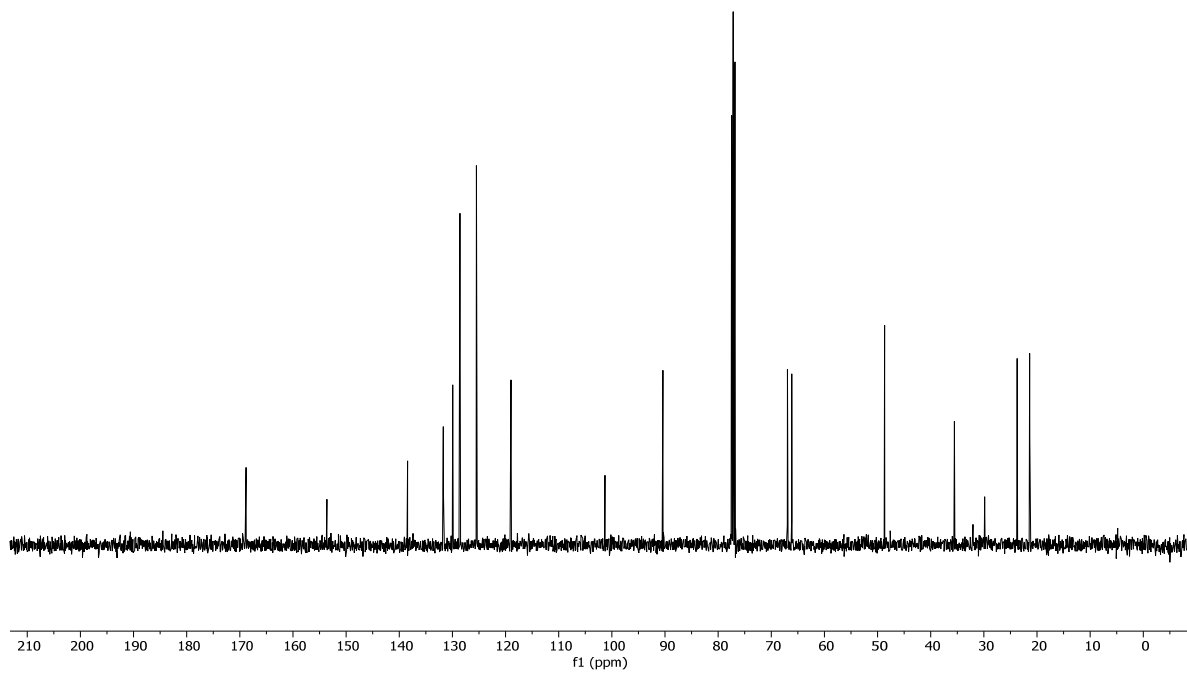
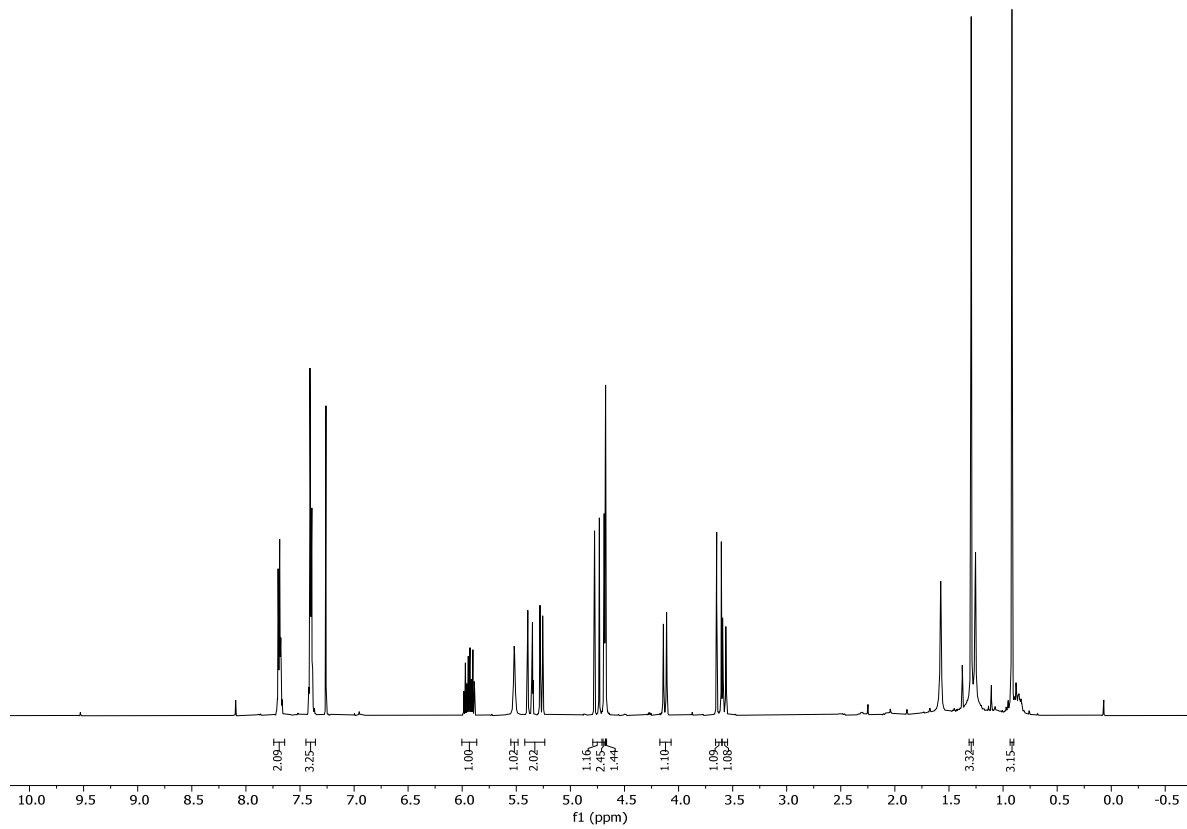
TLC: R_f = 0.40 (EtOAc/hexane 1:2). **¹H-NMR** (400 MHz, CDCl₃): δ = 8.21 – 8.15 (m, 2H), 7.68 – 7.57 (m, 1H), 7.50 – 7.44 (m, 2H), 5.95 – 5.79 (m, 1H), 5.54 (s, 1H), 5.36 – 5.13 (m, 2H), 4.81 (d, *J* = 17.6 Hz, 1H), 4.64 (dt, *J* = 5.8, 1.5 Hz, 2H), 3.95 (d, *J* = 17.5 Hz, 1H), 3.53 (d, *J* = 10.5 Hz, 1H), 3.29 (d, *J* = 10.4 Hz, 1H), 1.11 (s, 3H), 0.91 (s, 9H), 0.86 (s, 3H), 0.09 (d, *J* = 4.8 Hz, 6H). **¹³C-NMR** (101 MHz, CDCl₃): δ = 168.8, 167.0, 155.3, 133.9, 131.6, 129.9, 129.5, 128.7, 119.0, 92.4, 68.3, 66.2, 48.5, 44.9, 26.0, 21.0, 18.7, 18.6, 18.3, -5.4, -5.5. **IR** (neat): $\tilde{\nu}$ = 2955, 2931, 2858, 1751, 1688, 1609, 1575, 1471, 1453, 1362, 1319, 1304, 1290, 1261, 1188, 1092, 1065, 990, 838, 779, 698 cm⁻¹. **HRMS** (ESI): calcd for C₂₄H₃₇N₂O₅Si [(M+H)⁺]: 461.2466; found: 461.2464.



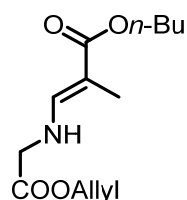
**DS5**

Allyl 2-(2-(1-hydroxy-2-methylpropan-2-yl)-4-oxo-6-phenyl-2H-1,3,5-oxadiazin-3(4H)-yl)acetate (DS5). To a solution of **D20** (80.0 mg, 0.17 mmol, 1.0 equiv.) in THF (4 mL) was added TBAF (0.21 mL, 0.21 mmol, 1.2 equiv.) at rt. After stirring for 15 min at rt sat. aq. NaHCO₃ (10 mL) was added, the layers were separated and the aqueous layer was extracted with CH₂Cl₂ (3x 10 mL). The combined organic extracts were dried over MgSO₄ and then concentrated. Purification of the residue by FC (EA/hexane 1:4 → 1:3, + 2% Et₃N) afforded **DS5** (43.4 mg, 0.13 mmol, 72%) as colorless oil.

TLC: R_f = 0.30 (EtOAc/hexane 1:1). **¹H-NMR** (400 MHz, CDCl₃): δ = 7.69 (ddt, *J* = 4.8, 3.4, 1.4 Hz, 2H), 7.44 – 7.36 (m, 3H), 5.94 (ddt, *J* = 17.2, 10.4, 5.7 Hz, 1H), 5.52 (s, 1H), 5.42 – 5.24 (m, 2H), 4.75 (d, *J* = 17.7 Hz, 1H), 4.70 – 4.68 (m, 2H), 4.67 (d, *J* = 1.8 Hz, 1H), 4.13 (d, *J* = 11.8 Hz, 1H), 3.63 (d, *J* = 17.7 Hz, 1H), 3.58 (dd, *J* = 11.8, 1.6 Hz, 1H), 1.29 (s, 3H), 0.92 (s, 3H). **¹³C-NMR** (101 MHz, CDCl₃): δ = 168.8, 153.6, 138.4, 131.7, 129.9, 128.6, 125.5, 119.0, 101.3, 90.4, 67.0, 66.1, 48.7, 35.6, 23.7, 21.4. **IR** (neat): $\tilde{\nu}$ = 3331, 2962, 2935, 2886, 2864, 1751, 1688, 1609, 1575, 1542, 1453, 1363, 1304, 1261, 1093, 1066, 990, 930, 698, 617 cm⁻¹. **HRMS** (ESI): calcd for C₁₈H₂₃N₂O₅ [(M+H)⁺]: 347.1601; found: 347.1600.



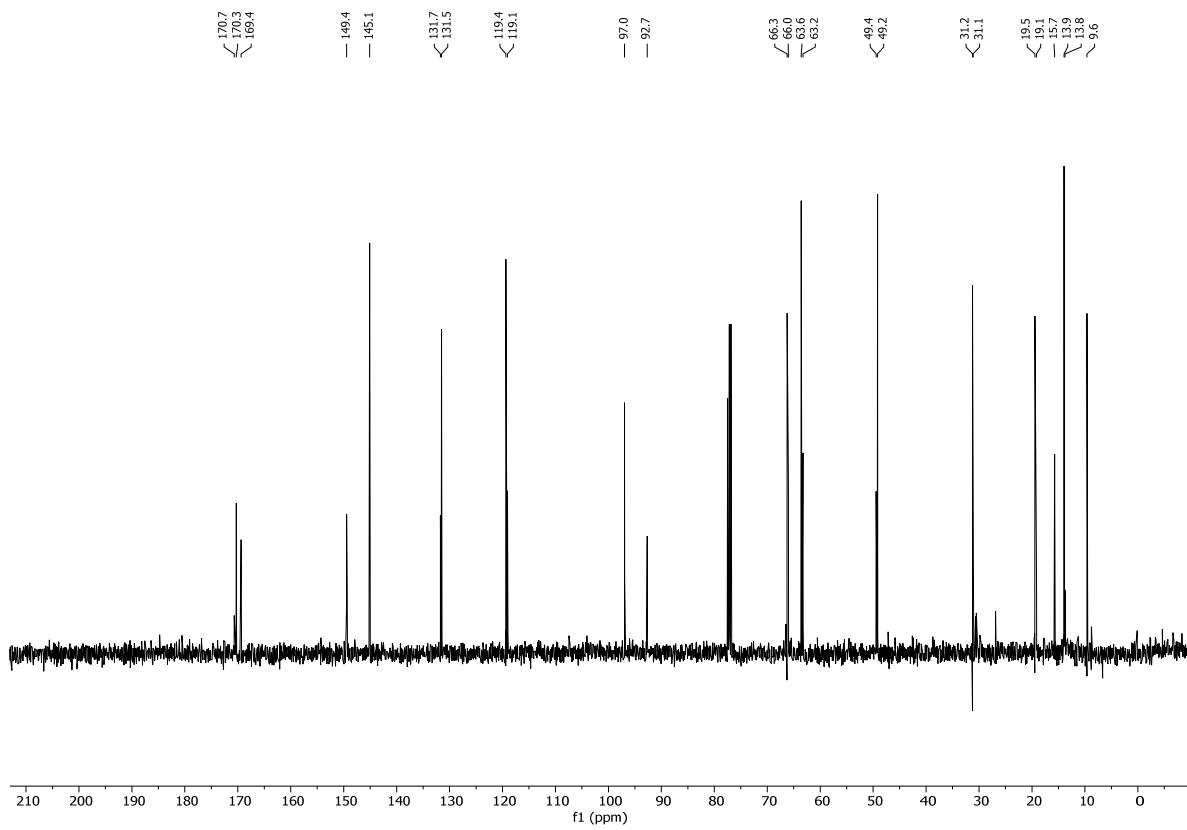
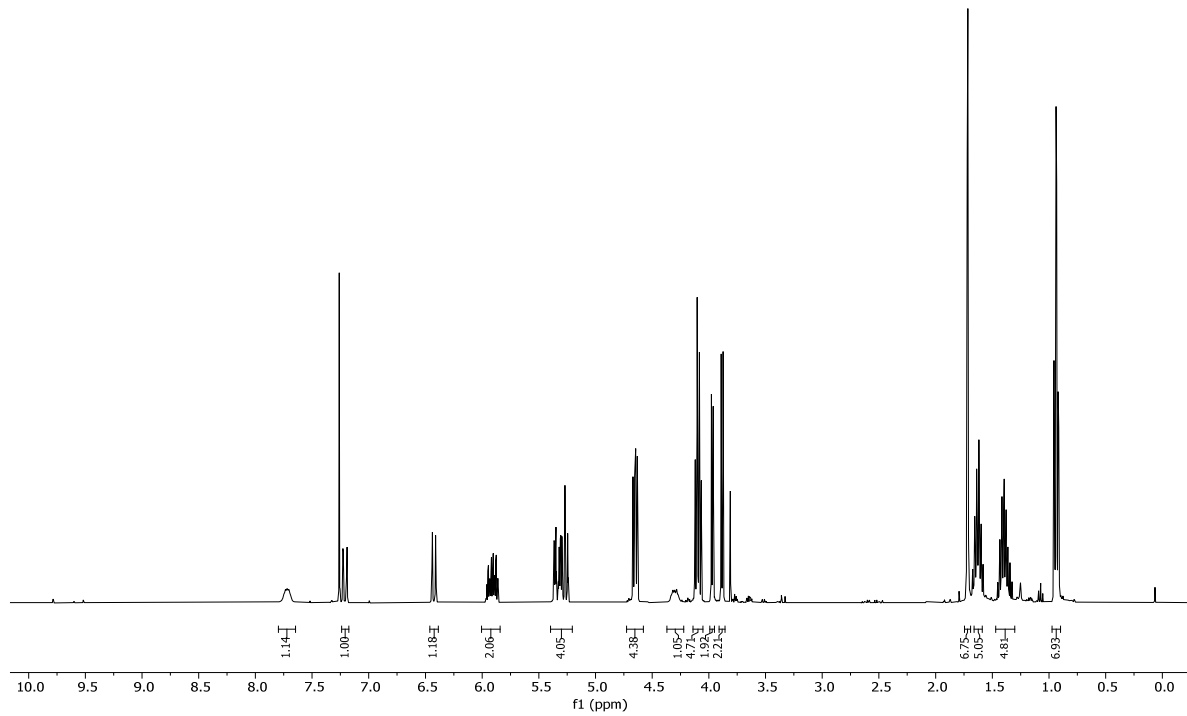
4.3.1.4 Synthesis of 24 and attempted conversion into D25

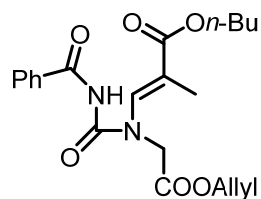


D23 (E/Z = 1.2:1)

Butyl 3-((2-(allyloxy)-2-oxoethyl)amino)-2-methylacrylate (D23). Allyl glycinate hydrochloride (**D9**•HCl)^[231,316] (0.48 g, 3.17 mmol, 1.00 equiv.) was dissolved in CH₂Cl₂ (31 mL) and Et₃N (4.39 mL). The solution was stirred for 20 min at rt. A solution of **D22**^[233] (0.50 g, 3.17 mmol, 1.00 equiv.) in CH₂Cl₂ (31 mL) and MgSO₄ (1.90 g) were added and the mixture was stirred for 3 h. Afterwards the MgSO₄ was removed *via* filtration, H₂O (50 mL) was added, the phases were separated and the aqueous layer was extracted with EtOAc (3 x 50 mL). The organic layer was washed with H₂O (70 mL) and brine (70 mL). The organic layer was dried over MgSO₄ and the solvent was removed under reduced pressure to afford **D23** (0.58 g, 2.26 mmol, 71%, E/Z = 1.2:1) as a colorless oil that was used in the next step without further purification

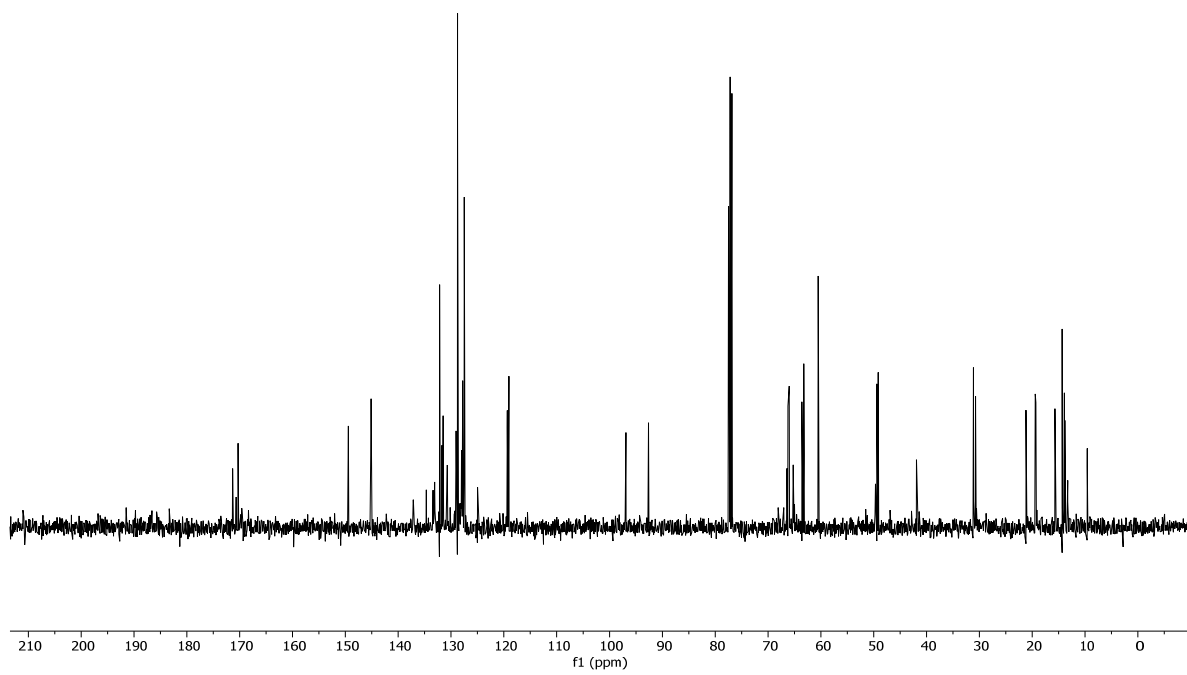
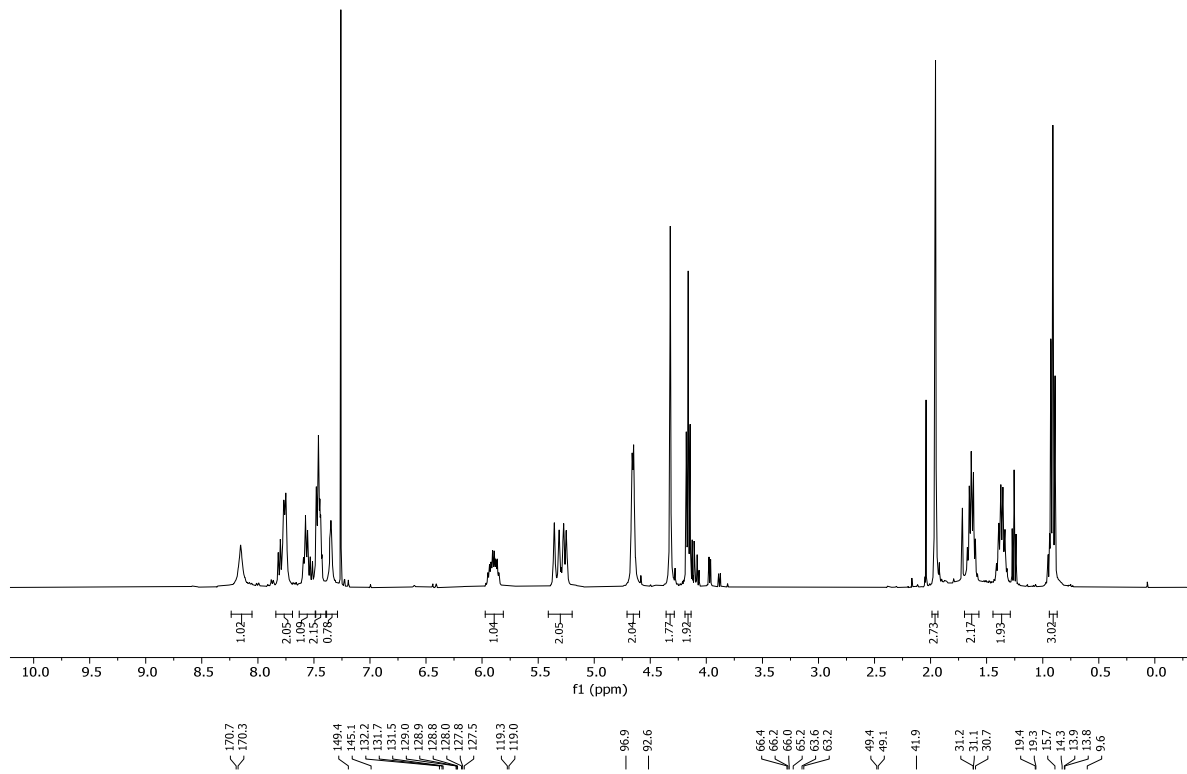
TLC: R_f = 0.35 (EtOAc/hexane 1:9). **¹H-NMR** (400 MHz, CDCl₃): δ = ¹H NMR (400 MHz, CDCl₃) δ 7.80 – 7.65 (m, 1H), 7.21 (dq, *J* = 13.3, 1.1 Hz, 1H), 6.42 (dd, *J* = 12.6, 1.0 Hz, 1H), 5.91 (ddtd, *J* = 17.1, 10.4, 5.9, 2.3 Hz, 2H), 5.40 – 5.20 (m, 3H), 4.65 (ddt, *J* = 9.5, 5.8, 1.3 Hz, 4H), 4.37 – 4.22 (m, 1H), 4.09 (dt, *J* = 8.1, 6.6 Hz, 4H), 3.97 (d, *J* = 5.8 Hz, 2H), 3.88 (d, *J* = 6.3 Hz, 2H), 1.72 (dd, *J* = 2.1, 1.0 Hz, 6H), 1.66 – 1.59 (m, 4H), 1.47 – 1.30 (m, 4H), 0.93 (td, *J* = 7.4, 2.1 Hz, 6H). **¹³C-NMR** (101 MHz, CDCl₃): δ = 170.7, 170.3, 169.4, 149.4, 145.1, 131.7, 131.5, 119.4, 119.1, 97.0, 92.7, 66.3, 66.0, 63.6, 63.2, 49.4, 49.2, 31.2, 31.1, 19.5, 19.1, 15.7, 13.9, 13.8, 9.6. **IR** (neat): $\tilde{\nu}$ = 3283, 2960, 2875, 1735, 1710, 1644, 1577, 1505, 1480, 1418, 1374, 1240, 1183, 1136, 1116, 1045, 987, 932, 847, 755, 707, 636, 563, 550 cm⁻¹. **HRMS** (ESI): calcd for C₁₃H₂₂NO₄ [(M+H)⁺]: 256.1543; found: 256.1542.

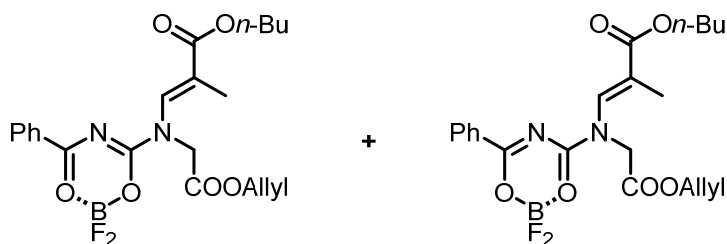


**D24**

Butyl (*E*)-3-(1-(2-(allyloxy)-2-oxoethyl)-3-benzoylureido)-2-methylacrylate (D24). To a solution of **D23** (0.10 g, 0.39 mmol, 1.00 equiv.) in CH₂Cl₂ (8 mL) was added a solution of benzoyl isocyanate (0.20 mL, 1.57 mmol, 4.00 equiv.) in CH₂Cl₂ (8 mL) at rt. The mixture was stirred at that temperature for 1.5 h. Afterwards H₂O (15 mL) was added, the phases were separated and the aqueous phase was extracted with CH₂Cl₂ (3 x 15 mL), washed with brine (25 mL), the combined organic phases were dried over MgSO₄, concentrated under reduced pressure and purified by FC (EtOAc/hexane 1:2) to afford **D24** (152 mg, 0.38 mmol, 96%) as colorless oil.

TLC: R_f = 0.65 (EtOAc/hexane 1:1). **¹H-NMR** (400 MHz, CDCl₃): δ = 8.15 (s, 1H), 7.84 – 7.69 (m, 2H), 7.63 – 7.49 (m, 1H), 7.45 (td, *J* = 7.4, 4.7 Hz, 2H), 7.35 (s, 1H), 5.97 – 5.81 (m, 1H), 5.41 – 5.20 (m, 2H), 4.71 – 4.60 (m, 2H), 4.32 (s, 2H), 4.16 (t, *J* = 6.7 Hz, 2H), 1.96 (d, *J* = 1.5 Hz, 3H), 1.64 (p, *J* = 6.9 Hz, 2H), 1.37 (qd, *J* = 7.7, 2.6 Hz, 2H), 0.91 (t, *J* = 7.4 Hz, 3H). **¹³C-NMR** (101 MHz, CDCl₃): δ = 170.7, 170.3, 149.4, 145.1, 132.2, 131.7, 131.5, 129.1, 128.9, 128.8, 128.0, 127.8, 127.5, 119.3, 119.1, 96.9, 92.6, 66.4, 66.2, 66.0, 65.2, 63.6, 63.2, 49.4, 49.1, 41.9, 31.2, 31.1, 30.7, 19.4, 19.3, 15.7, 14.3, 13.9, 13.8, 9.6. **IR** (neat): $\tilde{\nu}$ = 3277, 3069, 2959, 2935, 2875, 1740, 1701, 1699, 1677, 1653, 1642, 1602, 1577, 1506, 1480, 1448, 1418, 1382, 1349, 1258, 1183, 1137, 117, 1066, 1026, 985, 931, 844, 797, 755, 705, 644, 615, 557, 544 cm⁻¹. **HRMS** (ESI): calcd for C₂₁H₂₆N₂NaO₆ [(M+Na)⁺]: 425.1683; found: 425.1680.

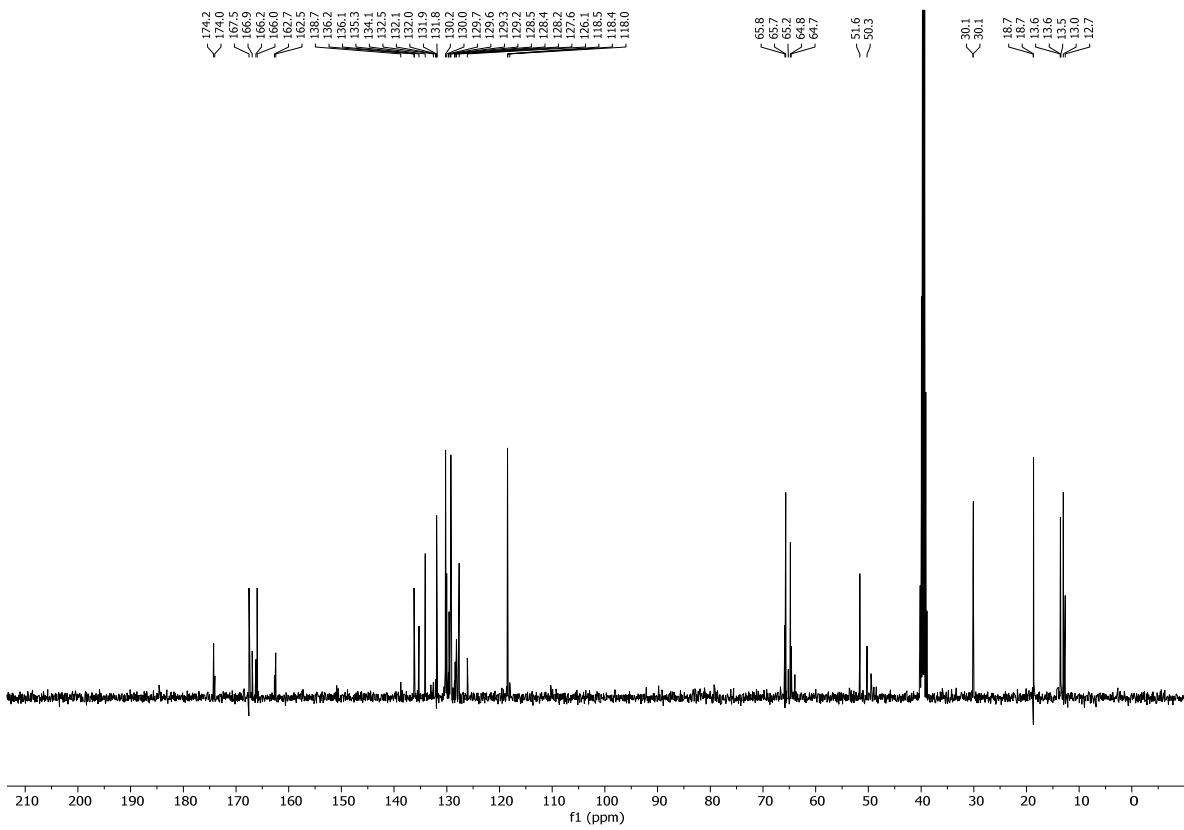
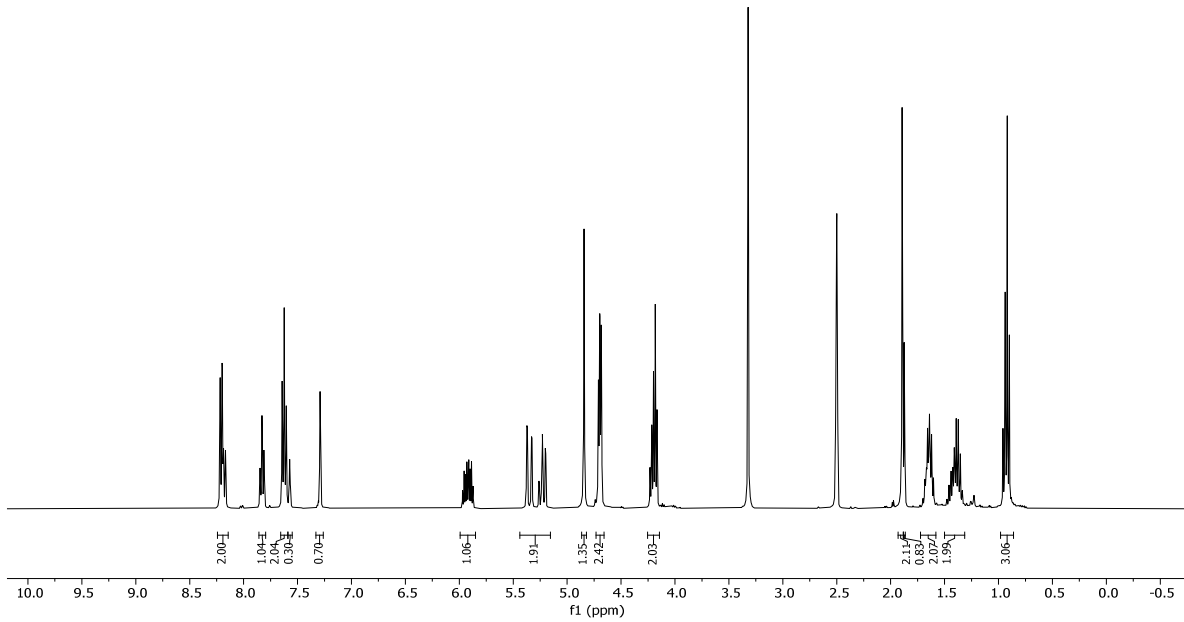


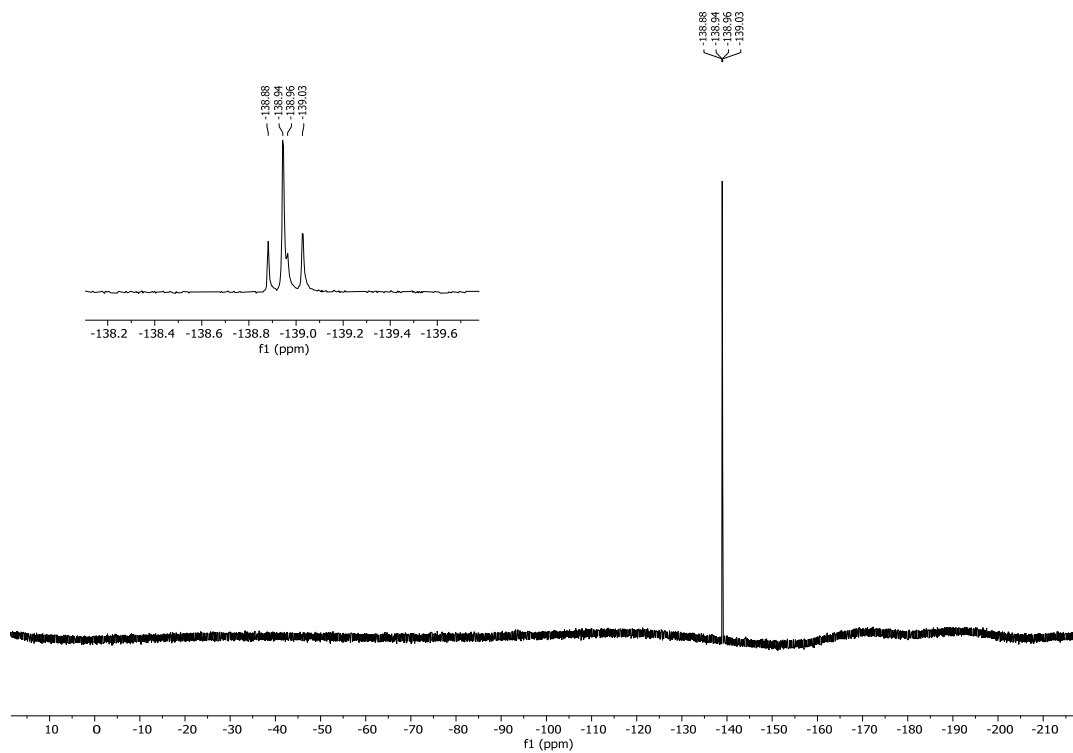
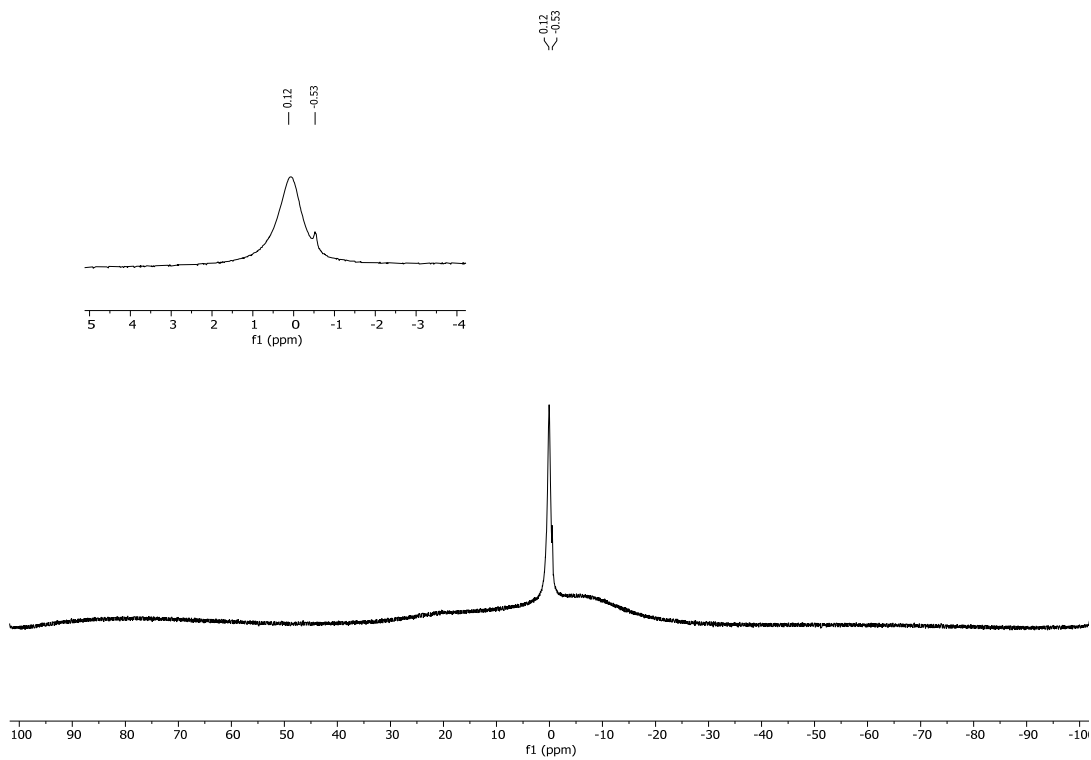
**DS6**

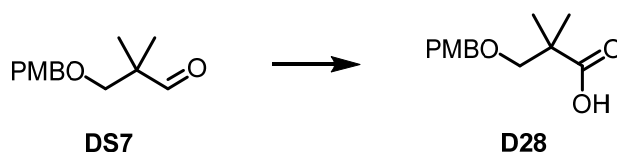
(tentative structures)

Butyl (E)-3-((2-(allyloxy)-2-oxoethyl)(2,2-difluoro-6-phenyl-2H-1,3,5,2,4-dioxaboronin-4-yl)amino)-2-methylacrylate and butyl (E)-3-((2-(allyloxy)-2-oxoethyl)(2,2-difluoro-6-phenyl-2H-1,3,5,2,4-dioxaboronin-4-yl)amino)-2-methylacrylate (DS6). See Table S1 Entry 9. The ratio of isomers is 2.3:1. The structural assignment of these products as **DS6** is in line with all spectroscopic data but should still be considered tentative at this point.

TLC: $R_f = 0.85$ (EtOAc/hexane 1:1). ¹H-NMR (400 MHz, DMSO) $\delta = 8.19$ (ddd, $J = 12.2, 8.3, 1.4$ Hz, 2H), 7.83 (td, $J = 7.4, 1.3$ Hz, 1H), 7.62 (t, $J = 7.9$ Hz, 2H), 7.57 (p, $J = 1.8$ Hz, 0H), 7.29 (q, $J = 1.5$ Hz, 1H), 5.92 (ddt, $J = 17.3, 10.8, 5.5$ Hz, 1H), 5.44 – 5.15 (m, 2H), 4.84 (s, 1H), 4.73 – 4.66 (m, 2H), 4.20 (dt, $J = 13.1, 6.5$ Hz, 2H), 1.89 (d, $J = 1.5$ Hz, 2H), 1.87 (d, $J = 1.5$ Hz, 1H), 1.65 (tq, $J = 8.4, 6.6$ Hz, 2H), 1.50 – 1.31 (m, 2H), 0.92 (h, $J = 7.5$ Hz, 3H). ¹³C-NMR (101 MHz, DMSO) $\delta = 174.2, 174.0, 167.5, 166.9, 166.2, 166.0, 162.7, 162.5, 138.8, 136.2, 136.1, 135.3, 134.1, 132.6, 132.1, 132.0, 131.9, 131.8, 130.2, 130.0, 129.7, 129.6, 129.3, 129.2, 128.5, 128.4, 128.2, 127.6, 126.1, 118.5, 118.4, 118.1, 65.8, 65.7, 65.2, 64.8, 64.7, 51.6, 50.3, 30.1, 30.1, 18.7, 18.7, 13.6, 13.6, 13.5, 13.0, 12.7$. ¹⁹F NMR (376 MHz, DMSO) $\delta = -138.88, -138.94, -138.96, -139.03$. ¹¹B NMR (160 MHz, DMSO) $\delta = 0.12, -0.53$. IR (neat): $\tilde{\nu} = 2956, 2931, 2857, 2359, 1737, 1464, 1389, 1371, 1251, 1167, 1097, 1031, 959, 912, 836, 808, 775, 742$ cm⁻¹. HRMS (ESI): calcd for C₂₁H₂₆N₂NaO₆ [(M+Na)⁺]: 425.1683; found: 425.1687.

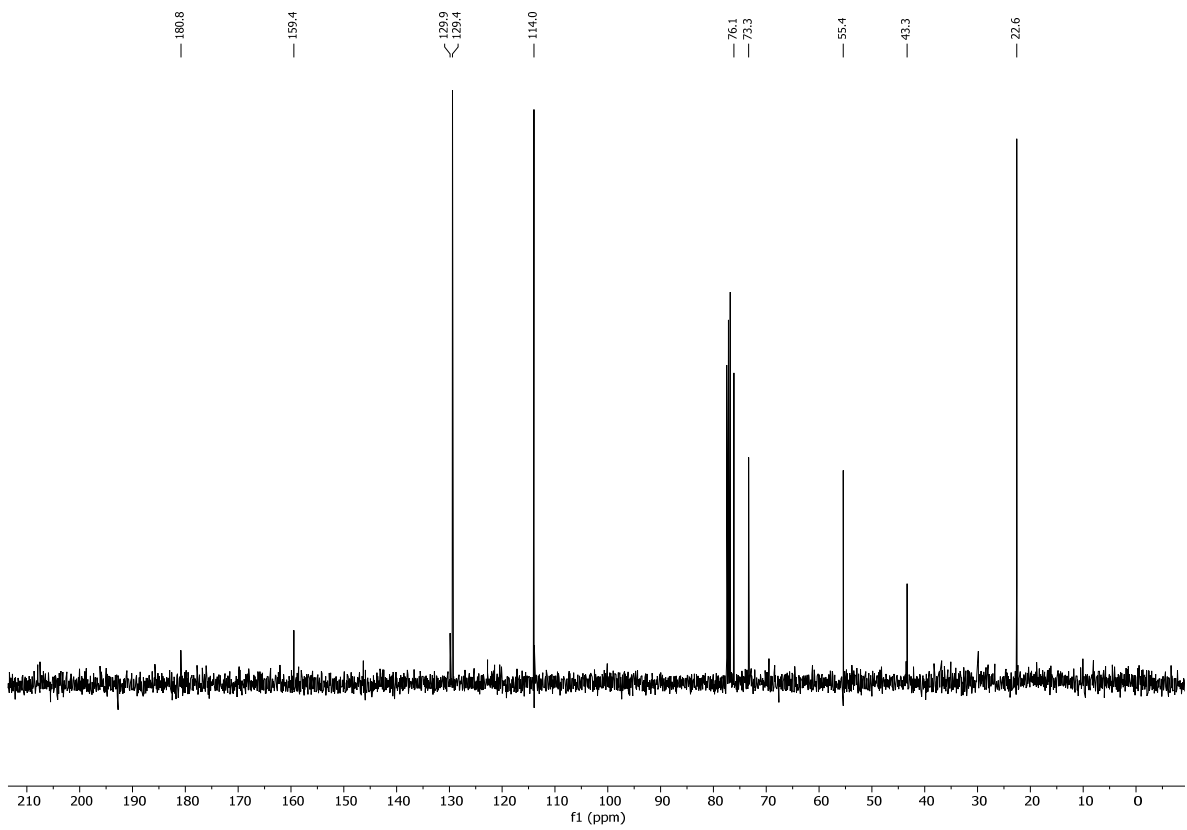
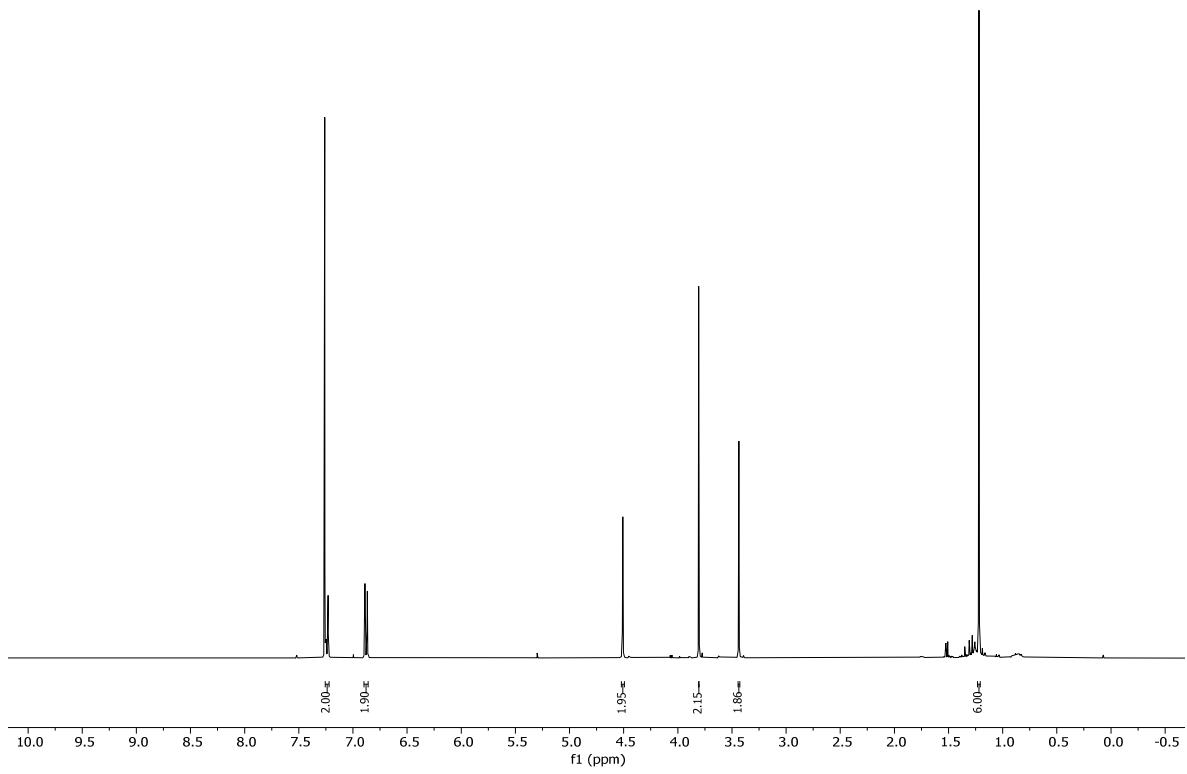


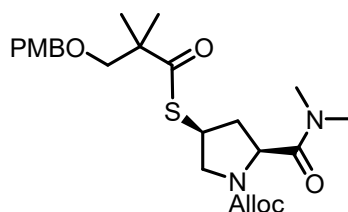
^{19}F -NMR of tentative structures **DS6**: ^{11}B -NMR of tentative structures **DS6**:

4.3.1.5 Synthesis of D26 and D33 and attempted conversion into D27, D34-D35

3-((4-Methoxybenzyl)oxy)-2,2-dimethylpropanoic acid (D28). To a solution of **DS7**^[235] (2.97 mg, 13.38 mmol, 1.00 equiv.) in a mixture of *t*-BuOH (45 mL) and 2-methyl-2-butene (45 mL) was added a solution of NaClO₂ (80%, 3.87 g, 42.80 mmol, 3.20 equiv.) and NaH₂PO₄ dihydrate (8.35 g, 42.80 mmol, 4.00 equiv.) in H₂O (15 mL) dropwise at 0 °C. The reaction mixture was stirred at the same temperature for 2 h and 1 h at rt before it was diluted with CH₂Cl₂ (200 mL) and brine (200 mL). The layers were separated and the aqueous layer was extracted with CH₂Cl₂ (3 x 200 mL). The combined organic layers were washed with brine (300 mL), dried over MgSO₄ and concentrated under reduced pressure to afford **D28** (3.20 g, 13.38, quant.) of as pale yellow oil that was used in the next step without further purification.

TLC: R_f = 0.40 (EtOAc/hexane 1:4, + 1% AcOH). **¹H-NMR** (400 MHz, CDCl₃): δ = 7.29 – 7.23 (m, 2H), 6.93 – 6.87 (m, 2H), 4.46 (s, 2H), 3.83 (s, 3H), 3.47 (d, *J* = 5.6 Hz, 2H), 3.32 (s, 2H), 2.65 (t, *J* = 5.9 Hz, 1H), 0.94 (s, 6H). **¹³C-NMR** (101 MHz, CDCl₃): δ = 180.8, 159.4, 129.9, 129.4, 114.0, 76.1, 73.3, 55.4, 43.3, 22.6. **IR** (neat): $\tilde{\nu}$ = 2927, 2857, 1701, 1612, 1586, 1513, 1477, 1464, 1417, 1381, 1364, 1302, 1245, 1173, 1092, 1035, 950, 921, 846, 819, 792, 753, 580, 518 cm⁻¹. **HRMS** (ESI): calcd for C₁₃H₁₈NaO₄ [(M+Na)⁺]: 261.1097; found: 261.1091.

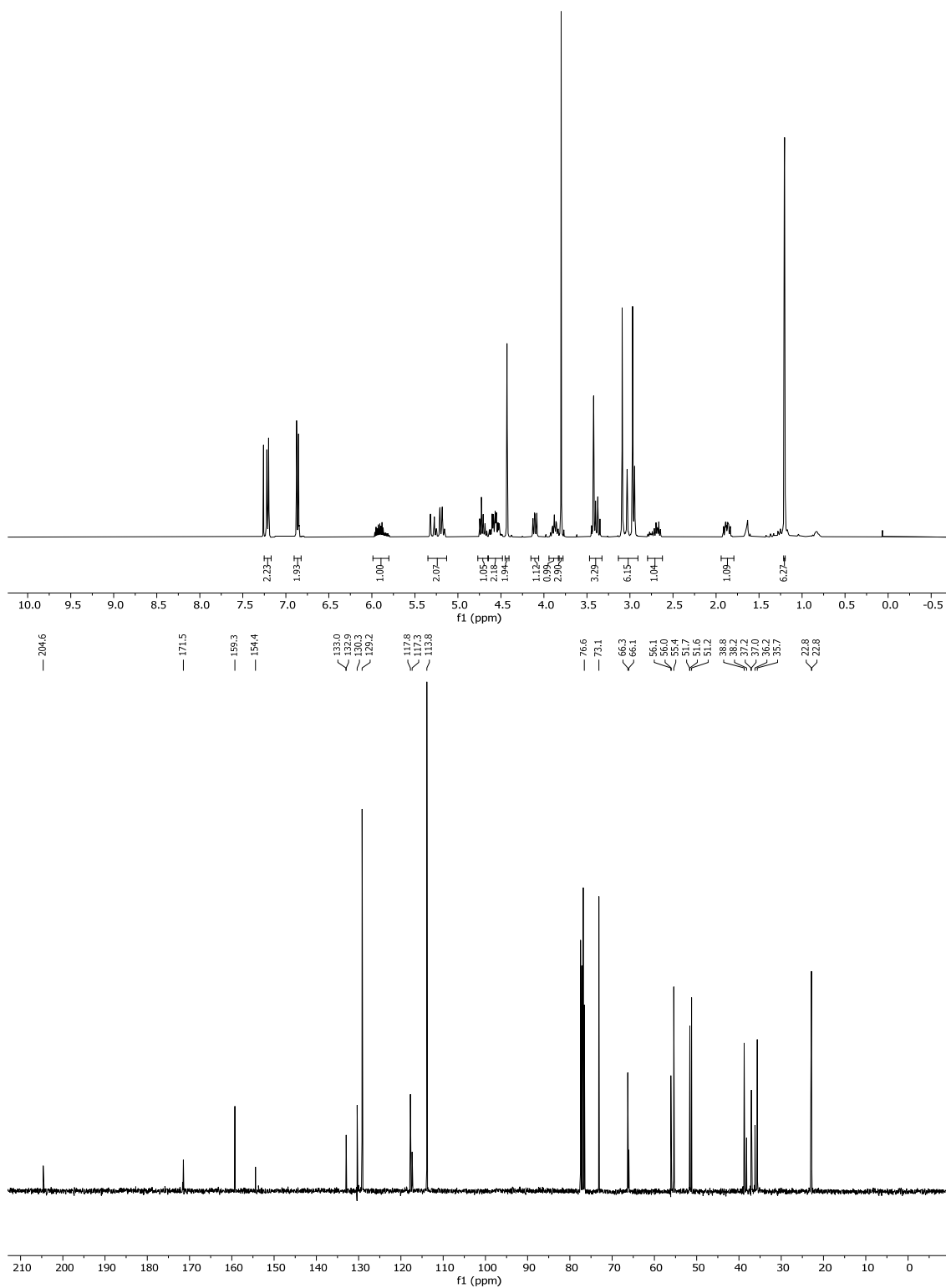




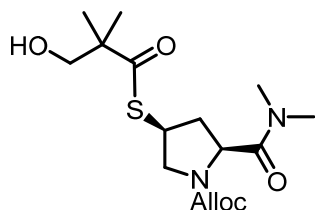
DS8

Allyl (2S,4S)-2-(dimethylcarbamoyl)-4-((3-((4-methoxybenzyl)oxy)-2,2-dimethylpropanoyl)thio)pyrrolidine-1-carboxylate (**DS8**). To a solution of **D28** (1.59 g, 6.66 mmol, 2.00 equiv. co-evaporated twice with 15 mL of toluene immediately before use) in CH₂Cl₂ (26 mL) were added EDC•HCl (2.55 g, 13.32 mmol, 4.00 equiv.) and DMAP (0.98 g, 7.99 mmol, 2.40 equiv.) at 0 °C. After stirring for 30 min at 0 °C, **D5a** (0.86 g, 3.33 mmol, 1.00 equiv.) was added and stirring was continued for 4 h at rt. The reaction mixture was washed with H₂O, dried over anhydrous MgSO₄ and evaporated. The residue was purified by FC (EtOAc/hexane 1:1 → 5:1) to give **DS8** (1.52 g, 3.17 mmol, 95%) as pale yellow oil.

TLC: R_f = 0.20 (EtOAc/hexane 2:1). **¹H-NMR** (400 MHz, CDCl₃): δ = 7.25 – 7.17 (m, 2H), 6.90 – 6.82 (m, 2H), 5.99 – 5.80 (m, 1H), 5.35 – 5.13 (m, 2H), 4.71 (dt, *J* = 16.6, 7.9 Hz, 1H), 4.58 (qdt, *J* = 13.4, 5.6, 1.5 Hz, 2H), 4.43 (s, 2H), 4.11 (dd, *J* = 10.6, 7.6 Hz, 1H), 3.94 – 3.83 (m, 1H), 3.80 (s, 3H), 3.47 – 3.33 (m, 3H), 3.13 – 2.91 (m, 6H), 2.72 (ddt, *J* = 28.6, 12.8, 7.9 Hz, 1H), 1.94 – 1.79 (m, 1H), 1.20 (d, *J* = 1.7 Hz, 6H). **¹³C-NMR** (101 MHz, CDCl₃): δ = 204.6, 171.5, 159.3, 154.4, 133.0, 132.9, 130.3, 129.2, 117.8, 117.3, 113.8, 76.6, 73.1, 66.3, 66.1, 56.1, 56.0, 55.4, 51.7, 51.6, 51.2, 38.8, 38.2, 37.2, 37.0, 36.2, 35.7, 22.8, 22.8. **IR** (neat): $\tilde{\nu}$ = 3684, 3674, 2987, 2971, 2901, 1704, 1658, 1612, 1513, 1442, 1406, 1362, 1301, 1286, 1248, 1196, 1173, 1143, 1079, 1066, 1056, 1038, 980, 936, 880, 867, 822, 767 cm⁻¹. **HRMS** (ESI): calcd for C₂₄H₃₄N₂NaO₆S [(M+Na)⁺]: 501.2030; found: 501.2026. $[\alpha]_D^{20}$: -5.80 (c = 1.00 in CHCl₃).



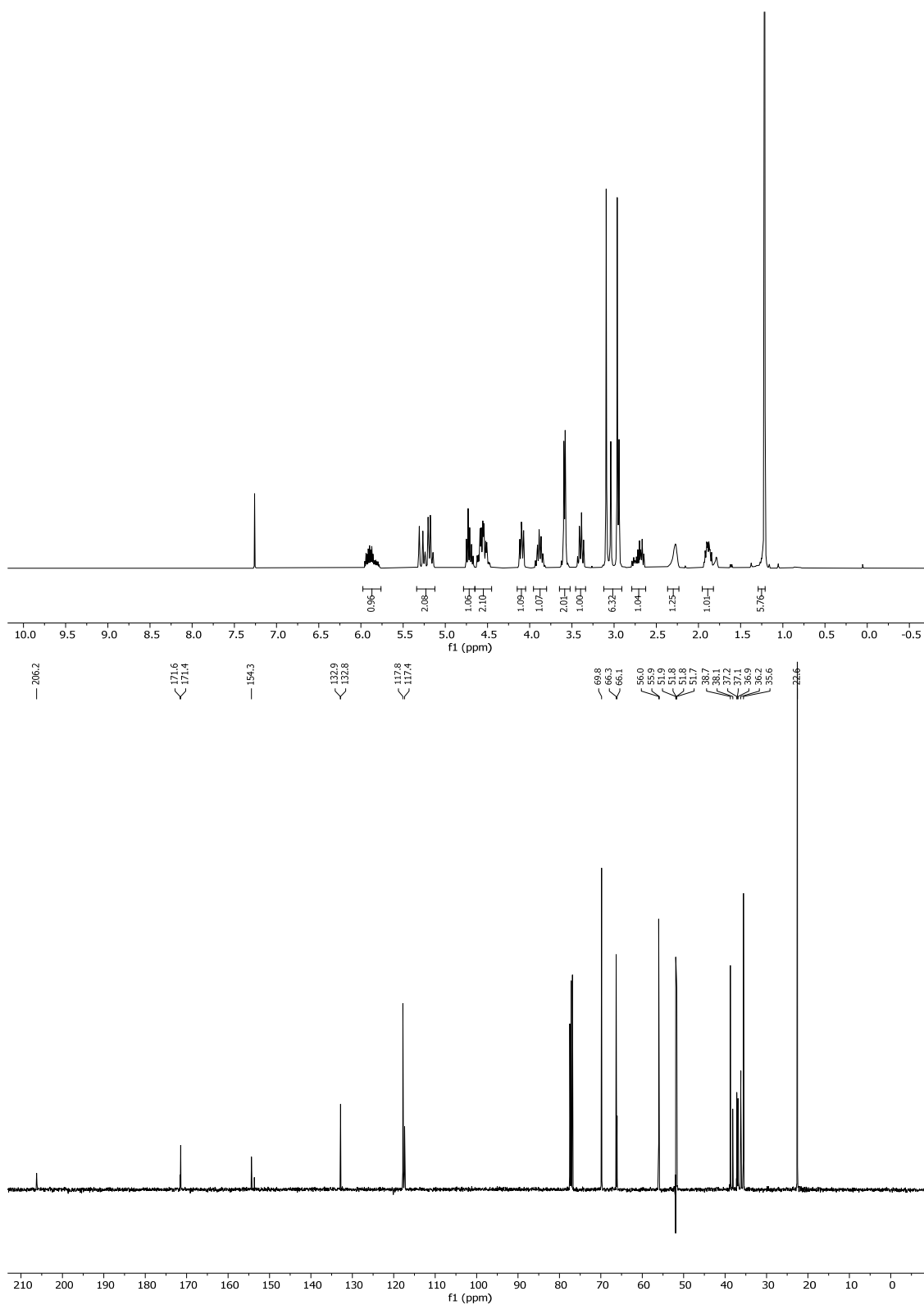
Remark: Peaks in ^1H and ^{13}C -NMR spectra broad and split due to the presence of *N*-Alloc and *N*-Me₂ rotamers.



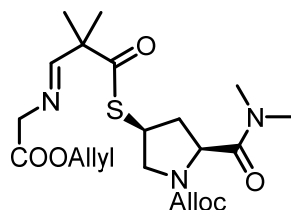
DS9

Allyl (2S,4S)-2-(dimethylcarbamoyl)-4-((3-hydroxy-2,2-dimethylpropanoyl)thio)pyrrolidine-1-carboxylate (DS9). To a solution of **DS8** (0.39 g, 0.81 mmol, 1.00 equiv.) in CH₂Cl₂ (41 mL) was added phosphate buffer pH 7 (12 mL) followed by DDQ (0.64 g, 2.84 mmol, 3.50 equiv.) at rt. The mixture was vigorously stirred for 3 h; then sat. aq. NaHCO₃ (50 mL) and CH₂Cl₂ (100 mL) were added and the phases were separated. The aqueous phase was extracted with CH₂Cl₂ (3 x 100 mL) and the combined organic extracts were washed with brine (100 mL), dried over MgSO₄ and concentrated under reduced pressure. Purification of the residue by FC (EtOAc) gave **DS9** (0.25 g, 0.70 mmol, 86%) as white powder.

TLC: R_f = 0.30 (EtOAc). **MP** = 102 °C. **¹H-NMR** (400 MHz, CDCl₃): δ = 5.98 – 5.76 (m, 1H), 5.34 – 5.12 (m, 2H), 4.71 (dt, *J* = 16.2, 7.8 Hz, 1H), 4.65 – 4.45 (m, 2H), 4.10 (ddd, *J* = 10.6, 7.5, 2.7 Hz, 1H), 3.95 – 3.80 (m, 1H), 3.59 (d, *J* = 6.4 Hz, 2H), 3.46 – 3.34 (m, 1H), 3.12 – 2.91 (m, 6H), 2.27 (s, 1H), 1.22 (d, *J* = 1.5 Hz, 6H), 2.72 (ddt, *J* = 28.4, 12.9, 7.9 Hz, 1H), 1.96 – 1.82 (m, 1H). **¹³C-NMR** (101 MHz, CDCl₃): δ = 206.2, 171.6, 171.4, 154.4, 132.9, 132.8, 117.8, 117.4, 69.8, 66.3, 66.1, 56.0, 55.9, 51.9, 51.8, 51.8, 51.7, 38.7, 38.1, 37.2, 37.1, 36.9, 36.2, 35.6, 22.6. **IR** (neat): $\tilde{\nu}$ = 3685, 3675, 3425, 2987, 2972, 2901, 1689, 1649, 1449, 1408, 1251, 1228, 1198, 1173, 1146, 1074, 1065, 1057, 1028, 931, 893, 879, 870, 768 cm⁻¹. **HRMS** (ESI): calcd for C₁₆H₂₇N₂NaO₅S [(M+Na)⁺]: 381.1455; found: 381.1454. $[\alpha]_D^{20}$: -5.80 (c = 1.00 in CHCl₃).



Remark: Peaks in ^1H and ^{13}C -NMR spectra broad and split due to the presence of *N*-Alloc and *N*-Me₂ rotamers.

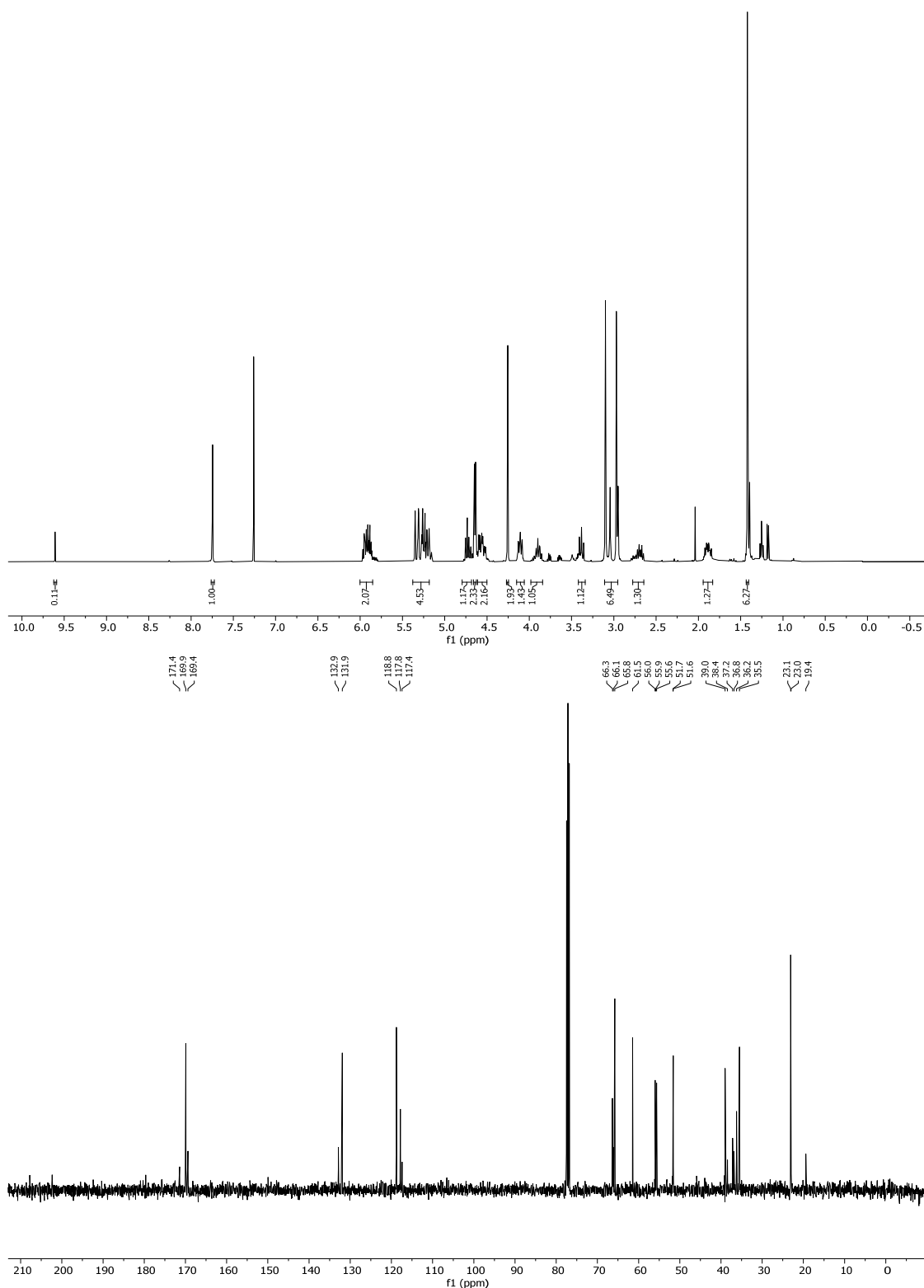
**D30**

Allyl (2S,4S)-4-(((E)-3-((2-(allyloxy)-2-oxoethyl)imino)-2,2-dimethylpropanoyl)thio)-2-(dimethylcarbamoyl)pyrrolidine-1-carboxylate (D30). To a solution of oxalyl chloride (0.29 mL, 3.33 mmol, 1.20 equiv.) in dry CH₂Cl₂ (10 mL) was added DMSO (0.47 mL, 6.66 mmol, 2.40 equiv.) in dry CH₂Cl₂ (5 mL) dropwise at -78 °C. The solution was stirred at the same temperature for 30 min and a solution of **DS9** (0.99 g 2.77 mmol, 1.00 equiv.) in dry CH₂Cl₂ (5 mL) was added dropwise. The reaction mixture was stirred for 1 h at -78 °C, before it was allowed to warm to -55 °C and Et₃N (1.92 mL, 13.87 mmol, 5.00 equiv.) was added dropwise. The mixture was stirred at -55 °C for 5 min and slowly allowed to warm to rt over 1 h. The slightly yellow reaction mixture was diluted with CH₂Cl₂ (25 mL) and washed with ice cold 0.5 M HCl (30 mL) and water (30 mL). The aqueous layers were extracted with CH₂Cl₂ (3 x 30 mL) and the combined organic layer were washed with H₂O (40 mL) and brine (40 mL), dried over MgSO₄ and concentrated under reduced pressure to afford crude **D29** as a yellow oil, which was used for the next step without further purification.

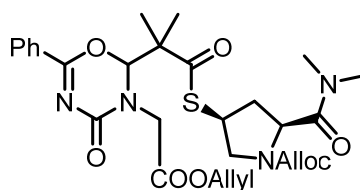
D9•HCl^[231,316] (0.49 g, 3.26 mmol, 1.00 equiv.) was dissolved in CH₂Cl₂ (32 mL) and Et₃N (4.52 mL). The solution was stirred for 30 min at rt before **D29** (0.99 g, 2.77 mmol, 0.85 equiv.) in CH₂Cl₂ (32 mL) and MgSO₄ (1.67 g) were added to the solution. The reaction mixture was stirred for 4.5 h. Afterwards the MgSO₄ was removed *via* filtration, the filtrate was diluted with EtOAc (60 mL) and H₂O (60 mL), the layers were separated and the aqueous layer was extracted with EtOAc (3 x 60 mL). The organic layer was washed with H₂O (150 mL) and brine (150 mL). The organic layer was dried over MgSO₄ and the solvent was removed under reduced pressure to afford crude **D30** (1.14g, 2.50 mmol, 90% over two steps, as a 9:1 mixture with **D29** (10%), calculated based on NMR spectroscopy).

TLC: R_f = 0.50 (EtOAc). **¹H-NMR** (400 MHz, CDCl₃): δ = 9.61 (s, 0H), 7.75 (t, J = 1.3 Hz, 1H), 6.00 – 5.85 (m, 2H), 5.38 – 5.18 (m, 5H), 4.79 – 4.68 (m, 1H), 4.64 (dt, J = 5.7, 1.5 Hz, 2H), 4.56 (dddd, J = 13.2, 11.7, 4.9, 3.4 Hz, 2H), 4.26 (d, J = 1.2 Hz, 2H), 4.11 (tdd, J = 7.4, 3.9, 1.8 Hz, 1H), 3.90 (tt, J = 10.1, 7.7 Hz, 1H), 3.42 – 3.34 (m, 1H), 3.11 – 2.95 (m, 6H), 2.78 – 2.65 (m, 1H), 1.94 – 1.83 (m, 1H), 1.42 (s, 6H). **¹³C-NMR** (101 MHz, CDCl₃): δ = 171.4, 169.9, 169.4, 132.9, 131.9, 118.8, 117.8,

117.4, 66.3, 66.1, 65.8, 61.5, 56.0, 55.9, 55.6, 51.7, 51.9, 39.0, 38.4, 37.2, 36.9, 36.2, 35.5, 23.1, 23.0, 19.4. **IR** (neat): $\tilde{\nu}$ = 2975, 2936, 2875, 1752, 1736, 1700, 1653, 1559, 1498, 2557, 1437, 1404, 1349, 1267, 1172, 1144, 1085, 977, 924, 863, 830, 791, 766, 734, 616, 577, 557, 536 cm^{-1} . **HRMS** (ESI): calcd for $\text{C}_{21}\text{H}_{32}\text{N}_3\text{O}_6\text{S}$ [(M+H)⁺]: 454.2006; found: 454.2003. $[\alpha]_D^{20}$: -6.00 (c = 1.00 in CHCl_3).

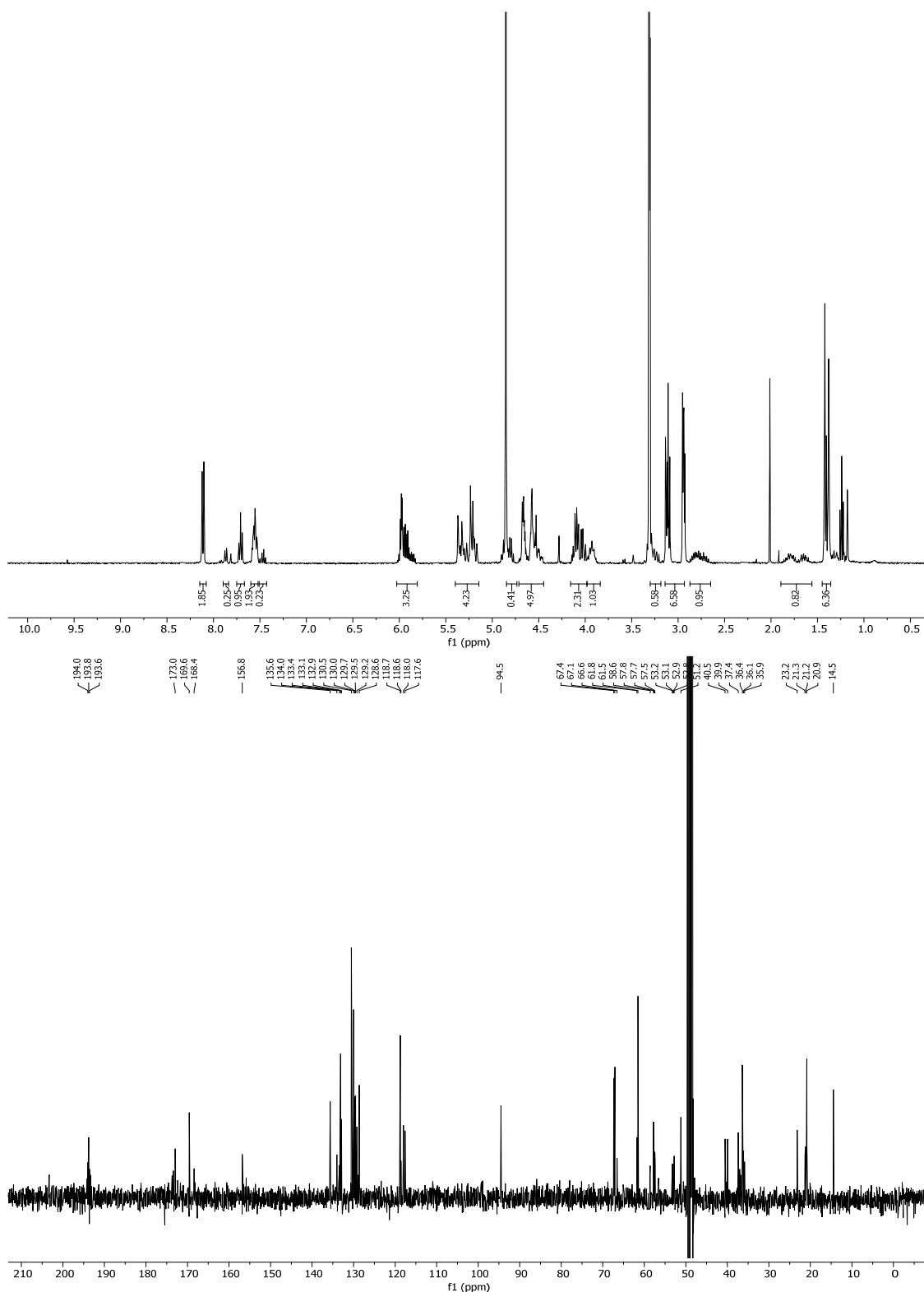


Remark: Peaks in ¹H and ¹³C-NMR spectra broad and split due to the presence of *N*-Alloc and *N*-Me₂ rotamers.

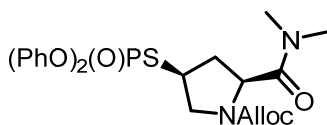
**D26**

Allyl (2*S*,4*S*)-4-((2-(3-(2-(allyloxy)-2-oxoethyl)-4-oxo-6-phenyl-3,4-dihydro-2*H*-1,3,5-oxadiazin-2-yl)-2-methylpropanoyl)thio)-2-(dimethylcarbamoyl)pyrrolidine-1-carboxylate (D26). To a solution of **D30** (180.0 mg, 0.40 mmol, 1.00 equiv.) in CH₂Cl₂ (4 mL) was added a solution of benzoyl isocyanate (0.15 mL, 1.20 mmol, 3.00 equiv.) in CH₂Cl₂ (4 mL) dropwise at 0 °C. The mixture was stirred at that temperature for 16 h. Afterwards H₂O (10 mL) was added, the phases were separated and the aqueous phase was extracted with CH₂Cl₂ (3 x 10 mL), washed with brine (30 mL), the combined organic phases were dried over MgSO₄, concentrated under reduced pressure and purified by FC (EtOAc/hexane 1:1 → 2:1 → 5:1 → EtOAc, + 2% Et₃N) to afford pressure to afford **D26** (160.0 mg, 0.27 mmol, 67%, as a 7:1 mixture with benzamide, calculated based on NMR spectroscopy) as colorless oil.

TLC: R_f = 0.45 (EtOAc). **¹H-NMR** (400 MHz, MeOD): δ = 8.15 – 8.08 (m, 2H), 7.90 – 7.84 (m, 0H), 7.71 (t, *J* = 7.5 Hz, 1H), 7.56 (ddt, *J* = 9.7, 7.0, 3.1 Hz, 2H), 7.51 – 7.43 (m, 0H), 6.03 – 5.81 (m, 3H), 5.40 – 5.14 (m, 4H), 4.81 (t, *J* = 7.5 Hz, 1H), 4.71 – 4.45 (m, 5H), 4.16 – 3.98 (m, 2H), 3.98 – 3.84 (m, 1H), 3.30 – 3.19 (m, 1H), 3.14 – 2.93 (m, 7H), 2.76 (dtd, *J* = 35.3, 14.0, 7.8 Hz, 1H), 1.89 – 1.56 (m, 1H), 1.45 – 1.36 (m, 6H). **¹³C-NMR** (101 MHz, MeOD): δ = 194.0, 193.8, 193.6, 173.0, 169.6, 168.4, 156.8, 135.6, 134.0, 133.4, 133.1, 132.9, 130.5, 130.0, 129.7, 129.5, 129.2, 128.6, 118.7, 118.6, 118.0, 117.6, 94.5, 67.4, 67.1, 66.6, 61.8, 61.5, 58.6, 57.8, 57.7, 57.5, 53.2, 53.2, 52.9, 52.8, 51.2, 40.5, 40.0, 37.4, 36.4, 36.1, 35.9, 23.2, 21.3, 21.2, 20.9, 14.5. **IR** (neat): $\tilde{\nu}$ = 2979, 2940, 2901, 1703, 1673, 1611, 1576, 1536, 1503, 1469, 1449, 1406, 1365, 1336, 1324, 1305, 1266, 1175, 1144, 1076, 1065, 1027, 983, 942, 786, 767, 701, 624 cm⁻¹. **HRMS** (ESI): calcd for C₂₉H₃₇N₄O₈S [(M+H)⁺]: 601.2327; found: 601.2323.

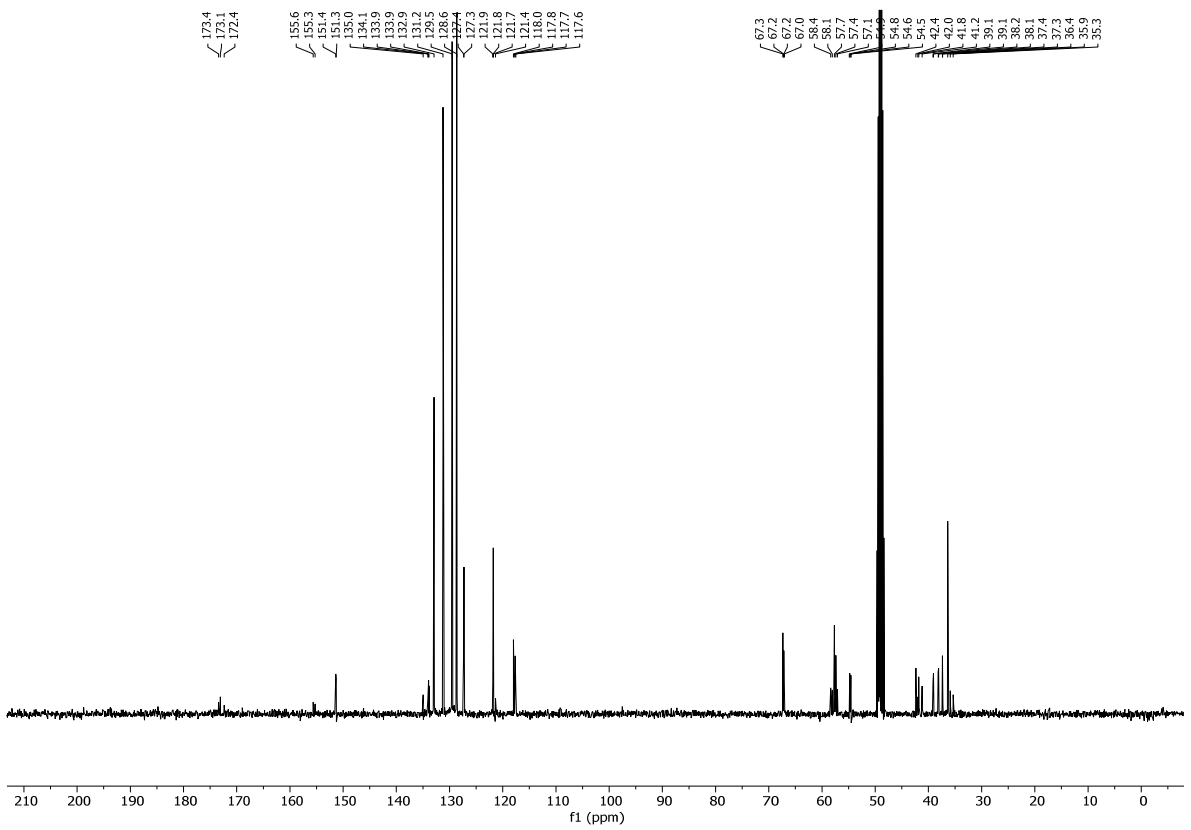
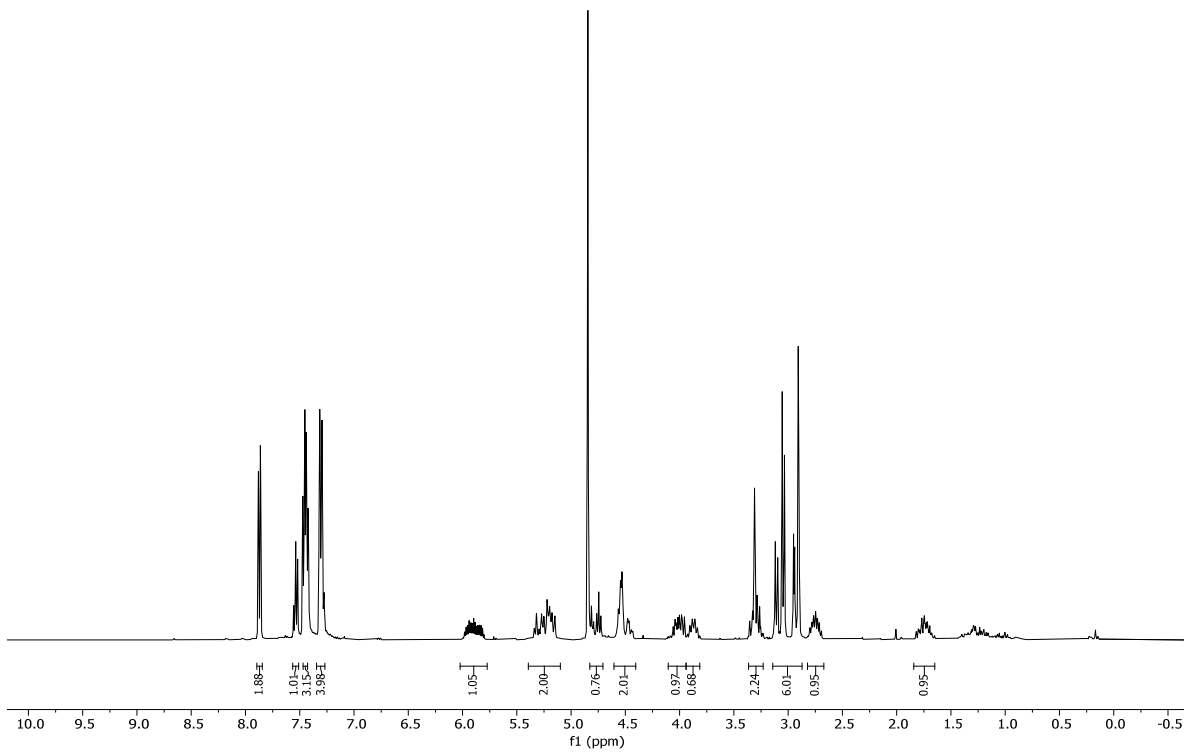


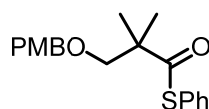
Remark: Peaks in ^1H and ^{13}C -NMR spectra broad and split due to the presence of *N*-Alloc and *N*-Me₂ rotamers.

**DS10**

Allyl (2*S*,4*S*)-2-(dimethylcarbamoyl)-4-((diphenoxyphosphoryl)thio)pyrrolidine-1-carboxylate (DS10). See Table 14, entries 1-3 and 5.

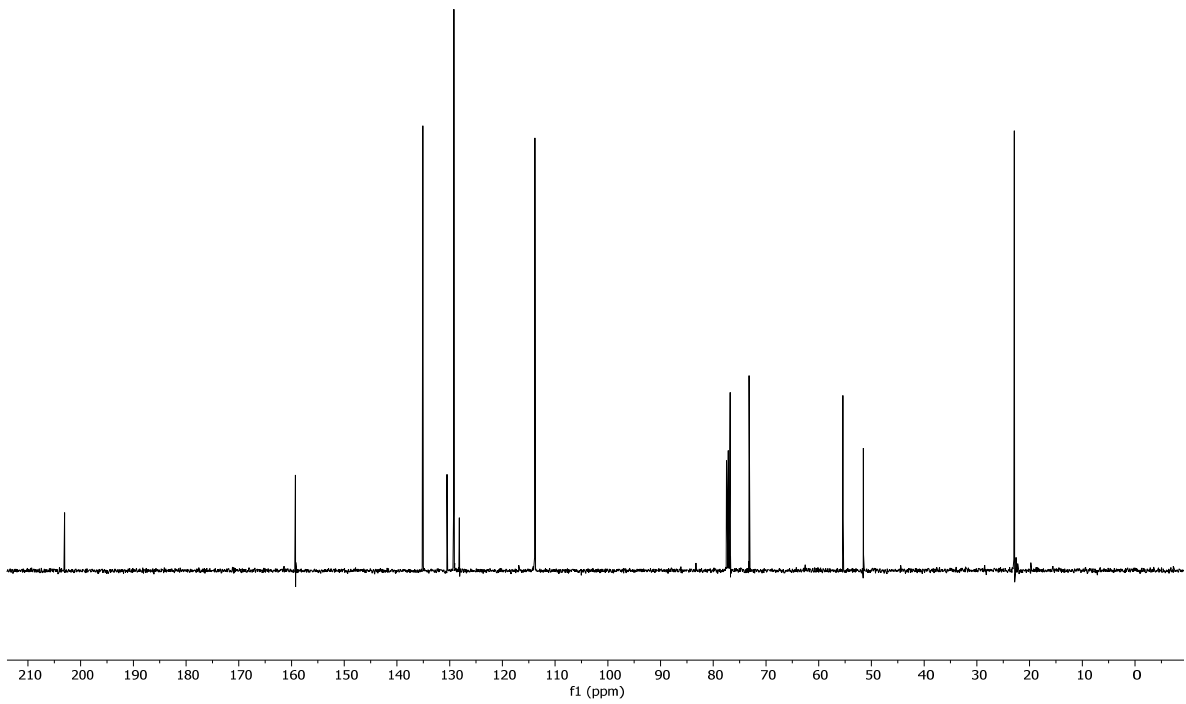
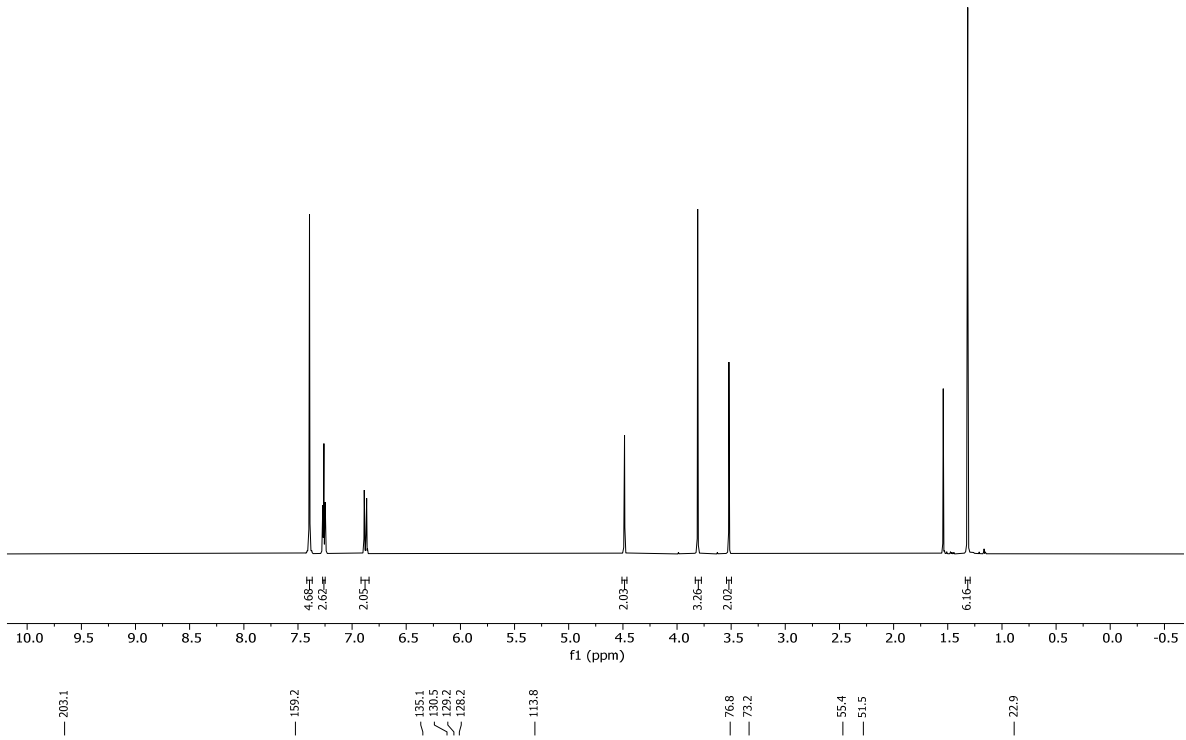
TLC: $R_f = 0.51$ (EtOAc). **¹H-NMR** (400 MHz, MeOD) $\delta = 7.90 - 7.84$ (m, 2H), 7.56 - 7.51 (m, 1H), 7.45 (ddd, $J = 7.1, 4.2, 2.3$ Hz, 3H), 7.34 - 7.27 (m, 4H), 6.02 - 5.77 (m, 1H), 5.39 - 5.10 (m, 2H), 4.83 - 4.71 (m, 1H), 4.61 - 4.40 (m, 2H), 4.11 - 3.94 (m, 1H), 3.94 - 3.81 (m, 1H), 3.36 - 3.23 (m, 2H), 3.14 - 2.87 (m, 6H), 2.82 - 2.67 (m, 1H), 1.84 - 1.65 (m, 1H). **¹³C-NMR** (101 MHz, MeOD) $\delta = 173.4, 173.1, 172.4, 155.6, 155.3, 151.4, 151.3, 135.0, 134.1, 133.9, 133.9, 132.9, 131.2, 129.5, 128.6, 127.4, 127.3, 121.9, 121.8, 121.7, 121.4, 118.0, 117.8, 117.7, 117.6, 67.4, 67.3, 67.2, 67.1, 58.4, 58.1, 57.7, 57.4, 57.1, 54.9, 54.8, 54.6, 54.5, 42.4, 42.0, 41.8, 41.2, 39.1, 39.1, 38.2, 38.1, 37.4, 37.3, 36.4, 35.9, 35.4$. **IR** (neat): $\tilde{\nu} = 3359, 3211, 3066, 2939, 1700, 1651, 1488, 1448, 1407, 1263, 1182, 1161, 1072, 1026, 1007, 940, 768, 692, 619, 593, 578, 547$ cm⁻¹. **HRMS** (ESI): calcd for C₂₃H₇N₂O₆PS [(M+H)⁺]: 491.1327; found: 491.1395. $[\alpha]_D^{20}$: -25.99 (c = 1.00 in CHCl₃).

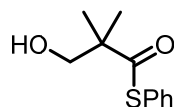


**DS11**

S-Phenyl 3-((4-methoxybenzyl)oxy)-2,2-dimethylpropanethioate (DS11). A solution of **D28** (4.40 g, 18.47 mmol, 1.00 equiv.) and HATU (14.04 g, 36.93 mmol, 2.00 equiv.) in DMF (60 mL) was stirred for 5 min before DIPEA (12.6 mL, 73.86 mmol, 4.00 equiv.) was added and stirring was continued for 10 more minutes. Afterwards thiophenol (3.78 mL, 4.07 mmol, 2.00 equiv.) was added. The mixture was stirred for 18 h. The solvent was evaporated under reduced pressure, the residue was dissolved in EtOAc (100 mL). The solution was washed with H₂O (40 mL), sat. aq. NaHCO₃ (40 mL) and brine (40 mL). The combined aqueous layers were re-extracted with CH₂Cl₂ (3 x 150) dried over MgSO₄, concentrated in vacuo and purified by FC (EtOAc/hexane 1:30 → 1:20 → 1:10) to give **DS11** (4.50 g, 13.62 mmol, 74%) as a colorless oil.

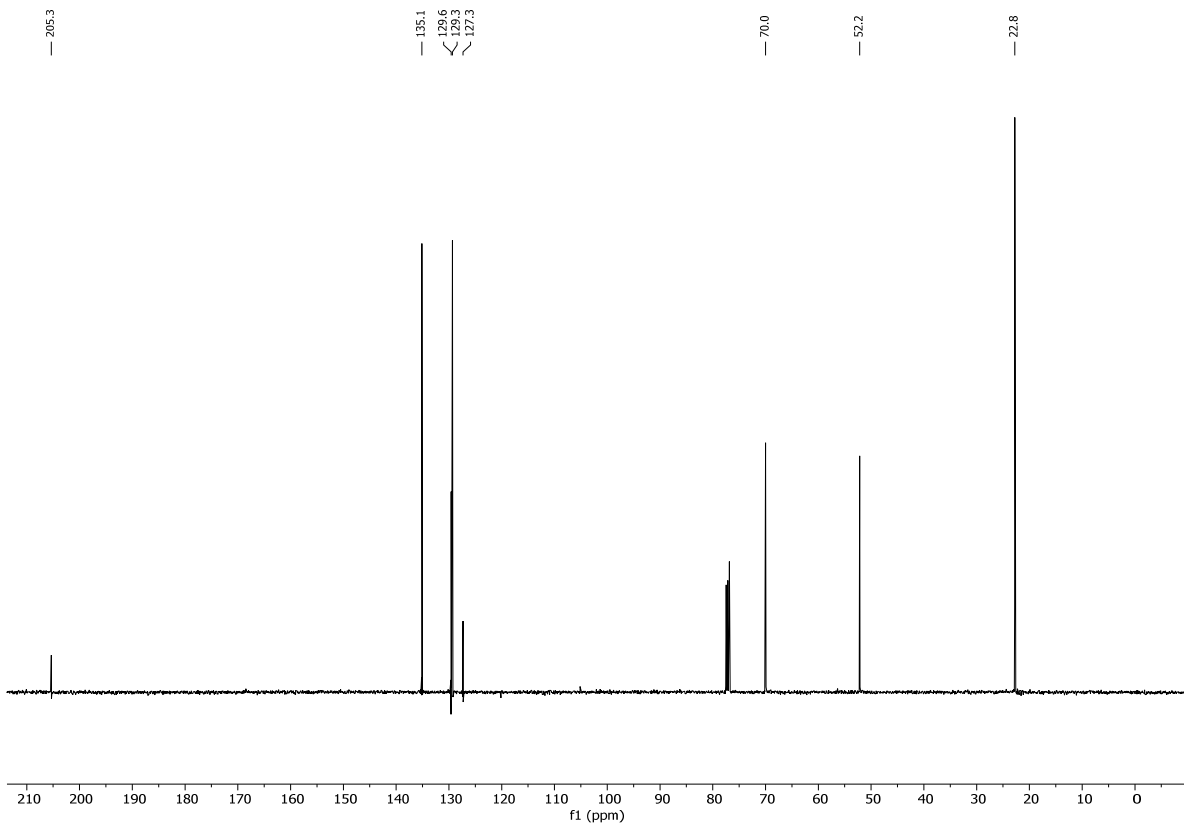
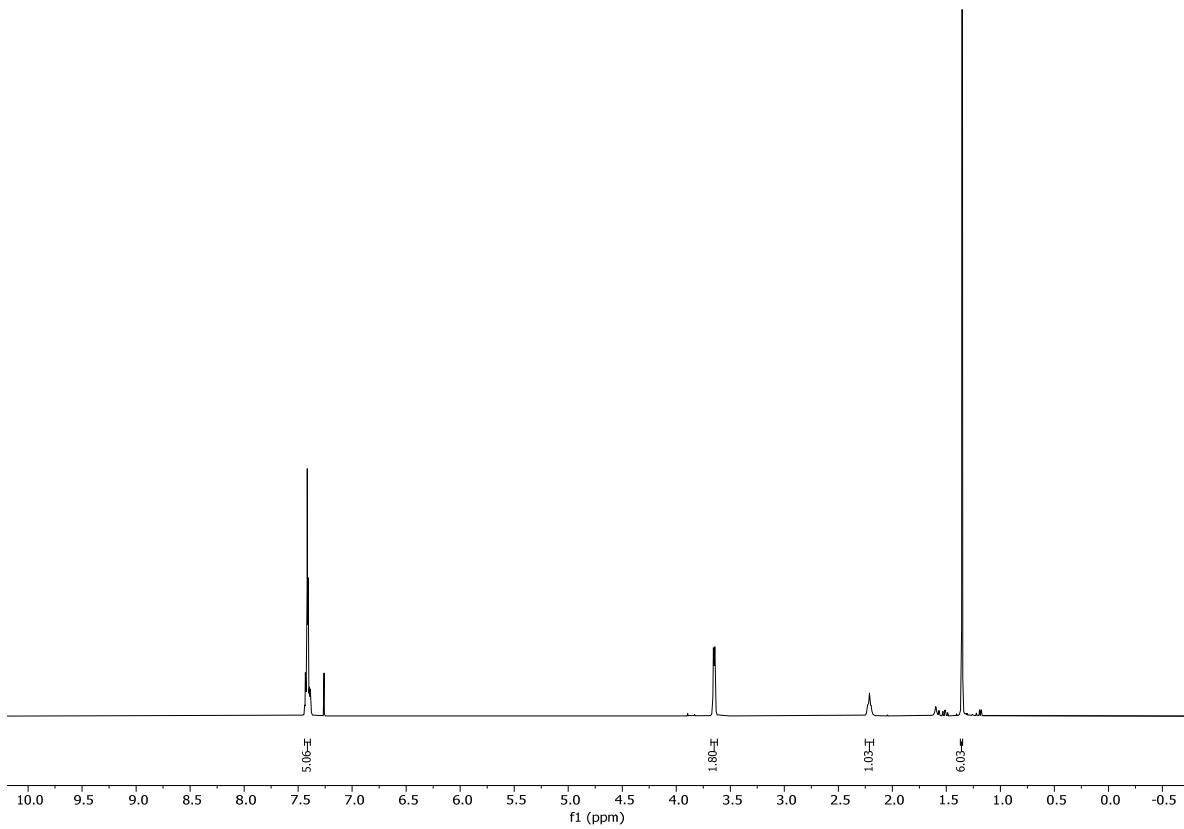
TLC: R_f = 0.50 (EtOAc/hexane 1:6). **¹H-NMR** (400 MHz, CDCl₃): δ = 7.39 (s, 5H), 7.26 (t, *J* = 4.3 Hz, 3H), 6.92 – 6.84 (m, 2H), 4.49 (s, 2H), 3.81 (s, 3H), 3.52 (s, 2H), 1.32 (s, 6H). **¹³C-NMR** (101 MHz, CDCl₃): δ = 203.1, 159.3, 135.1, 130.5, 129.2, 128.2, 113.8, 76.8, 73.2, 55.4, 51.5, 22.9. **IR** (neat): $\tilde{\nu}$ = 2967, 2933, 2902, 2856, 2837, 1693, 1611, 1585, 1512, 1476, 1466, 1441, 1381, 1362, 1302, 1256, 1209, 1173, 1093, 1034, 986, 927, 819, 745, 706, 689, 666, 623, 580, 532, 520 cm⁻¹. **HRMS** (ESI): calcd for C₁₉H₂₂NaO₃S [(M+Na)⁺]: 353.1182; found: 353.1176.

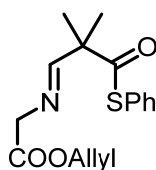


**DS12**

S-Phenyl 3-hydroxy-2,2-dimethylpropanethioate (DS12). To a solution of **DS11** (4.48 g, 13.56 mmol, 1.00 equiv.) in CH₂Cl₂ (225 mL) was added phosphate buffer pH 7 (85 mL) followed by DDQ (11.0 g, 47.45 mol, 3.50 equiv.) at rt. The mixture was vigorously stirred for 2.5 h; then sat. aq. NaHCO₃ (200 mL) and CH₂Cl₂ (300 mL) were added and the phases were separated. The aqueous phase was extracted with CH₂Cl₂ (3 x 200 mL) and the combined organic extracts were washed with brine (500 mL), dried over MgSO₄ and concentrated under reduced pressure. Purification of the residue by FC (EtOAc/hexane 1:15 → 1:10 → 1:5) furnished to **DS12** (2.68 g, 12.74 mmol, 94%) as a viscous liquid.

TLC: R_f = 0.25 (EtOAc/hexane 1:4). **¹H-NMR** (400 MHz, CDCl₃): δ = 7.44 – 7.39 (m, *J* = 2.0 Hz, 5H), 3.65 (d, *J* = 5.8 Hz, 2H), 2.25 – 2.17 (m, 1H), 1.36 (s, 6H). **¹³C-NMR** (101 MHz, CDCl₃): δ = 205.34, 135.12, 129.58, 129.34, 127.33, 70.00, 52.16, 22.77. **IR** (neat): $\tilde{\nu}$ = 3412, 3061, 2969, 2932, 2873, 1688, 1584, 1776, 1441, 1393, 1364, 1272, 1158, 1051, 1024, 985, 933, 822, 746, 706, 689, 672, 622, 532 cm⁻¹. **HRMS** (ESI): calcd for C₁₁H₁₄NaO₂S [(M+Na)⁺]: 233.0607; found: 233.0606.

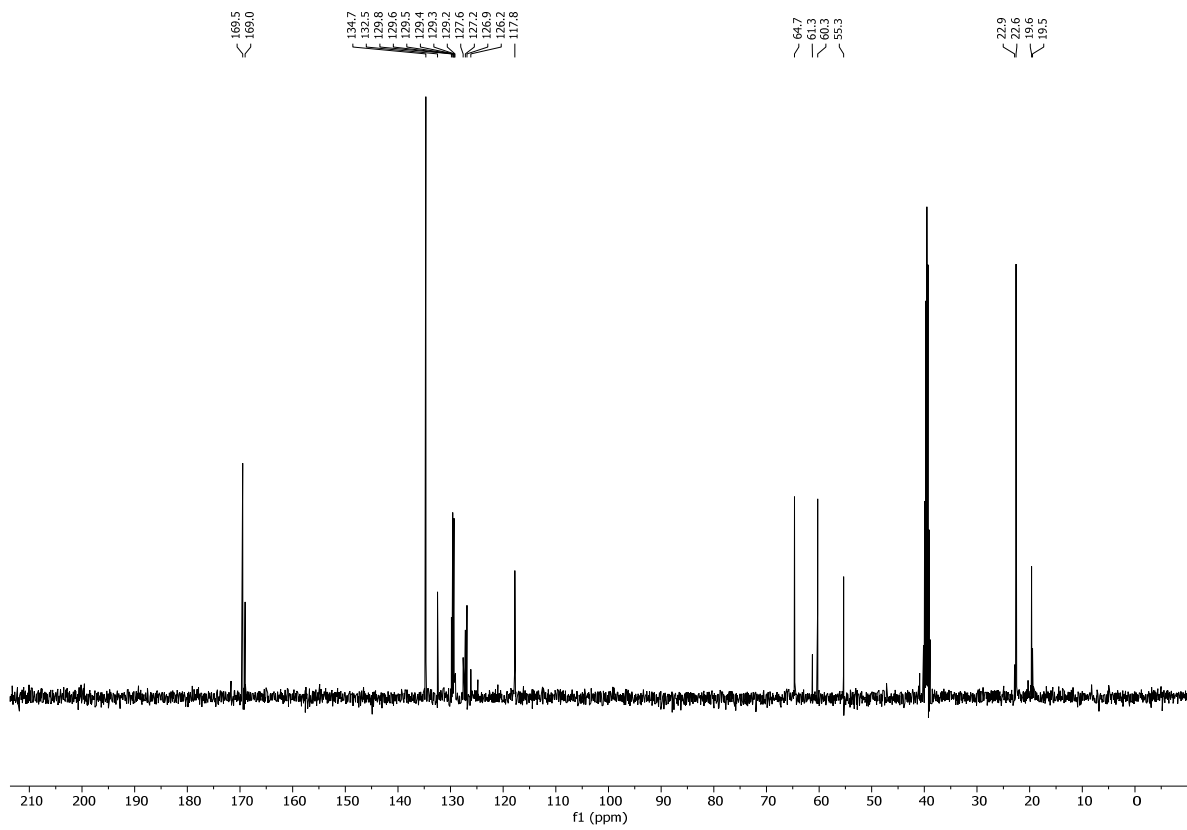
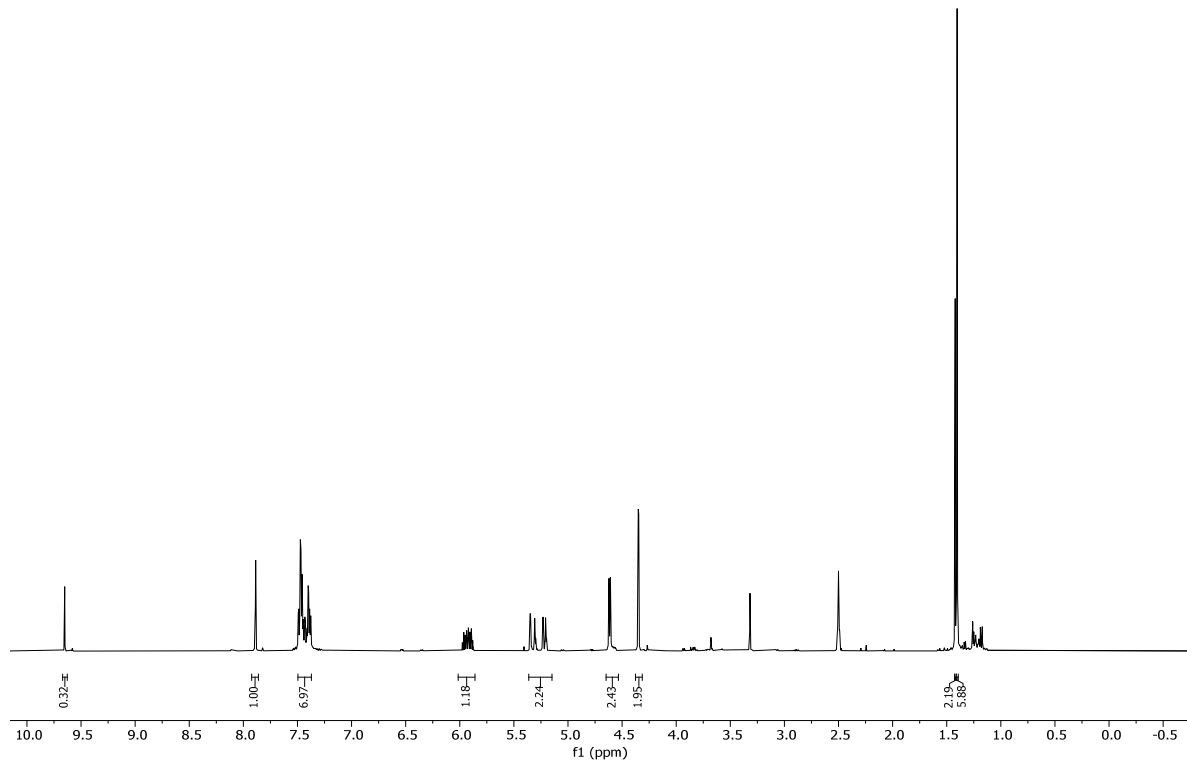


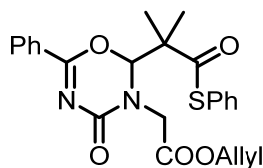
**D32**

Allyl (*E*)-2-((2,2-dimethyl-3-oxo-3-(phenylthio)propylidene)amino)acetate (D32). To a solution of oxalyl chloride (1.30 mL, 15.18 mmol, 1.20 equiv.) in dry CH₂Cl₂ (50 mL) was added DMSO (2.16 mL, 30.36 mmol, 2.40 equiv.) in dry CH₂Cl₂ (30 mL) dropwise at -78 °C. The solution was stirred at the same temperature for 30 min and **DS12** (2.66 g 12.65 mmol, 1.00 equiv.) in dry CH₂Cl₂ (30 mL) was added dropwise. The reaction mixture was stirred for 1 h at -78 °C, before it was allowed to warm to -55 °C and Et₃N (8.77 mL, 63.25 mmol, 5.00 equiv.) was added dropwise. The mixture was stirred at -55 °C for 5 min and allowed to slowly warm to rt over 1 h. The slightly yellow reaction mixture was diluted with CH₂Cl₂ (100 mL) and washed with ice cold 0.5 M HCl (120 mL) and water (120 mL). The aqueous layers were extracted with CH₂Cl₂ (3 x 200 mL) and the combined organic layers were washed with H₂O (400 mL) and brine (400 mL), dried over MgSO₄ and concentrated under reduced pressure to afford **D31** (2.68 g, 12.65 mmol, quant.) as crude colorless oil, which was used for the next step without further purification.

Allyl glycinate hydrochloride (**D9•HCl**)^[231,316] (2.12 g, 13.96 mmol, 1.00 equiv.) was dissolved in CH₂Cl₂ (85 mL) and Et₃N (19.39 mL, 139.85 mmol, 10.0 equiv.). The solution was stirred for 30 min before a solution of **D31** (2.62 g, 12.59 mmol, 0.90 equiv.) in CH₂Cl₂ (85 mL) and MgSO₄ (7.58 g) were added. The reaction mixture was stirred for 3 h at rt. Afterwards the MgSO₄ was removed by filtration, the filtrate was diluted with EtOAc (200 mL) and H₂O (200 mL), the layers were separated and the aqueous layer was extracted with EtOAc (3 x 200 mL). The organic layer was washed with H₂O (400 mL) and brine (400 mL). The organic layer was dried over MgSO₄ and the solvent was removed under reduced pressure to afford **D32** (2.91 g, 9.52 mmol, 76%, as a 3:1 mixture with **D31** (24%), calculated based on NMR spectroscopy).

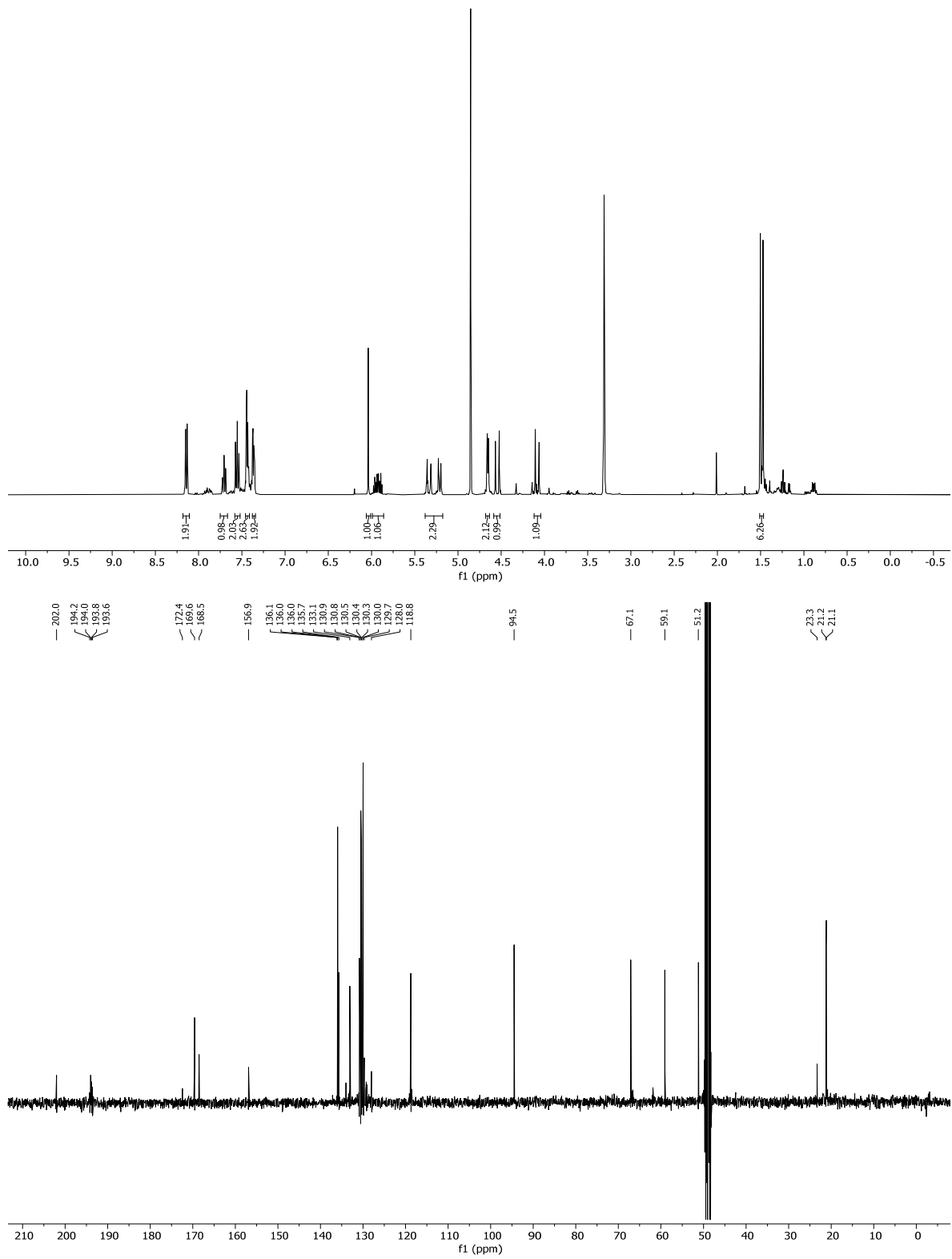
TLC: R_f = 0.50 (EtOAc). **¹H-NMR** (400 MHz, DMSO) δ = 9.65 (s, 0H), 7.89 (t, *J* = 1.2 Hz, 1H), 7.50 – 7.37 (m, 7H), 6.01 – 5.86 (m, 1H), 5.36 – 5.15 (m, 2H), 4.65 – 4.53 (m, 2H), 4.35 (d, *J* = 1.3 Hz, 2H), 1.42 (s, 2H), 1.40 (s, 6H). **¹³C-NMR** (101 MHz, DMSO): δ = 169.5, 169.0, 134.7, 132.5, 129.8, 129.6, 129.5, 129.3, 129.3, 129.2, 127.6, 127.2, 126.9, 126.2, 117.8, 64.7, 61.3, 60.3, 55.3, 22.9, 22.6, 19.6, 19.5. **IR** (neat): $\tilde{\nu}$ = 3060, 2979, 2935, 2871, 1736, 1690, 1662, 1478, 1463, 1441, 1389, 1364, 1337, 1271, 1176, 1066, 1023, 985, 933, 827, 746, 706, 689, 580, 560 cm⁻¹. **HRMS** (ESI): calcd for C₁₆H₂₀NO₃S [(M+H)⁺]: 306.1158; found: 306.1157.



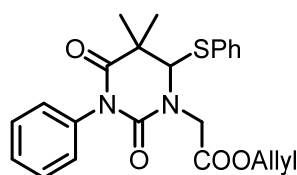
**D33**

Allyl 2-(2-(2-methyl-1-oxo-1-(phenylthio)propan-2-yl)-4-oxo-6-phenyl-2H-1,3,5-oxadiazin-3(4H)-yl)acetate (D33). To a solution of **D32** (0.37 g, 1.23 mmol, 1.00 equiv.) in CH₂Cl₂ (12 mL) was added a solution of benzoyl isocyanate (0.8 mL, 6.12 mmol, 5.00 equiv.) in CH₂Cl₂ (15 mL) dropwise at 0 °C. The mixture was stirred at that temperature for 2 h. Afterwards H₂O (20 mL) was added, the phases were separated and the aqueous phase was extracted with CH₂Cl₂ (3 x 30 mL), washed with brine (50 mL), the combined organic phases were dried over MgSO₄, concentrated under reduced pressure and purified by FC (EtOAc/hexane 1:4, 2% Et₃N) to afford **D33** (0.34 g, 0.75 mmol, 61%) as colorless oil.

TLC: R_f = 0.61 (1:1 EtOAc/hexane). **MP** = 98 °C. **¹H-NMR** (400 MHz, MeOD): δ = 8.18 – 8.11 (m, 2H), 7.75 – 7.67 (m, 1H), 7.58 – 7.52 (m, 2H), 7.44 (dd, *J* = 5.0, 2.0 Hz, 3H), 7.38 – 7.34 (m, 2H), 6.04 (s, 1H), 5.93 (ddt, *J* = 17.2, 10.9, 5.6 Hz, 1H), 5.38 – 5.18 (m, 2H), 4.65 (dt, *J* = 5.9, 1.6 Hz, 2H), 4.54 (d, *J* = 17.6 Hz, 1H), 4.08 (d, *J* = 17.6 Hz, 1H), 1.49 (d, *J* = 12.5 Hz, 6H). **¹³C-NMR** (101 MHz, MeOD): δ = 202.0, 194.2, 194.0, 193.8, 193.6, 172.4, 169.6, 168.5, 156.9, 136.1, 136.0, 136.0, 135.7, 133.1, 130.9, 130.8, 130.5, 130.4, 130.3, 130.0, 129.7, 128.0, 118.8, 94.5, 67.1, 59.1, 51.2, 23.3, 21.2, 21.1. **IR** (neat): $\tilde{\nu}$ = 2979, 2938, 1749, 1684, 1607, 1575, 1452, 1442, 1366, 1322, 1305, 1271, 1190, 1065, 1024, 984, 934, 780, 750, 691, 671, 613 cm⁻¹. **HRMS** (ESI): calcd for C₂₄H₂₅N₂O₅S [(M+H)⁺]: 453.1479; found: 453.1476.



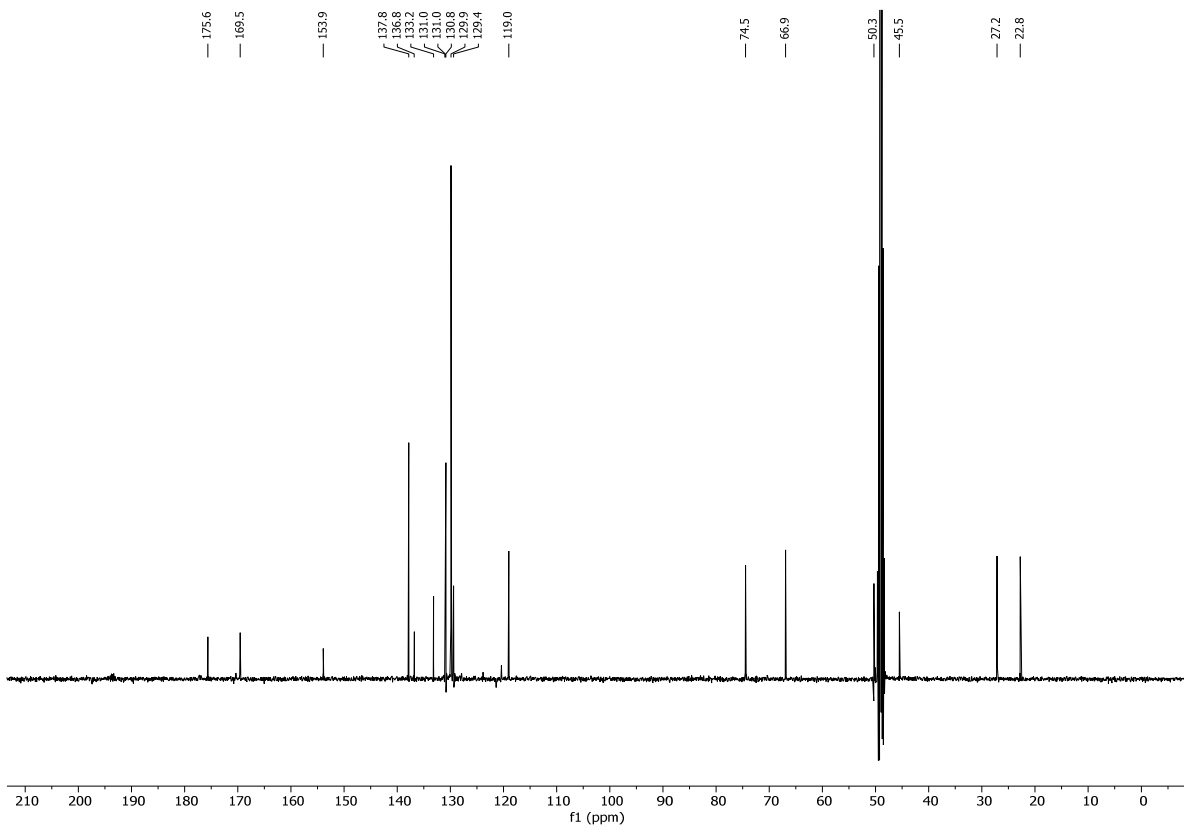
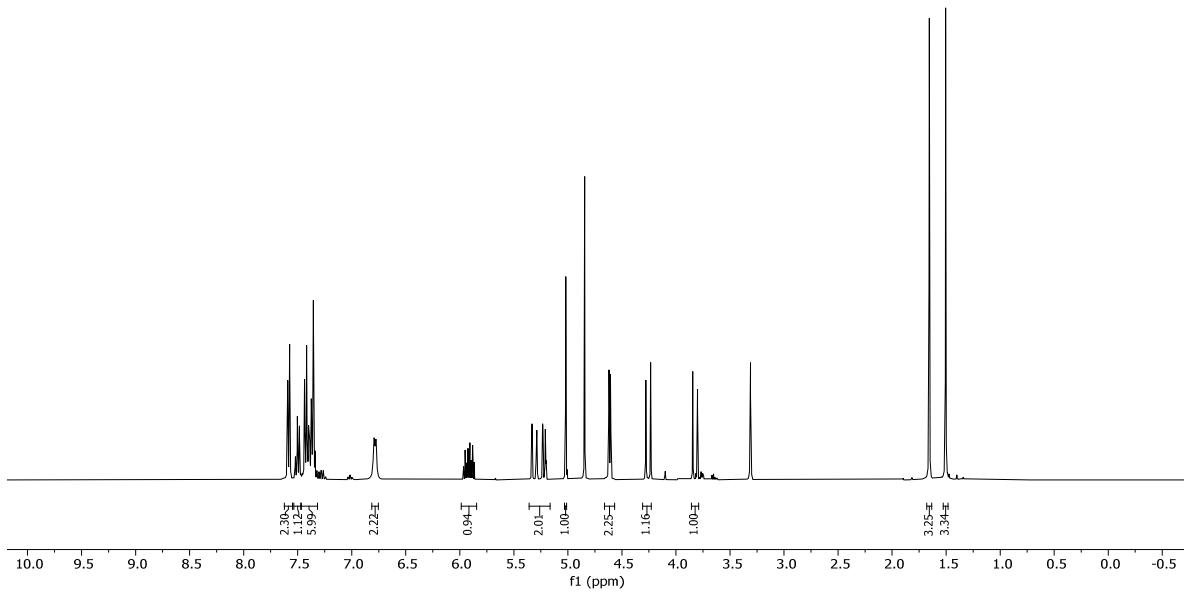
4.3.1.6 Synthesis of D42-D45

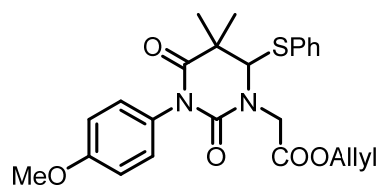


D42

Allyl 2-(5,5-dimethyl-2,4-dioxo-3-phenyl-6-(phenylthio)tetrahydropyrimidin-1(2H)-yl)acetate (D42). To neat **D33** (0.18 g, 0.60 mmol, 1.00 equiv.) was added neat phenyl isocyanate (**D37**) (0.33 mL, 3.00 mmol, 5.00 equiv.) at rt. The reaction mixture was heated to 70 °C and the mixture was stirred at that temperature for 18 h. Afterwards CH₂Cl₂ (20 mL) and H₂O (20 mL) were added, the phases were separated and the aqueous phase was extracted with CH₂Cl₂ (3 x 40 mL), washed with brine (60 mL), the combined organic phases were dried over MgSO₄, concentrated under reduced pressure and purified by FC (EtOAc/hexane 1:6 → 1:3) to afford **D42** (150.0 mg, 0.35 mmol, 58%) as colorless oil.

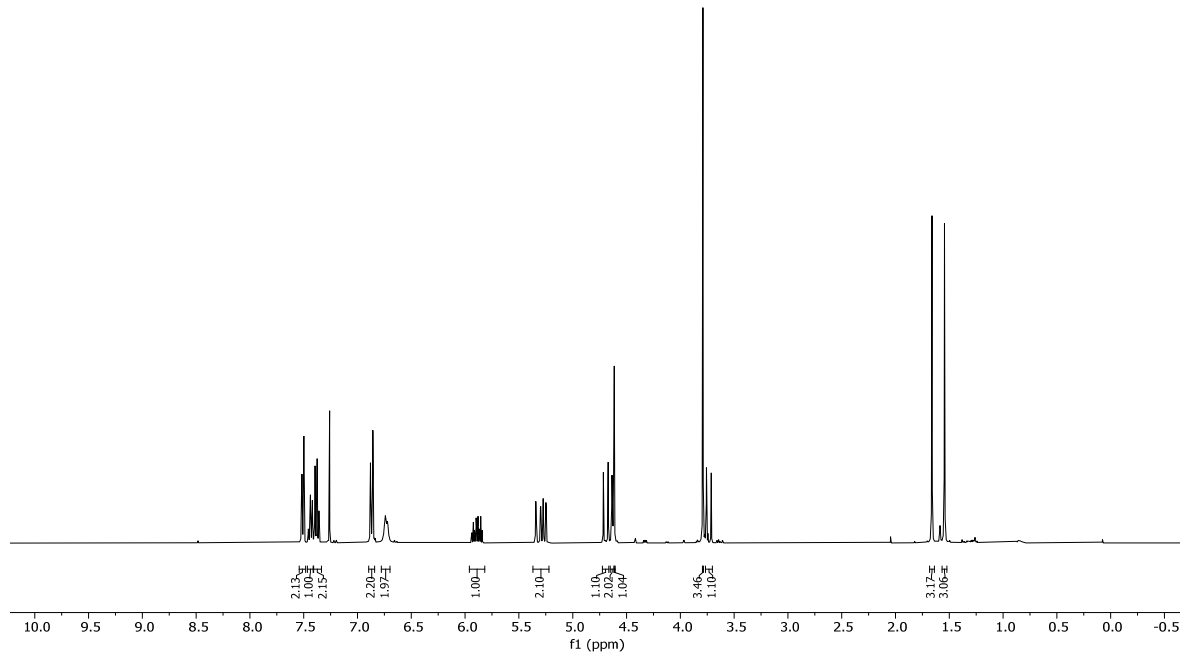
TLC: R_f = 0.58 (1:5 EtOAc/hexane). **¹H-NMR** (400 MHz, MeOD): δ = 7.62 – 7.55 (m, 2H), 7.54 – 7.47 (m, 1H), 7.47 – 7.32 (m, 6H), 6.78 (d, *J* = 6.9 Hz, 2H), 5.92 (ddt, *J* = 17.3, 10.4, 5.8 Hz, 1H), 5.36 – 5.16 (m, 2H), 5.02 (s, 1H), 4.61 (dt, *J* = 5.8, 1.4 Hz, 2H), 4.26 (d, *J* = 17.5 Hz, 1H), 3.82 (d, *J* = 17.5 Hz, 1H), 1.66 (s, 3H), 1.50 (s, 3H). **¹³C-NMR** (101 MHz, MeOD): δ = 175.6, 169.5, 153.9, 137.8, 136.8, 133.2, 131.0, 131.0, 131.0, 129.9, 129.4, 119.0, 74.5, 66.9, 50.3, 45.5, 27.2, 22.8. **IR** (neat): $\tilde{\nu}$ = 3065, 2979, 2933, 2868, 1750, 1724, 1679, 1597, 1527, 1493, 1468, 1440, 1404, 1395, 1379, 1352, 1312, 1222, 1183, 1087, 1070, 1024, 986, 936, 900, 836, 750, 719, 692, 662, 548, 518, 465 cm⁻¹. **HRMS** (ESI): calcd for C₂₃H₂₄N₂NaO₄S [(M+Na)⁺]: 447.1349; found: 447.1350.



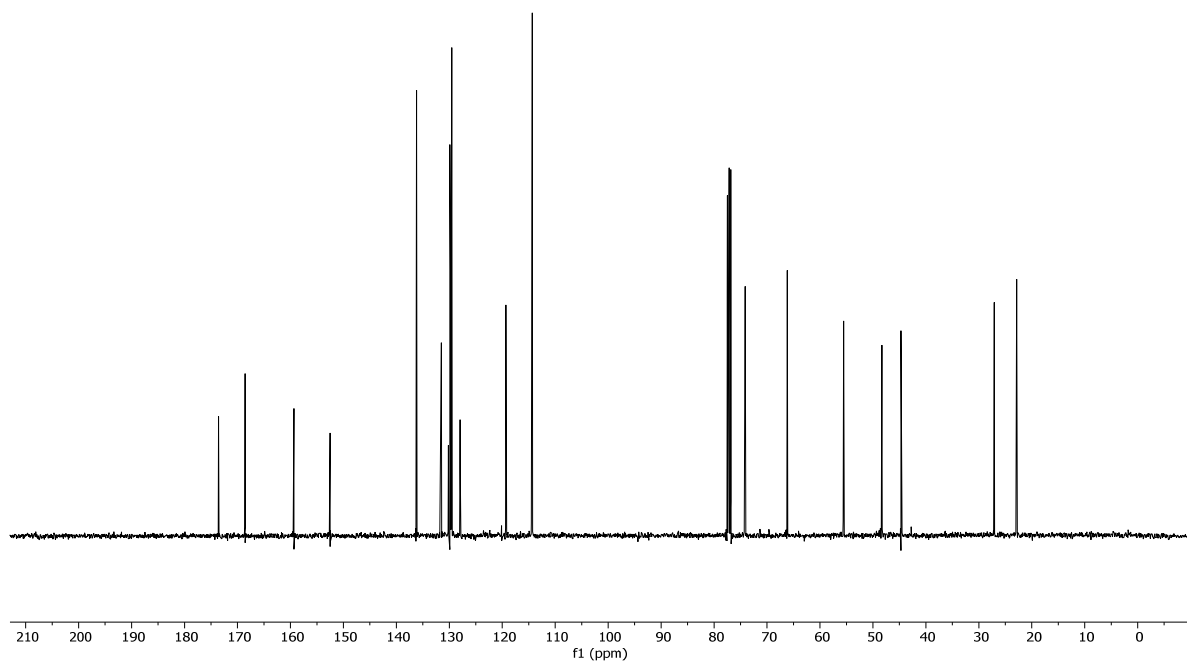
**D43**

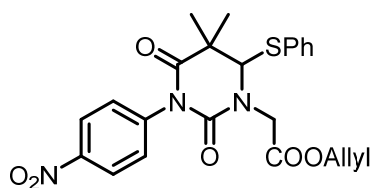
Allyl 2-(3-(4-methoxyphenyl)-5,5-dimethyl-2,4-dioxo-6-(phenylthio)tetrahydropyrimidin-1(2H)-yl)acetate (D43). To neat **D33** (0.27 mg, 0.87 mmol, 1.00 equiv.) was added neat PMP-isocyanate (**D38**) (0.57 mL, 4.35 mmol, 5.00 equiv.) at rt. The reaction mixture was heated to 70 °C and the mixture was stirred at that temperature for 18 h. Afterwards CH₂Cl₂ (20 mL) and H₂O (20 mL) were added, the phases were separated and the aqueous phase was extracted with CH₂Cl₂ (3 x 25 mL), washed with brine (60 mL), the combined organic phases were dried over MgSO₄, concentrated under reduced pressure and purified by FC (EtOAc/hexane 1:4 → 1:2) to afford pressure to afford **D43** (263.0 mg, 0.58 mmol, 67%) as colorless oil.

TLC: R_f = 0.55 (1:5 EtOAc/hexane). **¹H-NMR** (400 MHz, CDCl₃): δ = 7.54 – 7.48 (m, 2H), 7.47 – 7.41 (m, 1H), 7.41 – 7.34 (m, 2H), 6.90 – 6.84 (m, 2H), 6.74 (t, *J* = 6.6 Hz, 2H), 5.89 (ddt, *J* = 17.2, 10.4, 5.8 Hz, 1H), 5.37 – 5.22 (m, 2H), 4.69 (d, *J* = 17.7 Hz, 1H), 4.65 – 4.61 (m, 2H), 4.61 (s, 1H), 3.79 (s, 3H), 3.73 (d, *J* = 17.6 Hz, 1H), 1.66 (s, 3H), 1.54 (s, 3H). **¹³C-NMR** (101 MHz, CDCl₃): δ = 173.6, 168.6, 159.4, 152.5, 136.2, 131.5, 130.2, 129.9, 129.8, 129.5, 128.0, 119.3, 114.3, 74.1, 66.2, 55.5, 48.3, 44.7, 27.1, 22.8. **IR** (neat): $\tilde{\nu}$ = 2983, 2938, 1750, 1727, 1679, 1609, 1512, 1468, 1445, 1405, 1394, 1379, 1354, 1300, 1247, 1184, 1031, 988, 936, 827, 778, 753, 722, 693, 536 cm⁻¹. **HRMS** (ESI): calcd for C₂₄H₂₆N₂NaO₅S [(M+Na)⁺]: 477.1455; found: 477.1449.



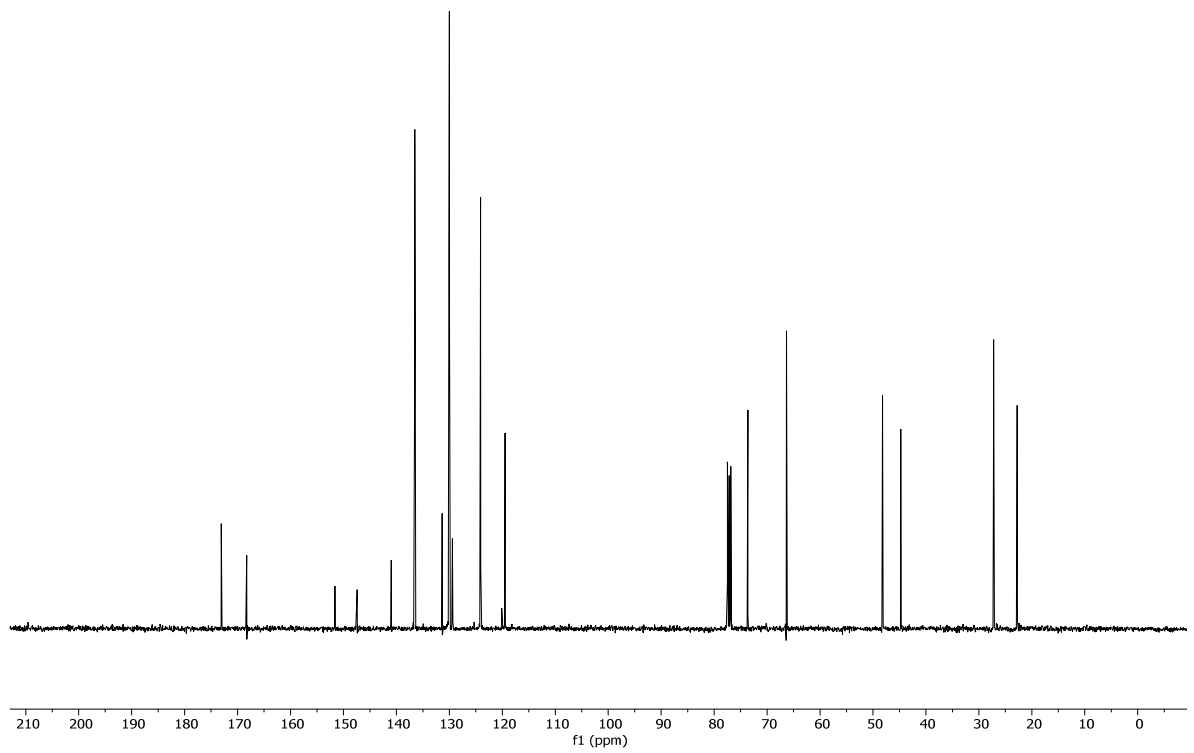
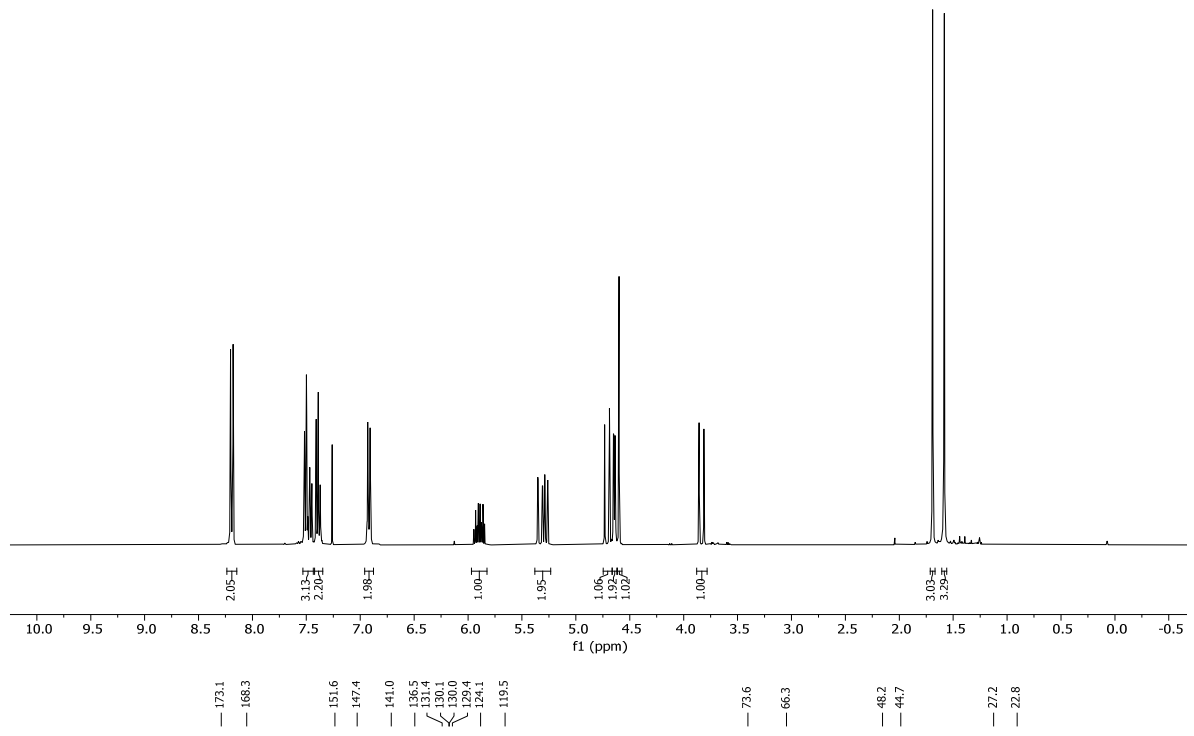
Chemical shift values (ppm): 173.6, 168.6, 158.3, 152.5, 136.2, 134.2, 130.2, 128.9, 128.7, 128.5, 128.0, 119.3, 114.3, 74.1, 66.2, 55.5, 48.3, 44.7, 27.1, 22.8.

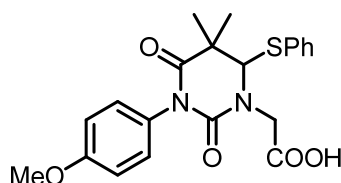


**D44**

Allyl 2-(5,5-dimethyl-3-(4-nitrophenyl)-2,4-dioxo-6-(phenylthio)tetrahydropyrimidin-1(2H)-yl)acetate (D44). To a mixture of **D33** (0.18 g, 0.60 mmol, 1.00 equiv.) in CCl_4 (0.3 mL) was added phenyl isocyanate (**D39**) (0.49 g, 3.00 mmol, 5.00 equiv.) at rt. The reaction mixture was heated to 70 °C and the mixture was stirred at that temperature for 18 h. Afterwards CH_2Cl_2 (20 mL) and H_2O (20 mL) were added, the phases were separated and the aqueous phase was extracted with CH_2Cl_2 (3 x 40 mL), washed with brine (60 mL), the combined organic phases were dried over MgSO_4 , concentrated under reduced pressure and purified by two consecutive FC (EtOAc/hexane 1st 1:3 and 2nd 1:5 → 1:3) to afford pressure to afford **D44** (180.0 g, 0.38 mmol, 64%) as pale yellow oil.

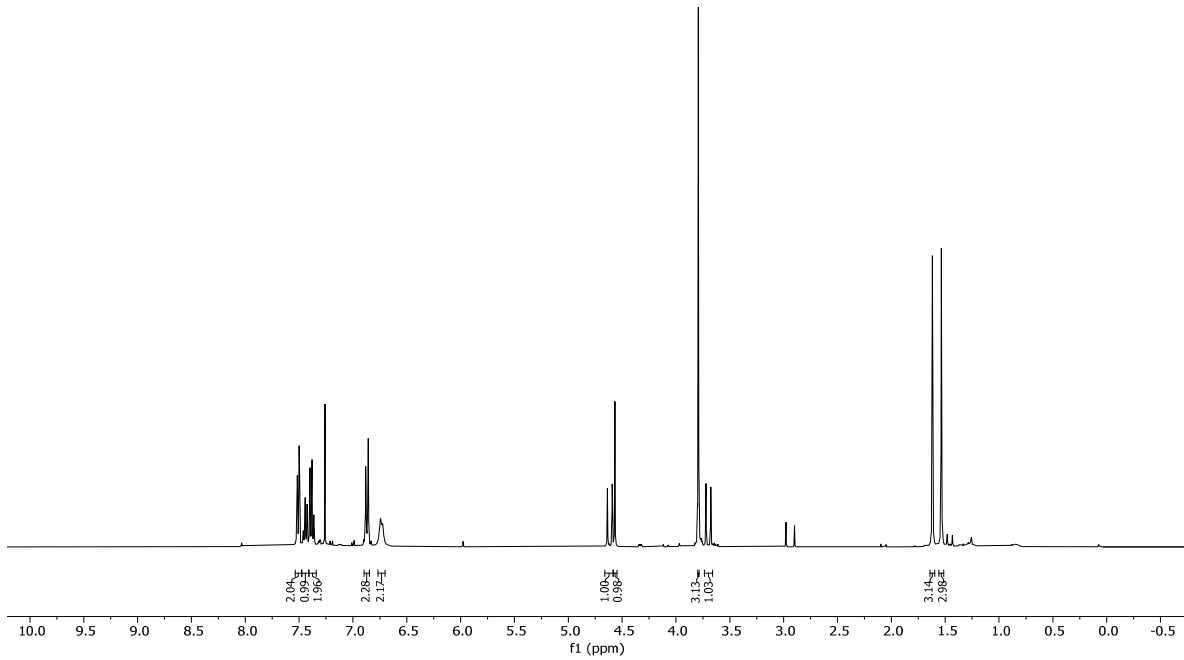
TLC: $R_f = 0.50$ (1:5 EtOAc/hexane). **$^1\text{H-NMR}$** (400 MHz, CDCl_3): $\delta = 8.24 - 8.15$ (m, 2H), 7.53 – 7.44 (m, 3H), 7.42 – 7.35 (m, 2H), 6.96 – 6.88 (m, 2H), 5.90 (ddt, $J = 17.4, 10.4, 5.9$ Hz, 1H), 5.38 – 5.23 (m, 2H), 4.71 (d, $J = 17.7$ Hz, 1H), 4.64 (dq, $J = 5.9, 1.3$ Hz, 2H), 4.60 (s, 1H), 3.83 (d, $J = 17.7$ Hz, 1H), 1.69 (s, 3H), 1.58 (s, 3H). **$^{13}\text{C-NMR}$** (101 MHz, CDCl_3): $\delta = 173.1, 168.3, 151.6, 147.4, 141.0, 136.5, 131.4, 130.1, 130.0, 129.4, 124.1, 119.5, 73.6, 66.3, 48.2, 44.8, 27.2, 22.8$. **IR** (neat): $\tilde{\nu} = 3083, 2987, 2940, 2127, 1748, 1730, 1682, 1613, 1523, 1440, 1395, 1344, 1300, 1313, 1182, 984, 937, 915, 849, 824, 752, 728, 692, 649, 552, 508$ cm^{-1} . **HRMS** (ESI): calcd for $\text{C}_{23}\text{H}_{23}\text{N}_3\text{NaO}_6\text{S}$ [(M+Na)⁺]: 492.1200; found: 492.1197.



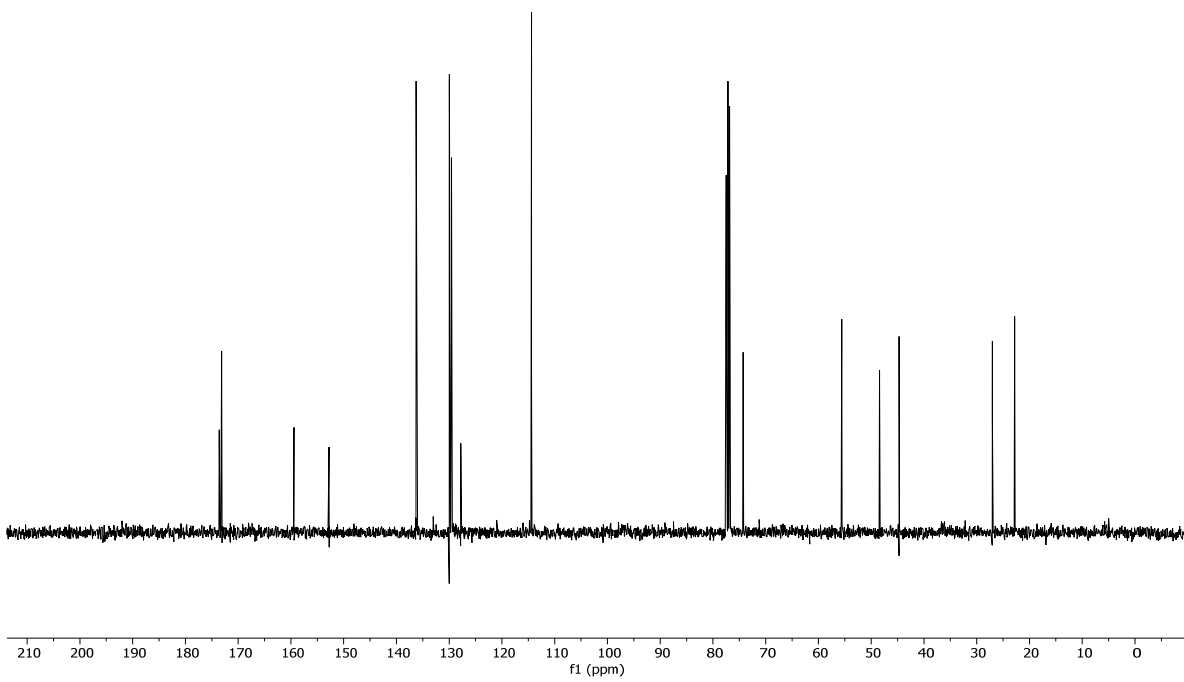
**D45**

2-(3-(4-Methoxyphenyl)-5,5-dimethyl-2,4-dioxo-6-(phenylthio)tetrahydropyrimidin-1(2H)-yl)acetic acid (D45). To a solution of **D43** (60 mg, 0.13 mmol, 1.00 equiv.) in MeOH (1.3 mL) and H₂O (0.4) was added 2M NaOH (0.21 mL, 0.41 mmol, 3.10 equiv.) at rt and the mixture was stirred for 2 h at that temperature. Afterwards CH₂Cl₂ (10 mL) and 1M HCl (1 mL) were added, the phases were separated and the aqueous phase was extracted with CH₂Cl₂ (3 x 15 mL), washed with brine (25 mL), the combined organic phases were dried over MgSO₄, concentrated under reduced pressure to afford **D45** (41.6 mg, 0.10 mmol, 77%) as white solid.

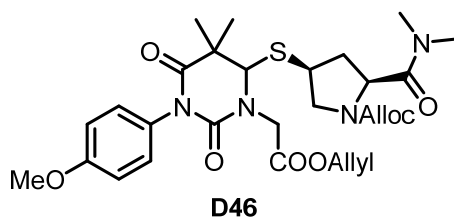
TLC: R_f = 0.25 (1:1 EtOAc/hexane, + 1% AcOH). **MP** = 82 °C. **¹H-NMR** (400 MHz, CDCl₃) δ = 7.54 – 7.48 (m, 2H), 7.47 – 7.41 (m, 1H), 7.41 – 7.34 (m, 2H), 6.90 – 6.85 (m, 2H), 6.73 (d, *J* = 8.3 Hz, 2H), 4.61 (d, *J* = 17.8 Hz, 1H), 4.57 (s, 1H), 3.79 (s, 3H), 3.70 (d, *J* = 18.0 Hz, 1H), 1.62 (s, 3H), 1.54 (s, 3H). **¹³C-NMR** (101 MHz, CDCl₃): δ = 173.6, 173.1, 159.4, 152.8, 136.3, 130.0, 129.9, 129.6, 127.8, 114.4, 74.3, 55.6, 48.4, 44.7, 27.0, 22.8. **IR** (neat): $\tilde{\nu}$ = 3059, 2982, 2936, 2839, 1723, 1673, 1609, 1510, 1441, 1395, 1353, 1300, 1246, 1182, 1030, 993, 911, 826, 752, 727, 692, 648, 602, 557, 535, 457 cm⁻¹. **HRMS** (ESI): calcd for C₂₁H₂₃N₂O₅S [(M+H)⁺]: 415.1322; found: 415.1322.



173.6
173.1
156.4
152.8
136.3
130.0
128.9
128.6
127.8
114.4
74.3
55.6
48.4
44.7
27.0
22.8



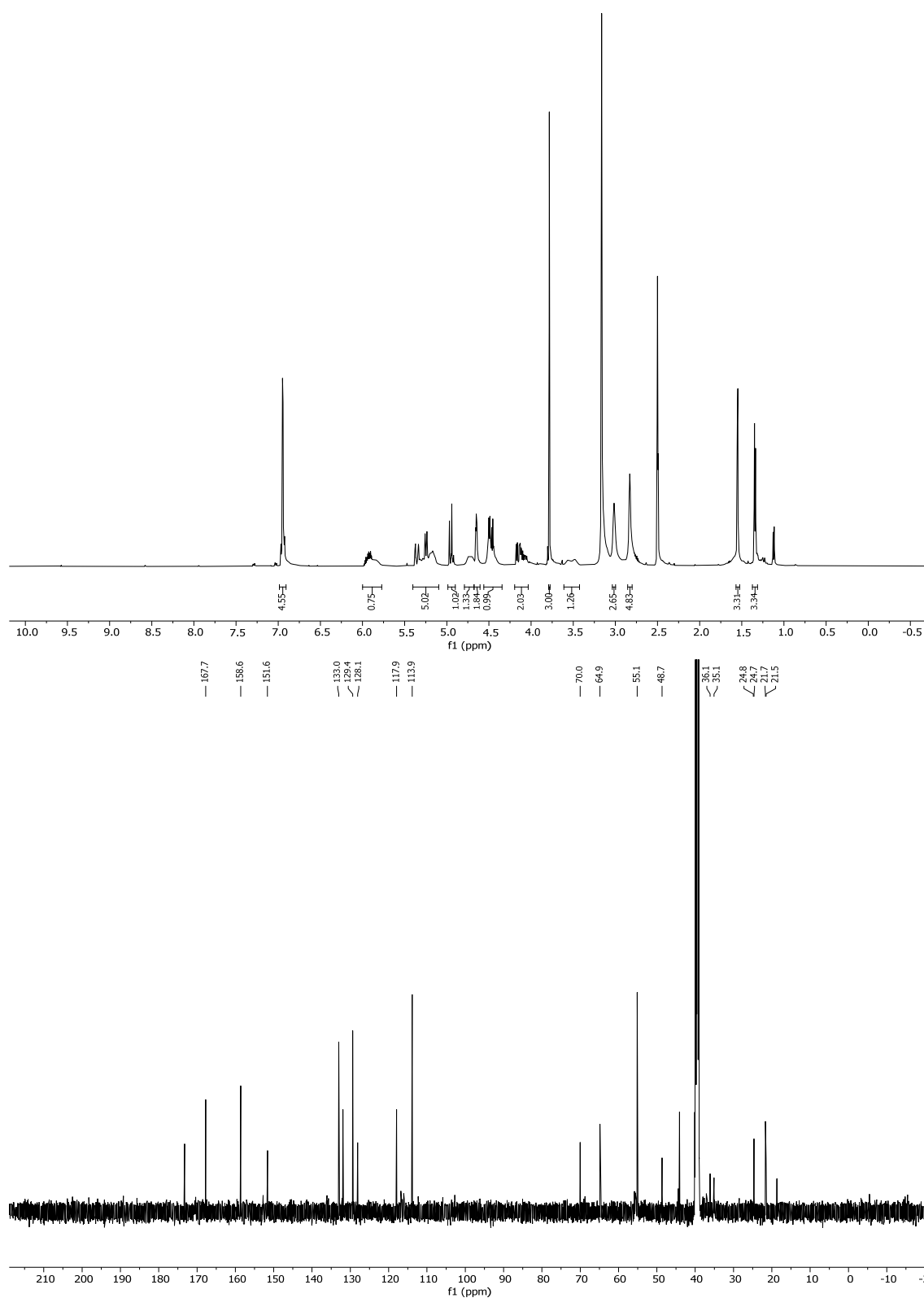
4.3.1.7 Synthesis of D46 and D48-D49



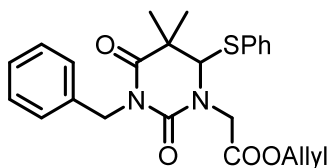
Allyl **(2S,4S)-4-((3-(2-(allyloxy)-2-oxoethyl)-1-(4-methoxyphenyl)-5,5-dimethyl-2,6-dioxohexahydropyrimidin-4-yl)thio)-2-(dimethylcarbamoyl)pyrrolidine-1-carboxylate (D46).**

To neat **D33** (0.20 mg, 0.44 mmol, 1.00 equiv.) was added neat PMP-isocyanate (**D38**) (0.29 mL, 2.21 mmol, 5.00 equiv.) at rt. The reaction mixture was heated to 70 °C and the mixture was stirred at that temperature for 18 h. Afterwards CH₂Cl₂ (20 mL) and H₂O (20 mL) were added, the phases were separated and the aqueous phase was extracted with CH₂Cl₂ (3 x 25 mL), washed with brine (60 mL), the combined organic phases were dried over MgSO₄, concentrated under reduced pressure and purified by FC (EtOAc/hexane 1:2 → 1:1) to afford **D46** (177.0 mg, 0.29 mmol, 67%) as colorless oil.

TLC: R_f = 0.30 (1:1 EtOAc/hexane). **¹H-NMR** (500 MHz, DMSO, 333.15 K) δ = 6.99 – 6.91 (m, 5H), 6.00 – 5.77 (m, 1H), 5.40 – 5.10 (m, 5H), 4.99 – 4.90 (m, 1H), 4.79 – 4.68 (m, 1H), 4.65 (ddq, J = 5.6, 2.7, 1.5 Hz, 2H), 4.47 (dt, J = 17.3, 5.4 Hz, 1H), 4.19 – 4.03 (m, 2H), 3.78 (s, 3H), 3.52 (d, J = 37.7 Hz, 1H), 3.02 (s, 3H), 2.83 (s, 5H), 1.55 (d, J = 3.1 Hz, 3H), 1.34 (d, J = 6.8 Hz, 3H). **¹³C-NMR** (126 MHz, DMSO, 333.15 K): δ = 167.7, 158.60, 151.6, 133.0, 129.4, 128.1, 117.9, 113.9, 70.0, 64.9, 55.2, 48.7, 36.1, 35.1, 24.8, 24.7, 21.7, 21.5. **IR** (neat): $\tilde{\nu}$ = 2980, 2938, 1752, 1682, 1651, 1609, 1512, 1444, 1405, 1352, 1299, 1247, 1179, 1146, 1126, 1109, 1030, 979, 932, 915, 827, 758, 733, 538 cm⁻¹. **HRMS** (ESI): calcd for C₂₉H₃₈N₄NaO₈S [(M+Na)⁺]: 625.2303; found: 625.2289. **[α]_D²⁰**: -20.00 (c = 1.00 in CHCl₃).

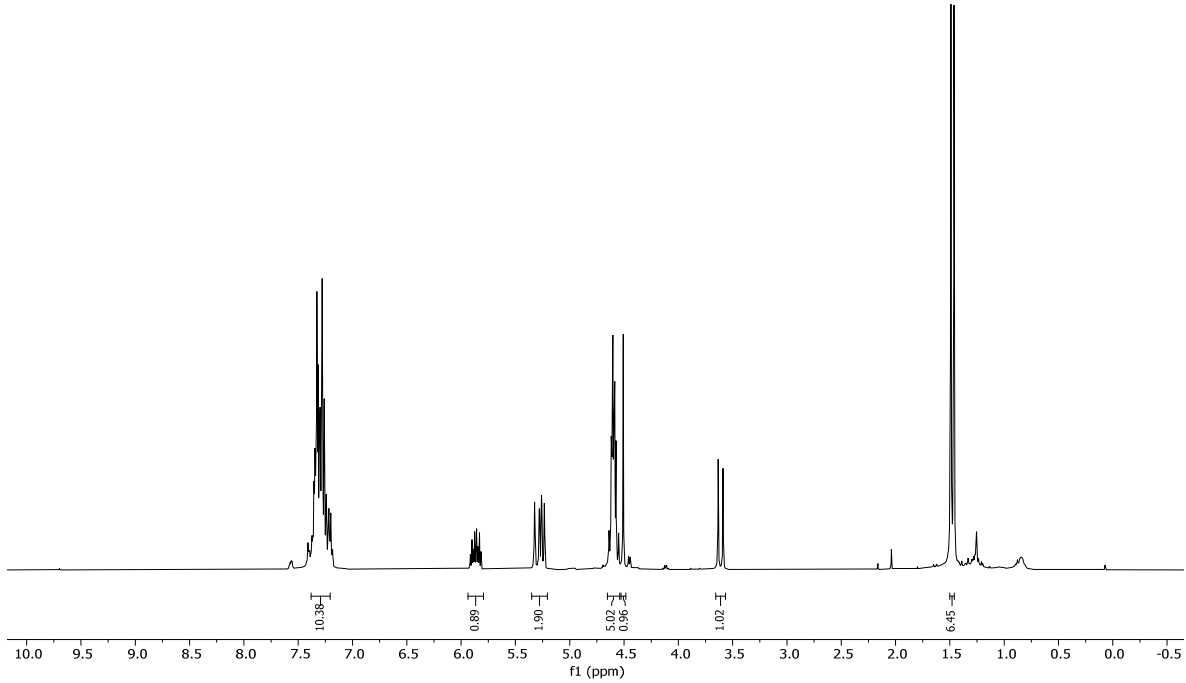


Remark: Peaks in ^1H and ^{13}C -NMR spectra broad and split due to the presence of *N*-Alloc and *N*-Me₂ rotamers partially suppressed by high temperature measurement.

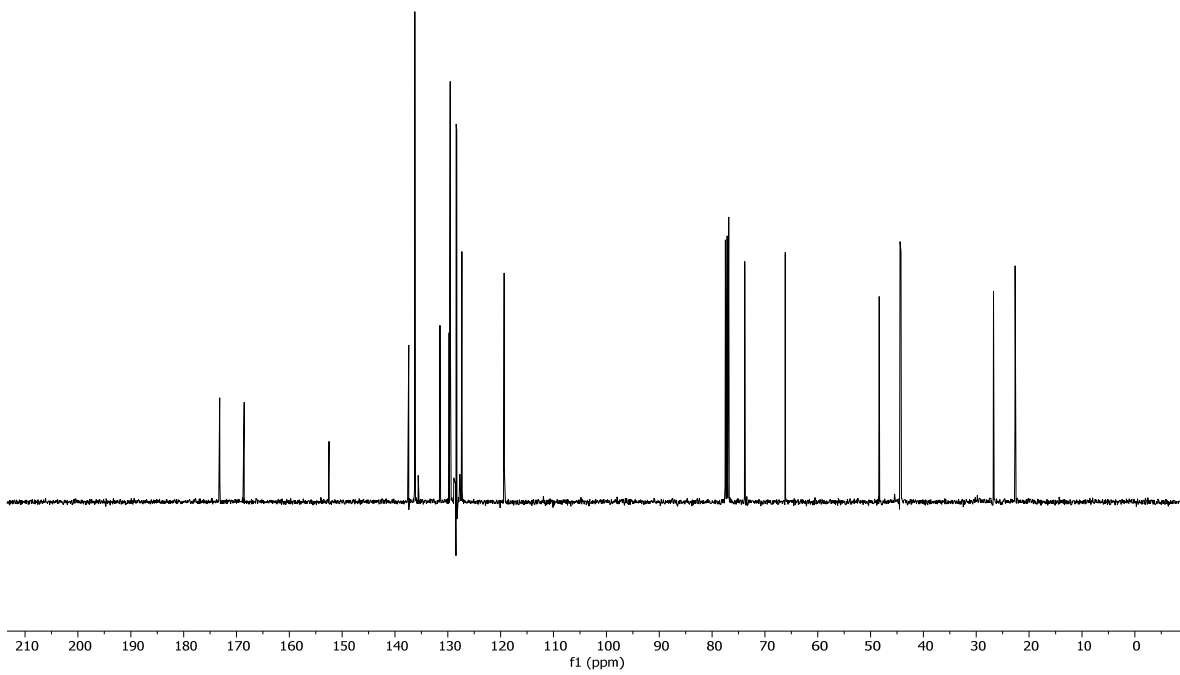
**D48**

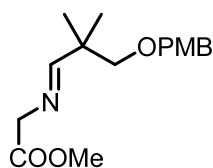
Allyl 2-(3-benzyl-5,5-dimethyl-2,4-dioxo-6-(phenylthio)tetrahydropyrimidin-1(2H)-yl)acetate (D48). To neat **D33** (27.0 mg, 0.09 mmol, 1.00 equiv.) was added benzyl isocyanate (**D47**) (54 μ L, 0.44 mmol, 5.00 equiv.) at rt under argon. The reaction mixture was heated to 70 °C and the mixture was stirred at that temperature for 3 h. Afterwards CH_2Cl_2 (1 mL) and H_2O (1 mL) was added, the phases were separated and the aqueous phase was extracted with CH_2Cl_2 (3 x 5 mL), washed with brine (10 mL), the combined organic phases were dried over MgSO_4 , concentrated under reduced pressure and purified by FC (EtOAc/hexane 1:6 \rightarrow 1:4) to afford **D48** (23.0 mg, 0.05 mmol, 59%) as colorless oil.

TLC: R_f = 0.30 (1:1 EtOAc/hexane). **$^1\text{H-NMR}$** (400 MHz, CDCl_3) δ = 7.38 – 7.21 (m, 10H), 5.87 (ddt, J = 16.3, 10.3, 5.9 Hz, 1H), 5.35 – 5.21 (m, 2H), 4.65 – 4.54 (m, 5H), 4.51 (s, 1H), 3.61 (d, J = 17.6 Hz, 1H), 1.48 (d, J = 11.5 Hz, 6H). **$^{13}\text{C-NMR}$** (101 MHz, CDCl_3): δ = 173.2, 168.6, 152.5, 137.4, 136.2, 135.6, 131.5, 129.8, 129.8, 129.6, 128.9, 128.5, 128.4, 128.3, 127.8, 127.3, 119.3, 73.8, 66.1, 48.4, 44.4, 44.3, 26.7, 22.7. **IR** (neat): $\tilde{\nu}$ = 2982, 2936, 1751, 1717, 1669, 1496, 1469, 1450, 1395, 1352, 1377, 1355, 1337, 1238, 1181, 1078, 1024, 985, 932, 752, 727, 695, 503 cm^{-1} . **HRMS** (ESI): calcd for $\text{C}_{24}\text{H}_{26}\text{N}_2\text{NaO}_4\text{S}$ [(M+Na) $^+$]: 461.1505; found: 461.1501.



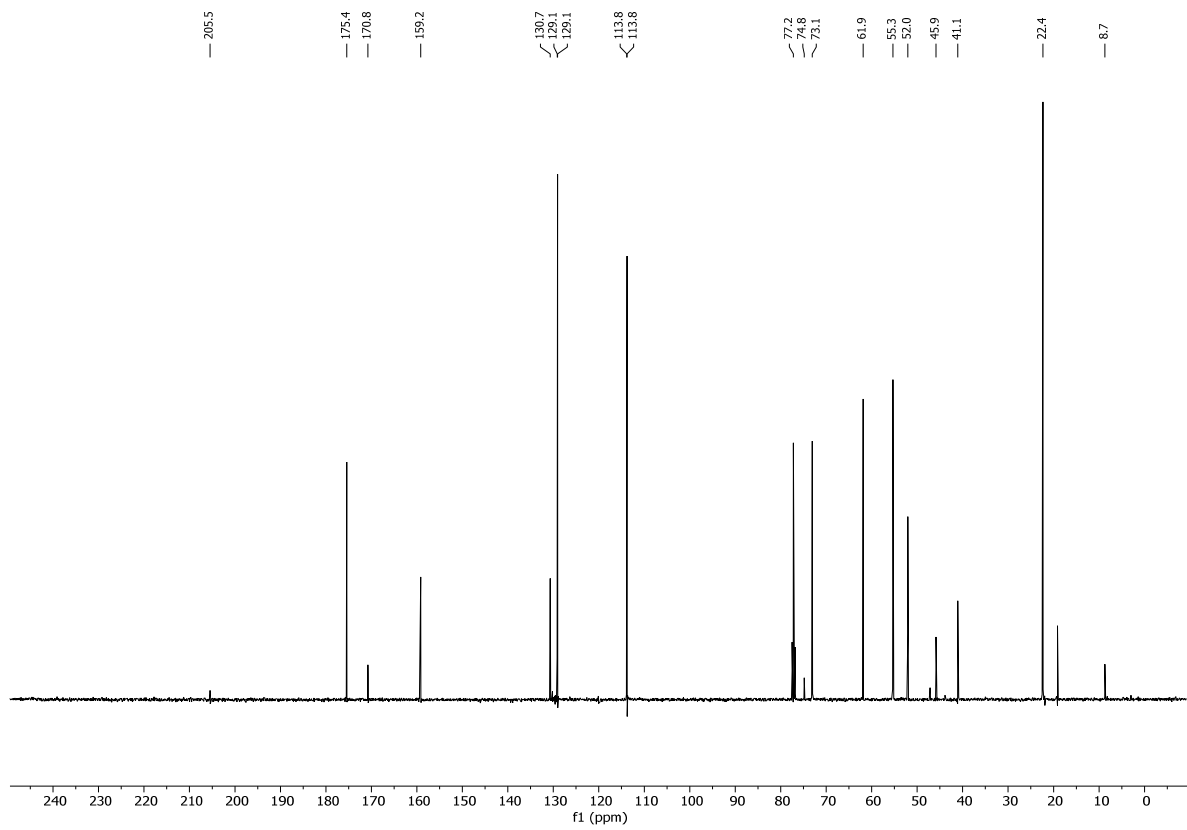
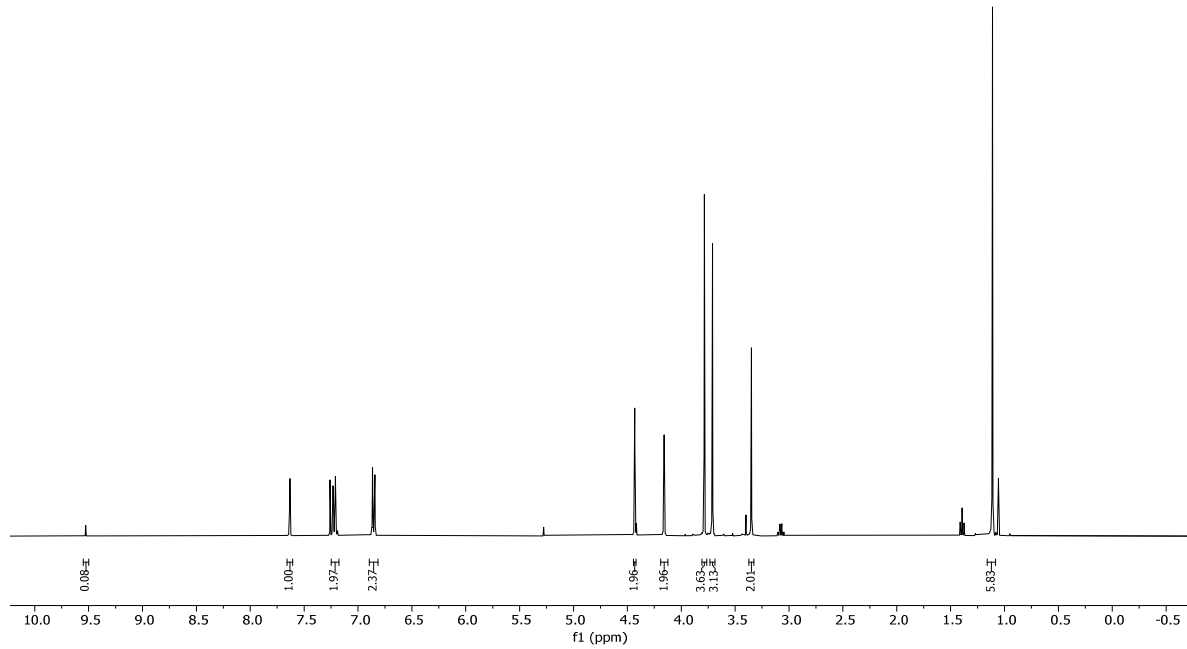
173.2, 168.6, 152.5, 137.4, 136.2, 135.6, 134.8, 129.8, 129.8, 129.6, 128.9, 128.5, 128.4, 127.7, 127.3, 119.3, 73.8, 66.1, 48.4, 44.4, 44.3, 26.7, 22.7



**D49**

Methyl (*E*)-2-((3-((4-methoxybenzyl)oxy)-2,2-dimethylpropylidene)amino)acetate (D49). H-Gly-OMe (1.86 g, 14.78 mmol, 1.00 equiv.) was dissolved in CH₂Cl₂ (90 mL) and Et₃N (15.00 mL, 147.75 mmol, 10.0 equiv.). The solution was stirred for 30 min before **DS7**⁷ (2.96 g, 13.30 mmol, 0.90 equiv.) in CH₂Cl₂ (90 mL) and MgSO₄ (8 g) were added to the solution. The reaction mixture was stirred for 3 h at rt. Afterwards the MgSO₄ was removed *via* filtration, the filtrate was diluted with CH₂Cl₂ (50 mL) and H₂O (50 mL), the layers were separated and the aqueous layer was extracted with EtOAc (1 x 100 mL). The combined organic layers were washed with brine (150 mL). The organic layer was dried over MgSO₄ and the solvent was removed under reduced pressure to afford **D49** (3.70 g, 12.60 mmol, 94%, as 13:1 mixture with **DS7** (7%), calculated based on NMR spectroscopy).

TLC: R_f = 0.70 (EtOAc/hexane 1:4). **¹H-NMR** (400 MHz, CDCl₃) δ = 9.53 (s, 0H), 7.63 (t, *J* = 1.3 Hz, 1H), 7.25 – 7.18 (m, 2H), 6.90 – 6.81 (m, 2H), 4.43 (s, 2H), 4.16 (d, *J* = 1.2 Hz, 2H), 3.79 (s, 4H), 3.71 (s, 3H), 3.35 (s, 2H), 1.11 (s, 6H). **¹³C-NMR** (101 MHz, CDCl₃): δ = 205.5, 175.4, 170.8, 159.2, 130.7, 129.2, 129.1, 113.9, 113.8, 77.2, 74.8, 73.1, 61.9, 55.3, 52.0, 45.9, 41.1, 22.4, 8.7. **IR** (neat): $\tilde{\nu}$ = 2955, 2905, 2859, 2370, 1747, 1667, 1612, 1586, 1462, 1438, 1360, 1301, 1196, 979, 916, 847, 819, 755, 710, 580, 516 cm⁻¹. **HRMS** (ESI): calcd for C₁₆H₃₂NO₃Si [(M+H)⁺]: 314.2146; found: 314.2145.



4.3.1.8 Crystallographic data for DS4, D12, D14, DS9, D33 and D44

Single crystals of **DS4**, **D12**, **D14**, **DS9**, **D33** and **D45** were analyzed on a Bruker Kappa APEX-II Duo diffractometer using microfocus sealed tube Cu-K α radiation and mirror optics ($\lambda = 1.54178 \text{ \AA}$). Measurements were carried out at 100K using an Oxford Cryosystems Cryostream 700 sample cryostat. Single crystals of **D33** were analyzed on a Rigaku Oxford Diffraction XtaLAB Synergy-R kappa diffractometer equipped with a Rigaku HyPix Arc150 HPAD detector and using microfocus rotating anode Cu-K α radiation with mirror optics ($\lambda = 1.54178 \text{ \AA}$). Measurements were carried out at 100K using an Oxford Cryosystems Cryostream 1000+ sample cryostat. Data were integrated using SAINT from the Bruker Apex-II program suite and corrected for absorption effects using the multi-scan method (SADABS).^[309] The structure was solved using SHELXT^[310] and refined by full-matrix least-squares analysis (SHELXL),^[311,312] using the program package OLEX2.^[313] All non-hydrogen atoms were refined anisotropically and non-donor hydrogen atoms were constrained to ideal geometries and refined with fixed isotropic displacement parameters (in terms of a riding model). CCDC's 2290115, 2290117, 2290124, 2290123, 2290121 and 2300752 contain the supplementary crystallographic data for this paper, including structure factors and refinement instructions. These data can be obtained free of charge from The Cambridge Crystallographic Data Centre, 12 Union Road, Cambridge CB2 1EZ, UK (fax: +44(1223)-336-033; e-mail: deposit@ccdc.cam.ac.uk), or via <https://www.ccdc.cam.ac.uk/structures>.

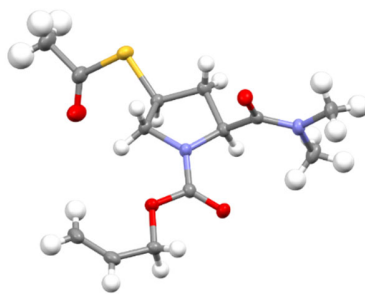


Figure 52: Asymmetric unit of the crystal structure of **DS4**. Ellipsoids depicted at 50% probability.

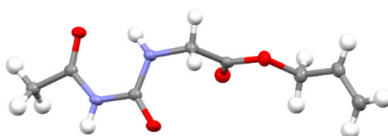


Figure 53: Asymmetric unit of the crystal structure of **D12**. Ellipsoids depicted at 50% probability.

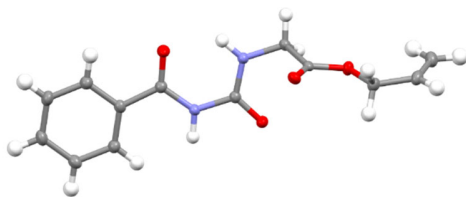


Figure 54: Asymmetric unit of the crystal structure of **D14**. Ellipsoids depicted at 50% probability.

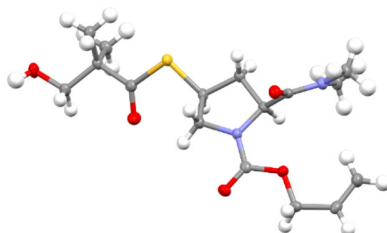


Figure 55: Asymmetric unit of the crystal structure of **D59**. Ellipsoids depicted at 50% probability.

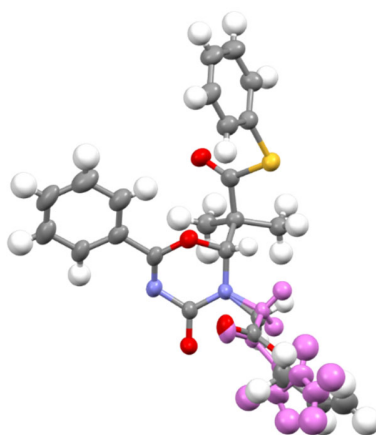


Figure 56: Asymmetric unit of the crystal structure of **D33**. Ellipsoids depicted at 50% probability. The minor (10%) *N*-Alloc conformer is shown in purple.

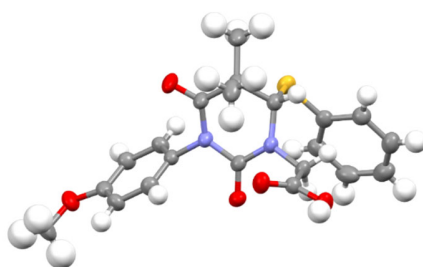


Figure 57: Asymmetric unit of the crystal structure of **D45**. Ellipsoids depicted at 50% probability.

Table 24. Crystal and structure refinement data for compounds **DS4**, **D12** and **D14**.

| Compound | DS4 | D12 | D14 |
|---|---|---|---|
| CCDC number | 2290115 | 2290117 | 2290124 |
| Empirical formula | C ₁₃ H ₂₀ N ₂ O ₄ S | C ₈ H ₁₂ N ₂ O ₄ | C ₁₃ H ₁₄ N ₂ O ₄ |
| Formula weight | 300.37 | 200.20 | 262.26 |
| Temperature [K] | 100.0(1) | 100.0(1) | 100.0(1) |
| Crystal system | orthorhombic | triclinic | triclinic |
| Space group | <i>P</i> 2 ₁ 2 ₁ 2 ₁ | <i>P</i> -1 | <i>P</i> -1 |
| <i>a</i> [Å] | 4.96170(10) | 4.98850(10) | 4.8164(2) |
| <i>b</i> [Å] | 8.30180(10) | 8.2867(2) | 8.4251(5) |
| <i>c</i> [Å] | 37.5677(3) | 11.9902(2) | 15.7190(7) |
| α [°] | 90 | 99.781(2) | 77.694(4) |
| β [°] | 90 | 94.822(2) | 87.043(4) |
| γ [°] | 90 | 94.976(2) | 83.321(4) |
| Volume [Å ³] | 1547.45(4) | 484.137(18) | 618.73(5) |
| <i>Z</i> | 4 | 2 | 2 |
| ρ_{calc} [g/cm ³] | 1.289 | 1.373 | 1.408 |
| μ [mm ⁻¹] | 1.994 | 0.946 | 0.886 |
| <i>F</i> (000) | 640.0 | 212.0 | 276.0 |
| Crystal size [mm ³] | 0.327 × 0.157 × 0.037 | 0.16 × 0.087 × 0.043 | 0.249 × 0.045 × 0.016 |
| Radiation | Cu K α (λ = 1.54184 Å) | Cu K α (λ = 1.54184 Å) | Cu K α (λ = 1.54184 Å) |
| 2 θ range [°] | 4.704 to 159.608 | 7.52 to 158.522 | 5.756 to 158.826 |
| Index ranges | -6 ≤ <i>h</i> ≤ 6, -10 ≤ <i>k</i> ≤ 10, -47 ≤ <i>l</i> ≤ 47 | -6 ≤ <i>h</i> ≤ 6, -10 ≤ <i>k</i> ≤ 9, -14 ≤ <i>l</i> ≤ 14 | -4 ≤ <i>h</i> ≤ 6, -9 ≤ <i>k</i> ≤ 10, -19 ≤ <i>l</i> ≤ 19 |
| Reflections collected | 34330 | 17768 | 5961 |
| Independent reflections | 3366 <i>R</i> _{int} = 0.0464, <i>R</i> _{sigma} = 0.0189 | 1906 <i>R</i> _{int} = 0.0391, <i>R</i> _{sigma} = 0.0185 | 2537 <i>R</i> _{int} = 0.0286, <i>R</i> _{sigma} = 0.0366 |
| Data/restraints/parameters | 3366/0/184 | 1906/2/134 | 2537/2/178 |
| Goodness-of-fit on <i>F</i> ² | 1.037 | 1.063 | 1.039 |
| Final <i>R</i> indexes [<i>I</i> ≥ 2 σ (<i>I</i>)] | <i>R</i> ₁ = 0.0304, <i>wR</i> ₂ = 0.0803 | <i>R</i> ₁ = 0.0284, <i>wR</i> ₂ = 0.0744 | <i>R</i> ₁ = 0.0354, <i>wR</i> ₂ = 0.0891 |
| Final <i>R</i> indexes [all data] | <i>R</i> ₁ = 0.0310, <i>wR</i> ₂ = 0.0807 | <i>R</i> ₁ = 0.0301, <i>wR</i> ₂ = 0.0755 | <i>R</i> ₁ = 0.0435, <i>wR</i> ₂ = 0.0933 |
| Largest diff. peak/hole [eÅ ⁻³] | 0.32/-0.31 | 0.17/-0.18 | 0.19/-0.21 |
| Flack X parameter | 0.003(6) | n/a | n/a |

Table 25. Crystal and structure refinement data for compounds **D59**, **D33** and **D45**.

| Compound | D59 | D33 | D45 |
|--|---|--|---|
| CCDC number | 2290123 | 2300752 | 2290121 |
| Empirical formula | C ₁₆ H ₂₆ N ₂ O ₅ S | C ₂₄ H ₂₄ N ₂ O ₅ S | C ₂₁ H ₂₂ N ₂ O ₅ S |
| Formula weight | 358.45 | 452.51 | 414.46 |
| Temperature [K] | 100.0(1) | 100.0(1) | 200.0(1) |
| Crystal system | monoclinic | monoclinic | orthorhombic |
| Space group | <i>P</i> 2 ₁ | <i>P</i> 2 ₁ / <i>c</i> | <i>P</i> 2 ₁ 2 ₁ 2 ₁ |
| <i>a</i> [Å] | 5.58700(10) | 10.0683(3) | 9.3960(2) |
| <i>b</i> [Å] | 19.4449(3) | 19.8478(5) | 12.7303(2) |
| <i>c</i> [Å] | 8.16410(10) | 11.4354(3) | 17.0795(3) |
| α [°] | 90 | 90 | 90 |
| β [°] | 98.0700(10) | 94.230(3) | 90 |
| γ [°] | 90 | 90 | 90 |
| Volume [Å ³] | 878.15(2) | 2278.94(11) | 2042.95(6) |
| <i>Z</i> | 2 | 4 | 4 |
| ρ_{calc} [g/cm ³] | 1.356 | 1.319 | 1.348 |
| μ [mm ⁻¹] | 1.888 | 1.581 | 1.711 |
| <i>F</i> (000) | 384.0 | 952.0 | 872.0 |
| Crystal size [mm ³] | 0.143 × 0.038 × 0.028 | 0.06 × 0.04 × 0.03 | 0.153 × 0.101 × 0.06 |
| Radiation | Cu K α (λ = 1.54184 Å) | Cu K α (λ = 1.54184 Å) | Cu K α (λ = 1.54184 Å) |
| 2 θ range [°] | 9.096 to 159.832 | 8.806 to 151.138 | 8.664 to 160.282 |
| Index ranges | -6 ≤ <i>h</i> ≤ 7, -24 ≤ <i>k</i> ≤ 24, -10 ≤ <i>l</i> ≤ 10 | -12 ≤ <i>h</i> ≤ 12, -24 ≤ <i>k</i> ≤ 23, -13 ≤ <i>l</i> ≤ 14 | -10 ≤ <i>h</i> ≤ 11, -16 ≤ <i>k</i> ≤ 14, -21 ≤ <i>l</i> ≤ 19 |
| Reflections collected | 18102 | 33561 | 30594 |
| Independent reflections | 3705 <i>R</i> _{int} = 0.0632, <i>R</i> _{sigma} = 0.0408 | 4491 <i>R</i> _{int} = 0.0903 <i>R</i> _{sigma} = 0.0572 | 4385 <i>R</i> _{int} = 0.0643, <i>R</i> _{sigma} = 0.0323 |
| Data/restraints/parameters | 3705/2/224 | 4491/301/325 | 4385/1/268 |
| Goodness-of-fit on <i>F</i> ² | 1.106 | 1.096 | 1.071 |
| Final <i>R</i> indexes [<i>I</i> >= 2 σ (<i>I</i>)] | <i>R</i> ₁ = 0.0328, <i>wR</i> ₂ = 0.0823 | <i>R</i> ₁ = 0.0651, <i>wR</i> ₂ = 0.1795 | <i>R</i> ₁ = 0.0346, <i>wR</i> ₂ = 0.0910 |
| Final <i>R</i> indexes [all data] | <i>R</i> ₁ = 0.0359, <i>wR</i> ₂ = 0.0846 | <i>R</i> ₁ = 0.0901, <i>wR</i> ₂ = 0.1981 | <i>R</i> ₁ = 0.0388, <i>wR</i> ₂ = 0.0953 |
| Largest diff. peak/hole [eÅ ⁻³] | 0.20/-0.30 | 0.48/-0.45 | 0.23/-0.22 |
| Flack <i>X</i> parameter | 0.021(11) | n/a | -0.037(11) |

4.3.1.9 Reaction Profiles and Transition States

TS of Reaction A

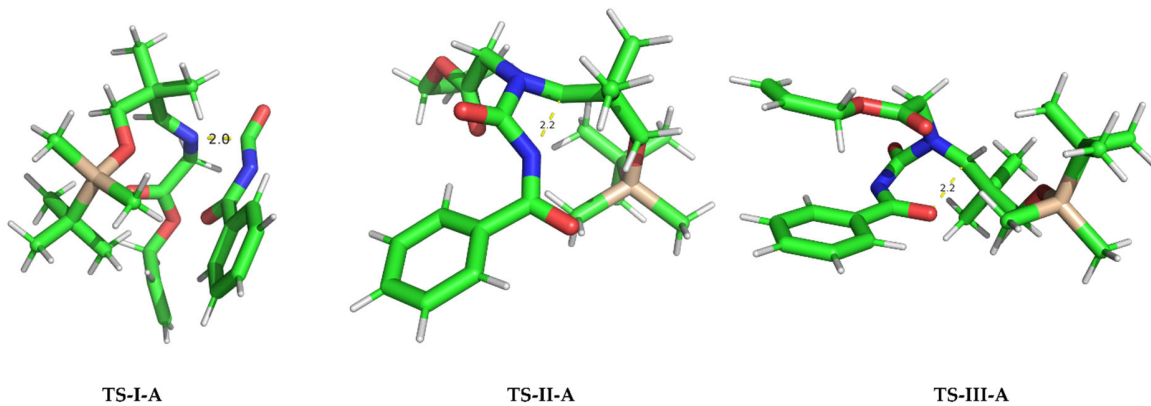


Figure 58: Transitions state structures and pertinent distances of newly formed bonds for Reaction A.

TS of Reaction C

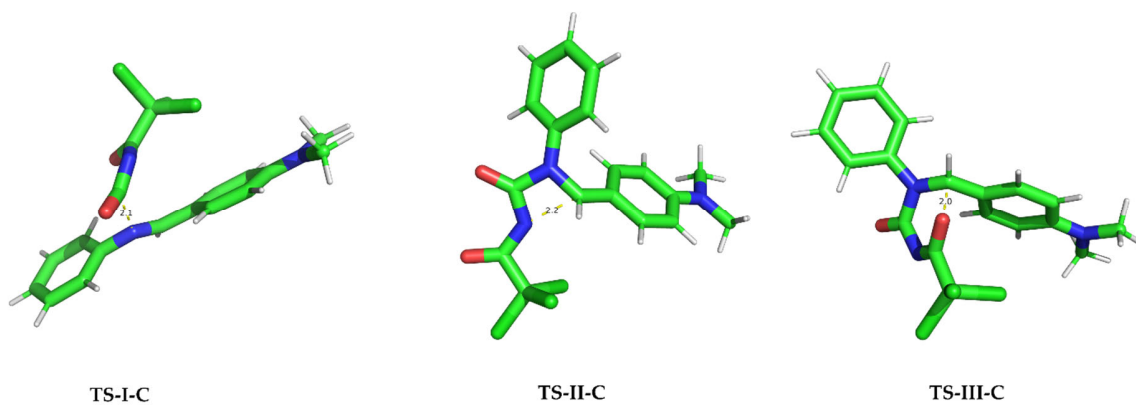


Figure 59: Transitions state structures and pertinent distances of newly formed bonds for Reaction C.

Energy Profile for Reactions B and D

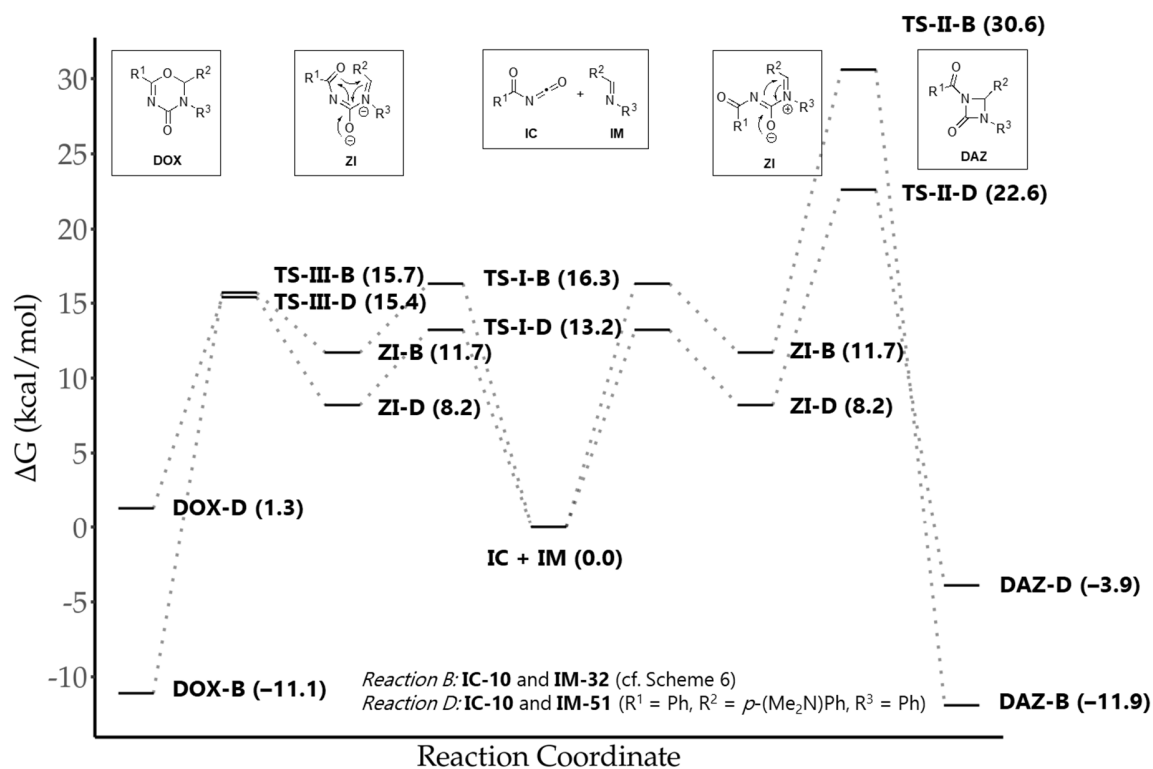


Figure 60: Reaction energy profiles for reactions B and D on the PBE0/def2-TZVP(D3BJ)-CPCM(dichloromethane) level of theory. The educt state isocyanate (IC) (**IC-10** = **D10**) and imine (IM) (**IM-32** = **D32** and **IM-51** = **D51**) is shown in the middle. The first step of the reaction (iminium formation, ZI) is the same for both directions. Subsequent *N*-centered nucleophilic attack to yield 4-membered ring DAZ is shown on the right, whereas *O*-centered nucleophilic attack to yield six-membered ring DOX is shown on the left. Gibbs free energies are provided in parentheses and are average values over four independent runs and reported relative to the respective starting materials IC and IM. The plot was visualized using EveRplot v.1.3.^[318] **DAZ-B** (**33**)/**DAZ-D** and **DOX-B**/**DOX-D** refer to the 1,3-diazetidiones and dihydro-oxadiazinones from reactions B and D.

Reaction C

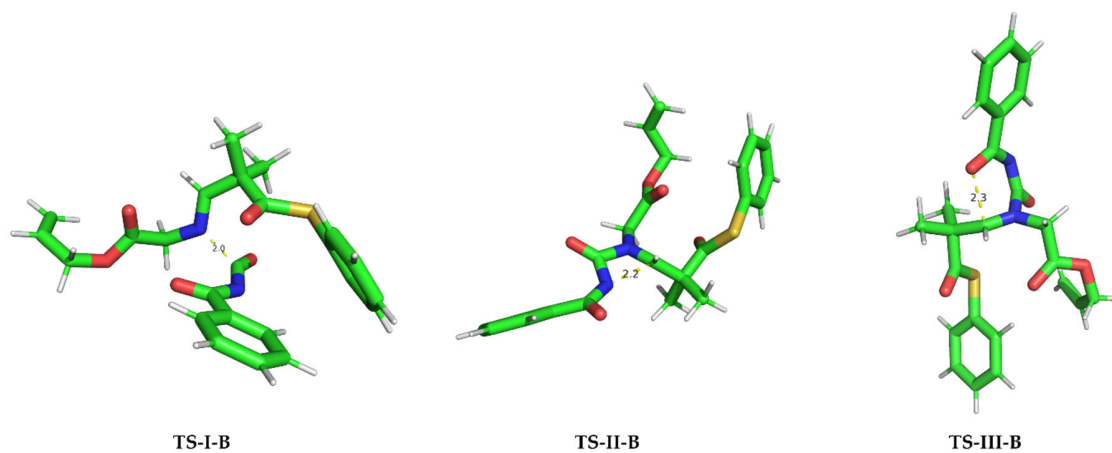


Figure 61: Transitions state structures and pertinent distances of newly formed bonds for Reaction B.

Reaction D

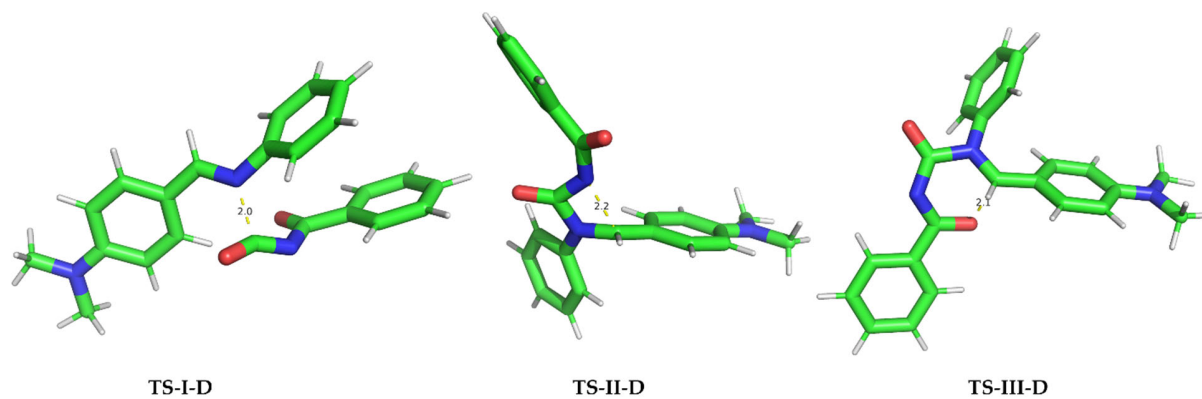


Figure 62: Transitions state structures and pertinent distances of newly formed bonds for Reaction D.

4.3.1.10 Unaligned Reference IR Spectra

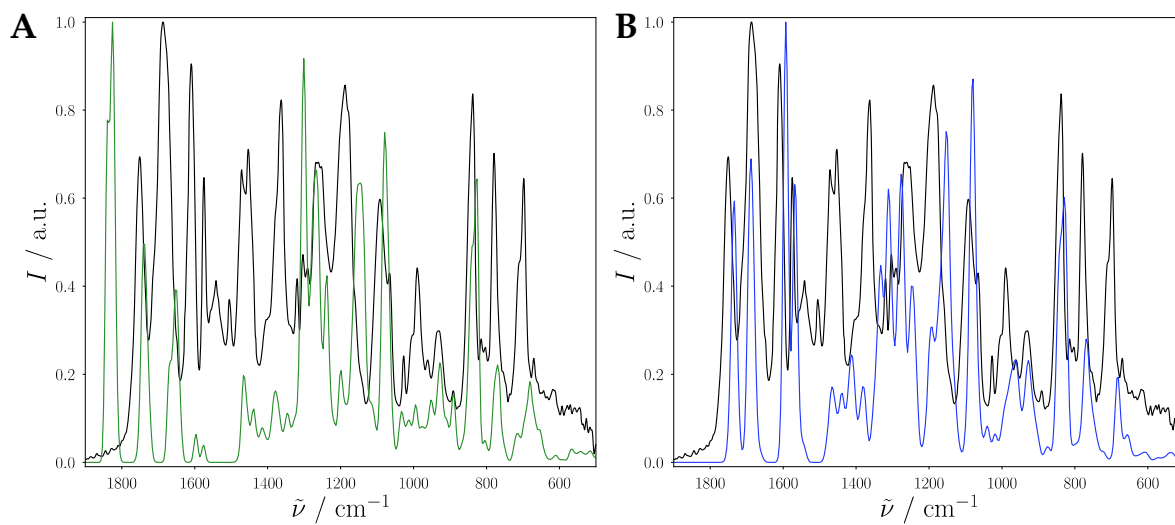
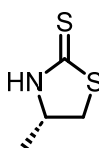


Figure 63: Unaligned theoretical spectra for four-membered **DAZ-A (D21)** (A, green) and six-membered **DOX-A (D20)** (B, blue) together with the experimentally recorded IR spectrum of **D20** (black).

4.3.2 Studies Towards the Synthesis of β -Sultam-Based Analogs of β -Lactam Antibiotics

Literature known compounds **S35**,^[295] **S33**,^[297] **S36**,^[297] and **S53**^[302] were prepared according to literature procedures.

4.3.2.1 Synthesis of (*S*)-3-Methyl Ethylsultam (**S32**)

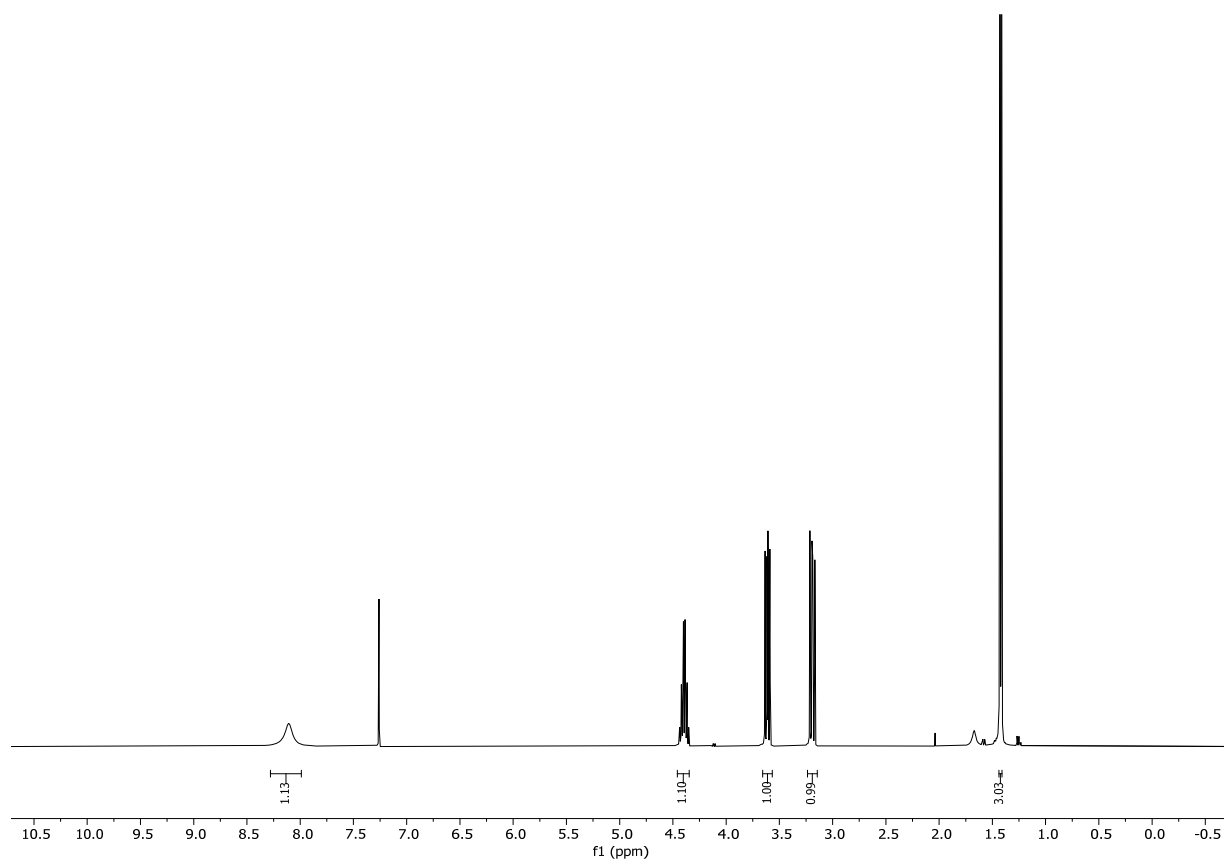


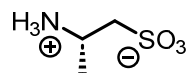
S36

(S)-4-methylthiazolidine-2-thione (S36).^[297] To a mixture of L-alaninol (**S34**) (1.14 mL, 14.65 mmol, 1.00 equiv.) in aq. KOH (1 M, 73.23 mL, 73.23 mmol, 5.00 equiv.) was added CS₂ (4.43 mL, 73.23 mmol, 5.00 equiv.) at rt. The resulting solution was refluxed at 100 °C for 16 h. Afterwards the cooled red reaction mixture was extracted with CH₂Cl₂ (3 x 30 mL), the combined organic extracts were dried over MgSO₄. The combined organic extracts were dried over MgSO₄, concentrated under reduced pressure, and the residue purified by flash chromatography (EtOAc/hexane 1:1) to give **S36** (1.91 g, 14.34 mmol, 98%) as a white powder.

TLC: R_f = 0.72 (EtOAc/hexane 1:1). **¹H-NMR** (400 MHz, CDCl₃) δ = 8.11 (s, 1H), 4.39 (ddt, *J* = 14.1, 7.6, 6.3 Hz, 1H), 3.61 (dd, *J* = 10.9, 7.6 Hz, 1H), 3.19 (dd, *J* = 11.0, 7.7 Hz, 1H), 1.42 (d, *J* = 6.3 Hz, 3H). **HRMS** (ESI): calcd for C₄H₈NS₂ [(M+H)⁺]: 134.0093; found: 134.0093.

Analytical data was in line with the reported data in ref. ^[297].

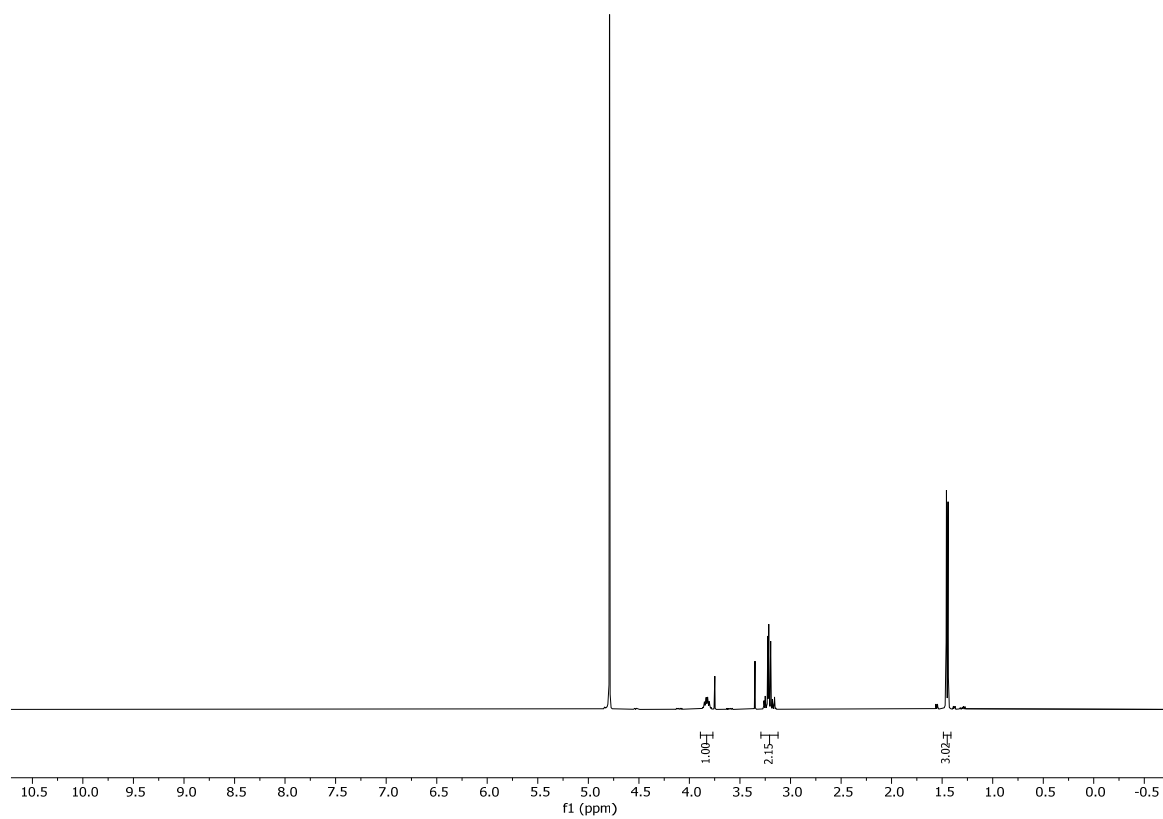


**S33**

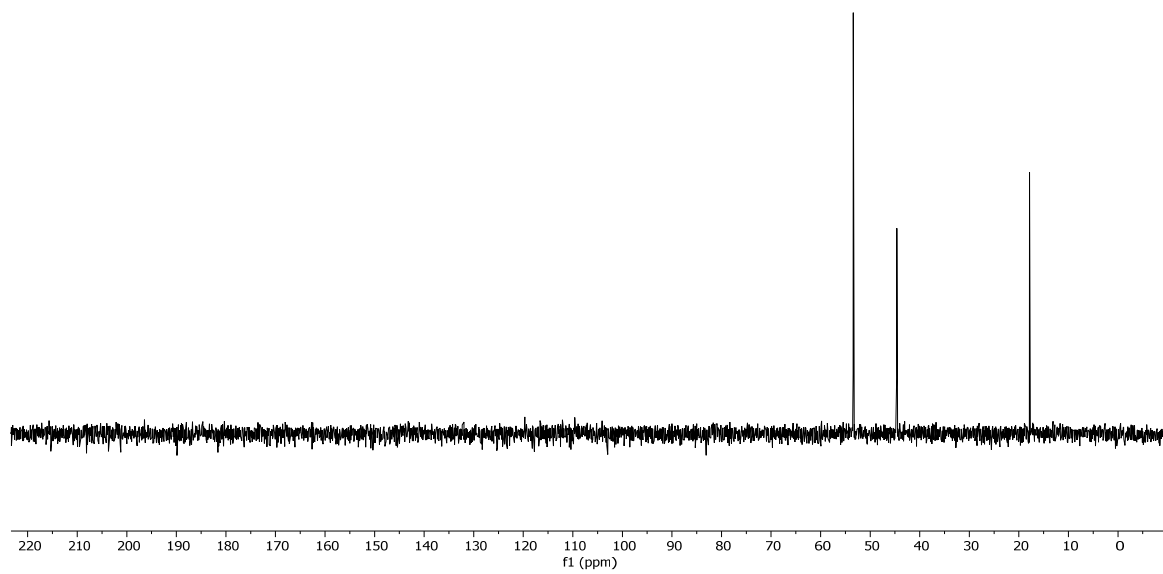
(S)-2-ammonio propane-1-sulfonate (S33).^[297] A solution of 35% H₂O₂ (13.86 ml, 142.61 mmol, 10.00 equiv.) was dissolved in 98% formic acid (65.65 mL, 1426.14 mmol, 100.00 equiv.) at 0 °C and stirring was continued for 1 h at that temperature. Afterwards **S36** (1.90 g, 14.26 mmol, 1.00 equiv.) was added portionwise at that temperature. The reaction mixture was stirred at 0 °C for 16 h and was then warmed to rt. The reaction mixture was filter and the solvents were removed under reduced pressure. The residue was crystallized from methanol to give **S33** (1.75 g, 12.57 mmol, 88%) as white crystals.

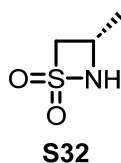
¹H-NMR (400 MHz, D₂O) δ = 3.83 (dq, J = 11.6, 6.9 Hz, 1H), 3.29 – 3.12 (m, 2H), 1.45 (d, J = 6.8 Hz, 3H). ¹³C-NMR (101 MHz, D₂O) δ = 53.4, 44.6, 17.8. IR (neat): $\tilde{\nu}$ = 3672, 2987, 2902, 1407, 1393, 1158, 1076, 1039, 978, 881, 821, 780, 604, 537. HRMS (ESI): calcd for C₃H₈NO₃S [(M-H)⁻]: 138.0230; found: 138.0229.

Analytical data was in line with the reported data in ref. ^[297] and obtained X-ray crystal structure was in line with data reported on the CSD database, structure code: TAYWEV ((S)-2-Aminopropanesulfonic acid)



53.40
44.64
17.84

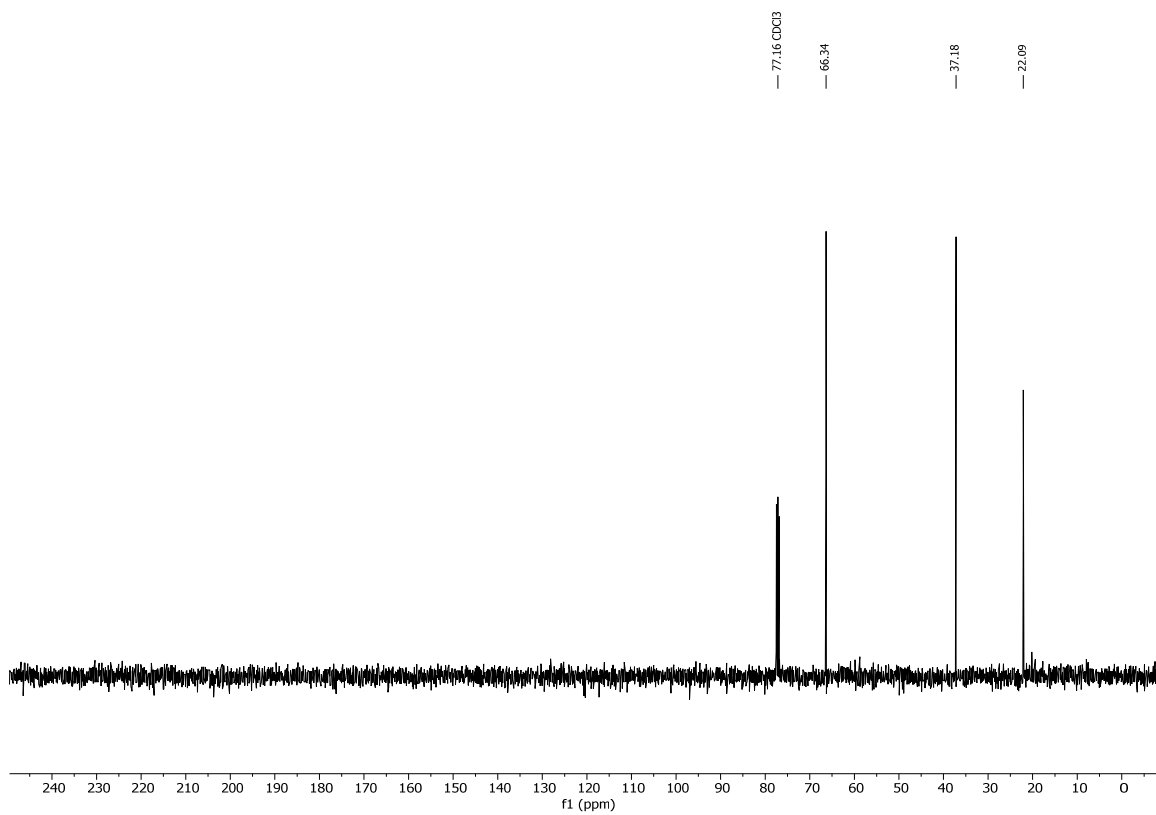
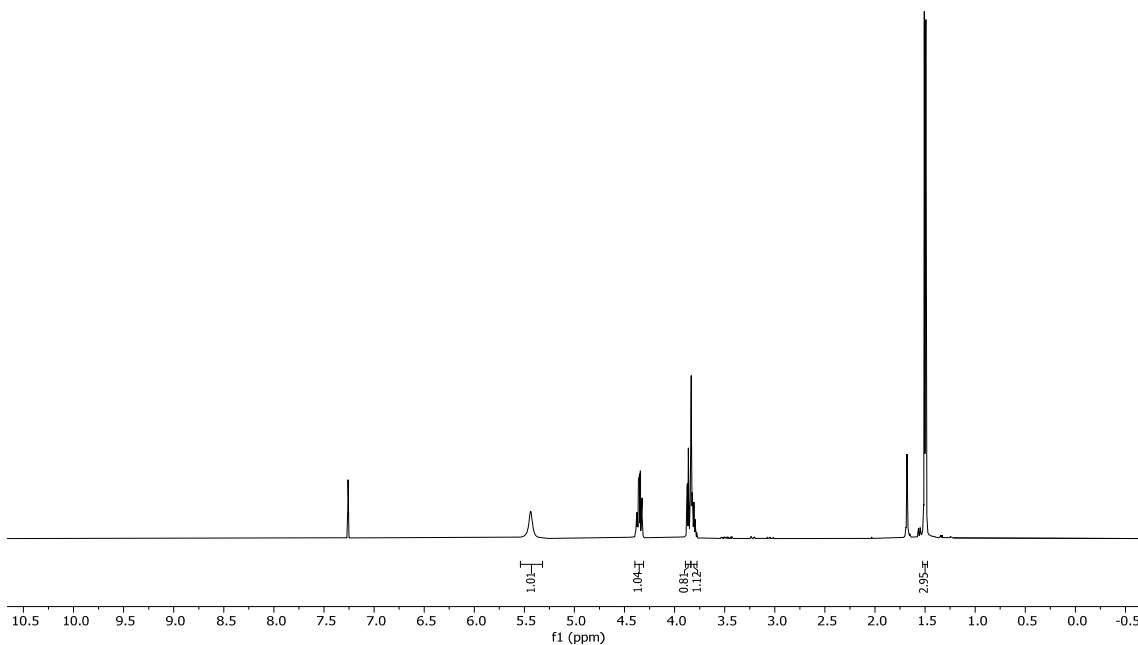


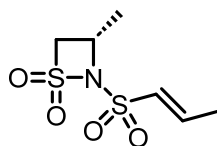


(S)-3-methyl-1,2-thiazetidine 1,1-dioxide (S32). To a solution of **S33** (4.00 g, 28.74 mmol, 1.00 equiv.) in MeCN (280 mL) was added POCl₃ (13.4 mL, 143.71 mmol, 5.0 equiv.) at rt. The reaction mixture was stirred heated at 60 °C for 18 h. Then the reaction mixture was concentrated under reduced pressure, the residue was triturated with Et₂O.

The residue was dissolved in EtOAc (700 mL) and Na₂CO₃ (26.44 g, 172.45 mmol, 10.00 equiv.) was added at rt stirring was continued for 18 h, before the suspension was filtered, washed with H₂O and the solvent was removed under reduced pressure and purified by FC (EtOAc/hexane 10:1 → EtOAc) to obtain **S32** (2.07 g, 17.11 mmol, 60%) as yellow oil.

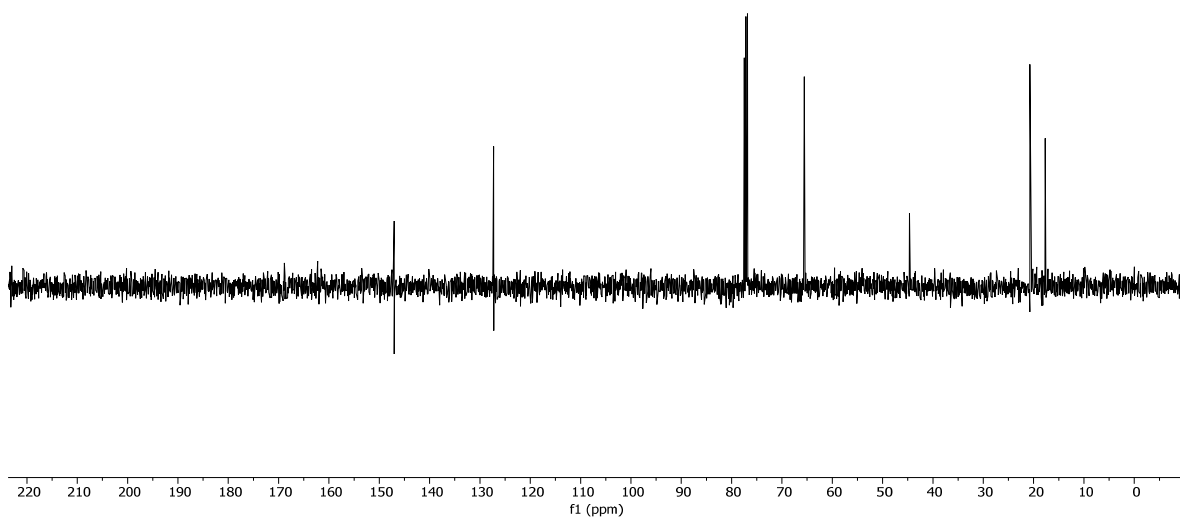
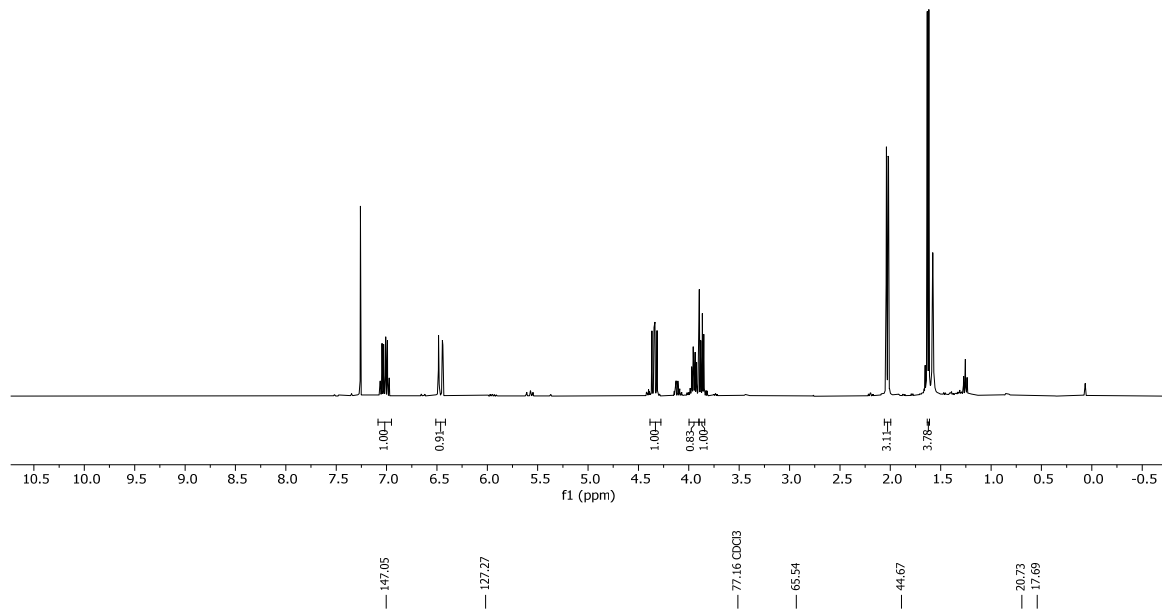
TLC: R_f = 0.86 (EtOAc). **¹H-NMR** (400 MHz, CDCl₃) δ = 5.54 – 5.32 (m, 1H), 4.40 – 4.31 (m, 1H), 3.89 – 3.84 (m, 1H), 3.84 – 3.78 (m, 1H), 1.50 (d, *J* = 6.0 Hz, 3H). **¹³C-NMR** (101 MHz, CDCl₃) δ = 66.3, 37.2, 22.1. **IR** (neat): $\tilde{\nu}$ = 3293, 3027, 2977, 2927, 2855, 1672, 1455, 1415, 1385, 1297, 1242, 1192, 1155, 1095, 1045, 940, 905, 807, 750, 648, 620. **HRMS** (ESI): calcd for C₃H₇NNaO₂S [(M+Na)⁺]: 144.0090; found: 144.0088. **[α]_D²⁰**: +7.00° (c = 1.00, CHCl₃).



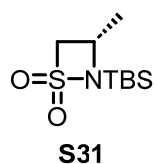
**S45**

(*S,E*)-3-methyl-2-(prop-1-en-1-ylsulfonyl)-1,2-thiazetidine 1,1-dioxide (S45). To a solution of **S33** (150.0 mg, 1.08 mmol, 1.00 equiv.) in MeCN (11 mL) was added POCl₃ (0.5 mL, 5.39 mmol, 5.0 equiv.) at rt. The reaction mixture was stirred heated at 60 °C for 18 h. Then, Et₃N (10.5 mL, 43.11 mmol, 40.00 equiv.) and stirring was continued at 60 °C for 18 h. Afterwards, EtOAc (12 mL) and sat. aq. NH₄Cl (15 mL) were added at rt, the phases were separated, the aqueous phase was extracted with EtOAc (3 x 15 mL) the organic layer was dried over MgSO₄, the solvent was removed under reduced pressure and purified by FC (EtOAc/hexane 4:1 → EtOAc) to obtain **S45** (5.0 mg, 0.022 mmol, 4%) as yellow liquid.

TLC: R_f = 0.55 (EtOAc). **MP** = 125 °C. **¹H-NMR** (400 MHz, CDCl₃) δ = 7.02 (dq, *J* = 15.2, 6.9 Hz, 1H), 6.46 (dq, *J* = 15.0, 1.7 Hz, 1H), 4.34 (dd, *J* = 12.2, 8.0 Hz, 1H), 4.00 – 3.90 (m, 1H), 3.87 (dd, *J* = 12.2, 5.8 Hz, 1H), 2.03 (dd, *J* = 7.0, 1.7 Hz, 3H), 1.62 (d, *J* = 6.0 Hz, 4H). **¹³C-NMR** (101 MHz, CDCl₃) δ = 147.1, 127.3, 65.5, 44.7, 20.7, 17.7. **IR** (neat): $\tilde{\nu}$ = 3043, 1978, 2924, 2853, 1643, 1445, 1411, 1361, 1354, 1338, 1292, 1212, 1173, 1165, 1145, 1105, 1059, 1011, 1003, 952, 917, 841, 814, 758, 701, 608, 561. **HRMS** (ESI): calcd for C₆H₁₁NNaO₄S₂ [(M+Na)⁺]: 248.0022; found: 248.0027. **[α]_D²⁰**: –28.42° (c = 0.63, CHCl₃).

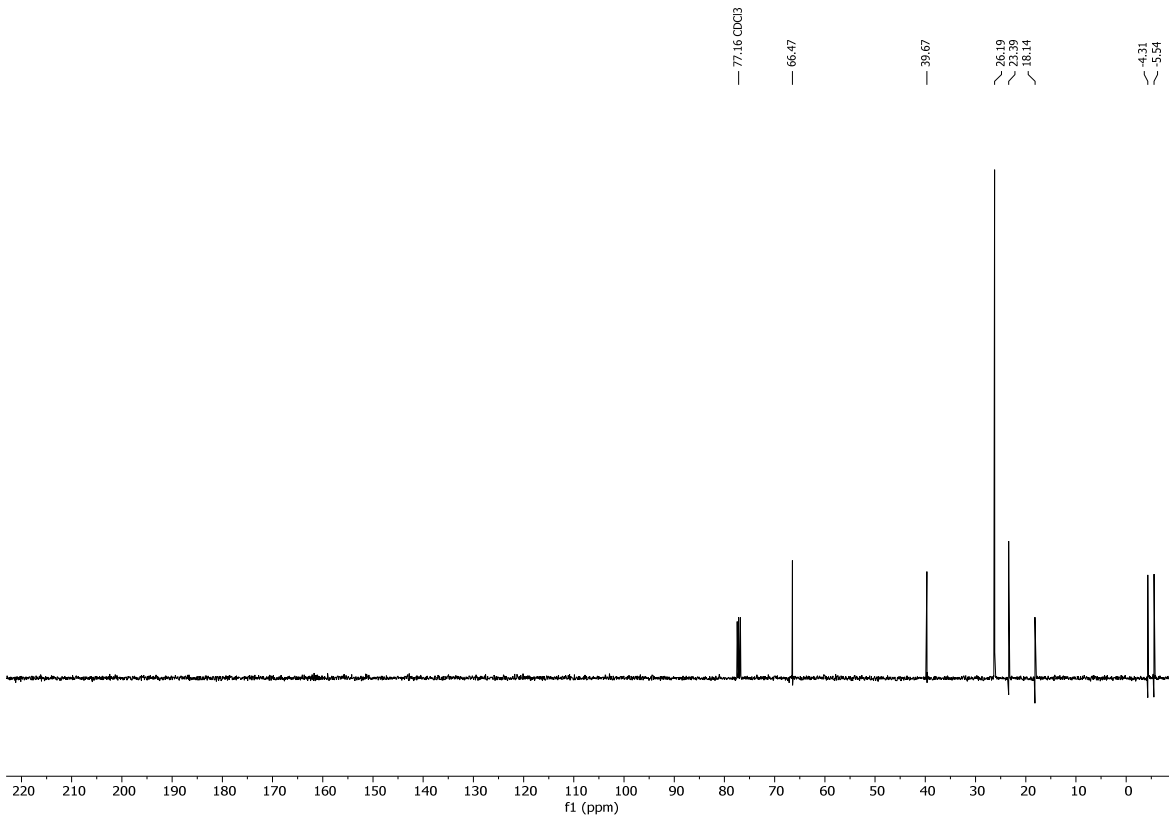
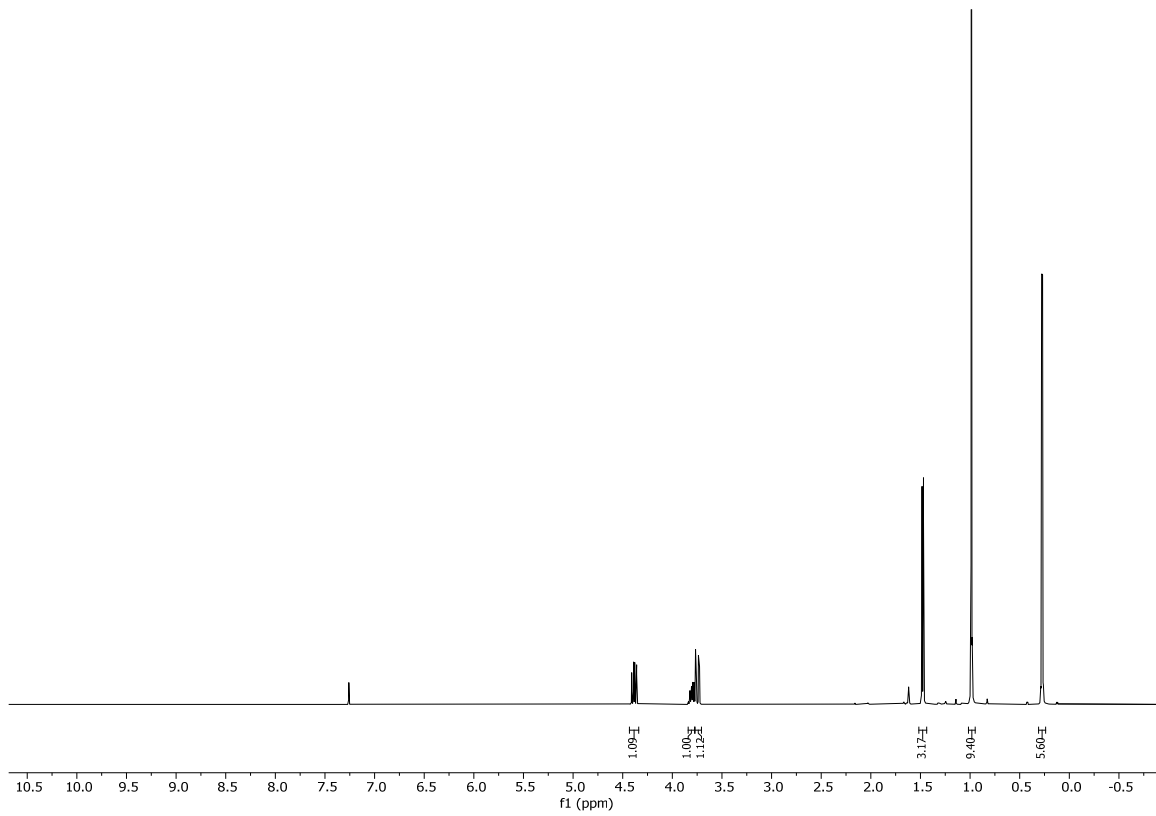


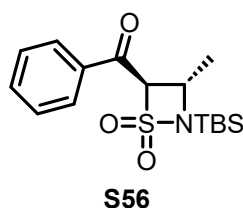
4.3.2.2 Studies Towards the Synthesis of Amine S29



(S)-2-(tert-butyldimethylsilyl)-3-methyl-1,2-thiazetidine 1,1-dioxide (S31). To a solution of **S32** (0.50 g 4.13 mmol, 1.00 equiv.) in THF (20 mL) was added LDA (2.0 M in THF/Heptane/Ethylbenzene, 2.2 mL, 4.33 mmol, 1.05 equiv.) at -78 °C and stirring was continued for 10 min. Then TBSCl (0.65 g, 4.33 mmol, 1.05 equiv.) was added and stirred for 2 h at -78 °C. Afterwards, EtOAc (12 mL) and sat. aq. NH₄Cl (15 mL) were added at rt, the phases were separated, the aqueous phase was extracted with EtOAc (3 x 15 mL) the organic layer was dried over MgSO₄, the solvent was removed under reduced pressure and purified by FC (EtOAc/hexane 1:4 → EtOAc) to obtain **S31** (0.95 g, 4.03 mmol, 98%) as yellow liquid.

TLC: R_f = 0.80 (EtOAc/hexane 1:1). **¹H-NMR** (400 MHz, CDCl₃) δ = 4.38 (dd, *J* = 12.1, 7.4 Hz, 1H), 3.84 – 3.78 (m, 1H), 3.75 (dd, *J* = 12.0, 4.1 Hz, 1H), 1.48 (d, *J* = 5.9 Hz, 3H), 0.99 (s, 9H), 0.27 (d, *J* = 4.0 Hz, 6H). **¹³C-NMR** (101 MHz, CDCl₃) δ = 66.5, 39.7, 26.2, 23.4, 18.1, -4.3, -5.5. **IR** (neat): $\tilde{\nu}$ = 2958, 2931, 2886, 2860, 1472, 1416, 1393, 1381, 1365, 1306, 1255, 1197, 1151, 1092, 1069, 1024, 1006, 939, 911, 881, 838, 824, 812, 772, 684, 655, 587. **HRMS** (ESI): calcd for C₉H₂₂NO₂SSi [(M+H)⁺]: 236.1135; found: 236.1135. **[α]_D²⁰**: +24.00° (c = 1.00, CHCl₃).

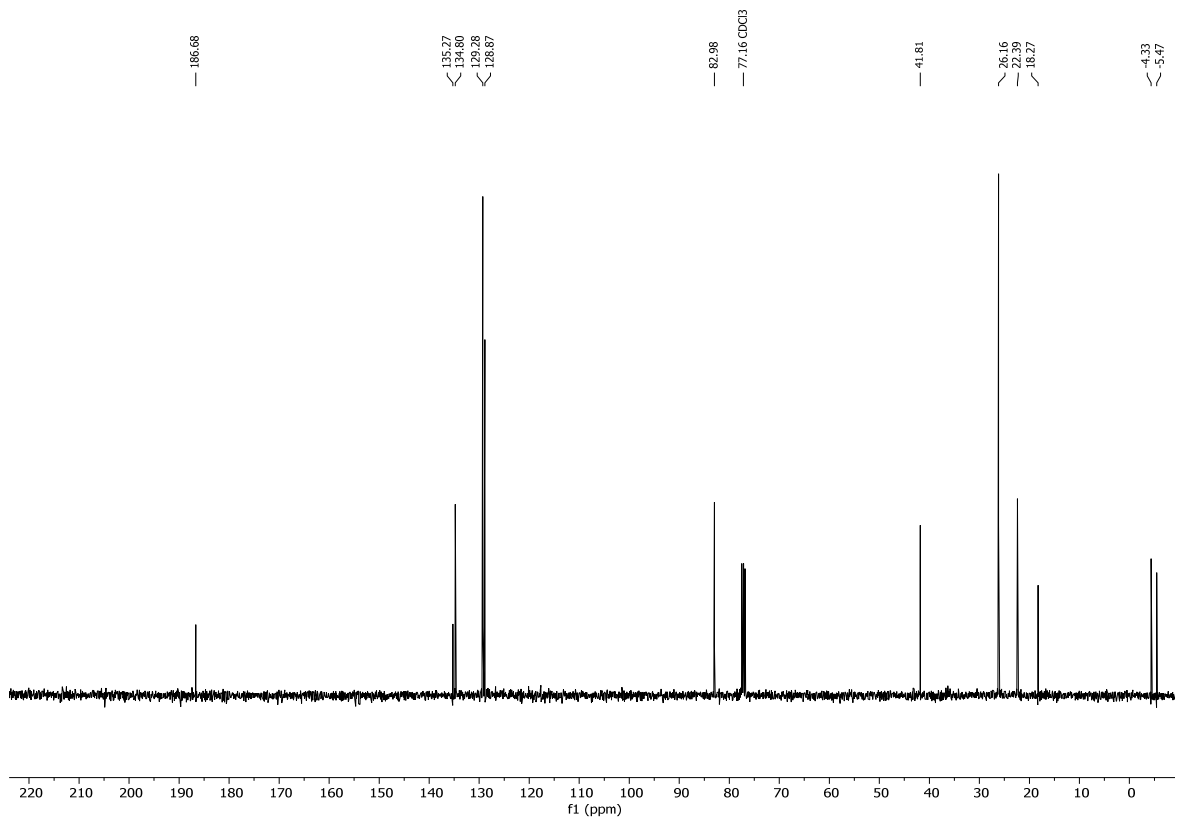
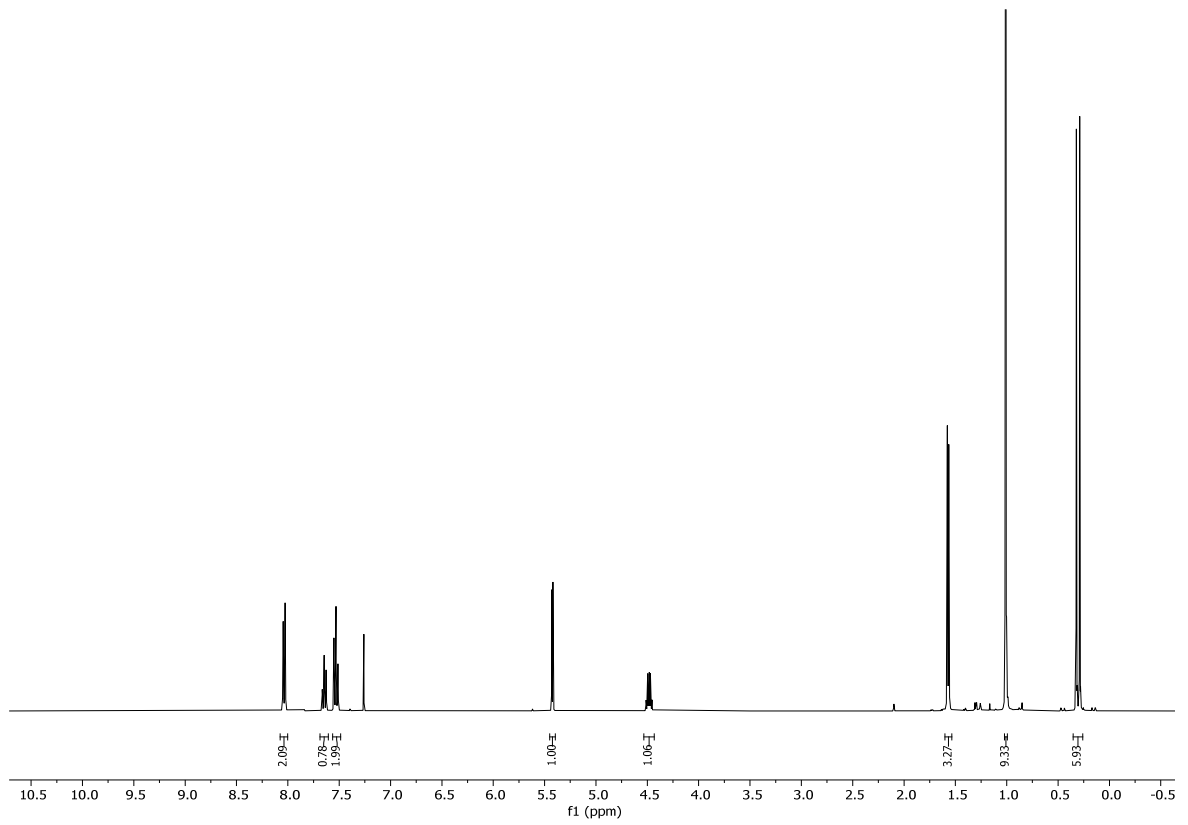


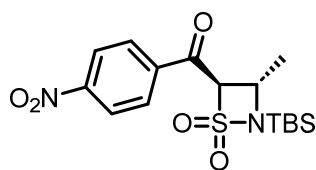


((3S,4R)-2-(tert-butyldimethylsilyl)-3-methyl-1,1-dioxido-1,2-thiazetid-4-yl)(phenyl)methanone (S56). To a solution of *n*-BuLi (1.6M in hexane, 0.16 mL, 0.26 mmol, 2.00 equiv.) in THF (0.5 mL) was added DIPA (36 μ L, 0.26 mmol, 2.00 equiv.) at -78 °C and stirred for 30 min at rt. Then, a solution of **S31** (30.0 mg 0.13 mmol, 1.00 equiv.) in THF (0.1 mL) was added at -78 °C and stirring was continued for 2 min. Then ethyl benzoate (**S55**) (36 μ L, 0.26 mmol, 2.00 equiv.) was added and stirred for 30 min at -78 °C and then for 2 h at rt. Afterwards, sat. aq. NH₄Cl (0.6 mL) was added at rt and the phases were separated, the organic layer was dried over MgSO₄, the solvent was removed under reduced pressure and purified by FC (EtOAc/hexane 1:6) to obtain **S56** (36.0 mg, 0.11 mmol, 88%) as a yellow oil.

When benzoyl chloride (**S57**) (2.00 equiv.) was used instead of ethyl benzoate (2.00 equiv.) under otherwise identical reaction conditions, **S56** was obtained in 67% yield (29.0 mg, 0.085 mmol).

TLC: R_f = 0.90 (EtOAc/hexane 1:1). **¹H-NMR** (400 MHz, CDCl₃) δ = 8.08 – 8.00 (m, 2H), 7.65 (t, *J* = 7.5 Hz, 1H), 7.56 – 7.49 (m, 2H), 5.42 (d, *J* = 4.2 Hz, 1H), 4.48 (qd, *J* = 6.1, 4.1 Hz, 1H), 1.57 (d, *J* = 6.1 Hz, 3H), 1.01 (s, 9H), 0.31 (d, *J* = 13.1 Hz, 6H). **¹³C-NMR** (101 MHz, CDCl₃) δ = 186.7, 135.3, 134.8, 129.3, 128.9, 83.0, 41.8, 26.2, 22.4, 18.3, -4.3, -5.5. **IR** (neat): $\tilde{\nu}$ = 2958, 2931, 2885, 2860, 1687, 1598, 1583, 1472, 1450, 1382, 1364, 1314, 1256, 1211, 1166, 1095, 1061, 1040, 993, 939, 904, 877, 839, 821, 780, 750, 691, 653. **HRMS** (ESI): calcd for C₁₆H₂₆NO₃SSi [(M+H)⁺]: 340.1397; found: 340.1396. **[α]₅₈₉²⁰**: -82.98° (c = 1.00, CHCl₃).

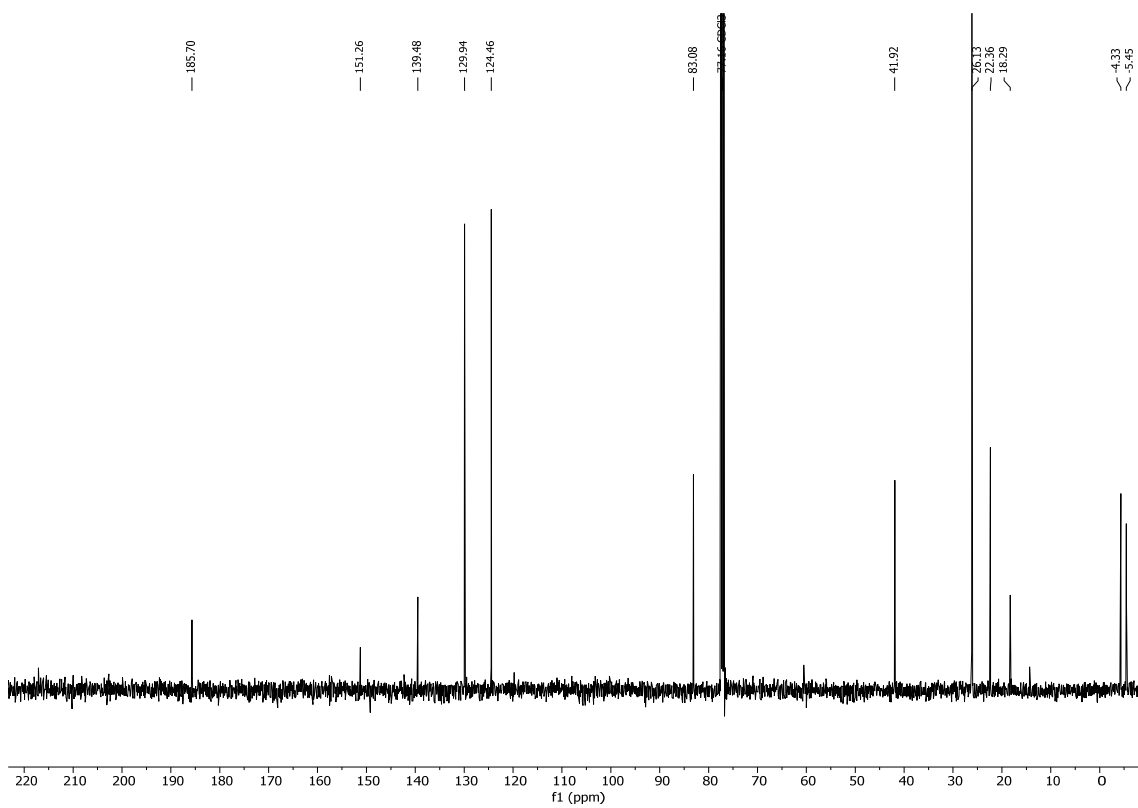
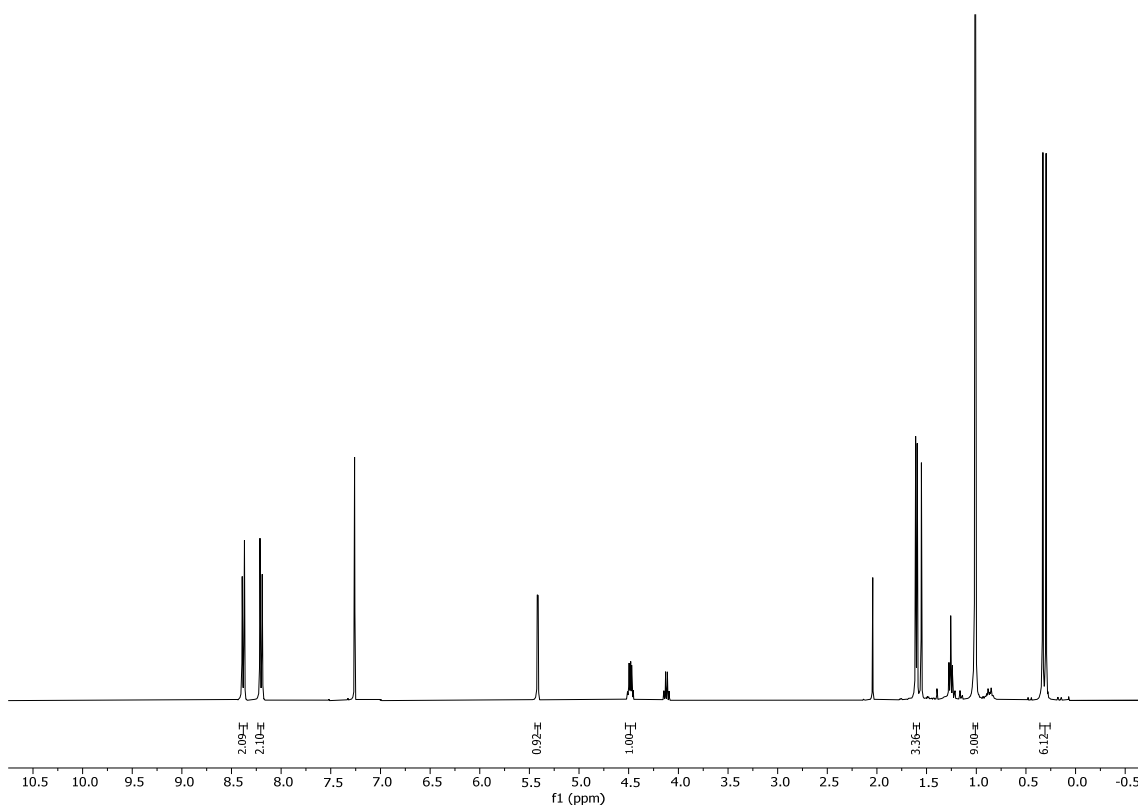


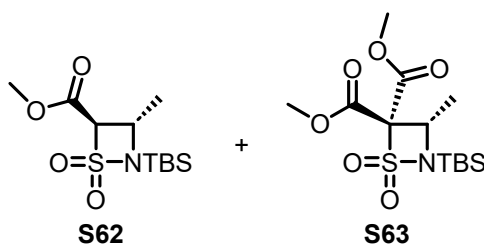
**S59**

((3*S*,4*R*)-2-(tert-butyldimethylsilyl)-3-methyl-1,1-dioxido-1,2-thiazetid-4-yl)(4-nitrophenyl)methanone (S59). To a solution of *n*-BuLi (1.6M in hexane, 0.11 mL, 0.17 mmol, 2.00 equiv.) in THF (0.5 mL) was added DIPA (24 μ L, 0.17 mmol, 2.00 equiv.) at -78 °C and stirred for 30 min at rt. Then, a solution of **S31** (20.0 mg 0.09 mmol, 1.00 equiv.) in THF (0.4 mL) was added at -78 °C and stirring was continued for 2 min. Then ethyl 4-nitrobenzoate (**S58**) (33.0 mg, 0.17 mmol, 2.00 equiv.) was added and stirred for 1 h min at -78 °C. Afterwards, sat. aq. NH₄Cl (0.5 mL) was added at rt and the phases were separated, the organic layer was dried over MgSO₄, the solvent was removed under reduced pressure and purified by FC (EtOAc/hexane 1:6) to obtain **S59** (29.0 mg, 0.075 mmol, 89%) as colorless crystals.

TLC: R_f = 0.88 (EtOAc/hexane 1:1). **MP** = 139 °C. **¹H-NMR** (400 MHz, CDCl₃) δ = 8.42 – 8.34 (m, 2H), 8.23 – 8.18 (m, 2H), 5.42 (d, *J* = 4.1 Hz, 1H), 4.48 (qd, *J* = 6.1, 4.1 Hz, 1H), 1.60 (d, *J* = 6.1 Hz, 3H), 1.01 (s, 9H), 0.31 (d, *J* = 13.2 Hz, 6H). **¹³C-NMR** (101 MHz, CDCl₃) δ = 185.7, 151.3, 139.5, 129.9, 124.5, 83.1, 41.9, 26.1, 22.4, 18.3, -4.3, -5.5. **IR** (neat): $\tilde{\nu}$ = 2958, 2932, 2861, 1697, 1605, 1528, 1472, 1408, 1350, 1314, 1257, 1209, 1165, 1095, 1064, 1040, 997, 908, 880, 857, 841, 824, 806, 782, 745, 711, 686, 646. **HRMS** (ESI): calcd for C₁₆H₂₅N₂O₅SSi [(M+H)⁺]: 385.1248; found: 385.1238. **$[\alpha]_{589}^{20}$** : -82.98° (c = 1.00, CHCl₃).

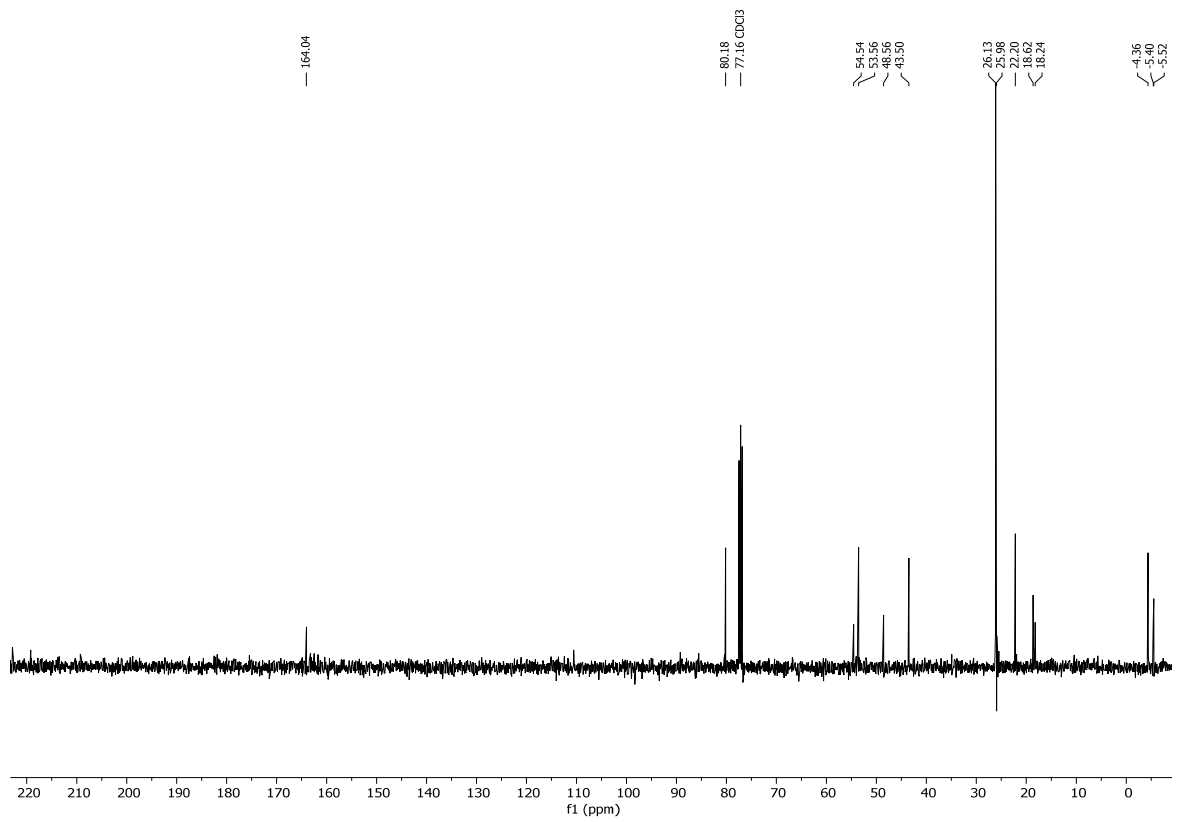
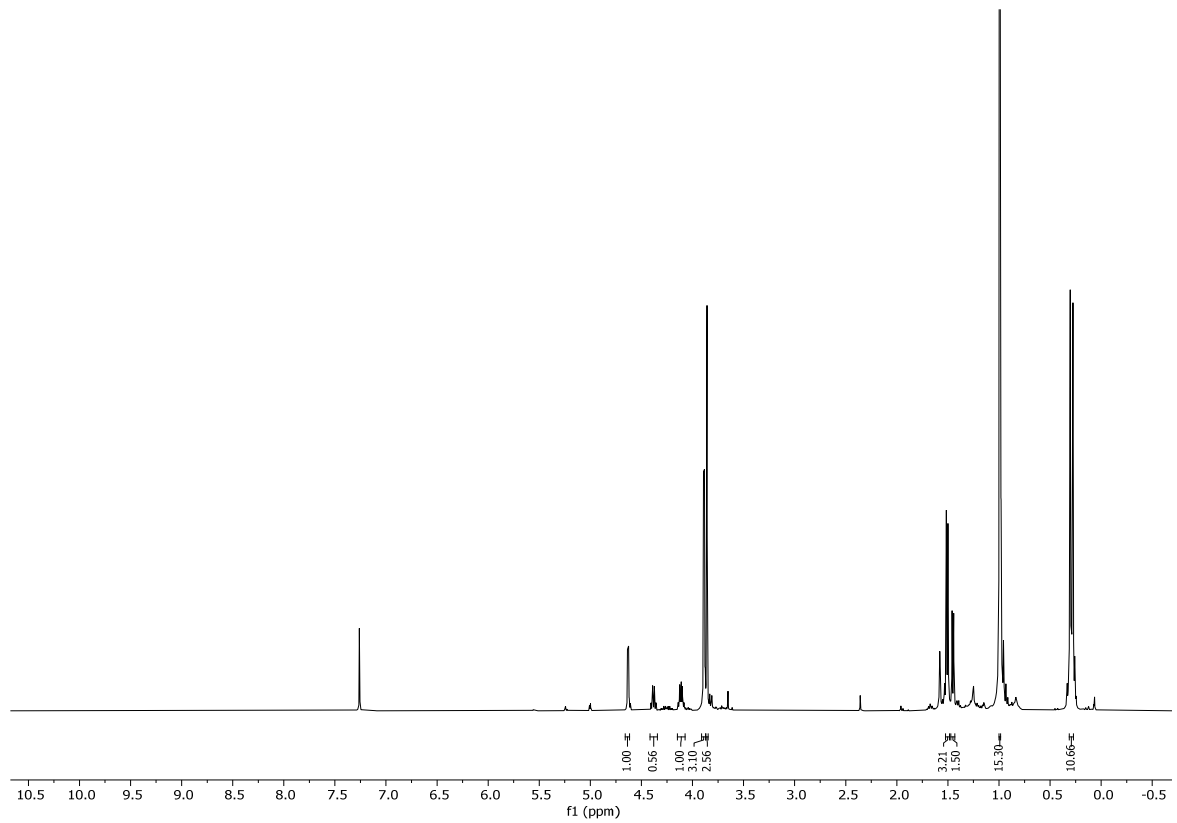
¹H-NMR- and ¹³C-NMR-spectra contain traces of EtOAc.

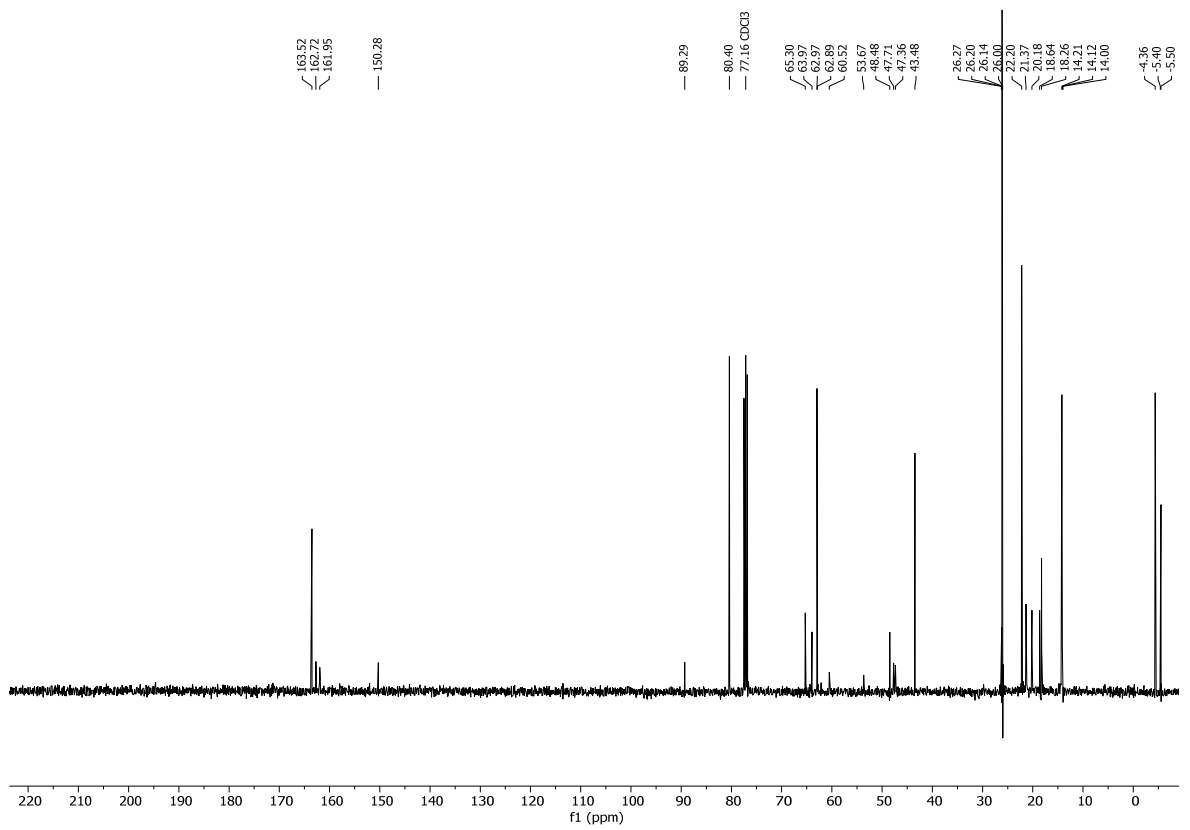
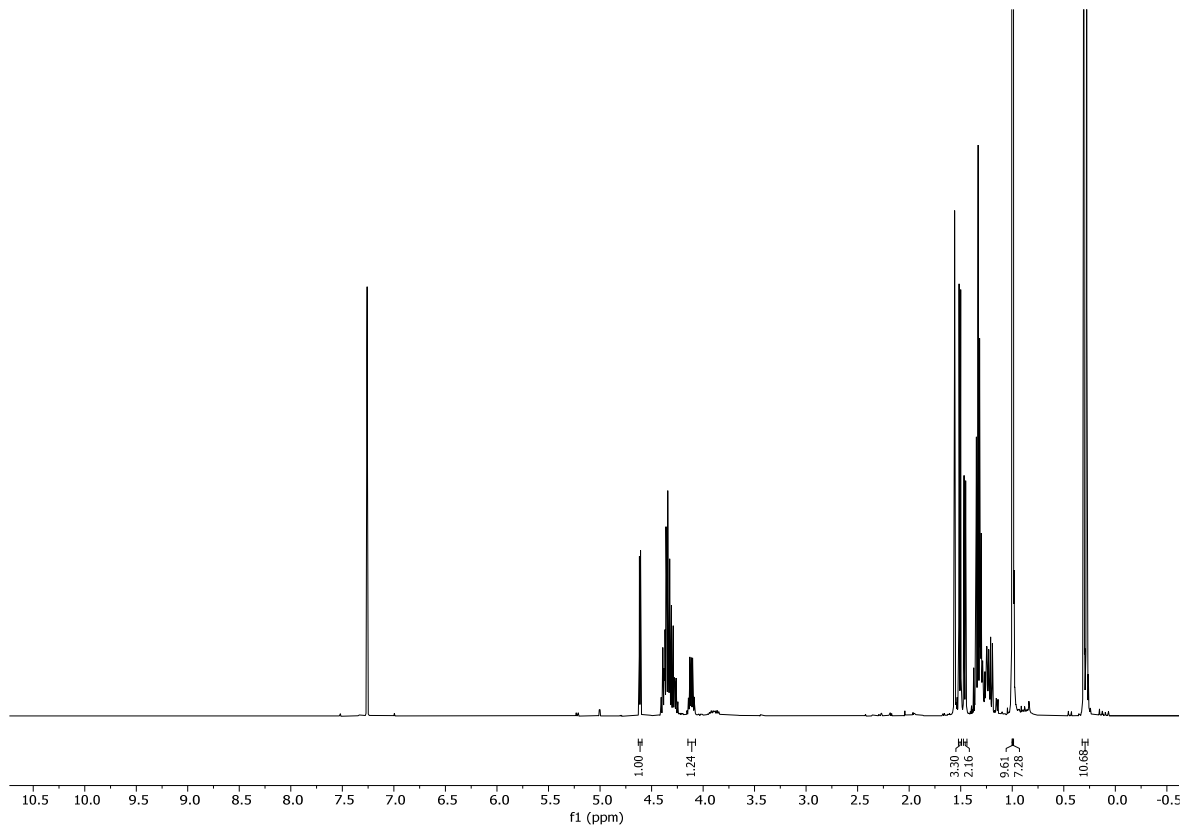


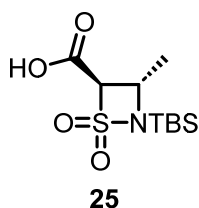


methyl (3*S*,4*R*)-2-(tert-butyldimethylsilyl)-3-methyl-1,2-thiazetidine-4-carboxylate 1,1-dioxide (S62) AND dimethyl (S)-2-(tert-butyldimethylsilyl)-3-methyl-1,2-thiazetidine-4,4-dicarboxylate 1,1-dioxide (S63). To a solution of *n*-BuLi (1.6M in hexane, 0.11 mL, 0.17 mmol, 2.00 equiv.) in THF (0.5 mL) was added DIPA (24 μ L, 0.17 mmol, 2.00 equiv.) at -78 $^{\circ}$ C and stirred for 30 min at rt. Then, a solution of **S31** (20.0 mg 0.09 mmol, 1.00 equiv.) in THF (0.5 mL) was added at -78 $^{\circ}$ C and stirring was continued for 2 min. Then methyl chloroformate (13 μ L, 0.17 mmol, 2.00 equiv.) was added and stirred for 2 h at -78 $^{\circ}$ C. Afterwards, sat. aq. NH₄Cl (0.6 mL) was added at rt and the phases were separated, the organic layer was dried over MgSO₄, the solvent was removed under reduced pressure and purified by FC (EtOAc/hexane 1:6) to obtain a mixture of **S62** (9.8 mg, 0.033 mmol, 40%) and **S63** (6.2 mg, 0.018, 22%) as colorless crystals. The chemical yield was calculated based on the ¹H-NMR spectrum of the obtained mixture after FC.

TLC: R_f = 0.86 (EtOAc/hexane 1:1). **MP** = 53 $^{\circ}$ C. **¹H-NMR** (400 MHz, CDCl₃) δ = 4.63 (d, *J* = 4.1 Hz, 1H), 4.38 (q, *J* = 6.5 Hz, 1H), 4.11 (qd, *J* = 6.3, 4.2 Hz, 1H), 3.89 (d, *J* = 3.5 Hz, 3H), 3.86 (s, 3H), 1.51 (d, *J* = 6.2 Hz, 3H), 1.45 (d, *J* = 6.5 Hz, 2H), 0.99 (d, *J* = 1.8 Hz, 15H), 0.29 (dd, *J* = 10.5, 1.8 Hz, 11H). **¹³C-NMR** (101 MHz, CDCl₃) δ = 164.0, 80.2, 54.5, 53.6, 48.6, 43.5, 26.1, 26.0, 22.2, 18.6, 18.2, -4.4, -5.4, -5.5. **IR** (neat): $\tilde{\nu}$ = 2957, 2932, 2860, 1747, 1618, 1465, 1437, 1283, 1322, 1257, 1234, 1204, 1167, 1088, 1063, 1037, 999, 940, 924, 876, 840, 821, 810, 781, 684, 653. **HRMS** (ESI): calcd for C₁₁H₂₄NO₄SSi [(M+H)⁺]: 294.1190; found: 294.1177; for C₁₃H₂₆NO₆SSi [(M+H)⁺]: 352.1245; found: 352.1233.







(3S,4R)-2-(tert-butyldimethylsilyl)-3-methyl-1,2-thiazetidine-4-carboxylic acid 1,1-dioxide (25).

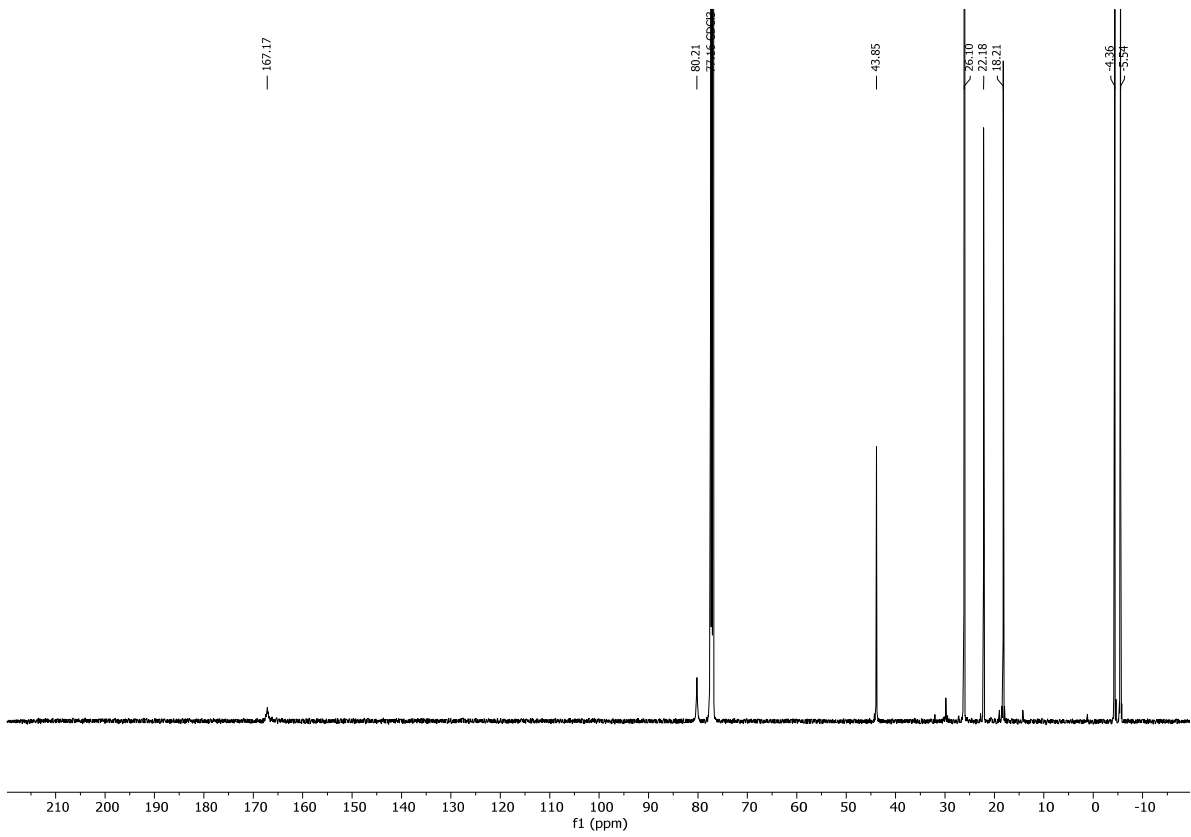
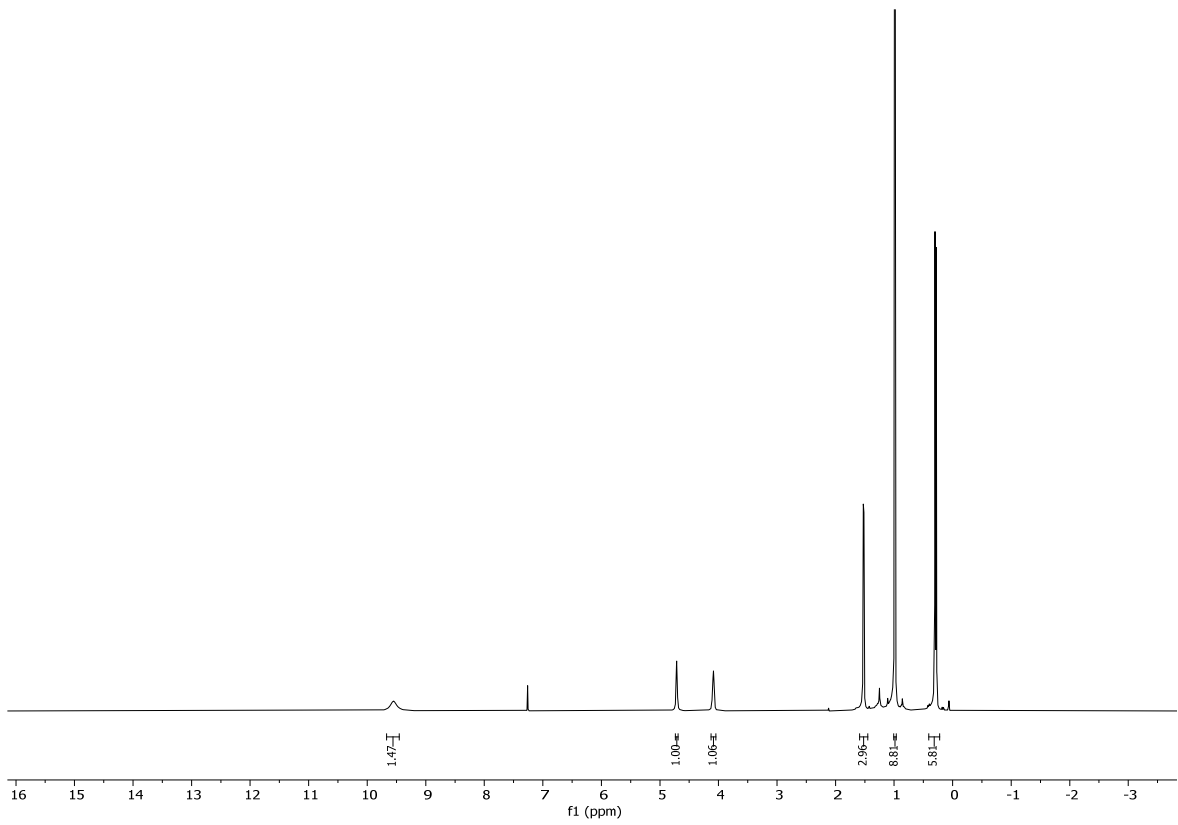
From a mixture of S62 and S63:

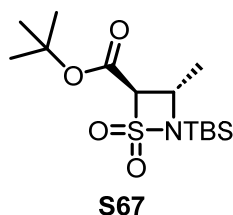
To a solution of **S62** (ca. 9.0 mg, 0.04 mmol, 1.00 equiv.) in THF (1 mL) was added LiOH (2.0 mg, 0.08 mmol, 2.00 equiv.) in H₂O (0.1 mL) stirred for 1 h at 0 °C. Afterwards, the solution was acidified to pH = 1 with a drop of con. HCl, the reaction mixture was dried over MgSO₄, the solvent was removed under reduced pressure and purified by FC (DCM/MeOH 30:1 + 1% acetic acid) to obtain **S60** (6.0 mg, 0.021 mmol, 25% over two steps from **S31**) as pale yellow crystals.

From a mixture of S64 and S65:

To a solution of **S64** (ca. 255.0 mg, 0.83 mmol, 1.00 equiv.) in THF (21 mL) was added LiOH (87.0 mg, 2.07 mmol, 2.50 equiv.) in H₂O (2.5 mL) stirred for 2 h at 0 °C. Afterwards, the solution was acidified to pH = 1 with con. HCl, the phases were separated, the organic phase was dried over MgSO₄, the solvent was removed under reduced pressure and purified by FC (DCM/MeOH 40:1 + 1% acetic acid) to obtain **S60** (60.0 mg, 0.21 mmol, 26% over two steps from **S31**) as pale yellow crystals.

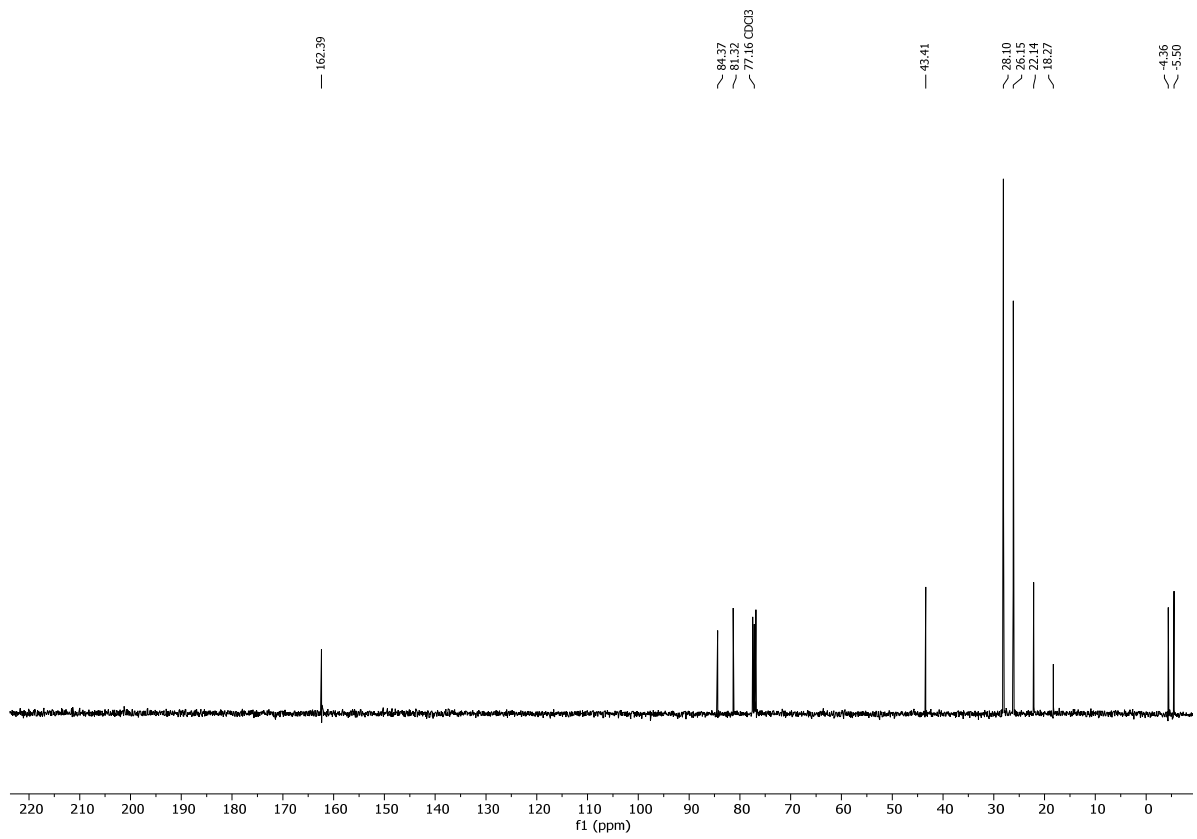
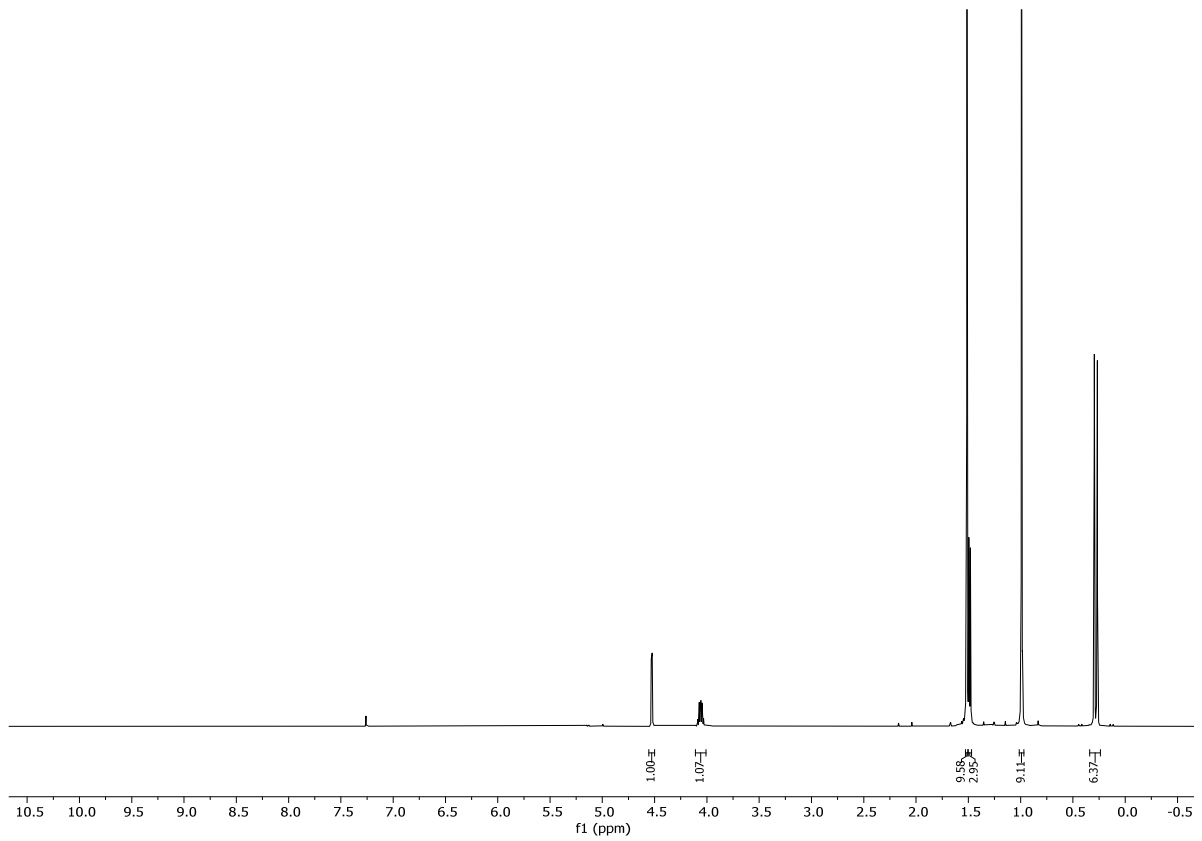
TLC: R_f = 0.20 (CH₂Cl₂/MeOH 20:1, +1% AcOH). **MP** = 45 °C. **¹H-NMR** (500 MHz, CDCl₃) δ = 9.55 (s, 1H), 4.74 – 4.69 (m, 1H), 4.09 (p, *J* = 5.8 Hz, 1H), 1.52 (d, *J* = 6.0 Hz, 3H), 0.99 (s, 9H), 0.29 (d, *J* = 10.8 Hz, 6H). **¹³C-NMR** (126 MHz, CDCl₃) δ = 167.2, 80.2, 43.9, 26.1, 22.2, 18.2, -4.4, -5.5. **IR** (neat): $\tilde{\nu}$ = 3183, 2958, 2933, 2861, 1733, 1473, 1394, 1366, 1319, 1258, 1170, 1093, 1060, 1032, 978, 939, 882, 841, 822, 811, 782, 684, 651. **HRMS** (ESI): calcd for C₁₀H₂₂NO₄SSi [(M+H)⁺]: 280.1033; found: 280.1033. **[α]_D²⁰**: -47.99° (c = 1.00, CHCl₃).

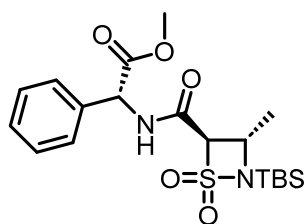




tert-butyl (3*S*,4*R*)-2-(tert-butyldimethylsilyl)-3-methyl-1,2-thiazetidine-4-carboxylate 1,1-dioxide (S67). To a solution of *n*-BuLi (1.6M in hexane, 0.27 mL, 0.43 mmol, 2.00 equiv.) in THF (1 mL) was added DIPA (60 μ L, 0.43 mmol, 2.00 equiv.) at -78 °C and stirred for 30 min at rt. Then, a solution of **S31** (50.0 mg 0.21 mmol, 1.00 equiv.) in THF (1 mL) was added at -78 °C and stirring was continued for 2 min. Then Boc₂O (93 mg, 0.43 mmol, 2.00 equiv.) was added and stirred for 1 h at -78 °C. Afterwards, sat. aq. NH₄Cl (1 mL) was added at rt and the phases were separated, the organic layer was dried over MgSO₄, the solvent was removed under reduced pressure and purified by FC (EtOAc/hexane 1:6) to obtain **S67** (53.0 mg, 0.16 mmol, 74%) as a colorless oil.

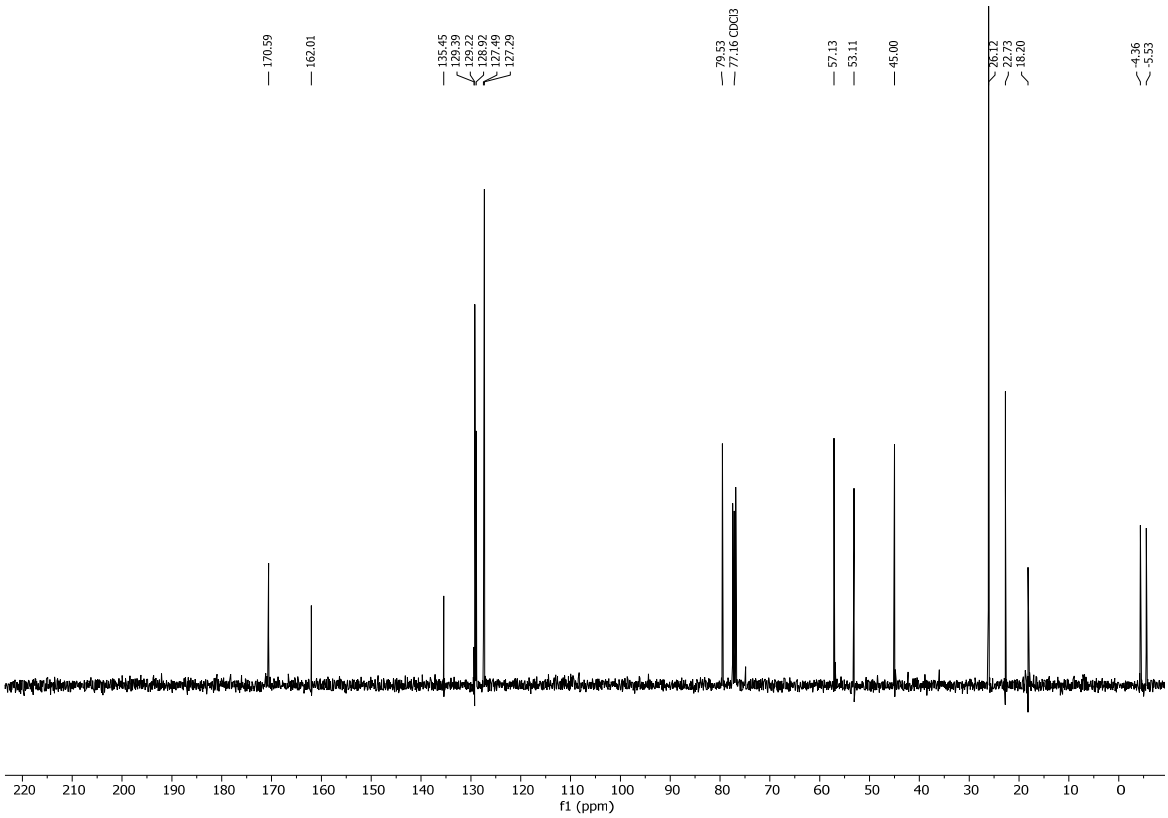
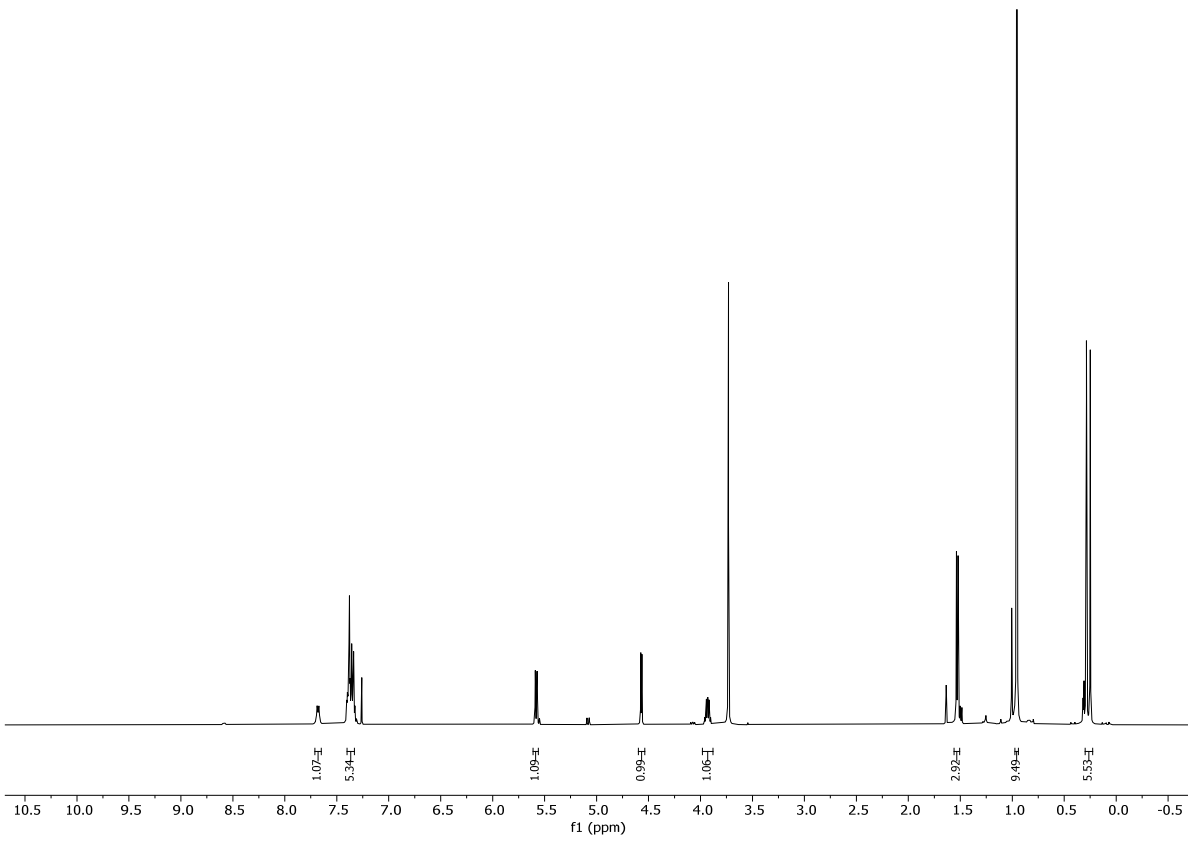
TLC: *R*_f = 0.92 (EtOAc/hexane 1:1). **¹H-NMR** (400 MHz, CDCl₃) δ = 4.53 (d, *J* = 3.9 Hz, 1H), 4.06 (qd, *J* = 6.2, 4.0 Hz, 1H), 1.51 (s, 10H), 1.49 (d, *J* = 6.2 Hz, 3H), 0.99 (s, 9H), 0.28 (d, *J* = 11.4 Hz, 6H). **¹³C-NMR** (101 MHz, CDCl₃) δ = 162.4, 84.4, 81.3, 43.4, 28.1, 26.2, 22.1, 18.3, -4.4, -5.5. **IR** (neat): $\tilde{\nu}$ = 2958, 2932, 2861, 1736, 1473, 1395, 1370, 1324, 1257, 1175, 1157, 1093, 1060, 1029, 986, 939, 899, 840, 821, 810, 782, 732, 685, 653. **HRMS** (ESI): calcd for C₁₄H₃₀NO₄SSi [(M+H)⁺]: 336.1659; found: 336.1654. **[α]₅₈₉²⁰**: -32.99° (c = 1.00, CHCl₃).



**C12**

methyl (R)-2-((3S,4R)-2-(tert-butyldimethylsilyl)-3-methyl-1,1-dioxido-1,2-thiazetidine-4-carboxamido)-2-phenylacetate (C12). To a solution of **S60** (20.0 mg, 0.72 mmol, 2.00 equiv. co-evaporated twice with 1 mL of toluene immediately before use) in toluene (1 mL) were added DCC (18.0 mg, 0.09 mmol, 1.20 equiv.) and DMAP (10 mg, 0.08 mmol, 1.10 equiv.) at 0 °C. After stirring for 30 min at 0 °C, (R)-(-)-2-Phenylglycine methyl ester hydrochloride (17.0 mg, 0.09 mmol, 1.20 equiv.) was added and stirring was continued for 7 h at rt. The reaction mixture was washed with H₂O, dried over anhydrous MgSO₄ and evaporated. The residue was purified by flash column chromatography (EtOAc/Hex 1:3 → 1:2) to give **C12** (14.0 mg, 0.03 mmol, 46%) as oil.

TLC: R_f = 0.71 (EtOAc/hexane 1:1). **¹H-NMR** (400 MHz, CDCl₃) δ = 7.68 (d, *J* = 6.8 Hz, 1H), 7.40 – 7.33 (m, 5H), 5.58 (d, *J* = 6.8 Hz, 1H), 4.57 (d, *J* = 4.2 Hz, 1H), 3.93 (qd, *J* = 6.1, 4.2 Hz, 1H), 1.53 (d, *J* = 6.1 Hz, 3H), 0.96 (s, 9H), 0.27 (d, *J* = 14.7 Hz, 6H). **¹³C-NMR** (101 MHz, CDCl₃) δ = 170.6, 162.0, 135.5, 129.4, 129.2, 128.9, 127.5, 127.3, 79.5, 57.1, 53.1, 45.0, 26.1, 22.7, 18.2, -4.4, -5.5. **IR** (neat): $\tilde{\nu}$ = 3337, 2956, 2932, 2886, 2860, 1748, 1690, 1531, 1472, 1456, 1438, 1382, 1315, 1257, 1211, 1169, 1092, 1062, 990, 911, 879, 840, 821, 811, 782, 731, 697, 656. **HRMS** (ESI): calcd for C₁₉H₃₀N₂NaO₅SSi [(M+Na)⁺]: 449.1537; found: 449.1531. **[α]_D²⁰**: -134.97° (c = 1.00, CHCl₃).



4.3.2.3 Crystallographic data for S45, S59, S63 and S64

Single crystals of **S45**, **S59**, **S63** and **S64** were analyzed on a Rigaku Oxford Diffraction XtaLAB Synergy-R kappa diffractometer equipped with a Rigaku HyPix Arc150 HPAD detector and using microfocus rotating anode Cu-K α radiation with mirror optics ($\lambda = 1.54178 \text{ \AA}$). Measurements were carried out at 100K using an Oxford Cryosystems Cryostream 1000+ sample cryostat. Data were integrated using SAINT from the Bruker Apex-II program suite and corrected for absorption effects using the multi-scan method (SADABS).^[309] The structure was solved using SHELXT^[310] and refined by full-matrix least-squares analysis (SHELXL),^[311,312] using the program package OLEX2.^[313] All non-hydrogen atoms were refined anisotropically and non-donor hydrogen atoms were constrained to ideal geometries and refined with fixed isotropic displacement parameters (in terms of a riding model). CCDC's 2344541, 2344542, 2344543 and 2344544 contain the supplementary crystallographic data for this paper, including structure factors and refinement instructions. These data can be obtained free of charge from The Cambridge Crystallographic Data Centre, 12 Union Road, Cambridge CB2 1EZ, UK (fax: +44(1223)-336-033; e-mail: deposit@ccdc.cam.ac.uk), or via <https://www.ccdc.cam.ac.uk/structures>.

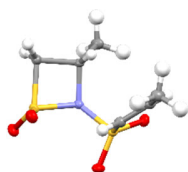


Figure 64: Asymmetric unit of the crystal structure of **S45**. Ellipsoids depicted at 50% probability.

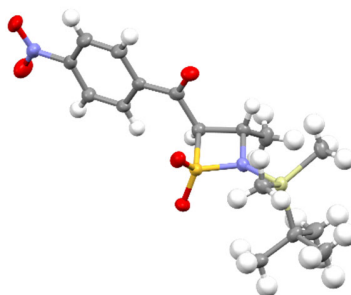


Figure 65: Asymmetric unit of the crystal structure of **S59**. Ellipsoids depicted at 50% probability.

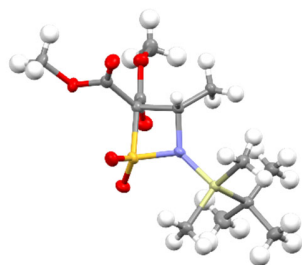


Figure 66: Asymmetric unit of the crystal structure of **S63**. Ellipsoids depicted at 50% probability.

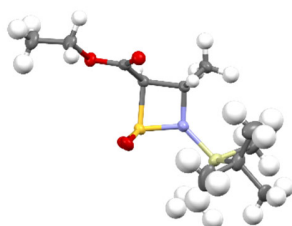


Figure 67: Asymmetric unit of the crystal structure of **S64**. Ellipsoids depicted at 50% probability.

Table 26. Crystal and structure refinement data for compounds **S45**, **S59**, **S63** and **S64**.

| Compound | S45 | S59 | S63 | S64 |
|---|---|--|---|---|
| CCDC number | 2344541 | 2344542 | 2344543 | 2344544 |
| Empirical formula | C ₆ H ₁₁ NO ₄ S ₂ | C ₁₆ H ₂₄ N ₂ O ₅ SiS | C ₁₃ H ₂₅ NO ₆ SiS | C ₁₂ H ₂₅ NO ₄ SiS |
| Formula weight | 225.28 | 384.52 | 351.49 | 307.48 |
| Temperature [K] | 100.0(1) | 100.0(1) | 100.0(1) | 100.0(1) |
| Crystal system | orthorhombic | orthorhombic | orthorhombic | orthorhombic |
| Space group | P2 ₁ 2 ₁ 2 ₁ | P2 ₁ 2 ₁ 2 ₁ | P2 ₁ 2 ₁ 2 ₁ | P2 ₁ 2 ₁ 2 ₁ |
| <i>a</i> [Å] | 7.10230(10) | 6.79760(10) | 7.67680(10) | 7.22300(10) |
| <i>b</i> [Å] | 11.4683(2) | 9.95240(10) | 14.03620(10) | 8.33700(10) |
| <i>c</i> [Å] | 11.8848(2) | 28.0879(3) | 16.29860(10) | 27.8801(2) |
| α [°] | 90 | 90 | 90 | 90 |
| β [°] | 90 | 90 | 90 | 90 |
| γ [°] | 90 | 90 | 90 | 90 |
| Volume [Å ³] | 968.03(3) | 1900.21(4) | 1756.22(3) | 1678.89(3) |
| <i>Z</i> | 4 | 4 | 4 | 4 |
| ρ_{calc} [g/cm ³] | 1.546 | 1.344 | 1.329 | 1.216 |
| μ [mm ⁻¹] | 4.907 | 2.370 | 2.533 | 2.484 |
| <i>F</i> (000) | 472.0 | 816.0 | 752.0 | 664.0 |
| Crystal size [mm ³] | 0.134 × 0.096 × 0.03 | 0.136 × 0.076 × 0.033 | 0.127 × 0.112 × 0.018 | 0.134 × 0.111 × 0.029 |
| Radiation | Cu K α (λ = 1.54184 Å) | Cu K α (λ = 1.54184 Å) | Cu K α (λ = 1.54184 Å) | Cu K α (λ = 1.54184 Å) |
| 2 θ range [°] | 10.72 to 158.858 | 6.294 to 149.688 | 8.314 to 149.218 | 6.34 to 149.602 |
| Index ranges | -8 ≤ <i>h</i> ≤ 9, -14 ≤ <i>k</i> ≤ 14, -14 ≤ <i>l</i> ≤ 15 | -8 ≤ <i>h</i> ≤ 8, -11 ≤ <i>k</i> ≤ 9, -34 ≤ <i>l</i> ≤ 34 | -9 ≤ <i>h</i> ≤ 9, -17 ≤ <i>k</i> ≤ 15, -19 ≤ <i>l</i> ≤ 20 | -9 ≤ <i>h</i> ≤ 8, -10 ≤ <i>k</i> ≤ 10, -34 ≤ <i>l</i> ≤ 34 |
| Reflections collected | 18989 | 36206 | 58905 | 51941 |
| Independent reflections | 2015 R _{int} = 0.0376, R _{sigma} = 0.0185 | 3780 R _{int} = 0.0355, R _{sigma} = 0.0192] | 3507 R _{int} = 0.0375, R _{sigma} = 0.0179 | 3330 R _{int} = 0.0314, R _{sigma} = 0.0146 |
| Data/restraints/parameters | 2015/0/120 | 3780/0/232 | 3507/0/207 | 3330/233/230 |
| Goodness-of-fit on <i>F</i> ² | 1.074 | 1.093 | 1.062 | 1.095 |
| Final <i>R</i> indexes [>=2 σ (<i>I</i>)] | R ₁ = 0.0224, wR ₂ = 0.0586 | R ₁ = 0.0297, wR ₂ = 0.0783 | R ₁ = 0.0253, wR ₂ = 0.0632 | R ₁ = 0.0245, wR ₂ = 0.0629 |
| Final <i>R</i> indexes [all data] | R ₁ = 0.0231, wR ₂ = 0.0591 | R ₁ = 0.0313, wR ₂ = 0.0791 | R ₁ = 0.0273, wR ₂ = 0.0638 | R ₁ = 0.0256, wR ₂ = 0.0634 |
| Largest diff. peak/hole [eÅ ⁻³] | 0.29/-0.36 | 0.31/-0.35 | 0.19/-0.28 | 0.20/-0.31 |
| Flack X parameter | -0.001(7) | 0.001(6) | 0.005(5) | -0.007(5) |

5 Bibliography

- [1] D. J. Newman, G. M. Cragg, *J. Nat. Prod.* **2020**, *83*, 770–803.
- [2] A. G. Atanasov, S. B. Zotchev, V. M. Dirsch, C. T. Supuran, *Nat. Rev. Drug Discov.* **2021**, *20*, 200–216.
- [3] V. Podwysotski, *Pharm. J. Trans.* **1881**, *12*, 217–218.
- [4] A. C. Ramos, R. Peláez, J. Luis López, E. Caballero, M. Medarde, A. San Feliciano, *Tetrahedron* **2001**, *57*, 3963–3977.
- [5] Z. Shah, U. F. Gohar, I. Jamshed, A. Mushtaq, H. Mukhtar, M. Zia-Ui-haq, S. I. Toma, R. Manea, M. Moga, B. Popovici, *Biomolecules* **2021**, *11*, 603.
- [6] T. J. Petcher, H. P. Weber, M. Kuhn, A. Von Wartburg, C. Keller-Juslh, H. Stahelin, E. Bianchi, K. Sheth, J. R. Cole, *J. Chem. Soc. Perkin Trans. 2* **1973**, *0*, 288–292.
- [7] F. Cortese, B. Bhattacharyya, J. Wolff, *J. Biol. Chem.* **1977**, *252*, 1134–1140.
- [8] M. Johansson, *Nat. Rev. Cancer* **2002**, *2*, 3–8.
- [9] D. J. N. Gordon M. Cragg, David G. I. Kingston, CRC Press, **2005**, p. 251.
- [10] S. Joel, *Cancer Treat. Rev.* **1996**, *22*, 179–221.
- [11] D. J. Newman, G. M. Cragg, *J. Nat. Prod.* **2020**, *83*, 770–803.
- [12] M. A. Koch, H. Waldmann, *Drug Discov. Today* **2005**, *10*, 471–483.
- [13] A. G. Atanasov et al., *Nat. Rev. Drug Discov.* **2021**, *20*, 200–216.
- [14] J. I. Tanaka, T. Higa, *Tetrahedron Lett.* **1996**, *37*, 5535–5538.
- [15] T. Taufaa, A. J. Singh, C. R. Harland, V. Patel, B. Jones, T. Halafihi, J. H. Miller, R. A. Keyzers, P. T. Northcote, *J. Nat. Prod.* **2018**, *81*, 2539–2544.
- [16] T. Matsumoto, M. Yanagiya, S. Maeno, S. Yasuda, *Tetrahedron Lett.* **1968**, *9*, 6297–6300.
- [17] R. A. Mosey, P. E. Floreancig, *Nat. Prod. Rep.* **2012**, *29*, 980–995.
- [18] L. K. Pannell, N. B. Perry, J. W. Blunt, M. H. Munro, *J. Am. Chem. Soc.* **1988**, *110*, 4850–4851.
- [19] H. Umezawa, S. Kondo, H. Iinuma, S. Kunimoto, Y. Ikeda, H. Iwasawa, D. Ikeda, T. Takeuchi, *J. Antibiot.* **1981**, *34*, 1622–1624.
- [20] F. Benz, F. Knüsel, J. Nüesch, H. Treichler, W. Voser, R. Nyfeler, W. Keller-Schierlein, *Helv. Chim. Acta* **1974**, *57*, 2459–2477.
- [21] J. J. Field, A. J. Singh, A. Kanakkanthara, T. Halafihi, P. T. Northcote, J. H. Miller, *J. Med. Chem.* **2009**, *52*, 7328–7332.
- [22] J. Uenishi, T. Iwamoto, J. Tanaka, *Org. Lett.* **2009**, *11*, 3262–3265.
- [23] Q. H. Chen, D. G. I. Kingston, *Nat. Prod. Rep.* **2014**, *31*, 1202–1226.
- [24] A. Cutignano, I. Bruno, G. Bifulco, A. Casapullo, C. Debitus, L. Gomez-Paloma, R. Riccio, *Eur. J. Org. Chem.* **2001**, *2001*, 775–778.
- [25] O. V. Sanjay Sarma, S. Palaparthi, R. Pidaparti, *Biomimetics* **2019**, *4*, 71.
- [26] H. Guo, X. Li, Y. Guo, L. Zhen, *Med. Chem. Res.* **2019**, *28*, 927–937.
- [27] L. A. Amos, D. Schlieper, *Adv. Protein Chem.* **2005**, *71*, 257–298.
- [28] T. Horio, T. Murata, T. Murata, *Front. Plant Sci.* **2014**, *5*, 108112.
- [29] “microtubule structure,” can be found under <https://nordicbiosite.com/news/microtubules-post-translational-modifications-of-tubulins-and-neurodegeneration>, **2024**.

- [30] M. A. Jordan, L. Wilson, *Nat. Rev. Cancer* **2004**, *4*, 253–265.
- [31] A. Aher, A. Akhmanova, *Curr. Opin. Cell Biol.* **2018**, *50*, 86–93.
- [32] V. I. Rodionov, G. G. Borisy, *Science* **1997**, *275*, 215–220.
- [33] T. Mitchison, M. Kirschner, *Nature* **1984**, *312*, 237–242.
- [34] A. Desai, T. J. Mitchison, *Annu. Rev. Cell Dev. Biol.* **1997**, *13*, 83–117.
- [35] C. Conde, A. Cáceres, *Nat. Rev. Neurosci.* **2009**, *10*, 319–332.
- [36] F. Borys, E. Joachimiak, H. Krawczyk, H. Fabczak, *Mol. 2020, Vol. 25, Page 3705* **2020**, *25*, 3705.
- [37] G. Varetto, A. Musacchio, *Curr. Biol.* **2008**, *18*, R591–R595.
- [38] C. Dumontet, M. A. Jordan, *Nat. Rev. Drug Discov.* **2010**, *9*, 790–803.
- [39] J. D. W. Bruce Alberts, Dennis Bray, Julian Lewis, Martin Raff, Keith Robert, *Molecular Biology of the Cell*, Garland Science, New York, **2015**.
- [40] M. O. Steinmetz, A. E. Prota, *Trends Cell Biol.* **2018**, *28*, 776–792.
- [41] X. Wang, B. Gigant, X. Zheng, Q. Chen, Q. Chen, *MedComm – Oncol.* **2023**, *2*, e46.
- [42] J. J. Field, J. F. Díaz, J. H. Miller, *Chem. Biol.* **2013**, *20*, 301–315.
- [43] P. B. Schiff, J. Fant, S. B. Horwitz, *Nature* **1979**, *277*, 665–667.
- [44] M. C. Wani, H. L. Taylor, M. E. Wall, P. Coggon, A. T. Mcphail, *J. Am. Chem. Soc.* **1971**, *93*, 2325–2327.
- [45] B. A. Weaver, *Mol. Biol. Cell* **2014**, *25*, 2677–2681.
- [46] Y. N. Cao, L. L. Zheng, D. Wang, X. X. Liang, F. Gao, X. L. Zhou, *Eur. J. Med. Chem.* **2018**, *143*, 806–828.
- [47] E. K. Rowinsky, L. A. Cazenave, R. C. Donehower, *JNCI* **1990**, *82*, 1247–1259.
- [48] S. Ezrahi, A. Aserin, N. Garti, *Adv. Colloid Interface Sci.* **2019**, *263*, 95–130.
- [49] D. M. Bollag, P. A. McQueney, J. Zhu, O. Hensens, L. Koupal, J. Liesch, M. Goetz, E. Lazarides, C. M. Woods, *Cancer Res.* **1995**, *55*, 2325–2333.
- [50] E. Ter Haar, R. J. Kowalski, E. Hamel, C. M. Lin, R. E. Longley, S. P. Gunasekera, H. S. Rosenkranz, B. W. Day, *Biochemistry* **1996**, *35*, 243–250.
- [51] T. Lindel, P. R. Jensen, W. Fenical, B. H. Long, A. M. Casazza, J. Carboni, C. R. Fairchild, *J. Am. Chem. Soc.* **1997**, *119*, 8744–8745.
- [52] E. Hamel, D. L. Sackett, D. Vourloumis, K. C. Nicolaou, *Biochemistry* **1999**, *38*, 5490–5498.
- [53] S. L. Mooberry, G. Tien, A. H. Hernandez, A. Plubrukarn, B. S. Davidson, *Cancer Res.* **1999**, *59*, 653–660.
- [54] B. Sato, H. Nakajima, Y. Hori, M. Hino, S. Hashimoto, H. Terano, *J. Antibiot.* **2000**, *53*, 204–206.
- [55] K. A. Hood, L. M. West, B. Rouwé, P. T. Northcote, M. V. Berridge, S. J. Wakefield, J. H. Miller, *Cancer Res.* **2002**, *62*, 3356–3360.
- [56] R. A. Isbrucker, J. Cummins, S. A. Pomponi, R. E. Longley, A. E. Wright, *Biochem. Pharmacol.* **2003**, *66*, 75–82.
- [57] T. L. Tinley, D. A. Randall-Hlubek, R. M. Leal, E. M. Jackson, J. W. Cessac, J. C. Quada, T. K. Hemscheidt, S. L. Mooberry, *Cancer Res.* **2003**, *63*, 3211–3220.
- [58] B. Pera, M. N. Calvo-Vidal, S. Ambati, M. Jordi, A. Kahn, J. F. Díaz, W. Fang, K. H. Altmann, L. Cerchietti, M. A. S. Moore, *Cancer Lett.* **2015**, *368*, 97–104.
- [59] L. Takahashi-Ruiz, J. D. Morris, P. Crews, T. A. Johnson, A. L. Risinger, *Molecules* **2022**, *27*, 4244.

- [60] J. J. Field et al., *Chem. Biol.* **2012**, *19*, 686–698.
- [61] A. E. Prota, K. Bargsten, D. Zurwerra, J. J. Field, J. F. Díaz, K.-H. Altmann, M. O. Steinmetz, *Science* **2013**, *339*, 587–590.
- [62] E. Nogales, M. Whittaker, R. A. Milligan, K. H. Downing, *Cell* **1999**, *96*, 79–88.
- [63] F. J. Fourniol, C. V. Sindelar, B. Amigues, D. K. Clare, G. Thomas, M. Perderiset, F. Francis, A. Houdusse, C. A. Moores, *J. Cell Biol.* **2010**, *191*, 463–470.
- [64] J. J. Field, B. Pera, J. E. Gallego, E. Calvo, J. Rodríguez-Salarichs, G. Sáez-Calvo, D. Zuwerra, M. Jordi, J. M. Andreu, A. E. Prota, G. Ménchon, J. H. Miller, K. H. Altmann, J. F. Díaz, *J. Nat. Prod.* **2018**, *81*, 494–505.
- [65] Y. Wang, Y. Yu, G. B. Li, S. A. Li, C. Wu, B. Gigant, W. Qin, H. Chen, Y. Wu, Q. Chen, J. Yang, *Nat. Commun.* **2017**, *8*, 1–8.
- [66] Q. Xiao, T. Xue, W. Shuai, C. Wu, Z. Zhang, T. Zhang, S. Zeng, B. Sun, Y. Wang, *Biochem. Biophys. Res. Commun.* **2021**, *534*, 330–336.
- [67] A. B. Smith, I. G. Safonov, R. M. Corbett, *J. Am. Chem. Soc.* **2001**, *123*, 12426–12427.
- [68] D. Zurwerra, F. Glaus, L. Betschart, J. Schuster, J. Gertsch, W. Ganci, K.-H. Altmann, *Chem. Eur. J.* **2012**, *18*, 16868–16883.
- [69] A. K. Ghosh, X. Cheng, R. Bai, E. Hamel, *Eur. J. Org. Chem.* **2012**, 4130–4139.
- [70] T. R. Hoye, M. Hu, *J. Am. Chem. Soc.* **2003**, *125*, 9576–9577.
- [71] A. K. Ghosh, X. Cheng, *Org. Lett.* **2011**, *13*, 4108–4111.
- [72] D. Zurwerra, J. Gertsch, K.-H. Altmann, *Org. Lett.* **2010**, *12*, 2302–2305.
- [73] F. Ding, M. P. Jennings, *J. Org. Chem.* **2008**, *73*, 5965–5976.
- [74] F. Ding, M. P. Jennings, *Org. Lett.* **2005**, *7*, 2321–2324.
- [75] I. Louis, N. L. Hungerford, E. J. Humphries, M. D. McLeod, *Org. Lett.* **2006**, *8*, 1117–1120.
- [76] S. Y. Yun, E. C. Hansen, I. Volchkov, E. Jin Cho, W. Yip Lo, D. Lee, *Angew. Chem. Int. Ed.* **2010**, *49*, 4261–4263.
- [77] A. B. Smith, I. G. Safonov, *Org. Lett.* **2002**, *4*, 635–637.
- [78] D. L. Aubele, S. Wan, P. E. Floreancig, *Angew. Chem. Int. Ed.* **2005**, *44*, 3485–3488.
- [79] C. C. Sanchez, G. E. Keck, *Org. Lett.* **2005**, *7*, 3053–3056.
- [80] K. Lee, H. Kim, J. Hong, *Angew. Chem. Int. Ed.* **2012**, *51*, 5735–5738.
- [81] A. B. Smith, I. G. Safonov, R. M. Corbett, *J. Am. Chem. Soc.* **2002**, *124*, 11102–11113.
- [82] T. M. Brütsch, S. Berardozi, M. L. Rothe, M. R. Horcajo, J. F. Díaz, K. H. Altmann, *Org. Lett.* **2020**, *22*, 8345–8348.
- [83] A. M. Rogan, T. C. Hamilton, R. C. Young, R. W. Klecker, R. F. Ozols, *Science* **1984**, *224*, 994–996.
- [84] R. J. Kowalski, P. Giannakakou, S. P. Gunasekera, R. E. Longley, B. W. Day, E. Hamel, *Mol. Pharmacol.* **1997**, *52*, 613–622.
- [85] G. Chen, R. Wang, B. Vue, M. Patanapongpibul, Q. Zhang, S. Zheng, G. Wang, J. D. White, Q. H. Chen, *Bioorganic Med. Chem.* **2018**, *26*, 3514–3520.
- [86] G. Chen, M. Patanapongpibul, Z. Jiang, Q. Zhang, S. Zheng, G. Wang, J. D. White, Q. H. Chen, *Org. Biomol. Chem.* **2019**, *17*, 3830–3844.
- [87] G. Chen, Z. Jiang, Q. Zhang, G. Wang, Q. H. Chen, *Molecules* **2020**, *25*, 362.
- [88] G. Chen, M. Gonzalez, Z. Jiang, Q. Zhang, G. Wang, Q. H. Chen, *Bioorg. Med. Chem. Lett.* **2021**, *40*, 127970.
- [89] C. P. Bold, M. Gut, J. Schürmann, D. Lucena-Agell, J. Gertsch, J. F. Díaz, K. H. Altmann, *Chem.*

- Eur. J.* **2021**, *27*, 5936–5943.
- [90] C. P. Bold, C. Klaus, B. Pfeiffer, J. Schürmann, R. Lombardi, D. Lucena-Agell, J. F. Díaz, K. H. Altmann, *Org. Lett.* **2021**, *23*, 2238–2242.
- [91] J. L. Henry, M. R. Wilson, M. P. Mulligan, T. R. Quinn, D. L. Sackett, R. E. Taylor, *MedChemComm* **2019**, *10*, 800–805.
- [92] C. A. Umaña, J. L. Henry, C. T. Saltzman, D. L. Sackett, L. M. Jenkins, R. E. Taylor, *ChemMedChem* **2023**, *18*, e202300292.
- [93] T. M. Brütsch, E. Cotter, D. Lucena-Agell, M. Redondo-Horcajo, C. Davies, B. Pfeiffer, S. Pagani, S. Berardozzi, J. Fernando Díaz, J. H. Miller, K. H. Altmann, *Chem. Eur. J.* **2023**, *29*, e202300703.
- [94] S. S. Bharate, S. Mignani, R. A. Vishwakarma, *J. Med. Chem.* **2018**, *61*, 10345–10374.
- [95] E. Patridge, P. Gareiss, M. S. Kinch, D. Hoyer, *Drug Discov. Today* **2016**, *21*, 204–207.
- [96] M. S. Butler, A. A. B. Robertson, M. A. Cooper, *Nat. Prod. Rep.* **2014**, *31*, 1612–1661.
- [97] U. Lindequist, *Biomol. Ther.* **2016**, *24*, 561–571.
- [98] W. H. Gerwick, B. S. Moore, *Chem. Biol.* **2012**, *19*, 85–98.
- [99] C. R. Pye, M. J. Bertin, R. S. Lokey, W. H. Gerwick, R. G. Linington, *PNAS* **2017**, *114*, 5601–5606.
- [100] Y. Hu, J. Chen, G. Hu, J. Yu, X. Zhu, Y. Lin, S. Chen, J. Yuan, *Mar. Drugs* **2015**, *13*, 202–221.
- [101] R. Montaser, H. Luesch, *Future Med. Chem.* **2011**, *3*, 1475–1489.
- [102] N. Papon, B. R. Copp, V. Courdavault, *Biotechnol. Adv.* **2022**, *54*, 107871.
- [103] W. Y. Lu, H. J. Li, Q. Y. Li, Y. C. Wu, *Bioorg. Med. Chem.* **2021**, *35*, 116058.
- [104] C. Jiménez, *ACS Med. Chem. Lett.* **2018**, *9*, 959–961.
- [105] K. H. Altmann, *Chimia* **2017**, *71*, 646–651.
- [106] “Marine Pharmacology,” can be found under <http://www.marinepharmacology.org/> [accessed Feb. 28, 2023], **2023**.
- [107] N. Fusetani, *Marine Toxins as Research Tools*, Springer, Berlin Heidelberg, **2009**.
- [108] T. F. Molinski, D. S. Dalisay, S. L. Lievens, J. P. Saludes, *Nat. Rev. Drug Discov.* **2009**, *8*, 69–85.
- [109] P. E. S. Munekata, M. Pateiro, C. A. Conte-Junior, R. Domínguez, A. Nawaz, N. Walayat, E. M. Fierro, J. M. Lorenzo, *Mar. Drugs* **2021**, *19*, 1–24.
- [110] M. J. Yu, W. Zheng, B. M. Seletsky, B. A. Littlefield, Y. Kishi, *Annu. Rep. Med. Chem.* **2011**, *46*, 227–241.
- [111] C. Cuevas, A. Francesch, *Nat. Prod. Rep.* **2009**, *26*, 322–337.
- [112] I. Paterson, E. A. Anderson, *Science* **2005**, *310*, 451–453.
- [113] T. R. Hoye, M. Hu, *J. Am. Chem. Soc.* **2003**, *125*, 9576–9577.
- [114] A. K. Ghosh, X. Cheng, R. Bai, E. Hamel, *Eur. J. Org. Chem.* **2012**, *2012*, 4130–4139.
- [115] A. P. Krapcho, J. F. Weimaster, J. M. Eldridge, E. G. E. Jahngen, A. J. Lovey, W. P. Stephens, *J. Org. Chem.* **1978**, *43*, 138–147.
- [116] D. B. Dess, J. C. Martin, *J. Org. Chem.* **1983**, *48*, 4155–4156.
- [117] J. M. Stevens, D. W. C. MacMillan, *J. Am. Chem. Soc.* **2013**, *135*, 11756–11759.
- [118] K. C. Nicolaou, K. C. Fylaktakidou, H. Monenschein, Y. Li, B. Weyershausen, H. J. Mitchell, H. X. Wei, P. Guntupalli, D. Hepworth, K. Sugita, *J. Am. Chem. Soc.* **2003**, *125*, 15433–15442.
- [119] N. D. Kjeldsen, E. D. Funder, K. V. Gothelf, *Org. Biomol. Chem.* **2014**, *12*, 3679–3685.
- [120] J. Inanaga, K. Hirata, H. Saeki, T. Katsuki, M. Yamaguchi, *Bull. Chem. Soc. Jpn.* **1979**, *52*,

- 1989–1993.
- [121] E. M. Larsen, M. R. Wilson, J. Zajicek, R. E. Taylor, *Org. Lett.* **2013**, *15*, 5246–5249.
- [122] W. S. Mahoney, D. M. Brestensky, J. M. Stryker, *J. Am. Chem. Soc.* **1988**, *110*, 291–293.
- [123] A. Renaldo, J. Labadie, J. Stille, *Org. Synth.* **1989**, *67*, 86–94.
- [124] D. M. Troast, J. Yuan, J. A. Porco, *Adv. Synth. Catal.* **2008**, *350*, 1701–1711.
- [125] M. Jiménez, W. Zhu, A. Vogt, B. W. Day, D. P. Curran, *Beilstein J. Org. Chem.* **2011**, *7*, 1372–1378.
- [126] P. X. T. Rinu, S. Radhika, G. Anilkumar, *ChemistrySelect* **2022**, *7*, e202200760.
- [127] D. Wang, S. Gao, *Org. Chem. Front.* **2014**, *1*, 556–566.
- [128] J. Franke, M. Bock, R. Dehn, J. Fohrer, S. B. Mhaske, A. Migliorini, A. A. Kanakis, R. Jansen, J. Herrmann, R. Müller, A. Kirschning, *Chem. Eur. J.* **2015**, *21*, 4272–4284.
- [129] C. Spino, M. C. Tremblay, C. Gobdout, *Org. Lett.* **2004**, *6*, 2801–2804.
- [130] Y. M. A. Mohamed, T. V. Hansen, *Tetrahedron* **2013**, *69*, 3872–3877.
- [131] K. C. K. Swamy, N. N. B. Kumar, E. Balaraman, K. V. P. P. Kumar, *Chem. Rev.* **2009**, *109*, 2551–2651.
- [132] K. Suzuki, K. Tomooka, E. Katayama, T. Matsumoto, G. ichi Tsuchihashi, *J. Am. Chem. Soc.* **1986**, *108*, 5221–5229.
- [133] M. Erdélyi, B. Pfeiffer, K. Hauenstein, J. Fohrer, J. Gertsch, K. H. Altmann, T. Carlomagno, *J. Med. Chem.* **2008**, *51*, 1469–1473.
- [134] R. M. Buey, J. F. Díaz, J. M. Andreu, A. O’Brate, P. Giannakakou, K. C. Nicolaou, P. K. Sasmal, A. Ritzén, K. Namoto, *Chem. Biol.* **2004**, *11*, 225–236.
- [135] E. Cotter, S. Glauser, A. Lelke, P. Scapozza, S. Berardozi, D. Lucena-Agell, R. Hortigüela, M. A. Oliva, J. Fernando Díaz, K.-H. Altmann, **2024**, DOI 10.26434/CHEMRXIV-2024-NWB48.
- [136] G. Chen, M. Patanapongpibul, Z. Jiang, Q. Zhang, S. Zheng, G. Wang, J. D. White, Q. H. Chen, *Org. Biomol. Chem.* **2019**, *17*, 3830–3844.
- [137] J. L. Henry, M. R. Wilson, M. P. Mulligan, T. R. Quinn, D. L. Sackett, R. E. Taylor, *MedChemComm* **2019**, *10*, 800–805.
- [138] K. Sun, X. Li, J. M. Liu, J. H. Wang, W. Li, Y. Sha, *J. Asian Nat. Prod. Res.* **2005**, *7*, 853–856.
- [139] S. Luo, Y. Wu, J. Huang, in *Int. Conf. BMSE*, **2012**, pp. 156–160.
- [140] W. S. Feng, C. G. Li, X. K. Zheng, L. L. Li, W. J. Chen, Y. L. Zhang, Y. G. Cao, J. H. Gong, H. X. Kuang, *Nat. Prod. Res.* **2016**, *30*, 1675–1681.
- [141] T. Liu et al., *J. Med. Chem.* **2012**, *55*, 8859–8878.
- [142] S. David, S. Hanessian, *Tetrahedron* **1985**, *41*, 643–663.
- [143] M. A. Leeuwenburgh, C. C. M. Appeldoorn, P. A. V. Van Hooft, H. S. Overkleeft, G. A. Van Der Marel, J. H. Van Boom, *Eur. J. Org. Chem.* **2000**, 873–877.
- [144] G. A. Kraus, M. T. Molina, J. A. Walling, *Chem. Comm.* **1986**, 1568–1569.
- [145] J. A. Frick, J. B. Klassen, A. Bathe, J. M. Abramson, H. Rapoport, *Synthesis* **1992**, *1992*, 621–623.
- [146] L. Wechteti, N. H. Mekni, M. Romdhani-Younes, *Heterocycl. Commun.* **2018**, *24*, 187–191.
- [147] G. Sosnovsky, *Tetrahedron* **1962**, *18*, 15–19.
- [148] G. Sosnovsky, *Tetrahedron* **1962**, *18*, 903–908.
- [149] D. Zhu, D. Chang, S. Gan, L. Shi, *RSC Adv.* **2016**, *6*, 27983–27987.
- [150] S. Guo, P. S. Kumar, Y. Yuan, M. Yang, *Eur. J. Org. Chem.* **2016**, *2016*, 4260–4264.
- [151] S. Wu, Y. Chen, *Adv. Synth. Catal.* **2023**, *365*, 2690–2696.

- [152] A. Fürst, P. A. Plattner, *Helv. Chim. Acta* **1949**, *32*, 275–283.
- [153] F. de A. Balaguer, T. Mühlethaler, J. Estévez-Gallego, E. Calvo, J. F. Giménez-Abián, A. L. Risinger, E. J. Sorensen, C. D. Vanderwal, K. H. Altmann, S. L. Mooberry, M. O. Steinmetz, M. Á. Oliva, A. E. Prota, J. F. Díaz, *Int. J. Mol. Sci.* **2019**, *20*, 1–17.
- [154] C. Stengel, S. P. Newman, M. P. Leese, B. V. L. Potter, M. J. Reed, A. Purohit, *Br. J. Cancer* **2010**, *102*, 316.
- [155] C. P. Bold, Synthesis and SAR of Morpholine- and Oxazole-Based Analogs of (–)-Zampanolide and Studies towards the Total Synthesis of Disorazole Z, Diss. ETH No. 27681, **2021**.
- [156] K. H. Altmann, G. Bold, G. Caravatti, N. End, A. Flörsheimer, V. Guagnano, T. O'Reilly, M. Wartmann, *Chimia* **2000**, *54*, 612–621.
- [157] C. N. Kuzniewski, S. Glauser, F. Z. Gaugaz, R. Schiess, J. Rodríguez-Salarichs, S. Vetterli, O. P. Horlacher, J. Gertsch, M. Redondo-Horcajo, A. Canales, J. Jiménez-Barbero, J. F. Díaz, K. H. Altmann, *Helv. Chim. Acta* **2019**, *102*, e1900078.
- [158] T. C. Chou, X. Zhang, Z. Y. Zhong, Y. Li, L. Feng, S. Eng, D. R. Myles, R. Johnson, N. Wu, Y. I. Yin, R. M. Wilson, S. J. Danishefsky, *PNAS* **2008**, *105*, 13157–13162.
- [159] R. Schiess, Total Synthesis of Cyclopropyl-Epothilone B Analogs and Studies Towards the Total Synthesis of Michaelide E, Diss. ETH No. 21597, **2013**.
- [160] M. Erdélyi, A. Navarro-Vázquez, B. Pfeiffer, C. N. Kuzniewski, A. Felser, T. Widmer, J. Gertsch, B. Pera, J. F. Díaz, K. H. Altmann, T. Carlomagno, *ChemMedChem* **2010**, *5*, 911–920.
- [161] J. Mulzer, A. Mantoulidis, E. Ohler, *J. Org. Chem.* **2000**, *65*, 7456–7467.
- [162] R. Schiess, J. Gertsch, W. B. Schweizer, K. H. Altmann, *Org. Lett.* **2011**, *13*, 1436–1439.
- [163] F. Z. Gaugaz, A. Chicca, M. Redondo-Horcajo, I. Barasoain, J. Fernando Díaz, K. H. Altmann, *Int. J. Mol. Sci.* **2019**, *20*, 1113.
- [164] S. E. Rossiter, M. H. Fletcher, W. M. Wuest, *Chem. Rev.* **2017**, *117*, 12415–12474.
- [165] G. Kapoor, S. Saigal, A. Elongavan, *J. Anaesthesiol. Clin. Pharmacol.* **2017**, *33*, 300.
- [166] R. B. Bhavsar, L. N. Makley, P. A. Tsonis, *Hum. Genomics* **2010**, *4*, 327–344.
- [167] K. M. Krause, A. W. Serio, T. R. Kane, L. E. Connolly, *Cold Spring Harb. Perspect. Med.* **2016**, *6*, a027029.
- [168] I. Chopra, M. Roberts, *Microbiol. Mol. Biol. Rev.* **2001**, *65*, 232–260.
- [169] S. R. Connell, D. M. Tracz, K. H. Nierhaus, D. E. Taylor, *Antimicrob. Agents Chemother.* **2003**, *47*, 3675–3681.
- [170] N. Vázquez-Laslop, A. S. Mankin, *Trends Biochem. Sci.* **2018**, *43*, 668–684.
- [171] S. Lohsen, D. S. Stephens, *Antibiot. Drug Resist.* **2019**, 97–117.
- [172] C. Foti, A. Piperno, A. Scala, O. Giuffrè, *Molecules* **2021**, *26*, 4280.
- [173] K. L. Leach, S. M. Swaney, J. R. Colca, W. G. McDonald, J. R. Blinn, L. M. M. Thomasco, R. C. Gadwood, D. Shinabarger, L. Xiong, A. S. Mankin, *Mol. Cell* **2007**, *26*, 393–402.
- [174] J. A. Ippolito, Z. F. Kanyo, D. Wang, F. J. Franceschi, P. B. Moore, T. A. Steitz, E. M. Duffy, *J. Med. Chem.* **2008**, *51*, 3353–3356.
- [175] A. K. McClendon, N. Osheroff, *Mutat. Res. Mol. Mech. Mutagen.* **2007**, *623*, 83–97.
- [176] C. Ma, X. Yang, P. J. Lewis, *Microbiol. Mol. Biol. Rev.* **2016**, *80*, 139–160.
- [177] R. Mariani, S. I. Maffioli, *Curr. Med. Chem.* **2009**, *16*, 430–454.
- [178] S. I. Maffioli, Y. Zhang, D. Degen, T. Carzaniga, G. Del Gatto, S. Serina, P. Monciardini, C.

- Mazzetti, P. Gugliera, G. Candiani, A. I. Chiriac, G. Facchetti, P. Kaltofen, H. G. Sahl, G. Dehò, S. Donadio, R. H. Ebricht, *Cell* **2017**, *169*, 1240-1248.e23.
- [179] M. Mora-Ochomogo, C. T. Lohans, *RSC Med. Chem.* **2021**, *12*, 1623–1639.
- [180] C. Watanakunakorn, *J. Antimicrob. Chemother.* **1984**, *14*, 7–18.
- [181] M. C. Bassik, M. Kampmann, *PNAS* **2011**, *108*, 11731–11732.
- [182] Z. Shi, J. Zhang, L. Tian, L. Xin, C. Liang, X. Ren, M. Li, *Mol.* **2023**, *Vol. 28*, Page 1762 **2023**, *28*, 1762.
- [183] M. A. Fischbach, C. T. Walsh, *Science* **2009**, *325*, 1089–1093.
- [184] A. Fleming, *Br. J. Exp. Pathol.* **1929**, *10*, 226.
- [185] J. Houbraken, J. C. Frisvad, R. A. Samson, *IMA Fungus* **2011**, *2*, 87–95.
- [186] R. Gaynes, *Emerg. Infect. Dis.* **2017**, *23*, 849–853.
- [187] In *Science*, American Association For The Advancement Of Science, **1945**, pp. 42–43.
- [188] T. C. on M. R. and T. M. Research, *Science* **1945**, *102*, 627–629.
- [189] A. L. Demain, R. P. Blander, *Antonie van Leeuwenhoek, Int. J. Gen. Mol. Microbiol.* **1999**, *75*, 5–19.
- [190] L. M. Lima, B. N. M. da Silva, G. Barbosa, E. J. Barreiro, *Eur. J. Med. Chem.* **2020**, *208*, 112829.
- [191] B. Thakuria, K. Lahon, *J. Clin. Diagn. Res.* **2013**, *7*, 1207.
- [192] M. I. El-Gamal, I. Brahim, N. Hisham, R. Aladdin, H. Mohammed, A. Bahaaeldin, *Eur. J. Med. Chem.* **2017**, *131*, 185–195.
- [193] S. Garde, P. K. Chodisetti, M. Reddy, *EcoSal Plus* **2021**, *9*, DOI 10.1128/ECOSALPLUS.ESP-0010-2020.
- [194] E. M. Darby, E. Trampari, P. Siasat, M. S. Gaya, I. Alav, M. A. Webber, J. M. A. Blair, *Nat. Rev. Microbiol.* **2022**, *21*, 280–295.
- [195] D. L. Paterson, R. A. Bonomo, *Clin. Microbiol. Rev.* **2005**, *18*, 657–686.
- [196] R. Laxminarayan, *Lancet* **2022**, *399*, 606–607.
- [197] K. S. Ikuta, *Lancet* **2022**, *400*, 2221–2248.
- [198] C. J. Murray, *Lancet* **2022**, *399*, 629–655.
- [199] J. I. Barrasa-Villar, C. Aibar-Remón, P. Prieto-Andrés, R. Mareca-Doñate, J. Moliner-Lahoz, *Clin. Infect. Dis.* **2017**, *65*, 644–652.
- [200] A. W. D’Souza, R. F. Potter, M. Wallace, A. Shupe, S. Patel, X. Sun, D. Gul, J. H. Kwon, S. Andleeb, C. A. D. Burnham, G. Dantas, *Nat. Commun.* **2019**, *10*, 1–19.
- [201] C. E. Luyt, N. Bréchet, J. L. Trouillet, J. Chastre, *Crit. Care* **2014**, *18*, 1–12.
- [202] C. L. Ventola, *Pharm. Therapeutics* **2015**, *40*, 277–283.
- [203] R. Mulchandaniid, Y. Wangid, M. Gilbert, T. P. Van Boeckelid, *PLOS Glob. Public Heal.* **2023**, *3*, e0001305.
- [204] WHO, “WHO antibacterial preclinical pipeline review,” can be found under <https://www.who.int/observatories/global-observatory-on-health-research-and-development/monitoring/who-antibacterial-preclinical-pipeline-review>, **2022**.
- [205] U. Theuretzbacher, K. Outtersson, A. Engel, A. Karlén, *Nat. Rev. Microbiol.* **2019**, *18*, 275–285.
- [206] M. Coll, J. Frau, B. Vilanova, J. Donoso, F. Muñoz, F. G. Blanco, *J. Phys. Chem. B* **2000**, *104*, 11389–11394.
- [207] A. Nangia, *J. Mol. Struct.* **1991**, *251*, 237–243.

- [208] A. Nangia, *Proc. Indian Acad. Sci. - Chem. Sci.* **1993**, *105*, 131–139.
- [209] A. Nangia, P. S. Chandrakala, M. V. Balaramakrishna, T. V. A. Latha, *J. Mol. Struct. THEOCHEM* **1995**, *343*, 157–165.
- [210] A. Nangia, P. S. Chandrakala, *Tetrahedron Lett.* **1995**, *36*, 7771–7774.
- [211] P. S. Chandrakala, A. K. Katz, H. L. Carrell, P. R. Sailaja, A. R. Podile, A. Nangia, G. R. Desiraju, *J. Chem. Soc. Perkin Trans. 1* **1998**, 2597–2608.
- [212] M. Coll, J. Frau, B. Vilanova, J. Donoso, F. Muñoz, *J. Comput. Aided. Mol. Des.* **2001**, *15*, 819–833.
- [213] R. C. Garcías, M. Coll, J. Donoso, F. Muñoz, *Chem. Phys. Lett.* **2003**, *372*, 275–281.
- [214] E. Cotter, F. Pultar, S. Riniker, K.-H. Altmann, *Chem. – A Eur. J.* **2024**, e202400619.
- [215] C. Mattar, S. Edwards, E. Baraldi, J. Hood, *Curr. Opin. Microbiol.* **2020**, *57*, 56–61.
- [216] “Antibiotic Resistance Threats Report,” can be found under <https://www.cdc.gov/drugresistance/Biggest-Threats.html> [accessed Jan. 2024], **2019**.
- [217] C. T. Walsh, T. A. Wencewicz, *J. Antibiot.* **2014**, *67*, 7–22.
- [218] M. Mora-Ochomogo, C. T. Lohans, *RSC Med. Chem.* **2021**, *12*, 1623–1639.
- [219] R. Li, X. Chen, C. Zhou, Q. Q. Dai, L. Yang, *Eur. J. Med. Chem.* **2022**, *242*, 114677.
- [220] D. E. Ehmann, H. Jahić, P. L. Ross, R. F. Gu, J. Hu, G. Kern, G. K. Walkup, S. L. Fisher, *PNAS* **2012**, *109*, 11663–11668.
- [221] D. E. Ehmann, H. Jahić, P. L. Ross, R. F. Gu, J. Hu, T. F. Durand-Réville, S. Lahiri, J. Thresher, S. Livchak, N. Gao, T. Palmer, G. K. Walkup, S. L. Fisher, *J. Biol. Chem.* **2013**, *288*, 27960–27971.
- [222] N. N. Zobova, G. N. Rusanov, B. A. Arbuzov, *Bull. Acad. Sci. USSR Div. Chem. Sci.* **1972**, *21*, 1957–1960.
- [223] B. A. Arbuzov, N. N. Zobova, *Bull. Acad. Sci. USSR Div. Chem. Sci.* **1973**, *22*, 2542–2543.
- [224] B. A. Arbuzov; N. N. Zobova, *Synthesis* **1974**, *July*, 461–476.
- [225] O. Tsuge, T. Hatta, R. Mizuguchi, T. Kobayashi, R. Kanzaki, *Heterocycles* **1996**, *42*, 533–536.
- [226] O. Tsuge, M. Tashiro, R. Mizuguchi, S. Kanemasa, *Chem. Pharm. Bull.* **1966**, *14*, 1055–1057.
- [227] R. Neidlein, R. Bottler, *Arch. Pharm.* **1969**, *302*, 306–309.
- [228] M. Seki, K. Kondo, T. Iwasaki, *J. Chem. Soc. Perkin Trans. 1* **1996**, 2851–2856.
- [229] E. De Lemos, F. H. Porée, A. Bourin, J. Barbion, E. Agouridas, M. I. Lannou, A. Commerçon, J. F. Betzer, A. Pancrazi, J. Ardisson, *Chem. Eur. J.* **2008**, *14*, 11092–11112.
- [230] M. S. Stanley, *J. Org. Chem.* **1992**, *57*, 6421–6430.
- [231] C. C. Hanna, S. S. Kulkarni, E. E. Watson, B. Premdjee, R. J. Payne, *Chem. Commun.* **2017**, *53*, 5424–5427.
- [232] D. Q. Song, N. N. Du, Y. M. Wang, W. Y. He, E. Z. Jiang, S. X. Cheng, Y. X. Wang, Y. H. Li, Y. P. Wang, X. Li, J. D. Jiang, *Bioorganic Med. Chem.* **2009**, *17*, 3873–3878.
- [233] H. Nakatsuji, H. Nishikado, K. Ueno, Y. Tanabe, *Org. Lett.* **2009**, *11*, 4258–4261.
- [234] F. Richter, M. Bauer, C. Perez, C. Maichle-Mössmer, M. E. Maier, *J. Org. Chem.* **2002**, *67*, 2474–2480.
- [235] T. Trieselmann, R. W. Hoffmann, K. Menzel, *Eur. J. Org. Chem.* **2002**, 1292–1304.
- [236] J. van Alphen, *Recl. des Trav. Chim. des Pays-Bas* **1935**, *54*, 885–887.
- [237] M. Tišler, B. Stanovnik, *Chem. Commun.* **1980**, *1980*, 313–314.
- [238] T. A. Young, J. J. Silcock, A. J. Sterling, F. Duarte, *Angew. Chem. Int. Ed.* **2021**, *60*, 4266–4274.

- [239] C. Bannwarth, E. Caldeweyher, S. Ehlert, A. Hansen, P. Pracht, J. Seibert, S. Spicher, S. Grimme, *Wiley Interdiscip. Rev. Comput. Mol. Sci.* **2021**, *11*, e1493.
- [240] F. Neese, F. Wennmohs, U. Becker, C. Riplinger, *J. Chem. Phys.* **2020**, *152*, 224108.
- [241] F. Neese, *Wiley Interdiscip. Rev. Comput. Mol. Sci.* **2022**, *12*, e1606.
- [242] S. Riniker, G. A. Landrum, *J. Chem. Inf. Model.* **2015**, *55*, 2562–2574.
- [243] G. Landrum et al., *Zenodo* **2023**, 7671152.
- [244] C. Bannwarth, S. Ehlert, S. Grimme, *J. Chem. Theory Comput.* **2019**, *15*, 1652–1671.
- [245] J. P. Perdew, K. Burke, M. Ernzerhof, *Phys. Rev. Lett.* **1996**, *77*, 3865–3868.
- [246] V. Barone, M. Cossi, *J. Phys. Chem. A* **1998**, *102*, 1995–2001.
- [247] C. Adamo, V. Barone, *J. Chem. Phys.* **1999**, *110*, 6158–6170.
- [248] F. Weigend, R. Ahlrichs, *Phys. Chem. Chem. Phys.* **2005**, *7*, 3297–3305.
- [249] F. Neese, F. Wennmohs, A. Hansen, U. Becker, *Chem. Phys.* **2009**, *356*, 98–109.
- [250] S. Grimme, J. Antony, S. Ehrlich, H. Krieg, *J. Chem. Phys.* **2010**, *132*, 154104.
- [251] S. Grimme, S. Ehrlich, L. Goerigk, *J. Comput. Chem.* **2011**, *32*, 1456–1465.
- [252] W. Clark Still, A. Tempczyk, R. C. Hawley, T. Hendrickson, *J. Am. Chem. Soc.* **1990**, *112*, 6127–6129.
- [253] F. Weigend, R. Ahlrichs, *Phys. Chem. Chem. Phys.* **2005**, *7*, 3297–3305.
- [254] M. K. Kesharwani, B. Brauer, J. M. L. Martin, *J. Phys. Chem. A* **2015**, *119*, 1701–1714.
- [255] S. Grimme, *Chem. – A Eur. J.* **2012**, *18*, 9955–9964.
- [256] E. Cotter, F. Pultar, S. Riniker, K.-H. Altmann, *Chem. – A Eur. J.* **2024**, e202304272.
- [257] M. K. Bogdos, B. Morandi, *J. Chem. Educ.* **2023**, *100*, 3641–3644.
- [258] L. Bösel, R. Dötzer, S. Steiner, M. Stritzinger, S. Salzmann, S. Riniker, *Anal. Chem.* **2020**, *92*, 9124–9131.
- [259] F. Pultar, M. E. Hansen, S. Wolfrum, L. Bösel, R. Fróis-Martins, S. Bloch, A. G. Kravina, D. Pehlivanoglu, C. Schäffer, S. LeibundGut-Landmann, S. Riniker, E. M. Carreira, *J. Am. Chem. Soc.* **2021**, *143*, 10389–10402.
- [260] L. Bösel, R. Aerts, W. Herrebout, S. Riniker, *Phys. Chem. Chem. Phys.* **2023**, *25*, 2063–2074.
- [261] S. Riniker, G. A. Landrum, *J. Chem. Inf. Model.* **2015**, *55*, 2562–2574.
- [262] T. A. Halgren, *J. Comput. Chem.* **1996**, *17*, 490–519.
- [263] T. A. Halgren, *J. Comput. Chem.* **1999**, *20*, 720–729.
- [264] D. Butina, *J. Chem. Inf. Comput. Sci.* **1999**, *39*, 747–750.
- [265] C. Adamo, V. Barone, *J. Chem. Phys.* **1999**, *110*, 6158–6170.
- [266] M. Feyereisen, G. Fitzgerald, A. Komornicki, *Chem. Phys. Lett.* **1993**, *208*, 359–363.
- [267] A. D. Becke, *Phys. Rev. A* **1988**, *38*, 3098.
- [268] E. P. Kohler, *Am. Chem. J.* **1897**, *19*, 728–752.
- [269] A. Le Berre, J. Petit, *Tetrahedron Lett.* **1972**, *13*, 213–216.
- [270] F. Cavagna, W. Koller, A. Linkies, H. Rehling, D. Reuschling, *Angew. Chem. Int. Ed.* **1982**, *21*, 548–549.
- [271] T. Iwama, T. Kataoka, *Rev. Heteroat. Chem.* **1996**, *15*, 25–60.
- [272] M. I. Page, P. S. Hinchliffe, J. M. Wood, L. P. Harding, A. P. Laws, *Bioorg. Med. Chem. Lett.* **2003**, *13*, 4489–4492.
- [273] M. I. Page, *Acc. Chem. Res.* **2004**, *37*, 297–303.
- [274] N. J. Baxter, A. P. Laws, L. J. H. Rigoreau, M. I. Page, *Chem. Commun.* **1999**, 2401–2402.
- [275] N. J. Baxter, L. J. M. Rigoreau, A. P. Laws, M. I. Page, *J. Am. Chem. Soc.* **2000**, *122*, 3375–

- 3385.
- [276] J. M. Wood, P. S. Hinchliffe, A. P. Laws, M. I. Page, *J. Chem. Soc. Perkin Trans. 2* **2002**, 2, 938–946.
- [277] A. Llinás, N. Ahmed, M. Cordaro, A. P. Laws, J. M. Frère, M. Delmarcelle, N. R. Silvaggi, J. A. Kelly, M. I. Page, *Biochemistry* **2005**, 44, 7738–7746.
- [278] W. Y. Tsang, N. Ahmed, P. S. Hinchliffe, J. M. Wood, L. P. Harding, A. P. Laws, M. I. Page, *J. Am. Chem. Soc.* **2005**, 127, 17556–17564.
- [279] M. Barwick, T. Abu-Izneid, I. Novak, *J. Phys. Chem. A* **2008**, 112, 10993–10997.
- [280] R. Kolb, N. C. Bach, S. A. Sieber, *Chem. Commun.* **2013**, 50, 427–429.
- [281] F. Cavagna, W. Koller, A. Linkies, H. Rehling, D. Reuschling, *Angew. Chem. Int. Ed.* **1982**, 21, 1201–1212.
- [282] V. A. Rassadin, D. S. Grosheva, A. A. Tomashevskii, V. V. Sokolov, *Chem. Heterocycl. Compd.* **2013**, 49, 39–65.
- [283] O. O. Grygorenko, B. V. Vashchenko, O. P. Blahun, S. Zherish, *Eur. J. Org. Chem.* **2020**, 2020, 5787–5800.
- [284] H. H. Otto, P. Schwenkkraus, *Tetrahedron Lett.* **1982**, 23, 5389–5390.
- [285] H. Plagge, N. Manicone, H. H. Otto, *Helv. Chim. Acta* **2004**, 87, 1574–1590.
- [286] A. Meinzer, A. Breckel, B. A. Thaher, N. Manicone, H. Otto, *Helv. Chim. Acta* **2004**, 87, 90–105.
- [287] E. Meyle, H. Otto, *Chem. Comm.* **1984**, 673, 1084–1085.
- [288] E. Meyle, H. -H Otto, E. Keller, *Liebigs Ann. Chem.* **1985**, 1985, 802–812.
- [289] M. Müller, E. Meyle, H. -H Otto, E. F. Paulus, H. Plagge, *Liebigs Ann. Chem.* **1989**, 1989, 975–983.
- [290] E. Meyle, P. Schwenkkraus, M. Zsigmondy, H. -H Otto, *Arch. Pharm.* **1989**, 322, 17–20.
- [291] P. Schwenkkraus, H. -H Otto, *Arch. Pharm.* **1990**, 323, 93–97.
- [292] M. Müller, H. -H Otto, *Arch. Pharm.* **1991**, 324, 15–17.
- [293] P. Schwenkkraus, H. -H Otto, *Arch. Pharm.* **1993**, 326, 437–441.
- [294] S. Merkle, H. -H Otto, *Arch. Pharm.* **1994**, 327, 657–660.
- [295] A. Holewinski, M. A. Sakwa-novak, C. W. Jones, *J. Am. Chem. Soc.* **2015**, 137, 11749–11759.
- [296] G. Abbenante, R. Hughes, R. H. Prager, *Aust. J. Chem.* **1997**, 50, 523–528.
- [297] N. Chen, W. Jia, J. Xu, *Eur. J. Org. Chem.* **2009**, 2009, 5841–5846.
- [298] D. Delaunay, L. Toupet, M. Le Corre, *J. Org. Chem.* **1995**, 60, 6604–6607.
- [299] C. Morrill, J. E. Gillespie, R. J. Phipps, *Angew. Chem. Int. Ed.* **2022**, 61, e202204025.
- [300] M. J. Szymonifka, J. V. Heck, *Tetrahedron Lett.* **1989**, 30, 2873–2876.
- [301] L. G. O’Neil, J. F. Bower, *Angew. Chem. Int. Ed.* **2021**, 60, 25640–25666.
- [302] S. Lee, M. S. Love, R. Modukuri, A. K. Chatterjee, L. Huerta, A. P. Lawson, C. W. McNamara, J. R. Mead, L. Hedstrom, G. D. Cuny, *Bioorganic Med. Chem. Lett.* **2023**, 90, 129328.
- [303] S. R. Crabtree, W. L. A. Chu, L. N. Mander, *Synlett* **1990**, 1990, 169–170.
- [304] H. Alper, D. Delledonne, M. Kameyama, D. Roberto, *Organometallics* **1990**, 9, 762–765.
- [305] R. Kumar, V. Sharma, S. Jain, H. Sharma, K. Vanka, S. S. Sen, *ChemCatChem* **2022**, 14, e202101788.
- [306] H. Breuer, C. M. Cimarusti, T. Denzel, W. H. Koster, W. A. Slusarchyk, U. D. Treuner, *J. Antimicrob. Chemother.* **1981**, 8, 21–28.
- [307] J. Fernando Díaz, R. Strobe, Y. Engelborghs, A. A. Souto, J. M. Andreu, *J. Biol. Chem.* **2000**,

- 275, 26265–26276.
- [308] J. F. Díaz, I. Barasoain, J. M. Andreu, *J. Biol. Chem.* **2003**, *278*, 8407–8419.
- [309] G. M. Sheldrick, *Program for Empirical Absorption Correction of Area Detector Data*, Univ. Of Göttingen, Göttingen, Germany, **1996**.
- [310] G. M. Sheldrick, *Acta Cryst.* **2015**, *A71*, 3–8.
- [311] G. M. Sheldrick, *Acta Cryst.* **2008**, *A64*, 112–122.
- [312] G. M. Sheldrick, *Acta Cryst.* **2015**, *C71*, 3–8.
- [313] O. V. Dolomanov, L. J. Bourhis, R. J. Gildea, J. A. K. Howard, H. J. Puschmann, *Appl. Crystallogr.* **2009**, *42*, 339–341.
- [314] O. Flögel, M. G. O. Amombo, H. U. Reißig, G. Zahn, I. Brüdgam, H. Hartl, *Chem. Eur. J.* **2003**, *9*, 1405–1415.
- [315] B. Narasimhan, V. Judge, R. Narang, R. Ohlan, S. Ohlan, *Bioorganic Med. Chem. Lett.* **2007**, *17*, 5836–5845.
- [316] M. S. Stanley, *J. Org. Chem.* **1992**, *57*, 6421–6430.
- [317] S. J. Gregson, P. W. Howard, J. A. Hartley, N. A. Brooks, L. J. Adams, T. C. Jenkins, L. R. Kelland, D. E. Thurston, *J. Med. Chem.* **2001**, *44*, 737–748.
- [318] L. Bösel, R. Dötzer, S. Steiner, M. Stritzinger, S. Salzmann, S. Riniker, *Anal. Chem.* **2020**, *92*, 9124–9131.

Curriculum Vitae

Etienne Victor Cotter

| | |
|----------------|---------------------------|
| Date of Birth | 28.September.1994 |
| Place of Birth | Sursee LU, Switzerland |
| Hometown | Anniviers VS, Switzerland |
| Nationality | Swiss |
| OrcID: | 0000-0001-9809-6343 |

Education

| | |
|-------------------|--|
| 10 2019 – 04 2024 | PhD in Organic & Medicinal Chemistry with Prof. Dr. Karl-Heinz Altmann, ETH Zurich Total synthesis of bioactive natural products |
| 02 2018 - 09 2019 | MSc in Interdisciplinary Sciences , ETH Zurich Organic Chemistry & Biological Chemistry major |
| 09 2014 - 02 2018 | BSc in Interdisciplinary Sciences , ETH Zurich Organic Chemistry & Biological Chemistry major |
| 08 2007 - 06 2013 | Swiss Academic Baccalaureate , Kantonsschule Willisau Biology & Chemistry major, Physics minor |

Scientific Experience

| | |
|-------------------|--|
| 06 2023 – 07 2023 | Research Exchange , CIB Madrid Together with Dr. Fernando Diaz <i>In vitro</i> testing of own synthesized compounds |
| 02 2019 – 09 2019 | Master Thesis , ETH Zurich Together with Prof. Dr. Karl-Heinz Altmann Total synthesis of bioactive natural products |
| 02 2018 - 07 2018 | Research Project , MIT Boston Together with Prof. Dr. Robert S. Langer Implementation & release studies on injectable hydrogels |
| 03 2017 - 06 2017 | BSc Thesis , ETH Zurich |

Together with Prof. Dr. Helma Wennemers
Molecular templates for length-controlled oligomerization

09|2016 - 02|2017

Research Project, ETH Zurich

Together with Prof. Dr. Jeffrey W. Bode
Synthesis of bicyclic peptides

Teaching Experience

10|2019 – 10|2023

Supervisor, ETH Zurich

Supervision of Several Master Thesis/Project Students
Total synthesis of bioactive natural products

10|2019 – 05|2023

Teaching Assistant, ETH Zurich

Practicum of Dr. Bernhard Pfeiffer
Isolation & quantification of natural products
with pharmaceutical sciences students

10|2019 – 01|2020

Teaching Assistant, ETH Zurich

Practicum of Dr. Stefan Gruber
General chemistry practicum for pharmaceutical sciences students

09|2017 – 06|2019

Teaching Assistant, ETH Zurich

Lecture of Prof. Dr. Helma Wennemers
Organic chemistry for chemistry students

02|2017 – 06|2019

Teaching Assistant, ETH Zurich

Lecture of Prof. Dr. Carlo Thilgen
Organic chemistry for biology & pharmacy students

Scientific Output

Publications

- (1) Cotter, E.; Glauser, S.; Lelke, A.; Scapozza, P.; Berardozi, S.; Lucena-Agell, D.; Hortigüela, R.; Oliva, M. A.; Fernando Díaz, J.; Altmann, K.-H. Synthesis and Structure-Activity Relationship Studies of Dioxane- and Oxathiane-Based Analogs of (–)-Zampanolide. *ChemRxiv*, **2024**. <https://doi.org/10.26434/CHEMRXIV-2024-NWB48>.
- (2) Cotter, E.; Pultar, F.; Riniker, S.; Altmann, K.-H. Experimental and Theoretical Studies on the Reactions of Aliphatic Imines with Isocyanates. *Chem. Eur. J.* **2024**, e202304272.
Associated cover page: *Chem. Eur. J.* **2024**, e202400619.

- (3) Brütsch, T. M*; Cotter, E*; Lucena-Agell, D.; Redondo-Horcajo, M.; Davies, C.; Pfeiffer, B.; Pagani, S.; Berardozzi, S.; Fernando Díaz, J.; Miller, J. H.; Altmann, K. H. Synthesis and Structure-Activity Relationship Studies of C(13)-Desmethylene(-)-Zampanolide Analogs. *Chem. Eur. J.* **2023**, e202300703. (*co-first authors)
Associated cover page: *Chem. Eur. J.* **2023**, 29 (36), e202301652.
Associated poster: <https://doi.org/10.1021/scimeetings.2c00480>
- (4) Lewandowski, B.; Schäfer, R. J. B.; Cotter, E.; Harangozo, D.; Wennemers, H. Catalytic Templated Length-Controlled Oligomerization. *Faraday Discuss.* **2023**, 244, 119–133.

Conferences

SCS Snow Symposium 2023, poster presentation

SICS 2023, poster presentation

Doktorandentag Spring 2022, IPW ETH Zurich, oral presentation

ACS Fall 2022, poster presentation <https://doi.org/10.1021/scimeetings.2c00480>

Several SCS Fall and Spring meetings, several poster presentations

Several SSCI Symposia, several poster presentations

Technical Skills

10|2019 – 04|2024

NMR Assistant

For the NMR Service in the Institute for Pharmaceutical Sciences (IPW), ETH

10|2019 – 04|2024

LC-MS Responsible

For the Altmann group

10|2019 – 04|2024

HPLC Responsible

For the Altmann group

Non-Scientific Working Experience

01|2014 - 04|2014

Quality controller, Flugzeugwerke Pilatus

Calibration laboratory in Stans

07|2013 - 12|2013

Swiss Military service

Air Force in Dübendorf

02 | 2013 – to date

Disc Jockey

Performing as DJ in clubs, bars & festivals

Summer jobs:

Stiftung Brändi, Emmi Käserei, Interio AG, Nussbaum AG

Language Skills

German

Mother Tongue

Graduate of Swiss Academic Baccalaureate in German

English

6 months staying at MIT, Boston, USA

Cambridge C1 diploma (advanced CAE),

2 months staying at St Giles International, London, GB

Graduate of Swiss Academic Baccalaureate in English

French

Graduate of Swiss Academic Baccalaureate in French

Extracurricular Activities

Sports

Soccer (leader of the weekly LOC soccer)

Surfing

Tennis

Skiing

Gym